
RUTHENIUM(II) AND IRIDIUM(III) COMPLEXES AS
PHOTOSENSITISERS TOWARDS LIGHT-DRIVEN
BIOCATALYSIS

A thesis submitted to the University of Manchester for the degree of
Doctor of Philosophy in the Faculty of Life Sciences

2012

Martyn Kyle Peers

TABLE OF CONTENT

List of Figures	7
List of Schemes	14
List of Tables	17
List of Abbreviations	19
Abstract	22
Declaration	23
Copyright Statement	23
Acknowledgements	24
Dedication	25
1. INTRODUCTION	26
1.1. Photophysical and Photochemical Processes	26
1.1.1. Absorption	26
1.1.2. Photophysical Processes	27
1.1.3. Photochemical Processes	28
1.2. Photosynthesis and Photosynthetic systems	28
1.3. Artificial Photosynthetic Systems	33
1.3.1. Photosensitizers	34
1.3.1.1. Flavins and deazariboflavins	34
1.3.1.2. Nicotinamide Adenine Dinucleotide	36
1.3.1.3. Thiouredopyrene-3,6,8-trisulfonates	36
1.3.1.4. Metal substituted Porphyrins	38
1.3.1.5. Transition Metal Complexes	38
1.4. Artificial Photosystems Inspired by Photosynthesis	42
1.4.1. Dye Sensitized Solar Cells	42
1.4.2. Solar Hydrogen Production	45
1.4.2.1. Photosystem I	45
1.4.2.2. Artificial Photosensitisers	48
1.4.3. Light-Driven Biocatalysis	50
1.5. Aims and Objectives	56
2. METHODS AND MATERIALS	57
2.1. Materials and Procedures	57
2.2. General Physical Measurements	57
2.3. Synthetic Chemistry	58
2.3.1. Ligand and Organic Precursor synthesis	58

2.3.1.1. Synthesis of 2,2'-bipyrazine	58
2.3.1.2. Synthesis of 4,4'-disubstituted-2,2'-bipyridine	60
2.3.1.3. Synthesis of Bridging Ligands	64
2.3.1.3.1. Towards 2,2'-bipyrimidine	64
2.3.1.3.2. Towards Tetra[3,2- <i>a</i> :2',3'- <i>c</i> :3'',2''- <i>h</i> :2''',3'''- <i>j</i>]phenazine (tpphz)	65
2.3.1.3.3. Towards the Synthesis of 2,2':4',4'':2'',2'''-quaterpyridine	65
2.3.1.4. Synthesis of 2,2':4,4'':4',4'''-quaterpyridyl and quaterpyridinium ligands	67
2.3.1.5. Synthesis of cyclometalating ligands	69
2.3.2. Metal Precursors	72
2.3.2.1. Ruthenium Precursors	72
2.3.2.2. Iridium Precursors	73
2.3.3. Synthesis of Ruthenium Complexes	74
2.3.3.1. Synthesis of Complexes of the general formula [Ru(bpz) ₂ (L)](PF ₆) _n	74
2.3.3.2. Synthesis of Complexes of the general formula [Ru(bpz) ₂ (L)](Cl) _n	79
2.3.3.3. Synthesis of complexes of the general formula [Ru(bpy)(L) ₂](X) _n	81
2.3.4. Synthesis of Monometallic Iridium Complexes	82
2.3.4.1. Synthesis of complexes of the general formula [Ir(ppy) ₂ (L)]X _n	82
2.3.4.2. Synthesis of complexes of the general formula [Ir(C ^N) ₂ (L)]X _n	83
2.4. Procedures in Molecular Biology	89
2.4.1. Media and Buffer Solutions	89
2.4.2. Mutant Stand Synthesis	90
2.4.3. DNA Agarose Gel Electrophoresis	90
2.4.4. DNA Purification - Gel Extraction	90
2.4.5. DNA Quantitation	91
2.4.6. Transformation of <i>E. coli</i> cells	91
2.4.7. Plasmid DNA Purification – Mini Prep	91
2.4.8. SDS-PAGE	92
2.4.9. Native PAGE	92
2.4.10. PETN Reductase Expression and Purification	92
2.4.10.1. PETNR Expression	92
2.4.10.2. PETNR Purification	92
2.4.10.2.1. Buffer Solutions	92
2.4.10.2.2. Purification Procedure A	93
2.4.10.2.3. Purification Procedure B	93
2.4.11. Labelling studies of PETNR	94
2.4.12. Spectrophotometric Assays	94
2.4.12.1. Diffusion-Controlled Multicomponent Systems	94
2.4.12.2. Sensitiser-Enzyme Constructs	94

2.4.12. Light-Driven Biocatalysis Assays	94
2.4.12.1. Aqueous Light-Driven Biocatalytic Assays Using Diffusion- Controlled Multicomponent Systems	94
2.4.12.2. Aqueous Light-Driven Biocatalytic Assays Using Sensitiser-Enzyme Constructs	95
2.4.12.3. Biphasic Light-Driven Biocatalytic Assays	95
2.4.12.4. Biphasic Biocatalytic Assays Using an Enzyme-Coupled Regeneration System	95
2.4.12.5. Analytical Procedures: Determination of Yields and Percentage Conversions	95
2.4.12.6 Analytical Procedures: Determination of Enantiomeric Excesses	96
3. SYNTHESIS AND ANALYSIS OF RUTHENIUM(II) POLYHETEROARYL COMPLEXES	97
3.1 Introduction	97
3.2. Results and Discussion	98
3.2.1 Synthetic Studies	98
3.2.1.1. Optimization of the Synthesis of 2,2'-bipyrazine	98
3.2.1.2. Synthesis of 4,4'-disubstituted-2,2'-bipyridines	100
3.2.1.3. Synthesis of Bridging Ligands	104
3.2.1.4. Synthesis of Complexes of the General Formula $[\text{Ru}(\text{bpz})_2\text{L}](\text{X})_2$	106
3.2.1.5. Synthesis of Complexes of the General Formula $[\text{Ru}(\text{bpz})_2\text{L}](\text{X})_4$	107
3.2.1.6. Synthesis of Complexes of the General Formula $[\text{Ru}(\text{L})_2\text{L}'](\text{X})_6$	108
3.2.1.7. Towards bimetallic species of the general formula $\{[\text{Ru}(\text{bpz})_2]\text{L}\}(\text{X})_4$	110
3.2.2. $^1\text{H-NMR}$ Spectroscopy	114
3.2.3. Electronic Spectroscopy	119
3.2.4. Electrochemical Studies	125
3.2.5. Theoretical Studies	128
3.2.5.1. Structural Geometries	128
3.2.5.2. Absorption Properties	129
3.3. Conclusions	136
3.4. Further Work	136
4. SYNTHESIS AND ANALYSIS OF CATIONIC IRIDIUM(III) CYCLOMETALATED COMPLEXES	137
4.1 Introduction	137
4.2. Results and Discussion	141
4.2.1 Synthetic Studies	141
4.2.1.1. Synthesis of Complexes of the General Formula $[\text{Ir}(\text{ppy})_2\text{L}](\text{X})_n$	141
4.2.1.2. Synthesis of Complexes of Bipyridinium Cyclometalating Ligands	142

4.2.1.2.1. Synthesis of Bipyridinium Pro-ligands	142
4.2.1.2.2. Synthesis of $\{[\text{Ir}(\text{C}^{\wedge}\text{N})_2\mu\text{-Cl}]_2\}^{4+}$ Intermediates	144
4.2.1.2.3. Synthesis of Complexes of the General Formula $[\text{Ir}(\text{C}^{\wedge}\text{N})_2(\text{N}^{\wedge}\text{N})](\text{X})_n$	146
4.2.2. NMR Spectroscopy	147
4.2.2.1. ^1H -NMR Spectroscopy	147
4.2.2.1.1. Bipyridinium Pro-ligands	147
4.2.2.1.2. Chloro-bridged Dimeric Intermediates	149
4.2.2.1.3. Monomeric Complexes	150
4.2.2.2. ^{13}C -NMR Spectroscopy	156
4.2.3. Crystallographic Studies	158
4.2.4. Electronic Spectroscopy	162
4.2.5. Electrochemical Studies	168
4.2.6. Theoretical Studies	175
4.2.6.1. Structural Geometries	175
4.2.6.2. Absorption Properties	177
4.3. Further Discussion	185
4.4. Conclusions	187
4.5. Further Work	188
5. DEVELOPMENT OF LIGHT-DRIVEN BIOCATALYTIC SYSTEMS	190
5.1. Introduction	190
5.2. Results and Discussion	196
5.2.1. Site-Directed Mutagenesis of Pentaerythritol Tetranitrite Reductase	196
5.2.1.1. Mutant Strand Synthesis	196
5.2.1.2. Expression and Purification of PETNR Variants.	198
5.2.2. Labelling Studies of PETNR Variants	201
5.2.2.1. Synthesis of Ruthenium Labels	201
5.2.2.2. Enzyme Labelling Trials	202
5.2.3. Development of Photosynthetic Systems	207
5.2.3.1. Diffusion Controlled Multicomponent Systems	207
5.2.3.1.1. Spectrophotometric Assays	207
5.2.3.1.2. Light-Driven Biocatalytic Assays	209
5.2.3.1.2.1. Enzyme Systems	210
5.2.3.1.2.2. Control Assays	212
5.2.3.1.2.3. Photosensitisers	213
5.2.3.1.2.4. Photosensitiser Concentration	216
5.2.3.1.2.5. Sacrificial Electron Donor Concentration	217
5.2.3.1.2.6. pH Dependence	218

5.2.3.1.3. Expanding the System: Selective Photoexcitation Towards Targeted Light-Driven Biocatalysis	221
5.2.4.1.4. Expanding the System: Applications Towards Other Substrates.	224
5.2.4.1.4.1. Aldehydes and Ketones	225
5.2.4.1.4.2. Maleimides	226
5.2.4.1.4.3. α,β -unsaturated nitroalkenes	227
5.2.4.1.4.4. Terpenoids	228
5.2.4.1.5. Expanding the System: Biphasic Assays	229
5.2.3.2. Covalently Bound Sensitiser-Enzyme Constructs	234
5.2.3.2.1. Spectrophotometric Assays	234
5.2.3.2.2. Light-Driven Biocatalytic Assays	235
5.3. Conclusions	236
5.4. Future Work	237
6. SUMMARY	239
7. APPENDIX	242
8. REFERENCES	255

Total Word Count: 100,214

LIST OF FIGURES

Fig 1.1.	Simplified molecular orbital diagrams illustrating the electronic transitions of A) an organic chromophore and B) an octahedral transition metal complex of D3 symmetry.	27
Fig. 1.2.	A modified Jabłoński diagram displaying the potential photophysical processes accessible by a molecule excited from a singlet ground state	28
Fig. 1.3.	A) The structure of chlorophyll a where R = CH ₃ and chlorophyll b where R = CHO and R ₂ = phytol. B) The absorption spectra of chlorophylls a and b.	30
Fig 1.4.	Schematic drawing detailing the predominant electron transfer processes inherent in DSSCs on photovoltaic current generation, also highlighting the relative energy levels of individual components.	43
Fig 1.5.	Example dye photosensitisers that have been utilised in the preparation of DSSCs.	44
Fig. 1.6.	Illustrating A) potential molecular wires used in the study of PSI nanoparticle bioconjugates and B) the schematic of the subsequent PS I – molecular wire – [FeFe]-hydrogenase construct using 1,6-hexanedithiol.	47
Fig. 1.7.	A schematic representation of the Ru-MV-cyt c ₃ triad complex employed in conjunction with the [NiFe]-hydrogenase from <i>Desulfovibrio vulgaris</i> .	49
Fig. 1.8.	Representative schematic of the artificial hybrid photosynthetic system utilising [Ru(bpy) ₂ (d(PO ₃ H ₂)bpy)] and (Db[NiFeSe]-H) co-adsorbed to the surface of TiO ₂ nanoparticles.	50
Fig. 3.1.	Representative structures of the four bridging ligands investigated as part of this study; (a) 2,2'-bipyrimidine (bpm); (b) 2,3-dipyridylpyrazine (dpp); (c) 2,2':4',4'':2'',2'''-quaterpyridine and (d) tetrapyrido[3,2-a:2',3'-c:3'',2''-h:2''',3'''-j]phenazine (tpphz).	104
Fig. 3.2.	Representative structures for each of the synthesised complexes with the general formula [Ru(bpz) ₂ (N [^] N)] ⁿ⁺ . Complexes were isolated as both the hexafluorophosphate and chloride salts.	113
Fig. 3.3.	Representative structures for complexes of the general formula [Ru(bpz) ₂ (N [^] N)] ²⁺ with labelling schemes used for NMR assignments.	114
Fig. 3.4.	¹ H-NMR spectra of a) [Ru(bpz) ₂ dCF ₃ bpy](PF ₆) ₂ and b) [Ru(bpz) ₂ bpy](PF ₆) ₂ . A section of the COSY spectrum of c) [Ru(bpz) ₂ d ^t Bubpy](PF ₆) ₂ in the region 7.00-10.00 ppm used in the identification of individual spin systems within the complex.	115

Fig. 3.5.	Section of the NOESY spectrum of $[\text{Ru}(\text{bpz})_2\text{d}^t\text{Bubpy}](\text{PF}_6)_2$ recorded in CD_3CN . Depicted region of 7.3-8.7 ppm chosen for clarity of the most significant cross peaks used in the determination of the ^1H -NMR assignment.	117
Fig. 3.6.	Three dimensional model structure of complexes with the general formula $[\text{Ru}(\text{bpz})_2(\text{N}^{\wedge}\text{N})]$. NOE contacts used in the assignment of ^1H -NMR spectra are illustrated and the corresponding atoms highlighted. A) View focused on the NOE contacts of A(6) and B) displaying similar interactions of C(6).	118
Fig. 3.7.	UV-visible absorption spectra of the complexes $[\text{RuZ}_2\text{A}](\text{PF}_6)_2$ (purple), $[\text{RuZ}_2\text{B}](\text{PF}_6)_2$ (blue), $[\text{RuZ}_2\text{Y}](\text{PF}_6)_2$ (red) and $[\text{RuZ}_2\text{F}](\text{PF}_6)_2$ (green) displaying A) the full spectra and B) $320 \leq \lambda \leq 650\text{nm}$ expansion of the lower energy bands. Recorded in acetonitrile at 298 K.	120
Fig. 3.8.	Cyclic voltammograms of $[\text{Ru}(\text{bpz})_3](\text{PF}_6)_2$ (orange), $[\text{Ru}(\text{bpz})_2(\text{bpy})](\text{PF}_6)_2$ (red) and $[\text{Ru}(\text{bpy})_3](\text{PF}_6)_2$ (dark red) recorded at 100 mVs^{-1} in $0.1 \text{ M } n\text{-Bu}_4\text{NPF}_6$ acetonitrile at 298 K.	126
Fig. 3.9.	Cyclic voltammograms of $[\text{Ru}(\text{bpz})_2\text{dNH}_2\text{bpy}](\text{PF}_6)_2$ (purple), $[\text{Ru}(\text{bpz})_2\text{d}^t\text{Bubpy}](\text{PF}_6)_2$ (blue), $[\text{Ru}(\text{bpz})_2\text{bpy}](\text{PF}_6)_2$ (red) and $[\text{Ru}(\text{bpz})_2\text{dCF}_3\text{bpy}](\text{PF}_6)_2$ (green) recorded at 100 mVs^{-1} in $0.1 \text{ M } n\text{-Bu}_4\text{NPF}_6$ acetonitrile at 298 K.	127
Fig. 3.10.	Representative structures for complexes of the general formula $[\text{Ru}(\text{bpz})_2(\text{N}^{\wedge}\text{N})]^{2+}$ with labelling schemes used in the discussion of optimized geometries.	129
Fig. 3.11.	Experimental (green) and the DFT calculated (blue dash) UV-Visible spectra of (a) $[\text{Ru}(\text{bpz})_2\text{dNH}_2\text{bpy}]^2$, (b) $[\text{Ru}(\text{bpz})_2\text{bpy}]^2$ and (c) $[\text{Ru}(\text{bpz})_2\text{dCF}_3\text{bpy}]^2$.	131
Fig. 3.12.	DFT calculated electron density maps (isosurface value $0.03 \text{ e}/\text{\AA}^3$) and respective energies for orbitals involved in the lower energy absorption ($>350 \text{ nm}$) ascribed to MLCT transitions of $[\text{Ru}(\text{bpz})_2\text{bpy}]^{2+}$. Energies of the respective orbitals of $[\text{Ru}(\text{bpz})_2\text{d}^t\text{Bubpy}]^{2+}$ and $[\text{Ru}(\text{bpz})_2\text{dCF}_3\text{bpy}]^{2+}$ are also listed.	132
Fig. 3.13.	Experimental (green) and the TD-DFT calculated (blue dash) UV-visible spectra of $[\text{Ru}(\text{bpz})_2\text{Me}_2\text{qpy}]^{4+}$.	133
Fig. 3.14.	DFT calculated electron density maps (isosurface value $0.03 \text{ e}/\text{\AA}^3$) and respective energies for orbitals of $[\text{Ru}(\text{bpz})_2\text{Me}_2\text{qpy}]^{4+}$ involved in ILCT centered upon the ancillary ligand.	134
Fig. 3.15.	Energy level diagram for complexes of the general formula $[\text{Ru}(\text{bpz})_2\text{L}]^{n+}$ displaying the TD-DFT calculated MOs within the range	134

	of -1.5 and -9.0 eV.	
Fig. 4.1.	General structure of the bis cyclometalated iridium(III) compounds	137
Fig. 4.2.	Examples of water soluble Iridium cyclometalated compounds.	139
Fig. 4.3.	Representative structure of the bipyridinium cyclometalating and bipyridyl ancillary ligands with labeling schemes used in ¹ H-NMR assignments.	148
Fig. 4.4.	The linkage isomers that may be adopted on cyclometalation of 1-methyl-3-(2-pyridyl)pyridinium; a) (1-methyl-3-(2-pyridyl)pyridin-4-yl-ium-C ⁴ ,N') and b) (1-methyl-3-(2-pyridyl)pyridin-2-yl-ium-C ² ,N').	150
Fig. 4.5.	¹ H-NMR spectra of a) [Ir(42) ₂ Y](PF ₆) ₃ (green) and b) [Ir(32) ₂ Y](PF ₆) ₃ (red). c) A section of the 2D-COSY spectrum of [Ir(22) ₂ Y](PF ₆) ₃ (blue) in the region of 6.80 - 8.90 ppm, as used in the assignment of individual resonances.	151
Fig 4.6.	DQF-COSY spectra of [Ir(22) ₂ F](PF ₆) ₃ in CD ₃ CN. a) Displaying the regions 4.5-4.8 and 7.0-9.2 ppm. b) A magnification of the cross peaks assigned to long range coupling of the methyl protons.	153
Fig. 4.7.	Section of the NOESY spectrum of [Ir(22) ₂ B](PF ₆) ₃ in the regions of 4.5-4.8 and 7.0-8.8 ppm, illustrating the interactions of the aromatic protons and the long-range NOE contacts of the methyl group of the pyridinium ring.	154
Fig. 4.8.	Heteronuclear spectra of [Ir(32) ₂ Y](PF ₆) ₃ as used in the assignment of individual resonances of the ¹³ C-NMR spectra. a) Sections of the HMQC and b) Sections of the HMBC spectra recorded in CD ₃ CN.	157
Fig. 4.9.	Representation of the crystal structure of {Ir(ppy) ₂ [(Pym) ₂ qpy]}(PF ₆) ₃ with counter anions and solvent molecules omitted for clarity. Displacement ellipsoids are set at the 30 % probability level.	158
Fig. 4.10.	Representation of the crystal structures of a) [Ir(22) ₂ Y](PF ₆) ₃ and b) [Ir(42) ₂ Y](PF ₆) ₃ with counter anions and solvent molecules omitted for clarity. Displacement ellipsoids are set at the 30 % probability level.	159
Fig. 4.11.	Representation of the crystal structure of [Ir(32) ₂ B](PF ₆) ₃ with counter anions and solvent molecules omitted for clarity. Displacement ellipsoids are set at the 30 % probability level.	161
Fig. 4.12.	UV-visible absorption spectra of the complexes [Ir(ppy) ₂ qpy](PF ₆) ₃ (blue), [Ir(ppy) ₂ Me ₂ qpy](PF ₆) ₃ (red) and [Ir(ppy) ₂ Pym ₂ qpy](PF ₆) ₃ (green) displaying a) the full spectra and b) 350 ≤ λ ≤ 700 nm expansion of the lower energy bands. Recorded in MeCN at 298 K.	163
Fig. 4.13.	UV-visible absorption spectra of the complexes [Ir(22) ₂ Y](PF ₆) ₃ (blue),	166

	[Ir(32) ₂ Y](PF ₆) ₃ (red) and [Ir(42) ₂ Y](PF ₆) ₃ (green) displaying a the full spectra and b) 320 ≤ λ ≤ 500 nm expansion of the lower energy bands. Recorded in acetonitrile at 298 K.	
Fig. 4.14.	UV-visible absorption spectra of the complexes [Ir(22) ₂ Y](PF ₆) (blue), [Ir(22) ₂ B](PF ₆) ₃ (red) and [Ir(22) ₂ F](PF ₆) ₃ (green) displaying a the full spectra and b) 320 ≤ λ ≤ 500 nm expansion of the lower energy bands. Recorded in acetonitrile at 298 K.	167
Fig. 4.15.	Cyclic voltammograms of [Ir(ppy) ₂ qpy](PF ₆) (blue), [Ir(ppy) ₂ Me ₂ qpy](PF ₆) ₃ (red) and [Ir(ppy) ₂ Pym ₂ qpy](PF ₆) ₃ (green) recorded at 100 mVs ⁻¹ in 0.1 M <i>n</i> -Bu ₄ NPF ₆ acetonitrile at 298 K.	169
Fig. 4.16.	Pulse differential voltammograms depicting the oxidation processes of [Ir(ppy) ₂ qpy](PF ₆) (orange), [Ir(22) ₂ Y](PF ₆) ₃ (blue), [Ir(32) ₂ B](PF ₆) ₃ (red) and [Ir(42) ₂ F](PF ₆) ₃ (green) recorded in 0.1M <i>n</i> -Bu ₄ NPF ₆ acetonitrile at 298 K.	170
Fig. 4.17.	Cyclic voltammograms depicting the reduction processes of [Ir(22) ₂ Y](PF ₆) ₃ (blue), [Ir(22) ₂ B](PF ₆) ₃ (red) and [Ir(22) ₂ F](PF ₆) ₃ (green) recorded at 100 mVs ⁻¹ in 0.1M <i>n</i> -Bu ₄ NPF ₆ acetonitrile at 298 K.	172
Fig. 4.18.	Cyclic voltammograms depicting the reduction processes of [Ir(22) ₂ Y](PF ₆) ₃ (blue), [Ir(32) ₂ Y](PF ₆) ₃ (red) and [Ir(42) ₂ Y](PF ₆) ₃ (green) recorded at 100 mVs ⁻¹ in 0.1M <i>n</i> -Bu ₄ NPF ₆ acetonitrile at 298 K.	172
Fig.4.19.	Cyclic voltammograms depicting the reduction processes of [Ir(32) ₂ Y](PF ₆) ₃ (blue), [Ir(32) ₂ B](PF ₆) ₃ (red) and [Ir(32) ₂ F](PF ₆) ₃ (green) recorded at 100 mVs ⁻¹ in 0.1M <i>n</i> -Bu ₄ NPF ₆ acetonitrile at 298 K.	174
Fig. 4.20.	Schematic of the optimized structure of [Ir(22) ₂ Y] ³⁺ ; highlighting the interatomic distances between the <i>N</i> -methyl group of the bipyridinium ring and the hydrogen in the 3-position of the pyridyl ring.	176
Fig. 4.21.	Experimental (green) and the DFT calculated (blue dash) UV-Visible spectra of a) [Ir(22) ₂ Y] ³⁺ , b) [Ir(32) ₂ Y] ³⁺ and c) [Ir(42) ₂ Y] ³⁺ .	178
Fig. 4.22.	DFT calculated electron density maps (isosurface value 0.03 e/Å ³) and respective energies selected orbitals of [Ir(22) ₂ Y] ³⁺ . Energies of corresponding orbitals of [Ir(42) ₂ Y] ³⁺ are also listed.	179
Fig. 4.23.	DFT calculated electron density maps (isosurface value 0.03 e/Å ³) and respective energies for selected orbitals of [Ir(32) ₂ Y] ³⁺ .	180
Fig. 4.24.	Experimental (green) and the TD-DFT calculated (blue dash) UV-Visible spectra of a) [Ir(ppy) ₂ qpy] and b) [Ir(ppy) ₂ Me ₂ qpy] ³⁺ .	182

Fig. 4.25.	DFT calculated electron density maps (isosurface value $0.03 \text{ e}/\text{\AA}^3$) and respective energies for the LUMO of a) $[\text{Ir}(\text{ppy})_2\text{qpy}]^+$ and b) $[\text{Ir}(\text{ppy})_2\text{Me}_2\text{qpy}]^{3+}$.	183
Fig. 4.26.	Energy level diagram for complexes of the general formula $[\text{Ir}(\text{C}^{\wedge}\text{N})_2(\text{N}^{\wedge}\text{N})]^{n+}$ displaying the TD-DFT calculated MOs between -2.0 and -9.0 eV.	183
Fig. 4.27.	Potential alternate cyclometalating ligands incorporating the pyridinium or pyridinium-type moiety. a) 1-methyl-3-phenylpyrazinium; b) 1-methyl-4-phenylpyrimidinium; c) 1-methyl-2'-phenyl-[4,4'-bipyridin]-1-ium; d) 1-methyl-4-(3-(pyridin-3-yl)phenyl)pyridin-1-ium and e) 1-methyl-2'-(3-(1-methylpyridin-1-ium-4-yl)phenyl)-[4,4'-bipyridin]-1-ium.	188
Fig. 5.1.	Crystal structure of TOYE displayed as a rainbow coloured cartoon N- (blue) to C- (red) terminus	194
Fig. 5.2.	The x-ray crystal structure of the active site of PETNR, highlighting the target residues for mutagenesis studies and their relative positions with respect to FMN.	196
Fig. 5.3.	Agarose gel showing final results achieved via PCR in the preparation of PETNR variants; (left to right) 1kb ladder, PETNR _{Q241C} , PETNR _{G301C} and PETNR _{R324C} .	197
Fig. 5.4.	UV-vis absorption profile recorded on purification of PETNR _{Q241C} by column chromatography utilising an AKTA purifier 100 system	198
Fig. 5.5.	SDS-PAGE of protein expression trials of the PETNR variants	200
Fig. 5.6.	SDS-PAGE of fractions collected on purification using a Hi-Prep Q Sepharose column. Stained with Coomassie Brilliant Blue R250.	200
Fig. 5.7.	Native PAGE of the two different products isolated on purification using a Hi-Prep Q Sepharose column	200
Fig. 5.8.	The X-ray crystal structure of PETNR, highlighting the relative positions of the C222 residue and the enzyme bound FMN of the active site.	203
Fig. 5.9.	UV-visible absorption spectra of the photosensitiser-PETNR _{Q241C} constructs using the labelling reagents (a) $[\text{Ru}(\text{bpy})_2(4\text{-hydroxymethyl-4'-methyl-2,2'-bipyridine})]^{2+}$ or (b) $[\text{Ru}(\text{bpz})_2(4\text{-hydroxymethyl-4'-methyl-2,2'-bipyridine})]^{2+}$.	204
Fig. 5.10.	Difference spectra recorded in the spectrophotometric studies of diffusion controlled multicomponent biocatalytic systems.	208
Fig. 5.11.	Time course of the bioreduction of 2-cyclohexenone by a number of OYEs in conjunction with a light-driven biocatalytic system.	210
Fig. 5.12.	Crystal structures of (A) TOYE (PDB code: 3KRU) and (B) PETNR	211

	(PDB code 1H50) focused upon the active site. (C) side view of the active site in native PETNR and (D) the R324C variant, the mutated residue is highlighted in purple for clarity.	
Fig. 5.13.	a) Time course illustrating the influence of changes in photosensitiser in the bioreduction of 2-cyclohexenone by TOYE. b) Plot of redox potentials of the Ru(II/III) couple vs TOF highlighting the impact of changes of photosensitizer upon the activity of the system.	215
Fig. 5.14.	Time course indicating the influence of photosensitiser concentration upon the light-driven biocatalytic reduction of 2-cyclohexen-1-one by A) PETNR and B) TOYE.	216
Fig. 5.15.	Time course highlighting the impact of the concentration of TEOA in the light-driven PETNR catalysed reduction of 2-cyclohexen-1-one using A) [Ru(bpz) ₂ dClbpy]Cl ₂ and B) [Ir(22) ₂ bpy]Cl ₃ as photosensitisers.	218
Fig. 5.16.	Time course indicating the influence of pH upon the light-driven PETNR catalysed reduction of 2-cyclohexen-1-one using a) [Ru(bpz) ₂ dClbpy]Cl ₂ and b) [Ir(22) ₂ bpy]Cl ₃ .	219
Fig. 5.17.	Proposed structures for the protonated bpz ligand radical formed on excitation of [Ru(bpz) ₃] ²⁺ in an acidic solution. a) N protonation b) H-adduct.	220
Fig. 5.18.	UV-visible absorption spectra of [Ir(32) ₂ dCF ₃ bpy]Cl ₃ (blue); [Ir(22) ₂ bpy]Cl ₃ (green); [Ru(bpz) ₂ dClbpy]Cl ₂ (purple) and [Rubpy(Me ₂ qpy) ₂]Cl ₆ (red) recorded in deionized water and highlighting the various longpass filters employed in the study of selective photoexcitation.	221
Fig. 5.19.	The influence of photosensitisers and the wavelength of incident irradiation upon the activity of PETNR towards the bioreduction of 2-cyclohexen-1-one, as demonstrated employing long pass filters at a) 530 b) 460 c) 360 and d) 305 nm.	223
Fig. 5.20.	Spectral changes afforded over the course of 30 minutes on illumination of a solution containing PETNR _{R324CRu} in Tris-HCl (5 mM, pH 8.0) and in the presence of TEOA (25 mM, pH 8.0).	235
Fig. A.1.	Representative structures of the prepared photosensitisers containing the bis(2,2'-bipyrazyl)ruthenium(II) moiety and a neutral polyheteroaryl ancillary ligand.	242
Fig. A.2.	Representative structures of the prepared photosensitisers containing the bis(2,2'-bipyrazyl)ruthenium(II) moiety and a 4,4':2',2'':4'':4'''-quaterpyridinium ancillary ligand.	243
Fig. A.3.	Structure of [Ru(bpy)(Me ₂ qpy) ₂] ⁶⁺ that was prepared in an effort to	243

	access complex salts of higher overall positive charge. The complex was isolated as both the hexafluorophosphate and chloride salts.	
Fig. A.4.	Representative structures of the cationic cyclometalated iridium(III) complexes of 2-phenylpyridine utilising the 4,4':2',2'':4'':4'''-quaterpyridyl or 4,4':2',2'':4'':4'''-quaterpyridinium ancillary ligands.	243
Fig. A.5.	Representative structures of the bis-cyclometalated iridium(III) complexes of the 2,2'-, 3,2' and 4,2'- isomers of methylated bipyridinium.	244
Fig. B.1.	UV-visible absorption spectra of the complexes [Ru(bpy) ₂ (Me ₂ qpy)](PF ₆) ₄ (red), [Ru(bpy)(Me ₂ qpy) ₂](PF ₆) ₆ (blue) and [Ru(Me ₂ qpy) ₃](PF ₆) ₈ (green) in acetonitrile at 298 K	245
Fig. D.1.	Representation of the crystal structure of [Ir(22) ₂ ClMeCN](PF ₆) ₃ with counter anions and solvent molecules omitted for clarity. Displacement ellipsoids are set at the 30% probability level.	248
Fig. D.2.	A section of the 2D-COSY spectrum of [Ir(22) ₂ Y](PF ₆) ₃ in the region 6.75 – 10.50 ppm used in the assignment of the ¹ H-NMR resonances. Spectra recorded in CD ₃ CN.	248
Fig. E.1.	Normalized UV-visible absorption spectra of [1-Me-2,2'-bpy]PF ₆ (blue), [1-Me-3,2'-bpy]PF ₆ (red) and [1-Me-4,2'-bpy]PF ₆ (green) displaying the region of 200 ≤ λ ≤ 360nm. Recorded in acetonitrile at 298 K.	249
Fig. E.2.	Cyclic voltammograms depicting the reduction processes of [1-Me-2,2'-bpy]PF ₆ (blue), [1-Me-3,2'-bpy]PF ₆ (red) and [1-Me-4,2'-bpy]PF ₆ (green) recorded at 100 mVs ⁻¹ in 0.1M n-Bu ₄ NPF ₆ acetonitrile at 298 K.	249
Fig. F.1.	Experimental (green) and the TD-DFT calculated (blue dash) UV-Visible spectra of (a) [Ir(22) ₂ B] ³⁺ and (b) [Ir(22) ₂ F] ³⁺ .	250
Fig. G.1.	UV-visible absorption spectra of [Ru(bpy) ₂ (4-hydroxymethyl-4'-methyl-2,2'-bipyridine)]Cl ₂ (blue), [Ru(bpz) ₂ (4-hydroxymethyl-4'-methyl-2,2'-bipyridine)]Cl ₂ (red) and {[Ru(bpz) ₂ [(HOCH ₂ Ph) ₂ qpy]}Cl ₄ (green) in deionised water at 293 K displaying a) the full spectra and b) 300 ≤ λ ≤ 050nm expansion of the lower energy bands. Recorded in deionised water at 298 K.	252
Fig. H.1.	Time courses highlighting the relative activity of PETNR _{R324C} and TOYE in the homogenous light-driven bioreductions of a variety of α,β-disubstituted alkene substrates.	254

LIST OF SCHEMES

Scheme 1.1.	Redox chemistry of the plastoquinone transfer mediator employed in the electron transport chain of photosystem II.	30
Scheme 1.2.	Sequence of electron transfer from water to NADP ⁺ via the photosystems PSII and PSI as part of oxygenic photosynthesis.	32
Scheme 1.3.	Generalized schematic energy diagram highlighting the key components and electron transfer processes within a simplified photosynthetic system.	33
Scheme 1.4.	Schematic illustrating the redox chemistry of the isoalloxazine ring of the flavin cofactors and the structures of the resultant products/intermediates.	34
Scheme 1.5.	Photoexcitation of NAD(P)H via two photon absorption and subsequent reduction of ferric BM3 haem domain to yield the BM3 Fe ^{II} -CO complex.	36
Scheme 1.6.	Formation of thiouredopyrene-3,6,8-trisulfonates on reaction of 2-isothiocyanatopyrene-3,6,8-trisulfonate with cystamine, where R = NH ₂ C ₂ H ₄ - or TUPS-.	37
Scheme 1.7.	Reaction scheme for the preparation of Ru ^(II) (bpy) ₂ (dcbpy-cytochrome c) derivatives.	39
Scheme 1.8.	Proposed mechanisms of a) photooxidation and b) photoreduction of an enzyme cofactor by an excited ruthenium complex; where M = enzyme redox cofactor, A = acceptor, D = donor and P = oxidation/reduction products.	40
Scheme 1.9.	Synthesis of the Ru ₂ Z bimetallic photosensitizer via a two stages reaction. i) Synthesis of the bis(2,2'-bipyrazyl)dichlororuthenium(II) precursor. ii) Subsequent reaction with 0.5 equivalence of the 2,2':4',4'':2'',2'''-quaterpyridine bridging ligand to yield the bimetallic species.	42
Scheme 1.10.	Proposed mechanism of the proflavine photosensitized NADH regeneration system employing [Cp*Rh(bpy)H ₂ O] ⁺ as an electron mediator and TEOA as a sacrificial donor.	53
Scheme 1.11.	Outline of the mechanism for the light-driven cofactor regeneration of a Baeyer-Villiger monooxygenase and subsequent oxidation reaction of the ketone substrate.	54
Scheme 1.12.	Schematic highlighting the individual processes involved in the photochemical initiated reduction of a flavoenzyme using free flavin as a photosensitizer.	54

Scheme 1.13.	Representative schematic of electron transfer processes postulated for the biocatalytic reduction of ketoisophorone to (R)-levodione employing CdSe quantum dots as a photosensitiser.	55
Scheme 3.1.	Schematic of the final procedure developed in the synthesis of 2,2'-bipyrazine.	99
Scheme 3.2.	Reaction scheme for the synthesis of 4,4'-disubstituted-2,2'-bipyridine ancillary ligands.	101
Scheme 3.3.	Mechanism of the Zincke reaction.	103
Scheme 3.4.	Reaction scheme for the synthesis of 4-iodo-2,2'-bipyridine from 4-nitro-2,2'-bipyridine.	105
Scheme 3.5.	Reaction schemes utilized in the preparation of (2,2'-bipyridyl)-bis-(quaterpyridinium)ruthenium(II) complexes via a Ru(bpy)(X) ₄ intermediate, where R = Me or 2-pyrimidyl.	109
Scheme 3.6.	Coordination reactions highlighting the two potential routes towards ruthenium(II) bimetallic complexes using the bridging ligands a) 2,2'-bipyrimidine and b) 2,3-(2'-pyridyl)pyrazine.	110
Scheme 3.7.	Attempted reaction pathway towards [Ru(bpz) ₂ (N ^N)] ²⁺ via the dicarbonyl intermediate, [Ru(bpz) ₂ (CO) ₂] ²⁺ .	111
Scheme 3.8.	Preparation of complexes of the general formula [Ru(bpz) ₂ L] ²⁺ via the diaqua intermediate, demonstrated with the use of the dCF ₃ bpy ancillary ligand.	112
Scheme 4.1.	Reaction scheme detailing the general procedure used in the preparation of bis-cyclometalated cationic iridium(III) complexes.	141
Scheme 4.2.	Catalytic cycle of the palladium catalysed Negishi cross-coupling reactions.	142
Scheme 4.3.	Synthesis of the <i>N</i> -substituted 3-(2'-pyridyl)pyridinium and 4-(2'-pyridyl)pyridinium pro-ligands.	143
Scheme 4.4.	Reaction scheme for the preparation of complexes with the general formula [Ir(C ^N) ₂ (N ^N)] ³⁺ , illustrating representative structures of the complexes and ligands to be utilised as part of this investigation.	145
Scheme 4.5.	Resonance structures inherent within the pyridyl ring resulting in partial positive charges in the α and γ positions with respect to the heteroatom.	147
Scheme 4.6.	Resonance structures of the deprotonated pyridinium ring of a) 1-methyl-2-(2-pyridyl)pyridin-3-yl-ium; b) 1-methyl-3-(2-pyridyl)pyridin-4-yl-ium; c) 1-methyl-4-(2-pyridyl)pyridin-3-yl-ium and d) 1-methyl-3-(2-pyridyl)pyridin-2-yl-ium. The pyridyl ring has been omitted for clarity.	189
Scheme 5.1.	Mechanism for the reductive half reaction of the OYE family	190

	highlighting the reduction of the FMN cofactor by NAD(P)H.	
Scheme 5.2.	Mechanism for the oxidative half-reaction of the OYE family, catalyzing the reduction of an α , β -unsaturated alkene.	191
Scheme 5.3.	Asymmetric bioreduction of a variety of α , β -unsaturated carbonyl compounds catalyzed by OYEs.	192
Scheme 5.4.	The proposed mechanism of biocatalytic reduction of α , β -unsaturated nitroalkenes, by the OYE family.	193
Scheme 5.5.	a) Synthesis of the 4-hydroxymethyl-4'-methyl-2,2'-bipyridine pro-ligand; b) Coordination of the pro-ligand to the Ru(bpy) ₂ Cl ₂ precursor and subsequent bromination reaction to yield the final complex to be used in labeling studies.	201
Scheme 5.6.	Electron transfer processes that are proposed to contribute towards enzyme reduction, and ultimately total catalytic turnover, in the light-driven catalytic cycles of PETNR and TOYE.	212
Scheme 5.7.	Reactions of the sacrificial electron donor in photosensitised reactions.	220
Scheme 5.8.	The proposed mechanism in the photochemical reduction of nitro-compounds, proceeding via hydrogen abstraction by the ³ n, π * excited state.	227
Scheme 5.9.	Proposed schematic for the light-driven biocatalytic reduction of activated alkenes by the flavin containing OYE using a transition metal photosensitiser and methyl viologen as an electron transfer mediator.	236

LIST OF TABLES

Table 1.1.	Reduction potentials of the Ru ₂ C and Ru ₂ Z complexes vs normal hydrogen electrode.	42
Table 3.1.	UV-visible absorption data for complexes of ruthenium containing the quaternised quaterpyridinium ligands, recorded as both the hexafluorophosphate and chloride salts.	122
Table 3.2.	UV-Visible absorption data for complexes of the general formula [Ru(bpz) ₂ L] ⁿ⁺ recorded as the hexafluorophosphate salt.	123
Table 3.3.	UV-Visible absorption data for complexes of the general formula [Ru(bpz) ₂ L] ⁿ⁺ recorded as the chloride salt.	124
Table 3.4.	Redox properties for compounds of the general formula [Ru(bpz) ₂ L] ⁿ⁺ .	125
Table 3.5.	Selected bond lengths (Å) and bond angles (°) taken from X-ray crystallography and from the DFT calculated optimized geometries of complexes of the general formula [Ru(bpz) _{3-x} L _x] ⁿ⁺ .	129
Table 3.6.	Select vertical transitions obtained by TD-DFT calculations performed for the complex cations of the general formula [Ru(bpz) _{3-x} L _x] ⁿ⁺ .	136
Table 4.1.	¹ H-NMR assignments (δ, ppm) for complexes of the general formula [Ir(C [^] N) ₂ (N [^] N)](PF ₆) ₃ containing the bipyridinium cyclometalating ligands.	148
Table 4.2.	¹³ C-NMR assignments (δ, ppm) for complexes [Ir22Y](PF ₆) ₃ , [Ir32Y](PF ₆) ₃ and [Ir42Y](PF ₆) ₃ .	157
Table 4.3.	Selected bond lengths (Å), angles (°) and torsional angles (°) taken from single crystal X-ray structures for complexes [Ir(22) ₂ Y](PF ₆) ₃ ; [Ir(22) ₂ B](PF ₆) ₃ ; [Ir(42) ₂ F](PF ₆) ₃ ; [Ir(32) ₂ Y](PF ₆) ₃ ; [Ir(32) ₂ B](PF ₆) ₃ ; [Ir(42) ₂ Y](PF ₆) ₃ and [Ir(ppy) ₂ (Me ₂ Qpy)](PF ₆) ₃ .	159
Table 4.4.	UV-Visible absorption data for the complexes of the general formula [Ir(ppy) ₂ (N [^] N)] ⁿ⁺ containing quaterpyridyl ancillary ligands.	162
Table 4.5.	UV-Visible absorption data for the complexes of the general formula [Ir(C [^] N) ₂ (N [^] N)] ³⁺ containing the bipyridinium cyclometalating ligands recorded as the hexafluorophosphate salt.	164
Table 4.6.	UV-Visible absorption data for the complexes of the general formula [Ir(C [^] N) ₂ (N [^] N)] ³⁺ containing the bipyridinium cyclometalating ligands recorded as the chloride salt.	165
Table 4.7.	Electrochemical data for the methylated quaternized bipyridinium pro-ligands and complexes of the general formula [Ir(C [^] N) ₂ (N [^] N)](PF ₆) _n .	168
Table 4.8.	Selected bond lengths (Å) and bond angles (°) taken from DFT calculated optimized geometries of [Ir(22) ₂ Y] ³⁺ , [Ir(32) ₂ Y] ³⁺ , [Ir(42) ₂ Y] ³⁺ , [Ir(ppy) ₂ ppy] ⁺ and [Ir(ppy) ₂ Me ₂ ppy] ³⁺ .	175

Table 4.9.	Select vertical transitions obtained by TD-DFT calculations performed for the complex cations $[\text{Ir}(\text{22})_2\text{Y}]^{3+}$, $[\text{Ir}(\text{32})_2\text{Y}]^{3+}$, $[\text{Ir}(\text{42})_2\text{Y}]^{3+}$, $[\text{Ir}(\text{ppy})_2\text{qpy}]^+$ and $[\text{Ir}(\text{ppy})_2\text{Me}_2\text{qpy}]^{3+}$.	184
Table 5.1.	List of primers used in the sequencing of PETNR variants, displaying both the forward and complementary sequences.	197
Table 5.2.	PCR cycling parameters used in the preparation of plasmid DNA towards the required PETNR variants.	197
Table 5.3.	Results of purification of PETNR _{Q241C} variant, highlighting the respective protein content at each individual stage of the procedure.	200
Table 5.4.	Comparison of the relative activities obtained for a number of OYEs towards the light-driven bioreduction of 2-cyclohexenone.	210
Table 5.5.	Influence of modifications made to the photosensitiser upon the activity of light driven biocatalytic systems in the reduction of 2-cyclohexenone by PETNR _{R324C} and TOYE.	214
Table 5.6.	Impact of changing photosensitiser concentration upon the rates of light driven biocatalytic reduction of 2-cyclohexenone by PETNR _{R324C} and TOYE.	216
Table 5.7.	Influence of changes in sacrificial electron donor concentrations upon the rates of light driven biocatalytic reduction of 2-cyclohexenone by PETNR _{R324C} and TOYE.	217
Table 5.8.	pH dependency of the light driven biocatalytic reduction of 2-cyclohexenone by PETNR _{R324C} and TOYE.	219
Table 5.9.	Influence of the wavelength of incident irradiation in the light driven bioreduction of 2-cyclohexene by PETNR _{R324C} .	222
Table 5.10.	Reduction of various activated alkenes by PETNR _{R324C} and TOYE in light-driven biocatalytic systems employing $(\text{Ru}(\text{bpz})_2\text{dClbpy})(\text{Cl})_2$ as a photosensitiser.	224
Table 5.11.	Biphasic reduction of various activated alkenes by PETNR _{R324C} and TOYE using a photosensitiser or a NADP ⁺ /G6PDH co-factor regeneration system.	231
Table B.1.	Redox properties for compounds of the general formula $[\text{Ru}(\text{bpy})_{3-n}(\text{Me}_2\text{qpy})_n]^{(n+2)+}$.	245
Table C.1.	Crystallographic data for complexes $\{\text{Ir}(\text{ppy})_2[(\text{Pym})_2\text{qpy}]\}(\text{PF}_6)_3$, $[\text{Ir}(\text{22})_2\text{Y}](\text{PF}_6)_3$, $[\text{Ir}(\text{22})_2\text{B}](\text{PF}_6)_3$, $[\text{Ir}(\text{22})_2\text{F}](\text{PF}_6)_3$, $[\text{Ir}(\text{32})_2\text{Y}](\text{PF}_6)_3$, $[\text{Ir}(\text{32})_2\text{B}](\text{PF}_6)_3$ and $[\text{Ir}(\text{42})_2\text{B}](\text{PF}_6)_3$.	247
Table F.1.	Select vertical transitions obtained by TD-DFT calculations performed for the complex cations $[\text{Ir}(\text{22})_2\text{F}]^{3+}$ and $[\text{Ir}(\text{22})_2\text{B}]^{3+}$.	251
Table G.1.	UV-visible absorption data of the labelling reagents with the general formula $[\text{Ru}(\text{L})_{(2)}(\text{L})]^{n+}$.	253

LIST OF ABBREVIATIONS

δ	Chemical shift
ε	Extinction Coefficient
λ	Wavelength
λ_{em}	Wavelength of maximum emission
λ_{max}	Wavelength of maximum absorption
λ_{onset}	Wavelength of absorption onset
(22) ₂	Bis-(1-methyl-2-(2-pyridyl)pyridin-3-yl-ium-C ⁴ ,N')
(32) ₂	Bis-(1-methyl-3-(2-pyridyl)pyridin-4-yl-ium-C ⁴ ,N')
(42) ₂	Bis-(1-methyl-4-(2-pyridyl)pyridin-3-yl-ium-C ⁴ ,N')
2-MeOEtOH	2-methoxyethanol
ADH	Alcohol dehydrogenase
bpm	2,2'-bipyrimidine
bpp	2,3-bis-(2-pyridyl)pyrazine
bpy	2,2'-bipyridine
bpz	2,2'-bipyrazine
BV	Benzyl viologen
<i>ca.</i>	Approximately
COD	1,5-octadiene
COSY	Correlation Spectroscopy
Cp*	1,2,3,4,5-pentamethylcyclopentadiene
CPCM	Conductor-like screening model
CPR	Cytochrome P450 reductase
CV	Cyclic Voltammetry
Cyt	Cytochrome
D	Donor
d(CO ₂ Me)	di-methoxycarbonyl
dCF ₃	di-trifluoromethyl
dCl	di-chloro
DCMU	3-(3,4-dichlorophenyl)-1,1-dimethylurea
DCPIP	2,6-dichlorophenolindophenol
DFT	Density Functional Theory
dMe	di-methyl
dMebpy	4,4'-dimethyl-2,2'-bipyridine
DMF	dimethylformamide
DMSO	Dimethylsulfoxide
dNH ₂	di-amino

dNO ₂	dinitro
dNTP	Deoxyribonucleotide
dPh	di-phenyl
DQF	Double quantum filtered
dRf	Deaza-riboflavin
dRfH	Deaza-riboflavin semiquinone
DSSC	Dye-sensitised solar cells
d ^t Bu	di- <i>tert</i> -butyl
d ^t Bu	di- <i>tertiary</i> -butyl
DTT	Dithiothreitol
$E_{1/2}$	Electrochemical gap
E_{max}	Energy Maximum
E_{pa}	Anodic peak potential
E_{pc}	Cathodic peak potential
eT	Electron transfer
FAD	Flavin adenine dinucleotide
F _c	Ferrocene
Fd	Ferredoxin
FMN	Flavin mononucleotide
f_{os}	Oscillator strength
FWHM	Full-width at half-maximum
G6PDH	Glucose 6-phosphate dehydrogenase
GC	Gas Chromatography
GDH	Glucose dehydrogenase
H ₂ ase	Hydrogenase
HMBC	Heteronuclear multibond correlation
HMQC	Heteronuclear multiple-quantum correlation
HOMePh	Hydroxymethylphenyl
HOMO	Highest Occupied Molecular Orbital
IC	Internal Conversion
ICT	Intramolecular charge transfer
ILCT	Intraligand Charge Transfer
IPTS	2-isothiocyanatopyrene-3,6,8-trisulfonate
KPO ₄	Potassium Phosphate Buffer (KH ₂ PO ₄ /K ₂ HPO ₄)
LLCT	Ligand-to-ligand charge-transfer
LMCT	Ligand to Metal Charge Transfer
LUMO	Lowest Unoccupied Molecular Orbital
MC	Metal Centered
Me	Methyl

MLCT	Metal to Ligand Charge Transfer
MMCT	Metal to metal charge transfer
MMLL'CT	Mixed metal/ligand-to-ligand charge transfer
MO	Molecular orbital
MV	Methyl viologen
NADH	Reduced nicotinamide adenine dinucleotide
NADPH	Reduced nicotinamide adenine dinucleotide diphosphate
NHC	<i>N</i> -heterocyclic carbene
NMR	Nuclear magnetic resonance
nNOS	Neuronal nitric oxide synthase
NOESY	Nuclear overhauser effect spectroscopy
OEC	Oxygen evolution center
OYE	Old yellow enzyme
PCR	Polymerase chain reaction
PETNR	Pentaerythritol tetranitrate reductase
Ph	Phenyl
ppm	Parts per million
ppy	2-phenylpyridine
PS	Photosensitiser
Pym	2-pyrimidyl
QD	Quantum dot
qpy	4,4':2',2'':4'',4'''-quaterpyridine
RT	Room temperature
SDS-PAGE	Sodium Dodecyl Sulfate Polyacrylamide Gel Electrophoresis
SOC	Super optimal broth with catabolite repression
TB	Terrific broth
TBME	<i>tert</i> -Butylmethyl ether
TD-DFT	Time dependant Denisty Functional Theory
TEA	Triethylamine
TEOA	Triethanolamine
TiO ₂	Titanium dioxide
TOF	Turn-over frequency
TON	Turn-over numbers
TOYE	Thermophillic old yellow enzyme
tpphz	Tetra[3,2-a:2',3'-c:3'',2''-h:2''',3'''-j]phenazine
VR	Vibrational Relaxation
VUV	Vacuum ultraviolet
WT	Wild type

ABSTRACT

Biocatalysis is becoming an increasingly attractive alternative to more traditional chemical transformations for use in pharmaceutical and industrial applications. This interest is primarily a consequence of the high regio-, stereo- and enantioselectivity that is associated with enzyme catalysed reactions. However, the proliferation of such techniques has been limited due to the dependence of enzyme activity upon the presence of redox cofactors, which are typically expensive and must be used in conjunction with efficient regeneration systems. Whilst numerous methods have been described, of particular potential are those that employ exogenous photosensitisers as a means of generating reducing equivalents to promote catalytic turnover.

In this study the potential of transition metal complexes as photosensitisers towards the development of light-driven biocatalytic systems is evaluated. Use of such compounds gives great scope towards fine-tuning the spectral and redox properties of the sensitisers with the aim of optimising catalytic efficiency. Detailed herein is an extensive study towards the synthesis and characterisation of a range of ruthenium(II) and iridium(III) coordination compounds. Using NMR, UV-vis, and electrochemical techniques, all complexes were fully characterised and the origins of the photophysical properties further investigated using time-dependent density functional theory (TD-DFT) calculations.

A series of ruthenium compounds were synthesised containing the bis(2,2'-bipyrazyl)ruthenium(II) moiety, investigating the impact of changes made to the functionality of the ancillary ligand upon the overall properties of the complex. New synthetic procedures have been developed towards the preparation of both 2,2'-bipyrazine and the related complexes, exhibiting significant benefits over previously established methods. Through manipulating the electron density of the ancillary ligand it is shown that the redox properties may be effectively tuned upon inducing changes in the energy of the metal-based HOMO.

The utilisation of cyclometalated iridium(III) complexes in aqueous systems has been limited due to a poor water solubility that is typically associated with these compounds. Herein it is demonstrated that this issue may be effectively circumvented on inclusion of the positively charged pyridinium moiety. Upon incorporation of this functional group into either the cyclometalating or ancillary ligands, two distinct series of compounds were successfully prepared. Complexes of the substituted quaterpyridinium ligands possess complicated UV-vis spectra that exhibit low intensity absorbance up to 650 nm. A number of monoquaternised bipyridinium compounds were also utilised as pyridine derived *N*-heterocyclic carbene cyclometalating ligands, to afford a range of complexes with unique redox properties.

The prepared photosensitisers were subsequently used to induce catalytic turnover in light-driven biocatalytic systems utilising the flavin dependent oxidoreductase enzymes, pentaerythritol tetranitrate reductase (PETNR) and the thermophilic old yellow enzyme (TOYE). Through an extensive investigation, optimal reaction conditions have been identified and a mechanism of electron transfer proposed. These systems were successfully implemented in the reduction of a broad range of substrates under both aqueous and biphasic conditions, delivering yields and enantiomeric excesses comparable to those obtained utilising an enzyme coupled regeneration system. This study clearly demonstrates that transition metal complexes are excellent candidates in developing practical light-driven biocatalytic systems. It is expected that, with further investigation, this approach can be readily expanded to incorporate a variety of applications and provide an effective alternative to the use of costly redox cofactors and a reliance upon complex regeneration techniques.

DECLARATION

I declare that no portion of the work referred to in the thesis has been submitted in support of an application for another degree or qualification of this or any other university or other institute of learning.

COPYRIGHT STATEMENT

The following four notes on copyright and the ownership of intellectual property rights must be included as written below:

i. The author of this thesis (including any appendices and/or schedules to this thesis) owns certain copyright or related rights in it (the "Copyright") and s/he has given The University of Manchester certain rights to use such Copyright, including for administrative purposes.

ii. Copies of this thesis, either in full or in extracts and whether in hard or electronic copy, may be made **only** in accordance with the Copyright, Designs and Patents Act 1988 (as amended) and regulations issued under it or, where appropriate, in accordance with licensing agreements which the University has from time to time. This page must form part of any such copies made.

iii. The ownership of certain Copyright, patents, designs, trade marks and other intellectual property (the "Intellectual Property") and any reproductions of copyright works in the thesis, for example graphs and tables ("Reproductions"), which may be described in this thesis, may not be owned by the author and may be owned by third parties. Such Intellectual Property and Reproductions cannot and must not be made available for use without the prior written permission of the owner(s) of the relevant Intellectual Property and/or Reproductions.

iv. Further information on the conditions under which disclosure, publication and commercialisation of this thesis, the Copyright and any Intellectual Property and/or Reproductions described in it may take place is available in the University IP Policy (see <http://www.campus.manchester.ac.uk/medialibrary/policies/intellectual-property.pdf>), in any relevant Thesis restriction declarations deposited in the University Library, The University Library's regulations (see <http://www.manchester.ac.uk/library/aboutus/regulations>) and in The University's policy on presentation of Theses

ACKNOWLEDGEMENTS

Throughout my PhD I have been extremely lucky to have the opportunity to work with some fantastic people, all of whom have helped me get to where I am today and who deserve a great many thanks. Firstly to my supervisor Professor Nigel Scrutton for giving me the opportunity to work on this project and for his guidance during the past four years. To my chemistry advisor Dr Ben Coe, for welcoming me into his lab and his group and for giving me a true appreciation for the world of statistics. Of those in the MIB I'd like to say a special thank you to Dr Derren Heyes for all his help and for showing me the way around a laser. A huge thank you goes to Dr Helen Toogood for being such a great mentor and for teaching a chemist the tips and tricks of the enzymology trade. Thanks also to Dr David Mansell for all his time and help with the GC and his tolerance of all the emails along the lines of 'Is the GC free tonight?' I'd also like to express my gratitude to Dr Karl Fisher for all his advice and his insights in choices of substrates, not to mention for being a friendly face during all those early mornings. Amongst those in the Chemistry Department the first and foremost I would like to mention is Dr Daniela Rusanova-Naydenova to whom I owe more than I can say; for her friendship, her guidance and for helping me become a better researcher (and for teaching me never to settle for a $R^2=0.95$). A big thank you must go to Dr Octavia Blackburn for her tutorials in the daunting world of DFT, for her encouragement in pursuing the iridium chemistry and for always having my back. To Dr Yien Ta for being a great lab partner for two years and for proof reading my introduction (you deserve a medal for that alone) and to Rachel Pilkington for putting up with me for the other two years. To Amber-Marie Pearce (yes I did have to put the 'Marie' in there) for being a good friend and for sticking around since the start of our undergraduate days and putting up with my frequent ranting, although I could have perhaps done without the added risk of chemical exposure over the years. Thanks must also go to Dr Madeleine Helliwell for her skill and perseverance with my crystal structures and to Dr Juan Aguilar and Mr Ian Goodbody for their help with setting up the DQF-COSY and NOESY NMR experiments. And of course a thank you to all Scrutton/Munro/Leys and Coe group members past and present and to all the technical staff that have supported this work in one way or another.

Thanks to you all!

Martyn Peers

September 27th 2012

DEDICATION

To my family. To my Mum. To my Dad. And to my sister. For their continued love, support and for always being there. None of this would have been possible without them.

SECTION ONE

INTRODUCTION

1.1 Photophysical and Photochemical processes

1.1.1. Absorption

All photo-initiated processes begin with the absorption of a photon, a quantum of electromagnetic energy of a given frequency, by a molecular entity. If the photon is of sufficient energy the population of previously inaccessible higher energy electronic states may occur, resulting in the formation of a photoexcited state.

Absorption in organic chromophores may be discussed in terms of excitation from the σ - and π -bonding orbitals to the unoccupied σ^* - and π^* -antibonding orbitals. For those chromophores where atoms with a lone pair of electrons are present, additional transitions originating from non-bonding orbitals, denoted as n , must also be considered. Due to the strength of the σ bond, σ - σ^* transitions occur at relatively high energies and exhibit absorption maxima within the vacuum ultraviolet (VUV) region of the electromagnetic spectrum. With the experimental difficulties associated with performing measurements in the VUV region and strong absorbance by atmospheric and solvent molecules, transitions of such energy are not recorded as part of standard UV-vis techniques (200-700 nm).^[1] n - σ^* transitions occur at lower energies, 150-250 nm, although these too may be relatively difficult to observe. The UV-visible absorption profiles of most organic compounds are dominated by the π - π^* and n - π^* transitions, which involve unsaturated functional groups. On increasing the conjugation of the π -system, a bathochromic shift in the absorbance maxima to longer wavelengths is observed. This is a consequence of a decrease in the energy gap between the highest occupied molecular orbitals (HOMOs) and the lowest unoccupied molecular orbitals (LUMOs). n - π^* transitions occur at lower energies but exhibit low extinction coefficients due to symmetry constraints.

The photoexcitation of a coordination compound is considerably more varied and complex by comparison and may best be described with regards to the relative distribution of electron density in the ground and excited states. Transitions between orbitals that are primarily metal in character are defined as being metal-centred (MC). For a complex of a d-block metal in an octahedral geometry, this can be considered as a promotion of an electron from the stabilised t_{2g} orbital to the destabilised e_g orbital. The terms used in defining the absorption processes of the organic chromophores accurately describe the ligand-centred (LC) transitions, though the influence of the coordinated metal centre must also be accounted for. Transitions that result in a redistribution of electron density from one discrete region of a species to another are referred to as intramolecular charge-transfer transitions (ICT). Those involving the promotion of an electron from the t_{2g} orbital of the metal ion to a π^* -antibonding orbital of a ligand are described as metal to ligand charge transfers (MLCT), whilst

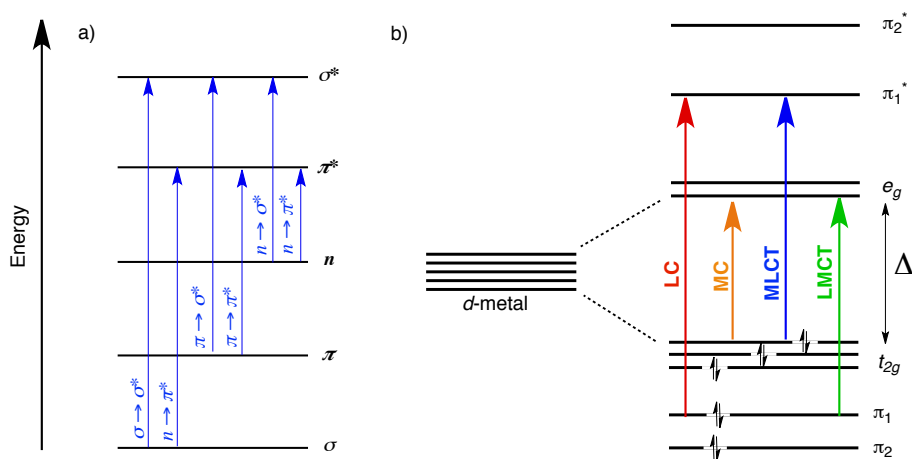


Fig. 1.1. Simplified molecular orbital diagrams illustrating the electronic transitions of A) an organic chromophore and B) an octahedral transition metal complex of D_3 symmetry.

promotion from a ligand π -bonding orbital to the e_g orbital gives rise to a ligand to metal charge transfer (LMCT). Under suitable conditions a ligand-to-ligand charge transfer (LLCT) may occur and involves a shift in electron density between ligands coordinated to the same metal centre. An intraligand charge transfer (ILCT) is analogous to the ICT processes within an organic chromophore, which typically describe a redistribution of charge density from an electron rich donor moiety to an electron deficient acceptor. In polymetallic complexes, additional intervalence or metal-to-metal charge transfer (MMCT) may be observed.

The means by which a molecule loses the excess energy gained on absorption and subsequently returns to the ground state, may proceed through a number of different photophysical or photochemical pathways.

1.1.2. Photophysical Processes

Photophysical processes are those that involve transitions between various electronic states within a molecule though do not result in a chemical change of the species. These processes can be categorised as being either radiative or radiationless in nature, the former involving the absorption/emission of a photon whilst the latter does not.

The relationship of these processes is most effectively illustrated through the use of a modified Jabłoński diagram, Fig. 1.2. Individual eigenstates are represented as horizontal lines and are stacked vertically to indicate their relative energies. Bold lines are used to define the limits of the various electronic states, which are divided into discrete vibrational energy levels and grouped into columns according to multiplicity. Transitions are depicted with the use of straight and wavy lines for radiative and radiationless processes respectively.

Vibrational relaxation (VR) is the loss of vibrational excitation energy by transfer of kinetic energy to other vibrational modes within the molecule or to the surrounding environment by thermal equilibration; the process occurs over a time scale of 10^{-14} – 10^{-11} s. If vibrational levels of two electronic states of the same multiplicity sufficiently overlap it is possible that a transition to a lower electronic energy state may occur via internal

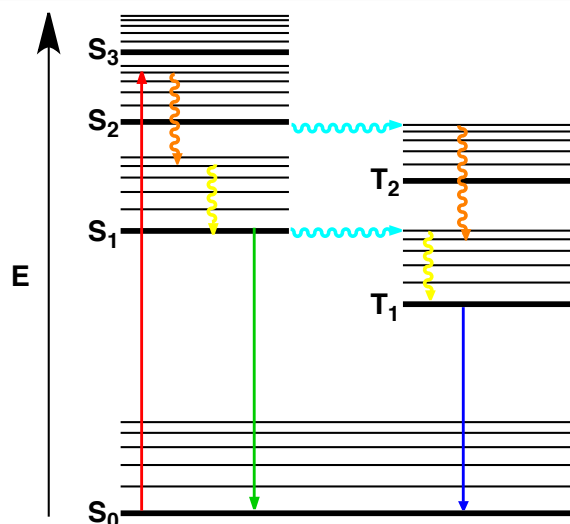


Fig. 1.2. A modified Jablonski diagram displaying the potential photophysical processes accessible by a molecule excited from a singlet ground state S_0 ; Absorption (red); Internal Conversion (orange); Vibration Relaxation (yellow); Intersystem Crossing (aqua); Fluorescence (green); Phosphorescence (blue).

conversion (IC). The resultant molecular entity is typically of an excited vibrational level and rapidly undergoes VR to the zeroth vibrational level of the lower energy electronic state. As a result of the large energy gap between the ground state and the first excited state, relaxation to the former via IC is very slow.

The absorbed energy may instead be dissipated by means of fluorescence, describing a transition from the first excited singlet state to the ground state via emission of a photon. As stated by Kasha's rule, it is only the lowest excited state of a given multiplicity that appreciably contributes to the overall emission. This is attributed to the relatively slow time scale with which emissive processes occur so that at higher energy states it is more probable that relaxation proceed via VR and IC. As such the emitted photon is typically of a longer wavelength than that absorbed due to energy loss from these radiationless processes.

It is also possible that an excited electron may undergo intersystem crossing, a spin forbidden transition that results in a change of spin multiplicity, such as in the transition from a singlet to a triplet excited state. Occurring on a time scale of 10^{-8} – 10^{-3} s, this process may effectively compete with fluorescence should sufficient vibrational coupling between energy levels of the two multiplicities be in effect. Emission from an excited triplet state is called phosphorescence which, due to the forbidden nature of the transition, has a decay time in the range of 10^{-4} – 10^{-1} s, considerably longer than that seen for fluorescent processes and giving rise to the characteristic 'afterglow' of the process.

Another potential route of relaxation is that of delayed fluorescence, whereby the excited singlet state is repopulated from the excited triplet state prior to the radiative transition. This process may proceed via one of two mechanisms. The first is by a thermally active radiationless transition whilst the second occurs on triplet-triplet annihilation and are referred to as E-type and P-type delayed fluorescence respectively.^[2]

1.1.3. Photochemical Processes ^[3]

Photochemical reactions are processes that are initiated from a photoexcited state and result in a chemical transformation of a species. The energy absorbed on photoexcitation is typically sufficient to overcome large activation barriers, thus providing access to a variety of reaction pathways. The products of a photochemical process may be the same as those of the thermal reactions, although requiring comparatively milder reaction conditions to achieve the same outcome. Alternatively the reactions may yield products that are inaccessible using conventional techniques either via an electronic configuration not attainable in the ground state or by overcoming an activation barrier not possible using other means. The excited state may also undergo secondary reactions to yield more stable photoproducts that may themselves display activity not observed with the species in the ground state. The effectiveness of these photochemical reactions is dependent upon the efficiency of the competing photophysical processes and as such typically proceeds from the longest-lived excited states.

The intramolecular photochemical reactions encompass a variety of processes including photoisomerisation, photodissociation and photoionisation. A primary example of these monomolecular processes is the *cis-trans* isomerisation of the C=C double bond, which proceeds on excitation of an electron to the π^* -orbital thus weakening the bond and enabling free rotation about the C-C axis.

Should the excited state be sufficiently long-lived, additional pathways of deactivation may be accessed on interaction with a second molecular entity or quencher. These intermolecular photochemical reactions can be discussed in terms of a number of broad categories including, photopolymerisation, photosubstitution, photoaddition and photoredox chemistry. A photosensitised reaction is one whereby a species in an excited state induces a physical or chemical change within a second molecule upon energy transfer to the latter. The chromophore in such processes is referred to as a photosensitiser and by definition is itself not consumed during the course of the reaction. When the reaction proceeds via photoinduced electron transfer, the process may also be referred to as an electron transfer photosensitisation, be it oxidative or reductive in nature. In such instances the ground state of photosensitiser is regenerated by the presence of a sacrificial electron donor or acceptor, which itself undergoes an irreversible chemical change.

1.2 Photosynthesis and Photosynthetic systems

Photosynthesis is the process by which the energy absorbed from light is converted to and stored as chemical energy. Aerobic photosynthesis that occurs in algae, higher plants and a variety of bacteria is the photo-initiated conversion of carbon dioxide into simple sugars and is the primary route of carbon fixation and oxygen production within the biosphere. The overall process may actually be considered in terms of two distinct subprocesses, the light and dark reactions. The light reaction uses the energy of absorbed photons to drive the phosphorylation

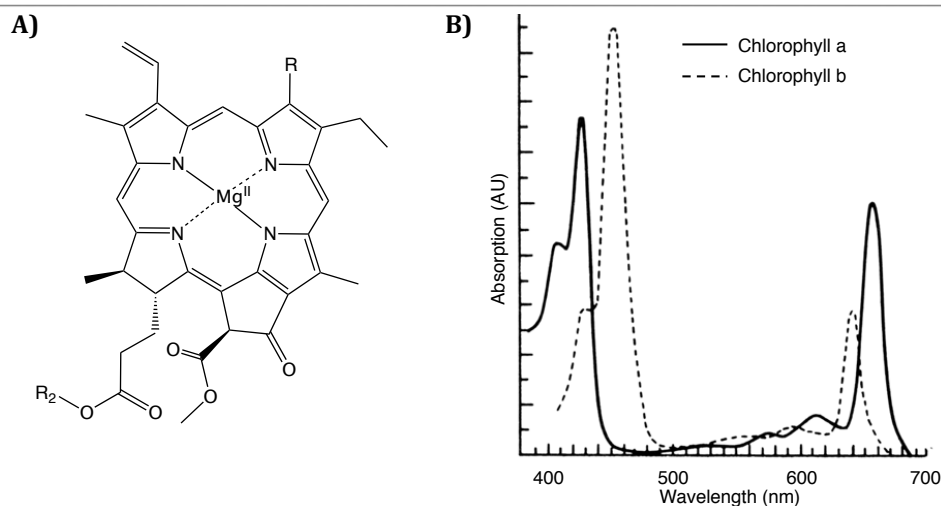
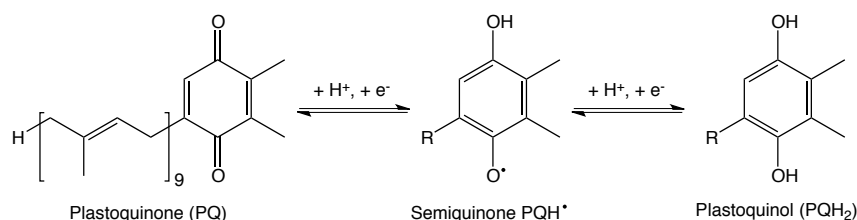


Fig. 1.3. A) The structure of chlorophyll *a* where $R = \text{CH}_3$ and chlorophyll *b* where $R = \text{CHO}$ and $R_2 = \text{phytyl}$. **B)** The absorption spectra of chlorophylls *a* and *b*.

reaction of ADP to yield ATP and the biosynthesis of NADPH on reduction of NADP^+ . The dark reaction utilises both of these components towards the synthesis of carbohydrates on reduction of CO_2 .^[4]

The light reaction is itself comprised of two distinct photochemical reactions involving an electron transport chain that is facilitated by two membrane bound pigment-protein complexes, photosystem I and photosystem II. Energy absorbed from solar radiation is maximised by a multi-subunit protein referred to as the light-harvesting complex. Utilising a series of auxiliary chromophores or antenna, the complex absorbs strongly across the entire visible region of the spectrum and efficiently channels energy to a pair of chlorophyll molecules that function as the reaction centre. It is the absorption profiles of these chlorophyll molecules that define the individual photosystems; PSI exhibits absorption up to wavelengths of 700 nm whilst PSII absorbs only to 680 nm.

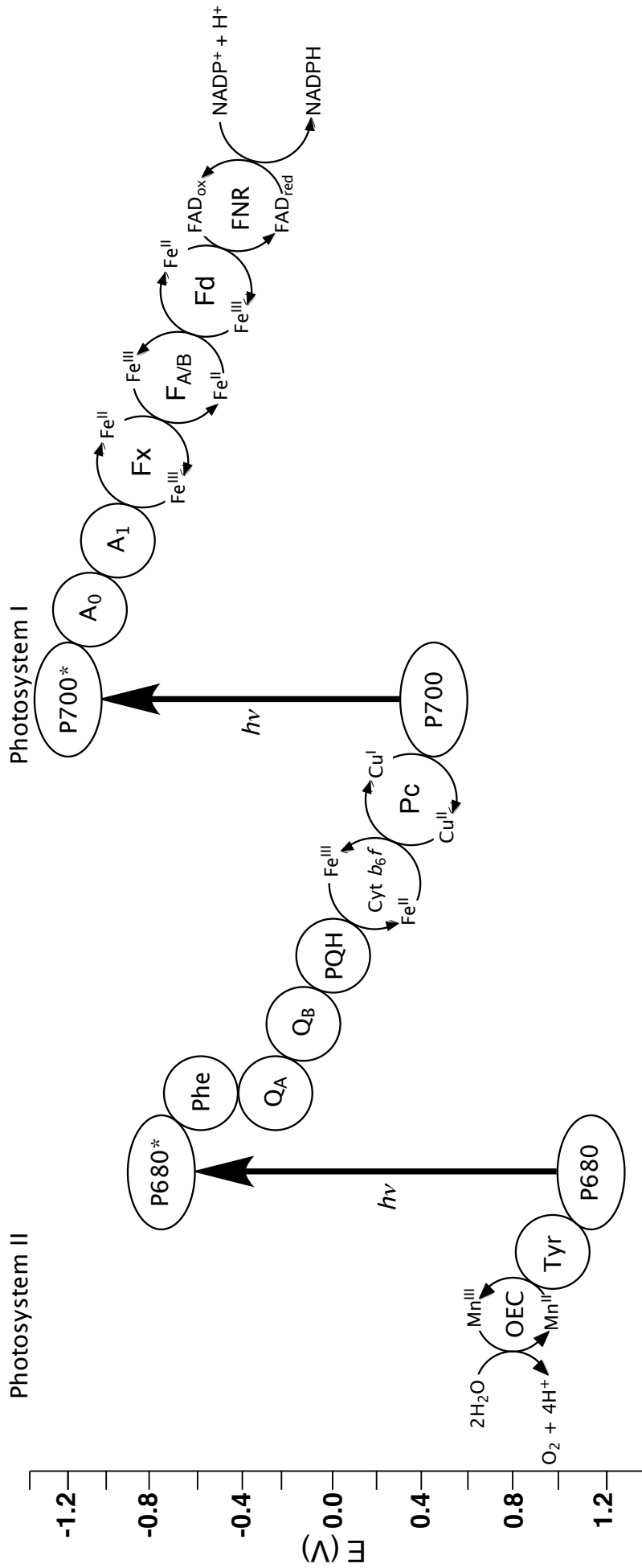
The sequence of electron transfer processes begins on the photoexcitation of the P680 reaction centre of PSII. The resultant excited singlet state, P680^* , is oxidatively quenched by a neighbouring pheophytin *a* molecule to yield an anionic radical. This transfer mediator is isostructural to chlorophyll *a* with the exception that the central Mg^{2+} ion has been substituted with two protons bound to the heteroatoms of the macrocycle. The primary stable acceptor of PSII is the first of a series of plastoquinone molecules (Q_A). Reduction by the pheophytin radical, affords a semiquinone, which is readily oxidised on electron transfer to a second more



Scheme 1.1. Redox chemistry of the plastoquinone transfer mediator employed in the electron transport chain of photosystem II.

loosely bound plastoquinone (Q_B). On accepting a second reducing equivalence from Q_A and two protons extracted from the stromal side of the membrane, Q_B is fully reduced to yield plastoquinol (PQH_2). On formation, PQH_2 is released from the lipid portion of the membrane, through which it can readily diffuse to then interact with the cytochrome *b₆f* complex. The latter facilitates electron transfer to the mobile copper containing protein plastocyanin, which acts as the primary donor towards PSI. On oxidation PQH_2 releases two protons into the thylakoid lumen thus establishing a transmembrane proton gradient that is essential in the biosynthesis of ATP. The oxidised $P680^+$ is returned to the original oxidation state on reduction by a redox active tyrosine residue, which is itself reduced by a solvent derived electron on oxidation of water via activity of the oxygen-evolving complex (OEC). The OEC is a Mn_4Ca cluster which acts as the necessary intermediate to couple a four electron oxidation process to a single electron acceptor. Water oxidation is achieved as the cluster cycles through five distinct oxidation states, S_0 to S_4 . The precise mechanism of oxygen evolution remains somewhat controversial due to uncertainty about the identity of the S_0 and S_3 states and the nature of the S_2 to S_3 transition within the cycle. In the case of the latter it is unclear as to whether this proceeds via oxidation of one of the Mn nuclei or is instead ligand centred in nature, be it a side chain residue, bound water or an oxo-bridge. A single cycle results in the decomposition of a pair of water molecules to yield dioxygen in addition to four protons and four electrons, the latter ultimately used in the formation of two PQH_2 molecules by PSII.

The second of the electron transport chains begins upon photoexcitation of P700 in photosystem I, yielding an excited state of significantly more negative potential than that of P680. The primary acceptor is the modified chlorophyll monomer A_0 that facilitates transfer to phylloquinone, A_1 , also known as vitamin K_1 . This acts as the donor to the first of three [4Fe-4S] clusters, F_X , which is a interpolypeptide [4Fe-4S] cluster bound by two cysteinyl residues from subunits PsaA and PsaB.^[5] The F_A and F_B [4Fe-4S] clusters are bound to the PsaC subunit via sites comprised from two consensus sequences containing four cysteinyl residues each. The first three cysteines of each sequence bind one of the [4Fe-4S] clusters whilst the fourth completes the binding site of a second cluster. F_B subsequently transfers an electron to ferredoxin (Fd), a water-soluble protein containing a [2Fe-2S] cluster. The electron is then transferred to the FAD cofactor of ferredoxin NADP⁺ reductase (FNR), an oxidoreductase flavoenzyme used in the regeneration of NADPH from NADP⁺. The reaction proceeds via the stable semiquinone form of the cofactor, which is fully reduced to the dihydroflavin on accepting an electron from a second ferredoxin protein. The final step of the electron transport chain is the reduction of NADP⁺ via hydrid transfer from the N5 of dihydroflavin to yield NADPH.

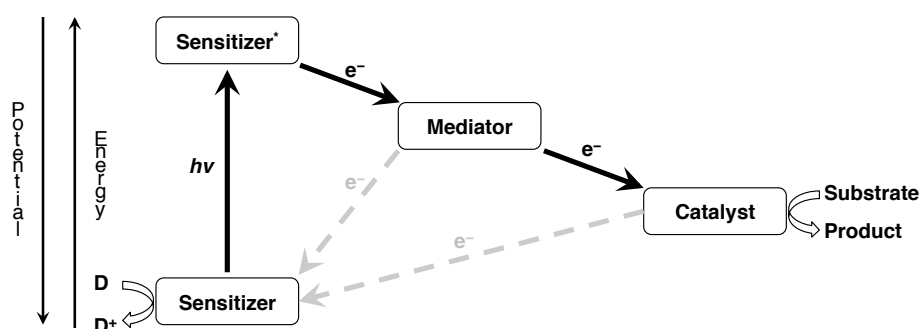


Scheme 1.2. Sequence of electron transfer from water to NADP⁺ via the photosystems PSII and PSI as part of oxygenic photosynthesis.
 Key: OEC, oxygen evolution centre; Tyr, tyrosine mediator; P680, chlorophyll a; Phe, pheophytin a; Q_A, Q_B protein bound plastoquinones; PQH, plastoquinol; Cyt *f*, cytochrome *b₆f* complex; Pc, plastocyanin; P700, chlorophyll b; A₀, modified chlorophyll acceptor; A₁ phylloquinone; F_A, F_B, F_X, iron sulphur clusters; F_d, ferredoxin; FNR, ferredoxin-NADP⁺ oxidoreductase.

1.3. Artificial Photosynthetic systems

Artificial photosynthetic systems function by adopting the same basic principles as the naturally occurring counterparts. When considered in the most simplistic of terms, the photosynthetic system may be described with regards to three or four different components, and allows the construction of a basic model that may be used as a template towards the design of artificial systems. The first component is a photosensitiser that, on excitation, is able to act as the source of low potential electrons for the system, emulating the function of the light-harvesting units of PSI and PSII. In an ideal system this would undergo direct electron transfer to the terminal acceptor, though typically an intermediary, in the form of an electron transfer mediator or relay, is required to provide an efficient transport chain between the two components. A catalytic module typically acts as the terminal acceptor, utilising the electrons in subsequent chemical transformations. If the system were comprised of just these components, minimal accumulation of the reduced acceptors would occur as rapid charge recombination through back electron transfer would predominate or the active chromophore would be consumed. Addition of a sacrificial electron donor offers a pathway to regenerate the photosensitiser and promote forward electron transfer. A variety of suitable sacrificial donors have been demonstrated, though the effectiveness is dependent upon the respective redox potentials of the other components within the system. Examples of such compounds are EDTA, triethanolamine, ascorbate, aniline or those containing the thiol functional group.

A number of ideal properties pertaining to the photosensitiser have been identified.^[6] The first is that the sensitiser be panchromatic and absorb across all wavelengths to maximise energy absorption under irradiation by white light. In those systems where specific wavelengths of incident irradiation are to be used, the absorption profile may instead be manipulated to absorb more strongly within the desired region. Photoexcitation and subsequent charge separation should be highly efficient, with each absorption event resulting in the injection of an electron into the transport chain. Catalytic activity is dependent upon the charge-separated state being of a sufficient lifetime to allow for effective electron transfer to the catalytic module with minimal charge recombination and energy loss on stabilisation of unnecessarily long-lived intermediary states. The photosensitiser needs also to be robust, displaying enhanced photostability during long periods of illumination so as to afford



Scheme 1.3. Generalised schematic energy diagram highlighting the key components and electron transfer processes within a simplified photosynthetic system.

continuous turn over without any loss of efficiency. If appropriate, an antenna assembly may be employed to further augment energy absorption within the system.

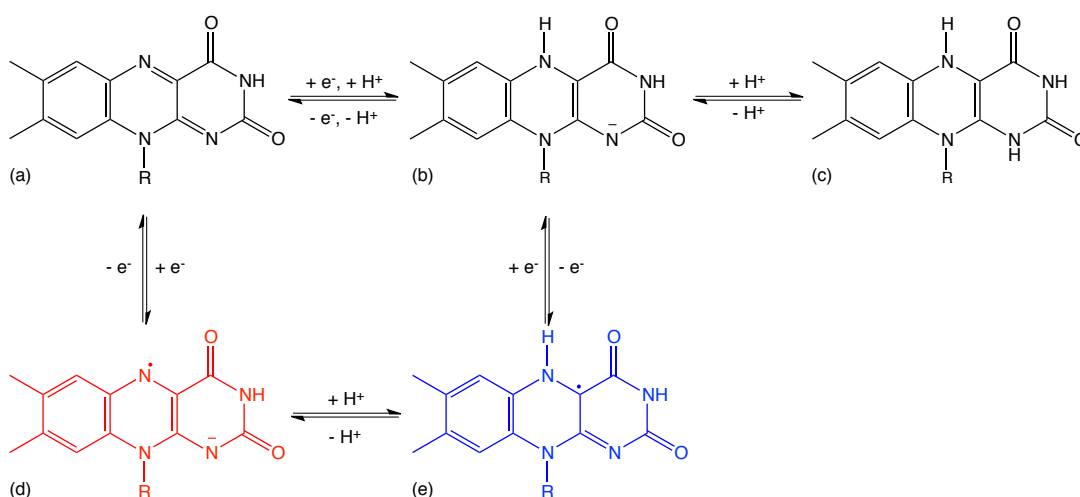
Of particular interest as potential catalytic modules are the natively non-photosynthetic redox enzymes. The basic premise would be to replace the endogenous electron donor with a photoinitiated transport chain to afford enzyme activity. Such endeavours have been successfully realised in the investigation of electron transfer processes within a variety of redox enzymes using techniques such as laser flash photolysis.

1.3.1. Photosensitisers

A broad range of photosensitisers have shown potential as electron transfer probes in the study of redox enzymes. It has been demonstrated that, dependent upon sufficient interactions occurring between the two, on excitation a sensitizer may be utilised to initiate electron transfer to or from a redox centre of a non-photosynthetic enzyme and thus promote subsequent electronic or chemical transformations.

1.3.2.1. Flavins and deazariboflavins

Free flavins have been proven to act as efficient single electron reducing agents on photoexcitation.^[7] The reductant is generated *in situ* on laser flash photolysis and subsequent reductive quenching of the flavin triplet state by a sacrificial electron donor.^[8] In the presence of organic donors such as EDTA this proceeds via hydrogen abstraction to result in the formation of a neutral semiquinone. This may undergo either direct electron transfer to the protein bound redox centre or disproportionation to form the oxidised and fully reduced flavin.^[9] The latter is also capable of providing reducing equivalents to the protein although the observed rate constants are appreciably lower than for the semiquinone. This is surmised to



Scheme 1.4. Schematic illustrating the redox chemistry of the isoalloxazine ring of the flavin cofactors and the structures of the resultant products/intermediates: a) oxidised flavoquinone, b) anionic hydroquinone, c) protonated hydroquinone, d) anionic “red” radical semiquinone and e) neutral “blue” radical semiquinone. Where R is indicative of the different functionality of the various flavins.

be a result of the smaller reactive surface of FMN⁻ in comparison to FMN[•] and the electron is localised on the N5 atom in comparison to delocalisation about the pyrazine and xylene rings of the isoalloxazine moiety of FMN[•].^[10] Walker *et al.* demonstrated the use of deazariboflavin (dRf) as a photosensitiser in the study of flavocytochrome *b*₂ from *Saccharomyces cerevisiae*.^[11] An increase in absorbance at 557 nm corresponded to the reduction of the haem centre by the deazariboflavin semiquinone (dRfH[•]). In the presence of pyruvate, the product of enzymatic transformation of L-lactate, this initial increase in absorption is followed by a steady decrease with a rate that is independent of enzyme concentration. This is assigned to the consumption of the reduced haem centre by intramolecular eT to the FMN cofactor of the enzyme. In the absence of pyruvate no such transfer is observed and is evidence of a ligand-gated intramolecular electron transfer process.

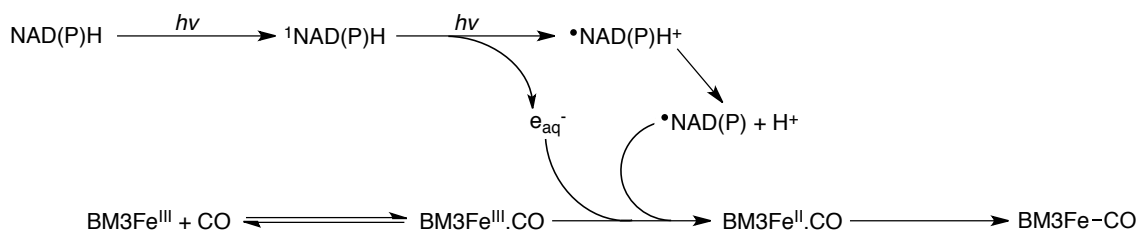
Using deazariboflavin and EDTA as a sacrificial donor, the interprotein electron transfer between ferredoxin (Fd) and ferredoxin:NAD(P)⁺ reductase (FNR) from the cyanobacterium *Anabaena* PCC 7119 has been directly observed.^[12] Transient spectra were recorded at 507 nm, which corresponds to an isosbestic point of the enzyme bound FAD of the reductase. An initial increase in absorbance is associated with the formation of (dRfH[•]) and is followed by a rapid decrease on oxidative quenching by ferredoxin. A subsequent gradual increase in absorption corresponds to the reoxidation of the ferredoxin on electron transfer to the reductase enzyme. This is confirmed by a concomitant increase in optical density at 610 nm, which is indicated of an accumulation of the FAD semiquinone. In the presence of ferredoxin, direct electron transfer to FAD from dRfH[•] was minimal due to steric hindrance resulting on formation of the Fd-FNR complex.

The flavins have also been shown to act as photooxidants, with the excited triplet state directly oxidising the redox centre of the enzyme.^[13] In the studies of the metalloenzyme ascorbate oxidase, oxidation of the reduced Type I Cu centre was achieved on irradiation of an anaerobic sample in the presence of dRf, as monitored at 610 nm. The increase in absorbance was attributed to a biphasic process, both components being independent of enzyme concentration. On consideration of this and the relatively slow rates, both these processes were assigned to intramolecular electron transfer processes. It was therefore surmised that initial photooxidation occurs at the trimetallic Type II/III cluster with subsequent electron transfer from the Type I centre. Whilst the Type II centre cannot be detected spectrophotometrically, the Type III bimetallic centre may be observed at 330 nm. A major limitation in the use of exogenous flavins as photosensitisers is the spectral overlap with the inherent cofactors of the enzyme system, thus making spectral analysis problematic as individual absorption patterns cannot be resolved. In this instance the transients were completely obscured by processes involving dRf.

1.3.1.2. Nicotinamide Adenine Dinucleotide

The use of NADPH as a photoreductant was initially demonstrated in the mechanistic studies of cytochrome *c* utilising flow-flash techniques. Under anaerobic conditions in sodium phosphate buffer (pH 7.4) a single laser pulse at 355 nm resulted in 90 % reduction yields of cytochrome *c* within 1-2 ms.^[14] Photoexcitation of NAD(P)H is proposed to occur via a sequential two photon absorption process with an intermediary long-lived singlet excited state $^1\text{NAD(P)H}$.^[15] This results in the ejection of a hydrated electron, e_{aq}^- , and the formation of the neutral $\bullet\text{NAD(P)}$ radical which is formed on deprotonation of the initially generated cationic $\bullet\text{NAD(P)H}^+$ radical. Both e_{aq}^- and $\bullet\text{NAD(P)}$ are potential reductants with redox potentials of -2.9 V^[16] and -0.94 to -0.92 V, respectively.^[17, 18] Generation of the reduced cytochrome *c* was monitored by a characteristic increase in absorbance at 418 nm with the concomitant decrease at 340 nm associated with NADPH consumption. Electron transfer was attributed to a biphasic process, the first of which involves the reduction of the cytochrome by a hydrated electron and is followed by transfer from $\bullet\text{NAD(P)}$ upon formation of the encounter complex. Under aerobic conditions photoreduction yields were decreased to *ca.* 25 % and is expected to be caused by quenching of $\bullet\text{NAD(P)}$ by molecular oxygen to form the superoxide anion. The latter becomes almost the sole reducing agent for the system and leads to the development of an additional third reduction phase, which becomes predominant at 20 % O_2 saturation.

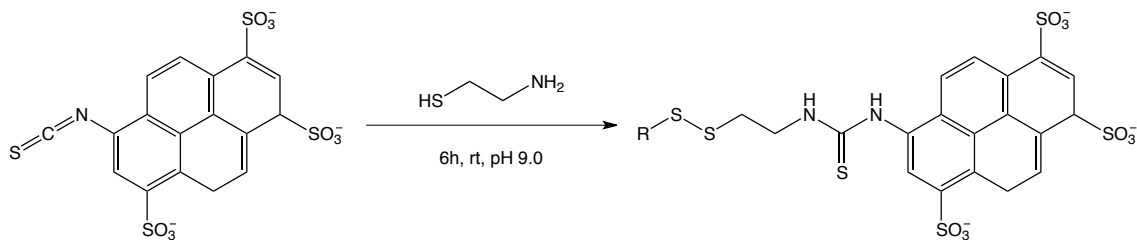
This method was subsequently adapted to study the reduction of the haem domain of P450 BM3 whereby near complete reduction was achieved following *ca.* 50 laser flashes at 355 nm.^[19] The reaction was monitored by a decrease in absorbance at 418 nm, which is associated with the ferric form of the enzyme, and a simultaneous increase at 450 nm attributed to an accumulation of the $\text{Fe}^{\text{II}}\text{-CO}$ complex. Minimal formation of the inactive form of the enzyme, was noted during photolysis experiments, as indicated by a lack of the characteristic Soret band at 420 nm. The process is typically observed on utilising chemical mediators such as sodium dithionite in the reduction of the haem iron as a result of protonation of the cysteine thiolate and subsequent ligation of the ferrous haem.



Scheme 1.5. Photoexcitation of NAD(P)H via two photon absorption and subsequent reduction of the ferric BM3 haem domain to yield the BM3 $\text{Fe}^{\text{II}}\text{-CO}$ complex.^[19]

1.3.1.3. Thiouredopyrene-3,6,8-trisulfonates

Thiouredopyrene-3,6,8-trisulfonates (TUPS) have also been identified as potential photosensitisers^[20], derived from the use of pyrene to form reactive radicals in aqueous and organic solutions^[21]. The effectiveness of pyrene had been limited due to the need for high



Scheme 1.6. Formation of thiouredopyrene-3,6,8-trisulfonates on reaction of 2-isothiocyanatopyrene-3,6,8-trisulfonate with cystamine, where $R = \text{NH}_2\text{C}_2\text{H}_4$ - or TUPS-

light intensities that cause the formation of solvated electrons that in turn can initiate a number of unwanted side reactions. However, TUPS has proven to efficiently undergo a singlet-triplet transition, forming a long-lived excited state under anaerobic conditions, which is oxidised in the presence of an electron acceptor. TUPS excitation occurs at much lower excitation intensity and offers higher quantum yields for excitation to the triplet state. It has also been shown that in the presence of a suitable donor, such as ascorbic acid, TUPS is also capable of acting as an electron acceptor and forming an anionic radical that can act as a reducing agent.^[22]

The compounds are synthesised on the reaction of 2-isothiocyanatopyrene-3,6,8-trisulfonate (IPTS) with the α -amino nitrogen of an amino acid or ϵ -amino nitrogen of lysine. The benefit of this approach being that it can be employed to selectively covalently bind to lysine residues that are native in a redox enzyme. On treatment of TUPS with cysteamine, this specificity can be altered to instead selectively target cysteinyl residues.^[23] Reaction of a two-fold excess of IPTS with cystamine formed the “(di-TUPS)”-cystamine derivative, which gave higher labelling yields of *ca.* 85 % compared to the mono substituted counterpart. Labeling of the enzyme proceeded via thiol-disulfide exchange between the cysteinyl group of the protein side chain and the cystamine disulfide of TUPS. Use of the symmetrical “(di-TUPS)”-cystamine derivative prevents the formation of unwanted coupling reactions involving the cystamine half of the mono reagent. Adapting this methodology, the internal electron transfer processes of Cytochrome P₄₅₀ Reductase (CPR) and neuronal Nitric Oxide Synthase (nNOS) were investigated.^[24] Upon laser photoexcitation of TUPS, rapid electron transfer to the flavin cofactors was observed. This was monitored by characteristic spectral changes between 600-700 nm, which corresponds to the formation of a neutral flavin semiquinone. When TUPS is employed in free solution, electron transfer was shown to proceed with a second order rate constant of $3.38 \pm 0.75 \times 10^8 \text{ M}^{-1} \text{ s}^{-1}$ and $3.55 \pm 0.45 \times 10^8 \text{ M}^{-1} \text{ s}^{-1}$ for CPR and nNOS reductase respectively. This is congruent with a diffusion controlled reaction and is in agreement with the rates calculated in the study of cytochrome *c*.^[25] The initial rapid increase in absorbance due to the formation of the semiquinone is followed by a slower decay fitted to a double exponential function indicating a biphasic process. The faster phase of this decay is attributed to back electron transfer to the oxidised form of TUPS, whilst the slower is representative of an intramolecular process such as interflavin electron transfer. Preparation of the S1233C variant of the nNOS reductase domain allowed for covalent binding of TUPS in close proximity to the

FAD cofactor. Formation of the semiquinone on excitation of the complex was fitted to a single exponential with a rate constant of $3.87 \pm 0.16 \times 10^4 \text{ s}^{-1}$. Whilst yields of reduction were greater than seen for experiments with the unbound TUPS, the efficiency of back electron transfer was likewise enhanced with a rate constant of $575 \pm 7 \text{ s}^{-1}$. The rate of the slower phase at 630 nm remained consistent with values obtained previously.

1.3.1.4. Metal Substituted Porphyrins

Metal-substituted porphyrins take advantage of the inherent photochemical properties of haem.^[26] On substitution of the iron with a different transition metals (predominately Zn, Sn or Mg) the lifetime of the excited state can be increased on enhancement of inter system crossing to yield a long-lived triplet state.^[27]

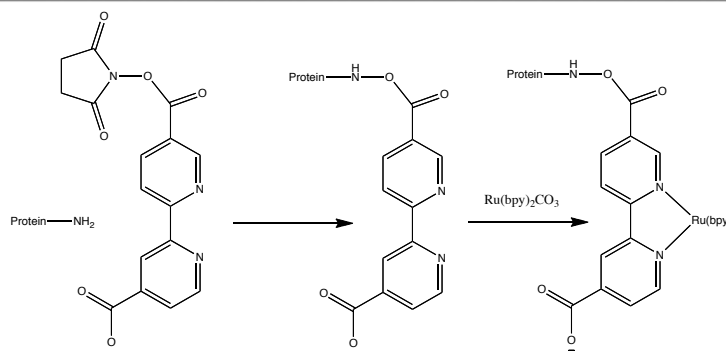
These compounds are typically employed on substitution of the native haem of an enzyme, which may be achieved in one of two ways. The first is the removal of the entire porphyrin cofactor followed by reconstitution with the metal substituted analogue. The second involves extracting the metal via chemical means and subsequent insertion of the required metal into the free coordination site. Modification of metalloenzymes such as cytochrome *c* allows for the study of interprotein electron transfer processes between itself and a suitable redox partner such as with cytochrome *c* oxidase.^[28] However, replacement of the native haem can be difficult and may bring about structural changes within the modified protein. Quantum yields are often low and the exact redox potentials of the resultant porphyrin are also dependent upon the protein environment; these therefore must be determined before interpretation of results concerning the electron transfer processes can be undertaken.

1.3.1.5. Transition Metal Complexes

Of all the photoactivated reagents, those that have perhaps proven the most practical and versatile are the coordination compounds of ruthenium. Due to a unique combination of chemical stability, redox activity, and long-lived excited states, the ruthenium polypyridyl complexes have been extensively employed as exogenous photochemical initiators in a variety of studies.^[29, 30]

Initial investigations into the electron transfer processes of biological systems focused upon the use of compounds that were bound directly to the enzyme. The first of these utilised $[(\text{NH}_3)_5\text{Ru}(\text{OH}_2)]^{n+}$ that had been bound to the protein via coordination to a surface histidine residue proceeding via displacement of the aqua ligand.^[31] The complex was chosen for its selectivity of binding to nitrogen and sulphur^[32] and its kinetic inertness towards substitution in the $n = 3$ and $n = 2$ states; this stability allowing the use of analytical methods, e.g. NMR, to accurately characterise the site of binding between the complex and the protein.^[33]

In experiments of horse heart cytochrome *c* it was discovered that the complex would selectively bind to the His-33 residue at physiological pH. As the pentaamine complex was itself not photoactive, $[\text{Ru}(\text{bpy})_3]^{2+}$ was employed as a photosensitiser.^[31]

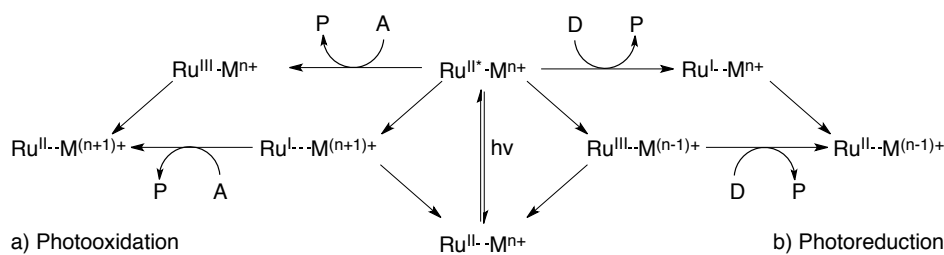


Scheme 1.7. Reaction scheme for the preparation of $Ru(bpy)_2(dcbpy\text{-}cytochrome\ c)$ derivatives.

The $Ru(NH_3)_5(His\text{-}33)^{3+}\text{-}cytochrome\ c$ complex ($PFe^{III}\text{-}Ru^{III}$) was readily reduced using laser flash photolysis techniques to yield ($PFe^{III}\text{-}Ru^{II}$) on photoexcitation in the presence of EDTA. Intramolecular electron transfer gave rise to reduction of the haem *c* centre, as evident by a characteristic increase in absorbance at 550 nm corresponding to the formation of ($PFe^{II}\text{-}Ru^{III}$).

Pan *et al.* diverged from this approach and introduced a novel procedure whereby lysine residues were labelled via amide bond formation using a highly reactive functionalised *N*-hydroxysuccinimide, Scheme 1.7.^[34, 35] The reaction between cytochrome *c* and the derivatised succinimide, resulted in the selective conversion of the positive lysine group to a negatively charged dicarboxybipyridine; this allowing the separation and purification of the singly labelled proteins by ion-exchange chromatography. The modified protein was then reacted with $Ru(bpy)_2(CO)_3$ at pH 4 to selectively yield the singly labelled $Ru(bpy)_2(dcbpy\text{-}cytochrome\ c)$ complex. At higher pH the His_{33} residue is also labelled as a consequence of deprotonation of the histidine group, which may act as a mono dentate ligand towards ruthenium.

Labelling of the sulfhydryl group of cysteine residues was also demonstrated with $[Ru(bpy)_2(4\text{-}bromomethyl\text{-}4'\text{-}methylbipyridine)](PF_6)_2$.^[36] The reaction proceeds via a S_N2 mechanism on nucleophilic attack of the α -carbon of the bromomethyl group by sulphur. This approach has been extensively exploited in conjunction with site directed mutagenesis in an effort towards a targeted labelling strategy. This provides the means to maximise the efficiency of electron transfer to the redox centres of the enzyme and to probe the mechanisms of specific processes of interest. Labelling of the C102T, H39C variant of yeast iso-1-cytochrome *c* has been achieved in up to 80% yields and the resultant bioconjugate, $Ru_p\text{-}39\text{-}cyt\ c$, utilised in the study of interprotein electron transfer in a number of redox partners of cytochrome *c*. In the presence of aniline and the carboxy-2,2,5,5-tetramethyl-1-pyrrolidinyloxy free radical (3CP) as sacrificial donors, laser flash photolysis of a solution containing $Ru_p\text{-}39\text{-}cyt\ c$ and beef heart cytochrome *c* oxidase lead to rapid formation of haem $Fe^{(II)}$ species of *cyt\ c*. This was quenched on reduction of the Cu_A centre of CcO, as monitored by a decrease in absorbance at 830 nm. The rate of recovery of $Cu^{(II)}$ was comparable to a concomitant decrease in absorbance at 605 nm, indicative of an intramolecular electron transfer from Cu_A to haem *a*. Similar investigations of *Rhodobacter sphaeroides* CcO were also undertaken using the ruthenium labelled K55C variant of horse heart cytochrome *c* as the electron donor.^[37]



Scheme 1.8. Proposed mechanisms of **a)** photooxidation and **b)** photoreduction of an enzyme cofactor by an excited ruthenium complex; where M = enzyme redox cofactor, A = acceptor, D = donor and P = oxidation/reduction products.

The specific pathway by which electron transfer occurs between a ruthenium photosensitiser and the redox cofactor of an enzyme is dependent upon the relative reduction potentials of each of the components involved, with two distinctly different mechanisms having been proposed, Scheme 1.8.B.^[29] The first involves direct reduction of the metal centre by the photoexcited sensitiser, $^*[\text{Ru}^{\text{II}}(\text{L})_3]^{2+}$, generating the reduced cofactor and the oxidised $[\text{Ru}^{\text{III}}(\text{L})_3]^{3+}$ complex. Back electron transfer is minimised on addition of a suitable sacrificial electron donor, which returns the sensitiser to the original oxidation state. In the presence of a donor of more negative potentials, or for complexes that are stronger oxidants in the excited state, a second mechanism that proceeds via reductive quenching of the excited sensitiser may occur. In the case of the ruthenium polypyridyls, it is suggested that the resultant negative charge is localised about one of the ligands to form the $[\text{Ru}^{\text{II}}(\text{L})_2\text{L}^-]$ species.

The ruthenium complexes may also be utilised in the photoinduced oxidation of a redox centre in accordance with Scheme 1.8.A. The intermolecular transfer processes of $\text{cyt } c_1$ in the yeast cytochrome bc_1 complex were probed in the physiological direction using the bioconjugate $\text{Ru}_z\text{-39-Cytc}$ as the electron acceptor.^[38] Coupling was achieved on reaction of $[\text{Ru}(2,2'\text{-bipyrazine})_2(4\text{-bromomethyl-4'-methylbipyridine})]^{2+}$ and the H39C;C102T variant of iso-1-cytochrome c . Photolysis of the $\text{Ru}_z\text{-39-Cytc}$ construct resulted in photooxidation of haem c in 20 % yields from a single flash. Under anaerobic conditions, back electron transfer dominates as reduction of haem by $[\text{Ru}^{\text{II}}(\text{L})_2\text{L}^-]^+$ results in the rapid recovery of the original oxidation states. Under aerobic conditions the reduced sensitiser was oxidatively quenched by molecular oxygen, effectively inhibiting back electron transfer resulting in an accumulation of the oxidised haem. Alternatively a sacrificial acceptor such as $[\text{CoCl}(\text{NH}_3)_5]^{2+}$ may be employed for systems that must be studied under inert atmospheres. Flash photolysis of $\text{Ru}_z\text{-39-Cytc}$ and reduced cytochrome bc_1 in a low strength ionic buffer lead to the rapid oxidation of $\text{cyt } c_1$ on electron transfer to the haem of $\text{Ru}_z\text{-39-Cytc}$. The former was monitored by a decrease in absorption at 557 nm with a concomitant recovery of the haem Fe(II) absorption at 550 nm.

The complex $[\text{Ru}(\text{bpy})_2(5\text{-iodoacetamido-1,10-phenanthroline})]^{2+}$ was used in the study of P450-BM3 from *Bacillus megaterium* so as to investigate the iron-oxo intermediates of the P450 catalytic cycle.^[39] Selective coupling was achieved on preparation of a triple mutant, C62A, C156S and K97C, to remove two native cysteine residues and to incorporate a solvent

exposed thiol group sufficiently close to haem to allow for eT between the two metal centres. Flash photolysis experiments in the presence of $[\text{Ru}(\text{NH}_3)_6]^{3+}$ afforded the ferric iron species upon oxidative quenching of the excited photosensitiser and subsequent reduction by haem. The resultant absorption kinetics were extremely complex and indicated at least five distinct phases contributing to the resultant recovery of the original state.

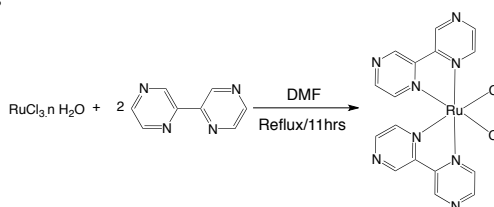
Nilsson^[40] first introduced the use of non-covalently bound ruthenium complexes for use in the photoactivated redox reactions of cytochromes. Tris(bipyridyl)ruthenium(II) complexes were found to inject a single electron into Cu_A of cytochrome *c* oxidase (CcO) during laser flash photolysis; the rate of electron donation was sufficiently rapid enough so as not to be rate determining of the subsequent processes. For successful transfer it was required to use a solution of high pH and low ionic strength, thus suggesting that electron transfer can only occur when the complex is electrostatically bound to the enzyme.

Zavlavsky *et al.* first reported the synthesis of the binuclear complexes Ru_2C $\{[\text{Ru}(\text{bpy})_2]_2(1,4\text{-bis}[2\text{-(4'-methyl-2,2'-bipyrid-4-yl)ethenyl}]benzene)(\text{PF}_6)_4$ and Ru_2D $\{[\text{Ru}(\text{bpy})_2]_2(2,2':4',4'':2'',2'''\text{-quaterpyridine})(\text{PF}_6)_4$ for use in subsequent studies of CcO.^[41] Results indicated an increase in photoreduction yields of the enzyme when compared to those attained for the mononuclear compounds. This was attributed to the increased positive charge of the complex allowing for more effective binding and improved interactions with the enzyme. The electrostatic nature of the binding with CcO was confirmed by a five-fold decrease in photoreduction yields upon increasing the ionic strength of solution. Likewise an eight-fold decrease resulted from the addition of an equivalence of cytochrome *c*. This indicated that electron transfer to the Cu_A centre is facilitated by interactions of the Ru_2C complex with the negatively charged cytochrome *c* binding domain.

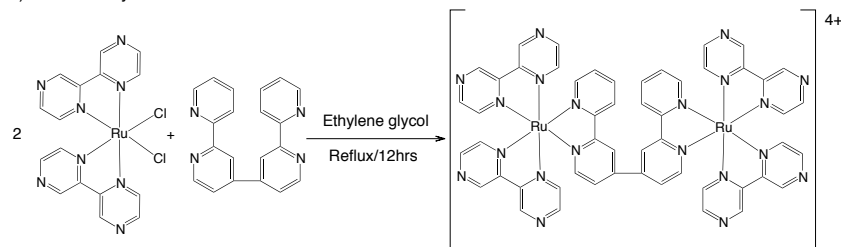
The use of 2,2':4',4'':2'',2'''-quaterpyridine as a ligand for ruthenium complexes was initially investigated in response to the increased interest shown in multi-nuclear systems.^[42] Though other bridging ligands have been synthesised that incorporate isolated bpy subunits inter-metal communication of the resultant polynuclear complexes has been relatively poor.^[43] This is due to a lack of conjugation between the two subunits as brought about by the use of a saturated alkyl chain as a linker unit. It has been demonstrated that for complexes of 2,2':4',4'':2'',2'''-quaterpyridine^[42] and *trans*-1,2-bis(4'-methyl-2,2'-bipyridyl-4-yl)-ethene^[44] limited communication between the two metal centres could be achieved. However, cyclic voltammograms showed a single $\text{Ru}^{\text{(II/III)}}$ couple similar to that of the analogous mononuclear systems thus indicating that the extent of this interaction was minimal. It is expected that as the metal-metal communication increases the redox couple would be split into two distinct waves due to a delocalisation of *d*-orbital between the two metal centres.^[45] The importance of this interaction with respect to the function of these systems as electron transfer agents is yet to be investigated.

Brand *et al.* synthesised a new binuclear complex for use in studies of the initial single electron reduction in the catalytic cycle of cytochrome *c* oxidase employing stopped-flow flash

i) Precursor synthesis



ii) Bimetallic synthesis



Scheme 1.9. Synthesis of the Ru_2Z bimetallic photosensitiser via a two stages reaction. **i)** Synthesis of the bis(2,2'-bipyrazyl)dichlororuthenium(II) precursor. **ii)** Subsequent reaction with 0.5 equivalence of the 2,2':4',4'':2'',2'''-quaterpyridine bridging ligand to yield the bimetallic species.

Table 1.1. Reduction potentials of the Ru_2C and Ru_2Z complexes vs normal hydrogen electrode

Complex	(II)/(III)	(II*)/(III)	(II)/(I)	(II*)/(I)
Ru_2C	1.27	-0.87	-1.31	0.83
Ru_2Z	1.7	-0.28	-0.82	+1.16

techniques.^[46] The Ru_2Z complex is a modification of the Ru_2D used by Zavlavsky, substituting the 2,2'-bipyridyl ligands with 2,2'-bypyrazine, synthesised using the method showed in Scheme 1.9. This resulted in a significant anodic shift in the redox potentials of the complex (Table 1.1); the calculated potential of the (II*)/(I) and (II*)/(III) couples suggests the excited state is a strong oxidant with subsequent electron transfer to Cu_A of CcO proceeding via the $[Ru^II(L)_2L^-]^+$ state, in accordance with Scheme 1.8.B. Yields of Cu_A photoreduction were ca. 60 % in the presence of aniline and 3CP as sacrificial donors under aerobic conditions, in comparison to ca. 10 and 2 % for Ru_2C and $[Ru(bpy)_3]^{2+}$ respectively. A lack of changes in absorbance at 436 nm indicated that reduction of haem a_3 had not occurred, implying that the Cu_B centre acts as the acceptor of the system.

1.4. Artificial Photosystems Inspired by Photosynthesis

1.4.1. Dye sensitised solar cells

The photovoltaic cell, more commonly known as the “solar cell”, converts light energy into electricity via the photovoltaic effect. The development of such devices has been extensively reported and perhaps shows the greatest potential towards a clean and renewable energy source.

The first-generation of solar cells are silicon-based and whilst these are the predominant devices employed at present they are typically of high manufacturing cost and

offer relatively low efficiencies. Second-generation devices that utilise thin films of amorphous silicon, CdTe or copper indium gallium selenides (CIGS) have exhibited greater efficiencies and are generally cheaper to produce. Perhaps the systems that most closely resemble that of naturally occurring photosynthesis are those of the dye-sensitised solar cells (DSSC).^[47] These systems typically employ transition metal complexes as a photosensitiser, closely mimicking the chlorophylls *a* and *b* of the light-harvesting complex of the naturally occurring photosystem.

A typical device is comprised of two plates of a glass or polymeric substrate that is coated with a transparent conductive film; the most common of these being the fluorine-doped tin oxide (FTO) and indium tin oxide (ITO) films. Upon one of these plates is deposited a mesoporous semiconductor layer, the most prolific material being TiO₂ though other semiconductors such as ZnO₂, SnO₂ and Nb₂O₅ have been utilised.^[48-51] A monolayer of a dye photosensitiser is adsorbed onto the semiconductor to complete the fabrication of the photoanode. Adsorption is facilitated on incorporation of appropriate anchoring groups into the molecular structure of the dye. Due to the ease of synthesis and a high stability, typically this takes the form of a carboxylic acid group (-CO₂H) although the phosphonic analogue (-PO₃H₂) has been shown to form more stable bonds to the oxide surface. Adsorption may be achieved through direct covalent and electrostatic bonding or upon the reliance of other weaker intermolecular interactions. Use of a mesoporous material aids to maximise light absorption owing to a large internal surface area to which the dye can bind. An organic electrolyte containing a redox couple such as iodide/triiodide is employed as a transfer mediator and to regenerate the photosensitiser by acting as an electron donor. The final component is a counter electrode that is constructed by deposition of a thin layer of platinum upon a second conductive glass substrate.

DSSCs operate via a sequence of electron transfer processes that are initiated on photoexcitation of the adsorbed dye and subsequent injection of an electron into the conduction band of the semiconductor. The oxidised dye is reduced by iodide in the electrolyte

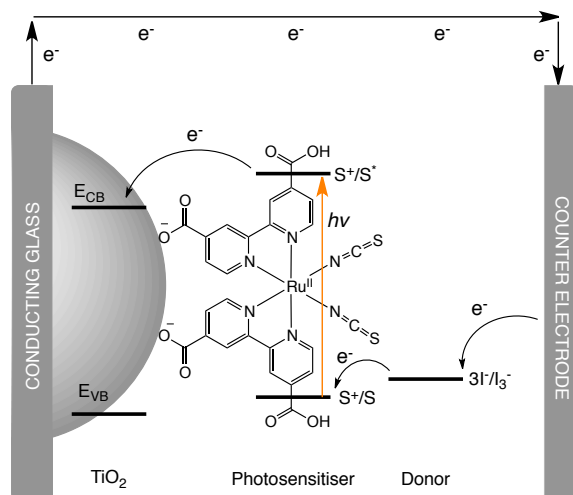


Fig. 1.4. Schematic drawing detailing the predominant electron transfer processes inherent in DSSCs on photovoltaic current generation, also highlighting the relative energy levels of individual components.^[52]

to yield the active photosensitiser and the oxidised donor, triiodide. The injected electron flows through an external circuit before being re-introduced into the cell via the Pt counter electrode; the circuit is completed on reduction of the oxidised donor, thus regenerating the cell. Additional processes may occur that diminish the overall efficiency of the device. As with all photosensitised reactions the associated radiative and non-radiative decay of the excited sensitiser may effectively compete with intermolecular electron transfer. Redox chemistry at the semiconductor surface may result in charge recombination with the oxidised dye or the direct reduction of tri-iodide, thus hindering current generation. A gradual deactivation of the cell is also expected due to the impact of irreversible chemical transformations.

The effectiveness of a cell is quantified by the overall conversion efficiency (η) which itself is derived from numerous other parameters including the photocurrent density, the open circuit voltage, the fill factor and light intensity. The incident photon to current efficiency (IPCE) describes the photocurrent density generated within the external circuit in relation to the monochromatic photon flux to which the cell is exposed.

Perhaps the most extensively researched of the photosensitisers is *cis*-Ru^{II}(NCS)₂(4,4'-dicarboxy-2,2'-bipyridyl)₂, the so called *N3* dye which boasts an impressive overall conversion efficiency of 10% and IPCE of $\geq 80\%$ for wavelengths between 480 – 600 nm.^[53] Whilst much of the focus has remained upon complexes of ruthenium, the utilisation of a variety of transition metals have also been studied including iron,^[54] osmium,^[55] rhenium,^[56] iridium^[57] and platinum.^[58] The use of purely organic dyes have also been demonstrated for DSSCs, the primary benefits being that the compounds offer high extinction coefficients and do not rely on the use of expensive transition metals. Organic dyes are based upon a donor-acceptor type structure, which constitutes an electron rich donor group separated from an electron deficient acceptor by a π -conjugated system or spacer. By altering the incorporated functionality of

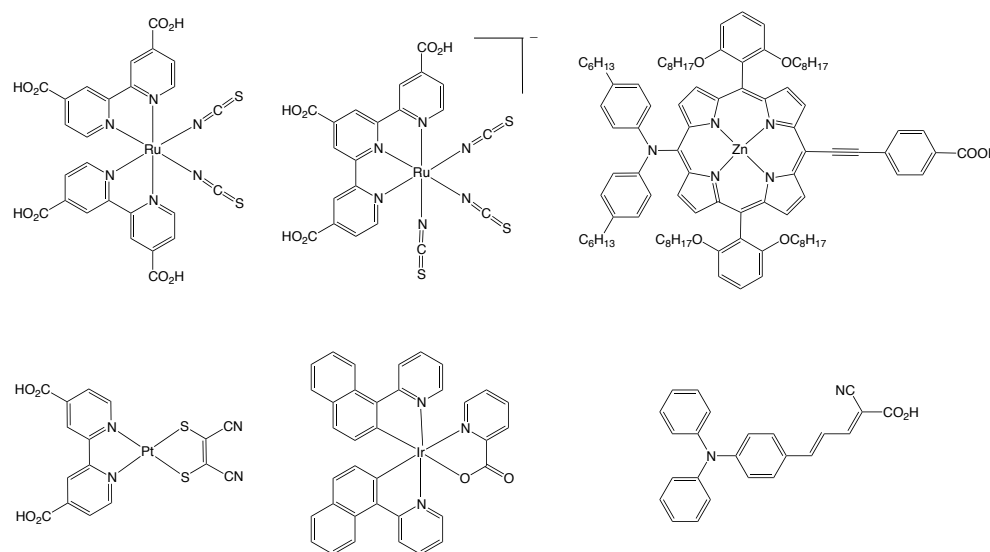


Fig. 1.5. Example dye photosensitisers that have been utilised in the preparation of DSSCs; a) the *N3* dye; b) the terpyridyl based 'black dye';^[59] c) the YD2-o-C8 dye;^[60] d) a maleonitriledithiolate based Pt dye;^[58] e) a neutral cyclometalated iridium(III) dye^[57] and f) a phenyl conjugated organic dye containing an electron rich $-NPh_2$ donor.^[61]

either of these groups it is possible to fine-tune the HOMO and LUMO energy gap and thus the overall properties of the sensitiser. On photoexcitation, the dyes undergo ILCT from the donor to the acceptor unit via the intervening π -bridge. The electron is then injected into the semiconductor via the acceptor group, the anchoring functionality is therefore typically in close proximity to the acceptor to facilitate electron transfer to the oxide surface.^[48]

The most efficient DSSC reported to date is the YD2-*o*-C8 dye that is based upon a modified zinc substituted porphyrin. The ligand has been designed to afford an effective donor- π -bridge-acceptor transfer towards the anchoring moiety.^[60] The reported IPCE value of 12.3 % under simulated sunlight was achieved utilising a redox electrolyte of tris-(2,2'-bipyridyl)cobalt^(II/III), *tert*-butylpyridine and LiClO₄ in acetonitrile. This value represents an unoptimised system as further investigations into the modification of this ligand to improve binding, etc. are currently on going.

1.4.2. Solar Hydrogen Evolution

Another viable alternative in the harvesting and storing of solar energy is the photosensitised decomposition of water to form H₂ and O₂ in the so-called water splitting reaction. An attractive route towards this goal is through the use of a family of metalloenzymes known as hydrogenases that catalyse the reversible reduction of protons to dihydrogen. As such within these systems, protons may be generated to act as a terminal acceptor in an electron transport chain whilst dihydrogen may be produced to be utilised as a source of low potential electrons.^[62] Replacement of the native electron donors with a photosensitiser has been demonstrated to be a viable route for greener and sustainable hydrogen production. Dihydrogen is an invaluable component in the synthesis of a variety of fuels and may itself be used as an energy source as part of a fuel cell.

1.4.2.1. Photosystem I

Initial attempts towards light-driven hydrogen production utilising hydrogenase enzymes focused upon the adaptation of PSI as the photosensitiser, chosen for the proffered high efficiencies that result from a number of contributing factors. The absorption profiles of the chromophores within PSI span all wavelengths below 700 nm, thus maximising energy absorption. The quantum yields of the formation of the charge separated P₇₀₀⁺F_B⁻ state are close to parity and offer thermodynamic efficiencies of between 38-59 % depending on the energy of the absorbed photon. The lifetime of this state is 60 ns and is sufficient to allow for electron capture and subsequent processes to occur. PSI has proven compatible with a variety of systems displaying extremely high photostability and a sufficient tolerance to changes in temperature.^[63] Of significant importance is the extent to which the cofactors and subunit proteins of the PSI construct may be manipulated so as to be adapted for a particular purpose, allowing for its inclusion in a variety of artificial systems.

Arnon *et al.* were amongst the first to describe a diffusion controlled light-driven hydrogen evolution system, coupling spinach chloroplasts to a hydrogenase from

Chromatium.^[64] Electron transfer was facilitated using ferredoxin as a mediator with cysteine and 2,6-dichlorophenolindophenol (DCPIP) as sacrificial electron donors to the chlorophyll of PSI.^[65, 66] Reactions were undertaken in the presence of 3-(3,4-dichlorophenyl)-1,1-dimethylurea (DCMU), which was used to inhibit PSII activity and subsequent water photolysis and oxygen production from the OEC. The presence of oxygen is typically detrimental to the activity of the system, either due to potential irreversible deactivation of the hydrogenase enzymes or by quenching of the reduced electron transfer mediators to form superoxide. Benemann *et al.* later demonstrated light-driven H₂ production employing water as the sole electron donor through PSII activity.^[67] The described system was comprised of spinach chloroplasts, ferredoxin and a hydrogenase from *Clostridium kluyveri*. Using glucose and glucose oxidase, oxygen formed on turnover of PSII was consumed to give gluconate and hydrogen peroxide thus perturbing the deactivation pathway.

The poor rates of hydrogen production in these initial systems was attributed to a lack of efficiency in electron transfer between PSI and the hydrogenase.^[68] It was demonstrated with the [FeFe]-hydrogenases of *Clostridium pasteurianum* that direct electron transfer between the two components could be achieved in the absence of a mediator.^[69] The native donors of these enzymes are the ferredoxins with which the terminal PsaC subunit of PSI shares sequence homology. Results suggested that the F_A and F_B iron-sulphur clusters of the PsaC subunit were acting as the primary donor to the hydrogenase, thus providing the necessary intermediary between the photoactive species and the catalytic site.

The assembly of a fusion protein containing PSI and an oxygen tolerant membrane bound [NiFe] hydrogenase from the β -proteobacterium, *Ralstonia eutropha* afforded a near five fold increase in the rate of electron transfer.^[70] The protein was prepared on substituting the C-terminal membrane anchor of the small HoxK subunit of the hydrogenase with a short linker peptide (Ser-Gly-Gly). This was subsequently fused to the PsaE subunit of PSI from the cyanobacterium *Thermosynechococcus elongates*. The active hydrogenase-PsaE/PSI complex was readily formed by self-assembly on incubation of the individual components at 4°C for 2 h. Using ascorbic acid, dithiothreitol (DTT) and *N,N,N,N*-tetramethyl-*p*-phenylenediamine (TMPD) as sacrificial electron donors, rates of H₂ production at 0.58 $\mu\text{mol H}_2$ (mg of Chl)⁻¹ h⁻¹ were achieved on illumination. Control reactions using chemically reduced methyl viologen as a source of reducing equivalents yielded an increased rate of 1.2 $\mu\text{mol H}_2$ (mg of Chl)⁻¹ h⁻¹, suggesting electron transfer from the PSI unit again being the rate determining step. It was concluded that a more rigid linker unit might further improve the efficiency of eT to the hydrogenase.

The use of molecular wires has been reported as a means of covalently linking PSI with a variety of catalytic modules.^[6] An early example of this approach is the PSI-molecular wire-nanoparticle bioconjugate, whereby PSI is used as a photosensitiser towards Au and Pt nanoparticles.^[71] Assembly of the system was achieved utilising the Cys₁₃Gly variant of the PsaC subunit. This mutation incorporates a solvent exposed differentiated site into the F_B

cluster which can be exploited to incorporate exogenous thiolated ligand and, through the use of dithiol compounds, provides the means to tether two entities to one another.^[72] In the initial experiments, 1,6-hexanedithiol was used to link the [4Fe-4S] cluster of PSI to the catalytic surface of a metallic nanoparticle. In the presence of DCPIP and sodium ascorbate as electron donors towards PS I, illumination with white light for 12 – 16 hours, yielded hydrogen production in the range of 3.4 – 9.6 $\mu\text{mol H}_2$ (mg of Chl)⁻¹ h⁻¹. Addition of the native electron donor Cyt *c*₆ yielded a five-fold increase in the rate of evolution for the Pt nanoparticle constructs.

Cross linking of plastocyanin to the PS I variant afforded a further two-fold increase compared to the non-covalently bound system.^[73] Cross linking was achieved on treatment of PS I with 1-ethyl-3-[3-dimethylaminopropyl]carbodiimide and *N*-hydroxysulfosuccinimide, proceeding via conversion of a carboxyl group into an activated isourea which in turn reacts with a primary amine residue of the cross linking partner. The increased rates of H₂ production were attributed to the elimination of diffusional rate control of electron transfer to P700⁺. The rate of electron transfer between the two units is highly dependent upon the molecular wire employed.^[73] Typically, increasing the length of the wire resulted in a decrease in H₂ production although this is with the exception of the shortest wire, 1,3-propanedithiol, which displayed a fraction of the activity of the hexyl analogue. This is surmised to be a result of steric hindrance preventing binding to the nanoparticle surface. The π -conjugated systems proved to be the most effective of the molecular wires; 1,4-benzene dithiol afforded a rate of 150.5 $\mu\text{mol H}_2$ (mg of Chl)⁻¹ h⁻¹, an increase of 50 % over the best performing saturated wire. Electron transfer to the hydrogenase is assumed to occur via quantum mechanical tunnelling as facilitated by the σ - and π - orbitals of the molecular wire, explaining the dependence of rates upon the nature of the linker. ^[63]

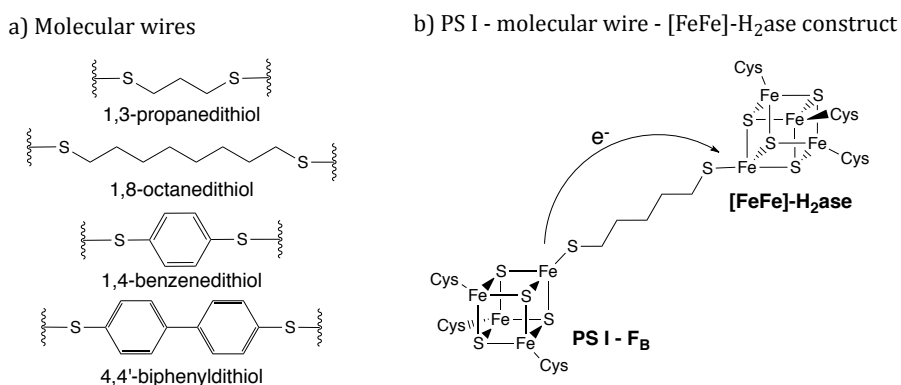


Fig. 1.6. Illustrating A) potential molecular wires used in the study of PSI nanoparticle bioconjugates and B) the schematic of the subsequent PS I – molecular wire – [FeFe]-hydrogenase construct using 1,6-hexanedithiol.

Using these same principles, tethering of PS I and the HydA[FeFe]-hydrogenase from *Clostridium acetobutylicum* was achieved with 1,6-hexanedithiol, forming a direct link between the redox cofactors.^[63] Samples were prepared on addition of the HydA_{C97G} variant to an equimolar quantity of the PS I–molecular wire construct, under stringent anaerobic conditions

and in the absence of light. On illumination with a broad spectrum white light the rate of H₂ production was measured at 30.3 μmol (mg of Chl)⁻¹ h⁻¹ when in the presence of Cyt c₆, sodium ascorbate and phenazine methosulphate as electron donors.

The coupling reaction suffers from poor selectivity, as the thiol group does not distinguish between the different iron clusters. It is therefore expected that the formation of non-active homodimers occur, meaning the reported rate does not represent the full capacity of the system. Using synthetic approaches it may be possible to gain a degree of control over the coupling of the two components although such methods would be difficult as the options available are fairly limited due to the restrictions set by the enzymes.

As with the nanoparticle bioconjugates the rate limitation by diffusion controlled electron donation to P700⁺ was negated on cross linking of Cyt c₆ to PS I. This subsequently afforded a bionanodevice that boasted a sevenfold increase in H₂ production yields to 200 ± 120 μmol mg Chl⁻¹ h⁻¹.^[74] From further investigation into the effects of pH, buffer solutions and wire lengths, an optimal system was identified. In a sodium phosphate buffer at pH 6.5 and employing the Cyt c₆-PS I_{C13G} construct tethered to the H₂ase via a 1,8-octanedithiol molecular wire, a hydrogen production rate of 2200 ± 460 μmol mg Chl⁻¹ h⁻¹ was achieved with an electron throughput of 105 ± 22 e PSI⁻¹s⁻¹. The latter is considerably larger than that found for naturally occurring photosynthesis in cyanobacteria under physiological conditions. These results substantiate the effectiveness of using molecular wires as a means of directly tethering two redox centres to optimise the rate of electron transfer.

1.4.2.2. Artificial Photosensitisers.

Extensive studies into the use of a variety of transition metal complexes as photosensitisers towards hydrogenase enzymes have also been undertaken. Okura *et al.* highlighted the use of zinc porphyrins as chlorophyll mimics towards the development of a number of diffusion-controlled multi-component systems.^[75] Initial studies focused upon zinc(II) tetraphenylporphyrin, Zn-TPP, and utilising the bipyridinium salts as electron transfer mediators.^[76] Hydrogen evolution was achieved using a [NiFe]-hydrogenase from *Desulfovibrio vulgaris* Miyazaki F in a phosphate buffer at pH 7.0 and using mercaptoethanol or triethanolamine as the electron donor, affording rates of 2.68 and 0.42 H₂ μmol h⁻¹ respectively. The significant difference in rates may be attributed to discrepancies in the relative concentrations of the donors used in the reaction mixtures. Similar systems utilising [Ru(bpy)₃]²⁺ and the organic dye 3,3'-sulfonic-propyl-5,5'-dichloro-9-ethylcarbocyanine have also been reported.^[77, 78]

Systems based upon Zn-TPP required the presence of a non-ionic surfactant, in this instance Triton X-100, to facilitate dissolution of the metalloporphyrin. The efficiency of hydrogen production has since been shown to be highly dependent upon the chemical composition of the surfactant employed; use of the PEGylated sorbitan, TWEEN 40, provided a significant rate enhancement as a consequence of changes in the micellar environment.^[79]

Modification of the porphyrin to incorporate the charged sulfonate groups sufficiently improved aqueous solubility to eliminate the need for additional surfactants. Zinc(II) *meso*-tetraphenylporphyrinsulfonic acid, Zn-PPS₃, also demonstrated increased activity towards reduction of methyl viologen in comparison to other studied sensitiser.^[80, 81]

The electron transfer mediator may be exchanged for one of numerous other bipyridinium salts. Whilst the functionality of the bipyridinium was shown to impact upon the rate of electron transfer to the hydrogenase, no clear correlation with the redox/structural properties of the compounds could be determined.^[82] In an approach similar to that described for systems of PSI, methyl viologen may alternatively be replaced with cytochrome *c*₃, the native redox partner of the hydrogenase.^[83] In the presence of triethanolamine, direct electron transfer from Zn-TPPS₃ to cytochrome *c*₃ affords near complete reduction of the latter in *ca.* 2 h. The process may be monitored by a decrease in absorbance at 419 nm with a concomitant increase at 432 nm that corresponds to the oxidised and reduced species respectively.

In an effort to further enhance the efficiency of the electron transport chain, a cytochrome *c*₃-viologen-ruthenium(II) triad complex was prepared with the viologen acting as a bridging unit between the sensitiser and the redox enzyme, Fig. 1.7.^[84] This was achieved by the selective mono-lithiation of 4,4'-dimethyl-2,2'-bipyridine and subsequent reaction with 1,4-dibromobutane to yield 4-(4-bromobutyl)-4'-methyl-2,2'-bipyridine. Reaction with 1-(2-carboxyethyl)-4,4'-bipyridine yields the diquaternary intermediate, which is covalent bound to cytochrome *c*₃ on reaction with the coupling reagents *N*-hydroxymethylsuccinimide and dicyclohexylcarbodiimide. The final complex was isolated on reaction of the functionalised cytochrome with Ru(bpy)₂CO₃ and purified by successive chromatography procedures using Sephadex-G25 and CM Sepharose.

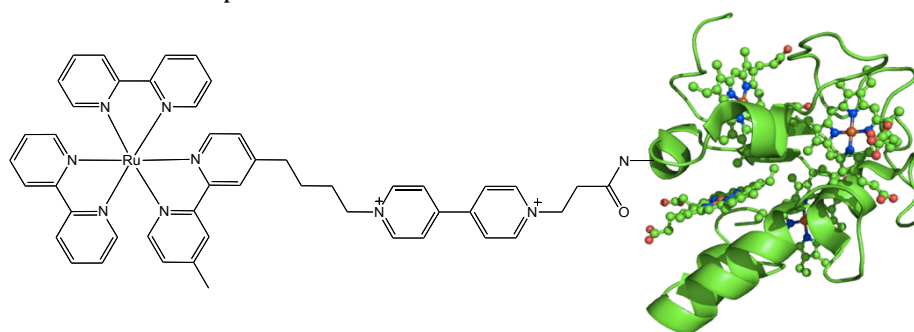


Fig. 1.7. A schematic representation of the Ru-MV-cyt *c*₃ triad complex employed in conjunction with the [NiFe]-hydrogenase from *Desulfovibrio vulgaris*.^[84]

Utilisation of colloidal TiO₂ nanoparticles as a semi-heterogeneous support for co-adsorbed photosensitiser and hydrogenase afforded efficient electron transfer between the two by adopting the basic principles of the DSSCs.^[85] The initial system was comprised of the [NiFeSe]-hydrogenase from *Desulfomicrobium baculatum* (*Db*[NiFeSe]-H₂ase) and proceeded via injection of an electron into the TiO₂ conduction band from the excited photosensitiser with subsequent electron transfer to the first of a series of [4Fe-4S] clusters and hence to the buried active site of the hydrogenase.

A number of ruthenium and platinum bipyridyl photosensitisers were tested, highlighting the effects of varying functionality and the anchoring groups.^[86] Of those studied the most effective was bis(2,2'-bipyridine)-(2,2'-bipyridine-4,4'-diylbis(phosphonic acid))ruthenium(II). This complex offered enhanced stability of attachment over the carboxylate analogue (>98 % adsorption versus <2 %) and significantly higher rates of hydrogen evolution compared to the most efficient Pt complex (3.56 ± 0.17 vs 0.30 ± 0.10 $\text{H}_2 \mu\text{mol h}^{-1}$). A number of alternate [NiFe]-, [NiFeSe]- and [FeFe]-hydrogenases were also investigated; results showed that activity is dependent upon the enzyme forming strong interactions with the TiO_2 surface whilst maintaining a conformation that is both catalytically active and allows for electron transfer to the hydrogenase. In *Db*[NiFeSe]-H₂ase this is facilitated by the electrostatic interactions of a large number of glutamate and aspartate surface residues in close proximity to the distal [4Fe4S] cluster, resulting in superior activity.

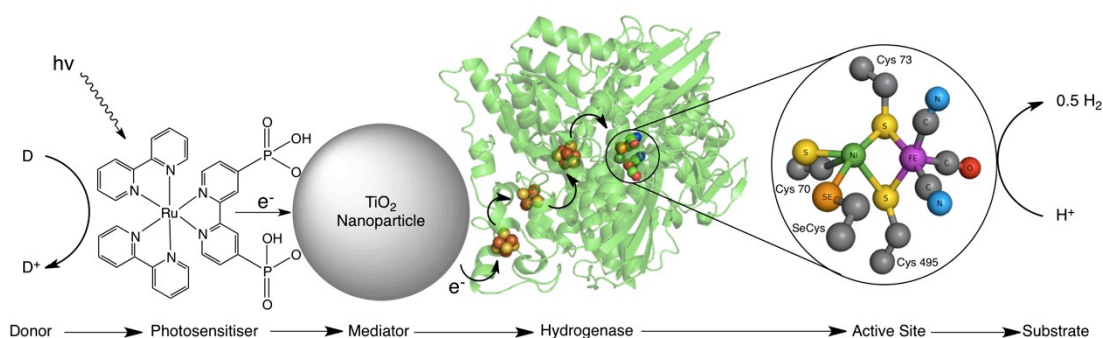


Fig. 1.8. Representative schematic of the artificial hybrid photosynthetic system utilising $[\text{Ru}(\text{bpy})_2(d(\text{PO}_3\text{H}_2)\text{bpy})]$ and *Db*[NiFeSe]-H co-adsorbed to the surface of TiO_2 nanoparticles.^[86]

This method was further modified to afford the efficient and clean photoreduction of CO_2 to CO utilising carbon monoxide dehydrogenase I enzyme (CODH I) from the anaerobic microbe *Carboxydotherrmus hydrogenoformans*.^[87] Whilst successful, the rates and stability of this system are low in comparison to that reported for the hydrogenase counterpart. This is believed to be a result of the smaller driving force for CO_2 reduction compared to H^+ and the potentially weaker binding of CODH I to the TiO_2 nanoparticles. The latter is supported by a significant drop in activity on centrifugation of the particles followed by buffer exchange, indicating the enzyme more readily desorbs.

1.4.3. Light-Driven Biocatalysis

The utilisation of enzymes in biocatalysis is becoming an increasingly attractive alternative to more traditional chemical transformations for pharmaceutical and industrial applications. This can be attributed to the proffered high regio-, stereo- and enantioselectivity that, in addition to substrate specificity, may also be tailored for specific purposes through the use of directed evolution. Furthermore this may avoid the use of protective groups, which can be laborious to incorporate though they are typically required in organic synthetic procedures if certain functionality is present. Enzymatically such groups can be selectively introduced into compounds of multiple functionality and likewise employed in subsequent deprotection

reactions.^[88] One disadvantage in employing enzymes in organic chemistry is a dependency upon the presence of redox cofactors. These compounds are typically highly expensive and thus require the use of efficient regeneration systems. Whole cell procedures are most often employed in industrial applications as the cofactor is biosynthesised along with the enzyme and regenerated by the native metabolic functions of the cell.^[89] Unfortunately due to the presence of additional enzymes in the wild type cells, undesired side reactions may occur. The carbonyl reductase enzymes present in whole cell baker's yeast result in the over reduction of the reduced enone products to form the corresponding saturated alcohols. A competing pathway involving direct consumption of the substrate may also occur to yield the allylic analogues. Enantiopurity may also be affected due to the competing activity of numerous oxidoreductases with opposite stereoselectivities.^[90]

Enzyme coupled systems employ regenerative enzymes such as the alcohol-, formate-, phosphate or glucose dehydrogenases.^[91-95] Regeneration is afforded on oxidation of the respective substrates which proceed with the concomitant reduction of NAD(P)⁺. However, this adds an extra level of complexity to the system and efficiency has been shown to be affected by changes in the substrate of the NAD(P)H dependent enzyme.^[96] For example, in the asymmetric bioreduction of the *cis*- α,β -unsaturated dicarboxylic acid, citraconic acid, regeneration of the cofactor failed outright. This was attributed to the ability of this substrate to act as a bidentate chelating agent that sequesters metal ions from solution. As the activity of the utilised dehydrogenases is dependent upon the presence of essential metal ions, the addition of equimolar quantities of the respective metal salts to the reaction mixture was required to negate this deactivating effect.

A range of electrochemical regeneration techniques have been developed based upon direct, indirect and enzyme-coupled methodologies.^[97] The efficiency of these processes tends to be rather poor with product concentrations of insufficient levels for practical purposes. As this approach requires the use of specialist equipment the potential applications in a synthetic laboratory are limited. Likewise it has been surmised that it will be some time until these electroenzymatic approaches may be viable for industrial scale processes.

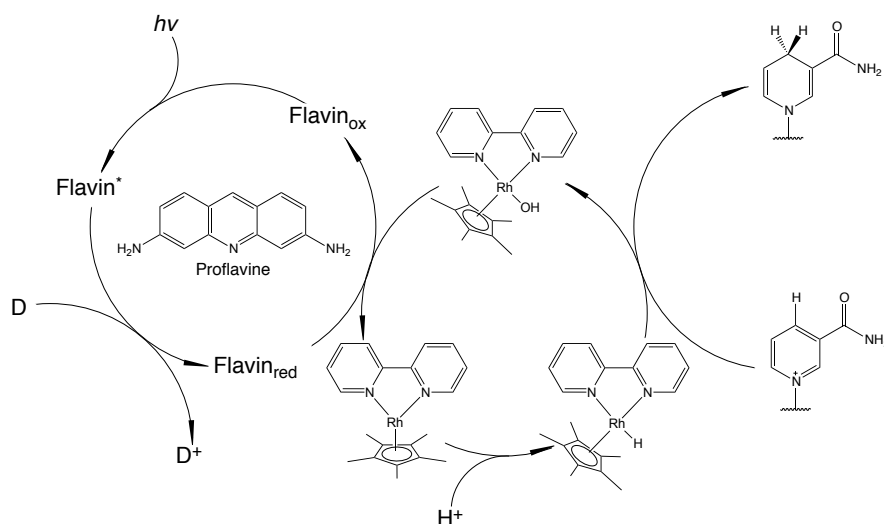
Chemical regeneration has been achieved with a variety of transition metal complexes including those of rhodium,^[98] platinum^[99] and ruthenium^[100] amongst others.^[101] Examples of this approach utilise dihydrogen as the reducing agent which is advantageous as no by-products are formed, as demonstrated for the *in situ* formation of NAD(P)H. Due to potential issues concerning the aqueous solubility of the catalysts and the associated expense of the reagents, this approach is perhaps less widely utilised than those discussed previously.

Photosensitised regeneration systems using visible light offer a simplified approach with additional economical and environmental benefits. One technique is to regenerate the native electron donor of the catalytic cycle. Gargiulo *et al.* demonstrated that flavins can be utilised in the photo-regeneration of NAD(P)⁺.^[102] Whilst FMN had been previously reported to be a potential candidate in non-enzymatic NAD(P)⁺ regeneration systems, the rate of hydride

transfer was slow and required a large excess of FMN to be viable.^[103] However, on illumination in the presence of a catalytic quantity of FMN, NAD(P)⁺ was rapidly generated as observed by a decrease in the characteristic NAD(P)H absorbance at 340 nm. Riboflavin delivered similar results though the rate of FAD catalysed oxidation was an order of magnitude slower as a result of intramolecular quenching of the excited state by the adenine moiety.^[104] The regeneration system underwent subsequent trials towards the oxidation reactions catalyzed by TADH and HLADH, alcohol dehydrogenase enzymes from *Thermus* sp.ATN1 and horse liver respectively. Initial trials with 2-octanol and cyclohexanol proved successful, though activity plateaued after *ca.* 3 hours, surmised to be a result of product inhibition of the enzyme. Using a biphasic system minimises this effect as the organic phase acts as both a substrate reservoir and product sink. Under these conditions, a steady rate of oxidation was afforded over a time period of at least nine hours with cyclohexanol as the substrate. Conversion rates were decreased by comparison to those of the homogenous system as a consequence of limitations in substrate diffusion across the phase boundary. The efficiency of photoexcitation may also be hampered due to an increased optical density caused by emulsion formation on mixing of the two phases. The HLADH catalysed oxidation reactions of the α,ω -diols, 1,4 butanediol and 1,5-pentanediol gave the respective lactones in 80 and 100 % yields via the hemiacetal intermediate. Whilst this approach has proven to be effective, the use of dioxygen as the terminal oxidant limits the potential applications of this system to those involving enzymes that are oxygen tolerant, unless an alternate sacrificial electron acceptor can be identified.

Willner *et al.* described the use of chlorotris[diphenyl(*m*-sulphonatophenyl)phosphine]rhodium(I), $[\text{Rh}^{\text{I}}\text{Cl}(\text{X})_3]^{3-}$ [$\text{X} = \text{P}(\text{Ph})_2(\text{C}_6\text{H}_4\text{SO}_3^-)$] as a catalyst in the regeneration of NAD(P)H.^[105] The system operates by employing $[\text{Ru}(\text{bpy})_3]^{2+}$ as a photosensitiser which is reductively quenched by sodium ascorbate to facilitate electron transfer to $[\text{Rh}^{\text{I}}\text{Cl}(\text{X})_3]^{3-}$. Disproportionation of the reduced hydride species $[\text{Rh}^{\text{II}}\text{HCl}(\text{X})_3]^{3-}$ yields $[\text{Rh}^{\text{I}}\text{HCl}(\text{X})_3]^{4-}$ which then acts as a hydride transfer agent towards NAD(P)⁺. When utilised in the biotransformation reactions of pyruvic acid with lactone dehydrogenase and alanine dehydrogenase, the resultant conversion yields were relatively low. The activity of the system was short lived and was attributed to enzyme inhibition by the free ligand $\text{P}(\text{Ph})_2(\text{C}_6\text{H}_4\text{SO}_3^-)$ which dissociates from the catalyst on illumination. On lowering the concentration of $[\text{Rh}^{\text{I}}\text{Cl}(\text{X})_3]^{3-}$ the system was successfully employed in the reduction of acetaldehyde by HLADH to give ethanol in 65 % yields over 10 hours.

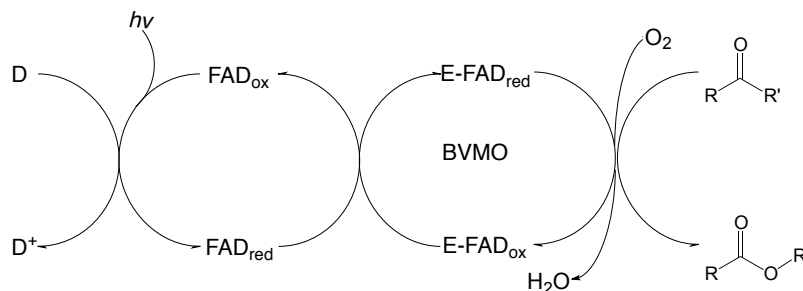
Alternatively, proflavine may also be used as a photosensitiser as demonstrated in the $[\text{Cp}^*\text{Rh}(\text{bpy})\text{H}_2\text{O}]$ where $\text{Cp}^* = 1,2,3,4,5$ -pentamethylcyclopentadiene mediated regeneration of NADH. At proflavine concentrations of 10 μM and in the presence of triethanolamine as a sacrificial donor, NADH regeneration yields of 63.4 % were achieved with a turnover frequency (TOF) of 127.8 h^{-1} .^[106] The system was subsequently applied in the biocatalytic reduction of α -ketoglutarate using the NADH-dependent L-glutamate dehydrogenase. On



Scheme 1.10. Proposed mechanism of the proflavine photosensitised NADH regeneration system employing $[\text{Cp}^*\text{Rh}(\text{bpy})\text{H}_2\text{O}]^+$ as an electron mediator and TEOA as a sacrificial donor.

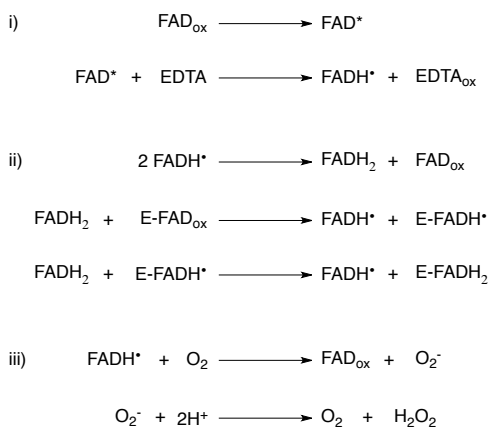
illumination with white light conversion yields of 65.3 % were achieved in 60 minutes. Control reactions in the absence of the mediator gave conversion rates of 5.7 % indicating that direct eT from the proflavine to NAD^+ is minimal. The mediator is reduced on accepting two photogenerated electrons from proflavine to yield the intermediary $[\text{Cp}^*\text{Rh}(\text{bpy})]$. The active species $[\text{Cp}^*\text{Rh}(\text{bpy})\text{H}]^+$ is formed on proton abstraction from the aqueous media and readily undergoes hydride transfer to $\text{NAD}(\text{P})^+$, Scheme 1.10. A similar method describes the production of formic acid from CO_2 by formate dehydrogenase using a novel photosensitiser, a multianthraquinone-substituted porphyrin, which had been covalently attached to a chemically converted graphene.^[107] On photoexcitation an electron is transferred to the graphene which subsequently acts as a mediator towards $[\text{Cp}^*\text{Rh}(\text{bpy})\text{H}_2\text{O}]^+$. In photocatalytic trials the graphene construct outperformed both the free photosensitiser and a standard of $\text{W}_2\text{Fe}_4\text{Ta}_2\text{O}_{17}$, with NADH regeneration yields of 45.5 % in comparison to 23.8 and 14.5 % respectively. This was likewise reflected in the yields of formic acid production, which after 2 h, were reported as $110.6 \mu\text{M}$ for the substituted graphene and 46.5 and $14.25 \mu\text{M}$ for each of the control reactions respectively.

Photosensitised reactions may also proceed via direct reduction of the redox centre of the enzyme. Hollmann *et al.* first demonstrated the potential of free flavin for this purpose in biocatalytic Baeyer-Villiger reactions of the flavoenzyme phenylacetone monooxygenase (PAMO-P3) from *Thermobifida fusca*.^[108, 109] This mutant was specifically engineered to catalyse the enantioselective reaction of a variety of substituted aromatic ketones to the respective lactones, towards which the wild type enzyme showed poor active and/or selectivity.^[110, 111] On illumination with white light and using EDTA as a sacrificial donor, FAD was successfully implemented in the PAMO-P3 catalyzed reaction of 2-phenylcyclohexane to give 7-phenyl-2-oxepanone in 48 % yield, close to the maximum theoretical conversion of 50 %, with a high enantiopurity (97 ee %). The presence of a catalytic quantity of NADP^+ was



Scheme 1.11. Outline of the mechanism for the light-driven cofactor regeneration of a Baeyer-Villiger monooxygenase and subsequent oxidation reaction of the ketone substrate.

also required for the reaction to proceed. NADP^+ was shown not to take part in the electron transfer process but instead allowed the enzyme to adopt an active conformation upon binding. The total turnover numbers (TON) and catalytic turnover frequency (TOF) of the light-driven system were at least an order of magnitude lower compared to those of the native catalytic cycle. This was attributed to an insufficient interaction between the enzyme bound cofactor and the free flavin as a consequence of steric hindrance about the active site. Catalysis was also limited by an uncoupling side reaction, whereby the photogenerated FAD semiquinone was quenched by molecular oxygen to reform the oxidised flavin and a superoxide radical that undergoes disproportionation to yield H_2O_2 and O_2 , Scheme 1.12. This particular issue may be counteracted by altering the photochemical initiator to a deazaflavin,^[112] which have demonstrated a low reactivity towards dioxygen thus minimising deactivation.^[114] This approach was successfully implemented in the P450-BM3 catalyzed hydroxylation reaction of lauric acid in the presence of a catalytic quantity of NAD(P)^+ .



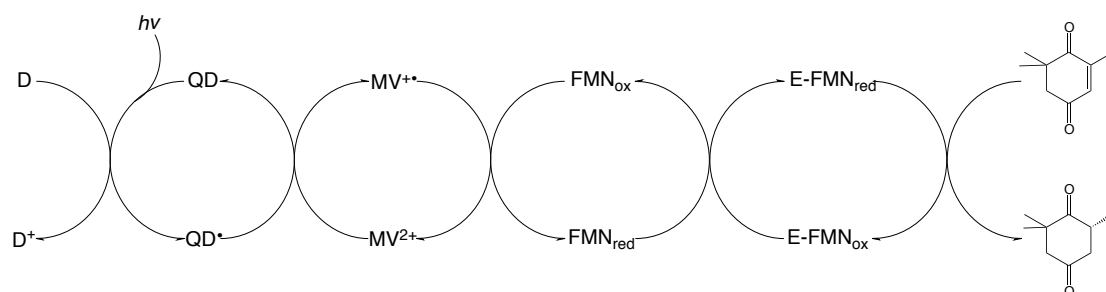
Scheme 1.12. Schematic highlighting the individual processes involved in the photochemical initiated reduction of a flavoenzyme using free flavin as a photosensitiser.^[113] i) Photoexcitation of the flavin and subsequent reductive quenching of the triplet state by EDTA to form the semiquinone. ii) synproportionation of the semiquinone yields an oxidised and fully reduced FAD molecule. The latter then undergoes a proportionation reaction with the enzyme bound cofactor, which on reaction with a second molecule of FADH_2 forms the catalytically active enzyme. iii) Oxidative quenching of the semiquinone by molecular oxygen to yield the oxidised cofactor and superoxide that readily undergoes disproportionation.

To determine the scope of this particular regeneration system, additional trials in conjunction with the oxygen independent old yellow enzyme homologue YqjM from *Bacillus subtilis* were undertaken.^[108] In comparison to PAMO, the enzyme bound FMN is more readily accessible owing to a considerably larger and more solvent exposed active site. The YqjM catalysed reduction of ketoisophorone in the presence of FMN and EDTA gave quantitative yields of (R)-levodione with an enantiomeric excess of 88 % and a turnover frequency of 194 h⁻¹. Evidence also supported a non-enzymatic reduction of the substrate to yield a racemic product at a rate *ca.* 10% of that proposed for the YqjM catalysed reaction. This along with a steady decrease of enantioselectivity on increasing reaction times indicates that under these conditions, a slow racemisation of the product is in effect.

Further study into the optimisation of this system showed a definitive dependence upon the concentration of both FMN and EDTA.^[115] The former is as expected on assuming that the formation of FMNH₂ be the rate-determining step. Whilst not affecting the initial rate of reaction, the concentration of the sacrificial electron donor did impact on the overall conversion of the substrate. Results suggested that EDTA does not undergo complete oxidation, requiring at least 0.6 equivalents, equating to *ca.* 2.4 equivalents of hydroxyl functionality, for full conversion of the substrate. This was attributed to a decrease in the rate of electron transfer on successive oxidative processes.

Adaptation of this approach allowed for the development of a photochemical initiated *in situ* H₂O₂ generation system.^[116, 117] Utilising the decoupling reaction of FMN with molecular oxygen the formed peroxide can subsequently be used to regenerate a catalytically active oxyferryl heme reaction centre. This was successfully implemented in the oxygenation reactions of Chloroperoxidase from *caldariomyces* (CPO) and *Agrocybe aegerita* aromatic peroxygenase (*AaeAPO*).

Most recently Burai *et al.* demonstrated the use of CdSe quantum dots (QDs) as a photosensitiser in the light driven reduction of ketoisophorone by YqjM.^[118] Reduction of the cofactor was facilitated by the use of methyl viologen and free FMN as electron transfer mediators. Generation of the methyl viologen cationic radical (MV^{•+}) was monitored spectrophotometrically and indicated yields of *ca.* 46 % (*ca.* 115 μM) as achieved within



Scheme 1.13. Representative schematic of electron transfer processes postulated for the biocatalytic reduction of ketoisophorone to (R)-levodione employing CdSe quantum dots as a photosensitiser. Where D = donor; QD = quantum dot; MV = methyl viologen and E-FMN = enzyme bound cofactor.^[118]

40 minutes. Subsequent reduction of free FMN was confirmed on a decrease in absorption at *ca.* 370 and 460 nm. Addition of YqjM and ketoisophorone resulted in minimal (*R*)-levodione formation with yields of *ca.* 10 % and an enantiomeric excess of 64 %. This is compared to *ca.* 60% for the NADPH-driven reaction using a glucose dehydrogenase regeneration system. It was also noted that in the absence of enzyme or cofactor, direct reduction of the substrate by MV⁺ occurred to yield a racemic product. Transient studies of MV⁺ formation indicated that ineffective eT from TEOA to the quantum dots equated to *ca.* 65 % of radical consumption by charge recombination. The efficiency of the system was further hindered due to inhibition of the reaction by decomposition products of TEOA, resulting in complete cessation of the reaction after 60 minutes. Studies are on-going to optimise the system through manipulation of the properties inherent in the quantum dots and the effects of alternative sacrificial donors.

1.5 Aims and Objectives

The primary objective of this project is the development of new light-driven biocatalytic systems derived from non-photosynthetic enzymes. Despite extensive precedent for the use of transition metal photosensitisers in the study of electron transfer processes in enzymatic systems, the application of such compounds in light-driven biocatalysis has yet to be described to an appreciable extent in the literature. Utilisation of transition metal complexes gives great scope towards fine-tuning the spectral and redox properties of the sensitiser to best suit the requirements of the system and maximise catalytic efficiency. The targets of the presented synthetic study are complexes of ruthenium(II) and iridium(III), which have been demonstrated to act as effective sensitisers in a variety of applications. Detailed is an extensive synthetic investigation towards the preparation of a variety of targets that have been chosen to create sensitisers of a broad range of properties as possible. Complete characterisation of the related structural, photophysical and electrochemical properties is achieved through the use of NMR, X-ray crystallography, electronic spectroscopy and electrochemistry techniques. The origins of such properties are also probed using computational methods. The biocatalytic systems that are the focus of this investigation are those of the FMN containing old yellow enzyme (OYE) family, specifically pentaerythritol tetranitrate reductase (PETNR) and the thermophilic old yellow enzyme (TOYE). The study examines the feasibility of such enzymes toward applications in artificial photosynthesis and the limitations thereof.

In overview, Section Three discusses the synthesis and characterisation of a series of ruthenium complexes incorporating the 2,2'-bipyrazyl pro-ligand in conjunction with a variety of other polyheteroaryl compounds. Section Four explores the development of water-soluble cyclometalated iridium(III) complexes through the use of ligands containing positively charged functionality. Section Five describes the utilisation of the prepared photosensitisers in the development of light-driven biocatalytic assays and the endeavour to optimise the reaction conditions to fully realise the potential of these artificial photosynthetic systems.

SECTION TWO

METHODS AND MATERIALS

2.1. Materials

The compounds $\text{NiBr}_2(\text{PPh}_3)_2$,^[119] $\text{NiCl}_2(\text{PPh}_3)_2$,^[119] $\text{PdCl}_2(\text{MeCN})_2$, $[\text{Ru}(\text{bpz})_3](\text{PF}_6)_2$,^[120] $\{[\text{Ru}(\text{bpy})_2]_2\text{bpm}\}(\text{PF}_6)_4$,^[121] $\{[\text{Ru}(\text{bpy})_2]_2\text{bpp}\}(\text{PF}_6)_4$,^[122] and $\{[\text{Ru}(\text{bpy})_2]_2\text{tpphz}\}(\text{PF}_6)_4$,^[123] were prepared using literature procedures. $[\text{Ru}(\text{CO})_2\text{Cl}_2]_n$ was synthesised according to Anderson *et al.*; purification achieved on trituration in boiling *n*-hexane with vigorous stirring over 8 hours.^[124] Copper powder (20 g) was activated prior to use on washing with Acetone:HCl_(aq) (1:1, 150 mL); Acetone (150mL); deionized water (150 mL) and aqueous ammonia (5% v/v; 150 mL). The solid was further washed with absolute ethanol until no colour was evident in the filtrate before a final wash with acetone (150 mL); diethyl ether (200 mL) and dried *in vacuo*. Zinc powder (20.0 g) was activated on stirring with HCl (10% v/v; 20 mL) and subsequent washing with deionised water (100 mL), acetone (100 mL) and dried *in vacuo*. Ruthenium(III) chloride and iridium(III) chloride were purchased from Precious Metals Online. 2-chloropyrazine, ammonium hexafluorophosphate and tetrakis(triphenylphosphine) palladium(0) was purchased from Fluorochem. Oligonucleotide primers were purchased from MWG. Complete mini Ethylenediaminetetraacetic acid (EDTA) free protease inhibitor cocktail tablets were purchased from Roche. Agar, ampicillin, carbenicillin and tris base were purchased from Formedium. Other chemicals were supplied by Sigma Aldrich, Alfa Aesar, Fisher Scientific or VWR. Products were dried in a desiccator (silica gel) overnight under high vacuum prior to characterization. All chemicals were of reagent grade purity or higher and were used without further purification unless otherwise stated. TOYE was kindly supplied by Dr Björn V. Adalbjörnsson and was prepared according to the literature procedure.^[125]

2.2. General Physical Measurements

¹H NMR spectra were recorded on a Bruker UltraShield or AV-400 spectrometer. Chemical shifts are reported in parts per million relative to SiMe₄ as referenced to the proton resonances of residual solvent using values reported in literature.^[126, 127] The fine splitting of pyridyl or phenyl ring AA'BB' patterns are reported herein. Elemental analyses were performed by the Microanalytical Laboratory, University of Manchester. Electrospray ionization, MALDI and gas chromatography mass spectrometry were performed by the Mass Spectrometry Services, School of Chemistry, University of Manchester. UV-vis spectra were obtained using either a Shimadzu UV-2401 PC or a Varian Cary UV-50 Bio spectrophotometer. Cyclic voltammetric measurements were obtained using an Ivium CompactStat and a BASi VC-2 voltammetry cell. A platinum disk electrode and a platinum wire were employed as the working and auxiliary electrodes respectively. A glass-bodied aqueous silver/silver chloride electrode (3 M NaCl, saturated AgCl) fitted with a Vycor porous junction was used as a

quasi-reference electrode using the ferrocene/ferrocenium couple as an internal standard. Acetonitrile used in experiments was of HPLC grade as supplied by Fisher Scientific. $[\text{nBu}_4\text{N}]\text{PF}_6$ was of electrochemical grade and used as supplied by Sigma Aldrich. Solutions containing *ca.* 10^{-3} M analyte in 0.1 M electrolyte were deaerated on purging with dried N_2 . $E_{1/2}$ values were calculated from the average of the anodic and cathodic peak potentials ($E_{1/2} = (E_{\text{pa}} + E_{\text{pc}})/2$) at a scan rate of 100 mV s^{-1} . GC analysis was performed on a Varian CP-3800 gas chromatograph equipped with a CombiPAL auto sampler and operated using the Varian Star Workstation software package.

2.3. Synthetic Chemistry

2.3.1. Ligand and Organic Precursor Synthesis

2.3.1.1. Preparation of 2,2'-bipyrazine

2-Iodopyrazine, (IPz): Hydriodic Acid (57 % *v/v*, 35 mL) was added to a round-bottomed flask and cooled to 0°C using a water/acetone/ice bath. 2-chloropyrazine (10 g, 87.7 mmol) was added drop-wise with vigorous stirring to afford an orange solution. The temperature was maintained for 1 h then gradually heated to 40°C and left to stir for a further 1h. The resultant yellow suspension was cooled to 0°C and basified to pH 8.0 with saturated K_2CO_3 (aq). The solution was extracted with DCM ($4 \times 50 \text{ mL}$) and the organic layers combined, washed with saturated $\text{Na}_2\text{S}_2\text{O}_3$ (aq) and dried over anhydrous MgSO_4 . Solvents were removed by rotary evaporation to afford the crude product, which was of sufficient purity for use in subsequent reactions but may be purified further using vacuum distillation.

Yield: Pale Yellow Oil 16.21 g, (90 %). **$^1\text{H-NMR}$:** δ_{H} (400 MHz, CDCl_3) 8.84 (1H, d, $J = 1.5 \text{ Hz}$), 8.482(1, d, $J = 2.51\text{Hz}$), 8.365 (1H, dd, $J = 4.0, 0.9$).

2,2'-bipyrazine; Method A: Palladium catalysed: Palladium acetate (0.09 g, 0.4 mmol), tetrabutylammonium bromide (1.29 g, 4 mmol), *N,N*- diisopropylamine (0.48 g, 8 mmol) and chloropyrazine (0.92 g, 8 mmol) were added to a double necked round bottomed flask and the vessel purged with argon. Dry, degassed toluene (1.5 mL) was added and the mixture refluxed for 1 h, at which time isopropanol (0.5 g) was added. The temperature was maintained at 105°C for 24 h. After cooling to *ca.* 35°C water and diethyl ether were added, the organic was separated, washed with water and dried over MgSO_4 .

Yield: Tan Solid 113 mg, (18 %).

2,2'-bipyrazine; Method B: Nickel catalysed reaction: A suspension of NaH (0.96, 40 mmol), $\text{Ni}(\text{OAc})_2$ (1.76 g, 10 mmol) and triphenylphosphine (10.48, 40 mmol) in DME (30 mL) was heated to 65°C under argon prior to the dropwise addition of a solution of *tert*-butanol (1.48 g, 20 mM) in DME (10 mL). After 2h stirring the temperature was reduced to 45°C and a solution of 2-chloropyrazine (1.14 g, 10 mmol) in DME (5 mL) was gradually added to the reaction

mixture and the temperature maintained for 12 h. Upon cooling, unreacted NaH was quenched upon careful addition of EtOH (*ca.* 5 mL) and the resultant mixture poured into water and exhaustively extracted with diethyl ether. The combined organic phases were dried over MgSO₄ and solvents removed by rotary evaporation. The product was purified by column chromatography (SiO₂, Ethyl acetate : Hexane; 4:6).

Yield: Pale yellow solid, 253 mg (32 %).

2,2'-bipyrazine; Method C: Nickel catalysed homocoupling: NiBr₂(PPh₃)₂ (2.23 g, 3 mmol), activated zinc powder (981 mg, 15 mmol) and [Et₄N]I (2.57 g, 10 mmol) were loaded to a three-necked round-bottomed flask and the vessel back filled with argon. Anhydrous THF (10 mL) was added via syringe and the mixture left to stir at room temperature for 30 mins. An argon-sparged solution of 2-iodopyrazine (2.05 g, 10 mmol) was then added and the temperature increased to 55°C and was maintained for 18 h. On cooling to room temperature the mixture was poured into aqueous ammonia (2M; 100 mL) and the mixture extracted with ethyl acetate (3 × 150 mL). The organic layers were combined, dried over MgSO₄ and solvents removed by rotary evaporation. The product was purified by column chromatography (SiO₂, Ethyl acetate : Hexane; 4:6).

Yield: Pale yellow solid, 278 mg (35 %).

2,2'-bipyrazine; Method D: Ullman-type reaction: 2-Iodopyrazine (5.0 g, 24.3 mmol) and activated copper powder (6.0 g, 94 mmol) were added to a double necked round bottomed flask equipped with a condenser and N₂ inlet. Anhydrous DMF (20 mL) was added and the reaction vessel purged with argon for 10 minutes before the temperature was increased to 80-85°C. After 3.25 h, activated copper powder (1.33 g, 21 mmol) was added and the N₂ inlet replaced with a calcium chloride tube. After a further 3.25 h, the temperature was increased to 120-130°C and stirred for 2 h. The suspension was then cooled to 0°C before being drowned in a solution of potassium cyanide (7.7 g) in ammonia (38 mL, 25 % w/v). The resultant suspension was filtered and the solid residue extracted with an equal volume of cyanide solution. The filtrate was treated with potassium cyanide (0.4 g) and extracted with chloroform (5 × 100 mL). The organic phase was dried over MgSO₄, filtered, evaporated and recrystallised from ethyl acetate/methanol 19:1 to yield a pale tan solid.

Yield: Pale Yellow Solid, 938 mg (48 %).

2,2'-bipyrazine (bpz); Final Method: 2-iodopyrazine (5.0 g, 24.3 mmol), Pd(OAc)₂ (34 mg, 0.15 mmol), K₂CO₃ (3.4 g, 24.6 mmol) and polyethylene glycol (Mw4000, 24.0 g) were added to a round bottomed flask (100 mL) and the vessel purged with argon. The mixture was gradually heated to 120°C and the temperature maintained for 48 h with stirring. The mixture was cooled to approximately 80°C and deionized water (30 mL) added. On further cooling to room temperature the solution was diluted with deionized water (100 mL) and exhaustively

extracted with ethyl acetate. The combined organic layers were washed with a saturated sodium thiosulphate solution and thrice with brine. The organic layer was dried over magnesium sulphate and solvents removed under reduced pressure. The residue was triturated *n*-pentane and the solid collected by filtration, which was washed with a further volume of *n*-pentane (50 mL) and dried *in vacuo*.

Yield: White crystalline solid, 1.35 g (70 %). **¹H-NMR:** δ_{H} (400 MHz, CDCl₃) 9.60 (2H, d, *J* = 1.1 Hz), 8.68 – 8.66 (4H, m) ppm. **GC-MS (*m/z*):** 158 [M]. **Anal. Calcd (%)** for formula C₈H₆N₄; C, 60.75; H, 3.82; N, 35.42. Found C, 60.36; H, 3.35; N, 35.80.

2.3.1.2. Synthesis of 4,4'-disubstituted-2,2'-bipyridine

2,2'-bipyridyl-N,N'-dioxide: A solution of 2,2'-bipyridine (10.0g, 64.1 mmol) in glacial acetic acid (65 mL) was heated to 75-80°C. To this H₂O₂ (20 mL, 35 % w/v) was added drop-wise at a rate to maintain the temperature between to 75-80°C. After two hours a further volume of H₂O₂ (20 mL, 35 % w/v) was added and the mixture stirred for 18 h. The solution was cooled to room temperature and the product precipitated on addition to acetone (750 mL), the solid was collected by filtration, washed with acetone and dried under vacuum.

Yield: Pearlescent white crystalline solid, 10.52 g (86 %) **¹H-NMR:** δ_{H} (400 MHz, D₂O) 8.46 – 8.44 (2H, m), 7.85 – 7.81 (2H, m), 7.76 – 7.72 (2H, m) ppm.

4,4'-dinitro-2,2'-bipyridyl-N,N'-dioxide: Fuming nitric acid (20 mL) was added dropwise to a stirred solution of 2,2'-bipyridyl-N,N'-dioxide (10.0 g, 52.6 mmol) in fuming sulphuric acid (30 mL) cooled to 0-5°C using a water/ice bath. The mixture was then gradually heated to 100°C and stirred for 20 h. The resultant orange solution was cooled to 0°C and then poured onto ice. The solid was then collected by vacuum filtration and the product washed with a copious volume of ice-cold water until the filtrate had become neutral.

Yield: Pale yellow powder, 6.25 g (42 %). **¹H-NMR:** δ_{H} (400 MHz, (CD₃)₂SO) 8.69 (2H, d, *J* = 3.3 Hz), 8.60 (2H, d, *J* = 7.2 Hz), 8.37 (1H, dd, *J* = 7.2, 3.3 Hz).

4,4'-dichloro-2,2'-bipyridyl-N,N'-dioxide: A suspension of 4,4'-dinitro-2,2'-bipyridyl-N,N'-dioxide (6.23 g, 22.3 mmol) in glacial acetic acid (60 mL) was warmed to 50°C under argon. Upon complete dissolution, acetyl chloride (20 mL) was added dropwise and the mixture heated at 80°C for 18 h with vigorous stirring. The mixture was cooled to room temperature and then cautiously poured over ice prior to basification to pH 9 using 8.3 M NaOH_(aq). The precipitate was collected by vacuum filtration and the filtrand washed with copious amounts of cold water prior to being dried *in vacuo*.

Yield: Pale tan powder, 4.37 g (76 %). **¹H-NMR:** δ_{H} (400 MHz, (CD₃)₂SO) 8.36 (2H, d, *J* = 7.0 Hz), 7.92 (2H, d, *J* = 3.1 Hz), 7.64 (2H, dd, *J* = 7.0, 3.0 Hz) ppm.

4,4'-dibromo-2,2'-bipyridyl-N,N'-dioxide: This was prepared in a similar manner to 4,4'-dichloro-2,2'-bipyridine instead using acetyl bromide (20 mL) in place of acetyl chloride.

Yield: Pale tan powder, 5.69 g (77 %). **¹H-NMR:** δ_{H} (400 MHz, (CD₃)₂SO) 8.28, (2H, dd, $J = 7.0$, 0.4 Hz), 8.02 (2H, dd, $J = 2.9$, 0.3 Hz), 7.78 (2H, dd, $J = 7$, 2.9 Hz) ppm.

4,4'-dinitro-2,2'-bipyridine: A suspension of 4,4'-dinitro-2,2'-bipyridyl-N,N'-dioxide (2.0 g, 7.2 mmol) in PCl₃ (20 mL) was heated at reflux for 21 h with vigorous stirring. Upon cooling to room temperature the solution was poured onto ice and basified to pH 10 using 25 % NaOH aqueous solution. This was extracted with CH₃Cl (3 × 250 mL), the organic layers combined, dried over magnesium sulphate and the product isolated on removal of solvents by rotary evaporation.

Yield: Yellow-tan crystalline solid, 1.21 g (68 %). **¹H-NMR:** δ_{H} (400 MHz, CDCl₃) 9.21 (2H, dd, $J = 2.2$, 0.6 Hz), 9.04 (2H, dd, $J = 5.3$, 0.6 Hz), 8.13 (2H, dd, $J = 5.3$, 2.2 Hz) ppm.

4,4'-dichloro-2,2'-bipyridine: To a suspension of 4,4'-dichloro-2,2'-bipyridyl-N,N'-dioxide (0.9 g, 3.5 mmol) in anhydrous acetonitrile (125 mL), PCl₃ (6 mL, 69 mmol) was added under argon. The mixture was refluxed for 4 h with vigorous stirring. On cooling to room temperature the solution was poured onto ice and basified to pH 10 using 25 % NaOH aqueous solution. This was extracted with CH₃Cl (3 × 250 mL), the organic layers combined, dried over magnesium sulphate and the product isolated on removal of solvents by rotary evaporation.

Yield: Off-white solid, 732 mg (93 %). **¹H-NMR:** δ_{H} (400 MHz, CDCl₃) 8.57 (2H, d, $J = 5.1$ Hz), 8.45 (2H, d, $J = 1.8$ Hz), 7.35 (2H, dd, $J = 5.2$, 2.0 Hz) ppm. **GC-MS (m/z) = 224 [M].**

4,4'-dibromo-2,2'-bipyridine: This was prepared in a similar manner to 4,4'-dichloro-2,2'-bipyridine instead using 4,4'-dibromo-2,2'-bipyridyl-N,N'-dioxide (1.5 g, 4.3 mmol) and PBr₃ (8.0 mL, 86 mmol) in place of 4,4'-dichloro-2,2'-bipyridyl-N,N'-dioxide and PCl₃ respectively.

Yield: Off-white solid, 1.26 mg (94 %). **¹H-NMR:** δ_{H} (400 MHz, CDCl₃) 8.60 (2H, dd, $J = 1.8$, 0.6 Hz), 8.48 (2H, dd, $J = 5.4$, 0.6 Hz), 7.50 (2H, dd, $J = 5.2$, 2.0 Hz)

4,4'-diamino-2,2'-bipyridine^[128]: 4,4'-dinitro-2,2'-bipyridine-N,N'-dioxide (2.0 g, 7.0 mmol) was dissolved in ethanol (45 mL) and 10 % Pd/C (0.35 g) added with stirring. A solution of hydrazine monohydrate (2.0 mL, 40.8 mmol) in ethanol (15 mL) was added dropwise over a period of 1 h and the mixture gradually heated to reflux and the temperature maintained for 8 h. The resultant suspension was then filtered whilst still hot and the filtrand washed with cold diethyl ether. The solvent was removed by rotary evaporation and the residue recrystallised from ethanol.

Yield: Pale tan crystalline solid, 1.19 g (91 %). **¹H-NMR:** δ_{H} (400 MHz, (CD₃)₂SO) 8.02 (2H, d, $J = 5.5$ Hz), 7.53 (2H, d, $J = 2.0$ Hz), 6.44 (2H, dd, $J = 5.5$, 2.4 Hz), 6.03 (4H, s) ppm.

4,4'-diphenyl-2,2'-bipyridine: A solution of 4,4'-dibromo-2,2'-bipyridine (1.2 g, 4.0 mmol) in toluene (60 mL) and an aqueous solution of Na₂CO₃ (2M; 40 mL) were charged to a round-bottomed flask and the mixture purged with argon for 30 mins before addition of Pd(PPh₃)₄ (220 mg, 5 mol%). An ethanolic solution of benzeneboronic acid (1.22 g, 10 mmol; 30 mL) was gradually added via syringe and the mixture heated at reflux with vigorous stirring for 48 h. On cooling to room temperature the ethanol was removed by rotary evaporation and the phases separated. The aqueous phase was extracted with CHCl₃ (3 × 50 mL) and the combined organic phases washed with brine (2 × 50 mL). The latter were dried over magnesium sulphate and solvents removed under vacuum. The product was purified by column chromatography (SiO₂; DCM:MeOH 95:5).

Yield: Pale tan solid, 580 mg (47 %). **¹H-NMR:** δ_H (400 MHz, CDCl₃) 8.76 (2H, dd, *J* = 5.1, 0.8 Hz), 8.74 (2H, dd, *J* = 1.9, 0.8 Hz), 7.81 – 7.78 (4H, m), 7.57 (2H, dd, *J* = 5.1, 1.9 Hz), 7.54 – 7.44 (6H, m) ppm. **GC-MS (*m/z*) = 308 [M].**

4,4'-di(trifluoromethyl)-2,2'-bipyridine: 2-bromo-4-(trifluoromethyl)pyridine (2.25 g, 10.0 mmol), Pd(OAc)₂ (56 mg, 0.25 mmol), K₂CO₃ (1.38 g, 10 mmol) and polyethylene glycol (Mw4000, 10.0 g) were added to a round bottomed flask (100 mL) and the vessel purged with argon. The mixture was gradually heated to 120°C and the temperature maintained for 48 h with stirring. The mixture was cooled to approximately 80°C and deionized water (30 mL) added. On further cooling to room temperature the solution was diluted with deionized water (100 mL) and exhaustively extracted with ethyl acetate. The combined organic layers were washed with a saturated sodium thiosulphate solution and thrice with brine. The organic layer was dried over magnesium sulphate and solvents removed under reduced pressure. The residue was purified by column chromatography (SiO₂, DCM).

Yield: White crystalline solid, 811 mg (56 %). **¹H-NMR:** δ_H (400 MHz, CDCl₃) 8.89 (2H, dt, *J* = 5.0, 0.7 Hz), 8.73 (2H, dt, *J* = 1.6, 0.8 Hz), 7.59 (2H, ddd, *J* = 5.0, 1.7, 0.7 Hz) ppm. **GC-MS (*m/z*) = 291.9 [M]. Anal. Calcd (%) for C₁₂H₁₀F₆N₂: C, 49.33; H, 2.07; N, 9.59. Found C, 49.26; H, 2.08; N, 9.82.**

4,4'-bis(*N,N'*-dimethylaminovinyl)-2,2'-bipyridine: *tert*-Butoxy-bis(dimethylamino)methane was added to a solution of 4,4'-dimethyl-2,2'-bipyridine in DMF and mixture heated at 140°C for 20 h under argon. The resultant dark orange solution was cooled to room temperature and deionised water added to yield a yellow-orange suspension. The mixture was extracted DCM (4 × 50 mL) and the combined organic layers dried over magnesium sulphate and solvents removed *in vacuo*.

Yield: Orange-yellow solid, 2.45 g (91.1 %). **¹H-NMR:** δ_H (400 MHz, CDCl₃) 8.34 (2H, d, *J* = 5.3 Hz), 8.11 (2H, d, *J* = 1.8 Hz), 7.20 (2H, d, *J* = 13.6 Hz), 6.95 (2H, dd, *J* = 5.3, 1.9 Hz), 5.08 (2H, d, *J* = 13.6 Hz), 2.87 (6H, s) ppm.

4,4'-diformyl-2,2'-bipyridine: A solution of NaIO_4 (13 g, 60 mmol) in deionised water (100 mL) was added to a 500 mL round bottomed flask containing 4,4'-bis(*N,N'*-dimethylaminovinyl)-2,2'-bipyridine (2.11 g, 9.72 mmol) and THF (150 mL). The mixture was heated to 40°C and stirred for 18 h, over which time the solution became paler in colour. On cooling to room temperature the mixture was filtered to remove a white precipitate, NaIO_3 , and extracted with DCM (4 × 60 mL). The combined organic layers were washed with brine (2 × 50 mL) and dried over magnesium sulphate. Solvents were removed under vacuum and the residue redissolved in CHCl_3 (250 mL) before filtration and removal of solvents.

Yield: Pale orange solid, 1.61g (78 %). **¹H-NMR:** δ_{H} (400 MHz, CDCl_3) 10.22 (2H,s), 8.96 (2H, d, $J = 5.1$ Hz), 8.89 (2H, d, $J = 1.5$ Hz), 7.78 (2H, dd, $J = 5.0, 1.5$ Hz) ppm.

4,4'-dicyano-2,2'-bipyridine: A solution of hydroxylamine hydrochloride (1.69 g, 24.3 mmol) in pyridine (20 mL) was added drop-wise to a pre-cooled (5°C) suspension of 4,4'-diformyl-2,2'-bipyridine (1.29 g, 6.1 mmol) in pyridine (30 mL). After 5 mins with vigorous stirring, acetic anhydride (50 mL) was added to yield a yellow solution. The temperature was gradually increased to reflux and maintained for 1 h. The resultant mixture was cooled to room temperature and poured into water (500 mL) to yield a cream coloured precipitate. The solid was collected by vacuum filtration, washed with water and dried *in vacuo*.

Yield: Beige solid, 865 mg (69 %). **¹H-NMR:** δ_{H} (400 MHz, CDCl_3) 8.87 (2H, dd, $J = 4.9, 0.9$ Hz), 8.71 (2H, dd, $J = 1.5, 0.9$ Hz), 7.60 (2H, dd, $J = 4.9, 1.5$ Hz) ppm.

4-hydroxymethyl-4'-methyl-2,2'-bipyridine: Selenium dioxide (2.0 g, 18 mmol) was added to a stirred suspension of 4,4'-dimethyl-2,2'-bipyridine (2.0 g, 11 mmol) in dioxane (100 mL), the mixture then refluxed for 24 h. The resultant green suspension was cooled to room temperature and filtered removal of solvents under reduced pressure. The pale pink solid was redissolved in ethyl acetate (600 mL) and treated with aqueous 0.1M Na_2CO_3 (20 mL), before being dried over magnesium sulphate and removal of solvents. The residue was then suspended in methanol (15 mL) and sodium borohydride (0.3 g) in NaOH (0.2 M, 2.5 mL) added drop-wise whilst cooled on ice. On completion the mixture was stirred at room temperature for 1h before the methanol was removed under reduced pressure. The resultant suspension was diluted with saturated Na_2CO_3 aqueous solution (6 mL) and extracted with chloroform (4 × 25 mL), the organic phase collected, dried and evaporated to afford an off-white solid.

Yield: Off white solid, 1.2 g (55 %). **¹H-NMR:** δ_{H} (400 MHz, CDCl_3) 8.64 (1H, dd, $J = 5.0, 0.8$ Hz), 8.53 (1H, dd, $J = 5.0, 0.5$ Hz), 8.34 (1H, dd, $J = 1.7, 0.8$ Hz), 8.22 (1H, dt, $J = 1.6, 0.8$ Hz), 7.33 (1H, ddt, $J = 5.0, 1.7, 0.8$ Hz), 7.15 (1H, ddd, $J = 5.0, 1.7, 0.7$ Hz), 4.82 (2H, d, $J = 4.0$ Hz), 2.44 (3H, s) ppm.

4,4'-dicarboxy-2,2'-bipyridine: Potassium dichromate (20 g, 68.0 mmol) was gradually added to solution of 4,4'-dimethyl-2,2'-bipyridine (5.0, 27.2 mmol) in 98% H₂SO₄ (100 mL). The mixture was heated at 70°C for 45 min and cooled to room temperature. The resulting mixture was carefully added to ice-cold water (750 mL) to form a yellow-green suspension. The solid was collected on filtration, washed extensively with deionised water and was redissolved in aqueous KOH (50 mL, 10 % w/w). The solution was acidified to pH 2 using HCl (10 %) to yield a white precipitate which was filtered, washed with water, methanol and diethyl ether before being dried *in vacuo*.

Yield: White Powder, 5.9 g (89 %). **¹H-NMR:** δ_H (400 MHz, (CD₃)₂SO): 8.91 (2H, d, *J* = 4.8 Hz), 8.84 (2H, s), 7.91 (2H, dd, *J* = 4.8, 1.3 Hz) ppm.

4,4'-dimethoxycarbonyl-2,2'-bipyridine: A suspension of 4,4'-dicarboxy-2,2'-bipyridine (5.0 g, 20.5 mmol) in methanol (100 mL) and 98 % H₂SO₄ (10 mL) was heated at reflux for 48 h. On cooling to room temperature the resultant deep pink solution was poured into deionised water (300 mL) and basified to pH 8 using 1M NaOH. The mixture was extracted with CHCl₃ (3 × 150 mL) and the combined organic layers dried over magnesium sulphate prior to the removal of solvents by rotary evaporation.

Yield: White crystalline solid, 4.64 g (82 %). **¹H-NMR:** δ_H (400 MHz, CDCl₃): 8.95 (2H, s), 8.85 (2H, d, *J* = 5.0 Hz), 7.89 (2H, dd, *J* = 4.9, 1.5 Hz) ppm.

2.3.1.3. Synthesis of Bridging Ligands

2.3.1.3.1. Towards 2,2'-bipyrimidine

2-iodopyrimidine: 2-chloropyrimidine (5.0 g, 43.9 mmol) was added in small portions to a stirred solution of hydriodic acid (20 mL, 57 % w/w) precooled to 0°C. After completion of addition the reaction mixture was left to stir vigorously for 1 h at 0°C before being neutralised with a saturated solution of K₂CO₃ with cooling. The resultant solution was then decolourised using potassium disulfite. The aqueous solution was then extracted using diethyl ether (5 × 100 mL), dried over MgSO₄, filtered and evaporated before recrystallisation from boiling petroleum ether (bp 40-60°C).

Yield: White crystalline solid, 6.98 g, (77.3 %). **¹H-NMR:** δ_H (400 MHz, CDCl₃) 8.45 (2H, d, *J* = 4.8 Hz), 7.32 (1H, t, *J* = 4.8 Hz) ppm.

2,2'-bipyrimidine: This compound was prepared in a manner similar to 2,2'-bipyrazine (method D), instead using 2-iodopyrimidine (5.0 g, 24.3 mmol) in place of 2-iodopyrazine.

Yield: Pale tan solid, 0.44 g, (23.1 %). **¹H-NMR:** δ_H (400 MHz, CDCl₃) 9.03 (4H, d, *J* = 4.8 Hz), 7.49 (1H, t, *J* = 4.9 Hz) ppm.

2.3.3.2. Towards Tetra[3,2-a:2',3'-c:3'',2''-h:2''',3'''-j]phenazine (tpphz)

1,10-phenanthroline-5,6-dione:^[129] 1,10-phenanthroline (2.0 g, 11 mmol) and potassium bromide (2.0 g, 16.8 mmol) were charged to a round-bottomed flask cooled in an actone-ice bath. An ice-cold solution of H₂SO₄ (20 mL) and HNO₃ (10 mL) was added drop-wise and the mixture gradually heated to reflux where the temperature for 3 h. This was cooled to *ca.* 60°C and poured over ice (500 g) and neutralised using 8M NaOH. The suspension was extracted with chloroform (3 × 100 mL) and the combined organic phases dried over magnesium sulphate before evaporation of solvents *in vacuo*. The product was purified by recrystallisation from ethanol.

Yield: Canary yellow solid, 1.89 g, (81 %). **¹H-NMR** δ_H (400 MHz, CDCl₃) 9.08 (2H, dd, *J* = 4.7, 1.8 Hz), 8.47 (2H, dd, *J* = 7.9, 1.8 Hz), 7.57 (2H, dd, *J* = 7.9, 4.7 Hz) ppm.

Tetra[3,2-a:2',3'-c:3'',2''-h:2''',3'''-j]phenazine (tpphz):^[123] 1,10-phenanthroline-5,6-dione (2.0 g, 9.6 mmol), ammonium acetate (10.2 g) and sodium hydrosulfite (0.235 g, 1.4 mmol) was gradually heated under argon to 180 °C and the temperature maintained for 2h. On cooling to room temperature, deionized water (30 mL) was added and the resultant suspension filtered. The filtrand was extensively washed with water, methanol and acetone before the solid was triturated in boiling ethanol and hot filtered. The solid was further washed with a further volume of ethanol, then diethyl ether and dried *in vacuo*.

Yield: Golden tan solid, 808 mg, (44 %). **¹H-NMR:** δ_H (400 MHz, CDCl₃) 9.60 (2H, dd, *J* = 8.1, 1.8 Hz), 9.33 (2H, dd, *J* = 4.4, 1.8 Hz), 7.83 (2H, dd, *J* = 8.1, 4.4 Hz) ppm.

2.3.1.3.3. Towards the Synthesis of 2,2':4',4'':2'',2'''-quaterpyridine

2,2'-bipyridyl-N-oxide: 2,2'-bipyridine (10.0 g, 64.1 mmol) was dissolved in glacial acetic acid (125 mL) and the solution heated to 70°C prior to the gradual addition of magnesium bis-monoperoxyphalate (20.0 g, 40.4 mmol). On completion the temperature was increased to 90°C and maintained for 18 h. The solution was cooled to room temperature and evaporated to near-dryness. The resultant residue was dissolved in chloroform (150 mL) and washed with a 0.1 M Na₂CO₃ (2 × 50 mL) aqueous solution. The organic layer was separated and the combined aqueous layers extracted with chloroform (3 × 100 mL). The combined organic layers were dried over anhydrous magnesium sulphate and solvents evaporated. The resultant residue was then purified by column chromatography with silica eluting with acetone: triethylamine (97:3).

Yield: Cream solid, 5.63 g, (51.1 %). **¹H-NMR:** δ_H (400 MHz, CDCl₃) 8.88 (1H, dt, *J* = 8.1, 1.1 Hz), 8.72 (1H, ddd, *J* = 4.8, 1.8, 1.0 Hz), 8.31 (1H, ddd, *J* = 6.5, 1.3, 0.6, Hz), 8.17 (1H, ddd, *J* = 8.0, 2.2, 0.5 Hz), 7.83 (1H, ddd, *J* = 8.1, 7.6, 1.9 Hz), 7.39-7.33 (2H, m), 7.27 (1H, ddd, *J* = 7.5, 6.5, 2.2 Hz) ppm.

4-nitro-2,2'-bipyridyl-1-oxide: 2,2'-bipyridyl-*N*-oxide (5.0 g, 29.1 mmol) was dissolved in concentrated sulfuric acid (30 mL) and cooled to -10°C using an acetone/ice bath. To the stirred solution, fuming nitric acid (18 mL) was added drop-wise. The mixture was then gradually heated to 110°C and the temperature maintained for 4.5 h. The resultant solution was cooled to room temperature before being poured over ice and neutralized with a concentrate aqueous solution of sodium hydroxide under cooling. A large quantity of solid was collected by vacuum filtration and air-dried before being exhaustively extracted with chloroform. The organic solvents were collected, dried over magnesium sulphate and removed under reduced pressure.

Yield: Pale yellow solid, 3.14g, (49.8 %). **¹H-NMR:** δ_{H} (400 MHz, CDCl₃) 9.16 (1H, d, $J = 3.3$ Hz), 8.88 (1H, dt, $J = 8.1, 1.0$ Hz), 8.79 (1H, ddd, $J = 4.7, 1.8, 1.0$ Hz), 8.36 (1H, dd, $J = 7.2, 0.4$ Hz), 8.07 (1H, dd, $J = 7.2, 3.3$ Hz), 7.88 (1H, td, $J = 7.9, 1.8$ Hz), 7.44 (1H, ddd, 7.6, 4.8, 1.1 Hz) ppm.

4-Bromo-2,2'-bipyridyl-1-oxide: Acetyl bromide (7 mL) was added dropwise to a stirred solution of 4-nitro-2,2'-bipyridyl-*N*-oxide (1.5 g, 5.1 mmol) in glacial acetic acid (20 mL) and the mixture heated at 100°C for 4 h. Upon cooling to room temperature the solution was cautiously poured over ice prior to basification to pH 9 using 8.3 M NaOH_(aq). The resultant suspension was extracted with chloroform (3 × 100 mL) and the combined organic phases washed with brine and dried over magnesium sulphate. Solvents were removed by rotary evaporation and the solid dried *in vacuo*.

Yield: Off-white solid, 1.43 g, (83 %). **¹H-NMR:** δ_{H} (400 MHz, CDCl₃) 8.89 (1H, dt, $J = 8.1, 1.0$ Hz), 8.73 (1H, ddd, $J = 4.8, 1.8, 0.9$ Hz), 8.39 (1H, d, $J = 2.9$ Hz), 8.23 (1H, dd, $J = 6.9, 0.3$ Hz), 7.84 (1H, ddd, $J = 8.1, 7.6, 1.8$ Hz), 7.41–7.36 (2H, m) ppm.

4-Bromo-2,2'-bipyridine: This was prepared in a similar manner to 4,4'-dichloro-2,2'-bipyridine instead using 4-bromo-2,2'-bipyridyl-*N*-oxide (1.0 g, 4.6 mmol) and PBr₃ (5.0 mL, 43 mmol) in place of 4,4'-dichloro-2,2'-bipyridyl-*N,N'*-dioxide and PCl₃ respectively.

Yield: White solid, 830 mg (77 %). **¹H-NMR:** δ_{H} (400 MHz, CDCl₃) 8.65 (1H, ddd, $J = 4.8, 1.8, 0.9$ Hz), 8.59 (1H, dd, $J = 1.9, 0.4$ Hz), 8.45 (1H, d, $J = 5.2$ Hz), 8.35 (1H, dt, $J = 8.0, 1.0$ Hz), 7.79 (1H, td, $J = 7.8, 1.8$ Hz), 7.30 (1H, ddd, $J = 7.5, 4.8, 1.2$ Hz) ppm. **GC-MS (m/z) = 235.9 [M+H]⁺**

4-amino-2,2'-bipyridine:^[130] A mixture of 4-nitro-2,2'-bipyridine-*N*-oxide (1.1 g, 5.1 mmol) and 10 % Pd/C (0.23 g) were suspended in methanol (40 mL) and cooled in an ice bath under inert atmosphere. Sodium borohydride (2.5 g) was added in small portions with vigorous stirring. Once gas evolution had ceased the catalyst was removed by filtration and the methanol removed under reduced pressure. The residue was re-dissolved in deionized water (60 mL) and extracted with diethyl ether (5 × 50 mL). The organic extracts were combined, dried over magnesium sulphate and evaporated to dryness.

Yield: Off-white solid, 795 mg (91 %) **¹H-NMR:** δ_{H} (400 MHz, CDCl_3) 8.64 (1H, ddd, $J = 4.9, 1.6, 0.8$ Hz), 8.35 (1H, d, $J = 8.0$ Hz), 8.31 (1H, d, $J = 5.6$ Hz), 7.79 (1H, td, $J = 7.8, 1.8$ Hz), 7.67 (1H, d, $J = 2.3$ Hz), 7.28 (1H, ddd, $J = 7.6, 4.9, 1.2$ Hz), 6.55 (1H, dd, $J = 5.5, 2.4$ Hz), 4.25 (2H, s) ppm.

4-iodo-2,2'-bipyridine:^[131] A solution of 4-amino-2,2'-bipyridine (1.0 g, 5.8 mmol) in H_2SO_4 (7 M, 15 mL) was cooled in an acetone:ice bath to which an ice cold solution of NaNO_2 (1.6 g, 23.2 mmol) in deionized water (4 mL) was added dropwise. The mixture was stirred for a further 2 minutes before addition of a cold saturated aqueous KI solution (12 g, *ca.* 10 mL). The mixture was gradually warmed to room temperature and the reaction quenched on neutralization with NaOH. The mixture was exhaustively extracted with CHCl_3 and the combined organic layers washed with a saturated aqueous solution of $\text{Na}_2\text{S}_2\text{O}_3$ and Brine. The organic phase was dried over magnesium sulphate and solvents removed by rotary evaporation. The residue was purified on recrystallized from methanol.

Yield: Cream coloured solid, 795 mg (91 %) **¹H-NMR:** δ_{H} (400 MHz, CDCl_3) 8.82 (1H, d, $J = 1.7$ Hz), 8.67 (1H, dt, $J = 4.8, 0.9$ Hz), 8.37 (1H, dd, $J = 8.0, 0.6$ Hz), 8.31 (1H, d, $J = 5.1$ Hz), 7.82 (1H, td, $J = 7.7, 1.8$ Hz), 7.68 (1H, ddd, $J = 5.1, 1.7, 0.6$), 7.33 (1H, dd, $J = 7.5, 4.7$ Hz) ppm. **GC-MS** (m/z) = 281.9 [M].

2.3.1.4. Synthesis of 2,2':4,4'':4',4'''-Quaterpyridyl and quaterpyridinium ligands

2,2':4,4'':4',4'''-Quaterpyridyl, (Qpy): A mixture of 4,4'-bipyridine (10.0 g, 64.0 mmol) and 10% Pd on charcoal (2.00 g) was heated at $\sim 250^\circ\text{C}$ for 48 h and then cooled to room temperature. The resultant black solid was exhaustively extracted with hot ethanol and collected alcoholic solution evaporated to dryness. The crude product was purified by column chromatography using silica gel and eluting with 95:5 CH_2Cl_2 : MeOH. Solvents were removed by rotary evaporation and the resulting solid triturated with a minimum amount of boiling acetone. The final solid was collected by filtration and dried under vacuum.

Yield: Off-white solid, 2.11 g (21.2 %). **¹H-NMR:** δ_{H} (400 MHz, CDCl_3) 8.83 (2 H, dd, $J = 5.1, 0.8$ Hz), 8.79 - 8.77 (6 H, m), 7.69 (4 H, dd, $J = 4.4, 1.6$ Hz), 7.61 (2 H, dd, $J = 5.1, 1.9$ Hz) ppm.

N'',N'''-Di(2-pyrimidyl)-2,2':4,4'':4',4'''-quaterpyridinium dihexafluorophosphate, [(2-Pym)₂qpy](PF₆)₂: A mixture of Qpy (0.400 g, 1.29 mmol) and 2-chloropyrimidine (1.43 g, 12.54 mmol) was heated at 120°C for *ca.* 1 h to yield a green/brown slurry. Ethanol (12 mL) was then gradually added and the mixture was heated at reflux for 4 h. The solution was allowed to cool before water (50 mL) was added and the mixture extracted with chloroform (3 \times 50 mL). The aqueous layer was collected and concentrated by rotary evaporation before addition of solid NH_4PF_6 to yield a pale brown precipitate. The solid was dissolved in acetone (50 mL) filtered and reprecipitated on addition on diethyl ether to yield the pure product.

Yield: Pale brown powder, 454 mg (69 %). **¹H-NMR:** δ_{H} (400 MHz, CD₃CN) 10.07 (4 H, d, $J = 7.3$ Hz), 9.13 (4 H, d, $J = 4.8$ Hz), 9.07-9.05 (4 H, m), 8.66 (4 H, d, $J = 7.4$ Hz), 8.04 (2 H, dd, $J = 5.0, 2.1$ Hz), 7.88 (2 H, t, $J = 4.9$ Hz) ppm.

***N,N'*,*N,N''*-Dimethyl-2,2':4,4'':4',4'''-quaterpyridinium dihexafluorophosphate,**

[Me₂qpy](PF₆)₂: Methyl iodide (2 mL) was added to a stirred suspension of 2,2':4,4'':4',4'''-quaterpyridine (500 mg, 1.57 mmol) in acetone (50 mL) and then heated to reflux. After 4 h the mixture was cooled and the precipitate collected by filtration. The solid was washed with acetone (50 mL), chloroform (50 mL) and then triturated with boiling ethanol (250 mL) to yield a bright yellow solid. This was dissolved in water (200 mL) and solid NH₄PF₆ added to yield an off white precipitate which was collected by filtration, washed with water and dried *in vacuo*.

Yield: Off-white solid, 555 mg (88 %). **¹H-NMR:** δ_{H} (400 MHz, CD₃CN) 8.98 (2H, dd, $J = 5.1, 0.7$ Hz), (2H, dd, $J = 1.8, 0.6$ Hz), 8.75 (4H, d, $J = 6.7$ Hz), 8.40 (4H, d, $J = 6.9$ Hz), 7.90 (2H, dd, $J = 5.1, 1.9$ Hz), 4.36 (6H, s) ppm.

***N,N'*,*N,N''*-Di(2,4-dinitrophenyl)-2,2':4,4'':4',4'''-quaterpyridinium dichloride, [(2,4-**

DNPh)₂qpy]Cl₂: A mixture of 2,2':4,4'':4',4'''-quaterpyridine (0.400 g, 1.29 mmol) and 2,4-dinitrochlorobenzene (2.54 g, 12.56 mmol) in ethanol (25 mL) was heated at reflux for 72 h. On cooling to room temperature dichloromethane (20 mL) was added and the resulting precipitate collected by vacuum filtration. The solid was washed with diethyl ether and dried *in vacuo*.

Yield: Cream solid, 842 mg (91 %). **¹H-NMR:** δ_{H} (400 MHz, CD₃OD) 9.48 (4H, d, $J = 7.1$ Hz), 9.33 (2H, d, $J = 2.5$ Hz), 9.22 (2H, dd, $J = 1.9, 0.8$ Hz), 9.11 (2H, dd, $J = 5.1, 0.8$ Hz), 8.99-8.94 (6H, m), 8.39 (2H, d, $J = 8.7$ Hz), 8.23 (2H, dd, $J = 5.1, 1.9$ Hz) ppm.

***N,N'*,*N,N''*-Di(4-hydroxymethylphenyl)-2,2':4,4'':4',4'''-quaterpyridinium**

dihexafluorophosphate, [(4-HOCH₂Ph)₂qpy](PF₆)₂: A mixture of [(2,4-DNPh)₂Qpy]Cl₂ (400 mg, 0.55 mmol) and 4-aminobenzyl alcohol (677 mg, 5.50 mmol) in ethanol (25 mL) was heated at reflux for 48 h. On cooling to room temperature the mixture was reduced in volume and added to acetone (100 mL) and the precipitate collected by filtration. The solid was suspended in water (200 mL), filtered and extracted with chloroform until no further colour change of the organic layer was observed. To the aqueous layer solid NH₄PF₆ was added and the resultant precipitate collected by filtration.

Yield: Yellow brown solid, 340 mg (76 %). **¹H-NMR:** δ_{H} (400 MHz, CD₃CN) 9.07 (4H, d, $J = 7.1$ Hz), 9.03 (2H, dd, $J = 5.1, 0.8$ Hz), 9.01 (2H, dd, $J = 1.9, 0.8$ Hz), 8.59 (4H, d, $J = 7.1$ Hz), 7.99 (2H, dd, $J = 5.1, 1.9$ Hz), 7.73 (8H, d, $J = 2.1$ Hz), 4.77 (4H, d, $J = 5.8$ Hz), 3.55 (2H, t, $J = 5.8$) ppm.

***N''',N'''*-Di(4-hydroxymethylphenyl)-2,2':4,4'':4',4'''-quaterpyridinium dichloride, [(4-HOCH₂Ph)₂Qpy]₂Cl₂:** [(4-HOCH₂Ph)₂Qpy](PF₆)₂ was dissolved in a minimum of acetone and an excess of solid tetra-*n*-butyl ammonium chloride was added. The precipitate was collected by vacuum filtration and the filtrand washed with acetone and diethyl ether then dried *in vacuo* to afford the chloride salt in near quantitative yields.

¹H-NMR: δ_H (400 MHz, CD₃OD) 9.41 (4H, d, *J* = 6.9 Hz), 9.16 (2H, d, *J* = 1.0 Hz), 9.08 (2H, dd, *J* = 5.1, 0.5 Hz), 8.80 (4H, d, *J* = 7.1 Hz), 8.17 (2H, dd, *J* = 5.1, 1.8 Hz), 7.89 (4H, d, *J* = 8.6 Hz), 7.78 (4H, d, *J* = 8.63 Hz), 4.81 (4H, s) ppm.

2.3.1.5. Synthesis of cyclometallating ligands

2-phenylpyridine: 2-bromopyridine (1.58 g, 10 mmol), benzene boronic acid (1.83 g, 15 mmol) and K₃PO₄·7H₂O (4.2 g, 12.5 mmol) were suspended in an aqueous ^tPrOH solution (50%; 40 mL). Pd(OAc)₂ (34 mg, 0.15 mmol) was added and the mixture heated at 80°C for 12 hours. On cooling to room temperature the mixture was extracted with ethyl acetate and the combined organic layers washed with brine then dried over magnesium sulphate in the presence of activated charcoal. The mixture was filtered and solvents removed by rotary evaporation. The product was purified by column chromatography (SiO₂; CHCl₃:Ethyl Acetate, 3:1).

Yield: Pale yellow oil, 1.05 g (68 %). **¹H-NMR:** δ_H (400 MHz, CDCl₃) 8.62 (1H, d, *J* = 4.8 Hz), 7.92 – 7.90 (2H, m), 7.67 – 7.63 (2H, m), 7.42 – 7.38 (2H, m), 7.36 – 7.31 (1H, m), 7.18 – 7.13 (1H, m) ppm.

2,3'-bipyridine: A three-necked round-bottomed flask (250 mL) equipped with a condenser, thermometer and septum was back-filled with argon and charged with isopropylmagnesium chloride (2.0 M in THF, 11 mL, 22 mmol) via syringe. 2-bromopyridine (1.9 mL, 20 mmol) was then added at a rate to maintain the temperature below 30°C. After 4 h, zinc chloride (0.5 M in THF, 48 mL, 24 mmol) was added drop-wise and the resultant mixture stirred at room temperature for 1.5 h. A solution of 3-bromopyridine (1.45 mL, 15 mmol) in TBME (7 mL) was added followed by triphenylphosphine (393 mg, 1.5 mmol) and palladium(II) acetate (75 mg, 0.33 mmol); the mixture was then heated at 50°C for 18 h. On cooling to room temperature ammonium hydroxide (25 mL) was gradually added and the mixture left to stir for 20 mins. The organic layer was separated and the aqueous phase exhaustively extracted with ethyl acetate. The combined organic layers were washed with brine, dried over magnesium sulphate and solvents removed by rotary evaporation. The crude material was purified by column chromatography (SiO₂; Hexane:Ethyl Acetate (70:30)).

Yield: Pale yellow oil, 1.71 g (73 %). **¹H-NMR:** δ_H (400 MHz, CD₃CN) 9.22 (1H, dd, *J* = 2.3, 0.8 Hz), 8.69 (1H, ddd, *J* = 4.8, 1.6, 1.2 Hz), 8.62 (1H, dd, *J* = 4.8, 1.6 Hz), 8.37 (1H, ddd, *J* = 8.0, 2.3, 1.7 Hz), 7.91-7.85 (2H, m), 7.45 (1H, ddd, *J* = 8.0, 4.8, 0.9), 7.36 (1H, ddd, *J* = 6.8, 4.9, 1.8 Hz) ppm. **ES-MS (*m/z*):** 157 [M+H]⁺

2,4'-bipyridine: This compound was prepared as above by using 4-bromopyridine in place of 3-bromopyridine. This was prepared on neutralization of 4-bromopyridine hydrochloride (2.92 g, 15 mmol) partitioned between TBME and water using Na₂CO₃. The aqueous layer was extracted with a further volume of TBME and the combined organic layers dried over magnesium sulphate. The volume of solution was concentrated by rotary evaporation before addition to the reaction mixture.

Yield: Off-white powder, 1.88 g (80.3 %). **¹H-NMR:** δ_H (400 MHz, CD₃CN) 8.72 (1H, ddd, *J* = 4.8, 1.8, 1.0 Hz), 8.68 (2H, dd, *J* = 4.5, 1.7 Hz), 7.96 (2H, dd, *J* = 4.5, 1.7 Hz), 7.96 (1H, dt, *J* = 7.9, 1.1 Hz), 7.89 (1H, ddd, *J* = 8.0, 7.4, 1.8 Hz), 7.41 (1H, ddd, *J* = 7.4, 4.9, 1.2 Hz) ppm. **ES-MS (*m/z*):** 157 [M+H]⁺

1-methyl-2-(2'-pyridyl)pyridinium iodide: Methyl iodide (2.4 mL, 38.4 mmol) was added to a solution of 2,2'-bipyridine (2.0 g, 12.8 mmol) in acetonitrile (25 mL) and heated at 45°C for 48 h under inert atmosphere. On cooling to room temperature the mixture was filtered to remove a yellow precipitate of *N,N'*-dimethyl-2,2'-bipyridinium iodide. The filtrate was poured into diethyl ether (200 mL) and allowed to stand for five minutes where upon the product precipitated solution. The solid was collect by filtration and washed with diethyl ether then dried *in vacuo*.

Yield: Off-white powder, 1.81 g (71 %). **¹H-NMR:** δ_H (400 MHz, CD₃OD) 9.10 (1H, d, *J* = 6.1 Hz), 8.86 (1H, d, *J* = 4.7 Hz), 8.71 (1H, t, *J* = 7.6 Hz), 8.25 (1H, d, *J* = 8.0 Hz), 8.19-8.14 (2H, m), 7.95 (1H, d, *J* = 7.9 Hz), 7.70 (1H, ddd, *J* = 7.7, 4.8, 0.8 Hz), 4.37 (3H, s) ppm. **ES-MS (*m/z*):** 171 [M-I]⁺

1-methyl-3-(2'-pyridyl)pyridinium iodide: Methyl iodide (2 mL, 32.1 mmol) was added to a solution of 2,3'-bipyridine (500 mg, 3.2 mmol) in *tert*-butyl methyl ether (20 mL) and heated at reflux for 36 hours. On cooling to room temperature the solid was collected by filtration, washed with *tert*-butyl methyl ether and *n*-pentane before being dried under vacuum.

Yield: Off-white powder, 798 mg (83 %). **¹H-NMR:** δ_H (400 MHz, CD₃OD) 9.66 (1H, s), 9.21 (1H, d, *J* = 8.2 Hz), 8.96 (1H, d, *J* = 6.1 Hz), 8.80 (1H, dd, *J* = 4.7, 0.6 Hz), 8.22 – 8.19 (2H, m), 8.05 (1H, td, *J* = 7.81, 1.7 Hz), 7.56 (1H, ddd, *J* = 7.6, 4.8, 0.7 Hz), 4.54 (3H, s) ppm. **ES-MS (*m/z*):** 171 [M-I]⁺.

1-methyl-4-(2'-pyridyl)pyridinium iodide: This compound was prepared in a manner identical to 1-methyl-3-(2'-pyridyl)pyridinium iodide instead using 2,4'-bipyridine (500 mg, 3.2 mmol) in place of 2,3'-bipyridine.

Yield: Off-white powder, 915 mg (95.5 %). **¹H-NMR:** δ_H (400 MHz, CD₃OD) 8.98 (2H, d, *J* = 6.8 Hz), 8.86 (1H, ddd, *J* = 4.8, 1.8, 0.9 Hz), 8.77 (2H, d, *J* = 6.9 Hz), 8.34 (1H, dt, *J* = 8.0, 1.0 Hz), 8.08 (1H, td, *J* = 7.8, 1.8 Hz), 7.63 (1H, ddd, *J* = 7.65, 4.76, 1.0 Hz), 4.45 (3H, s) ppm. **ES-MS (*m/z*):** 171 [M-I]⁺.

1-methyl-2-(2'-pyridyl)pyridinium hexafluorophosphate: 1-methyl-2-(2'-pyridyl)pyridinium iodide was dissolved in a minimum of deionised water and filtered to give a pale yellow solution to which solid NH_4PF_6 was added. The precipitate was collected by filtration and washed extensively with cold water to afford the product as the hexafluorophosphate salt in near quantitative yields.

$^1\text{H-NMR}$: δ_{H} (400 MHz, CD_3CN) 8.82 (1H, d, $J = 4.2$ Hz), 8.73 (1H, d, $J = 6.3$ Hz), 8.58 (1H, t, $J = 7.9$ Hz), 8.11-8.04 (3H, m), 7.77 (1H, d, $J = 7.9$ Hz), 7.65 (1H, ddd, $J = 7.8, 4.8, 1.1$ Hz), 4.23 (3H, s) ppm. **ES-MS (m/z):** 171 $[\text{M-PF}_6]^+$. **Anal. Calcd (%)** for formula $\text{C}_{11}\text{H}_{11}\text{F}_6\text{N}_2\text{P}$; C, 41.79; H, 3.51; N, 8.86; Found C, 42.02; H, 3.06; N 8.79.

1-methyl-3-(2'-pyridyl)pyridinium hexafluorophosphate: This compound was prepared in a manner identical to 1-methyl-2-(2-pyridyl)pyridinium hexafluorophosphate instead using 1-methyl-3-(2-pyridyl)pyridinium iodide.

$^1\text{H-NMR}$: δ_{H} (400 MHz, CD_3CN) 9.33 (1H, s), 9.04 (1H, dt, $J = 8.3, 1.2$ Hz), 8.78 (1H, dt, $J = 5.0, 1.4$ Hz), 8.63 (1H, d, $J = 6.0$ Hz), 8.09 (1H, t, $J = 7.1$ Hz), 8.04-7.99 (2H, m), 7.54 (1H, ddd, $J = 6.4, 4.9, 2.3$ Hz), 4.39 (3H, s) ppm. **ES-MS (m/z):** 171 $[\text{M-PF}_6]^+$. **Anal. Calcd (%)** for formula $\text{C}_{11}\text{H}_{11}\text{F}_6\text{N}_2\text{P}$; C, 41.79; H, 3.50; N, 8.86; Found C, 42.03; H, 3.00; N 8.87.

1-methyl-4-(2-pyridyl)pyridinium hexafluorophosphate: This compound was prepared in a manner identical to 1-methyl-2-(2-pyridyl)pyridinium hexafluorophosphate instead using 1-methyl-4-(2-pyridyl)pyridinium iodide.

$^1\text{H-NMR}$: δ_{H} (400 MHz, CD_3CN) 8.83 (1H, d, $J = 4.7$ Hz), 8.67 (2H, d, $J = 6.8$ Hz), 8.62 (2H, d, $J = 6.7$ Hz), 8.19 (1H, d, $J = 8.0$ Hz), 8.04 (1H, td, $J = 7.8, 1.7$ Hz), 7.60 (1H, ddd, $J = 7.6, 4.7, 0.9$ Hz), 4.31 (3H, s) ppm. **ES-MS (m/z):** 171 $[\text{M-PF}_6]^+$. **Anal. Calcd (%)** for formula $\text{C}_{11}\text{H}_{11}\text{F}_6\text{N}_2\text{P}$; C, 41.79; H, 3.51; N, 8.86; Found C, 41.99; H, 3.19; N 8.89.

1-(2,4-dinitrophenyl)-3-(2'-pyridyl)pyridinium hexafluorophosphate: 1-chloro-2,4-dinitrobenzene (5.2 g, 27.2 mmol) was added to a solution of 2,3'-bipyridine (500 mg, 3.2 mmol) in *tert*-butyl methyl ether (20 mL) and heated at reflux for 48 hours. On cooling to room temperature the precipitate was collected by filtration and washed with *tert*-butyl methyl ether. This was then dissolved in cold deionised water and filtered to remove unreacted starting material. Excess solid NH_4PF_6 was added and the product collected via filtration prior to being washed extensively with cold deionised water and dried *in vacuo*.

Yield: Cream coloured powder, 996 mg (66 %). **$^1\text{H-NMR}$:** δ_{H} (400 MHz, CD_3CN) 9.59 (1 H, s), 9.40 (1H, ddd, $J = 8.4, 1.9, 1.2$ Hz), 9.19 (1H, d, $J = 2.5$), 8.90 (1H, dt, $J = 6.1, 1.4$ Hz), 8.84 (1H, dd, $J = 8.7, 2.5$ Hz), 8.78 (1H, ddd, $J = 4.8, 1.7, 1.0$ Hz), 8.38 (1H, ddd, $J = 8.3, 6.1, 0.6$ Hz), 8.17 (1H, d, $J = 8.7$ Hz), 8.10-8.01 (2H, m), 7.57 (1H, ddd, $J = 7.5, 4.8, 1.3$ Hz) ppm. **ES-MS (m/z):** 323 $[\text{M-PF}_6]^+$. **Anal. Calcd (%)** for formula $\text{C}_{16}\text{H}_{11}\text{F}_6\text{N}_4\text{O}_4\text{P}$; C, 41.04; H, 2.37; N, 11.97; Found C, 41.18; H, 2.52; N 11.90.

1-(2,4-dinitrophenyl)-4-(2'-pyridyl)pyridinium hexafluorophosphate: This compound was prepared as above using 2,4'-bipyridine (500 mg, 3.2 mmol) in place of 2,3'-bipyridine.

Yield: Cream coloured powder, 1.37 mg (91 %). **¹H-NMR:** δ_{H} (400 MHz, CD₃CN) 9.17 (1H, d, J = 2.5 Hz), 8.93-8.88 (5H, m), 8.83 (1H, dd, J = 8.7, 2.5 Hz), 8.34 (1H, dt, J = 8.0, 1.0 Hz), 8.14 (1H, d, J = 8.7 Hz), 8.11 (1H, td, J = 7.6, 2.0 Hz), 7.68 (1H, ddd, J = 7.7, 4.7, 1.0 Hz) ppm. **ES-MS (m/z):** 323 [M-PF₆]⁺. **Anal. Calcd (%)** for formula C₁₆H₁₁F₆N₄O₄P; C, 41.04; H, 2.37; N, 11.97; Found C, 41.36; H, 2.49; N 11.98.

2.3.2 Metal Precursors

2.3.2.1. Ruthenium Precursors

cis-RuCl₂(bpy)₂: RuCl₃·3H₂O (348 mg, 1.33 mmol), 2,2'-bipyridine (415 mg, 2.66 mmol) and LiCl (0.386 g, 9.31 mmol) were dissolved in DMF (8 mL). The mixture was refluxed with stirring for 8 hours before being cooled to room temperature. Acetone (10 mL) was then added and the solution stored in a refrigerator overnight. The resultant black solid was then collected by filtration and washed with distilled water and diethyl ether and dried under vacuum.

Yield: Dark purple microcrystalline solid, 0.47 g (73 %). **¹H-NMR:** δ_{H} (400 MHz, (CD₃)₂SO) 9.97 (2H, dd, J = 5.7, 0.9 Hz), 8.64 (2H, d, J = 7.2 Hz), 8.48 (2H, d, J = 7.9 Hz), 8.06 (2H, td, J = 7.8, 1.5 Hz), 7.77 (2H, ddd, J = 7.4, 5.8, 1.4 Hz), 7.68 (2H, td, J = 7.8, 1.4 Hz), 7.51 (2H, dd, J = 5.8, 0.7 Hz), 7.10 (2H, ddd, J = 7.4, 5.9, 1.4 Hz) ppm.

cis-RuCl₂(bpz)₂: RuCl₃·3H₂O (390 mg, 1.5 mmol) and 2,2'-bipyrazine (500 mg, 3.2 mmol) were dissolved in DMF (35 mL) and refluxed for 18 h under argon. After being cooled to room temperature the mixture was filtered and the product precipitated on addition of excess diethyl ether. The resultant solid was collected by vacuum filtration, washed with diethyl ether, methanol:ether (1:3) and once more with ether before being dried under vacuum.

Yield: Dark purple microcrystalline solid 580 g, (79 %). **¹H-NMR:** δ_{H} (400 MHz, (CD₃)₂SO) 10.00 (2H, d, 3.8, 1.1 Hz), 9.84 (2H, dd, J = 3.3, 1.2 Hz), 9.82 (2H, d, J = 1.2 Hz), 8.96 (2H, d, J = 3.3 Hz), 8.25 (2H, d, J = 3.4 Hz), 7.88 (2H, dd, J = 3.4, 1.2 Hz) ppm.

RuCl₃(bpy)(H₂O): 2,2'-bipyridine (0.719 g, 4.6 mmol) was added to 1M HCl (8 mL) and stirred until dissolved. To this solution RuCl₃·3H₂O (1.0 g, 3.8 mmol) was gradually added and stirring maintained for 10 minutes. The vessel was then stoppered and sealed and the mixture left to stand for seven days. The product was collected by filtration and washed with ice cold water.

Yield: Dark brown solid, 1.30 g (93 %).

trans-Ru(bpy)(CO)₂Cl₂: [Ru(CO)₂Cl₂]_n (1.0 g, 4.4 mmol) and 2,2'-bipyridine (1.03 g, 6.6 mmol) were added to a round bottomed flask and the vessel purged with an inert atmosphere and protected from light. To this argon-sparged methanol (15 mL) was added via syringe and the mixture heated to reflux with vigorous stirring. Upon cooling the resultant solid was collected

by vacuum filtration and the filtrand washed with warm methanol and dried *in vacuo*.

Yield: Fine pale yellow powder, 993.7 mg (59 %). **¹H-NMR:** δ_{H} (400 MHz, CDCl_3) 9.20 (2H, ddd, $J = 5.5, 1.5, 0.8$ Hz), 8.24 (2H, dt, $J = 8.1, 1.0$ Hz), 8.13 (2H, ddd, $J = 8.1, 7.7, 1.6$ Hz), 7.68 (2H, ddd, $J = 7.6, 5.5, 1.3$ Hz) ppm.

***cis*-[Ru(bpz)₂(MeCN)₂](PF₆)₂:** Ru(bpz)₂Cl₂ (250 mg, 0.51 mmol) and AgPF₆ (388 mg, 1.54 mmol) were added to deaerated acetonitrile (50 mL) and heated at 85°C for 96 h under argon. The suspension was filtered through celite to remove the AgCl precipitate and solvent removed under reduced pressure. The residue was suspended in deionised water, filtered and the brown solid dried under vacuum. The crude product was purified by column chromatography (SiO_2 , 0.1 M NH_4PF_6 in acetonitrile). After removal of solvents by rotary evaporation, the solid was washed with water and diethyl ether and dried *in vacuo*.

Yield: Orange Powder, 323 mg (80 %). **¹H-NMR:** δ_{H} (400 MHz, CD_3CN) 9.80 (2H, d, $J = 1.2$ Hz), 9.64 (2H, d, $J = 1.2$), 9.32 (2H, dd, $J = 3.2, 1.3$ Hz), 9.06 (2H, d, $J = 3.2$), 8.46 (2H, d, $J = 3.3$), 7.76 (2H, dd, 3.3, 1.2 Hz), 2.27 (6H, s) ppm. **ES-MS (m/z):** 645 [M-PF₆]⁺.

***cis*-RuCl₂(Me₂SO)₄** Dimethyl sulfoxide (25 mL) was added to a two-necked round-bottomed flask and sparged with argon for 15 minutes before being heated to reflux. After 30 minutes, RuCl₃·3H₂O (2.00 g, 7.72 mmol) was added and the reflux maintained for a further 5 minutes before the mixture was cooled to ambient temperature. The resultant solution was added to acetone (200 mL) and stored at 4°C for 48 h. The golden yellow crystalline product was collected by filtration and washed with acetone (5 × 30 mL) and dried *in vacuo*.

Yield: Canary yellow crystalline solid, 2.01 g (54 %)

2.3.2.2. Iridium Precursors

***Tetrakis*(2-phenylpyridine-*C*²,*N*¹)-bis-(μ -dichloro)diiridium, [Ir(ppy)₂Cl]₂:** Iridium(III) chloride hydrate (0.28 g, 0.80 mmol) and 2-phenylpyridine (0.28 g, 1.8 mmol) were added to an argon-sparged solution of 2-methoxyethanol (30 mL) in water (10 mL) and the mixture heated at 120°C for 18 h under argon. The resulting precipitate was collected via filtration, washed with water and diethyl ether then dried *in vacuo*. The mother liquor was collected and evaporated to dryness then redissolved in dichloromethane. The solution was then added to an excess of diethyl ether to precipitate a second batch of product, which was collected and treated as previous.

Yield: Bright Yellow Powder, 270 mg (63 %). **¹H-NMR:** δ_{H} (400 MHz, CDCl_3) 9.24 (2H, dd, $J = 5.8, 0.8$ Hz), 7.87 (2H, d, $J = 7.9$ Hz), 7.73 (2H, td, $J = 7.8, 1.5$ Hz), 7.48 (2H, dd, $J = 7.8, 1.1$ Hz), 6.79-6.72 (4H, m), 6.56 (2H, td, $J = 7.6, 0.9$ Hz), 5.93 (2H, dd, $J = 7.8, 0.8$ Hz) ppm.

Tetrakis(1-methyl-2,2'-bipyridin-3-yl-ium-*C*³,*N'*)-bis-(μ -dichloro)diiridium

tetra(hexafluorophosphate), {[Ir(22)₂Cl]₂}(PF₆)₄: Iridium (III) chloride hydrate (200 mg, 0.57 mmol) and 1-methyl-2-(2'-pyridyl)-pyridinium hexafluorophosphate (377 mg, 1.19 mmol) were added to an argon-sparged solution of 2-methoxyethanol (22 mL) in water (8 mL) and the mixture heated at 120°C for 48 h under argon. Upon cooling, the solution was filtered and an excess of solid ammonium hexafluorophosphate added followed by removal of solvents by rotary evaporation. The residue was suspended in ice-cold water and the solid collected by vacuum filtration where upon it was rinsed with a small volume of cold water and air-dried. The resultant solid was this was washed with acetone:diethyl ether (1:3, 4 × 5 mL) and then dried under vacuum.

Yield: Bright Red Powder, 331.2 mg (48.2 %). **¹H-NMR:** δ_{H} (400 MHz, CD₃CN) 10.20 (2H, ddd, $J = 5.7, 1.7, 0.7$ Hz), 8.51 (2H, d, $J = 8.4$ Hz), 8.16 (2H, ddd, $J = 8.5, 7.6, 1.7$ Hz), 8.10 (2H, dd, 5.9, 0.8 Hz), 7.74 (2H, ddd, $J = 7.6, 5.7, 1.3$ Hz), 7.26 (2H, dd, $J = 7.9, 1.2$ Hz), 7.11 (2H, dd, $J = 7.9, 5.9$ Hz), 4.58 (6H, s) ppm.

Tetrakis(1-methyl-3-(2-pyridyl)pyridin-4-yl-ium-*C*⁴,*N'*)-bis-(μ -dichloro)diiridium

tetra(hexafluorophosphate), {[Ir(32)₂Cl]₂}(PF₆)₄: This compound was prepared in a manner identical to {[Ir(22)₂Cl]₂}(PF₆)₄ instead using 1-methyl-3-(2'-pyridyl)-pyridinium hexafluorophosphate in place of 1-methyl-2-(2'-pyridyl)-pyridinium hexafluorophosphate.

Yield: Bright Yellow Powder, 351.3 mg (51.1 %). **¹H-NMR:** δ_{H} (400 MHz, CD₃CN) 9.85 (2H, ddd, $J = 5.8, 1.5, 0.8$ Hz), 8.59 (2H, d, $J = 1.3$ Hz), 8.18-8.10 (4H, m), 7.68 (2H, ddd, $J = 7.3, 7.8, 1.7$ Hz), 7.44 (2H, dd, $J = 6.5, 1.4$ Hz), 6.75 (2H, d, $J = 6.4$ Hz), 3.91 (6H, s) ppm.

Tetrakis(1-methyl-4-(2-pyridyl)pyridin-3-yl-ium-*C*³,*N'*)-bis-(μ -dichloro)diiridium

tetra(hexafluorophosphate), {[Ir(42)₂Cl]₂}(PF₆)₄: This compound was prepared in a manner identical to {[Ir(22)₂Cl]₂}(PF₆)₄ instead using 1-methyl-4-(2'-pyridyl)-pyridinium hexafluorophosphate in place of 1-methyl-2-(2'-pyridyl)-pyridinium hexafluorophosphate.

Yield: Red Powder, 318 mg (46 %). **¹H-NMR:** δ_{H} (400 MHz, CD₃CN) 9.97 (2H, ddd, $J = 5.7, 1.6, 0.7$ Hz), 8.33 (2H, ddd, $J = 8.1, 1.4, 0.7$ Hz), 8.13 (2H, td, $J = 7.8, 1.6$ Hz), 8.04 (2H, d, $J = 6.3$), 7.98 (2H, dd, $J = 6.5, 1.7$ Hz), 7.73 (2H, ddd, $J = 7.5, 5.8, 1.5$) 7.18 (2H d, $J = 1.6$ Hz), 3.90 (6H, s) ppm.

2.3.3. Synthesis of Ruthenium Complexes**2.3.3.1. Synthesis of complexes of the general formula [Ru(bpz)₂(L)](PF₆)_n**

[Ru(bpz)₂(2,2'-bipyridine)](PF₆)₂: Ru(bpz)₂Cl₂ (100 mg, 0.20 mmol) and 2,2'-bipyridine (64 mg, 0.41 mmol) were added to a round bottomed flask and the vessel purged with argon. To this, an argon-sparged solution of 2-methoxyethanol (7 mL) in water (3 mL) was added and the mixture heated at reflux for 24 h. Upon cooling to room temperature, solvents were removed by rotary evaporation and the residue redissolved in a minimum of deionised water. The resultant suspension was then filtered to remove unreacted starting materials and an

excess of solid NH_4PF_6 added to the filtrate to precipitate the crude product. The material was isolated by vacuum filtration and purification afforded by column chromatography (SiO_2 ; 0.1M NH_4PF_6 , MeCN). The resultant fractions were evaporated to dryness and the product washed with extensively ice-cold deionised water then dried *in vacuo*.

Yield: Orange Powder, 94.8 mg (56 %). **$^1\text{H-NMR}$** : δ_{H} (400 MHz, CD_3CN): 9.75 (4H, t, $J = 1.2$ Hz), 8.59 (4H, dd, $J = 3.2, 2.2$ Hz), 8.53 (2H, d, $J = 8.0$ Hz), 8.15 (2H, td, $J = 7.9, 1.5$ Hz), 7.85 (2H, dd, $J = 3.2, 1.2$ Hz), 7.78 (2H, dd, $J = 3.2, 1.2$ Hz), 7.69 (2H, ddd, $J = 5.6, 1.4, 0.7$ Hz), 7.46 (2H, ddd, $J = 7.7, 5.7, 1.3$ Hz) ppm. **ES-MS (m/z)**: 718 $[\text{M-PF}_6]^+$, 287 $[\text{M-2PF}_6]^{2+}$. **Anal. Calcd (%)** for $\text{C}_{26}\text{H}_{20}\text{F}_{12}\text{N}_{10}\text{P}_2\text{Ru}\cdot\text{H}_2\text{O}$; C, 35.43; H, 2.52; N, 15.89. Found C, 35.54; H, 2.13; N 15.72.

$[\text{Ru}(\text{bpz})_2(4,4'\text{-di-methyl-2,2'-bipyridine})](\text{PF}_6)_2$: This compound was prepared in a manner identical to $[\text{Ru}(\text{bpz})_2\text{bpy}](\text{PF}_6)_2$ instead using 4,4'-dimethyl-2,2'-bipyridine (75.5 mg, 0.41 mmol) in place of 2,2'-bipyridine.

Yield: Dark Red Powder, 91.2 mg (50 %). **$^1\text{H-NMR}$** : δ_{H} (400 MHz, CD_3CN) 9.74 (4H, dd, $J = 2.7, 1.2$ Hz), 8.62 (4H, dd, $J = 9.9, 3.2$ Hz), 8.38 (2H, dd, $J = 1.0, 0.6$ Hz), 7.84 (2H, dd, $J = 3.2, 1.2$ Hz), 7.77 (2H, dd, $J = 3.3, 1.3$ Hz), 7.48 (2H, d, $J = 5.9$ Hz), 7.30-7.28 (2H, m), 2.55 (6H, s) ppm. **ES-MS (m/z)**: 746 $[\text{M-PF}_6]^+$, 301 $[\text{M-2PF}_6]^{2+}$. **Anal. Calcd (%)** for $\text{C}_{28}\text{H}_{24}\text{F}_{12}\text{N}_{10}\text{P}_2\text{Ru}$; C, 37.72; H, 2.71; N, 15.71. Found C, 37.97; H, 2.65; N 15.35.

$[\text{Ru}(\text{bpz})_2(4,4'\text{-di-tertiary-butyl-2,2'-bipyridine})](\text{PF}_6)_2$: This compound was prepared in a manner identical to $[\text{Ru}(\text{bpz})_2\text{bpy}](\text{PF}_6)_2$ instead using 4,4'-di-tert-butyl-2,2'-bipyridine (110 mg, 0.41 mmol) in place of 2,2'-bipyridine.

Yield: Red Powder, 112.4 mg (56 %). **$^1\text{H-NMR}$** : δ_{H} (400 MHz, CD_3CN) 9.75 (4H, dd, $J = 3.6, 1.2$ Hz), 8.62 (2H, d, $J = 3.2$ Hz), 8.58 (2H, d, $J = 3.2$ Hz), 8.49 (2H, d, $J = 2.4$ Hz), 7.84 (2H, dd, $J = 3.2, 1.2$ Hz), 7.77 (2H, dd, $J = 3.2, 1.2$ Hz), 7.54 (2H, d, $J = 6.0$ Hz), 7.42 (2H, dd, $J = 6.1, 2.1$ Hz), 1.41 (18H, s) ppm. **ES-MS (m/z)**: 831 $[\text{M-PF}_6]^+$, 343 $[\text{M-2PF}_6]^{2+}$. **Anal. Calcd (%)** for $\text{C}_{34}\text{H}_{36}\text{F}_{12}\text{N}_{10}\text{P}_2\text{Ru}\cdot\text{H}_2\text{O}$; C, 41.09; H, 3.85; N, 14.09. Found C, 41.39; H, 3.42; N, 13.86.

$[\text{Ru}(\text{bpz})_2(4,4'\text{-dichloro-2,2'-bipyridine})](\text{PF}_6)_2$: This compound was prepared in a manner identical to $[\text{Ru}(\text{bpz})_2\text{bpy}](\text{PF}_6)_2$ instead using 4,4'-dichloro-2,2'-bipyridine (92 mg, 0.41 mmol) in place of 2,2'-bipyridine.

Yield: Orange Powder, 97.3 mg (51 %). **$^1\text{H-NMR}$** : δ_{H} (400 MHz, CD_3CN) 9.75 (4H, dd, $J = 4.8, 1.1$ Hz), 8.63 (4H, t, $J = 2.3$ Hz), 8.59 (2H, d, $J = 3.2$ Hz), 7.83 (4H, ddd, $J = 7.0, 3.2, 1.2$ Hz), 7.61 (2H, d, $J = 6.1$ Hz), 7.54 (2H, dd, $J = 6.2, 2.2$ Hz) ppm. **ES-MS (m/z)**: 787 $[\text{M-PF}_6]^+$, 321 $[\text{M-2PF}_6]^{2+}$. **Anal. Calcd (%)** for $\text{C}_{26}\text{H}_{18}\text{Cl}_2\text{F}_{12}\text{N}_{10}\text{P}_2\text{Ru}$; C, 33.49; H, 1.95; N, 15.02. Found C, 33.36; H, 1.77; N 14.61.

[Ru(bpz)₂(4,4'-diphenyl-2,2'-bipyridine)](PF₆)₂: This compound was prepared in a manner identical to [Ru(bpz)₂bpy](PF₆)₂ instead using 4,4'-phenyl-2,2'-bipyridine (126 mg, 0.41 mmol) in place of 2,2'-bipyridine.

Yield: Orange/Red Powder, 141 mg (68 %). **¹H-NMR:** δ_H (400 MHz, CD₃CN) 9.77 (4H, t, *J* = 1.4 Hz), 8.93 (2H, t, *J* = 1.2 Hz), 8.62 (4H, dd, *J* = 4.3, 3.3 Hz), 7.95–7.93 (4H, m), 7.90 (4H, ddd, *J* = 5.6, 3.3, 1.2 Hz), 7.72 (4H, d, *J* = 1.2 Hz), 7.64–7.60 (6H, m) ppm. **ES-MS (*m/z*):** 870 [M-PF₆]⁺, 363 [M-2PF₆]²⁺. **Anal. Calcd (%)** for formula C₃₈H₂₈F₁₂N₁₀P₂Ru·1.5H₂O; C, 43.77; H, 3.00; N, 13.43. Found C, 43.24; H, 2.60; N 13.29.

[Ru(bpz)₂(4,4'-diamino-2,2'-bipyridine)](PF₆)₂: This compound was prepared in a manner identical to [Ru(bpz)₂bpy](PF₆)₂ instead using 4,4'-diamino-2,2'-bipyridine (76 mg, 0.41 mmol) in place of 2,2'-bipyridine.

Yield: Dark Red/Brown Solid, 103.4 mg (56 %). **¹H-NMR:** δ_H (400 MHz, CD₃CN) 9.71 (2H, d, *J* = 1.3 Hz), 9.69 (2H, d, *J* = 1.3 Hz), 8.62 (2H, d, *J* = 3.3 Hz), 8.50 (2H, d, *J* = 3.3 Hz), 7.96 (2H, dd, *J* = 3.3, 1.3 Hz), 7.80 (2H, d, *J* = 3.3, 1.3 Hz), 7.40 (2H, d, *J* = 2.5 Hz), 6.92 (2H, d, *J* = 6.5 Hz), 6.53 (2H, d, *J* = 6.5, 2.5 Hz) 5.72 (4H, s) ppm. **ES-MS (*m/z*):** 748 [M-PF₆]⁺, 302 [M-2PF₆]²⁺. **Anal. Calcd (%)** for formula C₂₆H₂₂F₁₂N₁₂P₂Ru·1.5H₂O; C, 33.95; H, 2.74; N, 18.26. Found C, 33.71; H, 2.50; N 18.02.

[Ru(bpz)₂(4-hydroxymethyl-4'-methyl-2,2'-bipyridine)](PF₆)₂: This compound was prepared in a manner identical to [Ru(bpz)₂bpy](PF₆)₂ instead using 4-hydroxymethyl-4'-methyl-2,2'-bipyridine (82.0 mg, 0.41 mmol) in place of 2,2'-bipyridine.

Yield: Bright Orange Powder, 113.7 mg (61 %). **¹H-NMR:** δ_H (400 MHz, CD₃CN) 9.74 (4H, s), 8.60 (2H, dd, *J* = 3.2, 1.7 Hz), 8.58 (2H, dd, *J* = 3.2, 1.8 Hz), 8.49 (1H, d, *J* = 0.9 Hz), 8.43 (1H, s), 7.85 (2H, ddd, *J* = 3.2, 2.6, 1.2 Hz), 7.78 (2H, ddd, *J* = 5.2, 3.3, 1.3 Hz), 7.57 (1H, d, *J* = 5.8 Hz), 7.49 (1H, d, *J* = 5.8 Hz), 7.39 (1H, dt = 5.8, 0.9 Hz), 7.30 (1H, ddd, *J* = 5.8, 1.7, 0.7 Hz), 4.82 (2H, d, *J* = 5.5 Hz), 3.79 (1H, t, *J* = 5.5 Hz), 2.56 (3H, s) ppm. **ES-MS (*m/z*):** 761 [M-PF₆]⁺, 309 [M-2PF₆]²⁺.

[Ru(bpz)₂(2,2'-bipyrimidine)](PF₆)₂: This compound was prepared in a manner identical to [Ru(bpz)₂bpy](PF₆)₂ instead using 2,2'-bipyrimidine (64.8 mg, 0.41 mmol) in place of 2,2'-bipyridine.

Yield: Bright Orange Powder, 77.4 mg (44 %). **¹H-NMR:** δ_H (400 MHz, CD₃CN) 9.76 (4H, dd, *J* = 3.3, 1.2 Hz), 9.18 (2H, dd, *J* = 4.8, 2.0 Hz), 8.65 (2H, d, *J* = 3.2 Hz), 8.60 (2H, d, *J* = 3.2), 8.02 (2H, dd, *J* = 5.8, 2.0 Hz), 7.96 (2H, dd, *J* = 3.2, 1.1 Hz), 7.84 (2H, dd, *J* = 3.2, 1.1 Hz), 7.60 (2H, dd, *J* = 5.7, 4.9 Hz) ppm. **ES-MS (*m/z*):** 720 [M-PF₆]⁺, 288 [M-2PF₆]²⁺. **Anal. Calcd (%)** for formula C₂₄H₁₈F₁₂N₁₂P₂Ru; C, 33.31; H, 2.10; N, 19.42. Found C, 32.83; H, 2.22; N 18.94.

[Ru(bpz)₂(2,3-bis-(2-pyridyl)pyrazine)](PF₆)₂: This compound was prepared in a manner identical to [Ru(bpz)₂bpy](PF₆)₂ instead using 2,3-bis(2-pyridyl)pyrazine (95.9 mg, 0.41 mmol) in place of 2,2'-bipyridine.

Yield: Bright Orange Powder, 82.6 mg (42.8 %). **¹H-NMR:** δ_H (400 MHz, CD₃CN) 9.82-9.76 (4H, m), 8.70 (1H, d, *J* = 3.2 Hz), 8.67 (2H, m), 8.63 (2H, dd, *J* = 5.8, 3.2 Hz), 8.60 (1H, d, *J* = 3.1 Hz), 8.12 (1H, td, *J* = 7.8, 1.7 Hz), 8.06 (1H, dd, *J* = 3.3, 1.2 Hz), 7.96 (1H, d, *J* = 7.8 Hz), 7.84 (2H, dd, *J* = 3.2, 1.2 Hz), 7.83 (1H, d, *J* = 3.1 Hz), 7.79 (1H, dd, *J* = 3.2, 1.2 Hz), 7.75 (1H, ddd, *J* = 8.3, 7.9, 1.5 Hz), 7.70 (1H, ddd, *J* = 5.7, 1.4, 0.7 Hz), 7.65 (1H, ddd, *J* = 7.6, 4.9, 1.0 Hz), 7.37 (1H, ddd, *J* = 7.6, 5.7, 1.4 Hz), 7.26 (1H, ddd, *J* = 8.4, 1.2, 0.8 Hz) ppm. **ES-MS (*m/z*):** 796 [M-PF₆]⁺, 326 [M-2PF₆]²⁺

[Ru(bpz)₂(N'',N'''-Dimethyl-2,2':4,4'':4',4'''-quaterpyridinium)](PF₆)₄: This compound was prepared in a manner identical to [Ru(bpz)₂bpy](PF₆)₂ instead using N'',N'''-Dimethyl-2,2':4,4'':4',4'''-quaterpyridinium dihexafluorophosphate (193.7 mg, 0.31 mmol) in place of 2,2'-bipyridine.

Yield: Bright Orange Powder, 126.4 mg (46 %). **¹H-NMR:** δ_H (400 MHz, CD₃CN) 9.80 (4H, s), 9.15 (2H, d, *J* = 1.7 Hz), 8.83 (4H, d, *J* = 6.7 Hz), 8.65 (4H, dd, *J* = 3.2, 2.4 Hz), 8.49 (4H, d, *J* = 7.0 Hz), 7.98 (2H, d, *J* = 6.0 Hz), 7.90-7.85 (6H, m), 4.39 (6H, s) ppm. **ES-MS (*m/z*):** 1192 [M-PF₆]⁺, 524 [M-2PF₆]²⁺, 302 [M-3PF₆]³⁺, 253 [M-4PF₆]⁴⁺. **Anal. Calcd (%)** for C₃₈H₃₂F₂₄N₁₂P₄Ru; C, 34.12; H, 2.41; N, 12.57. Found C, 33.70; H, 2.43; N 12.22.

[Ru(bpz)₂(N'',N'''-Di(4-hydroxymethylphenyl)-2,2':4,4'':4',4'''-

quaterpyridinium)](PF₆)₄: This compound was prepared in a manner identical to [Ru(bpz)₂bpy](PF₆)₂ instead using N'',N'''-di(4-hydroxymethylphenyl)-2,2':4,4'':4',4'''-quaterpyridinium dihexafluorophosphate (250 mg, 0.31 mmol) in place of 2,2'-bipyridine.

Yields: Bright orange powder, 101.0 mg (32 %). **¹H-NMR: δ_H (400 MHz, CD₃CN)** 9.82 (4H, s), 9.25 (2H, s), 9.14 (4H, d, *J* = 7.1 Hz), 8.69-8.68 (8H, m), 8.03 (2H, d, *J* = 6.0 Hz), 7.95 (2H, dd, *J* = 6.0, 1.9 Hz), 7.92 (4H, dd, *J* = 3.2, 1.2 Hz), 7.74 (8H, d, *J* = 3.5 Hz), 4.76 (4H, d, *J* = 5.6), 3.53 (2H, t, *J* = 5.7 Hz) ppm. **ES-MS (*m/z*):** 616 [M-2PF₆]²⁺, 363 [M-3PF₆]³⁺. **Anal. Calcd (%)** for C₅₀H₄₀F₂₄N₁₂P₄Ru·1.5H₂O; C, 38.77; H, 2.80; N, 10.85. Found C, 38.37; H, 2.68; N 10.51.

[Ru(bpz)₂(4,4'-di-trifluoromethyl-2,2'-bipyridine)](PF₆)₂: Ru(bpz)₂Cl₂ (100 mg, 0.20 mmol) and AgNO₃ (76.8 mg, 0.45 mol) were heat at reflux for 48 h in deionized water (25 mL). On cooling the mixture was filtered through celite to remove AgCl precipitate and the filtrate subsequently evaporated to dryness. The residue was redissolved in DMF (15 mL) and the resultant solution purged with argon for 15 minutes. 4,4'-di-trifluoromethyl-2,2'-bipyridine (121.4 mg, 0.41 mmol) was added and the mixture heated at 100°C for 24 h under argon. On cooling the solution was concentrated and diethyl ether (150 mL) added. The resultant precipitate was collected by filtration and redissolved in a minimum of cold water to which

solid NH_4PF_6 was added. The solid was isolated by vacuum filtration and purification afforded by column chromatography (SiO_2 ; 0.1M NH_4PF_6 , MeCN). The resultant fractions were evaporated to dryness and the product washed extensively with ice-cold deionised water then then dried *in vacuo*.

Yield: Orange powder, 73.4 mg (36 %). **$^1\text{H-NMR}$: δ_{H} (400 MHz, CD_3CN)** 9.77 (4H, d, $J = 1.2$ Hz), 8.96 (2H, t, $J = 3.2$ Hz), 8.63 (4H, d, $J = 3.2$ Hz), 7.97 (2H, d, $J = 5.9$ Hz), 7.84 (2H, dd, $J = 3.2, 1.2$ Hz), 7.80 (2H, dd, $J = 3.2, 1.2$ Hz), 7.75 (2H, dd, $J = 6.0, 1.4$ Hz) ppm. **$^{19}\text{F-NMR}$: δ_{F} (400 MHz, CD_3CN)** -63.89 (6H, s), -71.36 (12H, d, $J = 707$ Hz). **ES-MS (m/z):** 854 $[\text{M-PF}_6]^+$, 355 $[\text{M-2PF}_6]^{2+}$. **Anal. Calcd (%)** for $\text{C}_{28}\text{H}_{18}\text{F}_{18}\text{N}_{10}\text{P}_2\text{Ru}\cdot\text{H}_2\text{O}$; C, 33.05; H, 1.98; N, 13.77. Found C, 32.69; H, 1.48; N, 13.73.

$[\text{Ru}(\text{bpz})_2(4,4'\text{-di(methoxycarbonyl)-2,2'\text{-bipyridine)}](\text{PF}_6)_2$: This compound was prepared in a manner identical to $[\text{Ru}(\text{bpz})_2(4,4'\text{-di(trifluoromethyl)-2,2'\text{-bipyridine)}](\text{PF}_6)_2$ by instead using 4,4'-di(methoxycarbonyl)-2,2'-bipyridine (111.5 mg, 0.41 mmol) in place of 4,4'-di-trifluoromethyl-2,2'-bipyridine.

Yield: Orange powder, 98.2 mg (49 %). **$^1\text{H-NMR}$: δ_{H} (400 MHz, CD_3CN)** 10.02 (4H, t, $J = 1.48$ Hz), 9.25 (2H, d, $J = 1.1$ Hz), 8.72 (2H, d, $J = 3.2$ Hz), 8.69 (2H, d, $J = 3.24$), 8.07 (2H, dd, $J = 5.8, 0.5$ Hz), 8.05-8.02 (4H, m), 7.94 (2H, dd, $J = 3.2, 1.2$ Hz), 3.35 (6H, s) ppm. **ES-MS (m/z):** 835 $[\text{M-PF}_6]^+$, 345 $[\text{M-2PF}_6]^{2+}$. **Anal. Calcd (%)** for $\text{C}_{30}\text{H}_{24}\text{F}_{12}\text{N}_{10}\text{O}_4\text{P}_2\text{Ru}\cdot\text{H}_2\text{O}$; C, 36.12; H, 2.63; N, 14.04. Found C, 35.98; H, 2.32; N, 13.88.

$[\text{Ru}(\text{bpz})_2(4\text{-bromomethyl-4'\text{-methyl-2,2'\text{-bipyridine)}](\text{PF}_6)_2$: To a round bottomed flask $[\text{Ru}(\text{bpz})_2(4\text{-hydroxymethyl-4'\text{-methyl-2,2'\text{-bipyridine)}](\text{PF}_6)_2$ (100 mg, 0.11 mmol) and acetonitrile (20 mL) were added and sparged with argon for 15 minutes. To this stirred solution, phosphorus tribromide (0.2 mL) was added dropwise via syringe. The mixture was gradually heated to 60°C and the temperature maintained for 14 h with vigorous stirring. On cooling to room temperature the crude product was isolated as the bromide salt by precipitation on addition of diethyl ether (150 mL). The solid was collected by filtration, and washed with diethyl ether and DCM. The material was then dissolved in cold water and solid NH_4PF_6 was added to precipitate the product as the hexafluorophosphate salt. This was washed with cold water, air dried, dissolved in acetone and reprecipitated from diethyl ether to afford the product which was collected by filtration, washed with diethyl ether and dried *in vacuo*.

Yield: Brown orange powder, 68.3 mg (64 %). **$^1\text{H-NMR}$: δ_{H} (400 MHz, CD_3CN)** 9.77 (4H, s), 8.64 (2H, dd, $J = 3.2, 0.8$ Hz), 8.61 (2H, dd, $J = 3.2, 2.1$ Hz), 8.57 (1H, d, $J = 1.8$ Hz), 8.44 (1H, d, 0.9 Hz), 7.86 (2H, ddd, $J = 5.5, 3.2, 1.3$ Hz), 7.83 (1H, dd, $J = 3.2, 1.3$ Hz), 7.78 (1H, dd, $J = 3.2, 1.2$ Hz), 7.65 (1H, d, $J = 5.4$ Hz), 7.52 (1H, d, $J = 5.8$ Hz), 7.49 (1H, dd, $J = 5.9, 1.9$ Hz), 7.34 (1H, ddd, $J = 5.9, 1.9, 0.7$ Hz), 4.68 (2H, s), 2.60 (3H, s) ppm. **ES-MS (m/z):** 825 $[\text{M-PF}_6]^+$, 340 $[\text{M-2PF}_6]^{2+}$

[Ru(bpz)₂(N'',N'''-Di(4-bromomethylphenyl)-2,2':4,4'':4',4''')-

quaterpyridinium)](PF₆)₄: This compound was prepared in a manner similar to [Ru(bpz)₂(4,-bromomethyl-4'-methyl-2,2'-bipyridine)](PF₆)₂ instead using [Ru(bpz)₂(N'',N'''-Di(4-hydroxymethylphenyl)-2,2':4,4'':4',4''')-quaterpyridinium)](PF₆)₄ (50 mg, 0.03 mmol) in place of [Ru(bpz)₂(hydroxymethyl-4'-methyl-2,2'-bipyridine)](PF₆)₂.

Yield: Brown-red solid, 42.0 mg (78 %). **¹H-NMR:** δ_H (400 MHz, CD₃CN) 9.82 (4H, s), 9.22 (2H, s), 9.14 (4H, d, *J* = 6.7 Hz), 8.68 (8H, d, *J* = 3.4 Hz), 8.03 (2H, d, *J* = 6.2 Hz), 7.97 – 7.92 (6H, m) 7.80 (8H, q, *J* = 10.3 Hz), 4.73 (4H, s) ppm. **ES-MS (*m/z*):** 678 [M-2PF₆]²⁺, 405 [M-3PF₆]³⁺.

2.3.3.2. Preparation of complexes of the general formula [Ru(bpz)₂(L)]Cl_n

[Ru(bpz)₂(2,2'-bipyridine)]Cl₂: This compound was prepared by metathesis of the analogous complex as the hexafluorophosphate salt. On dissolution in acetone, an excess of solid tetra-*n*-butyl ammonium chloride was added and the precipitate collected by vacuum filtration. The filtrand was washed with acetone and diethyl ether then dried *in vacuo* to give the chloride salt in near quantitative yields.

¹H-NMR: δ_H (400 MHz, CD₃OD) 10.00 (4H, t, *J* = 1.4 Hz), 8.78 (2H, d, *J* = 8.1 Hz), 8.69 (2H, d, *J* = 3.3 Hz), 8.68 (2H, d, *J* = 3.3 Hz), 8.25 (2H, td, *J* = 7.9, 1.3 Hz), 8.05 (2H, dd, *J* = 3.2, 1.2 Hz), 7.94 (2H, dd, *J* = 3.2, 1.2 Hz), 7.85 (2H, dt, *J* = 5.7, 0.7 Hz), 7.58 (2H, ddd, *J* = 7.6, 5.7, 1.3 Hz) ppm. **ES-MS (*m/z*):** 608 [M-Cl]⁺, 287 [M-Cl]²⁺. **Anal. Calcd (%)** for C₂₆H₂₀Cl₂N₁₀Ru·2H₂O; C, 45.89; H, 3.55; N, 20.58. Found C, 45.89; H, 3.55; N, 20.58.

[Ru(bpz)₂(4,4'-dimethyl-2,2'-bipyridine)]Cl₂: This compound was prepared in a manner identical to that used for [Ru(bpz)₂(2,2'-bipyridine)]Cl₂.

¹H-NMR: δ_H (400 MHz, CD₃OD) 9.99 (4H, t, *J* = 1.3 Hz), 8.69 (2H, d, *J* = 3.3 Hz), 8.67 (2H, d, *J* = 3.2 Hz), 8.65 (2H, s), 8.04 (2H, dd, *J* = 3.3, 1.2 Hz), 7.95 (2H, dd, *J* = 3.3, 1.2 Hz), 7.63 (2H, d, *J* = 5.8 Hz), 7.40 (2H, ddd, *J* = 5.8, 1.8, 0.7 Hz) 2.62 (6H, s) ppm. **ES-MS (*m/z*):** 637 [M-Cl]⁺, 300 [M-Cl]²⁺. **Anal. Calcd (%)** for C₂₈H₂₄Cl₂N₁₀Ru·1.5H₂O; C, 48.07; H, 3.89; N, 20.02. Found C, 48.40; H, 3.89; N, 20.02.

[Ru(bpz)₂(4,4'-di-tertiary-butyl-2,2'-bipyridine)]Cl₂: This compound was prepared in a manner identical to that used for [Ru(bpz)₂(2,2'-bipyridine)]Cl₂.

¹H-NMR: δ_H (400 MHz, CD₃OD) 10.00 (4H, t, *J* = 1.0 Hz), 8.80 (2H, dd, *J* = 3.7, 1.3 Hz), 8.70 (2H, d, *J* = 3.3 Hz), 8.68 (2H, d, *J* = 3.2 Hz), 8.04 (2H, dd, *J* = 3.3, 1.2 Hz), 7.93 (2H, dd, *J* = 3.2, 1.2 Hz), 7.70 (2H, dd, *J* = 6.0 Hz), 7.58 (2H, dd, *J* = 6.1, 2.1 Hz), 1.46 (18H, s) ppm. **ES-MS (*m/z*):** 720 [M-Cl]⁺, 342 [M-2Cl]²⁺. **Anal. Calcd (%)** for C₃₄H₃₆Cl₂N₁₀Ru·3H₂O; C, 50.37; H, 5.22; N, 17.28. Found C, 50.37; H, 5.03; N, 17.12.

[Ru(bpz)₂(4,4'-dichloro-2,2'-bipyridine)]Cl₂: This compound was prepared in a manner identical to that used for [Ru(bpz)₂(2,2'-bipyridine)]Cl₂.

¹H-NMR: δ_H (400 MHz, CD₃OD) 10.01 (2H, d, *J* = 1.2 Hz), 10.00 (2H, d, *J* = 1.2 Hz), 9.01 (2H, d, *J* = 3.2 Hz), 8.72 (2H, d, *J* = 3.2 Hz), 8.68 (2H, d, *J* = 3.2 Hz), 8.03 (2H, dd, *J* = 3.3, 1.2 Hz), 8.01 (2H, dd, *J* = 3.2, 1.2 Hz), 7.79 (2H, dd, *J* = 6.1, 0.2 Hz), 7.67 (2H, dd, *J* = 6.2, 2.2 Hz) ppm. **ES-MS (*m/z*)**: 629 [M-Cl]⁺, 321 [M-2Cl]²⁺. **Anal. Calcd (%)** for C₂₆H₂₈Cl₄N₁₀Ru·2H₂O; C, 41.67; H, 2.96; N, 18.69. Found C, 41.81; H, 2.73; N, 18.35.

[Ru(bpz)₂(4,4'-diphenyl-2,2'-bipyridine)]Cl₂: This compound was prepared in a manner identical to that used for [Ru(bpz)₂(2,2'-bipyridine)]Cl₂.

¹H-NMR: δ_H (400 MHz, CD₃OD) 10.04 (4H, s), 9.27 (2H, d, *J* = 1.2 Hz), 8.72 (4H, dd, 3.2, 1.6 Hz), 8.10 (4H, td, *J* = 3.20, 1.1 Hz), 8.03 (4H, dd, *J* = 7.9, 1.6 Hz), 7.88-7.84 (4H, m), 7.64-7.58 (6H, m) ppm. **ES-MS (*m/z*)**: 761 [M-Cl]⁺, 363 [M-2Cl]²⁺. **Anal. Calcd (%)** for C₃₈H₂₈Cl₂N₁₀Ru·1.5H₂O; C, 55.41; H, 3.79; N, 17.00. Found C, 55.21; H, 3.70; N 16.50.

[Ru(bpz)₂(4,4'-diamino-2,2'-bipyridine)]Cl₂: This compound was prepared in a manner identical to that used for [Ru(bpz)₂(2,2'-bipyridine)]Cl₂.

¹H-NMR: δ_H (400 MHz, CD₃OD) 9.94 (2H, dd, *J* = 7.9, 1.2 Hz), 8.72 (2H, d, *J* = 3.3 Hz), 8.59 (2H, d, *J* = 3.3 Hz), 8.09 (2H, dd, *J* = 3.3, 1.2 Hz), 7.98 (2H, dd, *J* = 3.3, 1.2 Hz), 7.51 (2H, d, *J* = 2.5 Hz), 6.98 (2H, d, *J* = 6.5 Hz), 6.58 (2H, dd, *J* = 6.5, 2.5 Hz) ppm. **ES-MS (*m/z*)**: 302 [M-2Cl]²⁺. **Anal. Calcd (%)** for C₂₆H₂₂Cl₂N₁₂Ru·4H₂O; C, 41.83; H, 4.05; N, 22.51. Found C, 41.55; H, 3.85; N 22.08.

[Ru(bpz)₂(4-hydroxymethyl-4'-methyl-2,2'-bipyridine)]Cl₂: This compound was prepared in a manner identical to that used for [Ru(bpz)₂(2,2'-bipyridine)]Cl₂.

¹H-NMR: δ_H (400 MHz, CD₃OD) 9.99 (4H, s), 8.68 (6H, dt, *J* = 10.0, 6.9 Hz), 8.05 (2H, d, *J* = 3.1 Hz), 7.95 (2H, d, *J* = 2.9 Hz), 7.74 (1H, d, *J* = 5.8 Hz), 7.64 (1H, d, *J* = 5.9 Hz), 7.55 (1H, d, *J* = 6.1 Hz), 7.41 (1H, d, *J* = 5.7 Hz), 2.62 (3H, s) ppm. **ES-MS (*m/z*)**: 652 [M-Cl]⁺, 308 [M-2Cl]²⁺.

[Ru(bpz)₂(2,2'-bipyrimidine)]Cl₂: This compound was prepared in a manner identical to that used for [Ru(bpz)₂(2,2'-bipyridine)]Cl₂.

¹H-NMR: δ_H (400 MHz, CD₃OD) 10.01 (2H, d, *J* = 1.1 Hz), 10.00 (2H, d, *J* = 1.1 Hz), 9.26 (2H, dd, *J* = 4.8, 1.9 Hz), 8.74 (2H, d, *J* = 3.2 Hz), 8.70 (2H, d, *J* = 3.2 Hz), 8.28 (2H, dd, 5.8, 1.9 Hz), 8.16 (2H, dd, *J* = 3.2, 1.1 Hz), 8.02 (2H, dd, *J* = 3.2, 1.1 Hz), 7.75 (2H, t, *J* = 5.3 Hz) ppm. **ES-MS (*m/z*)**: 610 [M-Cl]⁺, 288 [M-2Cl]²⁺. **Anal. Calcd (%)** for C₂₄H₁₈Cl₂N₁₂Ru·2.5H₂O; C, 41.69; H, 3.35; N, 24.31. Found C, 41.66; H, 2.94; N, 24.55.

[Ru(bpz)₂(Me₂Qpy)]Cl₄: This compound was prepared in a manner identical to that used for [Ru(bpz)₂(2,2'-bipyridine)]Cl₂.

¹H-NMR: δ_H (400 MHz, CD₃OD) 10.05 (2H, d, *J* = 1.1 Hz), 10.04 (2H, d, *J* = 1.1 Hz), 9.78 (2H, s), 9.14 (4H, d, *J* = 6.7 Hz), 8.85 (4H, d, *J* = 6.9 Hz), 8.74 (2H, d, *J* = 3.4 Hz), 8.73 (2H, d, *J* = 3.4 Hz), 8.17-8.13 (6H, m), 8.10 (2H, dd, *J* = 3.2, 1.1 Hz), 4.51 (6H, s) ppm. **ES-MS (*m/z*)**: 415 [M-2Cl]²⁺, 265 [M-3Cl]³⁺, [(M-4Cl)+H]³⁺, 190 [M-4Cl]⁴⁺. **Anal. Calcd (%)** for C₃₈H₃₂Cl₄N₁₂Ru·3H₂O; C, 47.86; H, 4.02; N, 17.62. Found C, 47.77; H, 3.89; N 17.34.

[Ru(bpz)₂(N'',N'''-Di(4-hydroxymethylphenyl)-2,2':4,4'':4',4'''-quaterpyridinium)]Cl₂:

This compound was prepared in a manner identical to that used for [Ru(bpz)₂(2,2'-bipyridine)]Cl₂.

¹H-NMR: δ_H (400 MHz, CD₃OD) 10.07 (4H, s), 9.91 (2H, s), 9.48 (4H, d, *J* = 7.0 Hz), 9.04 (4H, d, *J* = 6.9 Hz), 8.76 (4H, d, *J* = 3.2 Hz), 8.24-8.20 (4H, m), 8.19 (2H, dd, *J* = 3.3, 0.9 Hz), 8.12 (2H, dd, *J* = 3.3 0.9 Hz), 7.89 (4H, d, *J* = 8.6 Hz), 7.78 (4H, d, *J* = 8.6 Hz), 4.80 (4H, s) ppm. **ES-MS (*m/z*)**: 506 [M-2Cl]²⁺, 325 [M-3Cl]³⁺, 314 [(M-4Cl)+H]⁴⁺, 236 [M-4Cl]⁴⁺. **Anal. Calcd (%)** for C₅₂H₄₀Cl₄N₁₂O₂Ru·2H₂O; C, 53.63; H, 3.96; N, 15.01. Found C, 53.19; H, 4.01; N, 14.85.

[Ru(bpz)₂(4,4'-di(trifluoromethyl)-2,2'-bipyridine)]Cl₂: This compound was prepared in a manner identical to that used for [Ru(bpz)₂(2,2'-bipyridine)]Cl₂.

¹H-NMR: δ_H (400 MHz, CD₃OD) 10.03 (4H, t, *J* = 1.4 Hz), 9.41 (2H, s), 8.72 (4H, dd, *J* = 5.5, 3.2 Hz), 8.15 (2H, d, *J* = 5.8 Hz), 8.03 (2H, dd, *J* = 3.2, 1.1 Hz), 7.99 (2H, dd, *J* = 3.2 1.2 Hz), 7.84 (2H, dd, *J* = 6.1, 1.6 Hz) ppm. **ES-MS (*m/z*)**: 744 [M-Cl]⁺, 355 [M-2Cl]²⁺. **Anal. Calcd (%)** C₂₈H₁₈Cl₂F₆N₁₀Ru·4.5H₂O; C, 39.03; H, 3.16; N, 16.26. Found C, 38.65; H, 3.02; N, 16.06.

[Ru(bpz)₂(4,4'-di(methoxycarbonyl)-2,2'-bipyridine)]Cl₂: This compound was prepared in a manner identical to that used for [Ru(bpz)₂(2,2'-bipyridine)]Cl₂.

¹H-NMR: δ_H (400 MHz, CD₃OD) 10.01 (4H, t, *J* = 1.5 Hz), 9.25 (2H, d, *J* = 1.1 Hz), 8.72 (2H, d, *J* = 3.2 Hz), 8.69 (2H, d, *J* = 3.2 Hz), 8.08-8.02 (6H, m), 7.94 (2H, dd, *J* = 3.2, 1.2 Hz), 3.35 (6H, s) ppm. **ES-MS (*m/z*)**: 345 [M-2Cl]²⁺. **Anal. Calcd (%)** for C₃₀H₂₄Cl₂N₁₀O₄P₂Ru·5H₂O; C, 42.36; H, 4.03; N, 16.47. Found C, 41.87; H, 3.95; N 16.29.

2.3.3.3. Synthesis of complexes of the general formula [Ru(bpy)(L)₂](X)_n

[Ru(bpy)(N'',N'''-Dimethyl-2,2':4,4'':4',4'''-quaterpyridinium)]₂(PF₆)₆: Ru(bpy)(CO)₂Cl₂ (120 mg, 0.30 mmol), (N'',N'''-Dimethyl-2,2':4,4'':4',4'''-quaterpyridinium)(PF₆)₂ (441.1 mg, 0.7 mmol) and trimethylamine-*N*-oxide (210 mg, 1.83 mmol) were added to a round bottomed flask and the vessel purged with argon. Sparged 2-methoxyethanol (10 mL) was then added via syringe and the mixture heated at reflux for 24 h.

Yield: Dark red powder, 108.5 mg (21 %). **¹H-NMR**: δ_H (400 MHz, CD₃CN) 9.04 (2H, t, *J* = 1.9 Hz), 8.82 (2H, d, *J* = 6.6 Hz), 8.81 (2H, d, *J* = 6.6 Hz), 8.59 (1H, d, *J* = 8.4 Hz), 8.44 (2H, d, *J* = 7.2

Hz), 8.42 (2H, d, $J = 7.2$ Hz), 8.16 (1H, td, $J = 8.0, 1.4$ Hz), 8.09 (1H, d, $J = 6.2$ Hz), 8.04 (1H, d, $J = 6.2$ Hz), 7.87-7.81 (3H, m), 7.49 (1H, ddd, $J = 7.6, 5.8, 1.2$ Hz), 4.39 (3H, s), 4.38 (3H, s) ppm. **Anal. Calcd (%)** for $C_{54}H_{48}F_{36}N_{10}P_6Ru$; C, 35.88; H, 2.68; N, 7.75. Found C, 35.69; H, 2.52; N 7.50.

[Ru(bpy)(N'',N'''-Dimethyl-2,2':4,4'':4',4'''-quaterpyridinium)₂]Cl₆: To a solution of [Ru(bpy)(Me₂qpy)₂](PF₆)₆ in acetone, an excess of solid tetra-*n*-butyl ammonium chloride was added and the precipitate collected by vacuum filtration. The filtrand was washed with acetone and diethyl ether then dried *in vacuo* to give the chloride salt in near quantitative yields.

¹H-NMR: δ_H (400 MHz, CD₃OD) 9.75 (2H, dd, $J = 4.9, 1.5$ Hz), 9.13 (4H, t, $J = 6.9$ Hz), 8.85 (4H, dd, $J = 6.9, 4.8$ Hz), 8.82 (1H, d, $J = 8.1$ Hz), 8.31 (1H, d, $J = 6.1$ Hz), 8.23 (1H, td, $J = 7.9, 1.4$ Hz), 8.17-8.11 (3H, m), 8.02 (1H, d, $J = 4.9$ Hz), 7.59 (1H, ddd, $J = 7.6, 5.8, 1.2$ Hz), 4.51 (3H,s), 4.49 (3H,s) ppm.

2.3.4. Synthesis of Monometallic Iridium Complexes

2.3.4.1. Synthesis of complexes of the general formula [Ir(ppy)₂(L)]X_n

[Ir(ppy)₂(2,2':4,4'':4',4'''-quaterpyridine)]PF₆: To a round bottomed flask [Ir(ppy)₂Cl]₂ (40.0 mg, 0.037 mmol) and 2,2':4,4'':4',4'''-quaterpyridine (26 mg, 0.083 mmol) were added and the vessel purged an inert atmosphere. An argon-sparged solution of 2-methoxyethanol (10 mL) was added via syringe and the mixture heated at reflux for 20 h. After cooling, solvents were removed by rotary evaporation and the residue redissolved in a minimum volume of methanol to which was added an excess of solid NH₄PF₆. Cold deionized water was added and precipitate was collected by filtration and washed with water. The product was purified by column chromatography (SiO₂, 0.1M NH₄PF₆ MeCN).

Yield: Pale orange solid, 54.2 mg, (76 %). **¹H-NMR**: δ_H (400 MHz, CD₃CN) 8.96, (2H, dd, $J = 1.8, 0.4$ Hz), 8.81 (4H, dd, $J = 4.5, 1.7$ Hz), 8.10-8.09 (4H, m), 7.89-7.82 (10H, m), 7.69 (2H, ddd, $J = 5.9, 1.5, 0.8$ Hz), 7.10-7.04 (4H, m), 6.96 (2H, td, $J = 7.4, 1.4$ Hz), 6.32 (2H, dt, $J = 7.6, 0.6$ Hz) ppm. **ES-MS (*m/z*)**: 810 [M-PF₆]⁺. **Anal. Calcd (%)** for $C_{42}H_{30}F_6IrN_6P \cdot 0.5H_2O$; C, 52.28; H, 3.24; N, 8.71. Found C, 52.11; H, 2.89; N, 8.55.

[Ir(ppy)₂(N'',N'''-Dimethyl-2,2':4,4'':4',4'''-quaterpyridinium)](PF₆)₃: This compound was prepared as above by using [(2-Pym)₂Qpy]Cl₂ (44.2 mg, 0.08 mmol) in place of 2,2':4,4'':4',4'''-quaterpyridine.

Yield: Pale red solid, 73.8 mg (78 %). **¹H-NMR**: δ_H (400 MHz, CD₃CN) 9.03 (2H, d, $J = 1.4$ Hz), 8.82 (4H, d, $J = 6.6$ Hz), 8.42 (4H, d, $J = 6.8$ Hz), 8.23 (2H, d, $J = 5.8$ Hz), 8.11 (2H, d, $J = 8.0$ Hz), 7.93-7.84 (6H, m), 7.67 (2H, d, $J = 5.8$ Hz), 7.12-7.04 (4H, m), 6.98 (2H, td, $J = 7.4, 1.3$ Hz), 6.30 (2H, dd, $J = 7.5, 0.8$ Hz), 4.38 (6H, s) ppm. **ES-MS (*m/z*)**: 493 [M-2PF₆]²⁺. **Anal. Calcd (%)** for formula $C_{44}H_{36}F_{18}IrN_6P_3 \cdot 1H_2O$ C, 40.84; H, 2.96; N, 6.49. Found C, 40.92; H, 2.74; N 6.22.

{[Ir(ppy)₂(N'',N'''-Di(2-pyrimidyl)-2,2':4,4'':4',4''''-quaterpyridinium)](PF₆)₃}: This compound was prepared as above by using [Me₂Qpy]Cl₂ (33.7, 0.08 mmol) in place of 2,2':4,4'':4',4''''-quaterpyridine.

Yield: Brown-green solid, 68.4 mg (65 %). **¹H-NMR:** δ_H (400 MHz, CD₃CN) 10.12 (4H, dd, *J* = 7.5, 1.9 Hz), 9.18 (2H, d, *J* = 1.4 Hz), 9.13 (4H, d, *J* = 4.9 Hz), 8.68 (4H, dd, *J* = 7.4, 1.8 Hz), 8.31 (2H, d, *J* = 5.6 Hz), 8.13 (2H, dt, *J* = 8.1, 0.8 Hz), 8.05 (2H, dd, *J* = 5.7, 1.8 Hz), 7.93-7.87 (8H, m), 7.71 (2H, ddd, *J* = 5.9, 1.5, 0.7 Hz), 7.14-6.98 (8H, m), 6.33 (2H, dd, *J* = 7.6, 0.9 Hz) ppm. **MALDI-MS (*m/z*):** 1405 [M+H]⁺, 1260 [(M-PF₆)+H]⁺, 1115 [(M-2PF₆)+H]⁺, 970 [(M-3PF₆)+H]⁺. **Anal. Calcd (%)** for formula C₅₀H₃₆F₁₈IrN₁₀P₃·0.5H₂O; C, 42.50; H, 2.64; N, 9.91. Found C, 42.04; H, 2.48; N 9.56.

[Ir(ppy)₂(N'',N'''-Dimethyl-2,2':4,4'':4',4''''-quaterpyridinium)]Cl₃: This compound was prepared in near quantitative yields on dissolution of the corresponding hexafluorophosphate salt in acetone and subsequent addition of an excess of solid tetra-*n*-butyl ammonium chloride. The precipitate was collected by filtration, washed with acetone and dried *in vacuo*.

¹H-NMR: δ_H (400 MHz, CD₃OD) 9.84 (2H, d, *J* = 1.6 Hz), 9.11-9.10 (4H, m), 8.91 (4H, d, *J* = 7.0 Hz), 8.28 (2H, d, *J* = 5.7 Hz), 8.18 (2H, d, *J* = 8.2 Hz), 8.15 (2H, dd, *J* = 5.9, 1.9 Hz), 7.92-7.88 (4H, m), 7.78 (2H, d, *J* = 5.9 Hz), 7.10-7.07 (4H, m), 6.95 (2H, td, *J* = 7.5, 1.3 Hz), 6.33 (2H, dd, *J* = 7.7, 0.8 Hz), 4.49 (6H, s) ppm. **MALDI-MS (*m/z*):** 877 [M-2Cl]⁺, 842 [M-3Cl]⁺. **Anal. Calcd (%)** for C₄₄H₃₆Cl₂IrN₆·3H₂O; C, 52.77; H, 4.23; N, 8.39. Found C, 52.24; H, 4.10; N, 8.01.

{[Ir(ppy)₂(N'',N'''-Di(2-pyrimidyl)-2,2':4,4'':4',4''''-quaterpyridinium)]Cl₃}: This compound was prepared in a manner identical to that used for [Ir(ppy)₂(N'',N'''-Dimethyl-2,2':4,4'':4',4''''-quaterpyridinium)]Cl₃.

¹H-NMR: δ_H (400 MHz, CD₃OD) 10.36 (4H, d, *J* = 7.2 Hz), 9.93 (2H, d, *J* = 1.0 Hz), 9.21 (4H, dd, *J* = 5.2, 3.3 Hz), 9.13 (4H, d, *J* = 7.1 Hz), 8.38 (2H, d, *J* = 5.8 Hz), 8.29 (2H, dd, *J* = 5.8, 1.6 Hz), 8.21 (2H, d, *J* = 8.5 Hz), 7.94-7.90 (6H, m), 7.85 (2H, dd, *J* = 5.8, 0.6 Hz), 7.14-7.09 (4H, m), 6.98 (2H, t, *J* = 7.4 Hz), 6.35 (2H, d, *J* = 7.5 Hz) ppm. **ES-MS (*m/z*):** 1031 [M-PF₆]⁺, 501 [M-2PF₆]²⁺. **Anal. Calcd (%)** for C₅₀H₃₆Cl₂IrN₁₀·2H₂O; C, 54.03, H, 3.63; N, 12.60. Found C, 53.70; H, 3.46; N, 12.46.

2.3.6.1. Synthesis of complexes of the general formula [Ir(C[^]N)₂(L)]X_n

[Ir(1-Me-2,2'-bpy)₂(2,2'-bipyridine)](PF₆)₃, [Ir(22)₂Y](PF₆)₃:

[Ir(22)₂Cl]₂(PF₆)₄ (100 mg, 0.058 mmol), 2,2'-bipyridine (30 mg, 0.192 mmol) and silver hexafluorophosphate (37 mg, 0.146 mmol) were combined in a round bottomed flask and the vessel purged with an inert atmosphere. An argon-sparged solution of 2-methoxyethanol:H₂O (8:2, 15 mL) was added via syringe and the mixture heated at 100°C for 36 h. Upon cooling to room temperature the solution was filtered through celite to remove the silver chloride precipitate and the solvents removed by rotary evaporation. The residue was resuspended in

a minimum volume of acetone before addition of an excess of solid tetra-*n*-butyl ammonium chloride. The resultant precipitate was collected by filtration, washed with acetone and purified by column chromatography (Sephadex SP C-25; 0.025 M - 0.075 M NaCl, Acetone:H₂O (1:1)). The eluate was evaporated to dryness and the solid suspended in cold methanol followed by filtration to remove excess NaCl. Solvents were removed and the residue redissolved in cold water with the final product being isolated upon addition of NH₄PF₆ and subsequent filtration, the resultant solid was with ice-cold water then dried *in vacuo*.

Yield: Bright yellow powder, 76.5 mg (58 %). **¹H-NMR:** δ_H (400 MHz, CD₃CN) 8.60 (4H, d, *J* = 8.3 Hz), 8.42 (2H, dd, *J* = 6.0, 0.9 Hz), 8.26 (2H, td, *J* = 8.0, 1.5 Hz), 8.19 (2H, ddd, *J* = 8.6, 7.7, 1.6 Hz), 7.94 (2H, ddd, *J* = 5.5, 1.5, 0.7 Hz), 7.90 (2H, ddd, *J* = 5.7, 1.6, 0.6 Hz), 7.57 (2H, ddd, *J* = 7.7, 5.5, 1.3 Hz) 7.46 (2H, ddd, *J* = 7.7, 5.7, 1.2 Hz), 7.38 (2H, dd, *J* = 7.9, 6.0 Hz), 7.21 (2H, dd, *J* = 7.9, 1.3 Hz), 4.65 (6H, s) ppm. **ES-MS (*m/z*):** 417 [M-2PF₆]²⁺, 344 [M-3PF₆]²⁺, 230 [M-3PF₆]³⁺. **Anal. Calcd (%)** for C₃₂H₂₈F₁₈IrN₆P₃; C, 34.20; H, 2.51; N, 7.48. Found C, 33.76; H, 2.32; N 7.26.

[Ir(1-Me-2,2'-bpy)₂(4,4'-di-*tert*-butyl-2,2'-bipyridine)](PF₆)₃, [Ir(22)₂B](PF₆)₃:

This compound was prepared in a manner identical to [Ir(22)₂Y](PF₆)₃ instead using 4,4'-di-*tert*-butyl-2,2'-bipyridine (51.5 mg, 0.192 mmol) in place of 2,2'-bipyridine.

Yield: Canary yellow powder, 85.1 mg (59 %). **¹H-NMR:** δ_H (400 MHz, CD₃CN) 8.61 (2H, d, *J* = 8.6 Hz), 8.54 (2H, d, *J* = 1.7 Hz), 8.42 (2H, dd, *J* = 6.0, 0.9 Hz), 8.19 (2H, ddd, *J* = 8.6, 7.7, 1.5 Hz), 7.88 (2H, dd, *J* = 5.7, 1.0 Hz), 7.79 (2H, d, *J* = 5.9 Hz), 7.51-7.46 (4H, m), 7.37 (2H, dd, *J* = 7.9, 6.0 Hz), 7.21 (2H, dd, *J* = 7.9, 1.1 Hz), 4.65 (6H, s), 1.42 (18H, s) ppm. **ES-MS (*m/z*):** 1092 [M-PF₆]⁺, 472 [M-2PF₆]²⁺, 267 [M-3PF₆]³⁺. **Anal. Calcd (%)** for C₄₀H₄₄F₁₈IrN₆P₃; C, 38.87; H, 3.59; N, 6.80. Found C, 38.36; H, 3.12; N 6.51.

[Ir(1-Me-2,2'-bpy)₂(4,4'-di-trifluoromethyl-2,2'-bipyridine)](PF₆)₃, [Ir(22)₂F](PF₆)₃:

This compound was prepared in a manner identical to [Ir(22)₂Y](PF₆)₃ instead using 4,4'-di-trifluoromethyl-2,2'-bipyridine (56.9 mg, 0.192 mmol) in place of 2,2'-bipyridine.

Yield: Yellow powder, 71.1 mg (48 %). **¹H-NMR:** δ_H (400 MHz, CD₃CN) 9.04 (2H, s) 8.62 (2H, d, *J* = 8.5 Hz), 8.45 (2H, dd, *J* = 6.1, 0.9 Hz), 8.23-8.19 (4H, m), 7.91-7.87 (4H, m), 7.47 (2H, ddd, *J* = 7.7, 5.8, 1.2 Hz), 7.41 (2H, dd, *J* = 7.9, 6.0 Hz), 7.18 (2H, dd, 7.9, 1.2 Hz), 4.66 (6H, s) ppm. **ES-MS (*m/z*):** 1115 [M-PF₆]⁺, 485 [M-2PF₆]²⁺, 275 [M-3PF₆]³⁺. **Anal. Calcd (%)** for C₃₄H₂₆F₂₄IrN₆P₃; C, 32.42; H, 2.08; N, 6.67. Found C, 32.28; H, 1.64; N 6.65.

[Ir(1-Me-3,2'-bpy)₂(2,2'-bipyridine)](PF₆)₃, [Ir(32)₂Y](PF₆)₃: This compound was prepared in a manner identical to [Ir(22)₂Y](PF₆)₃ instead using {[Ir(32)₂Cl]₂}(PF₆)₄ in place of {[Ir(22)₂Cl]₂}(PF₆)₄.

Yield: Yellow-cream powder, 54.0 mg (41 %). **¹H-NMR:** δ_H (400 MHz, CD₃CN) 8.84 (2H, s), 8.60 (2H, d, *J* = 8.3 Hz), 8.29-8.24 (4H, m), 8.17 (2H, t, *J* = 8.5 Hz), 7.88 (2H, d, *J* = 5.5 Hz), 7.77-7.73 (4H, m), 7.58 (2H, t, *J* = 6.6 Hz) 7.41 (2H, t, *J* = 7.3 Hz), 6.87 (2H, d, *J* = 6.4 Hz), 4.12 (6H, s) ppm.

ES-MS (*m/z*): 979 [M-PF₆]⁺, 417 [M-2PF₆]²⁺, 230 [M-3PF₆]³⁺. **Anal. Calcd (%)** for C₃₂H₂₈F₁₈IrN₆P₃; C, 34.20; H, 2.51; N, 7.48. Found C, 33.93; H, 2.12; N 7.44.

[Ir(1-Me-3,2'-bpy)₂(4,4'-di-*tert*-butyl-2,2'-bipyridine)](PF₆)₃, [Ir(32)₂B](PF₆)₃: This compound was prepared in a manner identical to [Ir(22)₂B](PF₆)₃ instead using {[Ir(32)₂Cl]₂}(PF₆)₄ in place of {[Ir(22)₂Cl]₂}(PF₆)₄.

Yield: Yellow-cream powder, 41.3 mg (29 %). **¹H-NMR:** δ_H (400 MHz, CD₃CN) 8.85 (2H, s), 8.54 (2H, d, *J* = 1.8 Hz), 8.29 (2H, d, *J* = 8.2 Hz), 8.17 (2H, td, *J* = 7.9, 1.5 Hz), 7.79-7.69 (6H, m), 7.51 (2H, d, *J* = 5.9, 2.0 Hz), 7.43 (2H, ddd, *J* = 7.5, 5.9, 1.5 Hz), 6.86 (2H, d, *J* = 6.3 Hz), 4.12 (6H, s), 1.42 (18H, s) ppm. **ES-MS (*m/z*):** 1091 [M-PF₆]⁺, 472 [M-2PF₆]²⁺, 267 [M-3PF₆]³⁺. **Anal. Calcd (%)** for C₄₀H₄₄F₁₈IrN₆P₃; C, 38.87; H, 3.59; N, 6.80. Found C, 38.35; H, 3.42; N 6.66.

[Ir(1-Me-3,2'-bpy)₂(4,4'-di-trifluoromethyl-2,2'-bipyridine)](PF₆)₃, [Ir(32)₂F](PF₆)₃: This compound was prepared in a manner identical to [Ir(22)₂F](PF₆)₃ instead using {[Ir(32)₂Cl]₂}(PF₆)₄ in place of {[Ir(22)₂Cl]₂}(PF₆)₄.

Yield: Yellow-cream powder, 42.0 (28 %). **¹H-NMR:** δ_H (400 MHz, CD₃CN) 9.04 (2H, d, *J* = 0.6 Hz), 8.86 (2H, d, *J* = 0.6 Hz), 8.28 (2H, ddd, *J* = 8.1, 1.4, 0.7 Hz), 8.19 (2H, td, *J* = 7.9, 1.4 Hz), 8.13 (2H, d, *J* = 5.8 Hz), 7.89 (2H, dd, *J* = 5.8, 1.2 Hz), 7.79 (2H, dd, *J* = 6.4, 1.3 Hz), 7.74 (2H, ddd, *J* = 5.8, 1.4, 0.7 Hz), 7.42 (2H, ddd, *J* = 7.5, 5.9, 1.5 Hz), 6.84 (2H, d, *J* = 6.3 Hz), 4.14 (6H, s) ppm. **ES-MS (*m/z*):** 1115 [M-PF₆]⁺, 485 [M-2PF₆]²⁺, 275 [M-3PF₆]³⁺. **Anal. Calcd (%)** for C₃₄H₂₆F₂₄IrN₆P₃; C, 32.42; H, 2.08; N, 6.67. Found C, 32.16; H, 1.72; N 6.51.

[Ir(1-Me-4,2'-bpy)₂(bpy)](PF₆)₃, [Ir(42)₂Y](PF₆)₃: This compound was prepared in a manner identical to [Ir(22)₂Y](PF₆)₃ instead using {[Ir(42)₂Cl]₂}(PF₆)₄ in place of {[Ir(22)₂Cl]₂}(PF₆)₄.

Yield: Bright yellow powder, 73.0 mg (56 %). **¹H-NMR:** δ_H (400 MHz, CD₃CN) 8.59 (2H, d, *J* = 8.2 Hz), 8.44 (2H, d, *J* = 8.0 Hz), 8.32 (2H, d, *J* = 6.6 Hz), 8.27-8.23 (4H, m), 8.16 (2H, t, *J* = 8.2 Hz), 8.01 (2H, d, *J* = 5.6 Hz), 7.73 (2H, d, *J* = 5.6 Hz), 7.56 (2H, t, *J* = 6.7 Hz), 7.44 (2H, t, 6.7 Hz), 7.26 (2H, s), 4.01 (6H, s) ppm. **ES-MS (*m/z*):** 979 [M-PF₆]⁺, 417 [M-2PF₆]²⁺, 230 [M-3PF₆]³⁺. **Anal. Calcd (%)** for C₃₂H₂₈F₁₈IrN₆P₃; C, 34.20; H, 2.51; N, 7.48. Found C, 33.73; H, 2.41; N, 7.32.

[Ir(1-Me-4,2'-bpy)₂(4,4'-di-*tert*-butyl-2,2'-bipyridine)](PF₆)₃, [Ir(42)₂B](PF₆)₃: This compound was prepared in a manner identical to [Ir(22)₂B](PF₆)₃ instead using {[Ir(1-Me-4,2'-bpy)₂Cl]₂}(PF₆)₄ in place of {[Ir(22)₂Cl]₂}(PF₆)₄.

Yield: Canary yellow powder, 45.4 mg (32 %). **¹H-NMR:** δ_H (400 MHz, CD₃CN) 8.53 (2H, d, *J* = 1.7 Hz), 8.44 (2H, d, *J* = 8.1 Hz), 8.31 (2H, dd, *J* = 6.5, 1.4 Hz), 8.25 (2H, d, *J* = 6.4 Hz), 8.16 (2H, td, *J* = 7.9, 1.4 Hz), 7.88 (2H, d, *J* = 5.9 Hz), 7.72 (2H, d, *J* = 5.9 Hz), 7.72 (2H, d, *J* = 5.8 Hz), 7.50-7.45 (4H, m), 7.25 (2H, s), 4.01 (6H, s), 1.42 (18H, s) ppm. **ES-MS (*m/z*):** 1091 [M-PF₆]⁺, 472

$[\text{M-2PF}_6]^{2+}$, 267 $[\text{M-3PF}_6]^{3+}$ **Anal. Calcd (%)** for $\text{C}_{40}\text{H}_{44}\text{F}_{18}\text{IrN}_6\text{P}_3$; C, 38.87; H, 3.59; N, 6.80. Found C, 38.09; H, 3.64; N 6.78.

$[\text{Ir(1-Me-2,4'-bpy)}_2(4,4'\text{-di-trifluoromethyl-2,2'-bipyridine})](\text{PF}_6)_3$, $[\text{Ir(42)}_2\text{F}](\text{PF}_6)_3$:

This compound was prepared in a manner identical to $[\text{Ir(22)}_2\text{F}](\text{PF}_6)_3$ instead using $\{[\text{Ir(42)}_2\text{Cl}]_2\}(\text{PF}_6)_4$ in place of $\{[\text{Ir(22)}_2\text{Cl}]_2\}(\text{PF}_6)_4$.

Yield: Yellow powder, 63.1 mg (43 %). **$^1\text{H-NMR}$:** δ_{H} (400 MHz, CD_3CN) 9.03 (2H, d, $J = 0.7$ Hz), 8.45 (2H, dd, $J = 8.2, 0.7$ Hz), 8.35 (2H, dd, $J = 6.4, 1.0$ Hz), 8.28 (2H, d, $J = 5.7$ Hz), 8.27 (2H, d, $J = 6.4$ Hz), 8.18 (2H, td, $J = 7.9, 1.4$ Hz), 7.88 (2H, dd, $J = 5.8, 1.2$ Hz), 7.75 (2H, ddd, $J = 5.8, 1.4, 0.7$ Hz), 7.45 (2H, ddd, $J = 7.6, 5.9, 1.6$ Hz), 7.23 (2H, s), 4.02 (6H, s) ppm. **ES-MS (m/z):** 412 $[\text{M-3PF}_6]^{2+}$, 275 $[\text{M-3PF}_6]^{3+}$. **Anal. Calcd (%)** for $\text{C}_{34}\text{H}_{26}\text{F}_{24}\text{IrN}_6\text{P}_3$; C, 32.42; H, 2.08; N, 6.67. Found C, 32.26; H, 1.69; N 6.64.

$[\text{Ir(22)}_2\text{Y}]\text{Cl}_3$: This compound was prepared by metathesis of the analogous complex as the hexafluorophosphate salt. On dissolution in acetone, an excess of solid tetra-*n*-butyl ammonium chloride was added and the precipitate collected by vacuum filtration. The filtrand was washed with acetone and diethyl ether then dried *in vacuo* to give the chloride salt in near quantitative yields.

$^1\text{H-NMR}$: δ_{H} (400 MHz, $(\text{CD}_3)_2\text{SO}$) 8.99 (2H, d, $J = 8.4$ Hz), 8.90 (2H, d, $J = 5.1$ Hz), 8.86 (2H, d, $J = 8.6$ Hz), 8.37 (2H, td, $J = 7.9, 1.4$ Hz), 8.29 (2H, td, $J = 8.2, 1.4$ Hz), 7.99 (4H, m), 7.66 (2H, ddd, $J = 7.5, 5.6, 1.2$ Hz), 7.60-7.56 (4H, m), 7.17 (2H, dd, $J = 7.8, 0.9$ Hz), 4.80 (6H, s) ppm. **ES-MS (m/z):** 344 $[\text{M-3Cl}]^{2+}$, 230 $[\text{M-3Cl}]^{3+}$. **Anal. Calcd (%)** for $\text{C}_{32}\text{H}_{28}\text{Cl}_2\text{IrN}_6 \cdot 4\text{H}_2\text{O}$; C, 44.32; H, 4.18; N, 9.69. Found C, 44.08; H, 4.00; N 9.46.

$[\text{Ir(22)}_2\text{B}]\text{Cl}_3$: This compound was prepared in a manner identical to that used for $[\text{Ir(22)}_2\text{Y}](\text{Cl})_3$.

$^1\text{H-NMR}$: δ_{H} (400 MHz, $(\text{CD}_3)_2\text{SO}$) 9.00 (2H, s), 8.92 (2H, d, $J = 5.9$ Hz), 8.87 (2H, d, $J = 8.7$ Hz), 8.30 (2H, t, $J = 8.2$ Hz), 7.96 (2H, d, $J = 5.2$ Hz), 7.87 (2H, d, $J = 5.9$ Hz), 7.63-7.56 (6H, m), 7.07 (2H, d, $J = 7.9$ Hz), 4.81 (6H, s), 1.42 (18H, s) ppm. **ES-MS (m/z):** 400 $[\text{M-3Cl}]^{2+}$, 267 $[\text{M-3Cl}]^{3+}$. **Anal. Calcd (%)** for $\text{C}_{40}\text{H}_{44}\text{Cl}_2\text{IrN}_6 \cdot 2.5\text{H}_2\text{O}$; C, 50.44; H, 5.19; N, 8.82. Found C, 50.20; H, 5.55; N 8.80.

$[\text{Ir(22)}_2\text{F}](\text{Cl})_3$: This compound was prepared in a manner identical to that used for $[\text{Ir(22)}_2\text{Y}](\text{Cl})_3$.

$^1\text{H-NMR}$: δ_{H} (400 MHz, $(\text{CD}_3)_2\text{SO}$) 9.70 (2H, s), 8.96 (2H, d, $J = 5.6$ Hz), 8.87 (2H, d, $J = 8.8$ Hz), 8.31-8.28 (4H, m), 8.08 (2H, d, $J = 5.4$ Hz), 8.03 (2H, d, $J = 4.9$ Hz), 7.61 (2H, t, $J = 6.9$ Hz), 7.56 (2H, t, $J = 6.3$ Hz), 7.05 (2H, d, $J = 7.9$ Hz), 4.82 (6H, s) ppm. **ES-MS (m/z):** 895 $[\text{M-Cl}]^+$, 430 $[\text{M-2Cl}]^{2+}$, 413 $[\text{M-3Cl}]^{2+}$, 275 $[\text{M-3Cl}]^{3+}$. **Anal. Calcd (%)** for $\text{C}_{34}\text{H}_{26}\text{Cl}_2\text{F}_6\text{IrN}_6 \cdot 1.5\text{H}_2\text{O}$; C, 42.57; H, 3.15; N, 8.76. Found C, 42.15; H, 2.97; N 8.40.

[Ir(32)₂Y]Cl₃: This compound was prepared in a manner identical to that used for [Ir(22)₂Y](Cl)₃.

¹H-NMR: δ_H (400 MHz, (CD₃)₂SO) 9.85 (2H, s), 9.01 (2H, d, *J* = 8.2 Hz), 8.76 (2H, d, *J* = 7.9 Hz), 8.39 (2H, t, *J* = 7.8 Hz), 8.32 (2H, t, *J* = 7.9 Hz), 8.17 (2H, d, *J* = 6.9 Hz), 7.98 (2H, d, *J* = 4.7 Hz), 7.84 (2H, d, *J* = 5.5 Hz), 7.68 (2H, t, *J* = 6.5 Hz), 7.52 (2H, t, *J* = 6.5 Hz), 6.83 (2H, d, *J* = 6.3 Hz), 4.19 (6H, s) ppm. **ES-MS (*m/z*):** 362 [M-2Cl]²⁺, 344 [M-3Cl]²⁺, 230 [M-3Cl]³⁺. **Anal. Calcd (%)** for C₃₂H₂₈Cl₂IrN₆·2.5H₂O; C, 45.74; H, 3.96; N, 10.00. Found C, 45.57; H, 4.02; N 9.92.

[Ir(32)₂B]Cl₃: This compound was prepared in a manner identical to that used for [Ir(22)₂Y](Cl)₃.

¹H-NMR: δ_H (400 MHz, (CD₃)₂SO) 9.78 (2H, s), 8.99 (2H, d, *J* = 1.9 Hz), 8.73 (2H, d, *J* = 8.2), 8.33 (2H, td, *J* = 7.9, 1.3 Hz), 8.15 (2H, dd, *J* = 6.5, 0.9 Hz), 7.86 (2H, d, *J* = 5.9 Hz), 7.82 (2H, d, *J* = 5.7 Hz), 7.56-7.53 (4H, m), 6.80 (2H, d, 6.3 Hz), 4.18 (6H, s), 1.41 (18H, s) ppm. **ES-MS (*m/z*):** 418 [M-2Cl]²⁺, 400 [M-3Cl]²⁺, 267 [M-3Cl]³⁺. **Anal. Calcd (%)** for C₄₀H₄₄Cl₂IrN₆·2.5H₂O; C, 50.44; H, 5.19; N, 8.82. Found C, 50.21; H, 5.34; N 8.59.

[Ir(32)₂F]Cl₃: This compound was prepared in a manner identical to that used for [Ir(22)₂Y](Cl)₃.

¹H-NMR: δ_H (400 MHz, (CD₃)₂SO) 9.85 (2H, s), 9.69 (2H, s), 8.75 (2H, d, *J* = 8.1 Hz), 8.33 (2H, t, *J* = 7.6 Hz), 8.27 (2H, d, *J* = 5.6 Hz), 8.20 (2H, d, *J* = 6.2 Hz), 8.01 (2H, d, *J* = 5.6 Hz), 7.95 (2H, d, *J* = 5.6 Hz), 7.50 (2H, t, *J* = 6.5 Hz), 6.77 (2H, d, *J* = 6.3 Hz), 4.20 (6H, s) ppm. **ES-MS (*m/z*):** 895 [M-Cl]⁺, 430 [M-2Cl]²⁺, 275 [M-3Cl]³⁺. **Anal. Calcd (%)** for C₃₄H₂₆Cl₂F₆IrN₆·2H₂O; C, 42.22; H, 3.13; N, 8.69. Found C, 41.96; H, 3.07; N 8.51.

[Ir(42)₂Y]Cl₃: This compound was prepared in a manner identical to that used for [Ir(22)₂Y](Cl)₃.

¹H-NMR: δ_H (400 MHz, (CD₃)₂SO) 8.98 (2H, d, *J* = 8.2 Hz), 8.84 (2H, d, *J* = 8.2 Hz), 8.79 (2H, d, *J* = 6.5 Hz), 8.74 (2H, d, *J* = 6.4 Hz), 8.37 (2H, td, *J* = 8.0, 1.3 Hz), 8.29 (2H, td, *J* = 7.9, 1.3 Hz), 8.08 (2H, d, *J* = 5.5 Hz), 7.80 (2H, d, *J* = 5.5 Hz), 7.67 (2H, td, *J* = 6.6, 0.82 Hz), 7.56-7.53 (4H, m), 4.11 (6H, s) ppm. **ES-MS (*m/z*):** 362 [M-2Cl]²⁺, 344 [M-3Cl]²⁺, 230 [M-3Cl]³⁺. **Anal. Calcd (%)** for C₃₂H₂₈Cl₂IrN₆·2H₂O; C, 46.24; H, 3.88; N, 10.11. Found C, 45.90; H, 3.84; N 10.00.

[Ir(42)₂B]Cl₃: This compound was prepared in a manner identical to that used for [Ir(22)₂Y](Cl)₃.

¹H-NMR: δ_H (400 MHz, (CD₃)₂SO) 8.95 (2H, d, *J* = 1.6 Hz), 8.82 (2H, d, *J* = 7.9 Hz), 8.77 (2H, d, *J* = 6.3 Hz), 8.70 (2H, d, *J* = 6.4 Hz), 8.30 (2H, td, *J* = 7.9, 1.3 Hz), 7.94 (2H, d, *J* = 6.0 Hz), 7.77 (2H, d, *J* = 5.8 Hz), 7.60-7.56 (4H, m), 7.49 (2H, s), 4.10 (6H, s), 1.42 (18H, s) ppm. **ES-MS (*m/z*):** 400 [M-3Cl]²⁺, 267 [M-3Cl]³⁺. **Anal. Calcd (%)** for C₄₀H₄₄Cl₂IrN₆·3H₂O; C, 49.97; H, 5.24; N, 8.74. Found C, 49.54; H, 5.42; N 8.72.

[Ir(42)₂F]Cl₃: This compound was prepared in a manner identical to that used for [Ir(22)₂Y](Cl)₃.

¹H-NMR: δ_H (400 MHz, (CD₃)₂SO) 9.67 (2H, s), 8.82 (4H, t, *J* = 8.0 Hz), 8.74 (2H, d, *J* = 6.5 Hz), 8.38 (2H, d, *J* = 5.8 Hz), 8.30 (2H, t, *J* = 7.3 Hz), 8.03 (2H, d, *J* = 5.8 Hz), 7.90 (2H, d, *J* = 5.4 Hz), 7.52 (2H, t, *J* = 6.7 Hz), 7.46 (2H, s), 4.11 (6H, s) ppm. **ES-MS (*m/z*)**: 895 [M-Cl]⁻, 430 [M-2Cl]²⁺, 413 [M-3Cl]²⁺, 275 [M-3Cl]³⁺. **Anal. Calcd (%)** for C₃₄H₂₆Cl₂F₆IrN₆·1.5H₂O; C, 42.62; H, 3.05; N, 8.77. Found C, 42.37; H, 3.18; N 8.64.

2.4 Procedures In Molecular Biology

2.4.1. Media and Buffer Solutions

LB Media: Bacto-Tryptone (10 g), Bacto-Yeast extract (5 g), and NaCl (10 g) were dissolved in deionized H₂O (900 mL) and pH was adjusted to 7.0 using 1 M NaOH. The total volume adjusted to 1 L with distilled water and sterilized by autoclaving.

TB Auto-induction media: The powdered medium (55.85 g) was dissolved in deionized H₂O (1 L) and sterilized by autoclave. The medium was used as provided by the supplier, containing tryptone (12 g), yeast extract (24 g), (NH₄)₂SO₄ (3.3 g), KH₂PO₄ (6.8 g) Na₂HPO₄ (7.1 g), Glucose (0.5 g), α -lactose (2.0 g) and MgSO₄ (0.15 g).

Super Optimal Broth with Catabolite Repression (SOC) Medium: Bacto-Tryptone (20 g), Bacto-Yeast extract (5 g), NaCl (0.5 g), 1 M KCl(aq) (2.5 mL), sterile 1 M MgCl₂ (10 mL), and 1 M glucose (20 mL) were added to distilled water (900 mL). On complete dissolution the pH was adjusted to 7.0 using 1 M NaOH and the total volume adjusted to 1 L with deionized H₂O before sterilization by autoclaving.

TAE Buffer: Tris (48.4 g) was dissolved in deionized H₂O (500 mL), to which was added 0.5M Na₂EDTA (100 mL, pH 8) and glacial acetic acid (57.1 mL). The volume was adjusted to 1 L using deionized H₂O and stored at room temperature.

10X SDS Buffer: SDS (10 g), Tris (30.3 g) and glycine (144.1 g) were dissolved in deionized H₂O (800 mL). On complete dissolution the volume was adjusted to 1 L with deionized H₂O and stored at room temperature.

1X Native Gel Running Buffer: Glycine (14.41 g) was dissolved in deionized H₂O (800 mL) followed by addition of 1 M Tris (25 mL, pH 8.3). On complete dissolution the volume was adjusted to 1 L with deionized H₂O.

10X Agarose Gel Sample Buffer: Bromophenol blue (250 mg) was dissolved in 150 mM Tris (33 mL, pH 8), followed by the addition of glycerol (60 mL) and deionized H₂O (7 mL).

5X SDS-PAGE Sample Buffer: Glycerol (4 mL), 1 M Tris (2.5 mL, pH 6.8), SDS (0.82 g), β -mercaptoethanol (0.5 mL) and bromophenol blue (5 mg) were mixed together and the volume adjusted to 10 mL with deionized H₂O. The mixture was aliquoted into 100 μ L samples and stored at -20°C.

2X Native PAGE Sample Buffer: 1 M Tris (0.625 mL, pH 6.8), glycerol (4 mL) and 2.5 % bromophenol blue (40 μ L) were mixed together and the volume adjusted to 10 mL with deionized H₂O. The mixture was aliquoted into 1 mL samples and stored at -20°C.

2.4.2. Mutant Strand Synthesis

The reaction mixtures were prepared in a thin-walled tube and were comprised of 10x QuikChange Multi reaction buffer (5 μ L), $MgSO_4$ (2 μ L, 25 mM), template DNA (0.5 μ L, 20 ng/ μ L), dNTP (5 μ L, 10 mM), KOD polymerase (1 μ L, 1U/ μ L), dd H₂O (30.5 μ L) and where applicable DMSO (1 μ L). To the final mixture 3 μ L of both the forward and reverse direction primers (5 μ M) were added. The samples were loaded into a Techne TC512 thermal cycler and the parameters set appropriately for each reaction, as discussed in section 5.2.1.1. Removal of non-mutated template DNA was then achieved by digestion via the addition of *Dpn* I restriction enzyme (1 μ L). The mixture was thoroughly mixed by pipette before being spun down in a microcentrifuge for 1 minute and immediately incubated at 37°C for 1 hour. The resultant DNA was either frozen at - 20°C or purified and isolated by gel electrophoresis and subsequent extraction.

2.4.3. DNA Agarose Gel Electrophoresis

Agarose gel (0.6% v/v) was prepared by addition of agarose (6.0 g) to 1X TAE (100 mL) and heating to dissolution using a microwave. Ethidium bromide (5 μ L, 0.5 μ g/mL) was then added and the gel allowed to cool slightly, prior to being poured into the cast and left to set. The wells were loaded with 15 μ L sample, containing DNA (13.5 μ L) and 10X agarose gel sample buffer (1.5 μ L). A sample of 1kB DNA ladder was also loaded onto each gel. The gel was run at 100 mV for 20 minutes before the bands were visualized on exposure to UV light using a transilluminator.

2.4.4. DNA Purification - Gel Extraction

DNA gel extraction was carried out according to the QIAquick® Gel Extraction protocol and using the buffer solutions provided by the manufacturer. The DNA band of approximately correct molecular weight was excised from the gel using a clean sharp scalpel. Excess agarose was removed and the sample weighed prior to being dissolved in 3 volumes (w/v) of the QG buffer. The sample was incubated at 50°C for *ca.* 10 min or until complete dissolution had been attained. If required pH was readjusted on addition of sodium acetate (10 μ L, 3.0 M, pH 5.0). One gel volume (w/v) of isopropanol was added and the sample thoroughly agitated prior to loading onto a QIAquick® spin column set into a 2 mL collection tube. The sample was centrifuged at 13300 rpm for 1 min and the eluate discarded. The column was washed with the QG buffer (500 μ L) and subsequently the PE buffer (750 μ L) by centrifugation at 13300 rpm for 1 min, removing the eluate from the collection tube between each run. Additional centrifugation was performed to remove any remaining traces of ethanol from buffer PE. The column was set in a clean collection tube and the DNA eluted on addition of the EB buffer (50 μ L) with subsequent centrifugation at 13300 rpm for 1 min.

2.4.5. DNA Quantitation

DNA concentration was quantified using the Qubit® dsDNA BR assay kit using a Qubit® 2.0 Fluorometer and the reagents provided by the manufacturer, which were equilibrated to room temperature prior to use. The working solution was prepared in a clean plastic tube on dilution of the Qubit® dsDNA BR reagent by a factor of 200. Samples were prepared on addition of DNA (1-20 µL) to 500 µL clear assay tubes containing appropriate quantity of working solution to give a total volume of 200µL. Standard solutions were also prepared in a similar manner (10 µL Qubit® dsDNA BR #1 and #2, 0 and 10 ng/mL respectively). All samples were vortexed and incubated at room temperature for 2 min prior to analysis. The Qubit® Fluorometer was calibrated using the standard solutions before loading of the samples containing the DNA analyte. Final concentrations were determined using the following equation:

$$[\text{DNA}] = QF_{\text{val}} \times (200/x)$$

Where QF_{val} = value given by the Qubit® 2.0 Fluorometer and x = the number of microliters of sample added to the assay tube.

2.4.6. Transformation of *E. coli* cells.

XL-10 Gold ultracompetent cells were gradually thawed on ice before an aliquot of 45 µL was added to a pre-chilled eppendorf tube. β-mercaptoethanol (2.0 µL, 14.3 M) was added and the mixture incubated on ice for 10 min with gently agitation every 2 min. To this 1.0 µL of the appropriate DNA was added and the resultant mixture left to incubate on ice for a further 30 min. The samples were then heat-pulsed at 42°C for 30 seconds and then immediately placed on ice and left to cool for 2 min. SOC medium (0.45 mL) was added and the mixture incubated at 37°C with gentle shaking for 1 h. An appropriate volume of the transformation reaction was then plated onto agar plates containing 50 µg/mL ampicillin, which were inverted and incubated at 37°C overnight. Cultures were picked and inoculated in LB Media (4 mL, containing 1 µL/mL of ampicillin) and incubated at 37°C overnight. Glycerol stocks were prepared on combination of 0.5 mL of the resultant culture with an equal volume of to glycerol stock buffer (0.5 mL) before being quickly frozen and stored at -80°C. For transformation of *E. coli* JM109 competent cells the above procedure was implemented with the exception that the volume of β-mercaptoethanol and DNA used were change to 0.4 µL and 5 µL respectively.

2.4.7. Plasmid DNA purification – Mini-Prep

Plasmid DNA was purified using the QIAprep® Spin Miniprep kit implementing the procedure laid out by the manufacturer and using the buffer solutions provided. LB Media (4 mL, containing 1 µL/mL of ampicillin) was inoculated with a glycerol stock containing the appropriate transformed *E. coli* cells and incubated at 37°C overnight. The sample was then centrifuged at 13300 rpm and the supernatants discarded. The resultant pellet was

resuspended in the P1 buffer (250 μ L) also containing RNase (0.1 mg/mL) and LyseBlue (1 μ L/mL). The P2 buffer (250 μ L) was added and the sample gently agitated on inversion of the tube to give a viscous homogeneous suspension. Buffer N3 (350 μ L) was added and the sample mixed thoroughly to quench the lyase reaction. The lysate was centrifuged at 13300 rpm for 10 min and the supernatants loaded onto a QIAprep[®] spin column set into a 2 mL collection tube. DNA was bound to the column on centrifugation of the sample at 13300 rpm for 1 min and the resultant eluate discarded. The column was washed with the PB buffer (500 μ L) and subsequently with the PE buffer (750 μ L) by centrifuge at 13300 rpm for 1 min, removing the eluate from the collection tube between each run. An additional centrifugation step was performed to remove residual traces of the wash buffers. The column was set in a clean collection tube and the DNA eluted on addition of the EB buffer (40 μ L) upon centrifugation at 13300 rpm for 1 min. Plasmid DNA was stored at -80°C until such time as it was required.

2.4.8. SDS-PAGE

Samples were prepared on addition of 5X SDS-PAGE sample buffer (5 μ L) to the protein (25 μ L) prior to heating at 100°C for 5 minutes. The sample (5 μ L) and relevant protein ladder (10 μ L) were loaded onto a BioRad 10% Tris HCL precast polyacrylamide gel. The procedure was carried out using a Biorad Mini-PROTEAN[®] 3 module at 160 mV for 50 minutes in 1 X SDS buffer, prepared on dilution of a 10X stock solution. The gel was incubated in boiling Coomassie Brilliant Blue R-250 for 1 minute and destained via to a series of washes in boiling ddH₂O prior to final wash at room temperature with gentle agitation overnight.

2.4.9. Native-PAGE

Samples were prepared on addition of 2X Native PAGE sample buffer (10 μ L) to the protein (10 μ L) and the gently mixed. The sample was run as the SDS-PAGE with the exception that 1X Native gel running buffer was instead used.

2.4.10. PETN Reductase Expression and Purification

2.4.10.1. PETNR Expression

Cultures were prepared on inoculation of LB media (4 mL, containing 1 μ L/mL of ampicillin) with a glycerol stock of JM109 transformed cells. These were incubated overnight at 37°C with shaking. 3 mL aliquots of the culture were added to sterile TB AIM (1000 mL, containing 1 μ L/mL of ampicillin) and incubated at 37°C with shaking. The cells were collected on centrifuge at 5000 rpm for 10 minutes and the pellet frozen at -80°C after removal of supernatants.

2.4.10.2. PETNR Purification

2.4.10.2.1. Buffer Solutions

Buffer A: 50 mM KH₂PO₄/K₂HPO₄ solution, pH 8.0, filtered and degassed.

Buffer B: 50 mM KH₂PO₄/K₂HPO₄, pH 8.0, 300 mM NaCl, 20 mM imidazole and filtered.

Buffer C: 50 mM KH₂PO₄/K₂HPO₄, pH 8.0, 300 mM NaCl, 50 mM imidazole and filtered.

Buffer D: 50 mM KH₂PO₄/K₂HPO₄, pH 8.0 and 1 M NaCl, filtered and degassed.

Buffer E: 50 mM KH₂PO₄/K₂HPO₄ solution, pH 8.0, 2 mM β-mercaptoethanol, filtered and degassed.

Buffer F: 50 mM KH₂PO₄/K₂HPO₄, pH 8.0, 300 mM NaCl, 20 mM imidazole, 2 mM β-mercaptoethanol and filtered.

Buffer G: 50 mM KH₂PO₄/K₂HPO₄, pH 8.0, 300 mM NaCl, 50 mM imidazole, 2 mM β-mercaptoethanol and filtered.

2.4.10.2.2. Purification Procedure A

The cells were defrosted on ice and resuspended using buffer A (50 mL), also containing one dissolved CompleteTM protease inhibitor EDTA-free tablet, and stirred for five min at 4°C. Benzonase (2 μL) and lysozyme (1 μL) were then added and the mixture left to stir for a further 20 min. The resultant slurry was cooled on ice and sonicated at 50% amplitude for 30 seconds with a 50 second interval between pulses, this cycle was repeated a total of 5 times. The sample was then centrifuged at 20,000 rpm for 45 minutes at 4°C and the supernatants collected. An excess of FMN in aqueous solution was added and dialysed against buffer A. This protein was then loaded onto a nickel affinity column pre-equilibrated with buffer B. The column was washed with 3 column volumes of buffer B before elution of the protein was undertaken with buffer C. The fractions were analyzed by SDS-PAGE and the appropriate samples combined and dialysed against buffer A. The following day the protein would be loaded onto a Hi-Prep Q Sepharose column attached to automated AKTA purifier 100 system and pre-equilibrated with buffer A. A wash with this buffer was begun before a gradient to 100% buffer D was implemented. The composition of fractions was observed by UV-Vis absorption at 280 and 464 nm. The yellow fractions collected at analyzed by SDS-PAGE. Those fractions of correct composition were combined and concentrated before being aliquoted into 100 μL samples and frozen at -80°C.

2.4.10.2.3. Purification procedure B

The cells were defrosted on ice and resuspended using buffer A (50 mL), also containing 2 mM DTT and one dissolved CompleteTM protease inhibitor EDTA-free tablet, and stirred for five min at 4°C. Benzonase (2 μL) and lysozyme (1 μL) were then added and the mixture left to stir for a further 20 min. The resultant slurry was cooled on ice and sonicated at 50% amplitude for 30 seconds with a 50 second interval between pulses, this cycle was repeated a total of 5 times. The sample was then centrifuged at 20,000 rpm for 45 minutes at 4°C and the supernatants collected. An excess of FMN in aqueous solution was added and the dialysed against buffer E. This protein was then loaded onto a nickel affinity column pre-equilibrated with buffer F and. The column was washed with 3 column volumes of buffer F before elution of

the protein was undertaken with buffer G. The fractions were analyzed by SDS-PAGE and the appropriate samples combined and dialysed against buffer A also containing 2 mM DTT.

2.4.11. Labelling Studies of PETNR

An aliquot of PETNR (~1 mL) was exchanged into Tris-HCl (50 mM, pH 8.3) using an Amersham PD-10 Desalting column. The concentration of the enzyme was determined by UV-vis spectra on monitoring absorbance at 464 nm (extinction coefficient, $\epsilon_{464} = 11,300 \text{ M}^{-1}\text{cm}^{-1}$). The ruthenium label (1 – 10 equivalence) was added from a 50 mM stock solution in dry DMF. The sample was gently agitated at room temperature for 18 h and protected from light. On completion the sample was centrifuged at 13,300 rpm for 1 min and loaded onto a Amersham PD-10 Desalting column pre-equilibrated with Tris-HCl (5 mM, pH 8.3). The protein was eluted using the same buffer and the sample concentrated to *ca.* 0.5 mL using a Vivaspin™ 500 (MWCO 10,000) concentrator on centrifuge at 10,000 rpm. This was analysed by UV-vis spectroscopy and used in subsequent experiments without further purification. Of note, uncoupled label could be removed from the desalting column on elution with a buffer of higher ionic strength, Tris-HCl (50 mM pH 8.3).

2.4.12. Spectrophotometric Assays

2.4.12.1. Diffusion-Controlled Multicomponent Systems

Samples were prepared anaerobically in a 10 mm quartz cuvette (1 mL) and subsequently sealed with a suba-seal. Samples contained an appropriate combination of enzyme (10 μM), substrate (5mM), photosensitizer (20 μM) and methyl viologen (0.5 mM) made to a total volume of 1.0 mL using triethanolamine buffer (5 mM, pH 7.0) with 5 % ethanol. Samples were illuminated using a Schott 1500 LCD lamp fitted with a 360 nm long-pass filter. Reactions were monitored spectrophotometrically on recording UV-vis spectra every 1, 5 or 10 min in the range of 250 – 800 nm for 1 – 6 hours.

2.4.12. Light-Driven Biocatalytic Assays

2.4.12.1. Aqueous Light-Driven Biocatalytic Assays Using Diffusion-Controlled Multicomponent Systems

Samples were prepared anaerobically in a 5 mL vial and subsequently sealed with a suba-seal and secured with parafilm. Typical reaction mixtures contained enzyme (10 μM), substrate (5mM), photosensitizer (5-100 μM) and an electron transfer mediator (0.1 mM) made to a total volume of 3.5 mL using triethanolamine buffer (5-50 mM, pH 6.0-10.0) with 5 % ethanol. Samples were illuminated using a Schott 1500 LCD lamp fitted with a 360 nm long-pass filter. Periodically, 500 μL samples were collected via syringe under a positive pressure of nitrogen and subsequently extracted with 500 μL ethyl acetate containing limonene 5 % (v/v) as an internal standard. The organic phase was separated and dried over magnesium sulphate and analysed by gas chromatography. Products were identified on comparison to known standards.

2.4.12.2. Aqueous Light-Driven Biocatalytic Assays Using Sensitiser-Enzyme Constructs.

Samples were prepared anaerobically in a 5 mL vial and subsequently sealed with a suba-seal and secured with parafilm. Typical reaction mixtures contained the sensitiser-enzyme construct (*ca.* 10 μ M) and substrate (5mM) made to a total volume of 3.5 mL using triethanolamine buffer (25 mM, pH 8.0) with 5 % ethanol. Samples were illuminated using a Schott 1500 LCD lamp fitted with a 360 nm long-pass filter. Periodically, 500 μ L samples were collected via syringe under a positive pressure of nitrogen and subsequently extracted with 500 μ L ethyl acetate containing limonene 5 % (v/v) as an internal standard. The organic phase was separated and dried over magnesium sulphate and analysed by gas chromatography. Products were identified by comparison to known standards.

2.4.12.3. Biphasic Light-Driven Biocatalytic Assays

Standard reactions were carried out in 2 mL vials screw top vials sealed and secured with parafilm. In a typical reaction mixture the aqueous phase contained enzyme (10 μ M), photosensitizer (20 μ M) and methyl viologen (0.1 mM) made to a total volume of 1000 μ L using triethanolamine buffer (50 mM, pH 8.0). The substrate (200 μ L, 25 mM) was added directly from a stock solution made with the appropriate organic solvent. Samples were illuminated using a Schott 1500 LCD lamp fitted with a 360 nm long-pass filter and agitated at 450 rpm under ambient temperature for 24 h. The reaction mixture was subsequently extracted with 800 μ L ethyl acetate containing limonene 5 % (v/v) as an internal standard. Extracts were dried over magnesium sulphate and analysed by gas chromatography. Products were identified by comparison to known standards.

2.4.12.4. Biphasic Biocatalytic Assays Using an Enzyme-Coupled Regeneration System.

Standard reactions were carried out in 2 mL vials screw top vials sealed and secured with parafilm. In a typical reaction mixture the aqueous phase contained enzyme (10 μ M), NADP (10mM) glucose 6-phosphate (15 mM) and glucose 6-phosphate dehydrogenase 10 (units) made to a total volume of 1000 μ L using potassium phosphate buffer (50 mM, KPO₄, pH 8.0). The substrate (200 μ L, 25 mM) was added directly from a stock solution made with the appropriate organic solvent. Samples were agitated at 450 rpm under ambient temperature for 24 h and subsequently extracted with 800 μ L ethyl acetate containing limonene 5 % (v/v) as an internal standard. Extracts were dried over magnesium sulphate and analysed by gas chromatography. Products were identified by comparison to known standards.

2.4.12.5. Analytic procedures: Determination of Yields and Percentage Conversions

GC analysis of conversion and yields was performed using a DB-Wax column (30 m, 0.32 mm, 0.25 μ m) and results compared to known standards and associated calibration curves.

2-cyclohexenone: split 20, flow 1.0 mL min⁻¹, injector: 220°C, detector: 250°C, temperature programme: 40°C hold for 10 min, to 210°C at 20°C min⁻¹, hold for 1 min; retention times: Substrate: 15.19 min, Product 13.66 min.

Cinnamaldehyde: split 20, flow 2.0 mL min⁻¹, injector: 250°C, detector: 250°C, temperature programme: 100°C hold for 2 min, to 220°C at 20°C min⁻¹, hold for 5 min; retention times: Substrate: 6.55 min, Product 5.12 min.

α -methylcinnamaldehyde: As for cinnamaldehyde; retention times: Substrate: 6.35 min, Product: 5.04 min.

2-methylpentenal: split 20, flow 1.0 mL min⁻¹, injector: 220°C, detector: 250°C, temperature programme: 40°C hold for 10 min, to 200°C at 20°C min⁻¹, hold for 1 min; retention times: Substrate: 11.39 min, Product 5.61 min.

Ketoisophorone: split 20, flow 1.0 mL min⁻¹, injector: 220°C, detector: 150°C, temperature programme: 110°C hold for 5 min, to 210°C at 20°C min⁻¹, hold for 1 min; retention times: Substrate: 7.61 min, Product 8.32 min

N-phenyl-2-methylmaleimide: split 20, flow 1.0 mL min⁻¹, injector: 220°C, detector: 250°C, temperature programme: 110°C hold for 2 min, to 240°C at 20°C min⁻¹, hold for 10 min; retention times: Substrate: 9.72 min, Product 10.95 min

(S)-Carvone: split 20, flow 1.0 mL min⁻¹, injector: 220°C, detector: 250°C, temperature programme: 60°C hold for 2 min, to 210°C at 15°C min⁻¹, hold for 3 min; retention times: Substrate: 10.83, Products: (2R,5R)-dihydrocarvone and (2S,5R)-dihydrocarvone at 10.36 and 10.56 min, respectively.

2.4.12.6. Analytic procedures: Determination of Enantiomeric Excesses.

Absolute configurations were assigned on comparison to authentic samples of enantiomerically pure material.

2-methylpentenal: Rt-BDEXsa column (30 m, 0.25 mm, 0.25 μ m): split 100, flow 1.0 mL min⁻¹, injector: 180°C, detector: 250°C, temperature programme: 80°C hold for 10 min, to 120°C at 4°C min⁻¹, hold for 2 min, to 180°C at 20°C min⁻¹, hold for 1 min; retention times: (R)-2-methylpentanal and (S)-2-methylpentanal at 12.19 and 13.47 min, respectively.

α -methylcinnamaldehyde: Chirasil-DEX CB column (25 m, 0.32 mm, 0.25 μ m): split 100, flow 3.0 mL min⁻¹, injector: 250°C, detector: 150°C, temperature programme: 90°C hold for 30 min, to 180°C at 20°C min⁻¹, hold for 1 min; retention times: (S)-dihydrocinnamaldehyde and (R)-dihydrocinnamaldehyde at 27.14 and 27.64 min, respectively.

Ketoisophorone: Chirasil-DEX CB column (25 m, 0.32 mm, 0.25 μ m): split 100, flow 2.5 mL min⁻¹, injector: 250°C, detector: 250°C, temperature programme: 115°C hold for 10 min, to 180°C at 20°C min⁻¹, hold for 1 min; retention times: (R)-levodione and (S)-levodione at 7.80 and 8.25 min, respectively.

N-phenyl-2-methylmaleimide: Rt-BDEXsm column (30 m, 0.25 mm, 0.25 μ m): split 100, flow 2.5 mL min⁻¹, injector: 180°C, detector: 250°C, temperature programme: 80°C hold for 1 min, to 200°C at 2°C min⁻¹, hold for 1 min; retention times: (S)-N-phenyl-2-methylsuccinimide and (R)-N-phenyl-2-methylsuccinimide at 50.65 and 50.91 min, respectively.

SECTION THREE

SYNTHESIS AND ANALYSIS OF RUTHENIUM POLYHETEROARYL COMPLEXES

3.1. INTRODUCTION

As has been demonstrated in Section 1, the ability of the ruthenium(II) polypyridyl complexes to act as photosensitisers towards enzymatic systems has been extensively utilised. Whilst much of the focus has been upon complexes of the bis-(2,2'-bipyridyl)ruthenium(II) moiety, the potential of other ruthenium compounds is now being realised. One such series is that based upon the complex [Ru(bpz)₃]Cl₂, which was first isolated on reaction of Ru(DMSO)₄Cl₂ with an excess of 2,2'-bipyrazine (bpz) upon reflux in water.^[120] Preparation of Ru(bpz)₂Cl₂, analogous to the bipyridyl complex used as a precursor towards heteroleptic polypyridyl complexes, was initially achieved on irradiation of [Ru(bpz)₃](PF₆)₂ in the presence of [Et₄N]Cl.^[132] However, the first heteroleptic complexes were instead prepared from Ru(bpy)₂Cl₂ or Ru(bpy)Cl₄ on reflux in ethylene glycol with two to three equivalents of the pro-ligand to yield [Ru(bpy)₂bpz]²⁺ and [Ru(bpz)₂bpy]²⁺ respectively.^[133] Furthermore, Crutchley *et al.* prepared a series of complexes of the formula Ru(bpz)₂X₂, where X = Cl⁻; Br⁻; I⁻; NO₂⁻; NCS⁻, thus describing the ability to tune the overall properties by ligand exchange.^[134] The potential of [Ru(bpz)₃]Cl₂ to act as an efficient photosensitiser was demonstrated in the photochemical reduction of methylviologen (MV²⁺) in the presence of triethanolamine to yield the cationic radical, MV^{•+}.^[120] Results showed a significant improvement in the quantum yields in comparison to the bipyridyl analogue, with values of Φ_{MV} = 0.77 and Φ_{MV} = 0.19 for [Ru(bpz)₃]Cl₂ and [Ru(bpy)₃]Cl₂ respectively. Emission spectra displayed a 7 nm hypsochromic shift to 603 nm and longer lifetimes of 1.04 μs in comparison to 0.685 μs for [Ru(bpy)₃]Cl₂.

Despite the obvious beneficial properties offered by the bipyrazyl systems, they have yet to be investigated to the same extent as the bipyridyl analogues. This has been due in part to the difficulties associated with the preparation of the pro-ligand, 2,2'-bipyrazine. Synthesis is typically achieved through the homocoupling reactions of 2-substituted pyrazines in the presence of a variety of metal catalysts, the most common of these being a modified Ullman coupling reaction of 2-pyrazinecarboxylic acid using metallic copper as a catalyst.^[132, 135] However, such reactions require temperatures in excess of 350°C and suffer from relatively low yields.

Herein are described the trials undertaken to gain insight into the synthesis of 2,2'-bipyrazine with the aim to provide a more efficient and reliable synthesis of the pro-ligand. Following this an extensive study into the preparation of complexes based upon the bis(2,2'-bipyrazyl)ruthenium(II) moiety is discussed. The work will focus upon the incorporation of a variety of functional groups onto an ancillary ligand and investigate the relative effects this imposes upon the photophysical and redox properties of the compounds.

3.2 RESULTS AND DISCUSSION

3.2.1. Synthetic Studies

3.2.1.1 Optimisation of the synthesis of 2,2'-bipyrazine

In addition to the methods briefly discussed in section 3.1, a recently published procedure highlighted the potential of palladium catalysis in the formation of polyheteroaryl compounds from heteroaryl halides.^[136] Whilst the published material reported yields in excess of 97 %, such results could not be reproduced with initial trials yielding less than 10 % product formation. Isolation of the pro-ligand proved problematic due to the solidification of the reaction mixture on cooling to room temperature, yielding a dense brown/black solid of low solubility. Subsequent extraction required a significant volume of solvent to redissolve this material even for reactions performed on a small scale. Samples of this unknown material were analyzed using ¹H-NMR and mass spectroscopies, the results revealing a complex mixture of compounds from which individual components could not be identified.

It was determined that the reaction was both water and oxygen sensitive as yields were shown to improve on the use of anhydrous solvents and degassing of the reaction mixture using the freeze-pump-thaw method. Alternate palladium catalysts such as bis-(acetonitrile)-palladium(II) chloride were also investigated, although despite the enhanced solubility in less polar solvents, as provided by the presence of labile acetonitrile adducts, no discernable improvement in yields was observed. With consistently poor results and little scope for increasing the scale of the reaction, alternate approaches were investigated. It should be noted that since the completion of the work presented here a further method has been published that is related to this procedure, therein the catalyst has been changed to Pd(PPh₃)₄ and the reaction solvent to DMF. The increased polarity of the solvent circumvented the issues of solubility and allowed the reaction to be performed on the multi-gram scale.^[137] After extraction, column chromatography and subsequent trituration in MeOH, yields of 42 % were reported.

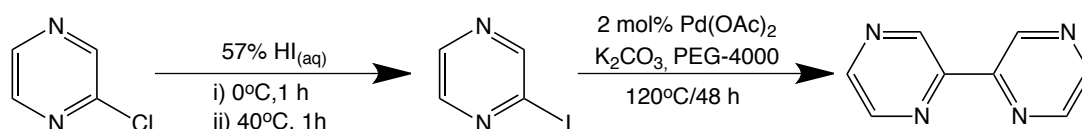
The second method to be investigated utilised a nickel complex reducing agent (t-BuONa-NiCRA-PPh₃) that was prepared *in situ* on reaction of *tert*-butanol, sodium hydride, nickel(II) acetate and triphenylphosphine in 1,2-dimethoxyethane.^[138] After 2 hours of stirring at 65°C the heteroaryl halide was added drop-wise and heating maintained for 12 hours. Whilst this procedure gave improved bipyrazine yields, issues of purification remained. The crude material was highly contaminated with triphenylphosphine and a second impurity, thought to be 2-phenylpyrazine, which proved difficult to isolate. The latter is a by-product resulting from the well documented side reaction of aryl-aryl exchange^[139] and is typically evident in coupling reactions involving a phosphine mediator.^[140-142] Another contributor to low yields in such reactions is the consumption of the aryl halide by the palladium catalysed formation of tetraarylphosphonium salts.^[140] It is for these two reasons that the utilisation of ligand-less coupling reactions are so attractive.

In a comparative study of the synthesis of 2,2'-bipyrimidine, Vlád *et al.* reported

similarly low yields for the nickel mediated coupling reactions. Furthermore they demonstrated that using a modification of the Ullmann reaction, excellent yields could be obtained through the homocoupling of 2-iodopyrimidine.^[143] The use of aryl iodides is necessary for this approach owing to the increased activity of the iodo group towards coupling reactions. The precursor could be synthesized by direct halogen exchange upon reaction of 2-chloropyrazine with with hydriodic acid. Lacking the activating influence of the two *ortho*-nitrogen atoms present in the pyrimidyl ring, by comparison the reaction of 2-chloropyrazine had to be undertaken at elevated temperatures. Allowing the reaction mixture to stir at 0°C before increasing the temperature to 40°C, yielded 2-iodopyrazine in 72 % yields, though a small quantity of unreacted 2-chloropyrazine remained, less than *ca.* 5 % as indicated by ¹H-NMR. Increasing the temperature further resulted in a decrease of both the yields and purity of the product. It is surmised that at higher temperatures the product decomposes to give the fully reduced pyrazine.^[144]

The coupling reaction proceeds on heating 2-iodopyrazine in the presence of an excess of activated metallic copper powder in anhydrous DMF. On heating the mixture at 85°C with vigorous stirring for 7 h, the temperature was increased to 130°C for a further 2 h before the suspension was cooled in an acetone-ice bath. The suspension was added to a concentrated KCN solution in 25 % aqueous ammonia to liberate the product via ligand exchange of the resultant copper complex salts. The pro-ligand was isolated on extraction with chloroform, removal of solvents and subsequent recrystallisation. Using this method, improved yields of *ca.* 49 % were obtained, although not on par with those reported for 2,2'-bipyrimidine the quantities of the pro-ligand that were synthesised were sufficient for subsequent coordination chemistry to be investigated. However, the scope to further increase the scale of the reaction was somewhat limited, as the reaction requires the use of a large quantity of metallic copper. Consequently, issues were encountered with stirring of the suspension, although this could perhaps be overcome by use of a mechanical stirrer. A second consideration was the significant quantities of KCN that would be required should a larger scale reaction be utilised.

Further trials led to the successful development of a new procedure based upon a modification of one previously used in the synthesis of biaryls.^[145] The homocoupling reaction of 2-iodopyrazine was undertaken in the presence of a catalytic quantity of palladium(II) acetate and potassium carbonate in polyethylene glycol (PEG-4000). The latter was chosen for the reaction medium as it acts as an effective phase transfer solvent allowing for sufficient interaction between the hydrophobic and hydrophilic components of the system.^[146] It has been suggested that PEG also plays a role in altering the microenvironment of the catalyst

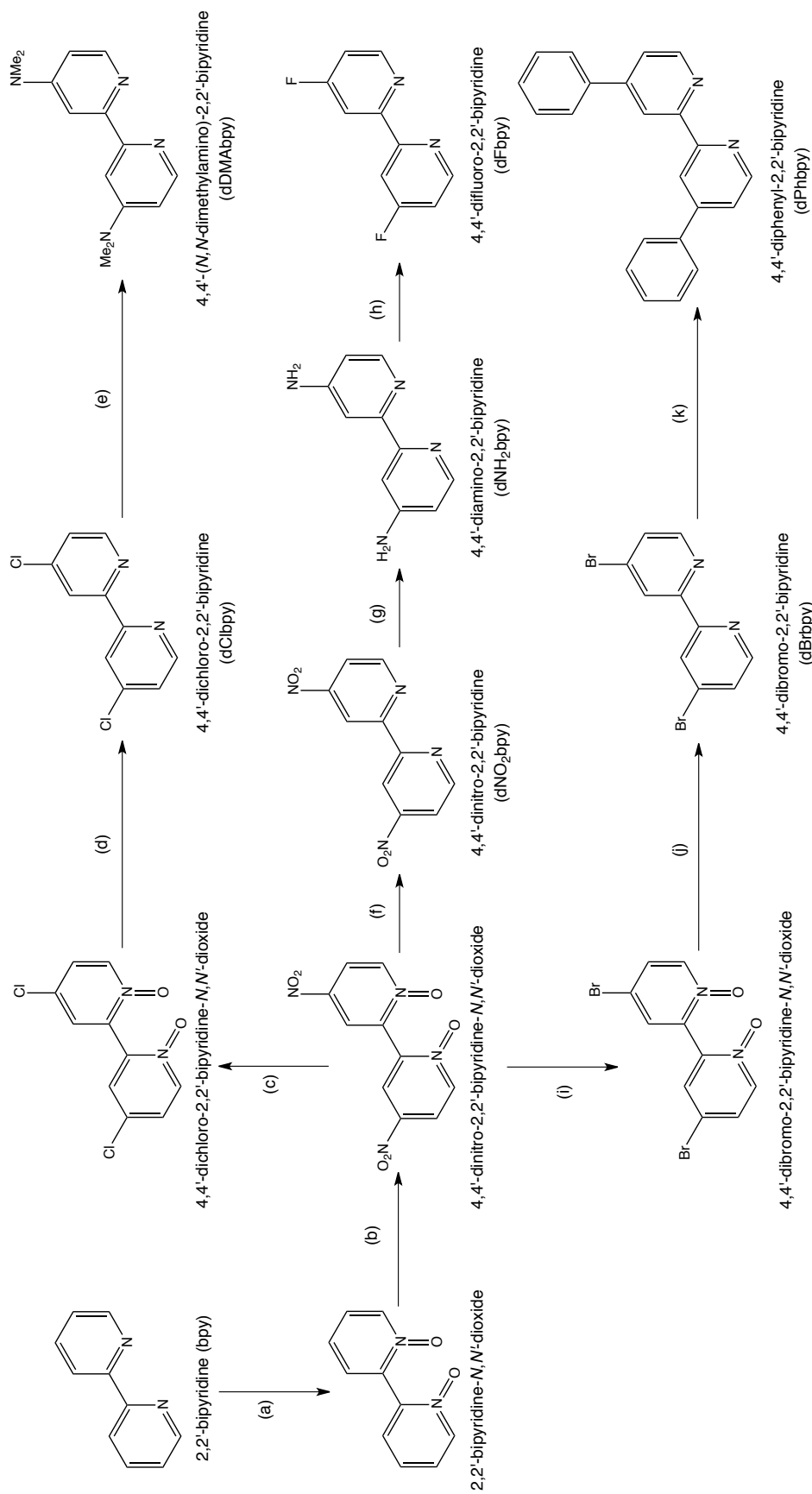


Scheme 3.1. Synthesis of 2,2'-bipyrazine proceeding via a) a halogen exchange reaction to yield 2-iodopyrazine followed by b) a PEG-mediated palladium catalyzed homocoupling reaction.

which ultimately facilitates catalytic turnover.^[147] Additionally, it has been surmised that the terminal hydroxyl group may act as the reductant in the catalytic cycle, although the exact nature of this mechanism is yet to be fully determined.^[145] On heating the mixture at 120°C for 48 hours, a viscous brown slurry was formed that solidified upon cooling and made subsequent isolation of the product laborious. Addition of hot water to the mixture before cooling prevented solidification and allowed for effective extraction of the crude product using ethyl acetate. Purification could be readily achieved upon first washing the combined ethyl acetate portions with sodium thiosulphate and brine to remove free iodide and palladium salts. On removing the solvent the residue was extensively washed with n-pentane to remove unreacted 2-iodopyrazine and afford a pure product in yields of 70 %. The reaction has been reproduced numerous times and has successfully been scaled up to the multi-gram scale without detriment to the efficiency of the procedure. Overall this method is much preferred over those previously reported as in addition to higher yields, it does not require extensive work up and utilises relatively cheap and benign starting materials.

3.2.1.2. Synthesis of 4,4'-disubstituted-2,2'-bipyridines

As stated previously the overall properties of the complexes may be fine tuned upon manipulation of the ligands included within the system. With this in consideration a variety of different functionalised ancillary pro-ligands were prepared, focusing primarily upon the 4,4'-disubstituted-2,2'-bipyridines. The majority of the required pro-ligands could be attained via the reactions of one particular intermediate, specifically 4,4'-dinitro-2,2'-bipyridine-*N,N'*-dioxide (Scheme 3.2.). This itself was readily synthesised by the oxygenation of 2,2'-bipyridine and the subsequent nitration of the resultant 2,2'-bipyridyl-*N,N'*-dioxide; the latter achieved on heating in concentrated sulfuric acid, fuming nitric acid and oleum. The dioxide was prepared in moderate yields on refluxing 2,2'-bipyridine in glacial acetic acid and containing a solution of hydrogen peroxide, the product readily isolated on subsequent precipitation in acetone. This sequence of reactions is required as direct halogenation of pyridine is not possible due to deactivation of the ring by the electronegative heteroatom. Whilst direct nitration can be achieved it requires considerably harsher conditions than those used in the analogous reactions of the phenyl moiety and selectively reacts to yield the β -substituted products. Through favourable resonance forms, incorporation of the *N*-oxide increases the electron density at the α - and γ -positions so as to increase their susceptibility towards electrophilic attack and, upon nitration, selectively yield the 4-nitropyridyl product. The nitro group may then readily undergo nucleophilic substitution on subsequent reaction with an appropriate nucleophile. 4,4'-dichloro-2,2'-bipyridine-*N,N'*-dioxide was synthesised upon heating of 4,4'-dinitro-2,2'-bipyridine-*N,N'*-dioxide in the presence of acetyl chloride and glacial acetic acid.^[148] The final pro-ligand, 4,4'-dichloro-2,2'-bipyridine (dClbpy), was prepared by subsequent deoxygenation on heating the *N*-oxide intermediate with phosphorous trichloride in anhydrous acetonitrile.



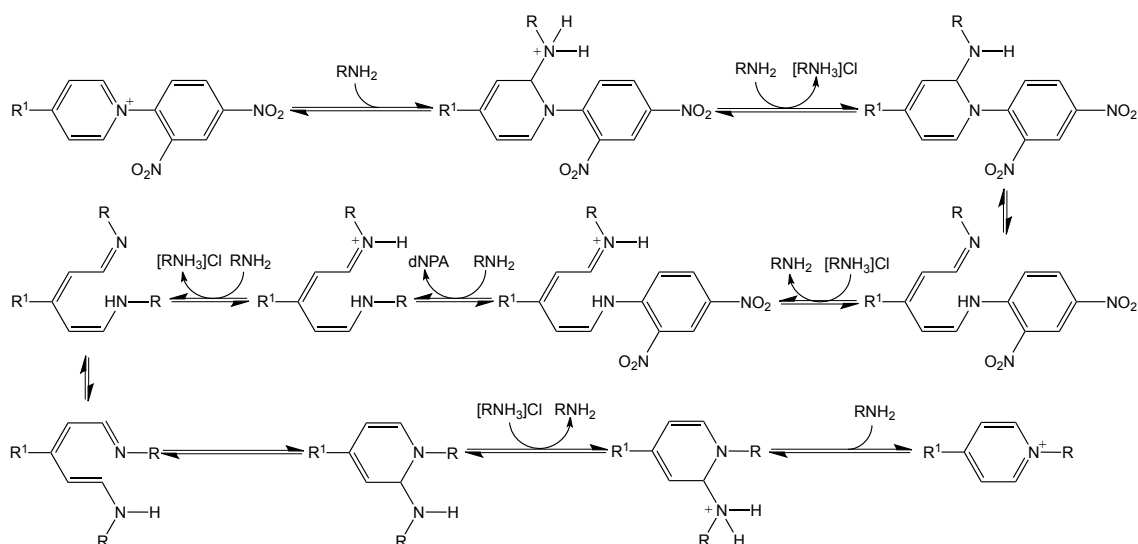
Scheme 3.2. Reaction scheme for the synthesis of 4,4'-disubstituted-2,2'-bipyridine pro-ligands; **(a)** H₂O₂, glacial acetic acid, 80 °C, 8 h; **(b)** HNO₃/H₂SO₄, 110 °C, 8 h; **(c)** acetyl chloride, glacial acetic acid, 100 °C, 4 h; **(d)** PCl₃, anhydrous acetonitrile, reflux, 4 h; **(e)** DMF, K₂CO₃, reflux 12 h; **(f)** PCl₃, reflux, 21 h; **(g)** Pd on C, hydrazine hydrate, ethanol, r.t. 15 h; **(h)** i) KNO₃, HBF₄, 0 °C ii) 160 °C, N₂ 160 °C; **(i)** acetyl bromide, glacial acetic acid, reflux, 18 h; **(j)** PBr₃, anhydrous acetonitrile, reflux, 4 h; **(k)** phenylboronic acid, tetrakis triphenylphosphine palladium, sodium carbonate, toluene/ethanol/water, 110 °C, 48 h.

Deoxygenation of 4,4'-dinitro-2,2'-bipyridine-*N,N'*-dioxide could likewise be achieved using phosphorous trichloride to yield 4,4'-dinitro-2,2'-bipyridine (dNO₂bpy). 4,4'-dibromo-2,2'-bipyridine (dBrbpy) was prepared by an analogous procedure upon substituting acetyl chloride and phosphorous trichloride for their bromide analogues. dBrbpy is an excellent intermediate towards incorporating further functionality, as the reactive heteroaryl bromide group allows for a range of coupling reactions to be undertaken. 4,4'-diphenyl-2,2'-bipyridine was prepared in good yields by the Suzuki-Miyaura coupling reaction between dBrbpy and benzenboronic acid using Pd(PPh₃)₄ as a catalyst in a toluene/water biphasic solvent system.

Whilst dClbpy and dBrbpy are readily accessible from the dinitro precursor, an analogous procedure towards 4,4'-difluoro-2,2'-bipyridine was not possible. The investigated route instead proceeded first via the palladium catalyzed hydrogenation reaction of 4,4'-dinitro-2,2'-bipyridine-*N,N'*-dioxide to afford 4,4'-diamino-2,2'-bipyridine in moderate to good yields. The next stage performed was a diazotisation, whereby the -NH₂ group was converted to -N₂⁺ by reaction with nitrous acid, which is formed *in situ* from sodium nitrite and tetrafluoroboric acid, to yield the product as the tetrafluoroborate salt. The final stage of the reaction was to be a modified version of the Balz-Schiemann reaction,^[149] itself a variant of the Sandmeyer reaction that involves the thermal decomposition of a diazo group and subsequent fluoride abstraction from the counteranion. Unfortunately this stage of the pathway proved unsuccessful, yielding none of the desired product. As such the target was changed to 4,4'-ditrifluoromethyl-2,2'-bipyridine (dCF₃bpy), a pro-ligand that is typically synthesised via nickel-catalysed homo-coupling reactions similar to those discussed in the section 3.2.2; the employed procedures are typically laborious and afford relatively poor yields of <35 %.^[150, 151] Here it was shown that dCF₃bpy could be readily synthesised from 2-bromo-4-trifluoromethylpyridine by employing the PEG-mediated palladium catalysis system used in the preparation of 2,2'-bipyrazine. The pro-ligand was isolated in yields of 63 %, the material readily purified by column chromatography on silica gel and eluting with DCM.

4,4'-di(methoxycarbonyl)-2,2'-bipyridine (dCMbpy) was prepared by a two-step reaction via the oxidation of 4,4'-dimethyl-2,2'-bipyridine using sodium dichromate to afford 4,4'-dicarboxy-2,2'-bipyridine in very high yields (>85 %). The final pro-ligand was obtained by esterification on refluxing the acid with methanol in the presence of conc. H₂SO₄, the product isolated on quenching in water and subsequent neutralisation.

Synthesis of 4,4'-dicyano-2,2'-bipyridine was achieved via a three stage reaction. The first being the preparation of 4,4'-bis(*N,N'*-dimethylaminovinyl)-2,2'-bipyridine, upon heating of 4,4'-dimethyl-2,2'-bipyridine with Brederick's reagent, [*tert*-butoxy bis(dimethylamino)methane, in DMF at 140°C.^[152] 4,4'-diformyl-2,2'-bipyridine was prepared on oxidative cleavage of the incorporated vinyl bond by reaction with an aqueous solution of sodium periodate in THF at 40°C for 18 h. Transformation of the aldehyde was achieved on reaction with hydroxylamine hydrochloride in pyridine at 5°C for approximately 10 minutes before the addition of acetic anhydride and heating at reflux for 1 hour. The reaction



Scheme 3.3. Mechanism of the Zincke reaction, where RNH_2 is an aryl amine, $[RNH_3]Cl$ is the chloride salt of the protonated aryl amine and dNPA is 2,4-dinitrophenylamine. The reaction proceeds first via nucleophilic attack at the α -carbon of the pyridinium moiety by RNH_2 . After protonation and subsequent ring opening of the dihydropyridine ring, dNPA is lost to yield an unsaturated iminium salt, which is readily deprotonated to give the neutral species. The latter readily undergoes isomerisation via an intermediate where all alkene bonds adopt a trans conformation (not shown). The reaction continues via a ring closing mechanism followed by protonation and loss of RNH_2 to yield the final substituted pyridinium product.

proceeds via oxime formation and subsequent dehydration by acetic anhydride to form the cyano group by a mechanism analogous to that seen in the Wohl degradation.

4,4':2',2'':4'',4'''-quaterpyridine (qpy) was prepared by the palladium catalyzed dimerisation reaction of 4,4'-bipyridine using a modified literature procedure.^[153] In place of dissolving the crude reaction material in 2 M HCl and subsequent neutralisation using 8 M NaOH, the material was extracted using boiling ethanol. This proved beneficial, as even at elevated temperatures, the higher molecular weight polymeric by-products are poorly soluble in ethanol, thus affording a purer crude material that simplified the final purification by column chromatography.

The quaternised pro-ligands N'',N''' -dimethyl-4,4':2',2'':4'',4'''-quaterpyridinium (Me_2qpy^{2+}) and N'',N''' -di(2-pyrimidyl)-4,4':2',2'':4'',4'''-quaterpyridinium (Pym_2qpy^{2+}) were prepared via the S_N2 and S_NAr reactions of qpy with methyl iodide or 2-chloropyrimidine respectively. N'',N''' -di(4-hydroxymethylphenyl)-4,4':2',2'':4'',4'''-quaterpyridinium, $[(4-HOCH_2Ph)_2Qpy]^{2+}$ was prepared by a Zincke type reaction^[154] of N'',N''' -di(2,4-dinitrophenyl)-4,4':2',2'':4'',4'''-quaterpyridinium chloride, $[(2,4dNO_2Ph)_2Qpy]Cl_2$, with an excess of 4-aminobenzyl alcohol in refluxing ethanol, Scheme 3.3. The $[(2,4dNO_2Ph)_2Qpy]Cl_2$ intermediate was prepared on reaction of 4,4':2',2'':4'',4'''-quaterpyridine with 1-chloro-2,4-dinitrobenzene.^[153] The compound is readily purified on extraction of an aqueous solution of the chloride salt with chloroform to remove unreacted starting materials and byproducts.

3.2.1.3. Synthesis of Bridging Ligands

Four potential bridging ligands were identified for this study; of these 2,3-bis(2-pyridyl)pyrazine (dpp) was obtained commercially whilst the others would have to be synthesised. 2,2'-bipyrimidine (bpm) was prepared using the reported Ullman reaction discussed in the section 3.2.1.1.^[143] Tetrapyrido[3,2-*a*:2',3'-*c*:3'',2''-*h*:2''',3'''-*j*]phenazine (tpphz) was formed from the imine condensation reaction of 1,10-phenanthroline-5,6-dione and ammonium acetate in the presence of sodium hydrosulphite.^[123]

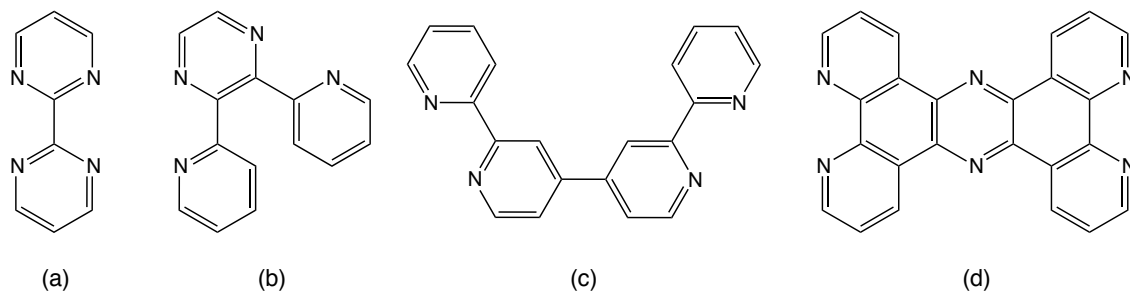


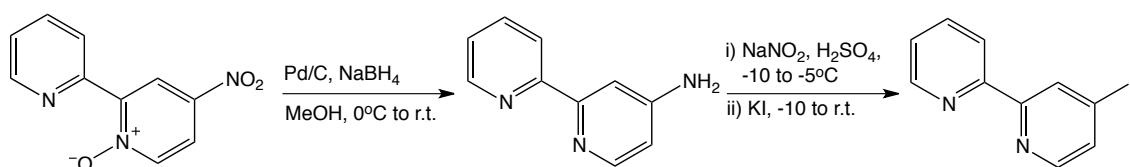
Fig. 3.1. Representative structures of the four bridging ligands investigated as part of this study; (a) 2,2'-bipyrimidine (bpm); (b) 2,3-dipyridylpyrazine (dpp); (c) 2,2':4',4'':2'',2'''-quaterpyridine and (d) tetrapyrido[3,2-*a*:2',3'-*c*:3'',2''-*h*:2''',3'''-*j*]phenazine (tpphz).

Synthesis of 2,2':4',4'':2'',2'''-quaterpyridine was reported to be achieved over three successive steps,^[42] the first of which is the monooxygenation of 2,2'-bipyridine to give 2,2'-bipyridyl-*N*-oxide. A number of different oxidising agents have been utilised towards the synthesis of this compound including hydrogen peroxide^[155], *m*-chloroperbenzoic acid^[156] and magnesium monoperoxyphthalate (MMPP).^[157] Of the three reagents, MMPP afforded the highest yields and the most consistent results after optimisation of the reaction conditions. Issues of purification hampered initial attempts using this reagent, as column chromatography failed due to precipitation of a solid within the column despite successful solubility trials previously being undertaken. In other instances, the crude product was obtained as a deep red 'gum-like' solid making further manipulation of the material difficult. Both of these issues were identified to be a consequence of insufficient quenching of unreacted MMPP during work-up of the reaction. Upon incorporating an additional basic wash during extraction the problem was resolved and subsequently yielded a crude material of higher purity. The product was isolated in yields of 51 % on final purification by column chromatography using silica gel and eluting with acetone containing 3 % triethylamine; the latter allows for bands of much higher definition and prevents the product from adhering to the silica.

The second stage described in literature was a direct chlorination reaction using phosphorus oxychloride to yield 4-chloro-2,2'-bipyridine and 6-chloro-2,2'-bipyridine in equimolar quantities.^[158] The reported method claimed that separation of the two products could be achieved through the selective coordination of the less sterically hindered isomer by nickel(II) salts in aqueous solution. The desired product could subsequently be isolated via liberation on addition of excess cyanide/ammonia and extraction with chloroform.^[42]

However, results obtained as part of this study indicated that only minimal improvements in purity were achieved using this method. Column chromatography likewise failed as the two separate isomers were of comparable R_f values with bands that displayed insufficient definition to afford a pure product.

An alternate approach via the 4-nitro-2,2'-bipyridine intermediate was also investigated as it allowed for directed halogenation, in a method similar to that used in preparation of the 4,4'-disubstituted-2,2'-bipyridines, as discussed in section 3.2.1.2. Such an approach also provided access to the more reactive 4-bromo- and 4-iodo-2,2'-bipyridine precursors. 4-nitro-2,2'-bipyridine was synthesised using a modification of the procedure used in the preparation of the dinitro analogue. Whilst the latter is isolated by precipitation on addition to ice-water, the former required an additional neutralisation step due to protonation of the unsubstituted pyridyl nitrogen.^[159] Bromination was achieved via nucleophilic substitution of the nitro group as discussed previously. 4-iodo-2,2'-bipyridine was prepared from 4-amino-2,2'-bipyridine using a Sandmeyer-type reaction which used potassium iodide as the halide source, Scheme 3.4.^[131]



Scheme 3.4. Reaction scheme for the synthesis of 4-iodo-2,2'-bipyridine from 4-nitro-2,2'-bipyridine; a) Pd/C reduction of the nitro group to yield 4-amino-2,2'-bipyridine and subsequent b) Sandmeyer type reaction with potassium iodide via a diazonium intermediate.

The final stage in the formation of 2,2':4',4'':2'',2'''-quaterpyridine was reported as the Ni(II) catalysed homocoupling of 4-chloro-2,2'-bipyridine.^[160] This was attempted for both of the synthesised halo- precursors in conjunction with nickel(II) catalysts with the general formula $NiX_2(PPh_3)_2$, where $X = Cl$ or Br . Reactions were performed in either THF or DMF in the presence of activated zinc powder and tetraethylammonium iodide, acting as the reducing agent and the phase transfer catalyst respectively. In each instance only minimal product formation was observed. Similar reactions where the catalyst was generated *in situ* from NiX_2 and PPh_3 were also attempted, although these likewise failed. The ineffectiveness of these nickel-catalysed coupling reactions has been previously demonstrated with related compounds, such as 4-(2-pyridyl)-5-chloropyrimidine^[161] and 5-chloro-1,10-phenanthroline.^[162] This failure has subsequently been attributed to sequestering of the nickel catalysts by the bipyridyl moiety upon coordination.

Attempts were also undertaken using the previously described PEG-mediated Pd catalysed reaction, although in both instances only unreacted starting material was isolated; this is surmised to be in part due to the decreased solubility of the precursors in PEG. Further attempts at the synthesis of this ligand were not undertaken.

3.2.1.4. Synthesis of complexes of the formula [Ru(bpz)₂(L)]X₂

The reported yields for the coordination reactions of Ru(bpz)₂Cl₂ are considerably lower than those typically attained for Ru(bpy)₂Cl₂. Jibril *et al*^[163] described that, on refluxing Ru(bpz)₂Cl₂ with an appropriate ligand in ethanol:water (1:1), yields of *ca.* 25 % were obtained, less than half that achieved with the bipyridyl analogue despite longer reaction times being employed. Similar observations were made as part of this study upon employing the same procedure in the reactions of Ru(bpz)₂Cl₂ with either bpy, dMebpy or dClbpy.

Initial optimisation trials were attempted via the diaqua intermediate, which has proven to be an effective route towards the synthesis of bis(2,2'-bipyridine) ruthenium complexes containing monodentate amine ligands.^[164] The reaction proceeded on heating of Ru(bpz)₂Cl₂ in deionised water at 60°C for 4 h, whereupon the mixture was injected into a refluxing ethanolic or propanolic solution of the ligand. After *ca.* 12 h the mixture was cooled and the organic solvent removed by rotary evaporation. A minimum quantity of crude material was collected on precipitation with ammonium hexafluorophosphate, the resultant filtrate a dark red/purple colour indicative of unreacted Ru(bpz)₂Cl₂. Yields were extremely poor at < 10 % as much of the crude material proved to be starting materials and a species which is consistent with [Ru(bpz)₂(H₂O)Cl]⁺.

The use of chloride abstraction agents was also investigated, specifically utilising silver salts that promote the forward reaction by the formation and subsequent precipitation of AgCl. By refluxing Ru(bpz)₂Cl₂ with 1.2 equivalents of the ancillary ligand in EtOH:H₂O (1:1) and in the presence of AgNO₃, improved yields of between 22–30 % were obtained. Concerning the more aliphatic or sterically bulky pro-ligands, issues of solubility were encountered with this particular solvent system. In such reactions the major product obtained was Ru(bpz)₂(NO₃)₂ as indicated by mass spectroscopy and ¹H-NMR, the latter spectra consistent with literature precedent.^[134] To accommodate more ligands the solvent was changed to a solely organic medium, though this also required a change in the chloride abstraction agent due to solubility considerations. Whilst trials with ethanol or *n*-propanol and using silver(I)triflate offered improved solubility, the poor product yields persisted. Changing the solvent to 2-methoxyethanol (MeOEtOH) proved greatly beneficial as yields increased to *ca.* 40%. This solvent was originally chosen for its enhanced polarity in relation to the other alcohols with the aim of improving ligand solubility, exhibiting a polarity index of 5.5 compared to 5.1 and 4.3 for MeOH and EtOH respectively. However, it is surmised that the increased boiling point of 125°C was also sufficient to aid in the promotion of the reaction through favourable thermodynamics. In an effort to avoid the use of chloride abstraction agents, and the additional purification steps such methods require, additional trials were undertaken in the absence of silver salts and using a mixed MeOEtOH:water reaction solvent. It was shown that on refluxing Ru(bpz)₂Cl₂ and 1.2 equivalents of the pro-ligand in MeOEtOH:H₂O (3:1) for 24-48 hours, yields in the range of 32 – 68 % could be achieved for a wide range of substituted bipyridine ancillary ligands. The crude product was isolated on removal of solvents and subsequent

metathesis to the hexafluorophosphate salt on dissolution of the residue in cold deionised water and addition of solid NH₄PF₆. Purification of the final complexes was readily achieved by column chromatography using silica gel and eluting with 0.1 M NH₄PF₆ in acetonitrile. The precise R_f value of the complexes are highly dependent upon the functionality of the ancillary ligand, though are typically in the range of 0.65 – 0.8. Observations made during the course of the reaction tend to suggest that it proceeds via the *in situ* generation of the diaqua intermediate. This is surmised from the characteristic red colour of the solution that forms during the first few hours of the reaction before developing the orange hue that is expected of the tris diimine complex.

Whilst attempts to synthesise the complex of dCNbpy yielded the desired product, as indicated by ¹H-NMR, the quantities formed were minimal. Attempts at purification indicated that a significant number of different ruthenium containing complexes were present in the sample, as evident by the numerous strongly coloured bands observed during trials using TLC. Reactions of dCNbpy described in literature have highlighted the deactivating effect afforded by the nitrile group when in the *para* position with respect to the chelating nitrogen.^[165-167] It is suggested that the electronegativity of the functional group is sufficient to perturb Ru – N bond formation by decreasing the σ-donor ability of the ligand. This rationale is also in agreement with the failure to synthesis complexes containing the more electron deficient ligands, dCF₃bpy and dNO₂bpy. It was also noted that the preparation of [Ru(bpz)₃](PF₆)₂ from the Ru(bpz)₂Cl₂ precursor was likewise unsuccessful.

3.2.1.5. Synthesis of complexes of the formula [Ru(bpz)₂(L)]X₄

It has been suggested that an increase in the charge of a complex may improve the electrostatic interactions with an enzyme and thus afford an increase in the efficiency of direct electron transfer to the redox centre on photoexcitation.^[46] This rationale has been used to explain in part the increased quantum yields of enzyme reduction using the Ru₂C dimer, and subsequently the Ru₂Z dimer, in comparison to the monometallic counterparts. Therefore, an investigation into the synthesis of a number of complexes that contain positively charged ligands was undertaken with the aim of identifying an alternate route for preparing complexes of increased overall charge without the need to incorporate additional nuclearity.

Potential pro-ligands of interest for this study were the 4,4':2',2'':4'',4'''-quaterpyridinium family of compounds. Complexes containing these groups typically exhibit a significant bathochromic shift in the MLCT absorption bands,^[168] a characteristic that is potentially desirable for complexes that are to be used as photosensitisers. The properties of the MLCT can also be further modified upon altering the functionality of the pendent pyridinium group. It has been shown that by increasing the electron withdrawing ability, it is possible to achieve a significant shift in absorption to longer wavelengths.

Coordination of the quaterpyridinium ligands to afford complexes of the general formula [Ru(bpz)₂L]⁴⁺ was achieved using the previously discussed procedure, although the purification method as described proved ineffective and had to be modified. The material

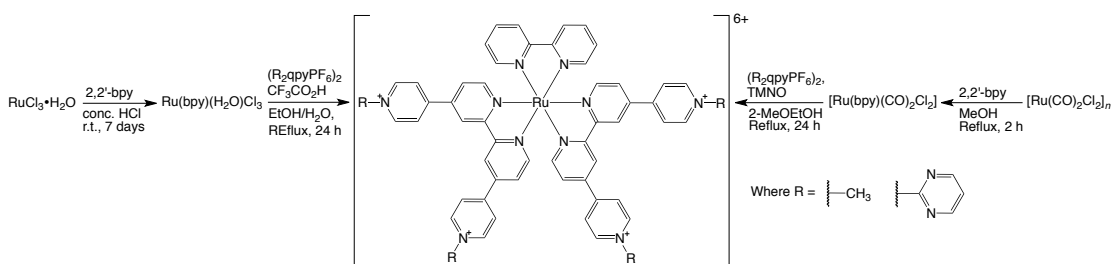
isolated on completion of the standard protocol contained at least one additional component that could not be removed by trituration, re-precipitation or re-metathesis via the chloride salt. After extensive trials it was discovered that by loading the partially purified material onto a silica column and eluting with 0.05 M NH_4PF_6 in acetonitrile:DCM (1:1), a near pure product could be obtained and also allowed for a sample of the impurity to be isolated. The progress of the column was monitored on illumination with a UV lamp (325 nm) with the impurity evident as a blue/green emissive band. On comparison of the recorded $^1\text{H-NMR}$ data, the identity of the impurity was confirmed as uncoordinated pro-ligand. Whilst this method proved partially successful towards purifying $\{\text{Ru}(\text{bpz})_2[(2\text{-Pym})_2\text{ppy}]\}^{4+}$ it was completely ineffective for the $[\text{Me}_2\text{ppy}]^{2+}$ and $[(\text{HOCH}_2\text{Ph})_2\text{ppy}]^{2+}$ analogues.

The final purification method utilised the cation exchange resin Sephadex-CM C-25 with an eluent of H_2O :acetone (5:3) and various concentrations of sodium chloride. Unreacted $\text{Ru}(\text{bpz})_2\text{Cl}_2$ was eluted as a purple/pink band on flushing the column with a 0.025 M NaCl solution. A second red/purple band and a pale yellow band were removed at a concentration of 0.075 M and are believed to be $[\text{Ru}(\text{bpz})_2\text{Cl}(\text{H}_2\text{O})]\text{Cl}$ and unreacted pro-ligand respectively. The final product was eluted on increasing the concentration of NaCl to 0.125 M and appeared as a red, strongly luminescent band. $\{\text{Ru}(\text{bpz})_2[(2\text{-Pym})_2\text{ppy}]\}^{4+}$ was incompatible with Sephadex C-25 and appeared to readily decompose over the time frame required to carry out the procedure. Once loaded onto the column minimal quantities of the material could be recovered, as the complex evidently adhered to the resin and could not be eluted using the methods employed. The related Sephadex SP-25 produced similar results and the aliphatic LH-20 resin failed to afford any separation between the two components. As a pure sample could not be obtained further studies with $\{\text{Ru}(\text{bpz})_2[(2\text{-Pym})_2\text{ppy}]\}^{4+}$ were not undertaken.

It should be noted that on purification of the bipyridyl analogues such issues were not encountered, as the compounds were readily purified by chromatography using silica gel and eluting with 0.1 M NH_4PF_6 in acetonitrile.^[153] It is surmised that due to the additional interactions occurring between the stationary phase and the distal nitrogens of bipyrazine ligands, the rate of elution of the product is sufficiently slowed so as to coincide with that of the pro-ligand. This is in agreement with observed R_f values for the $[\text{Ru}(\text{bpz})_2\text{L}]^{2+}$ complexes of the unquaternised ligands, which were consistently lower than those for the bipyridyl analogues.

3.2.1.6. Synthesis of complexes of the formula $[\text{Ru}(\text{L})_2(\text{L}')]\text{X}_6$

The overall charge of the complex may be further altered on incorporation of a varying number of quaterpyridinium ligands, thus allowing compounds of +4, +6 and +8 charge to be prepared. Complexes of +6 charge may be attained using two distinct approaches. The first proceeds via the preparation of a bis-(quaterpyridinium)dichlororuthenium(II) precursor followed by substitution of the chloride ligands with an appropriate diimine ligand. However, previous studies carried out within the Coe group have shown that synthesis and subsequent purification of this type of compound is difficult, with yields proving to vary significantly depending upon the functionality of the quaterpyridinium ligand.^[169]



Scheme 3.5. Reaction schemes utilised in the preparation of (2,2'-bipyridyl)-bis-(quaterpyridinylium)ruthenium(II) complexes via a Ru(bpy)(X)₄ intermediate, where R = Me or 2-pyrimidyl.

An alternate route is to proceed via the Ru(N[^]N)(X)₄ intermediate with subsequent coordination of the quaterpyridinium ligands to yield the tris polypyridyl complex. The first precursor to be used towards this method was RuCl₃(bpy)(H₂O), which was prepared from the reaction of 2,2'-bipyridine with RuCl₃·nH₂O in conc. HCl at room temperature over seven days.^[170] The subsequent reaction with [(2-Pym)₂qpy]Cl₂ was initially refluxed for 6 hours before a sample of the mixture was taken and purified on a small scale (less than 10 mg), at which point three distinct components were identified. The first, a pale yellow fraction was identified as uncoordinated pro-ligand. The second species was deep blue in colour, characteristic of a bis-substituted ruthenium compound containing a quaterpyridinium ligand, suggesting the formation of {Ru(bpy)[(2-Pym)₂qpy]Cl₂}²⁺.^[169] The final compound was an intense red colour, indicative of the tris-polypyridyl complexes. Due to the relative quantities of the two complexes, the reaction was allowed to proceed for a further 42 hours over which time the solution became increasingly red in colour. Isolated yields were as low as 4%, the problem attributed to the utilisation of the Sephadex C-25 ion exchange resin during the purification process. Due to the poor solubility and the paramagnetic nature of the RuCl₃(bpy)(H₂O) precursor it was unclear whether the low yields and numerous byproducts were associated with decomposition during the reaction or due to potential impurities present in the starting material.

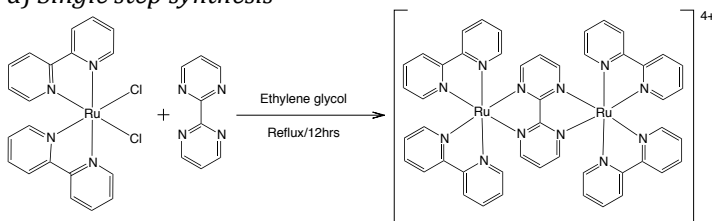
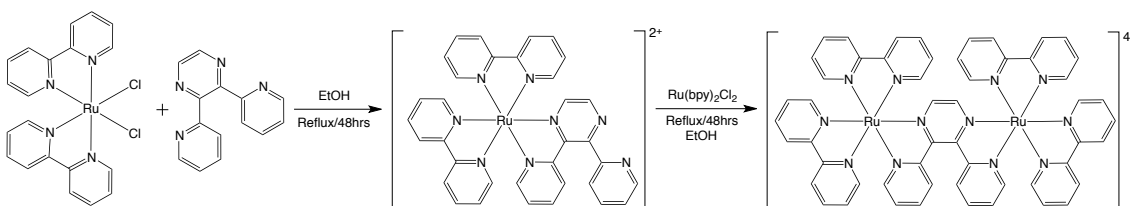
The second precursor to be tested was the polymeric *cis,cis*-[Ru^{II}(CO)₂Cl₂]_n complex which was formed upon reaction of RuCl₃·nH₂O with paraformaldehyde in refluxing formic acid.^[124] The subsequent reaction with 2,2'-bipyridine in refluxing methanol resulted in the breaking of the μ -dichloro bridge to yield [Ru(bpy)(CO)₂Cl₂], the resultant solid being readily soluble and can be fully characterised by ¹H-NMR, mass spectroscopy and elemental analysis. The final reaction with the quaterpyridinium pro-ligands was achieved on heating at 100°C in 2-methoxyethanol and in the presence of trimethylamine-*N*-oxide (TMAO). The latter is used as an oxidative decarbonylation reagent that reacts with the complex to form CO₂ and trimethylamine, thus promoting the forward reaction. This method was successfully used in the synthesis of [Ru(Me₂qpy)₂(bpy)](PF₆)₆, which was isolated in good yields on purification by chromatography using silica gel and eluting with 0.1 M NH₄PF₆ in acetonitrile. However, purification of the [(2-Pym)₂qpy]²⁺ and qpy analogues was unsuccessful as similar issues regarding the adherence of the compound to the stationary phase were encountered.

3.2.1.7. Towards bimetallic species of the general formula {[Ru(bpz)₂]L}(X)₄

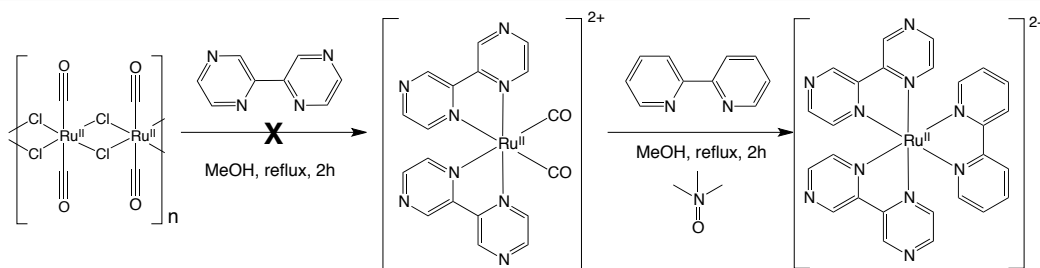
Initial reactions toward the bimetallic species were undertaken using the Ru(bpy)₂Cl₂ precursor to evaluate the efficiency of the published procedures. The first to be prepared was {[Ru(bpy)₂]₂(μ-2,2'-bipyrimidine)}(PF₆)₄ on reflux of two equivalents of Ru(bpy)₂Cl₂ with one equivalent of 2,2'-bipyrimidine in ethylene glycol.^[121] The product was isolated as a dark green solid on precipitation with NH₄PF₆ followed by column chromatography using silica gel and an eluent of 0.1M NH₄PF₆ acetone/toluene (6:1).

{[Ru(bpy)₂]₂(μ-2,3-bis(2-pyridyl)pyrazine)}(PF₆)₄ was prepared via two different routes. The first was similar to that used for the bipyrimidine complex except the solvent was changed to ethanol in place of ethylene glycol. This was required as the resultant material showed enhanced solubility in ethylene glycol and water, thus preventing precipitation on addition of NH₄PF₆. {[Ru(bpy)₂]₂(tpphz)}(PF₆)₄ was likewise prepared using this method. The second synthetic procedure adopted a step-wise approach, which proceeded on first synthesising the [Ru(bpy)₂(2,3-bpp)](PF₆)₂ complex upon reaction of Ru(bpy)₂Cl₂ with 1.25 equivalents of bpp. After purification and analysis the monometallic complex was subsequently reacted with 1.25 equivalents of Ru(bpy)₂Cl₂ to yield the final product, Scheme 3.6.^[122] On analysis of the material from both of these procedures it was evident that each gave comparable results, though bimetallic yields were slightly lower for the two-step procedure.

Efforts to prepare the bipyrazyl analogues with each of the three bridging ligands failed. Reactions were attempted using a number of different high boiling point solvents such as 2-methoxyethanol, DMF and ethylene glycol and also in the presence of a variety of chloride abstraction agents, though none of the desired bimetallic species could be isolated; in most instances the predominant component was either unreacted Ru(bpz)₂Cl₂, a solvento complex or the monometallic complex containing the bridging ligand. Trials using the step-wise approach were also undertaken using a large excess of the Ru(bpz)₂Cl₂ precursor in the final reaction, although this had no noticeable beneficial effects.

a) Single step synthesis**b) Two stage synthesis via a monometallic intermediate**

Scheme. 3.6. Coordination reactions highlighting the two potential routes towards ruthenium(II) bimetallic complexes using the bridging ligands a) bpm and b) bpp.

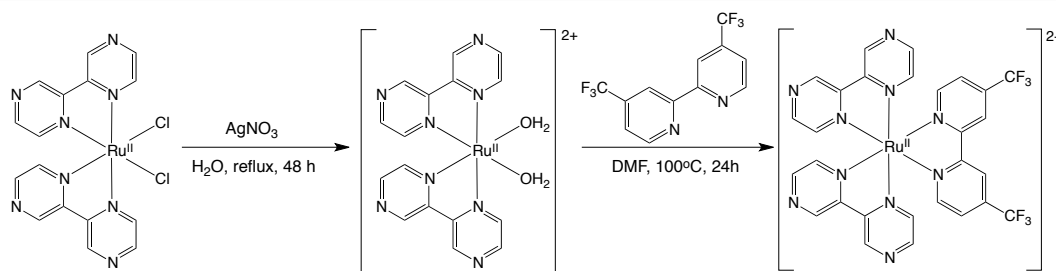


Scheme 3.7. Attempted reaction pathway towards $[Ru(bpz)_2(N^N)]^{2+}$ via the dicarbonyl intermediate, $[Ru(bpz)_2(CO)_2]^{2+}$.

With the continued failures using $Ru(bpz)_2Cl_2$, an investigation into the potential of alternate metal precursors was undertaken. The first of the new precursors to be studied was $[Ru(bpz)_2(CO)_2](PF_6)_2$. Addition of the polyheteroaryl ligands is typically undertaken in a the step-wise manner, proceeding first via formation of $[Ru(N^N)(CO)_2Cl_2]$ from *cis,cis*- $[Ru^{II}(CO)_2Cl_2]_n$, as described earlier.^[124] However, attempts to prepare $[Ru(bpz)(CO)_2Cl_2]$ failed as the reaction yielded a complex mixture of products as indicated in ¹H-NMR spectra. Similar observations have been reported for the reactions of 2-phenylpyrazine with $IrCl_3$, the numerous by-products were suggested to result from the reactions of the distal nitrogens of the pyrazyl ring.^[171] Using 2,2'-bipyridine, trials showed that $[Ru(bpy)_2(CO)_2]^{2+}$ may be formed directly from the polymeric starting material on reflux in methanol with 2.5 equivalents of the appropriate ligand. For the reaction of bipyrazine, the isolated product showed 12 distinct aromatic resonances in the ¹H-NMR spectra. Had $[Ru(bpz)_2(CO)_2]^{2+}$ been formed only three or six signals would be evident dependent upon whether the *trans*- or *cis*- isomer had been adopted, the results instead suggested that the bipyrazine ligands were of inequivalent environments. This was confirmed by ES-MS analysis which displayed a mass peak of 481 *m/z*, indicative of the formation of $[Ru(bpz)_2(CO)Cl]^+$. Subsequent reactions of this precursor were no more effective towards the preparation of the bimetallic complexes than $Ru(bpz)_2Cl_2$.

The other precursors studied were the bis-(bipyrazyl)-bis(solvento)ruthenium(II) complexes, the first being $[Ru(bpz)_2(MeCN)_2]^{2+}$. This was prepared by refluxing $Ru(bpz)_2Cl$ in acetonitrile in the presence of $AgPF_6$ for 48-60 hours and was isolated in excellent yields after purification by column chromatography. It should be noted that a similar result could be obtained for the bipyridyl analogue in only 1.5 hours and in the absence of a chloride abstraction agent.^[172] The choices of solvent and counter ion in subsequent reactions of this precursor were of the utmost importance. Due to the ease with which the acetonitrile adducts can be displaced, coordinative solvents had to be avoided due to competitive coordination with the desired pro-ligands. This was also true regarding the counter anion as exemplified in the reactions of $[Ru(bpz)_2(MeCN)_2]I_2$, where the main product that was isolated being $Ru(bpz)_2I_2$.

The second precursor of this type to be used was $[Ru(bpz)_2(OH_2)_2]^{2+}$, although due to the lability of the ligated water, attempts to isolate the compound were not undertaken. The crude material was prepared by refluxing $Ru(bpz)_2Cl_2$ in water for 24-48 hours in the presence of silver nitrate. On filtration through celite and removal of water the residue was redissolved in DMF and used in subsequent coordination reactions. Using this method, the previously



Scheme 3.8. Preparation of complexes of the general formula $[\text{Ru}(\text{bpz})_2\text{L}]^{2+}$ via the diaqua intermediate, demonstrated with the use of the $d\text{CF}_3\text{bpy}$ ancillary ligand.

unobtainable $[\text{Ru}(\text{bpz})_2(d\text{CF}_3\text{bpy})](\text{PF}_6)_2$ complex was successfully synthesised upon heating the DMF solution of the precursor in the presence of 1.5 – 2 equivalents of ancillary ligand for 24 hours at 100°C. The product was isolated as described previously although yields were reduced to 36 %, significantly lower than had been attained for the other ancillary ligands. Attempts to prepare the complex of $d\text{NO}_2\text{bpy}$ once again failed to yield the desired product. Synthesis of $[\text{Ru}(\text{bpz})_2d\text{CMbpy}]^{2+}$ from $\text{Ru}(\text{bpz})_2\text{Cl}_2$, whilst successful, resulted in partial trans-esterification of the ancillary ligand to the 2-methoxyethyl ester. This was evident in the ¹H-NMR spectra by two characteristic ethyl -CH₂- resonances, integration of which indicated that *ca.* 15-20 % of the material had undergone trans-esterification. Due to the similarities between the two compounds, separation could not be achieved. On proceeding via $[\text{Ru}(\text{bpz})_2(\text{OH}_2)_2]^{2+}$ the use of an alcoholic solvent was avoided and the $(\text{MeO}_2\text{C})_2\text{bpy}$ complex was isolated in comparable yields to the other ancillary ligands without evidence of ester hydrolysis.

Using this method the synthesis of bimetallic compounds proved partially successful. Isolation of a sample of $\{[\text{Ru}(\text{bpz})_2]_2(\text{tpphz})\}^{4+}$ was achieved, as suggested by ¹H-NMR and mass spectroscopy. However, the quantity obtained was small and the sample contained numerous minor impurities that could not be removed on additional chromatography steps or through recrystallisation as the material inevitably precipitated from solution or formed an oil or glass. Subsequently, further characterisation of the compound was not undertaken

The difficulties experienced in preparation of the bimetallic complexes of bipyridine are a consequence of a decrease in electron density at the metal centre in comparison to complexes of bipyridine; as is demonstrated in section 3.2.4. This may also be associated with the poor yields observed for the monometallic complexes of the more electron deficient ancillary ligands. This increased electron deficiency and the associated decrease in π -back bonding ability means that the metal centre would tend to favour strong σ -donor ligands, thus explaining the difficulties in displacing the chlorides of the $\text{Ru}(\text{bpz})_2\text{Cl}_2$ precursor. Likewise in the attempted synthesis of $[\text{Ru}(\text{bpz})_2(\text{CO})_2]^{2+}$, the electron deficiency at the metal centre is sufficient to promote the loss of CO in preference for retaining a chloride ligand. Concerning the preparation of bimetallic compounds, the changing electron density of the bridging ligand must be considered, as upon coordination the ligands become more electron deficient and are effectively deactivated towards coordination of a second metal centre. This effect is expected

to be enhanced considerably in complexes of the bis(bipyrazyl)ruthenium moiety as the bridging ligand is bound to a metal centre of greater electronegativity. It is therefore surmised that the larger and inherently more electron-rich bridging ligands are more likely to form bimetallic species, explaining the partial success that was achieved with $\{[\text{Ru}(\text{bpz})_2]_2\text{tpphz}\}^{4+}$. However in such systems the metal centres become increasingly isolated and the metal-metal interactions, and the subsequent influences on spectral and redox properties for which these compounds were targeted, would be lost.

3.2.1.8. Summary of Synthesised Complexes

A total of fourteen ruthenium complexes were synthesised and fully characterised for utilisation in photosensitiser trials. Of these, thirteen were of the general formula $[\text{Ru}(\text{bpz})_2(\text{N}^{\wedge}\text{N})]^{n+}$ and were prepared using a number of different synthetic procedures, as has been discussed. Representative structures for each of these complexes are presentation in Fig. 3.2, and in Appendix. A, Fig. A.1, and A.2.

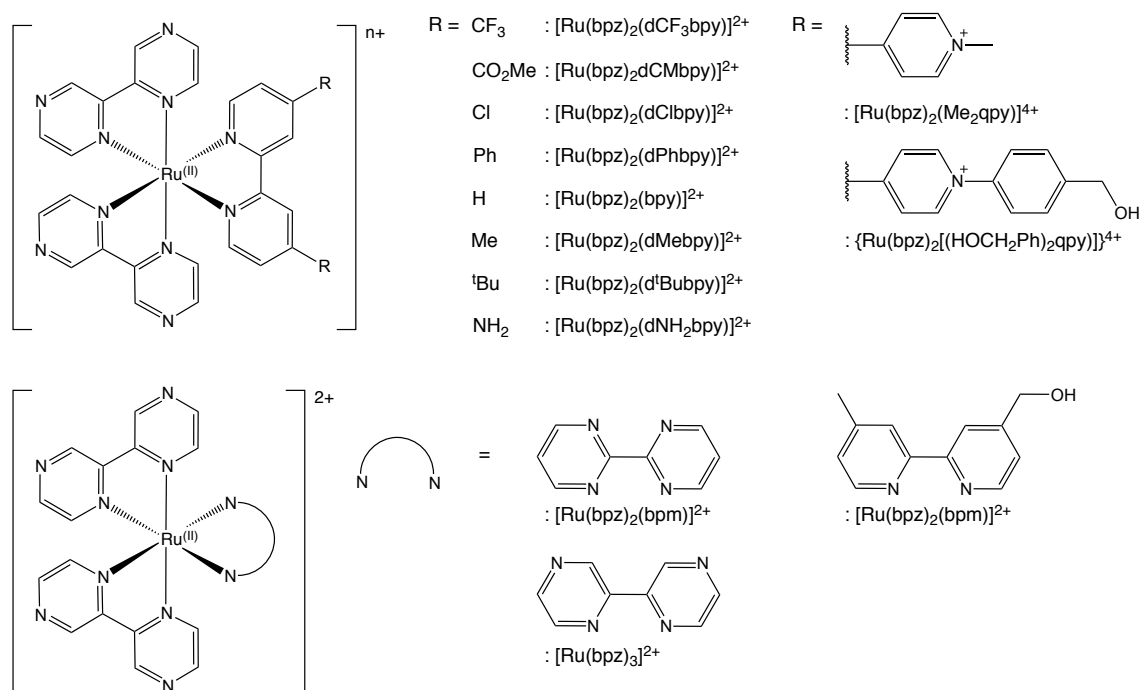


Fig. 3.2. Representative structures for each of the synthesised complexes with the general formula $[\text{Ru}(\text{bpz})_2(\text{N}^{\wedge}\text{N})]^{n+}$. Complexes were isolated as both the hexafluorophosphate and chloride salts.

3.2.2 ¹H-NMR Spectroscopy

The spectra for all complexes were recorded as both the hexafluorophosphate and chloride salts in CD₃CN and CD₃OD respectively. For comparison purposes all discussion contained herein refers to the spectra of complexes as the hexafluorophosphate salt, though general trends and observations remain true for both series of compounds

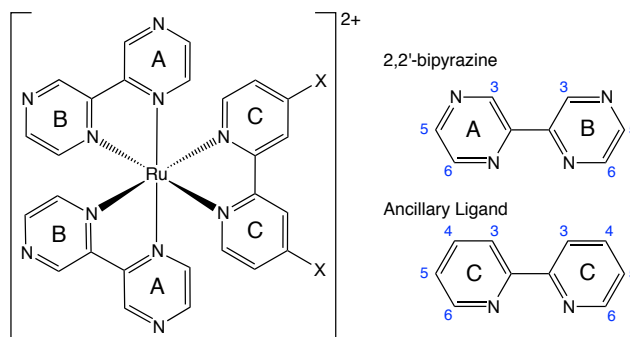


Fig. 3.3. Representative structures for complexes of the general formula $[Ru(bpz)_2(N^N)]^{2+}$ with labelling schemes used for NMR assignments.

The ¹H-NMR spectra for complexes of the general formula $[Ru(bpz)_2(N^N)](PF_6)_2$ show aromatic resonances between 10.10 and 6.53 ppm, the total number of protons this equates to is dependent upon the incorporated functionality of the ancillary ligand. Using COSY techniques at least three distinct spin systems were identified, Fig. 3.4; two of which are associated with the inequivalent rings of bipyrazine and the third with the rings of the bipyridyl unit of the ancillary ligand. In complexes of dPhppy, $[Me_2qpy]^{2+}$, $[(HOCH_2Ph)_2qpy]^{2+}$, $[(2-Pym)_2qpy]^{2+}$ and bpp, additional spin systems were identified and readily assigned by the characteristic splitting patterns of the phenyl, para-substituted pyridyl and/or pyrimidyl functional groups.

Typically the most downfield signals are assigned to A(3) and B(3) of the bipyrazine ligands, and are observed as two very closely spaced or overlapping doublets. The measured coupling constants of *ca.* 1.2 Hz are consistent with reported values of *para*-coupling within a mono-substituted pyrazine.^[173] In 4,4'-disubstituted bipyridines splitting of the H(3) proton signal is often attributed to *meta*-coupling with H(5), though the magnitude of this is dependent upon the nature of the functional group attached to the γ -carbon. The lack of observed *meta*-coupling in bipyrazine is attributed to the electronic effects induced by an intervening nitrogen atom upon the α protons.^[174] As was shown on analysis of the ¹H-NMR spectra of pyridine, the magnitude of $^4J_{(2,6)}$ is much smaller than that seen for $^4J_{(2,4)}$ and $^4J_{(3,5)}$, with an obtained value of 0.13 Hz in comparison to 1.4 and 1.8 Hz respectively.^[175, 176] An analogous effect would be expected for a pyrazyl ring and would explain the observations made here and the small value of the $^4J_{(3,5)}$ reported in literature.^[173]

The most downfield resonance of the bipyridyl spin system is assigned to the C(3) proton. The chemical shift of this and all other protons in the system are highly sensitive to the inductive effect of the substituted functional group. The most up-field signal, typically a finely

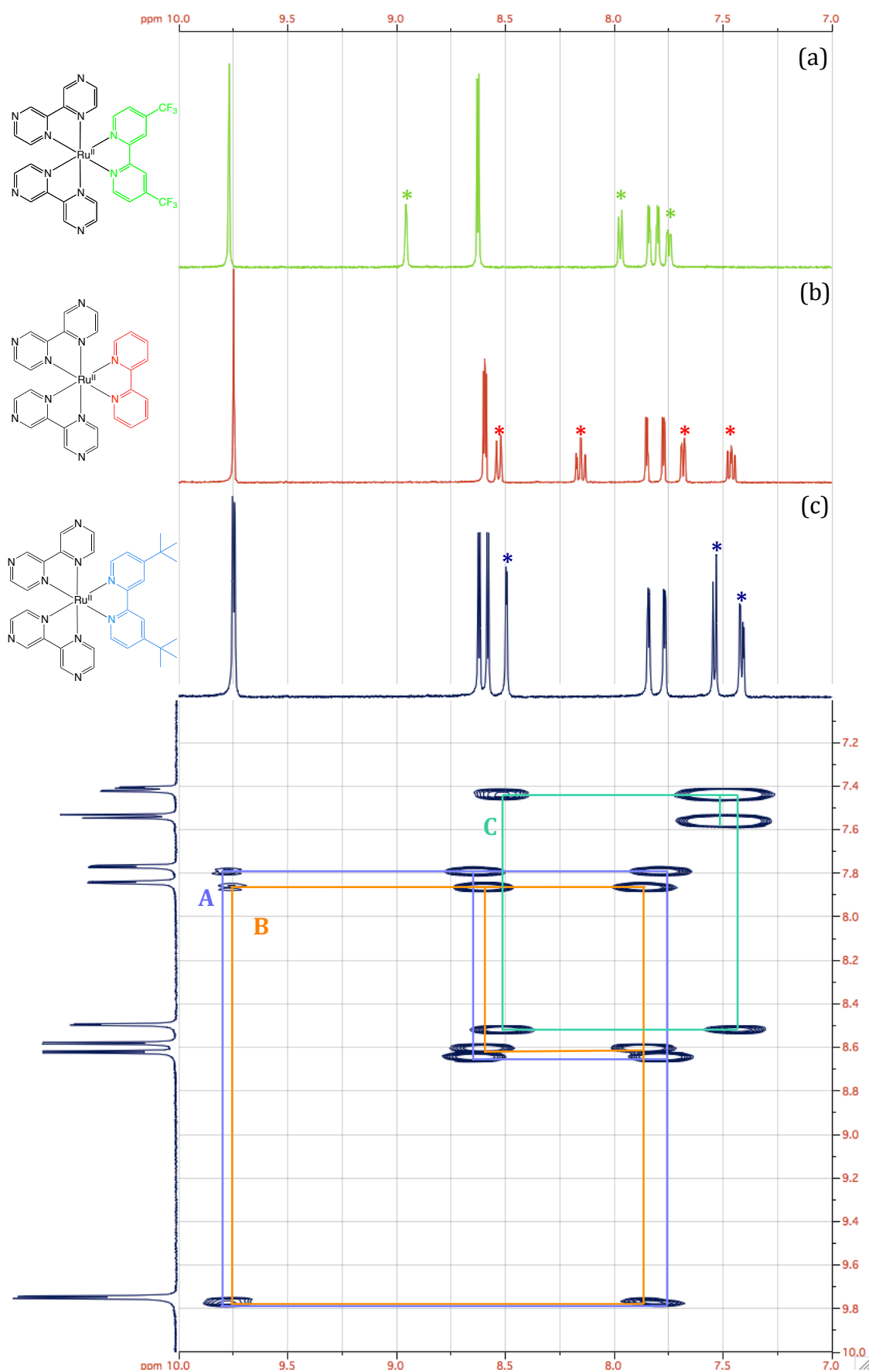


Fig. 3.4. ¹H-NMR spectra of a) [Ru(bpz)₂dCF₃bpy](PF₆)₂ and b) [Ru(bpz)₂bpy](PF₆)₂. A section of the COSY spectrum of c) [Ru(bpz)₂d^tBubpy](PF₆)₂ in the region 7.00-10.00 ppm used in the identification of individual spin systems within the complex; pyrazyl ring, A = purple; pyrazyl ring, B = orange; pyridyl ring, C = aqua. * = pyridyl resonance.

split doublet of doublets, with the exception of 2,2'-bipyridine where it is a triplet due to the presence of a hydrogen atom in the C(4) position, is assigned to the C(5) proton. Typically in ruthenium complexes of 2,2'-bipyridine the most up-field aromatic signals are assigned to the H(5) and H(5') protons. However, in the case of 2,2'-bipyrazine due to A(5) and B(5) being *ortho* to an electronegative nitrogen atom, these signals are significantly shifted downfield in comparison to the bipyridyl analogues. As such A(5) and B(5) are assigned to the two doublets at δ 8.5-8.7 ppm. The most up-field signals of the pyrazyl rings, a pair of doublets of doublets, are assigned to A(6) and B(6). In comparison to the resonances of the pro-ligand a significant negative coordination-induced shift (CIS) of *ca.* 0.9 ppm is observed, a result of extensive shielding induced by through-space ring current anisotropy from adjacent ligands. These assignments discussed for the pyrazyl rings are in agreement with those proposed by Crutchley *et al.* in their analysis of the ¹H-NMR spectra of [Ru(bpz)₃]²⁺[132]

The precise chemical shift of the resonances of the bipyrazine ligand, and the relative difference between equivalent protons of rings A and B, are dependent upon the nature of the ancillary ligand. This is attributed to changes in electron density within the bipyridyl unit that are afforded upon altering the functional group, the effects of which are communicated to the bipyrazine ligands primarily via one of two distinct mechanisms. The first is due to the variations induced in the metal centre by the relative σ -donor and π -acceptor abilities of the ancillary ligand. As the electron density of the metal centre fluctuates the overall electron withdrawing effect experienced by the coordinated nitrogen lone-pair of the pyrazyl ring is similarly altered. Subsequently these effects are transmitted to the protons of the bipyrazine ligand on polarisation of the σ -framework and through resonance of the π -conjugated system, thus inducing the changes observed in ¹H chemical shift.[177] This may also be discussed in terms of the relative trans influence,[178] or structural trans effect (STE),[179] of a pyrazyl and substituted pyridyl ring. It has been extensively shown for complexes of octahedral and square planar geometries that coordination of a ligand has an impact on the bonding between the metal centre and all other ligands, particularly for those that adopt mutually trans positions. As such it is surmised that the STE is a significant contributing factor to the inequivalency of spin systems A and B. In this instance it is expected that the increased σ -donor ability of the pyridyl ring in comparison to that of the pyrazyl would afford an upfield shift of the resonances associated with the trans pyrazyl rings (B).

Additionally the shielding effect induced upon A(6) and B(6) by through-space ring current anisotropy must be considered. It is the susceptibility of these protons to the influence of the π -system of the adjacent ligands that brings about the pronounced variations in chemical shift of these positions across the series of compounds. The difference between the two resonances is dominated by the relative magnitude of shielding afforded by the pyridyl ring in comparison to that of the pyrazyl.

The discussed assignments were confirmed using two-dimensional Nuclear Overhauser effect spectroscopy (NOESY). The NOE allows for the observation of through-space coupling of

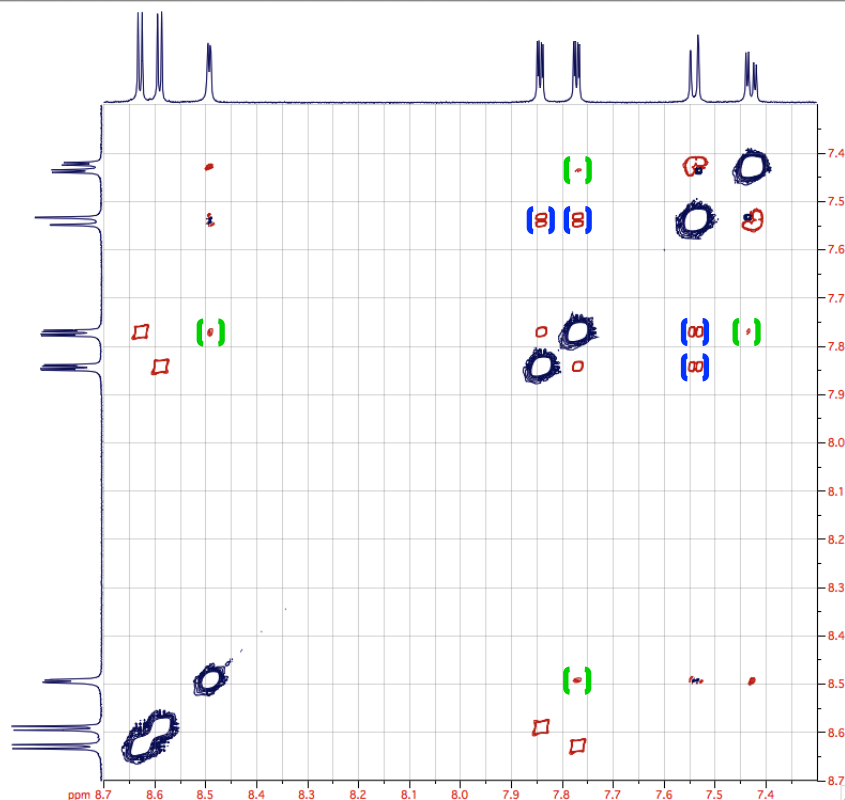


Fig. 3.5. Section of the 2D-NOESY spectrum of $[\text{Ru}(\text{bpz})_2\text{d}^t\text{Bubpy}](\text{PF}_6)_2$ recorded in CD_3CN . Depicted region of 7.3-8.7 ppm chosen for clarity of the most significant cross peaks used in the determination of the ^1H -NMR assignment. Contour peaks highlighted in blue illustrate the short range interactions of the A(6) and B(6) protons with C(6). The peaks highlighted in green indicate those of long range NOE contacts used in distinguishing between the two inequivalent pyrazyl rings to afford a complete spatial assignment, specifically the coupling of A(6) with the C(3) and C(5) resonances.

nuclei through dipolar interactions. This provides information pertaining to the distance between interacting nuclei, which subsequently may be used in determining their relative spatial arrangement. Xie *et al* demonstrated the use of this technique to determine the stereochemical assignment of tris-heteroleptic ruthenium(II) complexes by ^1H -NMR.^[180] This was achieved on observation of intraligand NOE contacts of H(6) and H(6') for each of the three unique ligands. Using this method it was possible to unambiguously assign the most up-field signals of the bipyrazyl rings to the H(6) and H(6') positions. A section of the 2D-NOESY spectra of $[\text{Ru}(\text{bpz})_2\text{d}^t\text{Bubpy}](\text{PF}_6)_2$ is shown in Fig. 3.5. Two strong cross peaks at 7.54-7.77 ppm and 7.54-7.84 ppm are assigned to the interaction of C(6) with the A(6) and B(6) protons.

Whilst COSY allowed for distinction between the two pyrazyl rings the relative stereochemistry could not be confirmed to any degree of certainty. Through the use of NOESY and analysis of the less intense cross peaks that correspond to long-range NOE contacts, a full assignment of the ^1H -NMR spectra can be achieved even for symmetrical octahedral complexes such as those of the general formula $[\text{Ru}(\text{N}^{\wedge}\text{N})_2(\text{N}^{\wedge}\text{N}')_2]^{2+}$ reported herein.

Cross signal peaks at 7.77-7.42 ppm and 7.77-8.49 ppm are indicative of additional

interactions of A(6) with C(5) and C(3) respectively. For an octahedral complex such interactions would only be possible should spin system A be mutually *cis* to the bipyridyl ring C and be perpendicular to the plane of the aromatic system of the ancillary ligand. If other geometries were adopted the resultant internuclear distances would exceed those for which the NOE would be monitored under these experimental conditions. A similar interaction is observed for C(6) with B(3) as indicated by a weak cross peak at 7.54-9.75 ppm, which would be in agreement with the spatial arrangement deduced from the interactions of A(6). Three-dimensional models illustrating these interactions are depicted in Figure 3.6.

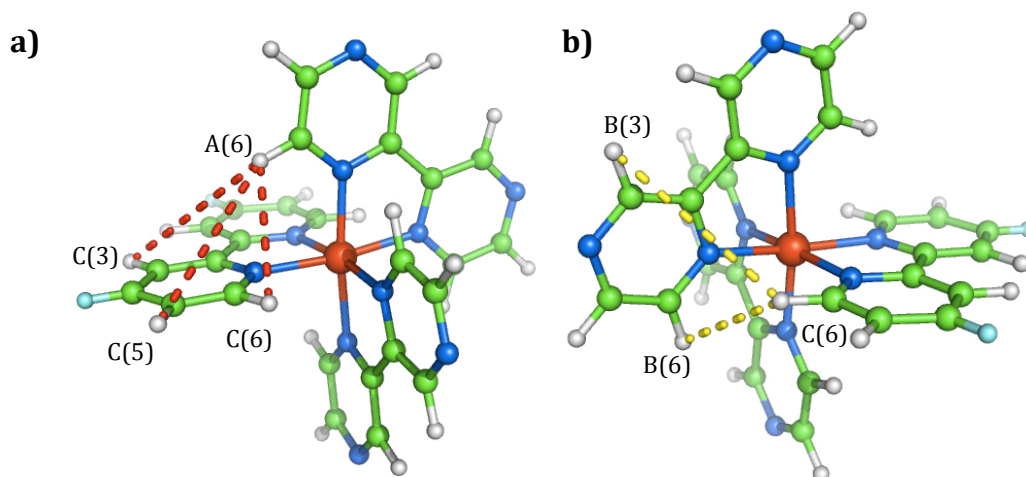


Fig. 3.6. Three dimensional model structures of complexes with the general formula $[Ru(bpz)_2(N^{\wedge}N)]^{n+}$. NOE contacts used in the assignment of 1H -NMR spectra are illustrated and the corresponding atoms highlighted. **a)** View focused upon the NOE contacts of A(6) and **b)** displaying similar interactions of C(6). Elements; C = green, H = white, N = blue, Ru = red and varying functional group = aqua. Image generated using MacPyMOL.

From the COSY experiments it is seen that the most shielded H(6) is coupled to the most deshielded H(5) and H(3) protons. This would be in agreement with the proposed assignment as in this geometry A(6) will be located above the plane of the more electron rich π -system of the bipyridyl ligand thus causing an increased shielding effect. Similarly in this position the pyrazyl ring will be trans to another pyrazine moiety which, considering the STE, would afford a decreased shielding effect compared to a pyridyl ring, resulting in lower field resonances for A(5) and A(3). This remains true for all complexes with the exception of $[Ru(bpz)_2dNH_2bpy]^{2+}$ whereby the A(6) proton is at higher ppm in comparison to B(6). The latter is more shielded than previously seen owing to the increased STE imposed by the improved σ -donation of the ancillary ligand. The former however is in fact considerably more deshielded in comparison to the A(6) resonances of the other $[Ru(bpz)_2L]^{2+}$ complexes by *ca.* 0.15–0.20 ppm, which is contradictory to the increased electron density of the adjacent pyridyl ligand. The electronic or structural origins of this anomaly are as of yet not fully understood though, as is demonstrated in the subsequent sections, $[Ru(bpz)_2dNH_2bpy]^{2+}$ displays considerably different properties in comparison to other members of the series.

3.3.3. Electronic Spectroscopy

Room temperature UV-visible absorption spectra were recorded for all complexes as both the hexafluorophosphate (Table 3.2) and chloride salts (Table 3.3) in acetonitrile and deionised water respectively. The lower energy absorption of $\lambda \geq 400$ nm is observed as two broad overlapping bands and is assigned to transitions of MLCT character. The trends in λ_{\max} show that an increase in the electron density of the ancillary ligand, and hence its pK_a , results in a bathochromic shift of the lower energy band. Upon changing the functional group of the ligand from the electronegative trifluoromethyl to the strongly donating amino, thus describing the two extremes of the series, a shift of *ca.* 52 nm is afforded. In most instances the λ_{\max} value of the higher energy MLCT could not be determined due to overlap with the more intense low energy band. However, on comparison between [Ru(bpz)₂bpy]²⁺, [Ru(bpz)₂d^tBubpy]²⁺ and [Ru(bpz)₂dNH₂bpy]²⁺, a similar bathochromic shift was identified upon increasing the electron density of the ancillary ligand. The magnitude of this shift is *ca.* 50 % of that observed for the lower energy band; the difference observed in the higher energy MLCT for [Ru(bpz)₂bpy]²⁺ and [Ru(bpz)₂dNH₂bpy]²⁺, is approximately 16 nm whilst for the lower energy band this is increased to 30 nm.

In resonance Raman (RR) and time-resolved resonance Raman (TR³) spectroscopy measurements of [Ru(bpz)₂bpy]²⁺ and [Ru(bpy)₂bpz]²⁺ the excitation of the lower energy MLCT resulted in the selectively enhancement of Raman bands associated with bipyrazine.^[181] Likewise excitation at higher energy enhanced the signals of the bipyridyl ligand by a comparable magnitude. Similar results were also presented for complexes of the general formula [Ru(N[^]N)₂bpz]²⁺ where (N[^]N) = 2,2'-bipyridine, 4,4'-dimethyl-5,5'-diethyl-2,2'-bipyridine and diazafluorene.^[182] From this it is possible to tentatively assign the lower energy band to transitions which are predominantly of $d \rightarrow \pi^*_{(\text{bpz})}$ character and those with higher energy to transitions with a larger $d \rightarrow \pi^*_{(\text{bpy})}$ contribution. Such an assignment is consistent with the relative order in energy of the π^* -orbitals of the two different ligands. The bathochromic shift observed on increasing the electron density of the ancillary ligand, suggests the destabilisation of the metal based HOMO through σ -donation. The energy of the π^* -orbitals of bipyrazine will also be altered as a consequence of the decreased electronegativity of the metal centre, although the magnitude of this change is expected to be smaller by comparison. Therefore, whilst both the HOMO and LUMO are expected to be destabilised with increasing pK_a of the ancillary ligand, a net decrease in energy of the MLCT and a subsequent bathochromic shift of λ_{\max} would result. The smaller magnitude of the shift observed for the higher energy band can be discussed in terms of the destabilisation of the metal centre being offset by a concomitant destabilisation of the ancillary ligand π^* -orbitals through the inductive effects of the functional group; this in agreement with the assignment of increased $d \rightarrow \pi^*_{(\text{bpy})}$ character for this band. However, such assignments may be over-simplified as the spectra of the tris homoleptic [Ru(bpz)₃]²⁺ complex also displayed two overlapping MLCT bands in this region, similar to that observed in the spectra of [Ru(bpy)₃]²⁺. Despite extensive experimental

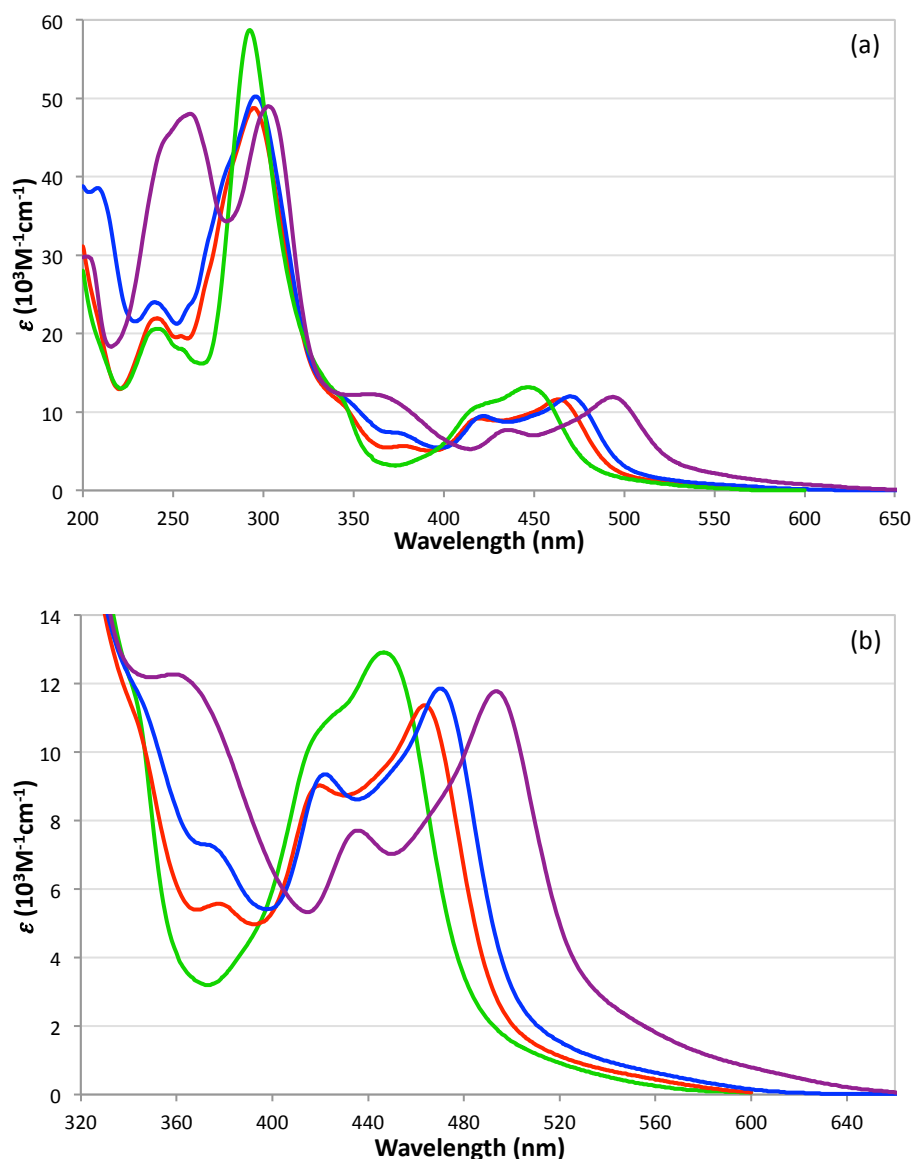


Fig. 3.7. UV-visible absorption spectra of the complexes $[Ru(bpz)_2dNH_2bpy](PF_6)_2$ (purple), $[Ru(bpz)_2d^tBubpy](PF_6)_2$ (blue), $[Ru(bpz)_2bpy](PF_6)_2$ (red) and $[Ru(bpz)_2dCF_3bpy](PF_6)_2$ (green) displaying **(a)** the full spectra and **(b)** $320 \leq \lambda \leq 650$ nm expansion of the lower energy bands. Recorded in acetonitrile at 298 K.

and theoretical studies the origins of these bands are still under debate, although it is suggested that they arise from transitions to π^* -orbitals of differing energy.^[183, 184] TD-DFT calculations, as discussed in Section 3.2.5, suggest that both of these bands instead involve MLCT that is predominately $d \rightarrow \pi^*_{(bpz)}$ in character. Whilst a contribution towards the higher energy band from the ancillary ligand is evident, the contribution is minor and is dependent upon the pK_a of the bipyridyl ligand. It is suggested that this assignment would be consistent with the evident trends of the higher energy band should the two inequivalent rings of bipyrazine be considered as two distinct moieties with their own discrete energy levels. Due to the STE, it would be expected that the π^* -orbitals of the pyrazyl rings *trans* to the ancillary ligand be increasingly destabilised with an increasing pK_a of the latter. Therefore the

associated transitions would be of comparatively higher energy and be subject to a similar dependence upon the ancillary ligand as is observed experimentally.

Higher energy MLCT bands are also evident at *ca.* 375 nm and as a shoulder at *ca.* 325 – 350 nm. The former is best defined for complexes of bpy, dMebpy, d^tBubpy and dPhbpy and is assigned to transitions primarily involving the ancillary ligand, as indicated in TD-DFT calculations. The shoulder at *ca.* 325-350 nm displays a shift of similar magnitude to those of the lowest energy MLCT band. Related transitions evident in the spectra of [Ru(bpz)₃]²⁺, [Ru(bpz)₂(MeCN)Cl]⁺ and Ru(bpz)₂Cl₂ likewise undergo a shift to progressively lower energies upon successive addition of the strong σ -donor chloride ligand.^[132] This suggests the band may be assigned to a higher energy MLCT associated with the bpz ligands.

The intense bands between *ca.* 200 – 320 nm are attributed to the π - π^* and n - π^* ligand centred (LC) transitions, with a contribution from higher energy MLCT. The band at *ca.* 300 nm corresponds to the LC transitions within the bipyrazine rings as evident on comparison with the spectra of [Ru(bpz)₃]²⁺. A modest bathochromic shift of *ca.* 10 nm for this band arises from the destabilisation of the metal-based HOMO and subsequent increase in energy of the bipyrazine π -orbitals on increasing the σ -donating ability of the ancillary ligand. The high energy shoulder is attributed to LC transitions of primarily bipyridine character and becomes more pronounced on increasing the electron donating ability of the functional group so that for [Ru(bpz)₂dNH₂bpy]²⁺ it is a fully resolved band. This observation is consistent with an increase in the energy of the π^* -orbitals of the ancillary ligand. The magnitude of this destabilisation is evidently greater than that experienced by the π -orbitals and the associated influence of the concomitant decrease in electron withdrawing ability of the metal centre.

The absorption spectrum of [Ru(bpy)(Me₂qpy)₂]⁶⁺ (Appendix A, Fig. A.1.) exhibits decidedly broadened MLCT absorption which can be described as three over-lapping bands; the third is evident as a poorly defined maximum centred between the two more intensely absorbing bands. In the related complexes of [Ru(bpy)₂(Me₂qpy)]⁴⁺ and [Ru(Me₂qpy)]⁶⁺, only two maxima can be distinguished, which correlate to the highest and lowest energy bands in the spectra of [Ru(bpy)(Me₂qpy)₂]⁶⁺. The higher energy band is assigned to a MLCT involving the pyridinium moieties of the quaterpyridinium ligand, the trends in λ_{max} describing a hypsochromic shift with an increasing number of quaterpyridinium ligands. This is consistent with the stabilisation of the metal based HOMO upon changing to a ligand with poorer donor/better acceptor ability as is the case upon changing from 2,2'-bipyridine to [Me₂qpy]²⁺. The MLCT transitions of predominantly 2,2'-bipyridine character are also expected to be within this range of 350-450 nm. The lower energy band is assigned to a MLCT with a greater contribution to the bipyridyl unit of the quaterpyridinium ligand. As no discernable trends in λ_{max} were apparent, an evaluation of the impact upon the energy levels of the respective HOMO and LUMO could not be made. The band at *ca.* 325 nm is evident in each of the three complexes and displays a systematic increase in ϵ values with each successive addition of a (Me₂qpy)²⁺ ligand with minimal variations of λ_{max} . This has been assigned to an ILCT that describes a

redistribution of electron density from the bipyridyl unit to the pyridinium moiety.^[185] These assignments were established in the photophysical studies of complexes with the general formula $[M(R_2qpy)_3]^{n+}$ investigating the impact of variations in the *N*-substituent of the quaterpyridinium ligand.^[186] It was demonstrated that the lower energy band showed only slight variations with changes in functionality, whilst the higher energy transitions showed a much greater dependence. It is expected that the pyridinium ring be more susceptible to changes in the *N*-substituent, hence this assignment. The scenario is more complex for the heteroleptic complexes due to the influence of the additional ligand environments, although processes involving the quaterpyridinium ligand are expected to be similar throughout the series.

Table 3.1 UV-visible absorption data for complexes with the general formula $[Ru(L)_{(3-n)}(L')_n]^{(n+2)+}$ containing quaterpyridinium ligands.

Complex	λ_{max} , nm	ϵ , $10^3 M^{-1} cm^{-1}$	E_{max} , eV	λ_{onset} , nm	Assignment
Hexafluorophosphate Salts^a					
[Ru(bpz) ₂ (Me ₂ qpy)] ⁴⁺	253	54.5	4.90	587	$\pi \rightarrow \pi^*$
	298	50.0	4.16		$\pi \rightarrow \pi^*$
	425 ^{sh}	17.1	2.92		$d \rightarrow \pi^*$
	453	21.3	2.74		$d \rightarrow \pi^*$
{Ru(bpz) ₂ [(HOCH ₂ Ph) ₂ qpy]} ⁴⁺	254	54.0	4.88	594	$\pi \rightarrow \pi^*$
	298	64.5	4.16		$\pi \rightarrow \pi^*$
	427 ^{sh}	20.0	2.90		$d \rightarrow \pi^*$
	455	24.3	2.73		$d \rightarrow \pi^*$
[Ru(bpy)(Me ₂ qpy) ₂] ⁶⁺	254	95.1	4.88	674	$\pi \rightarrow \pi^*$
	325	37.8	3.82		$\pi \rightarrow \pi^*$
	412	22.0	3.01		$\pi \rightarrow \pi^*$
	456	20.9	2.72		$d \rightarrow \pi^*$
	503	26.4	2.47		$d \rightarrow \pi^*$
Chloride Salts^b					
[Ru(bpz) ₂ (Me ₂ qpy)] ⁴⁺	250	50.0	4.96	588	$\pi \rightarrow \pi^*$
	304	51.5	4.08		$\pi \rightarrow \pi^*$
	426 ^{sh}	16.8	2.91		$d \rightarrow \pi^*$
	453	19.1	2.74		$d \rightarrow \pi^*$
{Ru(bpz) ₂ [(HOCH ₂ Ph) ₂ qpy]} ⁴⁺	249	49.8	4.98	592	$\pi \rightarrow \pi^*$
	305	65.0	4.07		$\pi \rightarrow \pi^*$
	430 ^{sh}	20.5	2.88		$d \rightarrow \pi^*$
	455	23.3	2.73		$d \rightarrow \pi^*$
[Ru(bpy)(Me ₂ qpy) ₂] ⁶⁺	255	88.2	4.86	665	$\pi \rightarrow \pi^*$
	323	34.2	3.84		$\pi \rightarrow \pi^*$
	411	20.2	3.02		$\pi \rightarrow \pi^*$
	454	18.7	2.73		$d \rightarrow \pi^*$
	503	23.8	2.47		$d \rightarrow \pi^*$

Solutions ca. 1.0×10^{-5} - 1.0×10^{-4} M. ϵ were determined from measurements at three or more different concentrations. ^{sh} denotes a shoulder or a poorly defined maximum. ^a Recorded in acetonitrile. ^b Recorded in deionised water

Table 3.2. UV-visible absorption data for complexes of the general formula [Ru(bpz)₂L]ⁿ⁺ recorded as the hexafluorophosphate salt.^a

Complex	λ_{\max} , nm	ϵ , 10 ³ M ⁻¹ cm ⁻¹	E_{\max} , eV	λ_{onset} , nm	Assignment
[Ru(bpz) ₃] ²⁺	239	19.6	5.18	568	$\pi \rightarrow \pi^*$
	292	53.3	4.25		$\pi \rightarrow \pi^*$
	338 ^{sh}	15.7	3.67		$d \rightarrow \pi^*$
	414 ^{sh}	10.5	3.00		$d \rightarrow \pi^*$
	441	13.0	2.81		$d \rightarrow \pi^*$
[Ru(bpz) ₂ dCF ₃ bpy] ²⁺	241	20.9	5.15	576	$\pi \rightarrow \pi^*$
	255 ^{sh}	18.4	4.86		$\pi \rightarrow \pi^*$
	293	60.1	4.23		$\pi \rightarrow \pi^*$
	344 ^{sh}	11.6	3.60		$d \rightarrow \pi^*$
	417 ^{sh}	10.6	2.97		$d \rightarrow \pi^*$
	447	13.3	2.77		$d \rightarrow \pi^*$
[Ru(bpz) ₂ bp _m] ²⁺	244	41.7	5.08	572	$\pi \rightarrow \pi^*$
	262	30.6	4.73		$\pi \rightarrow \pi^*$
	296	42.1	4.19		$\pi \rightarrow \pi^*$
	340 ^{sh}	15.1	3.65		$d \rightarrow \pi^*$
	413 ^{sh}	9.3	3.00		$d \rightarrow \pi^*$
	451	12.6	2.75		$d \rightarrow \pi^*$
[Ru(bpz) ₂ dCMbpy] ²⁺	220	29.9	5.64	580	$\pi \rightarrow \pi^*$
	298	65.1	4.16		$\pi \rightarrow \pi^*$
	343 ^{sh}	15.6	3.62		$d \rightarrow \pi^*$
	418 ^{sh}	13.9	2.97		$d \rightarrow \pi^*$
	449	17.0	2.76		$d \rightarrow \pi^*$
[Ru(bpz) ₂ dClbpy] ²	215	42.8	5.77	596	$\pi \rightarrow \pi^*$
	289	54.2	4.29		$\pi \rightarrow \pi^*$
	340 ^{sh}	13.3	3.65		$d \rightarrow \pi^*$
	430 ^{sh}	10.5	2.88		$d \rightarrow \pi^*$
	455	11.3	2.72		$d \rightarrow \pi^*$
[Ru(bpz) ₂ bpy] ²⁺	241	22.3	5.15	581	$\pi \rightarrow \pi^*$
	254 ^{sh}	20.0	4.88		$\pi \rightarrow \pi^*$
	295	49.3	4.20		$\pi \rightarrow \pi^*$
	342 ^{sh}	11.5	3.63		$d \rightarrow \pi^*$
	378	5.7	3.28		$d \rightarrow \pi^*$
	420	9.2	2.95		$d \rightarrow \pi^*$
	464	11.7	2.68		$d \rightarrow \pi^*$
[Ru(bpz) ₂ dPhbpy] ²⁺	243	37.2	5.10	603	$\pi \rightarrow \pi^*$
	262	39.3	4.73		$\pi \rightarrow \pi^*$
	298	80.2	4.16		$\pi \rightarrow \pi^*$
	388	9.5	3.20		$d \rightarrow \pi^*$
	425	15.4	2.92		$d \rightarrow \pi^*$
	465	13.8	2.67		$d \rightarrow \pi^*$
[Ru(bpz) ₂ dMebpy] ²⁺	241	21.2	5.15	605	$\pi \rightarrow \pi^*$
	296	45.6	4.19		$\pi \rightarrow \pi^*$
	374 ^{sh}	11.0	3.32		$d \rightarrow \pi^*$
	422	8.4	2.84		$d \rightarrow \pi^*$
	470	11.0	2.64		$d \rightarrow \pi^*$
[Ru(bpz) ₂ dtBubpy] ²⁺	208	39.3	5.96	608	$\pi \rightarrow \pi^*$
	240	22.7	5.17		$\pi \rightarrow \pi^*$
	296	51.2	4.19		$\pi \rightarrow \pi^*$
	345 ^{sh}	11.8	3.59		$d \rightarrow \pi^*$
	374 ^{sh}	7.4	3.32		$d \rightarrow \pi^*$
	422	9.5	2.94		$d \rightarrow \pi^*$
	470	12.1	2.64		$d \rightarrow \pi^*$
[Ru(bpz) ₂ dNH ₂ bpy] ²⁺	260	48.1	4.77	656	$\pi \rightarrow \pi^*$
	303	49.1	4.09		$\pi \rightarrow \pi^*$
	359	12.4	3.45		$d \rightarrow \pi^*$
	436	7.8	2.84		$d \rightarrow \pi^*$
	499	11.9	2.48		$d \rightarrow \pi^*$

^a Solutions ca. 1.0 × 10⁻⁵ - 1.0 × 10⁻⁴ M in acetonitrile. λ_{onset} defined as the wavelength above which $\epsilon > 100 \text{ M}^{-1}\text{cm}^{-1}$. ^{sh} denotes a shoulder or a poorly defined maximum.

Table 3.3. UV-visible absorption data for complexes of the general formula [Ru(bpz)₂L]ⁿ⁺ recorded as the chloride salt.^a

Complex	λ_{\max} , nm	ϵ , 10 ³ M ⁻¹ cm ⁻¹	E_{\max} , eV	λ_{onset} , nm	Assignment
[Ru(bpz) ₃] ²⁺	239	20.1	5.19	555	$\pi \rightarrow \pi^*$
	295	48.4	4.20		$\pi \rightarrow \pi^*$
	338 ^{sh}	16.9	3.67		$d \rightarrow \pi^*$
	413 ^{sh}	10.7	3.00		$d \rightarrow \pi^*$
	442	13.2	2.81		$d \rightarrow \pi^*$
[Ru(bpz) ₂ dCF ₃ bpy] ²⁺	241	22.6	5.15	564	$\pi \rightarrow \pi^*$
	292	54.3	4.25		$\pi \rightarrow \pi^*$
	335 ^{sh}	14.7	3.70		$d \rightarrow \pi^*$
	420 ^{sh}	11.2	2.95		$d \rightarrow \pi^*$
	450	12.9	2.76		$d \rightarrow \pi^*$
[Ru(bpz) ₂ bpm] ²⁺	244	30.7	5.08	561	$\pi \rightarrow \pi^*$
	260	30.7	4.77		$\pi \rightarrow \pi^*$
	299	41.6	4.15		$\pi \rightarrow \pi^*$
	340 ^{sh}	16.3	3.65		$d \rightarrow \pi^*$
	415 ^{sh}	9.7	2.99		$d \rightarrow \pi^*$
	452	12.8	2.74		$d \rightarrow \pi^*$
[Ru(bpz) ₂ dCMBpy] ²⁺	222	29.3	5.59	574	$\pi \rightarrow \pi^*$
	300	59.6	4.13		$\pi \rightarrow \pi^*$
	330 ^{sh}	21.3	3.76		$d \rightarrow \pi^*$
	425 ^{sh}	14.0	2.92		$d \rightarrow \pi^*$
	452	15.0	2.74		$d \rightarrow \pi^*$
[Ru(bpz) ₂ dClbpy] ²	215	36.1	5.77	599	$\pi \rightarrow \pi^*$
	299	41.2	4.15		$\pi \rightarrow \pi^*$
	333	12.7	3.72		$d \rightarrow \pi^*$
	383	5.2	3.23		$d \rightarrow \pi^*$
	423	9.1	2.93		$d \rightarrow \pi^*$
	463	10.4	2.68		$d \rightarrow \pi$
[Ru(bpz) ₂ bpy] ²⁺	240	23.1	5.17	593	$\pi \rightarrow \pi^*$
	274 ^{sh}	32.5	4.53		$\pi \rightarrow \pi^*$
	300	46.6	4.13		$\pi \rightarrow \pi^*$
	338 ^{sh}	12.5	3.67		$d \rightarrow \pi^*$
	374	6.6	3.32		$d \rightarrow \pi^*$
	421	8.4	2.95		$d \rightarrow \pi^*$
	469	11.9	2.64		$d \rightarrow \pi^*$
[Ru(bpz) ₂ dPhbpy] ²⁺	241	38.4	5.15	615	$\pi \rightarrow \pi^*$
	262	40.3	4.73		$\pi \rightarrow \pi^*$
	301	78.9	4.12		$\pi \rightarrow \pi^*$
	384	11.4	3.23		$d \rightarrow \pi^*$
	424	15.2	2.92		$d \rightarrow \pi^*$
	472	14.2	2.63		$d \rightarrow \pi^*$
[Ru(bpz) ₂ dMeppy] ²⁺	241	22.1	5.15	615	$\pi \rightarrow \pi^*$
	272	31.4	4.56		$\pi \rightarrow \pi^*$
	301	44.1	4.12		$\pi \rightarrow \pi^*$
	424	7.9	2.92		$d \rightarrow \pi^*$
	476	11.7	2.61		$d \rightarrow \pi^*$
[Ru(bpz) ₂ d ^t Bubpy] ²⁺	240	26.0	5.17	617	$\pi \rightarrow \pi^*$
	273 ^{sh}	36.7	4.54		$\pi \rightarrow \pi^*$
	301	49.7	4.12		$\pi \rightarrow \pi^*$
	340 ^{sh}	13.1	3.65		$d \rightarrow \pi^*$
	370 ^{sh}	8.9	3.35		$d \rightarrow \pi^*$
	424	9.0	2.92		$d \rightarrow \pi^*$
	475	12.7	2.61		$d \rightarrow \pi^*$
[Ru(bpz) ₂ dNH ₂ bpy] ²⁺	258	45.4	4.81	670	$\pi \rightarrow \pi^*$
	307	47.0	4.04		$\pi \rightarrow \pi^*$
	360	12.3	3.44		$d \rightarrow \pi^*$
	440	6.6	2.82		$d \rightarrow \pi^*$
	499	11.0	2.48		$d \rightarrow \pi^*$

^a Solutions *ca.* 1.0 × 10⁻⁵ - 1.0 × 10⁻⁴ M in deionised water. λ_{onset} defined as the wavelength above which $\epsilon > 100 \text{ M}^{-1}\text{cm}^{-1}$. ^{sh} denotes a shoulder or a poorly defined maximum.

3.3.4. Electrochemical Studies

Cyclic voltammograms were recorded for each of the complexes as the hexafluorophosphate salt at 50, 100 and 200 mV s⁻¹ with a supporting electrolyte of 0.1 M [nBu₄N]PF₆ in acetonitrile.

Table 3.4. Redox properties for compounds of the general formula [Ru(bpz)_(3-x)L_x]ⁿ⁺.^a

Cation	Ru(III/II)	E(2 ⁺ /1 ⁺)	E(1 ⁺ /0)	E(0/1 ⁻)	E(1 ⁻ /2 ⁻)
[Ru(bpz) ₃] ²⁺	+2.01 (90)	-0.66 (70)	-0.83 (70)	-1.10 (90)	-1.74 (90) ^b
[Ru(bpz) ₂ dCF ₃ bpy] ²⁺	+1.92 (120)	-0.69 (70)	-0.88 (60)	-1.13 (70)	
[Ru(bpz) ₂ bpm] ²⁺	+1.91 (90)	-0.71 (70)	-0.92 (60)	-1.17 (70)	-1.80 (100)
[Ru(bpz) ₂ dCMbpy] ²⁺	+1.89 (90)	-0.69 (70)	-0.89 (60)	-1.15 (70)	-1.65 (70)
[Ru(bpz) ₂ dClbpy] ²⁺	+1.82 (100)	-0.73 (80)	-0.95 (70)	-1.27 (80)	
[Ru(bpz) ₂ bpy] ²⁺	+1.79 (80)	-0.73 (70)	-0.96 (70)	-1.50 (70)	
[Ru(bpz) ₂ dPhbpy] ²⁺	+1.74 (90)	-0.73 (70)	-0.96 (70)	-1.43 (70)	-1.83 (70)
[Ru(bpz) ₂ dMebpy] ²⁺	+1.72 (80)	-0.75 (60)	-0.99 (60)	-1.58 (70)	
[Ru(bpz) ₂ d ^t Bubpy] ²⁺	+1.72 (100)	-0.75 (70)	-0.98 (60)	-1.58 (70)	
[Ru(bpz) ₂ dNH ₂ bpy] ²⁺	+1.43 (80)	-0.76 (60)	-1.06 (70)	-1.89 ^c	
[Ru(bpy) ₃] ²⁺	+1.32 (70)	-1.29 (70)	-1.27 (80)	-1.48 (70)	-1.73 (70)
	Ru(III/II)	E(4 ⁺ /3 ⁺)	E(3 ⁺ /2 ⁺)	E(2 ⁺ /1 ⁺)	E(1 ⁺ /0)
{Ru(bpz) ₂ [(HOCH ₂ Ph) ₂ Qpy]} ⁴⁺	+1.88 (90)	-0.43 ^c	-0.50 ^c	-0.75 ^c	-0.91 ^c
[Ru(bpz) ₂ Me ₂ Qpy] ⁴⁺	+1.85 (90)	-0.58 (70)	-0.69 (70)	-0.82 (60)	-1.044 ^c
	Ru(III/II)	E(6 ⁺ /5 ⁺)	E(5 ⁺ /4 ⁺)	E(4 ⁺ /3 ⁺)	E(3 ⁺ /2 ⁺)
[Ru(bpy)(Me ₂ qpy) ₂] ⁶⁺	+1.52 (90)	-0.62 ^c	-0.72 ^c	-1.19 ^c	-1.28 ^c

^a $E = 0.5 \times (E_{pc} + E_{pa})$ vs Ag/AgCl; Measurements performed in acetonitrile, 0.1 M [nBu₄N]PF₆. With a scan rate of 100 mV s⁻¹ at RT; Solutions ca. 1.5×10^{-4} M with respect to analyte; F_c/F_c⁺ internal reference, $E = 0.44$ V, $\Delta E_p = 70$ -90 mV; Pt disc working electrode and Pt wire auxiliary electrode. ^b quasi-reversible process; ^c irreversible process E_{pc} ; ^d irreversible process E_{pa} ; as determined using differential pulse voltammetry techniques, potential increment = 2 mV; amplitude = 50 mV; pulse width = 0.01 s.

Cyclic voltammograms for each of the complexes display a single reversible oxidation process with potentials in the range of 1.43 – 2.01 V and are assigned to the Ru(II/III) couple. On comparison of the potentials of [Ru(bpz)₃](PF₆)₂ and [Ru(bpz)₂bpy](PF₆)₂, the cathodic shift of 0.22 V that is evident in the latter is a consequence of the increased σ -donor ability of 2,2'-bipyridine in relation to 2,2'-bipyrazine.^[187] The difference in π -acceptor ability between these two ligands is expected to be minimal as is demonstrated in the comparative study regarding the coordination complexes of ruthenium(II) and nickel(II).^[132] In both instances an anodic shift of the oxidative couple was observed on substitution of bpy with bpz. As nickel(II) complexes exhibit minimal π -back bonding ability, the shift to more positive potentials may be described in terms of the inherent weaker σ -donor ability of bipyrazine.^[188] The relative influence of the two ligands is exemplified by a ca. 0.7 V cathodic shift of the Ru(II/III) couple for [Ru(bpy)₃](PF₆)₂ in relation to [Ru(bpz)₃](PF₆)₂, Fig. 3.8.

For the complexes of [Ru(bpz)₂L](PF₆)_n, the potential of the oxidative process directly correlates to the pK_a of the ancillary ligand and can be associated with the changes in σ -donor

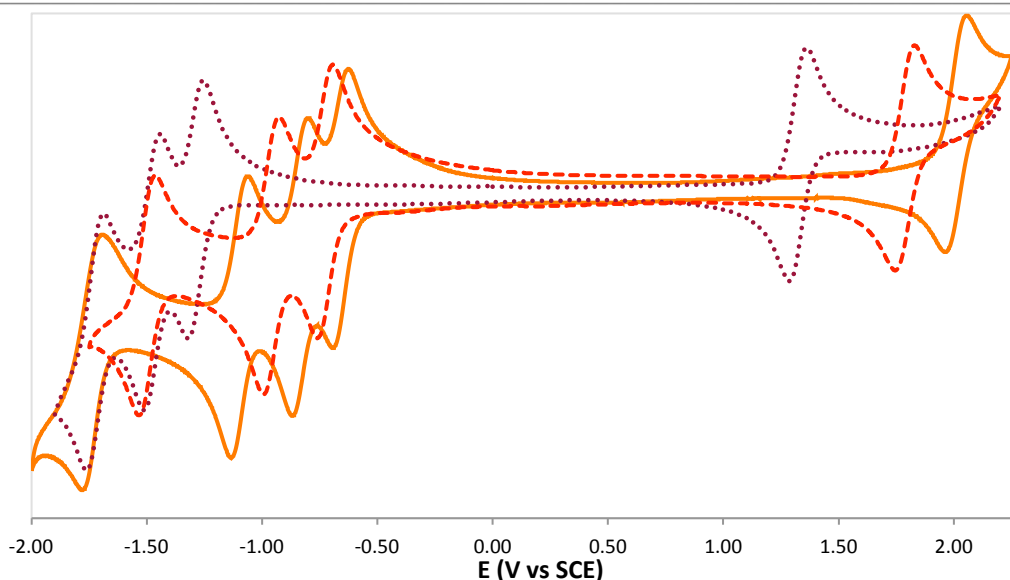


Fig. 3.8. Cyclic voltammograms of $[\text{Ru}(\text{bpz})_3](\text{PF}_6)_2$ (orange), $[\text{Ru}(\text{bpz})_2(\text{bpy})](\text{PF}_6)_2$ (red) and $[\text{Ru}(\text{bpy})_3](\text{PF}_6)_2$ (dark red) recorded at 100 mVs^{-1} in $0.1 \text{ M } n\text{-Bu}_4\text{NPF}_6$ acetonitrile at 298 K .

and π -acceptor abilities of the bipyridyl unit. In general an increasing $\text{p}K_a$ of the ancillary ligand results in an increasing cathodic shift in the $\text{Ru}^{\text{II/III}}$ couple with respect to $[\text{Ru}(\text{bpz})_3]^{2+}$. The shift is most pronounced for $[\text{Ru}(\text{bpz})_2\text{dNH}_2\text{bpy}]^{2+}$ with a value of *ca.* 0.58 V . This is afforded by delocalisation of the lone pair of the amine group into the π -system of the bipyridyl unit, which, through the available resonance forms, increases electron density at the relative *ortho/para* positions within the ring, thus significantly increasing the basicity of the coordinative nitrogen. The reverse is true for the related resonance forms within the diazine rings of bpz and bpm, which place a partial positive charge upon the *ortho* and *para* positions with respect to the electronegative heteroatoms. As such, for bpz the two nitrogens are mutually deshielded and therefore result in a ligand that acts as a poorer σ -donor; this is reflected by an anodic shift in the oxidation potential by 0.1 V for $[\text{Ru}(\text{bpz})_3]^{2+}$ in relation to $[\text{Ru}(\text{bpz})_2\text{bpm}]^{2+}$ and highlights the influence of the position of substitution upon the overall properties of the complexes.

The $\text{Ru}^{\text{II/III}}$ couple of $[\text{Ru}(\text{bpy})(\text{Me}_2\text{qpy})_2]^{6+}$ is at a potential approximating the mid point between those of $[\text{Ru}(\text{bpy})_2(\text{Me}_2\text{qpy})]^{4+}$ and $[\text{Ru}(\text{Me}_2\text{qpy})_3]^{8+}$, which were reported to be $+1.41 \text{ V}$ and $+1.60 \text{ V}$ respectively.^[153, 186] The trends therefore indicate a progressive anodic shift in potentials upon increasing the number of the more electron accepting $[\text{Me}_2\text{qpy}]^{2+}$ ligand. The additive effects of a ligand upon the oxidation potential within a series of complexes with the formula $[\text{Ru}(\text{L})_n(\text{L}')_{3-n}]^{2+}$ has been previously described and is in good agreement with the results presented here.^[189, 190]

The complexes of the disubstituted bipyridyl ancillary ligands display between three and four reversible reduction processes, with the exception of $[\text{Ru}(\text{bpz})_2\text{dNH}_2\text{bpy}]^{2+}$ which exhibits two reversible couples and an irreversible process at more negative potentials. Changes in the ancillary ligand induce shifts in $E(2^+/1^+)$ and $E(1^+/0)$ of 0.1 and 0.23 V

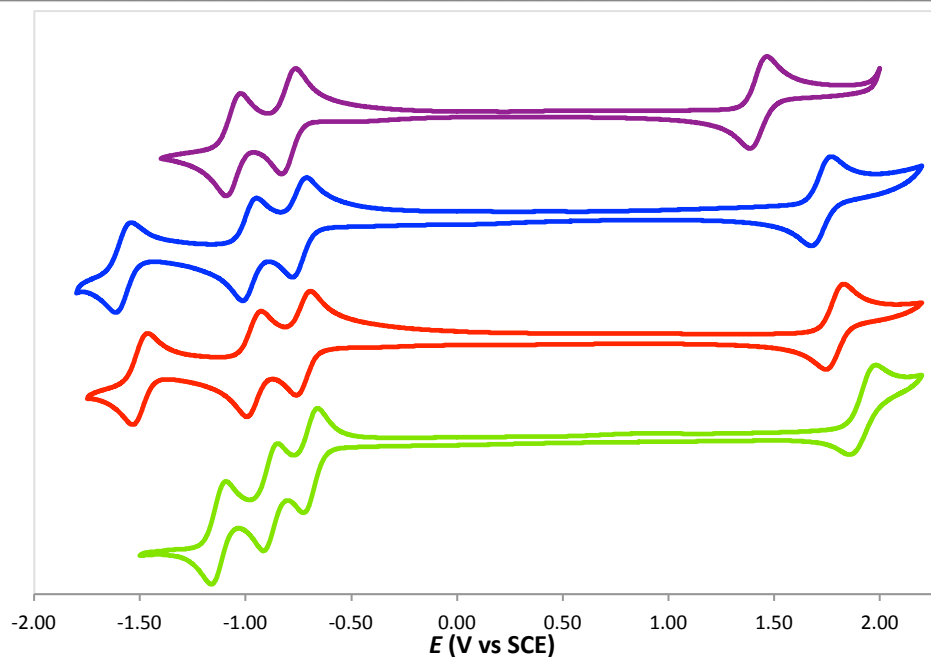


Fig. 3.9. Cyclic voltammograms of $[\text{Ru}(\text{bpz})_2\text{dNH}_2\text{bpy}](\text{PF}_6)_2$ (purple), $[\text{Ru}(\text{bpz})_2\text{d}^t\text{Bubpy}](\text{PF}_6)_2$ (blue), $[\text{Ru}(\text{bpz})_2\text{bpy}](\text{PF}_6)_2$ (red) and $[\text{Ru}(\text{bpz})_2\text{dCF}_3\text{bpy}](\text{PF}_6)_2$ (green) recorded at 100 mVs^{-1} in $0.1 \text{ M } n\text{-Bu}_4\text{NPF}_6$ acetonitrile at 298 K .

respectively between the extremes of the series. This effect is even more pronounced for $E(0/1^-)$, which is shifted by *ca.* 0.79 V , Fig. 3.9. Due to the decreased electron density of the pyrazyl ring it is expected that the respective π^* -orbitals be of the lowest energy; as exemplified on comparison of the reduction potentials of $[\text{Ru}(\text{bpz})_3](\text{PF}_6)_2$ and $[\text{Ru}(\text{bpy})_3](\text{PF}_6)_2$, Fig. 3.8. The $E(2^+/1^+)$ and $E(1^+/0)$ processes are therefore assigned to the single electron reduction of the individual bipyrazine ligands. $E(0/1^-)$ is subsequently associated with the reduction of the ancillary ligand which is in agreement with the susceptibility of this couple to changes in the 4,4'-substituents.

The reduction couples of the quaternised quaterpyridinium compounds are poorly defined due to extensive overlapping of multiple processes. Possible surface adsorption of the material also became evident on increasing the scan range to potentials greater than *ca.* -1.2 V . Through the use of pulse differential techniques, individual reduction waves could be sufficiently resolved to determine their potential. For both compounds, $E(4^+/3^+)$ and $E(3^+/2^+)$ are associated with the two single electron reductions of the pyridinium moieties. The anodic shift in potential for $[\text{Ru}(\text{bpz})_2(\text{HOCH}_2\text{Ph})_2\text{qpy}]^{4+}$ is a result of stabilisation of the pyridinium based LUMO on incorporation of the extended π -system of the hydroxymethylphenyl group. This is also reflected by a modest shift in the related oxidation couple, which is a consequence of the increased acceptor ability of quaterpyridinium upon changing the *N*-substituent. The influence of the metal centre upon the pendent pyridinium group appears to be relatively minor, as exemplified on comparison with the values obtained for the previously published bipyridyl analogues.^[153] Whilst the oxidation potential has shifted by an appreciable 0.44 V , the first reduction potential has undergone a shift of just *ca.* 0.04 V . The recorded potentials are also comparable to those obtained for $[\text{Ru}(\text{bpy})(\text{Me}_2\text{qpy})_2]^{6+}$.

The trends in the electrochemical gap, defined as $\Delta E = E_{\text{ox}} - E_{\text{red}}$, are in excellent agreement with the trends discussed concerning the MLCT bands of the UV-visible absorption spectra. Results demonstrate that effective tuning may be achieved through manipulation of the oxidation potential upon changes to the functionality of the ancillary ligand, thus affording ΔE values in the range of 2.19 – 2.67 V.

3.3.5. Theoretical Studies

In an effort to understand the origins of the measured UV-visible spectra, TD-DFT calculations were undertaken on a number of the report ruthenium complexes using Gaussian 09.^[191] Geometry optimisation and subsequent TD-DFT calculations were carried out at the B86,^[192, 193] B3LYP,^[194] PBE1PBE^[195] and M06^[196] levels with the Def2-QZVP^[197, 198] basis set and pseudopotential for ruthenium and Def2-SVP^[199] on all other atoms. Of these the M06 functional provided the best representation of the experimental data on inclusion of the CPCM^[200, 201] solvent model of acetonitrile. Using these parameters the first 100 excited singlet states were calculated and simulated UV-visible spectra were convoluted with Gaussian curves of fwhm of 3000 cm⁻¹ using GaussSum.^[202]

3.3.5.1. Structural geometries

Selected bond distances and bond angles describing the environment about the metal centre are presented in Table 3.5 for each of the optimised structures. Each of the cations exhibits a similarly distorted octahedral geometry. On comparison with the values determined by X-ray crystal diffraction of [Ru(bpz)₃](PF₆)₂^[203], Ru–N bond distances calculated for [Ru(bpz)₃]²⁺ are lengthened by *ca.* <0.025 Å. This is to be expected as coordination bond interactions are typically overestimated in DFT calculations employing hybrid functionals such as those used here;^[204] although those presented below prove to be a better representation of experimental data than those published previously at the B3LYP level.^[204-206]

On comparison of each of the distinct Ru–N bond lengths a definitive structural trans effect (STE) is evident. The Ru–N_B distances, describing the bond length between the metal centre and the nitrogen of the pyrazyl moiety trans to the pyridyl ring of the ancillary ligand, are consistently longer than those of Ru–N_A for the mutually trans pyrazyl rings. As discussed previously this is a result of the relative p*K*_a of the pyrazyl ring with respect to that of the pyridyl and variations induced in the latter on altering the substituted functional group. On increasing the electron density of the bipyridyl unit a general decrease in the Ru–N_A and Ru–N_B bond lengths are observed, although no discernable trend in the Ru–N_C distance is evident. It is surmised that the increased σ -donating ability of the more electron rich bipyridyl ligands affords an increase in the electron density at the metal centre. This subsequently allows for improved π -back bonding interactions with the bipyrazine ligands thus strengthening and shortening the bond. The Ru–N_C interatomic distances can be discussed in

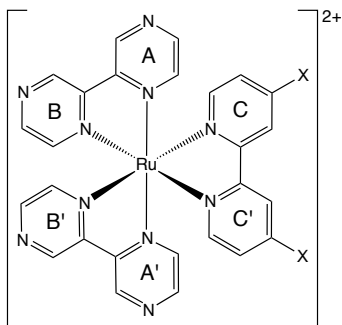


Fig. 3.10. Representative structures for complexes of the general formula $[Ru(bpz)_2(N^A N)]^{2+}$ with labelling schemes used in the discussion of optimised geometries.

Table. 3.5. Selected bond lengths (\AA) and bond angles ($^\circ$) taken from X-ray crystallography^[203] and from the DFT calculated optimised geometries of $[Ru(bpz)_{(3-X)}L_X]^{n+}$.

L =	Expt.	Calculated DFT-M06/Def2-QZVP(Ru) + Def2-SVP(C,H,N,F)					
	bpz	bpz	bpy	d ^t Bubpy	dCF ₃ bpy	dNH ₂ bpy	[Me ₂ qpy] ²⁺
Bond Lengths							
Ru–N _A	2.056	2.073	2.067	2.064	2.071	2.060	2.079
Ru–N _B	2.065	2.074	2.071	2.068	2.071	2.067	2.081
Ru–N _C	2.049	2.072	2.081	2.079	2.080	2.084	2.075
Bond Angles							
N _A –Ru–N _{A'}	172.66	174.19	174.91	175.67	174.24	175.36	171.83
N _B –Ru–N _{C'}	172.21	173.63	173.36	172.74	173.89	172.43	174.75
N _A –Ru–N _B	78.19	78.68	78.71	78.78	78.74	78.80	78.55
N _C –Ru–N _{C'}	78.71	78.63	78.34	78.25	78.52	77.81	77.58
N _A –Ru–N _C	89.77	87.96	87.85	88.11	87.94	95.12	88.56
N _A –Ru–N _{C'}	94.74	96.55	96.10	95.26	96.53	88.50	97.82
N _A –Ru–N _{B'}	96.78	97.09	97.56	98.05	97.04	97.81	95.40
N _B –Ru–N _{B'}	87.72	87.98	87.65	87.76	87.15	87.98	85.75
N _B –Ru–N _C	97.82	96.86	97.20	97.26	97.33	97.38	96.42

terms of a balance of increasing σ -donation and decreasing π -acceptor abilities of the ancillary ligand, which would result in no net change in the length of the bond.

Calculated bond angles are in good agreement with the experimental data, the greatest variation being 1.8° for $N_{z1}-Ru-N_{y1}$ and $N_{z1}-Ru-N_{y2}$. The bond angles between mutually trans heteroaryl rings are slightly overestimated in both instances though the relative magnitudes of the two values are correctly simulated. The optimised structure for $[Ru(bpz)_2Me_2qpy]^{4+}$ exhibits a torsion angle of 42.8° between the plane of the pyridyl ring of the bipyridyl moiety and the pendant pyridinium group. Whilst there are no published X-ray diffraction crystal structures for coordination compounds of $[Me_2qpy]^{2+}$, this value is consistent with those obtained for complexes of the analogous ligands 1-methyl-4-(4'-pyridyl)-pyridinium^[185, 207] and 4-(1-methyl-4-pyridinium)-2,2'-bipyridine.^[208]

3.3.5.2. Absorption properties

Calculated $S_0 \rightarrow S_1$ transition energies and the respective MO contributions for the cations $[Ru(bpz)_2bpy]^{2+}$, $[Ru(bpz)_2d^tBubpy]^{2+}$, $[Ru(bpz)_2d^tCF_3bpy]^{2+}$, $[Ru(bpz)_2dNH_2bpy]^{2+}$ and $[Ru(bpz)_2(Me_2qpy)]^{4+}$ are presented in Table 3.6. Comparisons of the experimental and

simulated UV-visible spectra are shown in Fig. 3.11 and Fig. 3.13. The calculated spectra are in very good agreement with those obtained experimentally though in each instance the low energy band is inaccurately represented as a single broad peak that is primarily comprised of two transitions of comparable oscillator strength. Separated by *ca.* 15 – 40 nm, these transitions directly correlate to the individual bands observed in the experimental data though are hypsochromically-shifted by *ca.* 5-10 nm. The exception to this are the results calculated for [Ru(bpz)₃]²⁺, which exhibits two transitions of almost identical energy corresponding to the mid-point between the absorption maxima and the higher energy shoulder of the experimental spectra.

The major orbital contribution of the lowest energy transition of significant oscillator strength is the same for each of the complexes, containing differing ratios of HOMO–2 → LUMO and HOMO–1 → LUMO+1. Both HOMO–2 and HOMO–1 are metal centred, the former derived from the d_{xy} and d_{xz} orbitals whilst the latter is predominantly $d_{x^2-y^2}$ in character with varying ratios of a d_{yz} contribution. A negligible component from the ligand π -system is also evident for these orbitals; in the HOMO and HOMO–1 this is situated about the ancillary ligand whilst for the HOMO–2 it is centred upon the pyrazyl rings *trans* to the substituted bipyridine. For [Ru(bpz)₂dNH₂bpy]²⁺ this contribution becomes significant with the additional electron density of the bipyridyl ligand localised about the amine group and the carbons in the relative *ortho* and *para* positions, thus reflecting the influence of the expected resonance structures within the pyridyl ring. The LUMO and LUMO+1 are predominantly bipyrazyl π^* -orbitals, where electron density is delocalised equally across the two ligands, although a minor metal d -orbital component is also apparent. Thus these transitions describe a MLCT with potentially a very minor LLCT component from the more electron rich bipyridyl moiety towards the bipyrazine ligands. Matching the related blue shift in the experimental data, on decreasing the electron donating ability of the substituent of the ancillary ligand, the energy of this transition increases owing to stabilisation of the HOMO. Calculations are successful in predicting the subtle difference in energy of 0.03 eV that is afforded on changing the ancillary ligand from 2,2'-bipyridine to 4,4'-di-*tert*-butyl-2,2'-bipyridine; exemplifying the accuracy of this approach.

The transition at a shorter wavelength is similarly a MLCT although to bipyrazyl π^* -orbitals of higher energy. A degree of HOMO–1 → LUMO+2 character is also evident, describing an MLCT towards the ancillary ligand. The LUMO+2 orbital, being predominantly localised upon the bipyridyl moiety, is highly dependent upon the relative pK_a of the ligand; for example, in relation to that of the bpy complex, for dNH₂bpy it is destabilised by 0.46 eV whilst for dCF₃bpy is stabilised by 0.36 eV. The extent of the contribution from this transition increases with decreasing pK_a of the ancillary ligand thus correlating to a decrease in the energy of LUMO+2. For [Ru(bpz)₂dNH₂bpy]²⁺ this orbital includes electron density delocalised across all three ligands. This is a consequence of the destabilising effects of the amine group so as the energy of the LUMO+2 is approximately equal to that of the LUMO+3 of the other cations; the latter being localised about the bipyrazyl ligands, thus explaining this additional contribution.

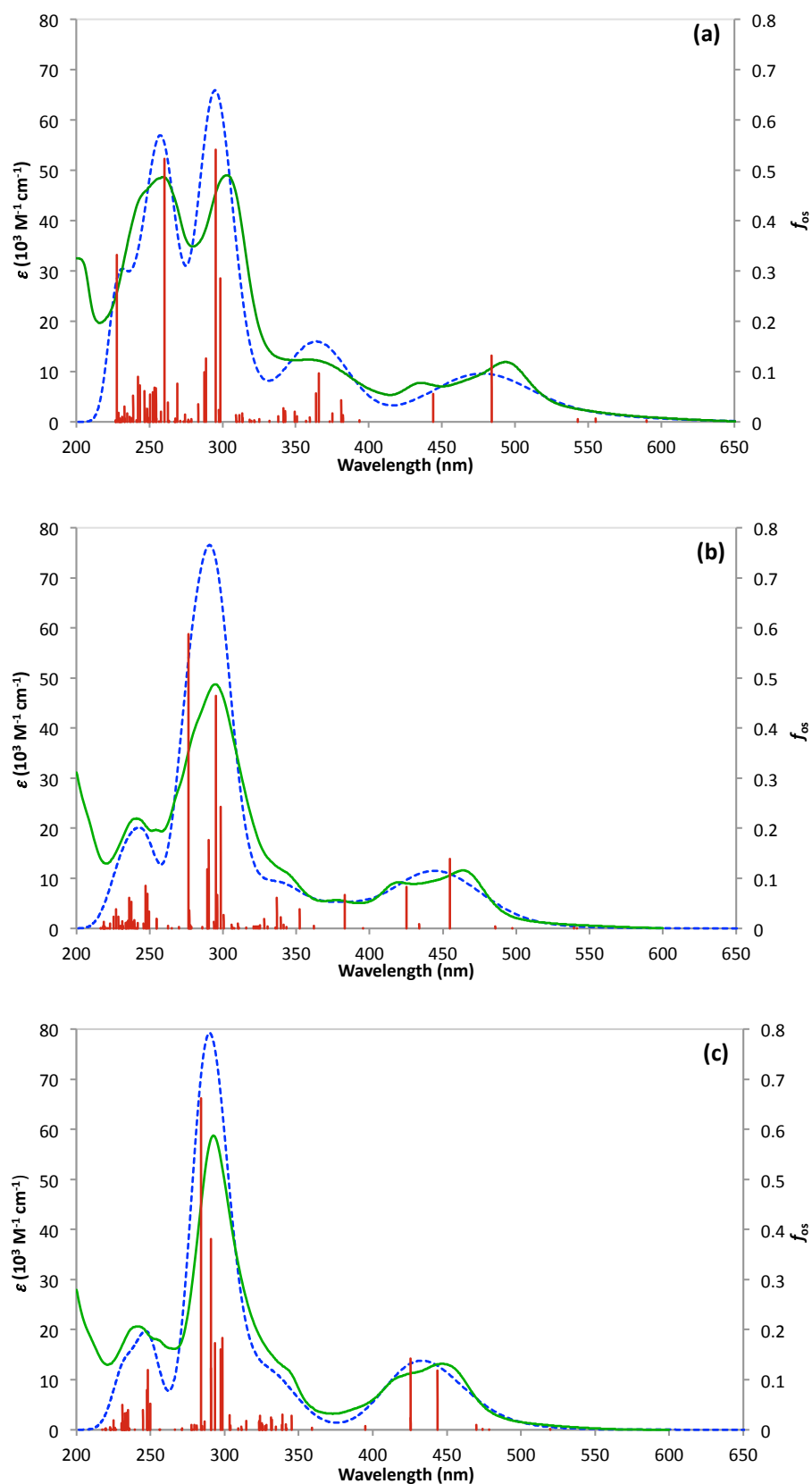


Fig. 3.11. Experimental (green) and the DFT calculated (blue dash) UV-Visible spectra of (a) $[\text{Ru}(\text{bpz})_2\text{dNH}_2\text{bpy}]^{2+}$, (b) $[\text{Ru}(\text{bpz})_2\text{bpy}]^{2+}$ and (c) $[\text{Ru}(\text{bpz})_2\text{dCF}_3\text{bpy}]^{2+}$. Experimental data is plotted against the primary ϵ -axes with calculated spectra scaled to match to allow for comparison of absorption bands. Individual calculated vertical transitions (red) are plotted versus the secondary oscillator strength (f_{os}) axes.

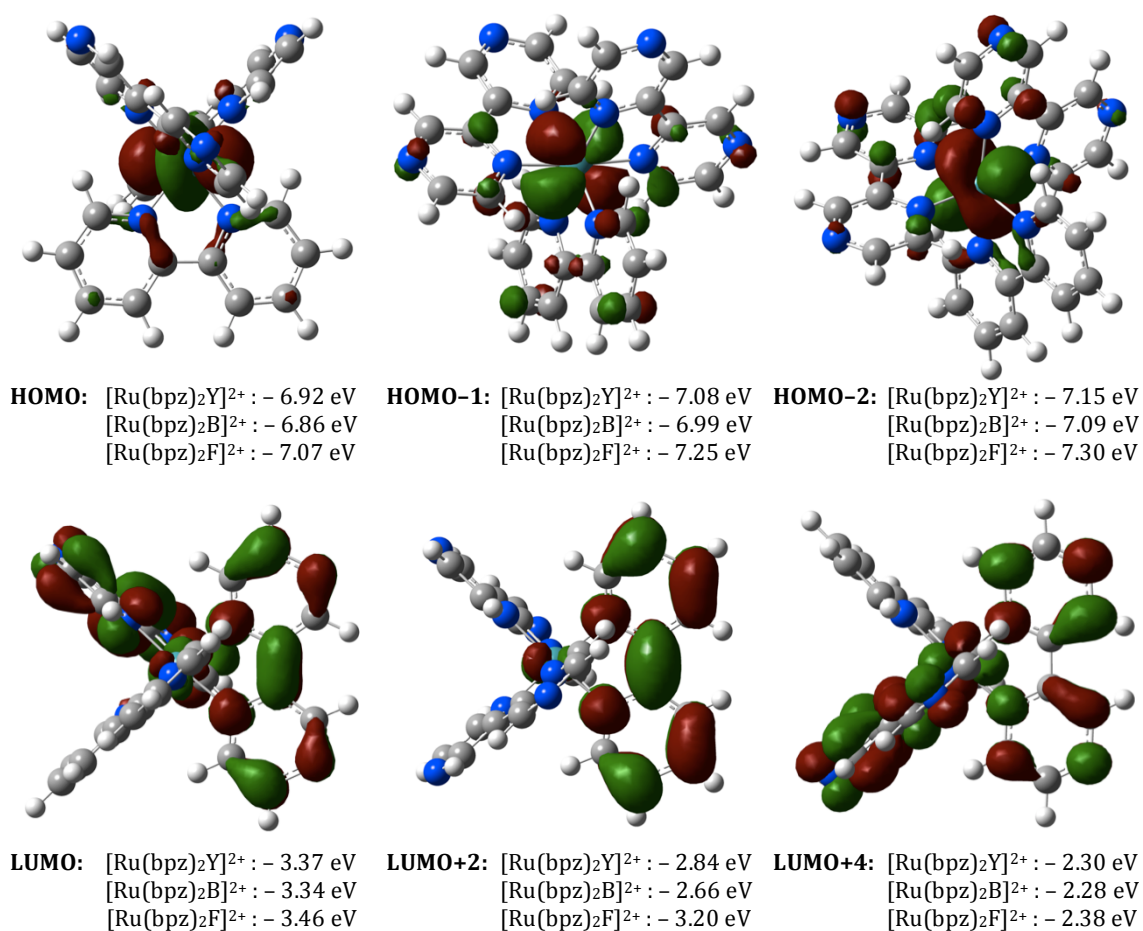


Fig. 3.12. DFT calculated electron density maps (isosurface value $0.03 e/\text{\AA}^3$) and respective energies for orbitals involved in the lower energy absorption (>350 nm) ascribed to MLCT transitions of [Ru(bpz)₂bpy]²⁺. Energies of the respective orbitals of [Ru(bpz)₂d^tBubpy]²⁺ and [Ru(bpz)₂dCF₃bpy]²⁺ are also listed.

The complexes of 2,2'-bipyridine and 4,4-di-*tert*-butyl-2,2'-bipyridine show an additional low intensity band at *ca.* 375 nm. Calculations show this correlates to a single transition at 383 and 375 nm for [Ru(bpz)₂bpy]²⁺ and [Ru(bpz)₂d^tBubpy]²⁺ respectively, both correspond to a predominantly HOMO-1 → LUMO+2 transition which originates from an MLCT involving the ancillary ligand as discussed. The shoulder between 325-350 nm is comprised of multiple transitions with oscillator strengths of ≤ 0.06 . The compositions suggest MLCT character involving bipyrazyl orbitals of energy equal to or higher than LUMO+4, in agreement with the assignment made in section 3.2.3.

The band at *ca.* 300 nm is derived from transitions primarily of LC character. The two predominant transitions of longer wavelengths describe the π - π^* transitions of bipyrazine and originate from two isostructural bonding orbitals, typically HOMO+4 and HOMO+5 which are separated by *ca.* 0.02 eV. Whilst the energies of these orbitals are minimally affected by changes in the ancillary ligand, the energy of the transition remains effectively constant throughout the series as the respective HOMOs and LUMOs are shifted by a similar magnitude. The intense higher energy transition models the equivalent process for the bipyridyl moiety

and is hypsochromically shifted with increasing pK_a of the ligand. The orbitals of the electron deficient dCF₃bpy are sufficiently close in energy to those of bipyrazine so as the LC transitions occur at similar wavelengths; this explains the narrowing of the absorption band and the lack of an observed shoulder for the intense band in the experimental data for [Ru(bpz)₂dCF₃bpy]²⁺.

Whilst LC transitions dominate the band at *ca.* 240 nm, a degree of ligand-to-ligand charge transfer (LLCT) character is evident. For the complexes of bpy, d^tBubpy and dNH₂bpy this is a clear transfer of electron density from the π -orbital of the ancillary ligand to the π^* -orbital of the bipyrazine ligands. However, for [Ru(bpz)₂dCF₃bpy]²⁺ this transition is less well defined as in this instance the electron density of the respective LUMO is delocalised across all three ligands. In no transition of significant oscillator strength were the reverse LLCT process observed, which is reasonable considering the relative pK_a of the ligands.

The calculated spectra for [Ru(bpz)₂(Me₂qpy)]⁴⁺ reveals a more complex origin of the lower energy MLCT band between 410 – 500 nm and is instead modelled upon four transitions of mixed bpz and (Me₂qpy)²⁺ character. The energy of the ill defined band at *ca.* 360 nm has been underestimated, resulting in a bathochromic shift of 20-30 nm and a subsequent broadening of the predicted profile. The HOMO, HOMO+1 and HOMO+2 are of equivalent composition to those previously discussed. The LUMO and LUMO+2 are now localised upon the ancillary ligand with the LUMO+1 and LUMO +3 of comparable energy and composition to the LUMO and LUMO+1 of the previously described cations respectively.

The low energy shoulder at *ca.* 330 nm is ascribed to a transition at 319 nm which corresponds to an ILCT within the ancillary ligand; analogous to the band at 325 nm in the experimental data of [Ru(bpy)(Me₂qpy)₂]⁶⁺ which was also assigned to an ILCT by literature precedent.^[185]

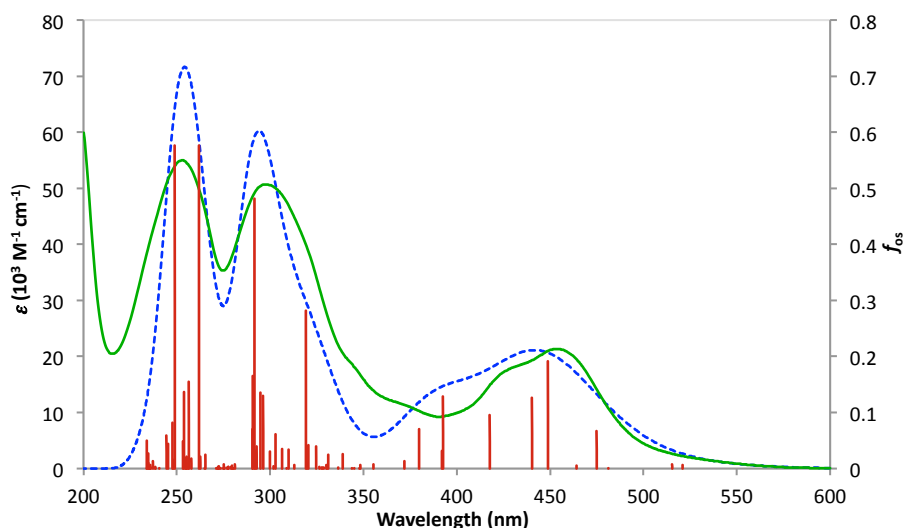


Fig. 3.13. Experimental (green) and the TD-DFT calculated (blue dash) UV-visible spectra of [Ru(bpz)₂Me₂qpy]⁴⁺. Experimental data is plotted against the primary ϵ -axes with calculated spectra scaled to match to allow for comparison of absorption bands. Individual calculated vertical transitions (red) are plotted versus the secondary oscillator strength (f_{os}) axes.

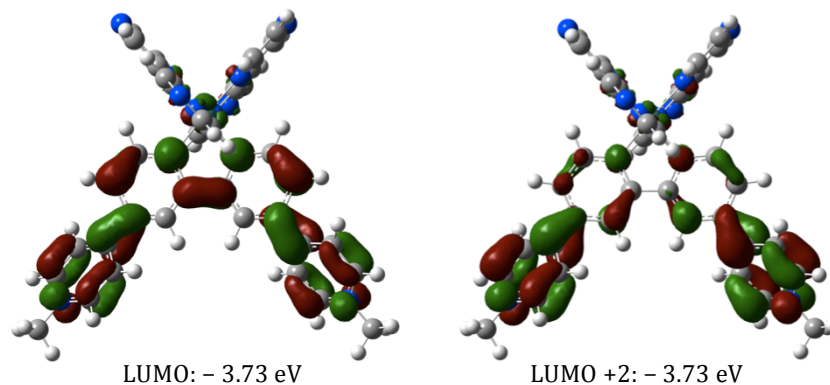


Fig. 3.14. TD-DFT calculated electron density maps (isosurface value $0.03 \text{ e}/\text{\AA}^3$) and respective energies for orbitals of $[\text{Ru}(\text{bpz})_2\text{Me}_2\text{qpy}]^{4+}$ involved in ILCT centred upon the ancillary ligand.

The trends in the relative energies of the HOMO and the LUMO are in excellent agreement with results obtained from cyclic voltammetry, Fig. 3.15. The composition of the LUMO, LUMO+1 and LUMO+2 corroborate the proposed assignments of the individual reduction couples as the bipyrazyl π^* -orbitals are typically of the lowest energy. The significant shifts in energy of the LUMO+2 orbital accurately describe those of $E(0/1^-)$ resulting from variations in the functionality of the ancillary ligand. The calculations also reflect the ease with which the pyridinium group is reduced as the LUMO of $[\text{Ru}(\text{bpz})_2\text{Me}_2\text{qpy}]^{4+}$ is stabilised by *ca.* 0.3 V and localised solely upon the ancillary ligand. The relative magnitude of destabilisation of the HOMO and LUMO on increasing the $\text{p}K_a$ of the ancillary ligand is well modelled. The variations in the energy gap are primarily a result of stabilisation of the metal-based HOMO and reflect the 0.58 V range in the recorded oxidation potentials. The differences in energy of the orbitals localised upon the bipyrazyl ligand are minimal by comparison, in agreement with the fairly consistent experimental values of the $E(2^+/1^+)$ and $E(1^+/0)$ couples.

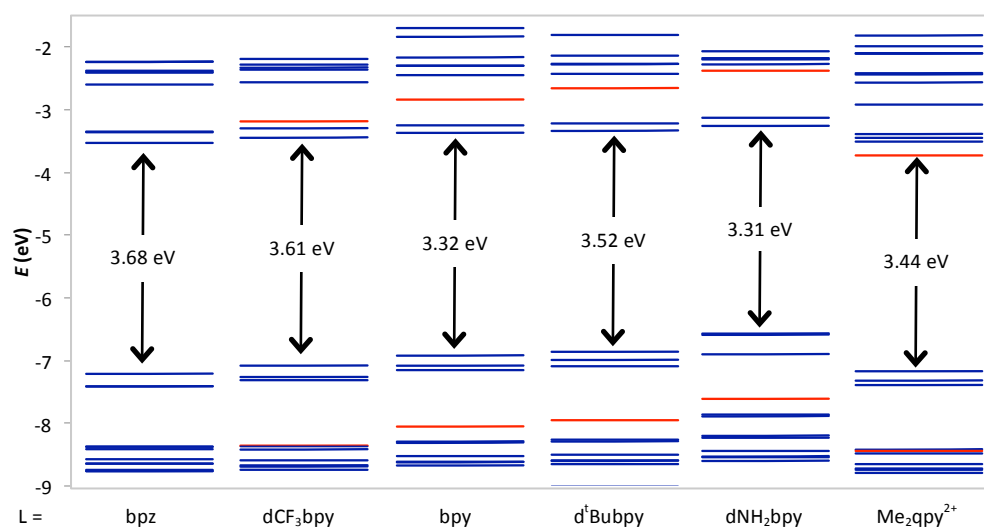


Fig. 3.15. Energy level diagram for complexes of the general formula $[\text{Ru}(\text{bpz})_2\text{L}]^{n+}$ displaying the TD-DFT calculated MOs within the range of -1.5 and -9.0 eV . Orbitals highlighted in red are the highest energy occupied and lowest energy unoccupied orbitals of considerable ancillary ligand contribution.

Table 3.6. Select vertical transitions obtained by TD-DFT calculations performed for the complex cations of the general formula $[Ru(bpz)_3-xLx]^{n+}$. Presented transitions chosen to represent the major contributors to each of the dominant bands in the UV-Visible spectra between 300 and 800 nm.

Cation	λ /nm	ΔE /eV	f_{os}	Major Contributions
[Ru(bpz) ₂ bpy] ²⁺	454.7	2.73	0.14	H-2 → LUMO (69 %), H-1 → L+1 (25 %)
	425.1	2.92	0.08	H-2 → L+1 (71 %), H-1 → LUMO (10 %), H-1 → L+2 (10 %)
	383.0	3.24	0.07	H-1 → L+2 (78 %), HOMO → L+5 (14 %)
	352.3	3.52	0.04	H-1 → L+5 (10 %), HOMO → L+4 (87 %)
	336.8	3.68	0.06	H-2 → L+3 (74 %), H-1 → L+5 (11 %)
[Ru(bpz) ₂ d ^t Bubpy] ²⁺	459.2	2.70	0.14	H-2 → LUMO (72 %), H-1 → L+1 (24 %)
	428.1	2.90	0.08	H-2 → L+1 (73 %), H-1 → LUMO (10 %)
	374.7	3.31	0.10	H-1 → L+2 (77 %), HOMO → L+5 (19 %)
	356.1	3.48	0.03	H-1 → L+5 (12 %), HOMO → L+4 (85 %)
	344.3	3.60	0.05	H-1 → L+5 (72 %), HOMO → L+4 (10 %)
[Ru(bpz) ₂ dNH ₂ bpy] ²⁺	484.1	2.56	0.132	H-2 → LUMO (79 %), H-1 → L+1 (13 %)
	444.0	2.79	0.0554	H-2 → L+1 (75 %)
	381.2	3.25	0.0428	H-1 → L+2 (65 %), HOMO → L+4 (26 %)
	365.9	3.39	0.096	H-1 → L+4 (35 %), HOMO → L+5 (56 %)
	363.9	3.41	0.0569	H-1 → L+3 (34 %), H-1 → L+5 (39 %), HOMO → L+4 (10 %)
[Ru(bpz) ₂ dCF ₃ bpy] ²⁺	443.7	2.79	0.12	H-2 → LUMO (75 %), H-1 → L+1 (20 %)
	425.5	2.91	0.14	H-2 → L+1 (50 %), H-1 → L+2 (38 %)
	345.3	3.59	0.03	HOMO → L+4 (71 %), HOMO → L+9 (19 %)
	339.0	3.66	0.03	H-1 → L+3 (78 %), HOMO → L+5 (12 %)
	331.9	3.74	0.02	H-1 → L+4 (14 %), HOMO → L+6 (58 %)
	331.4	3.74	0.02	H-1 → L+5 (56 %), HOMO → L+4 (10 %), HOMO → L+7 (14 %)
[Ru(bpz) ₂ (Me ₂ qpy) ⁴⁺	475.0	2.61	0.0671	H-1 → LUMO (43 %), H-1 → L+1 (53 %)
	448.8	2.76	0.1911	H-2 → L+3 (23 %), H-1 → LUMO (42 %), H-1 → L+1 (24 %)
	440.3	2.82	0.1263	H-2 → L+1 (68 %), H-1 → L+3 (23 %)
	417.7	2.97	0.0959	H-2 → L+3 (27 %), HOMO → L+2 (53 %)
	392.6	3.16	0.1283	H-1 → L+2 (86 %), H-1 → L+3 (11 %)
	379.8	3.27	0.07	H-2 → L+2 (62 %), H-2 → L+3 (21 %)
	319.2	3.89	0.282	H-5 → LUMO (47 %), H-4 → LUMO (14 %), H-2 → L+5 (16 %)

3.3. CONCLUSIONS

An extensive investigation into the synthesis of 2,2'-bipyrazine has been undertaken utilising a variety of coupling methods. This has allowed the development of an efficient and simplistic procedure that provides improved yields of upto 70 % and material of excellent purity. This has subsequently allowed the chemistry of the bis(2,2'-bipyrazyl)dichlororuthenium(II) precursor to be extensively explored and a number of new tris polypyridyl ruthenium complexes, including a variety of functional groups, to be synthesised. The experiments undertaken have allowed for the optimisation of these coordination reactions and has highlighted the relative differences in the chemistry of this precursor in comparison to the 2,2'-bipyridyl analogues. The photophysical and electrochemical properties have been probed using UV-visible absorption spectroscopy and cyclic voltammetry thus demonstrating the effectiveness with which the redox properties may be tuned upon manipulation of the ancillary ligand. TD-DFT calculations have provided further insight into the origins of the UV-visible absorption profile and has shown that the MLCT region is dominated by $d_{\text{Ru}} \rightarrow \pi^*_{(\text{bpz})}$ transitions, with a contribution of $d_{\text{Ru}} \rightarrow \pi^*_{(\text{bpy})}$ at higher energies.

3.4. FUTURE WORK

It is surmised that the insights gained through this work with 2,2'-bipyrazine may also prove valuable in the development of the ruthenium coordination chemistry of other electron deficient polypyridyl pro-ligands such as 2,2'-bipyridazine and dipyrido(3,2-*c*:2',3'-*e*)pyridazine (taphen). There is also further scope for fine-tuning the properties of complexes of 2,2'-bipyrazine on quaternisation of the distal nitrogens of the ligand to form compounds based upon the 4,4'-dimethyl-2,2'-bipyrazinium moiety.^[209, 210] It is expected that the first reduction process would undergo a significant anodic shift on quaternisation and provide a series of compounds with considerably different redox properties to those presented here. Whilst the ruthenium chemistry of these diquaternised heterocycles has been previously demonstrated, it has yet to be expanded to include the bis- or tris-complexes of such ligands.

Further work into the synthesis of bimetallic and higher order multimetallic compounds of the bis(2,2'-bipyrazyl)ruthenium moiety are still warranted. Whilst more conventional means of synthesis have been exhausted, a number of potential avenues of research remain. One such approach would be microwave-assisted or solvothermal reactions of bis(2,2'-bipyrazyl)dichlororuthenium(II); the high temperatures/pressures accessed under these conditions may be sufficient to overcome the lack of reactivity that has been previously displayed. Another approach would be that of the direct coupling reactions (for example the Suzuki-Miyaura reaction) of two monometallic tris-(polypyridyl)ruthenium(II) complex salts on inclusion of specific functional groups onto the ancillary ligand. However, such an approach has limited potential in investigating the intermetallic communication, as the number of potential bridging ligands that can be formed in this manner are few.

SECTION FOUR

SYNTHESIS AND ANALYSIS OF CATIONIC IRIDIUM(III) CYCLOMETALATED COMPLEXES.

4.1 INTRODUCTION

In an effort to prepare photosensitisers with as broad a range of properties as possible, the investigation would need to be expanded to incorporate metal centres other than ruthenium(II). Of particular interest are the cyclometalated iridium(III) complexes, which in recent years have demonstrated potential for a diverse range of photophysical and photochemical applications, including organic light emitting diodes (OLEDs);^[211-214] light-emitting electrochemical cells (LEECs);^[215, 216] bio labelling;^[217-219] chemosensors for a variety of species^[220, 221] and dye sensitised solar cells (DSSCs)^[57, 222, 223]. Such broad interest has been garnered as a result of the high quantum efficiencies, long-lived triplet states and strong photoluminescence typically displayed by such compounds owing to the large spin orbit coupling constant of the iridium metal centre; $\zeta = 3909 \text{ cm}^{-1}$ in comparison to $\zeta = 431, 1042, 3381 \text{ cm}^{-1}$ for iron, ruthenium and osmium respectively. The ability of these complexes to act as efficient photoreductants was first demonstrated for tris[2-phenylpyridinato-C²,N]iridium(III), Ir(ppy)₃, as indicated by the quenching of luminescence in the presence of a variety of oxidative quenchers.^[224] This has since been effectively adapted towards applications of photosensitised hydrogen production, boasting high H₂ yields and quantum efficiencies that are 16-37 times greater than those of a [Ru(bpy)₃]Cl₂ standard.^[225, 226]

The mononuclear cyclometalated iridium(III) compounds containing bidentate ligands may be discussed in terms of two broad categories, Fig. 4.1. The first are the charge neutral complexes with the general formulae Ir(C^N)₃ and Ir(C^N)₂(L^X) where C^N is a cyclometalated ligand and L^X is a monoanionic ancillary ligand. The second are bis-cyclometalated complexes that incorporate a neutral diimine (N^N), or an analogue thereof, as an ancillary ligand to give a cationic complex of the formula [Ir(C^N)₂(N^N)]ⁿ⁺.

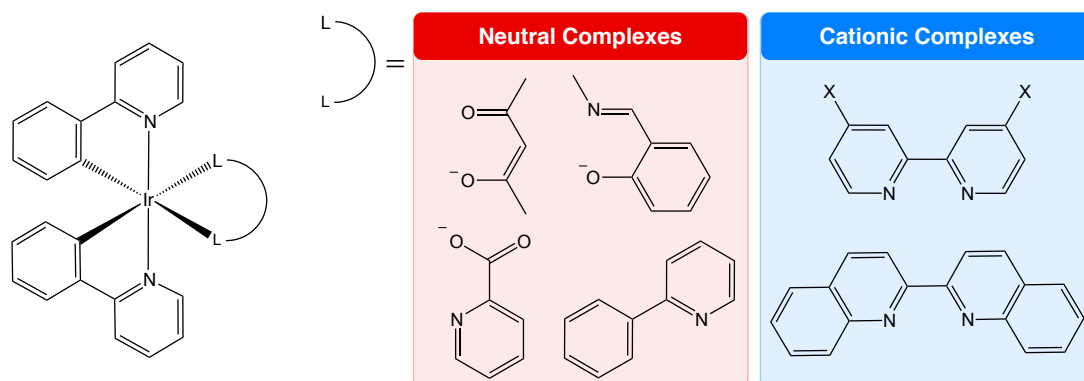


Fig. 4.1. General structure of the bis cyclometalated iridium(III) compounds highlighting potential ligands that may be used in the formation of neutral and cationic complexes.

As with ruthenium, the coordination compounds of iridium(III) have displayed an extensive chemistry that allows for the tuning of their photophysical and redox properties. For complexes of the general formula $[\text{Ir}(\text{C}^{\wedge}\text{N})_2(\text{N}^{\wedge}\text{N})]^{n+}$ this may be achieved using three distinct methods. The first involves making changes to the ancillary ligand, which is primarily utilised to modulate the energy of the metal-based HOMO. This is achieved through altering the σ -donating and π -accepting abilities of the ancillary ligand so as to influence the electron density at the metal centre.

Manipulation of the heteroaryl moiety of the cyclometalating ligand effects changes in the energy of the corresponding LUMO and subsequently the associated MLCT and LC transitions. For example, an extension of the π -system from 2-phenylpyridine to 1-phenylisoquinoline afforded a bathochromic shift of λ_{em} by 106 nm.^[214] Alternatively, a significant blue shift in emission was achieved upon replacing the pyridyl ring with a heteroaryl moiety with LUMOs of inherently higher energy; use of a pyrazoyl ring resulted in a hypsochromic shift of 80 nm whilst the use of *N*-heterocyclic carbene moieties, in ligands such as 1-phenyl-3-methylimidazolium, yielded complexes with $\lambda_{\text{em}} \approx 380$ nm in Me_2THF .^[227]

The final method is to make alterations to the cyclometalating moiety, which may be utilised towards the manipulation of the ligand and metal-centred HOMOs whilst affording minimal changes in energy of the ligand based LUMO. Consequently, on incorporation of electron withdrawing substituents, a significant increase in the energy of both the MLCT and LC transitions may be achieved owing to stabilisation of the HOMO. On substitution with fluorine at the 4-position of the phenyl ring, a hypsochromic shift in emission of 26 nm is observed.^[228] Further stabilisation was afforded on incorporation of a second fluorine in the 6-position to yield an overall shift of 42 nm with a $\lambda_{\text{em}} = 450$ nm.^[229, 230]

The use of cyclometalated iridium compounds for certain applications has been somewhat limited due to their inherently poor water solubility. In such cases the focus has predominantly been upon the cationic complexes containing a polypyridyl ligand, which display an increased ionic character. This property may be further augmented on incorporation of specific functionality, with particular success having been achieved through the use of bipyridyl ligands containing charged functional groups. Byun *et al* reported the use of the 3,3'-dihydroxy-2,2'-bipyridine ligand in the synthesis of bis(1-(phenyl)isoquinolinato)iridium(III) (2,2'-bipyridine-3-ol-3'-olate), Fig. 4.2.a.^[231] Under the reported reaction conditions deprotonation of a single hydroxyl group afforded a charge neutral zwitterionic complex. Characterisation suggested significant intramolecular H-bonding between the hydroxyl proton and the olate oxygen as demonstrated by the very short O-O distance of 2.39 Å. It is the stability of this $\text{O}^1\text{—H}\cdots\text{O}^2$ bond that is surmised to be the driving force for the complex adopting zwitterionic character and thus improving water solubility.

Jiang *et al* demonstrated the effectiveness of incorporating hydrophilic carboxylate functionality, synthesising a variety of complexes with the general formula $\text{Ir}(\text{C}^{\wedge}\text{N})_2(4\text{-carboxy-2,2'-bipyridyl-4'-carboxylate})$, where $(\text{C}^{\wedge}\text{N}) = 1\text{-phenylpyridine, 1 phenylpyrazole,}$

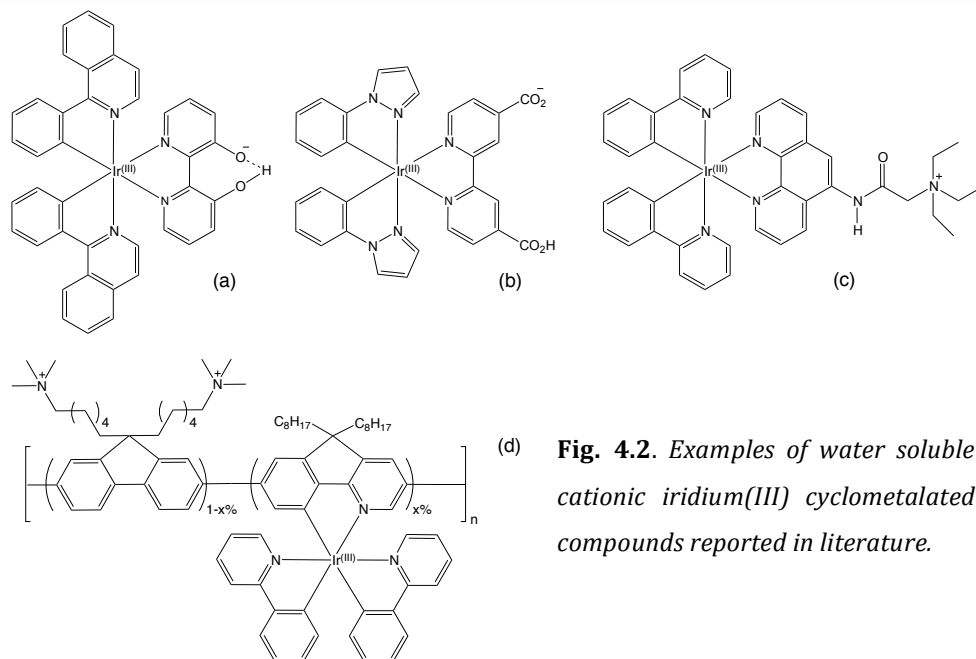


Fig. 4.2. Examples of water soluble cationic iridium(III) cyclometalated compounds reported in literature.

Fig.4.2.b, 2-(4',6'-difluoro-phenyl)pyridine, dibenzo[*f,h*]quinoxaline, and 1-phenylisoquinoline.^[232] The identity as a zwitterionic compound was confirmed by elemental analysis and X-ray crystallography, the latter indicating an inequivalency of the C—O bond lengths of the two carboxy- groups. After extended periods of sonication and stirring in 50 mM KPO₄ buffer at room temperature, solubilities ranging from 37-5096 μ M were achieved. The extent of solubility proved to be highly dependant upon the nature of the cyclometalating ligands used, as on increasing the steric bulk a marked decrease in water solubility was observed; this was exemplified by the complexes of dibenzo[*f,h*]quinoxaline which were only slightly soluble despite the measures employed.

More recently the potential of cationic ligands has also been investigated, specifically utilising quaternary amine functional groups. Sun *et al* reported the preparation of water soluble conjugated polyelectrolytes (CPEs) containing iridium(III) metal centres, Fig. 4.2.d.^[233] Quaternary amine functionality was introduced upon the reaction of trimethylamine with a bromoalkyl- group incorporated into the side chain of the neutral polymeric precursor complex. The latter was prepared over an extensive multistep synthesis involving the Suzuki-Miyaura coupling reaction of 2-(4',4',5',5'-tetra-methyl-1',3',2'-dioxaborolan-2'-yl)-7-bromo-9,9-dioctylfluorene with 2,5-dibromopyridine and subsequent cyclometalating reaction of the resultant 5-bromo-2-(2-bromo-9,9'-dioctyl-9H-fluoren-7-yl)pyridine with IrCl₃.H₂O. The final step was a Suzuki-Miyaura type polymerisation reaction of the complex with bis(bromohexyl)-2,7-dibromofluorene and bis[9,9'-bis(6''-bromohexyl)fluorenyl]-4,4,5,5-tetramethyl[1.3.2]dioxaborolane. Ma *et al* adopted a similar approach in utilising 2-((1,10-phenanthrolin-5-yl)amino)-*N,N,N*-triethyl-2-oxoethanaminium as an ancillary ligand, which was prepared from 1,10-phenanthroline via the 2-chloro-*N*-(1,10-phenanthrolin-5-yl) acetamide intermediate, Fig. 4.2.c.^[234]

The investigation presented here will instead focus upon the use of the pyridinium moiety as a means of enhancing aqueous solubility of the cationic cyclometalated iridium(III)

complexes by means of increasing the overall positive charge. This work will entail the synthesis of two distinct series of complexes that incorporate this functional group in one of two ways. Inclusion within the ancillary ligand will be achieved upon preparing complexes of the *N*-substituted quaterpyridinium compounds, as previously discussed in Section 3. The influence of these ligands upon the properties of the resultant complexes will be investigated through manipulation of the functionality of the pyridinium group.

The second approach will evaluate the potential of incorporating the functionality into the cyclometalating ligand by preparing complexes of the quaternised 2,2'-, 3,2'- and 4,2'-bipyridinium salts. Whilst considerable work has been undertaken concerning these compounds^[235] there is relatively little precedence for their utilisation as cyclometalating ligands. The focus of such work has primarily been towards the synthesis of complexes of Pd and Pt with the general formula $[M(C^N)LL'](X)_n$.^[236-241] Complexation to Group XII metals Zn(II), Hg(II) and Cd(II) has also been undertaken, although this resulted in the formation of complexes of the general formula $M(N-Me-2,2'bpy)X_3$, where X = Cl, Br and I, with the bipyridinium ligand acting in a monodentate fashion.^[242] A small series of ruthenium polypyridyl complexes has been reported, describing the reactions of 1-methyl-3-(2-pyridyl)pyridinium and 1-methyl-4-(2-pyridyl)pyridinium with $Ru(bpy)_2Cl_2$ in the presence of Et_3N or $AgPF_6$ to prepare compounds of the formula $[Ru(N^N)_2(C^N)](PF_6)_2$. Reactions of 1-methyl-2-(2-pyridyl)pyridinium failed to yield the desired cyclometalated product, instead resulting in demethylation to selectively form $[Ru(bpy)_3](PF_6)_2$.^[243] More recently, examples of similar ligands have been reported in the formation of a number of iridium(III) complexes of the formula $[Ir(COD)(L)HX]^+$; where COD = 1,5-octadiene, X = Br and I and L = 1-*n*-butyl-3-(2-pyridyl)pyridinium; 1-*n*-butyl-3-(2-pyridyl)-4-methylpyridinium; 7-*n*-butyl-1,7-phenanthroline-7-ium; 9-*n*-butyl-1,9-phenanthroline-9-ium or the quaternised benzyl derivatives of the latter two compounds.^[244] The focus of the study was the corresponding catalytic activity towards ketone transfer hydrogenation reactions; the spectroscopic and electrochemical properties of these complexes were not examined.

As part of this study, three series of complexes containing the bis-(*N*-substituted-bipyridinium)iridium(III) moiety will be prepared and a full characterisation of the photophysical and electrochemical properties undertaken. The influence of the unquaternised ancillary ligand will also be evaluated upon incorporation of varied functional groups.

4.2 RESULTS AND DISCUSSION

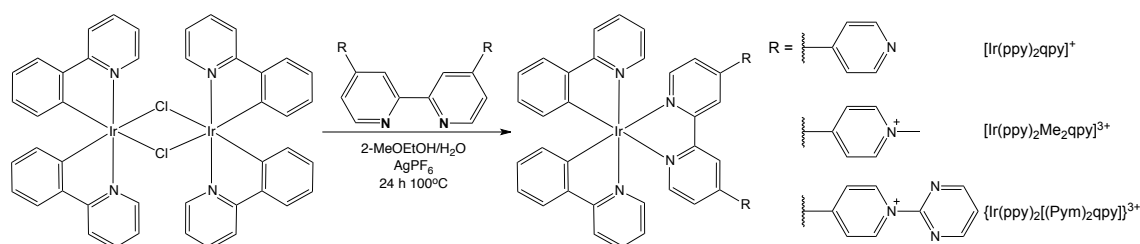
4.2.1. Synthetic Studies

4.2.1.1 Complexes of the General Formula [Ir(ppy)₂L]ⁿ⁺

The first iridium compounds to be synthesised were those of the quaternised quaterpyridinium ancillary ligands. 2-phenylpyridine was chosen as the cyclometalating ligand as it has been studied extensively in literature; thus providing the means of evaluating the effects of the ancillary ligand upon the properties of a well-established system.

The quaterpyridinium ligands were prepared as discussed in Section 3 and isolated as the hexafluorophosphate salt. 2-phenylpyridine was prepared in a single step by a ligand-free Suzuki-Miyaura coupling reaction between 2-bromopyridine and benzenboronic acid. Reactions employed Pd(OAc)₂ as a catalyst and were performed under aerobic conditions in 50% isopropanol and in the presence of K₃PO₄.^[245]

[Ir(ppy)₂Cl]₂ was synthesised upon the reaction of IrCl₃.nH₂O with 2-phenylpyridine in 2-methoxyethanol and water using modified Nonoyama conditions.^[246] On cooling of the reaction mixture the chloro-bridged dimer was readily isolated in good yields on collection of the resultant precipitate and washing with ethanol/water. Further material was collected by evaporation of the mother liquor and reprecipitation from DCM/diethyl ether, though the material obtained was of lower purity than that collected on initial filtration.

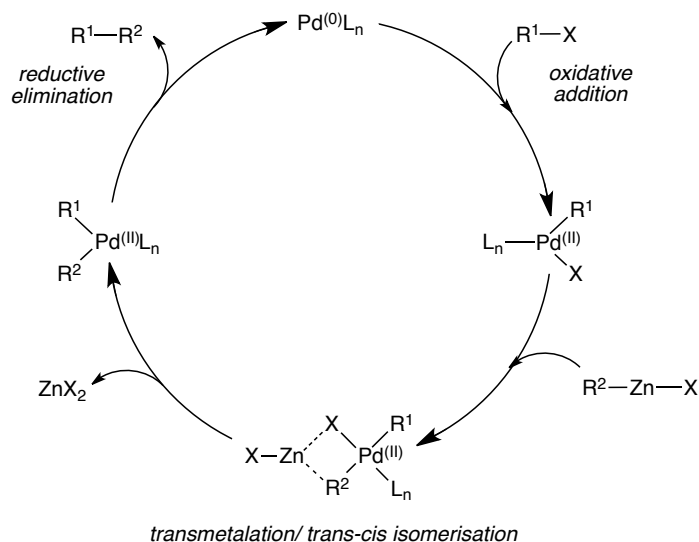


Scheme 4.1. Reaction scheme detailing the general procedure used in the preparation of bis-cyclometalated cationic iridium(III) complexes with general formula [Ir(ppy)₂(N[^]N)](PF₆)ⁿ⁺, specifically utilising a 4,4':2',2'':4'',4'''-quaterpyridinium ancillary ligand.

The monomeric compounds of general formula [Ir(ppy)₂L]ⁿ⁺ were prepared by reacting two equivalents of the appropriate quaterpyridyl or quaterpyridinium ligand with the chloro-bridged dimer in 2-methoxyethanol:water (3:1) under reflux. The crude material was isolated on concentration of the reaction mixture and precipitation by addition of a saturated NH₄PF₆ aqueous solution. Purification was achieved using column chromatography on silica gel and eluting with 0.1M NH₄PF₆ in acetonitrile, analogous to the method used in the purification of the [Ru(bpz)₂L]ⁿ⁺ complex salts. Each of the three compounds were isolated in moderate to good yields, ranging from 65 % for {Ir(ppy)₂[(2-Pym)₂qpy]}³⁺ to 78 % for [Ir(ppy)₂(Me₂qpy)]³⁺. Methathesis to the chloride salt was afforded on dissolution in acetone and subsequent addition of solid [ⁿBu₄N]Cl. Aqueous solubility trials showed that whilst [Ir(ppy)₂qpy]Cl was almost completely insoluble, the complexes of the quaternised ancillary ligands readily dissolved as the chloride salt.

4.2.1.2 Complexes of Bipyridinium**4.2.1.2.1 Pro-ligands for Cyclometalation**

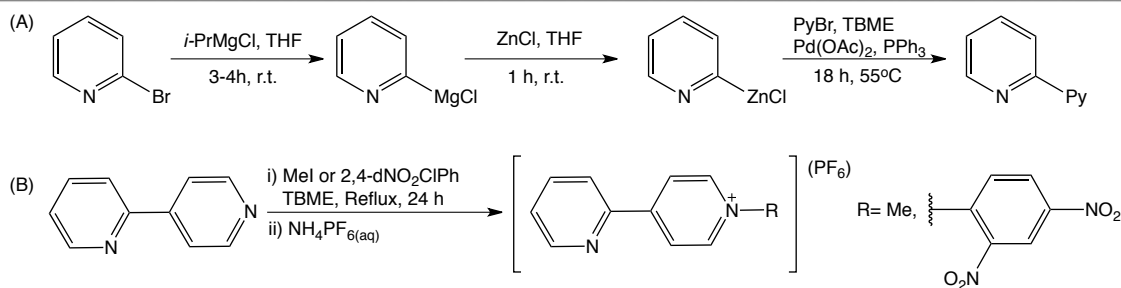
Whilst 2,2'-bipyridine is widely commercially available, the 2,3'- and 2,4'-analogues needed to be synthesised. A number of potential procedures such as the Suzuki-Miyaura^[247] or Stille^[248] coupling reactions have been previously utilised in the synthesis of a range of bipyridyls, although the method chosen here was that of the Negishi coupling of 2-pyridylzinc chloride with an appropriate heteroaryl bromide, Scheme 4.2.



Scheme. 4.2. Catalytic cycle of the palladium catalyzed Negishi cross-coupling reaction of an organozinc compound with an organic halide or triflate. Where R = aryl, heteroaryl, alkenyl, alkynyl or acyl. X = Cl, Br, I or OTf. L_n = ligand, PPh_3 , dba , $dppe$, etc.

2-pyridylzinc chloride was prepared at ambient temperature using modified Knochel conditions^[249-251]. 2-bromopyridine was converted to the intermediate Grignard reagent by metal-halogen exchange on reaction with isopropylmagnesium chloride. Transmetalation to the organozinc reagent was achieved *in situ* on addition of an anhydrous THF solution of zinc chloride. The resultant mixture was subsequently used in Negishi cross coupling reactions on addition of the required heteroaryl bromide, triphenylphosphine and a catalytic quantity of palladium(II) acetate, Scheme 4.3.

The next stage in the synthesis was the selective quaternisation of a single pyridyl ring with either methyl iodide or 1-chloro-2,4-dinitrobenzene; the reactions proceeding via a S_N2 and S_NAr mechanism respectively. The choice of reaction solvent proved crucial in the success of these procedures as demonstrated in the initial attempts to prepare the dinitrophenyl quaternised pro-ligands. Use of butyronitrile as reported in literature,^[252] resulted in poor product yields and afforded a material which was contaminated with a significant quantity of a dark coloured impurity. On changing the reaction solvent to *tert*-butyl methyl ether (TBME) the selective synthesis of the desired mono-quaternised bipyridinium compounds was achieved in excellent yields. The solubility of the material is such that, on formation, the product readily precipitates from solution preventing further reaction that would yield the unwanted diquaternary salts.



Scheme 4.3. Synthesis of the *N*-substituted 3-(2'-pyridyl)pyridinium and 4-(2'-pyridyl)pyridinium pro-ligands. **A)** Formation and subsequent Negishi coupling reaction of 2-pyridylzinc chloride. **B)** Selective quaternisation to yield the monoquaternised salts.

Isolation of the methylated compounds as the halide salt was achieved on simply washing the collected solid with TBME and drying *in vacuo*. For compounds of the dinitrophenyl group, additional purification steps were required. The contaminants were identified as unreacted starting material and could be readily removed upon filtration of an aqueous solution of the crude product. However, on removal of solvents, the material was inevitably isolated as a viscous oil due to the hygroscopic nature of the chloride salt. By subsequent dissolution in cold methanol and gradual addition of *n*-pentane:diethyl ether (1:1) it was possible to obtain the product as a pale yellow powder. Isolation as the hexafluorophosphate salt was also achieved on addition of NH₄PF₆ to an aqueous solution of the bipyridinium halide followed by vacuum filtration and extensive washing with cold deionised water. Using these methods the pro-ligands 1-methyl-3-(2-pyridyl)pyridinium, 1-(2,4-dinitrophenyl)-3-(2-pyridyl)pyridinium and the 4-(2-pyridyl)pyridinium analogues were obtained in excellent yields. In the case of 2,2'-bipyridine, using these conditions, the desired products were not isolated. The methylation reaction was instead repeated using one equivalent of methyl iodide in acetonitrile with heating at 40°C over 96 hours.^[253] Whilst this was successful, numerous attempts to prepare 1-(2,4-dinitrophenyl)-2-(2-pyridyl)pyridinium resulted in failure. This was attributed to issues of steric hindrance as a consequence of substitution at the α -position of the pyridyl ring and the increased steric bulk of the dinitrophenyl group in comparison to that of the methyl.

Attempts to prepare bipyridinium pro-ligands of more varied functionality via the Zincke reaction of *N*-(2,4-dinitrophenyl)bipyridinium failed, despite the use of a range of anilines of differing properties. In all instances the crude material collected was a dark tar-like substance from which a pure product could not be isolated. Purification trials using chromatography resulted in impure material as the individual components tended to be of similar *R_f* values and produced diffuse overlapping bands. Due to the decreased charge and the increased solubility in non-polar solvents, the bipyridinium compounds could not be purified using analogous methods employed for the quaterpyridinium pro-ligands. The purification of the latter is achieved through metathesis and is dependent upon distinct solubility profiles in different solvents, which these compounds lack. After numerous attempts without progress the work was discontinued instead focusing on the alkyl quaternised pro-ligands.

4.2.1.2.2 Synthesis of {[Ir(C[^]N)₂μ-Cl]₂}⁴⁺ intermediates

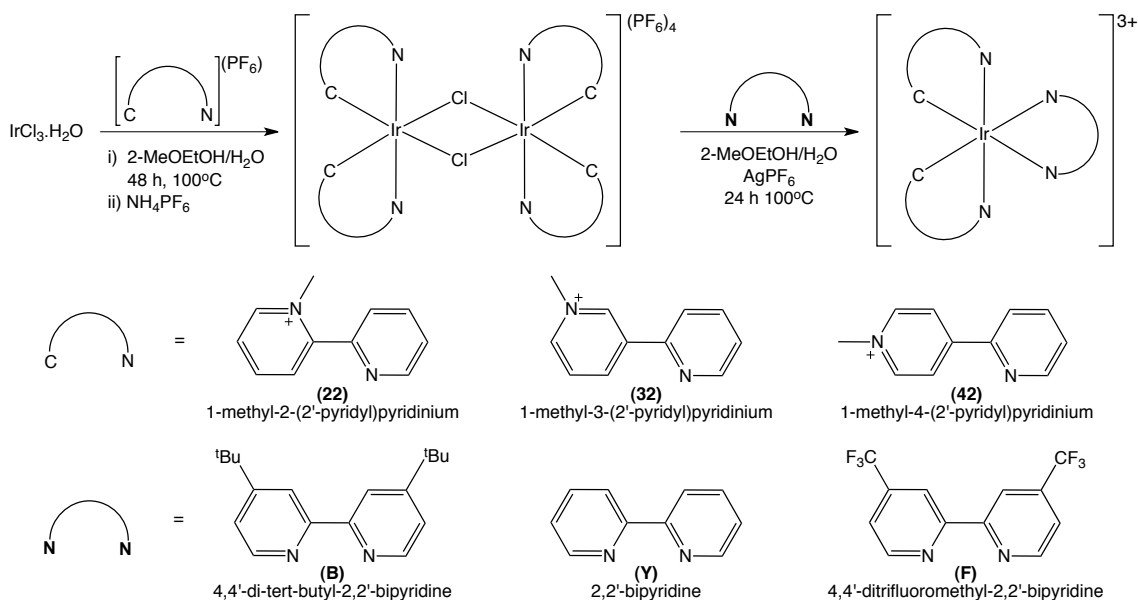
Inclusion of the quaternised ligands had a significant impact upon the experimental methods used in the preparation of the dichloro bridged bimetallic intermediates. The differences were primarily a consequence of changes in solubility afforded by the increased ionic character of these positively charged compounds in comparison to the neutral dimers that are typically synthesised. Initial cyclometalation reactions were carried out using the chloride or iodide salts of the quaternised pro-ligands. This was decided upon due to solubility considerations of the starting materials and potential products in the chosen alcohol-water solvent system. On completion of these reactions, it was observed that a significant quantity of near insoluble material had precipitated from solution, which was collected by filtration but could not be analysed directly. It was determined that on heating in acetonitrile and in the presence of KPF₆ that a small quantity of the [Ir(C[^]N)₂(MeCN)₂](PF₆)₃ species could be isolated after subsequent column chromatography. KPF₆ was added to metathesise the material to the hexafluorophosphate salt with the aim to improve solubility and potentially to aid in the abstraction of chlorides to promote the formation of the bis-solvento complex.

It is surmised that the desired product formation may have been perturbed due to the choice of counter-ion of the starting material, as both chloride and iodide are potential ligands towards iridium and may effectively compete with the cyclometalation reaction. As such experiments were subsequently repeated using the pro-ligands as the non-coordinative hexafluorophosphate salt. Whilst insoluble under ambient conditions, complete dissolution of the pro-ligands was achieved at elevated temperatures and the reaction proceeded without the formation of any precipitate, even upon cooling. The crude material was isolated on removal of solvents by rotary evaporation and resuspension in acetone/ether to yield a product that proved only partially soluble in most common solvents at ambient conditions. However, it did prove sufficiently soluble in dimethylsulfoxide to allow analysis by ¹H-NMR. The apparent poor solubility can be explained on consideration that the material had come from a mixed salt system as the chloride and hexafluorophosphate anions are expected to yield products of notably different solubility profiles. This problem was circumvented by addition of NH₄PF₆ to the reaction mixture directly after cooling and whilst all material was still in solution. The near complete metathesis to the hexafluorophosphate salt resulted in a great improvement in solubility of the isolated material. The identity of each of the chloro-bridged dimers was confirmed by ¹H-NMR in both (CD₃)₂SO and CD₃CN. In the instance of 1-methyl-3-(2-pyridyl)pyridinium, two potential products may have formed upon cyclometalation, namely the C⁴,N' and C²,N' linkage isomers. The data indicated that cyclometalation occurred at the *para* position with respect to the heteroatom, thus yielding the C⁴,N' isomer. This selectivity is surmised to be a consequence of favourable electronics within the adopted structure and the unfavourable sterics about the methyl group had the alternate isomer been formed.^[254]

Whilst the analysed materials were predominantly that of the desired products, minor impurity peaks were also evident. Unreacted pro-ligand could be selectively removed by

washing the solid with a mixture of methanol or acetone in diethyl ether (1:1). Careful attention to the relative ratios of both these solvents was required as too little of the polar component would fail to remove the charged pro-ligand whilst too much resulted in the loss of product. Attempts to recrystallise from acetonitrile either resulted in the failure to further purify the material or, in one particular instance, the breaking of the chloro-bridge to form the mono-chloro mono-solvento complex, $[\text{Ir}(\text{22})_2(\text{MeCN})\text{Cl}](\text{PF}_6)_3$. The identity of this species was determined by $^1\text{H-NMR}$, which showed 14 aromatic protons and two closely spaced methyl singlets, thus indicating two inequivalent cyclometalating ligands. An additional singlet at $\delta = 2.09$ ppm that equated to three protons was assigned to the methyl group of a coordinated acetonitrile molecule. Precedent for cleavage of the chloro-bridged dimers by coordinative solvents has been previously demonstrated in the selective low temperature synthesis of a variety of *fac*- and *mer*- tris-cyclometalated iridium(III) complexes.^[255] The proposed assignment was further corroborated on obtaining a single crystal x-ray structure, which is presented in appendix C with the associated $^1\text{H-NMR}$ and 2D-COSY spectra.

The cyclometalation reactions of both 1-(2,4-dinitrophenyl)-3-(2-pyridyl)pyridinium and 1-(2,4-dinitrophenyl)-4-(2-pyridyl)pyridinium did not yield the intended product. Results from $^1\text{H-NMR}$ obtained for the crude material were inconclusive, as it remained unclear whether the failure was caused by the formation of a number of different cyclometalation products or due to decomposition of the pro-ligand under the reaction conditions. Considering the reactivity of the nitro- group towards reduction and the relative instability of dinitrophenyl quaternised pyridiniums in comparison to other functional groups, it is believed that the latter is most likely. As such further studies concerning these pro-ligands were not explored.



Scheme 4.4. Reaction scheme for the preparation of complexes with the general formula $[\text{Ir}(\text{C}^{\text{A}}\text{N})_2(\text{N}^{\text{A}}\text{N})]^{3+}$, illustrating representative structures of the complexes and ligands to be utilised as part of this investigation. The complexes of formula $\{[\text{Ir}(\text{C}^{\text{A}}\text{N})_2(\mu\text{-Cl})]_2\}^{4+}$ were isolated as the hexafluorophosphate salt whilst those of the formula $[\text{Ir}(\text{C}^{\text{A}}\text{N})_2(\text{N}^{\text{A}}\text{N})]^{3+}$ were collected as both the hexafluorophosphate and chloride salts.

4.2.1.2.3 Synthesis of complexes of the general formula $[\text{Ir}(\text{C}^{\wedge}\text{N})_2(\text{N}^{\wedge}\text{N})](\text{X})_n$

Complexes of the general formula $[\text{Ir}(\text{C}^{\wedge}\text{N})_2(\text{N}^{\wedge}\text{N})](\text{X})_n$ were prepared by a method analogous to that used for $[\text{Ir}(\text{ppy})_2\text{L}](\text{PF}_6)_n$, with all reactions undertaken using the crude $[\text{Ir}(\text{C}^{\wedge}\text{N})_2\text{Cl}]^{4+}$ intermediate complex as the hexafluorophosphate salt. Whilst reactions of dCF_3bpy proceeded much more readily than those observed for ruthenium, as described in section 3, yields were significantly improved on addition of a chloride abstraction agent, as such AgPF_6 was included in all subsequent coordination reactions.

The primary complication with this procedure was one of purification. Initially, $[\text{Ir}(\text{22})_2\text{Y}]^{3+}$ and $[\text{Ir}(\text{42})_2\text{Y}]^{3+}$ were successfully isolated by column chromatography on silica gel using $\text{MeCN}:\text{H}_2\text{O}:\text{KNO}_3(\text{sat})$ (20:10:2) as the eluent. However, removal of excess KNO_3 from the product was problematic and attempts to purify $[\text{Ir}(\text{32})_2\text{Y}]^{n+}$ and complexes of the functionalised ancillary ligands proved unsuccessful. After extensive trials it was shown that by using Sephadex SP-C25 resin and eluting with acetone:water (1:1) containing an increasing concentration of NaCl , a pure product could be obtained in all instances. The column was first eluted with 0.025 M NaCl to remove unreacted pro-ligand. A stepped gradient to 0.05 M resulted in the removal of the majority of the impurities, although a minor component remained that eluted at a similar albeit slower rate to that of the titular complex salts. The product was eluted on gradual increase of the NaCl concentration to 0.10 M. Whilst this procedure is slow, using higher salt concentrations to increase the rate of elution resulted in insufficient separation between the two components. For the complexes of $[\text{Ir}(\text{22})_2\text{L}]^{3+}$ and $[\text{Ir}(\text{42})_2\text{L}]^{3+}$ the limits of the most concentrated product band were readily distinguished due to their strong yellow colour. Particular care was required in the purification of $[\text{Ir}(\text{32})_2\text{L}]^{3+}$ as these compounds and the related impurities are almost colourless in solution, the product band instead visualised using a long wave UV lamp (365 nm). As these compounds display intense luminescence even at very low concentrations, distinguishing the impurities can be difficult as they can be effectively masked by the diffuse tailing of the product band. Attempts to isolate and identify the impurity in complexes of $[\text{Ir}(\text{32})_2\text{L}]^{3+}$ were unsuccessful. The samples obtained were typically contaminated with the desired products, thus preventing full assignment by $^1\text{H-NMR}$ due to overlapping resonances. Initially it had been thought that the compound may have been one in which the bipyridinium ligand had adopted the alternate linkage isomer. However, the information that could be elucidated from the partial $^1\text{H-NMR}$ spectra was in disagreement with this proposal, although the data did not exclude the possibility of a geometric isomer. Alternately, mass spectra of the crude material suggested the potential formation of the diaqua species, $[\text{Ir}(\text{C}^{\wedge}\text{N})_2(\text{H}_2\text{O})]^{3+}$. However, upon repeating the reactions in the absence of water, the relative product to impurity ratios, as observed in $^1\text{H-NMR}$, were unaffected thus raising doubts concerning this assignment.

Final isolation of the product from the eluate was achieved on evaporation of solvents and resuspension of the residue in ice-cold methanol. The majority of the excess NaCl was removed by filtration prior to methathesis of the complex to the hexafluorophosphate salt.

4.2.2 NMR Spectroscopy**4.2.2.1 ¹H-NMR Spectroscopy**

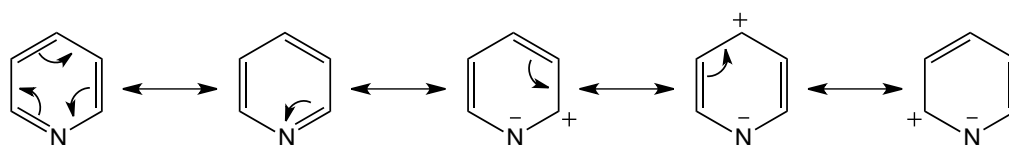
The spectra for all pro-ligands, intermediates and complexes were recorded as both the hexafluorophosphate and chloride salts in CD₃CN and (CD₃)₂SO respectively. Individual signals were assigned with the aid of 2D-COSY experiments. For comparison purposes the chemical shifts and subsequent assignments for all compounds containing the quaternised bipyridyl ligands are presented in Table 4.1. The discussion contained herein specifically refers to the spectra of complexes as the hexafluorophosphate salt, although general trends and observations remain true for both series of compounds.

4.2.2.1.1. Bipyridinium Pro-Ligands.

The spectra for each of the methylated pro-ligands show signals in the aromatic region between $\delta = 7.54 - 9.33$ ppm and equate to a total of eight protons. A singlet peak at $\delta 4.2 - 4.4$ ppm is of a chemical shift typically associated with the methyl group of a 1-alkyl pyridinium compound.^[256] This signal integrated to three protons indicating that the mono-methylated product had been synthesised. Unlike 2,2'-bipyridine, for the asymmetric 3,2'- and 4,2'-isomers the site of methylation must also be considered as two different products may be formed. Selective synthesis of the less sterically hindered isomers 1-methyl-3-(2'-pyridyl)pyridinium and 1-methyl-4-(2'-pyridyl)pyridinium was successful. This was indicated by a significant downfield shift of the resonances within the desired pyridyl spin system as a result of deshielding brought about by quaternisation.

The spectra of the *N*-dinitrophenyl derivitised compounds display a total of 11 resonances across three individual spin systems. In both cases a significant deshielding of the pyridinium protons in comparison to the methylated analogues is evident, thus reflecting the increased electron withdrawing capabilities of the dinitrophenyl group. In 1-(2,4-dinitrophenyl)-4-(2-pyridyl)pyridinium this equated to an downfield shift of *ca.* 0.25 ppm for all protons in the pyridinium ring. For 1-(2,4-dinitrophenyl)-3-(2-pyridyl)pyridinium, shifts of similar magnitude were evident for the protons *ortho* to the heteroatom. In the *para* position, the A₆ proton undergoes a more pronounced shift of 0.36 ppm to a lower field.

In the case of the 3,2'- isomer the resonances assigned to the unquaternised pyridyl ring remain largely unaffected by modifications in the *N*-substituent. However for the 4,2'- isomer a downfield shift is noted for all four protons, most notably for P₃ and to a lesser extent P₆ with a shift of + 0.15 and 0.08 ppm respectively. To explain this the resonance structures inherent in the pyridyl ring must be considered, Scheme 4.5.^[257]



Scheme 4.5. Resonance structures inherent within the pyridyl ring resulting in partial positive charges in the α and γ positions with respect to the heteroatom.

Table 4.1. (below). ¹H-NMR assignments (δ , ppm) for complexes of the general formula $[\text{Ir}(\text{C}^{\wedge}\text{N})_2(\text{N}^{\wedge}\text{N})](\text{PF}_6)_3$ containing the bipyridinium cyclometalating ligands. Spectra recorded in CD_3CN . Values reported are referenced with respect to TMS.

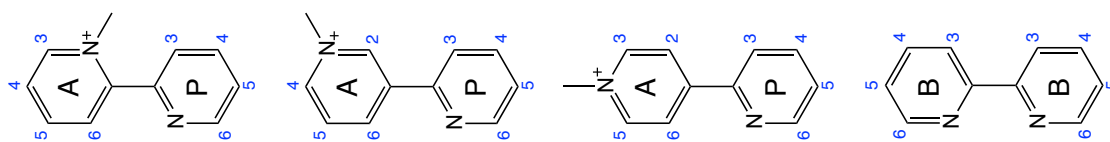


Fig. 4.3. (right). Representative structure of the bipyridinium cyclometalating and bipyridyl ancillary ligands with labelling schemes used in ¹H-NMR assignments.

Complex salt	(P) Pyridyl ring						(A) Cyclometalating ring						(B) Bipyridyl ring						Me	
	P3	P4	P5	P6	A2	A3	A4	A5	A6	B3	B4	B5	B6	Me	Me					
$(1\text{-Me-}2,2'\text{-bpy})^+$	8.07	8.07	7.65	8.82	---	8.73	8.07	8.58	7.77	---	---	---	---	---	4.23					
$[\text{Ir}(22)_2(\mu\text{-Cl})]_2^{4+}$	8.51	8.16	7.74	10.20	---	8.10	7.26	7.11	---	---	---	---	---	---	4.58					
$[\text{Ir}(22)_2\text{Y}]^{3+}$	8.60	8.19	7.46	7.90	---	8.42	7.37	7.20	---	8.60	8.26	7.57	7.94	4.65						
$[\text{Ir}(22)_2\text{F}]^{3+}$	8.62	8.21	7.47	7.89	---	8.45	7.41	7.18	---	9.04	---	---	8.21	4.66						
$[\text{Ir}(22)_2\text{B}]^{3+}$	8.61	8.19	7.49	7.88	---	8.42	7.37	7.20	---	8.54	---	7.49	7.80	4.65						
$(1\text{-Me-}3,2'\text{-bpy})^+$	8.02	8.02	7.54	8.77	9.33	---	9.04	8.09	8.63	---	---	---	---	4.39						
$[\text{Ir}(32)_2(\mu\text{-Cl})]_2^{4+}$	8.14	8.14	7.68	9.85	8.59	---	7.44	6.75	---	---	---	---	---	3.91						
$[\text{Ir}(32)_2\text{Y}]^{3+}$	8.26	8.17	7.41	7.73	8.84	---	7.76	6.87	---	8.60	8.26	7.58	7.88	4.12						
$[\text{Ir}(32)_2\text{F}]^{3+}$	8.28	8.19	7.42	7.74	8.86	---	7.79	6.84	---	9.04	---	---	8.13	4.14						
$[\text{Ir}(32)_2\text{B}]^{3+}$	8.29	8.17	7.43	7.71	8.85	---	7.74	6.86	---	8.54	---	7.51	7.75	4.12						
$(1\text{-Me-}4,2'\text{-bpy})^+$	8.19	8.04	7.60	8.83	8.62	8.67	---	8.67	8.62	---	---	---	---	4.31						
$[\text{Ir}(42)_2(\mu\text{-Cl})]_2^{4+}$	8.33	8.13	7.73	9.97	8.04	7.98	---	7.18	---	---	---	---	---	3.90						
$[\text{Ir}(42)_2\text{Y}]^{3+}$	8.44	8.16	7.44	7.73	8.25	8.32	---	7.26	---	8.59	8.25	7.56	8.01	4.01						
$[\text{Ir}(42)_2\text{F}]^{3+}$	8.45	8.16	7.47	7.75	8.28	8.35	---	7.23	---	9.03	---	7.87	8.27	4.02						
$[\text{Ir}(42)_2\text{B}]^{3+}$	8.43	8.18	7.45	7.72	8.25	8.31	---	7.25	---	8.53	---	7.47	7.88	4.01						

Due to the electronegativity of the nitrogen atom and the subsequent effects this has on the electron density of the delocalised π -system, the carbons in the α - and γ - positions experience a partial positive charge. These effects are enhanced further on quaternisation as the electron withdrawing capability of the nitrogen increases. As such it is expected that any substituents at the α - or γ - positions of the quaternised pyridyl ring would experience a greater electron withdrawing effect and thus be more susceptible to modifications of the *N*-substituent. This influence of the quaternised heteroatom upon the α - and γ - positions is observed through comparison of the chemical shift of the A₅ proton in each of the three isomers of the methylated pro-ligand. In 1-methyl-3-(2'-pyridyl)pyridinium the A₅ proton adopts the β -position with respect to the heteroatom and exhibits a resonance of 8.09 ppm. This is shifted up-field by 0.49 – 0.58 ppm in comparison to 1-methyl-2-(2'-pyridyl)pyridinium and 1-methyl-4-(2'-pyridyl)pyridinium, in which the A₅ proton adopts the γ - and α - positions respectively.

4.2.2.1.2. Chloro-Bridged Dimeric Intermediates

Whilst an entirely pure sample of the dimeric intermediates could not be obtained due to issues of solubility and reactivity, ¹H-NMR spectra were successfully acquired for all complexes in CD₃CN. This allowed for full proton assignments where the major component showed a total of seven aromatic resonances and a singlet associated with the *N*-methyl group. All complexes were comprised of two spin systems as identified by 2D-COSY techniques.

In each case the most upfield of the aromatic signals was assigned to the A₅ proton. This is expected due to extensive shielding by π -back bonding from the metal centre and the susceptibility of this position towards through-space ring current anisotropy from the pyridyl ring of the adjacent ligand. Making comparisons between the δ of equivalent protons within each of the three different isomers is made difficult due to the varying influence of the quaternised nitrogen upon the different positions within the pyridinium ring. However, it is clear on comparison with the δ of the pro-ligands that extensive shielding occurs on cyclometalation in all instances. Again this is attributed to extensive π -back-bonding from the iridium metal centre on formation of the Ir—C bond.

Significant variations within the chemical shift of the *N*-methyl substituent of the pyridinium ring were also noted. In comparison to the associated pro-ligand, the complexes {[Ir(32)₂Cl]₂}(PF₆)₄ and {[Ir(42)₂Cl]₂}(PF₆)₄ exhibit an upfield shift of 0.48 and 0.41 ppm respectively. The downfield shift of 0.35 ppm seen for {[Ir(22)₂Cl]₂}(PF₆)₄ can be attributed to additional van der Waals interactions between itself and the P₃ proton of the adjacent pyridyl ring. Similar observations were made on coordination of 1-methyl-2-(2'-pyridyl)pyridinium to palladium^[238] and for the methyl group and A₂ proton of the *ortho*-metalated iridium compounds of 3-methyl-2-phenylpyridine (mpppy).^[258, 259] Due to the steric hindrance caused by the *N*-methyl group, the two pyridyl rings of the pro-ligand most likely adopt an orthogonal conformation in solution.^[260] On cyclometalation the two rings are forced to adopt a planar geometry, thus resulting in a mutual deshielding of the methyl group and A₅ proton as the

nuclei are brought into close proximity to one another. This is evinced on comparison of the coordination-induced shift (CIS) of the P₃ protons of the three bipyridinium isomers. In compounds of 3,2' and 4,2'-bipyridinium a comparable downfield shift of 0.12 and 0.14 ppm is observed respectively, whilst for the 2,2'- isomer an increased shift of 0.44 ppm is apparent.

The proton signals of the pyridyl ring all undergo a downfield shift on coordination due to the electronegativity of the Ir(III) cation. The most pronounced shift is that of P₆, which is deshielded by 1.08 – 1.38 ppm as a consequence of this proton being positioned above the electronegative bridging chlorides.

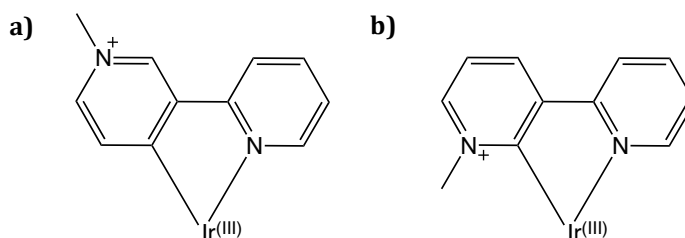


Fig. 4.4. The linkage isomers that may be adopted on cyclometalation of 1-methyl-3-(2-pyridyl)pyridinium; **a)** (1-methyl-3-(2-pyridyl)pyridin-4-yl-ium-C⁴,N') and **b)** (1-methyl-3-(2-pyridyl)pyridin-2-yl-ium-C²,N'). Other ligands about the metal centre are omitted for clarity.

The bonding mode of the cyclometalating ligand in the complex $\{[\text{Ir}(\text{32})_2\text{Cl}]_2\}(\text{PF}_6)_4$ was confirmed as (1-methyl-3-(2-pyridyl)pyridin-4-yl-ium-C⁴,N'), as indicated by an upfield doublet and a characteristic singlet at $\delta = 6.75$ and 8.59 ppm respectively. Had the (1-methyl-3-(2-pyridyl)pyridin-2-yl-ium-C²,N') linkage isomer been formed, the singlet resonance would have been lost upon cyclometalation and a significant upfield shift in the signal of the methyl group would also be expected as it would adopt the position *ortho* to the Ir—C bond and hence be subject to the effects of π -back bonding and through-space shielding as described for proton A₅.

4.2.2.1.3. Monometallic Complexes

The complexes of the general formula $[\text{Ir}(\text{C}^{\wedge}\text{N})_2\text{L}](\text{PF}_6)_3$ exhibit ten or eleven protons in the aromatic region, dependant upon the functionality of the ancillary ligand, with chemical shifts within the range of δ 6.8 to 9.1 ppm.

Using 2D-COSY techniques, three spin systems were identified. As with the dimers, the most up-field aromatic signal was assigned to the proton *ortho* to the cyclometalated bond and thus allowed unambiguous identification of the spin system. In complexes of $[\text{Ir}(\text{C}^{\wedge}\text{N})_2\text{Y}](\text{PF}_6)_3$ a distinction between the pyridyl rings of either 2,2'-bipyridine or of the cyclometalating ligand could only be achieved on comparison of the resonances from each of the three series of compounds. In the complexes of $[\text{Ir}(\text{C}^{\wedge}\text{N})_2\text{B}](\text{PF}_6)_3$ and $[\text{Ir}(\text{C}^{\wedge}\text{N})_2\text{F}](\text{PF}_6)_3$ one of these unidentified spin systems was instead comprised of only three protons allowing assignment of these resonances to the ancillary ligand. It then became evident that the δ of the protons in the P ring were largely unaffected by variations in the substituted-bipyridine and as such allowed for assignment of these resonances for each of the complexes. Likewise the δ of the protons in

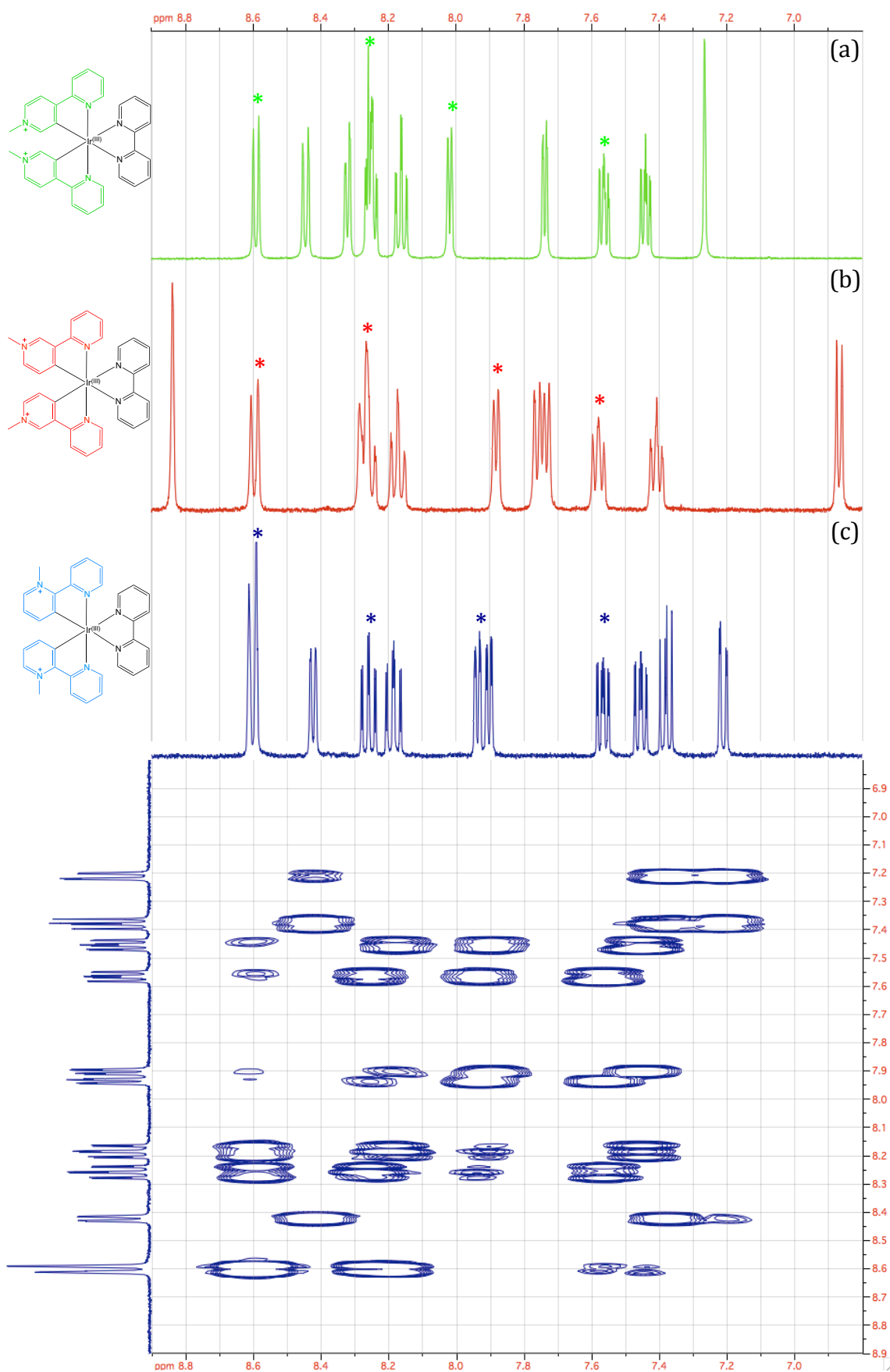


Fig. 4.5. $^1\text{H-NMR}$ spectra of (a) $[\text{Ir}(42)_2\text{Y}](\text{PF}_6)_3$ (green) and (b) $[\text{Ir}(32)_2\text{Y}](\text{PF}_6)_3$ (red). (c) A section of the 2D-COSY spectrum of $[\text{Ir}(22)_2\text{Y}](\text{PF}_6)_3$ (blue) in the region of 6.80 - 8.90 ppm, as used in the assignment of individual resonances. All spectra were recorded in CD_3CN . * = resonances of the ancillary ligand.

the ancillary ligand appear independent of the cyclometalating ligand employed and are instead dominated by the inductive effects of the incorporated functional groups. There is some variation in the signal of the B₆ proton which is expected due to the susceptibility of this position to through-space ring current anisotropy. The δ of this resonance in the [Ir(32)₂L](PF₆)₃ series is consistently shifted up-field with respect to the complexes of the other isomers of bipyridinium. This suggests an increased shielding effect from the adjacent cyclometalating ring and raises questions pertaining to the electron density localised about the pyridinium moiety in the 3,2'-isomer.

On coordination of the ancillary bipyridyl ligands the protons of the cyclometalating ring in each of the isomers undergoes a downfield shift of *ca.* 0.1-0.3 ppm. This is a result of the decreased donor ability of the bipyridyl ligand with respect to that of the chloride, the latter is therefore expected to exert a considerably stronger structural *trans* effect. This deshielding is also evident in the δ of the *N*-methyl group and is most pronounced for the complexes of [Ir(32)₂L](PF₆)₃, which display a downfield shift of 0.21-0.23 ppm in comparison to *ca.* 0.1 ppm for the other isomers. This again demonstrates the influence of resonance effects within the ring and highlights the sensitivity of the *para* position towards changes in the Ir—C bond.

The increased electronegativity of the iridium centre likewise results in a downfield shift of both the P₃ and P₄ resonances. The P₅ and P₆ signals are instead subject to shielding by through-space ring current anisotropy as they both now reside over the plane of the pyridyl ring of the ancillary ligand. Due to the relative positions, this shift is more pronounced for P₆ with $\Delta\delta$ values of 2.2 – 2.3 ppm.

On analysis of the resultant 2D-COSY spectra for these complexes, long-range proton-proton coupling interactions between the methyl and the aromatic protons of the cyclometalating ring were made apparent. The structure of the ligand can be considered analogous to that of a substituted toluene, within which similar interactions have been noted. This benzylic-type coupling has been extensively studied both experimentally and theoretically, with the relative magnitudes of *ortho*- (⁴J_{H,CH₃), *meta*- (⁵J_{H,CH₃) and *para*- coupling (⁶J_{H,CH₃) discussed.^[261] Whilst slight broadening of the methyl signal is observed, no defined splitting is evident in the results presented herein. Whilst no coupling constants could be determined it can be assumed from literature precedent that they are approximately less than or equal to 0.9 Hz. The presence of these interactions was confirmed on comparison of these observations with the experimental data obtained for each of the quaternised pro-ligands and chloro-bridged dimer intermediates.}}}

In the COSY spectra of 1-methyl-4-(2'-pyridyl)pyridinium a single cross peak indicates ⁴J_{H,CH₃ with the doublet assigned to the two protons in the *ortho* position with respect to the heteroatom. On cyclometalation these positions become inequivalent and two distinct cross coupling peaks can be observed. For 1-methyl-3-(2'-pyridyl)pyridinium, coupling of the methyl group to three of the aromatic protons is seen, ⁴J_{H,CH₃ to the A₂ and A₄ protons and ⁶J_{H,CH₃ to the A₆ proton. On cyclometalation the ⁶J_{H,CH₃ is no longer observed due to deprotonation and}}}}

formation of the Ir—C bond. Interestingly, for the complexes of 1-methyl-2-(2'-pyridyl)pyridinium in addition to ${}^4J_{\text{H,CH}_3}$ and ${}^6J_{\text{H,CH}_3}$ to the A₃ and A₅ protons respectively, potential ${}^6J_{\text{H,CH}_3}$ to the P₃ proton was also evident. Initially this interaction was disregarded as in most instances the magnitude of the cross peak was comparably to the more intense signals associated with the background noise. However, the peak was consistently seen in all complexes of the 2,2'-isomer thus lending credence to the actuality of this interaction. To confirm this, additional phase sensitive double quantum filtered-COSY (DQF-COSY) experiments were undertaken. DQF experiments work on the principles of double quantum coherence and as such remove signals of single quantum processes. This has the benefit of reducing the intensity of the diagonal cross peaks in addition to the associated t_1 noise and allows for the removal of artefacts towards providing a more simplified spectra. The results indicated the interaction was in fact present, as evident in the spectra of [Ir(22)₂F](PF₆)₃ as a well resolved cross peak at 4.66 – 8.62 ppm, Fig. 4.6. This also showed the previously unobserved ${}^5J_{\text{H,CH}}$ to the A₄ proton of the pyridinium ring, although the intensity of this signal was considerably smaller in comparison to the other three interactions discussed previously. It is typically expected that *meta* coupling constants be of much smaller magnitude in comparison to those of *ortho* and *para* coupling.^[262] This was exemplified in the ¹H-NMR study of mono-methylated pyrimidines, where it was demonstrated that whilst a ${}^6J_{\text{H,CH}_3}$ of 0.6-0.8 Hz was evident for 2-methylpyrimidine, no discernable ${}^5J_{\text{H,CH}_3}$ could be measured.^[263] These observations along with those presented here would reflect the relative weakness of ${}^5J_{\text{H,CH}_3}$ and explain the absence of such interactions in the original 2D-COSY spectra.

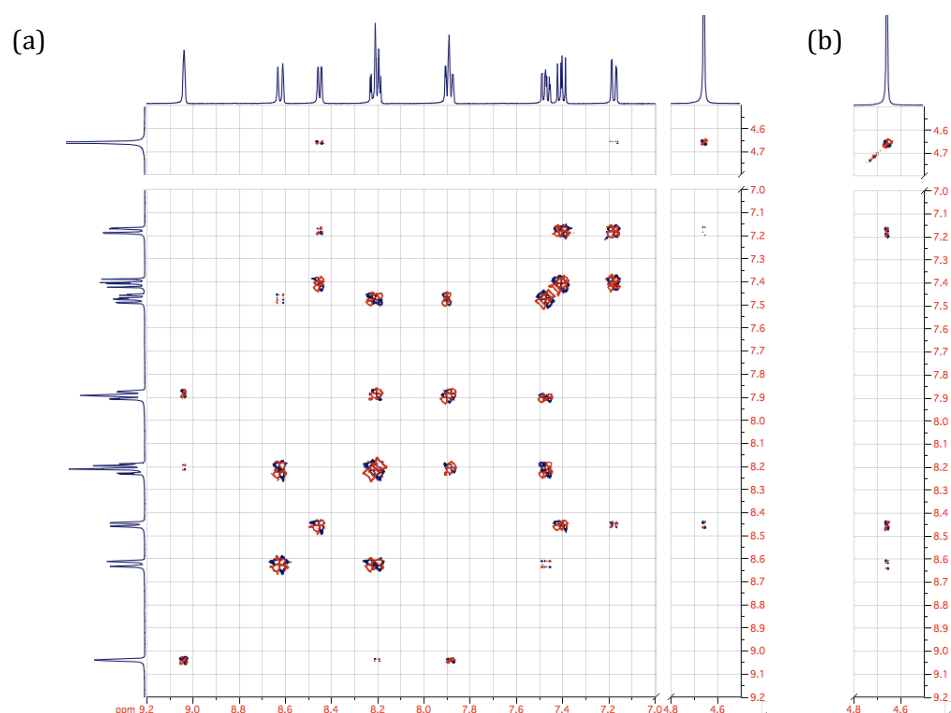


Fig. 4.6. DQF-COSY spectra of [Ir(22)₂F](PF₆)₃ in CD₃CN. **(a)** Displaying the regions 4.5-4.8 and 7.0-9.2 ppm. **(b)** A magnification of the cross peaks assigned to long range coupling of the methyl protons with the A₃, A₅ and P₃ protons.

The precise mechanism for ${}^6J_{\text{H,CH}_3}$ with the P_3 proton remains unclear. Partial delocalisation of the π -system across the two pyridyl rings could affect coupling via the σ - π spin polarisation mechanism under which the more orthodox benzylic-type coupling operates.^[264] It is also plausible that, due to the proximity of the methyl group and the P_3 hydrogen, a direct through-space coupling mechanism may also contribute.^[265, 266] This can be considered in terms of either an interaction between the $1s$ orbitals of the two protons or between the atomic orbital of the hydrogen and rear lobe of the $\text{C}-\text{H}$ bonding orbitals.^[267, 268] The latter interaction has been noted in a variety of rigid and/or sterically hindered systems and is typically only considered when the distance between the nuclei of interest is less than 220 pm.^[265, 269] In this instance, data collected from crystallographic studies and geometry optimisation calculations indicate that the intra-atomic distances between the P_3 proton and the methyl protons are expected to be less than *ca.* 2.05 Å, within the distance expected for these interactions to be valid.

To further establish the nature of this interaction the NOESY techniques discussed previously in section 3.2.2 were employed. In the spectra of $[\text{Ir}(\text{22})_2\text{F}](\text{PF}_6)_3$ two cross peaks of similar magnitude were observed at 4.66 – 8.45 and 4.66 – 8.62 ppm. These are assigned to short-range contacts of the methyl protons with the A_3 and P_3 protons respectively and demonstrate the magnitude of the through-space coupling interactions of the latter. The signal assignments determined by COSY experiments and the relative stereochemistry of the complex were also confirmed. In addition to the expected cross peaks associated with adjacent protons, the presence of contour signals at 7.18 – 7.89 and 7.18 – 8.21 ppm were observed, signifying the intraligand contacts of the A_5 proton with the P_6 and B_6 protons respectively. Additional

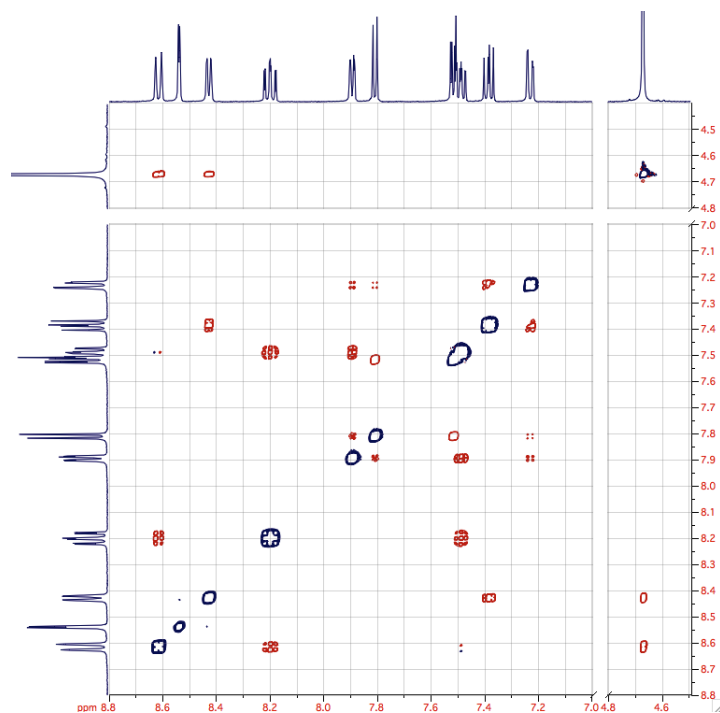


Fig. 4.7. Section of the NOESY spectrum of $[\text{Ir}(\text{22})_2\text{B}](\text{PF}_6)_3$ in the regions of 4.5–4.8 and 7.0–8.8 ppm, illustrating the interactions of the aromatic protons and the long-range NOE contacts of the methyl group of the pyridinium ring.

interactions that were expected between P₆ and B₆ could not be confirmed due to overlapping signals in the ¹H-NMR spectra, which effectively mask these contacts. Further experiments were performed using [Ir(22)₂B](PF₆)₃, which was chosen as the equivalent resonances are better resolved and as such allowed for the intraligand contacts between P₆ and B₆ to be observed in addition to those involving A₅, Fig. 4.7.

It was also noted that the ⁶J_{H,CH₃ with P₃ is not evident in the spectra of the pro-ligand. This is to be expected if the rings adopt a perpendicular orientation as the delocalised π-system does not extend between the two moieties nor is the methyl group within close enough proximity to afford through-space coupling. Overall it has been demonstrated that these interactions are useful tools in confirming the proton assignments used in the identification of alkylated pyridinium compounds. Similarly, as shown with the complexes of 1-methyl-3-(2-pyridyl)pyridinium, this can also act as a probe towards determining the site of cyclometalation and aid in making the distinction between different linkage isomers.}

The spectra for complexes containing 2-phenylpyridine exhibit a total of 15 to 18 aromatic resonances in the region of 6.0 – 10.3 ppm, the exact number of signals is dependant upon the functionality of the ancillary ligand. COSY experiments identified four spin systems for complexes of quaterpyridine and (Me₂qpy)²⁺ and five spin systems for that of [(Pym)₂qpy]²⁺. The pendant C₅H₄N ring of the ancillary ligand was readily identified by a characteristic pair of doublets that are associated with a *para*-substituted pyridine. On quaternisation, the resonances within this ring are shifted downfield in relation to the quaterpyridyl complex. For [Ir(ppy)₂(Me₂qpy)](PF₆)₃ this equates to a shift of 0.01 and 0.58 ppm for the *ortho*- and *meta*-protons respectively. The increased electron withdrawing ability of the 2-pyrimidyl group results in an increased deshielding of the pendent pyridinium group so as to afford a downfield shift of 1.34 and 0.85 ppm in the protons of the *ortho* and *meta* positions respectively. This is also reflected in the resonances within the bipyridyl unit, although of these only B₃ was sufficiently resolved in each of the three spectra to allow for a complete comparison. In relation to [Ir(ppy)₂qpy](PF₆), this signal is deshielded by 0.06 and 0.15 ppm upon inclusion of the *N*-methyl and *N*-(2-pyrimidyl) substituents respectively. A downfield shift of similar magnitude is also evident for B₅ between [Ir(ppy)₂(Me₂Qpy)](PF₆)₃ and {Ir(ppy)₂[(Pym)₂qpy]}(PF₆)₃, although the impact upon B₆ is diminished to just *ca.* 0.08 ppm. It was also noted that for [Ir(ppy)₂(Me₂qpy)](PF₆)₃ the aforementioned ⁴J_{H,CH} within the methylated pendant pyridinium group of the ancillary ligand was evident, thus providing confirmation of the proposed assignments. In comparison to the δ of the A₅ proton for complexes of bipyridinium, that of ppy is shielded by *ca.* 0.52-0.92 ppm, effectively demonstrating the magnitude of the increased electron density within the phenyl ring. The resonances within the pyridyl moiety are likewise shifted upfield as a consequence of the decreased electronegativity of the metal centre and through the effects of conjugation with the electron rich π-system of the phenyl moiety. The difference is most evident for the P₃ resonance, which is shifted upfield by *ca.* 0.13-0.51 ppm.

4.2.2.2 ¹³C-NMR Spectroscopy

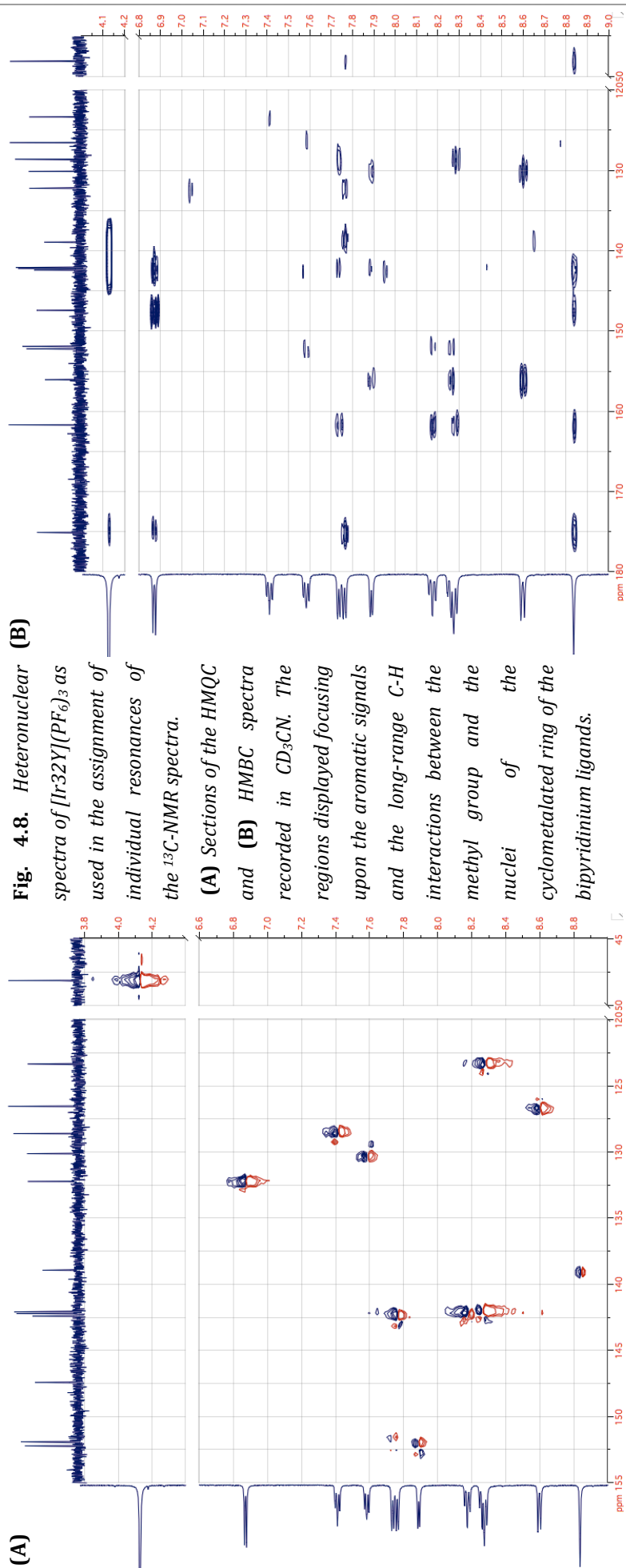
To further characterise the system, additional ¹³C-NMR experiments were undertaken for complexes [Ir(22)₂Y](PF₆)₃, [Ir(32)₂Y](PF₆)₃ and [Ir(42)₂Y](PF₆)₃ in CD₃CN. A total of sixteen individual resonances were evident in each of the spectra. The most upfield signal between 48-50 ppm was assigned to the methyl of the pyridinium moiety. In the region of 120 – 180 ppm fifteen distinct signals associated with the aromatic carbons of both the cyclometalating and ancillary ligands were apparent, equating to five carbon environments from each of the three unique pyridyl rings. Initial assignments were achieved through the use of heteronuclear multiple-quantum correlation (HMQC) spectroscopy, which provides information pertaining to heteronuclei that are separated by a single bond. The spectra displayed twelve contour signals, which in conjunction with the discussed proton assignments, allowed for identification of each of the corresponding carbon resonances and confirmation of the methyl signal. The four quaternary carbons were subsequently distinguished by a lack of a correlating proton signal. By means of heteronuclear multiple-bond correlation spectroscopic (HMBC) techniques, *J*_{C,H} through multiple bonds may be observed, thus facilitating the assignment of the individual quaternary carbons and the confirmation of results discerned using HMQC. The trends observed in the δ of the ¹H-NMR spectra are reflected in the values obtained from ¹³C-NMR. It is also of note that the aforementioned benzylic type coupling of the methyl group is also clearly observed in the HMBC experiments. In the case of [Ir(22)₂Y](PF₆)₃ a total of five contour signals involving the methyl group were evident. Cross peaks at 8.42 – 50.88 and 4.65 – 144.70 ppm describe the interactions of the methyl group with the A₃ proton and carbon respectively. Further peaks at 4.65 – 129.98 and 4.65 – 157.16 ppm refer to the ⁴*J*_{C,Me} of A₄ and A₆, whilst a weaker signal at 4.65 – 129.98 ppm is indicative of long-range coupling with the A₅ carbon. The ⁵*J*_{C,Me} interaction with P₃ could not be observed due to the proximity of the associated ¹³C resonance with that of the A₄ carbon, any potential interaction effectively masked by the intense contour peak of ⁴*J*_{C,Me} evident for the latter. Utilisation of these coupling interactions allowed for the distinction between a number of signals of similar chemical shift within the ¹³C-NMR spectra that HMQC and other contour signals obtained from HMBC could not elucidate.

A slight variation in the δ of the methyl peak of [Ir(22)₂Y](PF₆)₃ correlates to the extensive shift seen in ¹H-NMR, as afforded by mutual deshielding with the P₃ proton. Likewise a modest deshielding of the P₃ carbon is also observed, displaying a shift of similar magnitude to that reported on comparison between the related complexes of ppy, mppy and 2-(*p*-tolyl)pyridine.^[258]

Interestingly a deshielding of the A₆ carbon by 13.42 – 18.03 ppm is observed for [Ir(32)₂Y](PF₆)₃. This may be attributed to the electron withdrawing effect afforded on this position by the *para* quaternised heteroatom and is analogous to the comparative downfield shift of A₅ for [Ir(22)₂Y](PF₆)₃ and [Ir(42)₂Y](PF₆)₃ which is of similar magnitude.

Table 4.2. ¹³C-NMR assignments (δ , ppm) for complexes [Ir22Y](PF₆)₃, [Ir32Y](PF₆)₃, and [Ir42Y](PF₆)₃. Spectra run in CD₃CN. Reported values referenced to TMS.

Complex Salt	(P) Pyridyl ring						(A) Cyclometalating ring						(B) Bipyridyl ring						Me
	P2	P3	P4	P5	P6		A1	A2	A3	A4	A5	A6	B2	B3	B4	B5	B6	Me	
[Ir(22) ₂ (bpy)] ³⁺	157.16	130.02	141.47	129.98	153.64		149.91	---	144.70	127.28	149.91	157.05	156.23	126.55	141.91	129.87	152.44	50.88	
[Ir(32) ₂ (bpy)] ³⁺	161.69	123.35	142.22	128.61	151.91		147.43	138.94	---	142.41	132.23	175.08	156.07	126.55	142.10	130.13	152.22	48.14	
[Ir(42) ₂ (bpy)] ³⁺	161.59	126.46	141.76	130.14	152.41		143.79	122.31	141.68	---	147.02	161.66	156.43	126.46	141.92	129.90	152.58	48.44	



4.2.3. Crystallographic Studies

Single crystals were obtained for $\{[\text{Ir}(\text{ppy})_2[(\text{Pym})_2\text{qpy}]](\text{PF}_6)_3$, $[\text{Ir}(\text{22})_2\text{Y}](\text{PF}_6)_3$, $[\text{Ir}(\text{22})_2\text{B}](\text{PF}_6)_3$, $[\text{Ir}(\text{22})_2\text{F}](\text{PF}_6)_3$, $[\text{Ir}(\text{32})_2\text{Y}](\text{PF}_6)_3$, $[\text{Ir}(\text{32})_2\text{B}](\text{PF}_6)_3$ and $[\text{Ir}(\text{42})_2\text{Y}](\text{PF}_6)_3$. Crystallographic data and refinement details are presented in appendix C. Crystals of $[\text{Ir}(\text{22})_2\text{F}](\text{PF}_6)_3$ and $[\text{Ir}(\text{42})_2\text{Y}](\text{PF}_6)_3$ were grown by the slow evaporation of nitromethane or acetone from a mixture of 1,4-dioxane and the title compound. All other crystals were obtained by slow vapour diffusion of diethyl ether into an acetonitrile or acetone solution of the complex salt. Selected bond lengths and angles are presented in Table 4.3.

All complexes exhibit a pseudooctahedral geometry about the iridium centre with the pyridyl rings of the cyclometalating ligands adopting a mutual *trans* geometry. The latter is due to the strong kinetic *trans* effect (KTE) of the cyclometalating moiety and the labilising effect this exerts upon the bond *trans* to that position. Therefore, the cyclometalating rings adopt a mutual *cis* geometry and are positioned *trans* to the pyridyl rings of the ancillary ligand. The structural *trans* effect (STE) of the carbanion donor affords a lengthening of the Ir–N distances of bipyridine with respect to those of the pyridyl moiety of the cyclometalating ligand; this in the range of 0.022 – 0.135 Å. Bite angles of the cyclometalating and ancillary ligands are in the ranges of 79.5 – 84.9° and 76.3 – 77.0° respectively and are typical of a complex with the general formula $[\text{Ir}(\text{C}^{\wedge}\text{N})_2\text{bpy}]^{\text{n}+}$.^[218, 270, 271]

The bond lengths about the iridium centre of $\{[\text{Ir}(\text{ppy})_2[(2\text{-Pym})_2\text{qpy}]](\text{PF}_6)_3$, Fig. 4.9., are within the expected range for those of a $[\text{Ir}(\text{ppy})_2\text{R}_2\text{bpy}]^{\text{n}+}$ complex. The unit cell contains two pairs of cations that are stacked atop of one another and are aligned anti-parallel with respect to the dipole of the ancillary ligand. The cavity created by the two arms of the quaterpyridyl unit is occupied by three molecules of acetonitrile. The structure displays considerable twisting throughout the quaterpyridinium ligand, with the most significant deviation from planarity being between the pyridyl ring of the bipyridyl unit and the

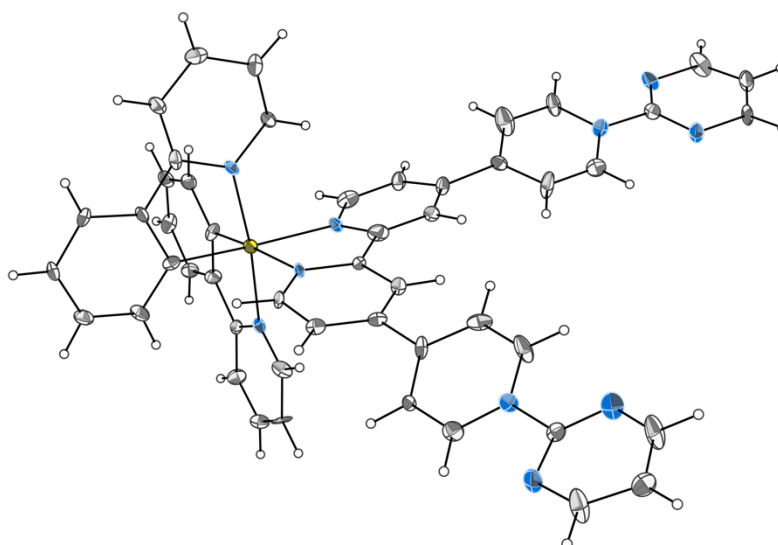


Fig. 4.9. Representation of the crystal structure of $\{[\text{Ir}(\text{ppy})_2[(2\text{-Pym})_2\text{qpy}]](\text{PF}_6)_3$ with counter anions and solvent molecules omitted for clarity. Displacement ellipsoids are set at the 30% probability level.

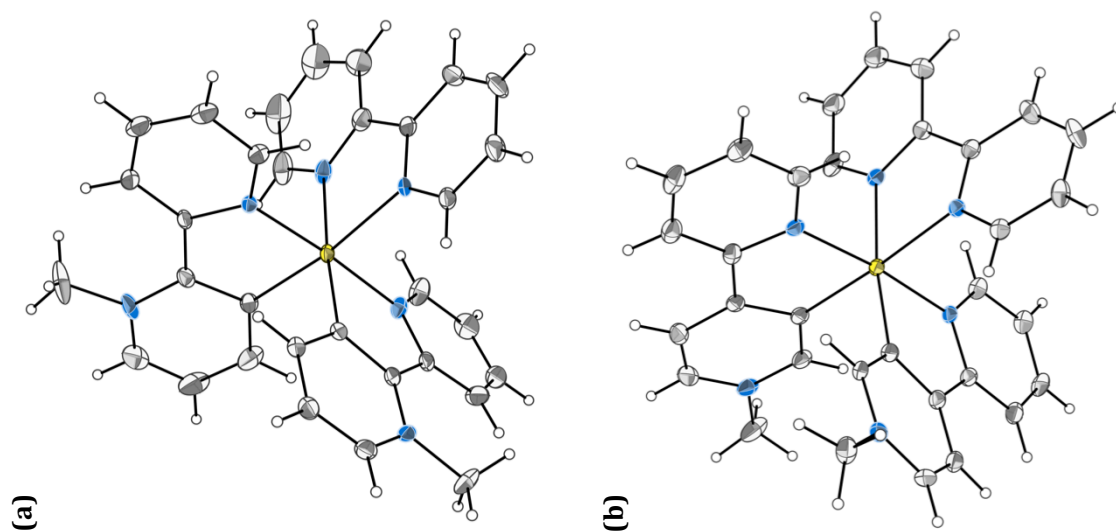


Fig. 4.10. (Right) Representation of the crystal structures of **(A)** $[\text{Ir}(22)_2\text{Y}](\text{PF}_6)_3$ and **(B)** $[\text{Ir}(42)_2\text{Y}](\text{PF}_6)_3$ with counter anions and solvent molecules omitted for clarity. Displacement ellipsoids are set at the 30% probability level.

Table 4.3. Selected bond lengths (Å), angles (°) and torsional angles (°) taken from single crystal X-ray structures for complexes $[\text{Ir}(22)_2\text{Y}](\text{PF}_6)_3$; $[\text{Ir}(22)_2\text{B}](\text{PF}_6)_3$; $[\text{Ir}(22)_2\text{F}](\text{PF}_6)_3$; $[\text{Ir}(32)_2\text{Y}](\text{PF}_6)_3$; $[\text{Ir}(32)_2\text{B}](\text{PF}_6)_3$; $[\text{Ir}(42)_2\text{Y}](\text{PF}_6)_3$ and $\{\text{Ir}(\text{ppy})_2[(2\text{-Pym})_2\text{ppy}]\}(\text{PF}_6)_3$, where N_B = bipyridyl nitrogen, C_c = cyclometalated carbon, N_p = nitrogen of the cyclometalating ligand

	$[\text{Ir}(22)_2\text{Y}]$	$[\text{Ir}(22)_2\text{B}]$	$[\text{Ir}(22)_2\text{F}]$	$[\text{Ir}(32)_2\text{Y}]$	$[\text{Ir}(32)_2\text{B}]$	$[\text{Ir}(42)_2\text{Y}]$	$[\text{Ir}(\text{ppy})_2\text{Pym}]$
Bond Distances							
Ir–C _{c1}	2.002(4)	1.993(3)	2.017(5)	1.880(19)	1.925(2)	2.010(6)	1.995(11)
Ir–C _{c2}	2.003(4)	2.002(3)	2.005(5)	1.959(19)	2.007(2)	2.014(6)	2.034(11)
Ir–N _{p1}	2.044(3)	2.042(3)	2.047(4)	2.054(16)	2.041(18)	2.050(5)	2.012(10)
Ir–N _{p2}	2.043(3)	2.041(3)	2.047(4)	2.052(17)	2.074(18)	2.052(5)	2.098(9)
Ir–N _B	2.128(3)	2.115(3)	2.135(4)	2.138(18)	2.138(18)	2.123(5)	2.120(8)
N–Me _{c1}	2.133(3)	2.129(3)	2.138(4)	2.099(18)	2.002(19)	2.128(9)	2.147(8)
N–Me _{c2}	1.489(5)	1.481(5)	1.486(6)	1.474(14)	1.470(13)	1.495(18)	---
	1.473(7)	1.481(5)	1.477(6)	1.464(14)	1.464(14)	1.472(8)	---
Bond Angles							
N _p –Ir–N _p	175.1(13)	174.7(10)	171.4(15)	171.9(6)	175.3(7)	174.3(4)	172.6(3)
C _c –Ir–N _p	172.1(12)	170.6(12)	173.7(16)	175.4(8)	172.8(8)	175.6(6)	172.5(4)
C _c –Ir–N _B	175.3(13)	175.7(11)	176.3(16)	177.4(8)	174.4(8)	175.8(4)	173.2(4)
N _p –Ir–C _c	79.6±0.3	79.8±0.21	79.7±0.07	80.7±0.6	80.2±0.4	82.8±2.1	80.5±0.6
N _p –Ir–C _c	97.3±0.2	96.4±0.18	94.1±1.00	93.7±1.5	96.4±0.9	93.1±1.3	95.9±0.2
N _p –Ir–N _B	96.7±2.3	95.7±0.52	99.1±0.93	97.1±0.1	95.1±0.3	97.5±0.3	94.1±0.6
N _p –Ir–N _p	86.6±2.2	87.8±1.43	87.6±0.07	88.8±2.0	88.6±0.8	86.9±0.5	91.7±0.9
C _c –Ir–C _c	87.3(16)	88.5(14)	86.5(18)	82.2(8)	85.8(9)	84.3(7)	86.1(4)
C _c –Ir–N _p	97.3(15)	95.1(12)	97.2(16)	99.8(8)	97.9(8)	99.6(6)	99.6(4)
C _c –Ir–N _B	99.0(13)	99.9(12)	99.7(17)	101.8(8)	100.1(8)	99.5(4)	98.1(4)
N _B –Ir–N _p	76.5(13)	76.5(11)	76.6(14)	76.3(7)	76.6(7)	76.5(3)	76.7(3)
Torsional/°							
N _p –C _{2p} –C _{1c} –X _{2c}	5.6±0.8	6.33±1.7	6.6±2.4	2.0±1.8	2.5±1.9	1.5±0.4	1.1±0.3
N _B –C _{2B} –C _{2B} –C ₃	2.2	0.8	3.7	5.9	3.4	8.1	11.5
						11.8	

pyridinium moiety, displaying a torsional angle of 21.1-31.6°. Similar twisting between the pyridinium and pyrimidyl rings was also noted although this was of a smaller angle of 12.7°, which is presumed to result from the decreased steric hindrance associated with a lack of hydrogens in the *ortho* position of the latter. Previously the only reported structure containing the [(Pym)₂qpy]²⁺ ligand was that of {Ru(bpy)₂[(Pym)₂qpy]}(PF₆)₄. This displays similar twisting, although the torsional angle between the pyridyl rings of the diimine unit is much closer to planarity.^[153]

The Ir–C distances of the bipyridinium complexes tend towards the shorter extremes typically expected for such compounds, with average bond lengths in the region 1.966 – 2.011 Å. Within the [Ir(22)₂L](PF₆)₃ series, all bond distances about the metal centre increase on decreasing the p*K*_a of the ancillary ligand, these differences being most pronounced for [Ir(22)₂F](PF₆)₃. The Ir–N distance of the ancillary ligand is particularly sensitive to changes in the functional group, displaying a variation of 0.015 Å across the series. Bond lengthening directly correlates to an increase in the electron withdrawing ability of the functional group and is therefore attributed to a decreased σ-donating ability of the ligand. The lengthening of the Ir–N distances of the cyclometalating ligand may be discussed in terms of the rationale presented in section 3.2.5.1. and are a consequence of a reduced electron density at the metal centre and a subsequent decrease in π-back bonding towards the pyridyl moiety. Incorporation of the trifluoromethyl group imparts a marked STE upon the Ir–C bond, resulting in a lengthening of 0.0135 Å in comparison to the average distances in [Ir(22)₂B](PF₆)₃. It is unclear whether this is a consequence of dCF₃bpy acting as poorer σ-donor or as an improved π-acceptor, although the concomitant lengthening of the Ir–N bond for the bipyridyl ligand indicates the former is more probable. In either scenario the STE is a consequence of perturbation of the back bonding from the metal centre to the pyridinium ring.

The crystals of [Ir(32)₂Y](PF₆)₃ displayed extensive twinning and yielded a unit cell containing two distinct structures. The first exhibits similar Ir–C and Ir–N distances to those of the other complexes with the exception of a significantly shortened Ir–N bond of 2.002(19) Å for the bipyridyl ring *trans* to the shorter of the two Ir–C bonds. In the second structure the cyclometalating ring is distorted, whereby C₃–C₄ and C₄–C₅ distances are lengthened by *ca.* 0.01-0.02 Å. Subsequently the C₃–C₄–C₅ angle is reduced to 104.2(17)°, in comparison to an expected value of *ca.* 115°, and results in a decrease in the Ir–C distance to 1.880(19) Å. For comparison purposes, the structure of [Ir(32)₂B](PF₆)₃ was also obtained although this was isolated as the (Δ)-enantiomer, the sole example of such presented herein. This too exhibited a decrease of the Ir–C distance to 1.925(19) Å, between 0.068-0.085 Å shorter than those seen in other structures, although no concomitant distortion of the cyclometalated ring was observed in this instance. One of the *tert*-butyl groups is disordered across two sites which are rotated by *ca.* 60° in relation to one another about the quaternary carbon. One of the cyclometalating moieties is also disordered, with the alternate conformation adopting a Ir–C distance that is lengthened by *ca.* 0.2 Å, thus resulting in an increase in the torsional angle

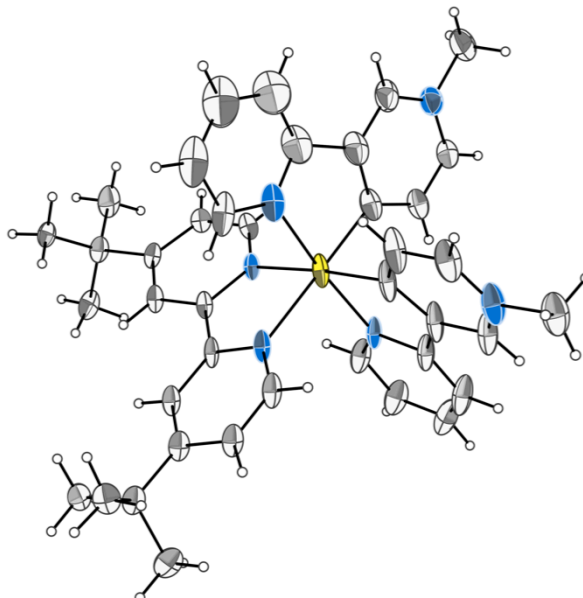


Fig. 4.11. Representation of the crystal structure of $[\text{Ir}(\text{32})_2\text{B}](\text{PF}_6)_3$ with counter anions and solvent molecules omitted for clarity. Displacement ellipsoids are set at the 30% probability level.

between the planes of the two rings of the cyclometalated ligand; no other significant differences were observed within the structure.

The N–Me distances vary by *ca.* 0.04 Å across the series of compounds and are in good agreement with the trends reported in literature for the pro-ligands and related metal complexes. The reported N – Me distances of 1-methyl-2-(2'-pyridyl)pyridinium^[272], $[\text{Pd}(\text{22})(\text{H}_2\text{O})(\text{ONO}_2)]\text{ClO}_4 \cdot \text{H}_2\text{O}$ ^[240] and $[\text{Pd}(\text{22})\text{Cl}_2]$ ^[273] at 1.489, 1.484 and 1.481 Å respectively indicate that only a minimal change in bond length is afforded upon cyclometalation. Unfortunately no crystal structure for 1-methyl-4-(2'-pyridyl)pyridinium has previously been published nor could one be obtained during this study. However, examples of the compound acting as both a monodentate, via pyridyl coordination, and a bidentate cyclometalated ligand have been reported in the form of $[\text{Pt}(\text{42})\text{Cl}_3]$ and $[\text{Pt}(\text{42})\text{Cl}_2]$, which exhibited N–Me distances of 1.471(7) and 1.466(1) respectively.^[274]

The trends of 1-methyl-3-(2'-pyridyl)pyridinium remain less clear. The reported N–Me bond length of 1.465 Å in the pro-ligand,^[243] is similar to that in both structures of $[\text{Ir}(\text{32})_2\text{Y}](\text{PF}_6)_3$. However, both the structure of $[\text{Ir}(\text{32})_2\text{B}](\text{PF}_6)_3$ and $[\text{Ru}(\text{bpy})_2(\text{32})](\text{PF}_6)$ ^[243] exhibit similar bond lengths which have been increased by *ca.* 0.035 Å with respect to the pro-ligand. One rationale that was presented for this observation was that an increase in the electron density of the pyridinium ring, as suggested by other experimental data, results in a diminished influence of the positive charge upon the N–Me distance, thus lengthening the bond.

4.2.4. Electronic Spectroscopy

The room temperature UV-visible absorption spectra were recorded for all complexes as both the hexafluorophosphate and chloride salts in acetonitrile and deionised water respectively. This is with the exception of [Ir(ppy)₂qpy](Cl) which was insoluble in water and hence could not be recorded. For comparison purposes all discussion contained herein refers to data collected as the hexafluorophosphate salt. General trends and observations remain true for both series of compounds and whilst there are slight variations in λ_{max} and ϵ , no distinct solvent dependency was apparent.

The intense bands at $\lambda < 320$ nm are assigned to spin allowed $\pi\text{-}\pi^*$ and higher energy MLCT transitions, involving both the cyclometalating and ancillary ligands. The low energy bands of modest extinction coefficients are assigned to an admixture of ¹MLCT and ¹LLCT transitions. A contribution from the spin forbidden ³MLCT and ³LC transitions are also expected, as facilitated by the large spin orbit coupling constant of the iridium metal centre. Whilst primarily obscured by the spin allowed processes, these transitions are still evident as a low intensity tailing which may be observed for all complexes, although they are particularly apparent for those of 2-phenylpyridine and 1-methyl-3-(2-pyridyl)pyridinium.

The spectra for complexes of the general formula [Ir(ppy)₂(N[^]N)]ⁿ⁺ display three distinct bands between 200 and 700 nm. These all undergo a bathochromic shift upon increasing the electron withdrawing ability of the pendent pyridyl group in the order of Pyr < N-MePyr < N-(2-Pym)Pyr and is similarly reflected in the reported λ_{onset} values. This correlates to a decreasing energy of the quaterpyridyl π^* -orbitals thus indicating the MLCT processes primarily involve the ancillary ligand. The increased extinction coefficients evident for

Table 4.4. UV-Visible absorption data for the complexes of the general formula [Ir(ppy)₂(N[^]N)]ⁿ⁺ containing quaterpyridyl ancillary ligands.

Complex salt	λ_{max} , nm	ϵ , 10 ³ M ⁻¹ cm ⁻¹	E_{max} , eV	λ_{onset} , nm ^c	Assignment
Hexafluorophosphate Salts^a					
Ir(ppy) ₂ Qpy ⁺	251	68.9	4.94	556	$\pi \rightarrow \pi^*$
	364	11.4	3.41		$d \rightarrow \pi^*$
	467	1.3	2.66		$d \rightarrow \pi^*$
Ir(ppy) ₂ MeQpy ³⁺	253	70.2	4.90	625	$\pi \rightarrow \pi^*$
	384	10.9	3.23		$d \rightarrow \pi^*$
	531	1.2	2.34		$d \rightarrow \pi^*$
Ir(ppy) ₂ PymQpy ³⁺	268	83.6	4.63	685	$\pi \rightarrow \pi^*$
	378	16.6	3.28		$d \rightarrow \pi^*$
	562	1.8	2.21		$d \rightarrow \pi^*$
Chloride Salts^b					
Ir(ppy) ₂ MeQpy ³⁺	252	53.8	4.92	610	$\pi \rightarrow \pi^*$
	381	8.2	3.25		$d \rightarrow \pi^*$
	543	0.9	2.28		$d \rightarrow \pi^*$
Ir(ppy) ₂ PymQpy ³⁺	267	75.4	4.64	674	$\pi \rightarrow \pi^*$
	374	15.0	3.32		$d \rightarrow \pi^*$
	542	1.6	2.29		$d \rightarrow \pi^*$

^a Solutions ca. 1.0×10^{-5} - 2.0×10^{-4} M in acetonitrile or ^b deionised water. ^c λ_{onset} defined as the wavelength above which $\epsilon > 100$ M⁻¹cm⁻¹. ϵ were determined from measurements at three or more different concentrations. ^{sh} denotes a shoulder or poorly defined maxima.

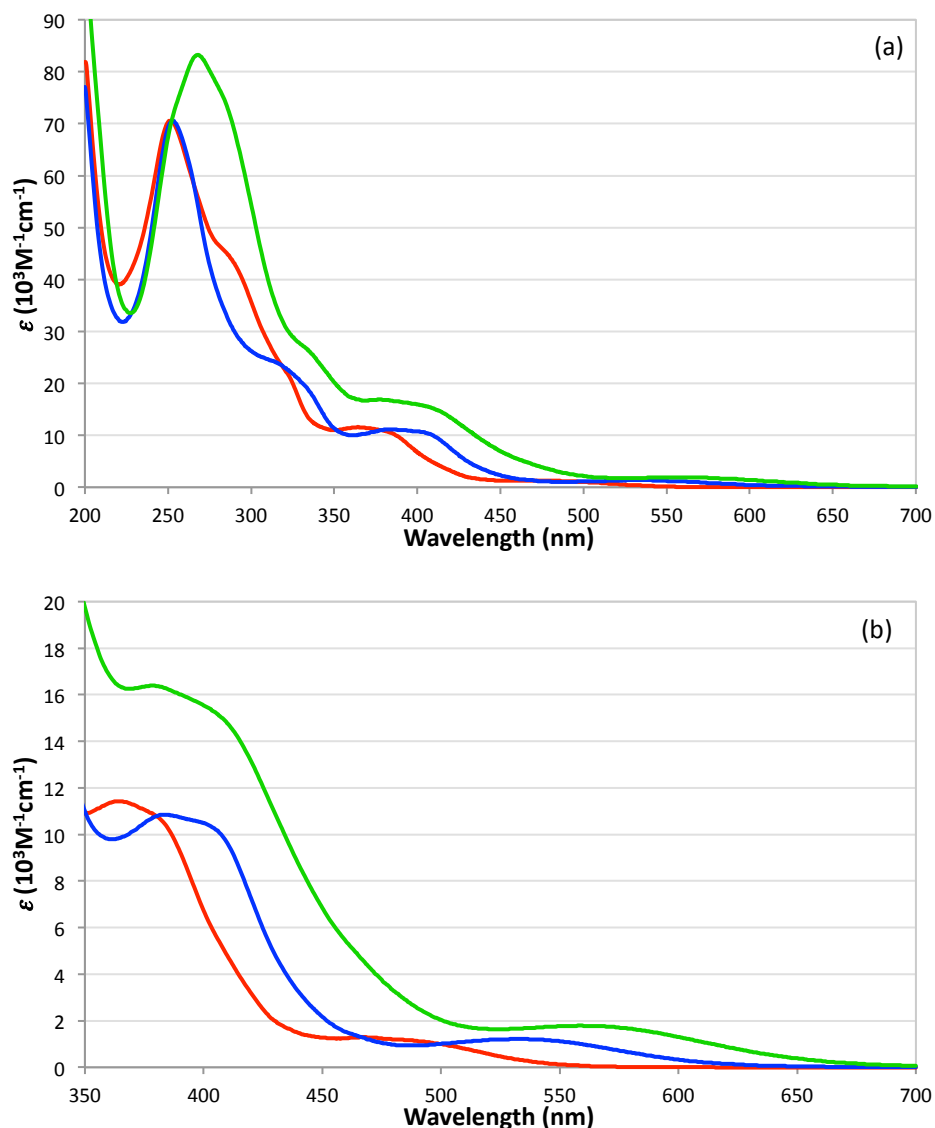


Fig. 4.12. UV-visible absorption spectra of the complexes $[\text{Ir}(\text{ppy})_2\text{qpy}](\text{PF}_6)$ (blue), $[\text{Ir}(\text{ppy})_2\text{Me}_2\text{qpy}](\text{PF}_6)_3$ (red) and $[\text{Ir}(\text{ppy})_2\text{Pym}_2\text{qpy}](\text{PF}_6)_3$ (green) displaying A) the full spectra and B) $350 \leq \lambda \leq 700\text{nm}$ expansion of the lower energy bands. Recorded in acetonitrile at 298 K.

$\{\text{Ir}(\text{ppy})_2[(\text{Pym})_2\text{qpy}]\}(\text{PF}_6)_3$ are associated with an extension of the π -conjugated system upon incorporation of pyrimidyl group.

The highest energy band with maxima between 250-270 nm also displays an additional shoulder extending to longer wavelengths. The latter is assigned to a higher energy MLCT and becomes more defined upon incorporation of the *N*-methyl substituent, as the causative transitions are bathochromically shifted. Further insight into the behaviour of these transitions are limited as once again they become indistinct on broadening of the more intense band in $\{\text{Ir}(\text{ppy})_2[(\text{Pym})_2\text{qpy}]\}(\text{PF}_6)_3$. The origin of the weak absorption in the range of $450 \leq \lambda \leq 700$ nm remains unclear, although from the relatively low ϵ values of 1.2 to $1.8 \times 10^3 \text{M}^{-1}\text{cm}^{-1}$ a contribution from the aforementioned spin forbidden transitions is expected to some to degree. TD-DFT calculations suggest a number of low intensity $^1\text{MLCT}$ transitions involving LUMOs localised about the pyridinium moiety of the ancillary ligand.

Table 4.5. UV-Visible absorption data for the complexes of the general formula [Ir(C[^]N)₂(N[^]N)]³⁺ containing the bipyridinium cyclometalating ligands recorded as the hexafluorophosphate salt.^a

Complex salt	λ_{\max} , nm	ϵ , 10 ³ M ⁻¹ cm ⁻¹	E_{\max} , eV	λ_{onset} , nm ^b	Assignment
Ir22Y	212 ^{sh}	53.1	5.85	502	$\pi \rightarrow \pi^*$
	257	34.4	4.82		$\pi \rightarrow \pi^*$
	297	33.3	4.18		$\pi \rightarrow \pi^*$
	354	9.4	3.50		$d \rightarrow \pi^*$
	437 ^{sh}	2.8	2.84		$d \rightarrow \pi^*$
Ir22B	213	60.4	5.82	507	$\pi \rightarrow \pi^*$
	258	35.2	4.81		$\pi \rightarrow \pi^*$
	299	34.0	4.15		$\pi \rightarrow \pi^*$
	312 ^{sh}	28.9	3.97		$d \rightarrow \pi^*$
	355	9.1	3.49		$d \rightarrow \pi^*$
Ir22F	212	48.2	5.85	492	$\pi \rightarrow \pi^*$
	263	32.3	4.71		$\pi \rightarrow \pi^*$
	298	29.7	4.16		$\pi \rightarrow \pi^*$
	350 ^{sh}	10.2	3.54		$d \rightarrow \pi^*$
	426 ^{sh}	3.4	2.91		$d \rightarrow \pi^*$
Ir23Y	237	54.3	5.23	434	$\pi \rightarrow \pi^*$
	255 ^{sh}	48.5	4.86		$\pi \rightarrow \pi^*$
	302	25.9	4.11		$\pi \rightarrow \pi^*$
	313	24.5	3.96		$d \rightarrow \pi^*$
	352 ^{sh}	5.3	3.52		$d \rightarrow \pi^*$
Ir23B	237	58.0	5.23	437	$\pi \rightarrow \pi^*$
	260	49.9	4.77		$\pi \rightarrow \pi^*$
	300	25.4	4.13		$\pi \rightarrow \pi^*$
	312	25.9	3.97		$d \rightarrow \pi^*$
	355 ^{sh}	5.5	3.49		$d \rightarrow \pi^*$
Ir23F	237	52.7	5.23	441	$\pi \rightarrow \pi^*$
	259	52.1	4.79		$\pi \rightarrow \pi^*$
	308	25.2	4.03		$\pi \rightarrow \pi^*$
	317	24.3	3.91		$d \rightarrow \pi^*$
	350 ^{sh}	5.8	3.54		$d \rightarrow \pi^*$
Ir24Y	254	44.8	4.88	498	$\pi \rightarrow \pi^*$
	280 ^{sh}	32.2	4.43		$\pi \rightarrow \pi^*$
	307	28.1	4.04		$\pi \rightarrow \pi^*$
	357	6.8	3.47		$d \rightarrow \pi^*$
	392 ^{sh}	3.8	3.16		$d \rightarrow \pi^*$
Ir24B	234	44.6	5.30	502	$\pi \rightarrow \pi^*$
	256	50.1	4.84		$\pi \rightarrow \pi^*$
	299	31.7	4.15		$\pi \rightarrow \pi^*$
	309	30.0	4.01		$\pi \rightarrow \pi^*$
	358	7.2	3.46		$d \rightarrow \pi^*$
Ir24F	252	46.2	4.92	488	$\pi \rightarrow \pi^*$
	295	32.7	4.20		$\pi \rightarrow \pi^*$
	307	31.7	4.04		$\pi \rightarrow \pi^*$
	350 ^{sh}	7.8	3.54		$d \rightarrow \pi^*$
	389	5.0	3.19		$d \rightarrow \pi^*$
Ir24F	425 ^{sh}	2.6	2.92		$d \rightarrow \pi^*$

^a Solutions ca. 1.0×10^{-5} - 2.0×10^{-4} M in acetonitrile. ^b λ_{onset} defined as the wavelength above which $\epsilon > 100 \text{ M}^{-1}\text{cm}^{-1}$. ϵ were determined from measurements at three or more different concentrations.

^{sh} denotes a shoulder or poorly defined maxima.

Table 4.6. UV-Visible absorption data for the complexes of the general formula $[Ir(C^{\wedge}N)_2(N^{\wedge}N)]^{3+}$ containing the bipyridinium cyclometalating ligands recorded as the chloride salt.^a

Complex salt	λ_{\max} , nm	ϵ , $10^3 M^{-1} cm^{-1}$	E_{\max} , eV	λ_{onset} , nm	Assignment
Ir22Y	209	52.0	6.08	501	$\pi-\pi^*$
	255	33.4	4.86		$\pi-\pi^*$
	300	32.4	4.13		$\pi-\pi^*$
	354	9.3	3.50		$d-\pi^*$
	438 ^{sh}	2.6	2.83		$d-\pi^*$
Ir22B	213	66.7	5.82	509	$\pi-\pi^*$
	257	38.3	4.82		$\pi-\pi^*$
	299	37.0	4.15		$\pi-\pi^*$
	312 ^{sh}	31.3	3.97		$\pi-\pi^*$
	355	9.5	3.49		$d-\pi^*$
	446 ^{sh}	2.3	2.78		$d-\pi^*$
Ir22F	212	45.6	5.85	477	$\pi-\pi^*$
	262	29.7	4.73		$\pi-\pi^*$
	296	27.6	4.19		$\pi-\pi^*$
	350 ^{sh}	9.4	3.54		$d-\pi^*$
	425 ^{sh}	3.0	2.92		$d-\pi^*$
Ir23Y	237	48.3	5.23	422	$\pi-\pi^*$
	255 ^{sh}	42.4	4.86		$\pi-\pi^*$
	302	22.8	4.11		$\pi-\pi^*$
	312	21.8	3.97		$\pi-\pi^*$
	353 ^{sh}	4.8	3.51		$d-\pi^*$
Ir23B	236	51.8	5.25	422	$\pi-\pi^*$
	259 ^{sh}	44.9	4.79		$\pi-\pi^*$
	299	23.9	4.15		$\pi-\pi^*$
	311	23.2	3.99		$\pi-\pi^*$
	356 ^{sh}	4.5	3.48		$d-\pi^*$
Ir23F	236	47.4	5.25	440	$\pi-\pi^*$
	257	43.2	4.82		$\pi-\pi^*$
	308	21.6	4.03		$\pi-\pi^*$
	316	20.9	3.92		$\pi-\pi^*$
	350 ^{sh}	5.4	3.54		$d-\pi^*$
Ir24Y	254	44.2	4.88	497	$\pi-\pi^*$
	277 ^{sh}	31.6	4.48		$\pi-\pi^*$
	300	28.4	4.13		$\pi-\pi^*$
	308	28.2	4.03		$\pi-\pi^*$
	358	6.7	3.46		$d-\pi^*$
	392 ^{sh}	3.6	3.16		$d-\pi^*$
Ir24B	233	44.9	5.32	504	$\pi-\pi^*$
	256	49.5	4.84		$\pi-\pi^*$
	298	31.6	4.16		$\pi-\pi^*$
	309	30.1	4.01		$\pi-\pi^*$
	357	7.0	3.47		$d-\pi^*$
	395 ^{sh}	3.6	3.14		$d-\pi^*$
	447 ^{sh}	1.6	2.79		$d-\pi^*$
Ir24F	252	42.4	4.92	487	$\pi-\pi^*$
	296	29.6	4.19		$\pi-\pi^*$
	307	29.5	3.56		$\pi-\pi^*$
	348	7.2	3.56		$d-\pi^*$
	388	4.5	3.20		$d-\pi^*$
	427 ^{sh}	2.2	2.90		$d-\pi^*$

^a Solutions ca. 1.0×10^{-5} - 2.0×10^{-4} M in deionised water. λ_{onset} defined as the wavelength above which $\epsilon > 100 M^{-1} cm^{-1}$. ϵ were determined from measurements at three or more different concentrations. ^{sh} denotes a shoulder or poorly defined maxima.

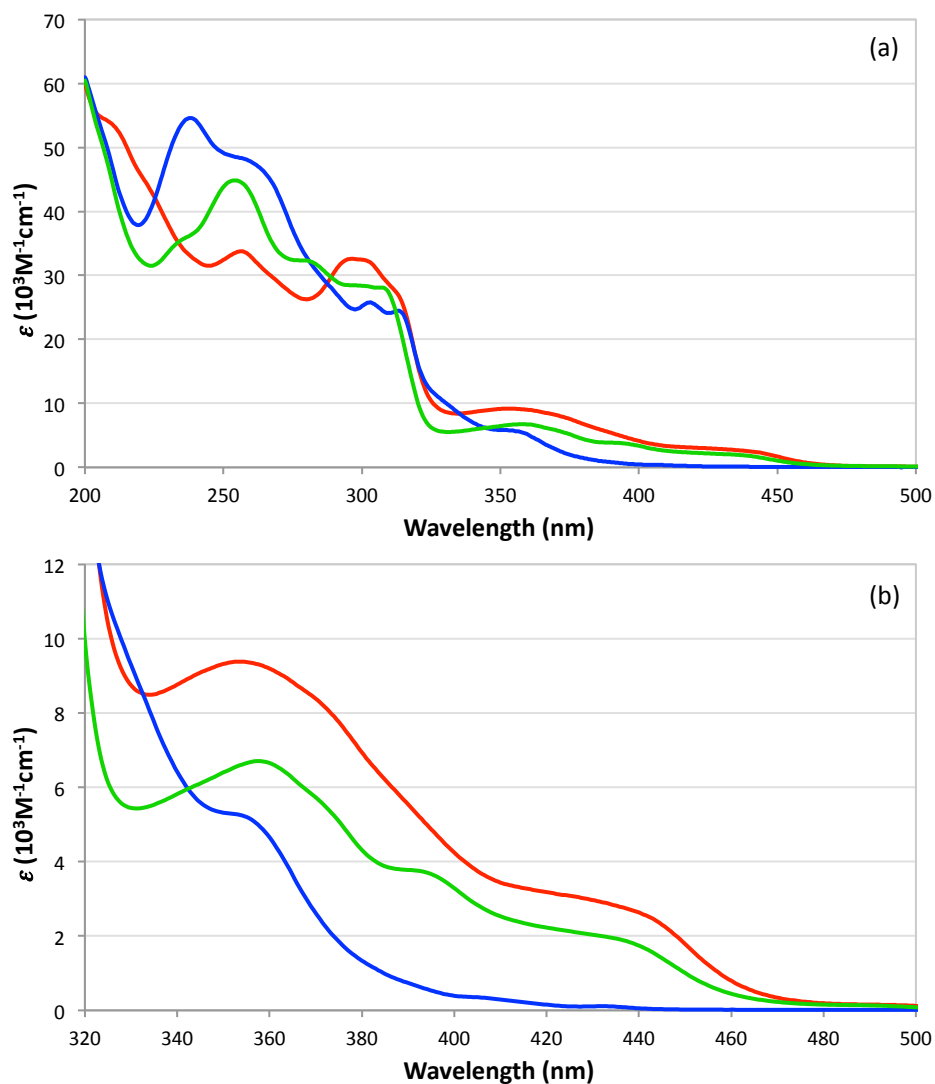


Fig. 4.13. UV-visible absorption spectra of the complexes [Ir(22)₂Y](PF₆)₃ (blue), [Ir(32)₂Y](PF₆)₃ (red) and [Ir(42)₂Y](PF₆)₃ (green) displaying A) the full spectra and B) 320 ≤ λ ≤ 500 nm expansion of the lower energy bands. Recorded in acetonitrile at 298 K.

A definitive comparison of the spectra for the complexes of bipyridinium is somewhat difficult due to the extensive overlapping and resultant poor definition of the bands in the low energy region. As such only two general trends can be discerned. The first is a bathochromic shift in the order of [Ir(32)₂L] << λ << [Ir(42)₂L] < λ < [Ir(22)₂L], which is accompanied by steadily increasing ϵ values, Fig. 4.13. The difference is most pronounced on comparison of the [Ir(32)₂L](PF₆)₃ series, which has undergone a shift of λ > 65 nm. Secondly, as the pK_a of the ancillary ligand increases on changing R in the order CF₃ < H < ^tBu, the lower energy bands undergo a bathochromic shift of ca. 20 nm between extremes of the series, Fig. 4.14. This relatively small change in absorption profile suggests the MLCT processes are localised about the cyclometalated ligand, the observed shift a result of stabilisation of the metal-based HOMOs on increasing the σ -donating or decreasing π -accepting abilities of the bipyridyl ligand. The exception to this trend is [Ir(32)₂F](PF₆)₃, which exhibits a tailing that extends to longer wavelengths and is of higher intensity than that of the bpy and ^tBubpy counterparts. This may be explained on assuming that the transition instead now describes a MLCT towards

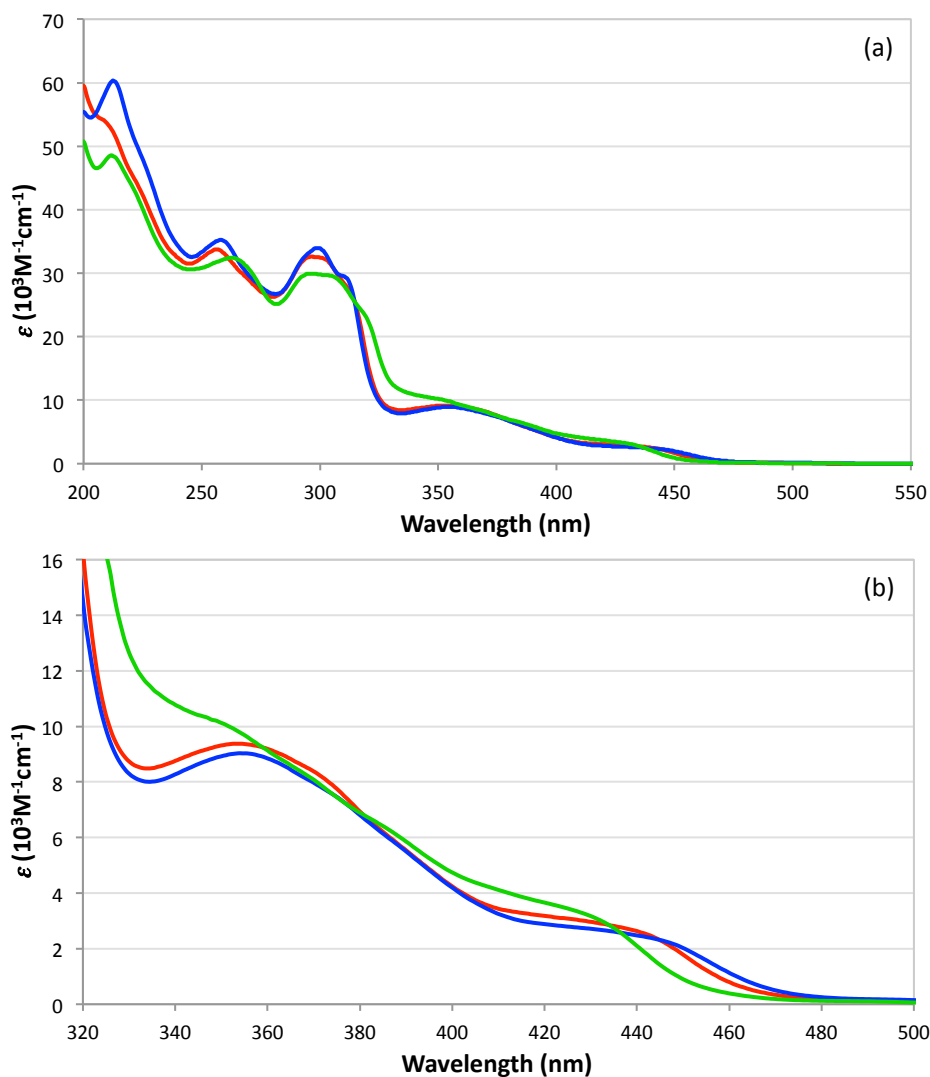


Fig. 4.14. UV-visible absorption spectra of the complexes $[\text{Ir}(22)_2\text{Y}](\text{PF}_6)_3$ (blue), $[\text{Ir}(22)_2\text{B}](\text{PF}_6)_3$ (red) and $[\text{Ir}(22)_2\text{F}](\text{PF}_6)_3$ (green) displaying A) the full spectra and B) $320 \leq \lambda \leq 500\text{nm}$ expansion of the lower energy bands. Recorded in acetonitrile at 298 K.

the ancillary ligand and thus results from the stabilisation of the π^* -orbitals by the electronegative trifluoromethyl group. This shift may also be evident in spectra of $[\text{Ir}(22)_2\text{F}](\text{PF}_6)_3$ and $[\text{Ir}(42)_2\text{F}](\text{PF}_6)_3$ but is obscured by other more intense MLCT transitions in this region, although this would explain in part the decreased definition of these bands in comparison to the complexes of bpy and d^tBubpy.

Each of the three series of compounds displays distinct absorption profiles in the region of $200 \leq \lambda \leq 320\text{ nm}$, although they do share some common features with one another and with those of the bipyridinium pro-ligands, as shown in appendix D. The band at 290-320 nm is more structured for compounds of $[\text{Ir}(32)_2\text{L}](\text{PF}_6)_3$ and $[\text{Ir}(42)_2\text{L}](\text{PF}_6)_3$, showing two defined maxima. For complexes of dCF₃bpy an additional shoulder extending to longer wavelengths becomes apparent. Considering the previously discussed rationale concerning the respective energy of the π^* -orbitals of the ancillary ligand, this would be in agreement with the assignment of a contribution to these bands from higher energy MLCT transitions as is also suggested by TD-DFT.

4.2.5. Electrochemistry

The cyclic voltammograms were recorded for each of the monometallic complexes as the hexafluorophosphate salt at 50, 100 and 200 mVs⁻¹ with a supporting electrolyte of 0.1 M tetra-*n*-butylammonium hexafluorophosphate in acetonitrile. For comparison purposes the methyl quaternised bipyridinium pro-ligands were also recorded under the same conditions.

Table 4.7. Electrochemical data for the methylated quaternised bipyridinium pro-ligands and complexes of the general formula $[\text{Ir}(\text{C}^{\wedge}\text{N})_2(\text{N}^{\wedge}\text{N})](\text{PF}_6)_n$.

Cation	Ir(III/IV)	$E(1^+/0)$	$E(0/1^-)$	$E(1^-/2^-)$	$E(2^-/3^-)$
(Me22bpy) ⁺	---	-1.07 ^c	---	---	---
(Me32bpy) ⁺	---	-1.15 ^c	---	---	---
(Me42bpy) ⁺	---	-1.00 (70)	-1.72 ^c	---	---
[Ir(ppy) ₂ qpy] ⁺	1.30 ^d	-1.12 (70)	-1.62 (70)	---	---
Cation	Ir(III/IV)	$E(3^+/2^+)$	$E(2^+/1^+)$	$E(1^+/0)$	$E(1^-/2^-)$
[Ir(ppy) ₂ Me ₂ qpy] ³⁺	1.34 ^b	-0.62 (70)	-0.73 (60)	-1.20 (60)	-1.43 (70)
{Ir(ppy) ₂ [(Pym) ₂ qpy]} ³⁺	1.35 ^b	-0.29 (80)	-0.79 ^c	---	---
[Ir(22) ₂ Y] ³⁺	2.18 ^d	-0.78 (60)	-0.94 (70)	-1.38 (70)	-1.65 (80)
[Ir(22) ₂ F] ³⁺	2.29 ^d	-0.72 (60)	-0.86 (70)	-1.03 (60)	-1.56 (90) ^b
[Ir(22) ₂ B] ³⁺	2.16 ^d	-0.78 (60)	-0.94 (70)	-1.45 (70)	-1.65 (70)
[Ir(32) ₂ Y] ³⁺	2.36 ^d	-1.09	-1.26 (60)	-1.47 ^c	---
[Ir(32) ₂ F] ³⁺	2.53 ^d	-0.72 (70)	-1.29 ^c	-1.44 ^c	-1.65 (br)
[Ir(32) ₂ B] ³⁺	2.34 ^d	-1.14 ^c	-1.31 ^c	-1.50 ^c	---
[Ir(42) ₂ Y] ³⁺	2.19 ^d	-0.83 (70)	-0.99 (60)	-1.41 (70)	---
[Ir(42) ₂ F] ³⁺	2.30 ^d	-0.73 (70)	-0.90 (60)	-1.07 (70)	---
[Ir(42) ₂ B] ³⁺	2.16 ^d	-0.82 (80)	-0.98 (80)	-1.48 (80)	-1.76 (80)

^a $E = 0.5 \times (E_{pc} + E_{pa})$ vs Ag/AgCl; Measurements performed in acetonitrile, 0.1 M [ⁿBu₄N]PF₆ with a scan rate of 100 mV s⁻¹ at RT; Solutions ca. 1.5×10^{-4} M with respect to analyte; F_c/F_c⁺ internal reference, $E = 0.44$ V, $\Delta E_p = 70$ -90 mV; Pt disc working electrode and Pt wire auxiliary electrode. ^b quasi-reversible process; ^c irreversible process, E_{pc} ; ^d irreversible process, E_{pa} ; as determined using differential pulse voltammetry techniques, potential increment = 2 mV; amplitude = 50 mV; pulse width = 0.01 s.

The complexes of the general formula $[\text{Ir}(\text{ppy})_2(\text{N}^{\wedge}\text{N})]^{n+}$ each exhibit a single oxidation process which is not fully chemically reversible and is associated with the Ir^(III/IV) couple; the recorded values typical of a $[\text{Ir}(\text{ppy})_2\text{bpy}]^+$ complex. The potential is anodically shifted by 0.04 V on quaternisation of the ancillary ligand, and is further shifted by +0.01 V on changing the *N*-substituent from the methyl to the pyrimidyl group. Concerning $[\text{Ir}(\text{ppy})_2\text{qpy}]^+$, the oxidation wave gradually became less distinct on multiple scans until it could no longer be observed. It was noted on inspection of the electrode, that an orange film had formed upon the working surface and could not be removed electrochemically. On cleaning of the electrode the oxidation wave once again became evident before diminishing during repeat scans. Issues of adsorption have been previously encountered within the Coe group upon analysis of compounds containing quaterpyridine and analogous ligands, a process that is promoted by the pendent pyridyl group.

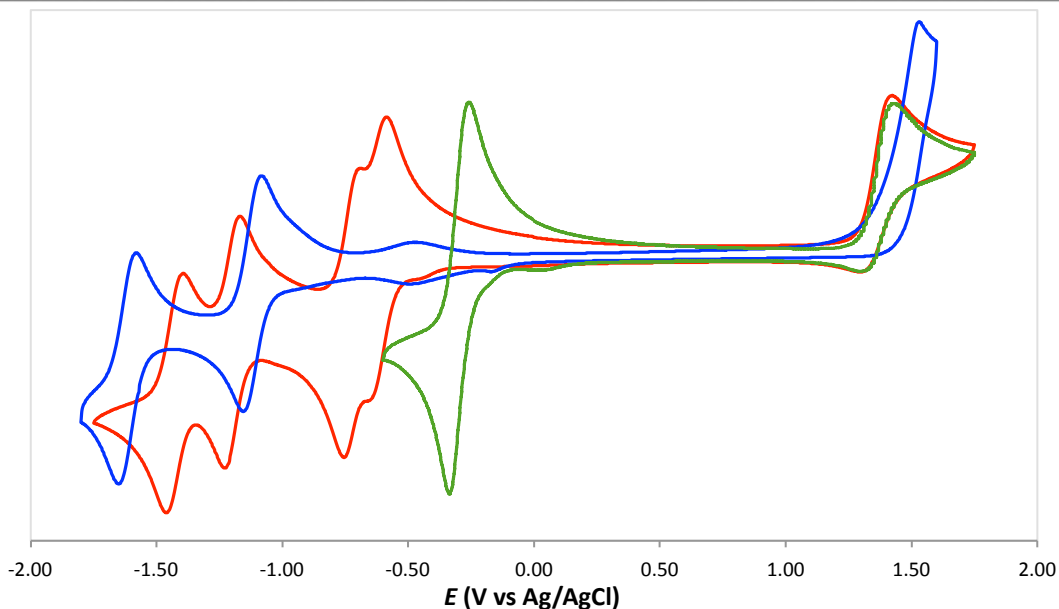


Fig. 4.15. Cyclic voltammograms of $[\text{Ir}(\text{ppy})_2\text{qpy}](\text{PF}_6)$ (blue), $[\text{Ir}(\text{ppy})_2\text{Me}_2\text{qpy}](\text{PF}_6)_3$ (red) and $[\text{Ir}(\text{ppy})_2\text{Pym}_2\text{qpy}](\text{PF}_6)_3$ (green) recorded at 100 mVs^{-1} in $0.1 \text{ M } n\text{-Bu}_4\text{NPF}_6$ acetonitrile at 298 K .

Each of the three compounds displays distinct reduction profiles, Fig. 4.15. The two reversible processes of $[\text{Ir}(\text{ppy})_2\text{qpy}]^+$ are of potentials expected for a complex with the general formula $[\text{Ir}(\text{ppy})_2(\text{bpy})]^{3+}$.^[218] As reduction of phenylpyridine is expected to occur at potentials more negative than -2.0 V vs SCE ^[218, 275, 276] the reported reduction couples are assigned to the ancillary ligand. Due to the stabilising effect of the metal centre it is expected that the first of these reductions be localised upon the bipyridyl unit of the ligand; an assumption that is supported by TD-DFT calculations indicating that the electron density of the LUMO is centred primarily about the bipyridyl rings. An additional process at $E \approx -0.1 \text{ V}$ is apparent when preceded by an oxidative scan, the intensity of which decreases with a decreasing scan rate. This appears to be related to the aforementioned adsorption processes as it is lost on cleaning of the electrode or, to a lesser extent, upon multiple reductive scans.

$[\text{Ir}(\text{ppy})_2\text{Me}_2\text{qpy}](\text{PF}_6)_3$ displays four reversible processes which are subject to a significant anodic shift in relation to the quaterpyridyl analogue. This is owing to the decrease in energy of the π^* -orbitals of the ligand upon quaternisation. The first two overlapping waves, which could only be resolved upon using pulse differential techniques, represent successive single electron reduction processes of the two pyridinium groups. The peak separation indicates a degree of electronic communication within the quaterpyridinium moiety; as previously demonstrated in the quaterpyridinium coordination complexes of ruthenium(II).^[153, 168] $\{\text{Ir}(\text{ppy})_2[(\text{Pym})_2\text{qpy}]\}(\text{PF}_6)_3$ displays a single reversible reduction couple of twice the current intensity to that of the oxidative wave. Presumably this is comparable to that seen for the complex of $(\text{Me}_2\text{qpy})^{2+}$ and is comprised of two individual single electron reductions of the pyridinium groups, although these are overlapping to a greater degree. The potential is shifted anodically by 0.33 V in comparison to the respective couple of the methyl analogue, a consequence of the increased electron withdrawing ability of

the pyrimidyl group. A second irreversible reduction is shifted by a similar magnitude with respect to the peak at -1.20 V in $[\text{Ir}(\text{ppy})_2\text{Me}_2\text{qpy}](\text{PF}_6)_3$, this wave is omitted from Fig. 4.15. for clarity of comparison. On extending the scan range beyond -1.2 V, broadening of the more negative wave occurs concomitant to an increase in the i_{pa} and ΔE of the couple at -0.29 V, the latter a result of the anodic peak shifting to more positive potentials.

The cyclic voltammograms for each of the complexes of bipyridinium display an indistinct irreversible process at potentials of $E \geq 2.10$ V. Using differential pulse techniques the anodic peak could be resolved and the potentials determined. In comparison to the complexes of 2-phenylpyridine, these oxidative processes are significantly anodically shifted by *ca.* $0.84 - 1.23$ V, Fig. 4.16. This is in agreement with the decreased σ -donating and increased π -accepting abilities that are expected of the pyridinium moiety in relation to the aryl ring of 2-phenylpyridine. The recorded potentials within the range of $2.16 - 2.53$ V are exceptionally high for bis-cyclometalated complexes of this type and are instead closer to values expected for the tricationic bis-terpyridyl compounds [277,278] or the di-/tricationic N⁺N linkage isomers of tris-2,2'-bipyridine.[279,280] Unfortunately, the degree to which this shift may be attributed to quaternisation cannot be properly evaluated as the analogous $[\text{Ir}(\text{bpy}-C,N')_2(\text{bpy}-N,N')^+]$ complex has yet to be reported, as such the relative effects of changing the cyclometalating ring from a phenyl to a pyridyl group cannot be quantified. It is surmised however that, by comparison, the more electron deficient pyridyl ring would afford an anodic shift of the oxidation couple. Upon quaternisation it is expected that the magnitude of this shift would increase owing to the stabilising effects of the positive charge upon the heteroatom.

Complexes of the formulae $[\text{Ir}(22)_2\text{L}](\text{PF}_6)_3$ and $[\text{Ir}(42)_2\text{L}](\text{PF}_6)_3$ exhibit comparable oxidation potentials and trends thereof, with a maximum variation of 0.03 V between the two series. In relation to these, the $[\text{Ir}(32)_2\text{L}](\text{PF}_6)_3$ complexes display an anodic shift of *ca.* 0.2 V, indicating that 1-methyl-3-(2'-pyridyl)pyridinium is acting as either a poorer σ -donor or an improved π -acceptor towards iridium than the other two isomers.

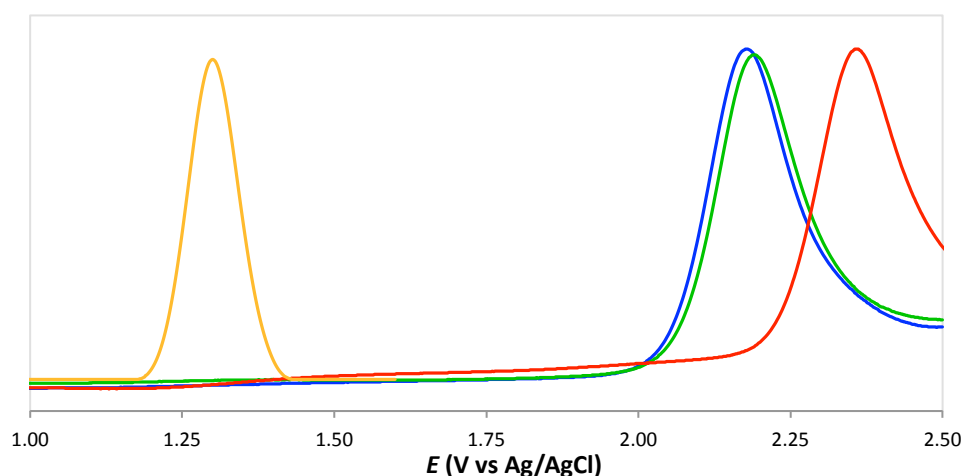


Fig. 4.16. Pulse differential voltammograms depicting the oxidation processes of $[\text{Ir}(\text{ppy})_2\text{qpy}](\text{PF}_6)$ (orange), $[\text{Ir}(22)_2\text{Y}](\text{PF}_6)_3$ (blue), $[\text{Ir}(32)_2\text{B}](\text{PF}_6)_3$ (red) and $[\text{Ir}(42)_2\text{F}](\text{PF}_6)_3$ (green) recorded in 0.1M $n\text{-Bu}_4\text{NPF}_6$ acetonitrile at 298 K.

Variations in the oxidation potential on changing the ancillary ligand from bpy to d^tBubpy are minimal and result in a cathodic shift of just 0.02 V. These results indicate that the *tert*-butyl group is of insufficient electron density to effect an appreciable change in the donor ability of the ligand. The inclusion of the trifluoromethyl group however afforded an anodic shift of *ca.* 0.1 – 0.2 V, owing to the decrease in σ -donation to the metal centre as a result of the electronegativity of the functionality.

It has been previously suggested that an irreversible oxidation process may be indicative of a loss of an electron from the Ir – C⁻ σ -bonding orbital rather than the metal centre itself.^[271, 281] The degree to which the bonding orbital contributes to the oxidative process is dependent upon the extent of the covalency of the Ir – C bond. For the complexes of bipyridinium it is difficult to fully evaluate the nature of this bond due to the unusual properties that have been made apparent. The anodic shift of the oxidative process and the expected poor σ -donor ability of the pyridinium moiety may suggest an increase in the ionic character. As such making a definitive assignment of the oxidation process for these complexes is untenable at present.

The cyclic voltammogram of the [1-Me-4,2'-bpy]PF₆ pro-ligand displays a reversible reduction at -1.00 V and a second irreversible process at -1.72 V. For [1-Me-2,2'-bpy]PF₆ and [1-Me-3,2'-bpy]PF₆ the first reduction process is irreversible and occurs at more negative potentials. The (1⁺/0) couple is assigned to the single electron reduction of the pyridinium moiety, with the irreversible (0/1⁻) process assigned to that of the unquaternised pyridyl ring. By comparison the first reduction of 2,2'-bipyridine in acetonitrile has been reported at - 2.21 V vs SCE.^[282] The anodic shift afforded on quaternisation demonstrates the extent of which the π^* -orbitals of the individual moieties, and thus the ligand as a whole, have been stabilised. The difference between the [1-Me-4,2'-bpy]PF₆ and [1-Me-2,2'-bpy]PF₆ may be explained by a decrease in the delocalisation within the π -system as a result of the steric interactions of the methyl group. The more significant shift seen for [1-Me-3,2'-bpy]PF₆ may be due to the relative position of the pyridyl moiety and the nitrogen of the pyridinium ring. Adopting a *meta*- position, the ligand does not benefit from the favourable resonance structures that are present in the other isomers and which facilitate a greater electronic communication between the two individual rings. This is reflected in ¹H-NMR results that show for *N*-substituted-3-(2'-pyridyl)pyridinium compounds, there is a decreased influence of the pyridinium moiety upon the resonances within the pyridyl ring.

The complexes of 2,2'- and 4,2'-bipyridinium display three or four reversible reduction processes in the region of -1.75 to 0 V, all being of equivalent current intensity as shown in both cyclic and pulse differential voltammograms. They are also of comparable intensity to the oxidative couple and are as such assigned as successive single electron processes. The influence of changes in the ancillary ligand are relatively small for $E(3^+/2^+)$ and $E(2^+/1^+)$, which exhibit a cathodic shift of *ca.* 0.1 V on changing the functional group from trifluoromethyl to *tert*-butyl. The value of $E(1^+/0)$ appears to be highly dependent upon the

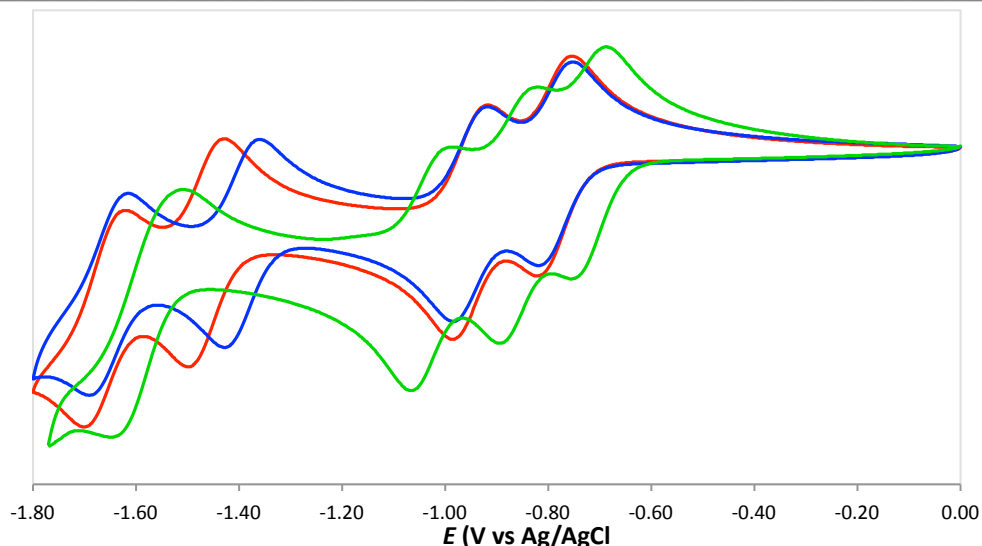


Fig. 4.17. Cyclic voltammograms depicting the reduction processes of [Ir(22)₂Y](PF₆)₃ (blue), [Ir(22)₂B](PF₆)₃ (red) and [Ir(22)₂F](PF₆)₃ (green) recorded at 100 mVs⁻¹ in 0.1M n-Bu₄NPF₆ acetonitrile at 298 K.

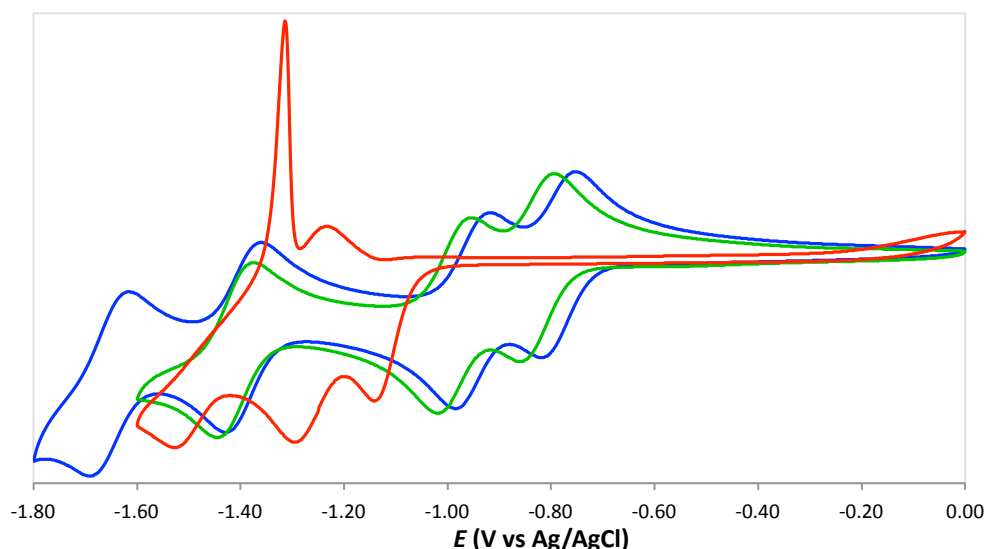


Fig. 4.18. Cyclic voltammograms depicting the reduction processes of [Ir(22)₂Y](PF₆)₃ (blue), [Ir(32)₂Y](PF₆)₃ (red) and [Ir(42)₂Y](PF₆)₃ (green) recorded at 100 mVs⁻¹ in 0.1M n-Bu₄NPF₆ acetonitrile at 298 K.

functionality of the bipyridyl ligand and is cathodically shifted with increasing pK_a thus affording a shift of *ca.* 0.43 V between extremes of the series, Fig. 4.17. This correlates to an increase in the energy of the π^* -orbital on increasing the electron donating ability of the substituent. This process is therefore assigned to the reduction of the ancillary ligand with the $E(3^+/2^+)$ and $E(2^+/1^+)$ processes assigned to the reduction of the cyclometalated ligands. The variations in the observed potential for the latter processes are a consequence of fluctuations in the relative electronegativity of the metal centre as imparted by the varying σ -donor abilities of the different ancillary ligands. This assignment also appears to be true for the complexes of the general formula [Ru(bpy)₂(C^N)](PF₆)₂, as reported by Koizumi *et al.*^[243] On comparison with [Ru(bpy)₃](PF₆)₂, a cathodic shift of the Ru^(II/III) couple by 0.45 V is evident for [Ru(bpy)₂(42)](PF₆)₂ with a concomitant anodic shift of the first reduction potential by 0.10 V.

Had the latter process been localised upon the bipyridyl ligands it is expected to have instead been cathodically shifted due to the influence of the increased electron density at the metal centre.

The complexes of $[\text{Ir}(\text{32})_2\text{L}](\text{PF}_6)_3$ exhibit three to four partially reversible or irreversible reduction processes with well defined cathodic peaks. For $[\text{Ir}(\text{32})_2\text{Y}](\text{PF}_6)_3$ a single sharp anodic peak at -1.28 V is observed with a broad anodic tailing, Fig. 4.18. The potential and current intensity of this peak are dependent upon the over-potential applied on reduction of the sample. Upon narrowing the scan range to less negative potentials the peak is cathodically shifted to -1.31 V with a concomitant decrease in the current intensity. As the extent of the tailing is minimised, the anodic peak of the $(2^+/1^+)$ couple became better resolved and was identified as a reversible or quasi-reversible process. The sharp anodic peak is indicative of adsorption of a reduced species onto the working surface of the electrode and is characteristic of the oxidation of a cationic radical, as demonstrated in the electrochemical analysis of *N,N'*-dialkyl-bipyridinium compounds.^[283, 284] In the studies of *n*-heptylviologen, equivalent tailing was observed and attributed to either a irreversible process or a diffusion controlled oxidation of an accumulated radical.^[285, 286] $[\text{Ir}(\text{32})_2\text{B}](\text{PF}_6)_3$ displayed a similar profile although the sharp peak was cathodically shifted to -1.47 V and no discernible anodic peak for the $(2^+/1^+)$ couple was evident. In addition to two irreversible processes, $[\text{Ir}(\text{32})_2\text{F}](\text{PF}_6)_3$ displays a single reversible reduction at more positive potentials, Fig. 4.19. The related cathodic shoulder at *ca.* -0.85 V is only apparent on increasing the over-potential beyond -1.30 V and decreases in current intensity upon using a slower scan rate. The $E(3^+/2^+)$ couple is anodically shifted by 0.37 and 0.42 V in relation to $[\text{Ir}(\text{32})_2\text{Y}](\text{PF}_6)_3$ and $[\text{Ir}(\text{32})_2\text{B}](\text{PF}_6)_3$ respectively. This is comparable to the trends observed for the reduction of the ancillary ligands in $[\text{Ir}(\text{22})_2\text{L}](\text{PF}_6)_3$ and $[\text{Ir}(\text{42})_2\text{L}](\text{PF}_6)_3$, albeit the potentials here are shifted by *ca.* $+0.3$ V. On considering the increased electronegativity of the iridium centre in this series of complexes, as evident by the shift in oxidation potentials, it would be expected that the reduction couple of the ancillary ligands be anodically shifted as seen here. Comparisons of $E(2^+/1^+)$ and $E(1^+/0)$ show similar trends to those of $E(3^+/2^+)$ and $E(2^+/1^+)$ in the isomeric counterparts, although the potentials have been cathodically shifted by 0.58 V. As such, for $[\text{Ir}(\text{32})_2\text{L}](\text{PF}_6)_3$, $E(3^+/2^+)$ is instead assigned to the reduction of the substituted bipyridine whilst $E(2^+/1^+)$ and $E(1^+/0)$ are centred upon the bipyridinium ligands. These results for $[\text{Ir}(\text{32})_2\text{L}](\text{PF}_6)_3$ clearly indicate a significant redistribution of electron density away from the metal centre and towards the cyclometalated ligands.

Questions pertaining to the localisation of electron density upon reduction of the cyclometalated ligands remain. Typically for complexes of phenylpyridine and analogous compounds, it is expected that reduction occurs at the heteroaryl moieties due to the decreased energy of the π^* -orbitals in relation to those of the more electron rich cyclometalated rings. Comparisons of the reduction potentials of the pro-ligands and the corresponding complexes precludes a pyridinium centred reduction if not for $[\text{Ir}(\text{32})_2\text{L}](\text{PF}_6)_3$

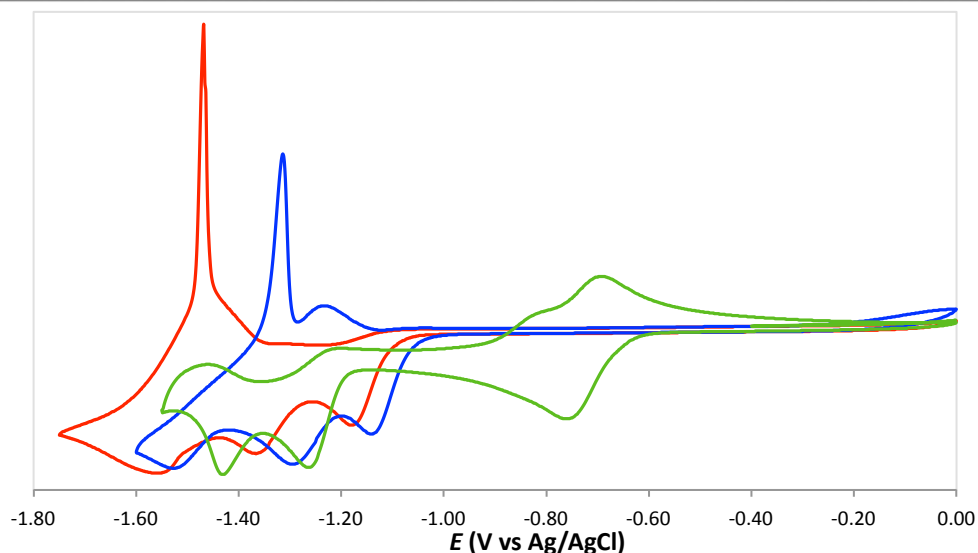


Fig. 4.19. Cyclic voltammograms depicting the reduction processes of $[\text{Ir}(32)_2\text{Y}](\text{PF}_6)_3$ (blue), $[\text{Ir}(32)_2\text{B}](\text{PF}_6)_3$ (red) and $[\text{Ir}(32)_2\text{F}](\text{PF}_6)_3$ (green) recorded at 100 mVs^{-1} in $0.1 \text{ M } n\text{-Bu}_4\text{NPF}_6$ acetonitrile at 298 K .

then certainly for $[\text{Ir}(22)_2\text{L}](\text{PF}_6)_3$ and $[\text{Ir}(42)_2\text{L}](\text{PF}_6)_3$. In the latter two instances $E(3^+/2^+)$ has moved to more positive potentials with respect to the $E(1^+/0)$ couple of the pro-ligand; this being contrary to an increase in electron density that is expected on cyclometalation of the pyridinium ring, as indicated by the CIS values determined in $^1\text{H-NMR}$. However, observations indicating the presence of a cationic radical suggest an involvement of the quaternised moiety. This is reasonable considering the energy of the π^* -orbitals has been significantly reduced in comparison to a phenyl moiety. TD-DFT calculations predict the lowest lying unoccupied orbital of the cyclometalated ligand in $[\text{Ir}(\text{ppy})_2\text{L}]^{n+}$ shows a preference for the pyridyl moiety, although for complexes of bipyridinium this is more equally delocalised about the entire ligand, thus reflecting the experimental observations.

The trends in ΔE are in excellent agreement with those discerned for the proposed MLCT transitions of the UV-visible absorption spectra. The recorded potentials demonstrate that relatively small manipulations of the ancillary ligand can afford large changes in the electrochemical gap; varying from 2.42 V for $[\text{Ir}(\text{ppy})_2\text{qpy}]\text{PF}_6$ to 1.64 V for $\{\text{Ir}(\text{ppy})_2[(\text{Pym})_2\text{qpy}]\}(\text{PF}_6)_3$. The ΔE values within the $[\text{Ir}(22)_2\text{L}](\text{PF}_6)_3$ and $[\text{Ir}(42)_2\text{L}](\text{PF}_6)_3$ series are fairly consistent ranging between $2.98 - 3.03 \text{ V}$. $[\text{Ir}(32)_2\text{L}](\text{PF}_6)_3$ displays a greater variation due to the dependency of the LUMO on the functionality of the ancillary ligand. Ranging between $3.25 - 3.48 \text{ V}$ this series of complexes exhibit ΔE values that are amongst the largest reported for a cationic cyclometalated Ir(III) complex incorporating a neutral diimine ligand.^[287] It is also of note that the results concerning $[\text{Ir}(32)_2\text{F}]^{3+}$ give insight into the assignment of the MLCT band in the UV-visible spectra. On consideration of the $(3^+/2^+)$ couple, the anomalous bathochromic shift of the absorption bands may be explained by the change in character of the LUMO from a bipyridinium centred orbital to one that is based upon the ancillary ligand. The observed shift in the MLCT transitions would therefore be expected due to stabilisation of the π^* -orbitals affected by the trifluoromethyl groups.

4.2.6. Theoretical Studies

In an effort to understand the origins of the measured UV-visible spectra, TD-DFT calculations were undertaken on a number of the report iridium complexes using Gaussian 09.^[191] Geometry optimisation and subsequent TD-DFT calculations were carried out at the B86,^[192, 193] B3LYP,^[194] PBE1PBE^[195] and M06^[196] levels with the Def2-QZVP^[197, 198] basis set and pseudopotential for iridium and Def2-SVP^[199] on all other atoms. Of these the M06 functional provided the best representation of the experimental data on inclusion of the CPCM^[200, 201] solvent model of acetonitrile. Using these parameters the first 100 excited singlet states were calculated and simulated UV-visible spectra were convoluted with Gaussian curves of fwhm of 3000 cm⁻¹ using GaussSum.^[202]

4.2.6.1. Structural geometries

Selected bond distances and bond angles describing the environment about the metal centre for each of the optimised structures are presented in Table 4.10. The data is in good agreement with that obtained experimentally as reported in Table 4.3. Bond lengths have been lengthened slightly but all values are within 0.04 Å of experimental; the largest deviations seen were those concerning the Ir–N distances of the bipyridyl ligand. Bond angles are likewise well represented with a maximum error of *ca.* 3.5°, although most values are within 2°.

The calculated Ir–C bond distances confirm the relative trends observed in the experimental data. In comparison to [Ir(22)₂Y]³⁺ the distance in [Ir(42)₂Y]³⁺ is lengthened by *ca.* 0.1 Å in both the experimental and optimised geometries. Whilst the experimental data of [Ir(32)₂Y]³⁺ is relatively unclear, due to the inequivalencies of the two Ir – C

Table 4.8. Selected bond lengths (Å) and bond angles (°) taken from DFT calculated optimised geometries of [Ir(22)₂Y]³⁺, [Ir(32)₂Y]³⁺, [Ir(42)₂Y]³⁺, [Ir(ppy)₂qpy]⁺ and [Ir(ppy)₂Me₂qpy]³⁺ where N_B = bipyridyl nitrogen, C_C = cyclometalated carbon, N_P = nitrogen of the cyclometalating ligand.

Distances/Å	[Ir(22) ₂ Y]	[Ir(22) ₂ B]	[Ir(22) ₂ F]	[Ir(32) ₂ Y]	[Ir(42) ₂ Y]	[Ir(ppy) ₂ Q]	[Ir(ppy)Me ₂ Q]
Ir–C _C	2.015	2.016	2.016	2.007	2.026	2.013	2.018
Ir–N _P	2.069	2.066	2.070	2.078	2.078	2.067	2.074
Ir–N _B	2.175	2.166	2.180	2.178	2.167	2.188	2.185
N–Me	1.474	1.474	1.475	1.474	1.472	---	1.474
Angles/°							
N _P –Ir–N _P	173.38	173.71	173.39	175.09	175.14	173.33	170.36
N _P –Ir–N _B	173.53	173.23	173.39	173.37	173.37	173.29	173.50
C _C –Ir–N _B	173.53	173.22	173.46	173.36	173.37	173.29	173.50
N _P –Ir–C _C	79.12	79.09	79.08	80.12	79.77	80.28	80.29
N _P –Ir–C _C	96.06	96.34	96.16	96.21	96.69	94.87	92.70
N _P –Ir–N _B	97.92	97.55	97.86	96.46	96.63	97.23	99.89
N _P –Ir–N _B	87.33	87.43	87.38	87.42	87.21	88.08	87.82
C _C –Ir–C _C	87.90	88.18	87.56	87.70	87.84	87.96	87.26
C _C –Ir–N _B	98.17	98.07	98.25	98.41	98.14	98.58	99.21
N _B –Ir–C _C	98.18	98.07	98.25	98.40	98.14	98.5	99.21
N _B –Ir–N _B	75.85	75.80	75.74	75.62	76.03	75.12	74.33
Torsional/°							
N _P –C _{2P} –C _{1C} –X _{2C}	7.4	7.3	7.7	0.87	0.62	2.31	3.6
N _B –C _{2B} –C _{2B'} –C _{3P}	0.98	0.11	1.41	1.59	1.89	1.81	11.69

distances and issues encountered with crystal twinning, results do suggest a general shortening of the bond. This was corroborated as the predicted structure also displays a decrease in the bond length in comparison to $[\text{Ir}(\text{22})_2\text{Y}]^{3+}$ by *ca.* 0.01 Å. The optimised structures however failed to display the related variation in the N–Me distance across the series, instead the values remain essential consistent at 1.47 Å in all the calculated structures, including that predicted for the pyridinium group of the $[\text{Me}_2\text{qpy}]^{2+}$ ancillary ligand.

As with $[\text{Ru}(\text{bpz})_2\text{Me}_2\text{qpy}]^{4+}$ the optimised structures of $[\text{Ir}(\text{ppy})_2\text{qpy}]^+$ and $[\text{Ir}(\text{ppy})_2\text{Me}_2\text{qpy}]^{3+}$ display a twisting of the quaterpyridyl ligand about the C–C bond between the bipyridyl unit and the pendent pyridyl groups, with comparable torsion angles of 34.8 and 35.9° respectively. Precedent for the twisting of the unquaternised quaterpyridyl ligand was established in the X-ray crystal structure of $[\text{Ru}(\text{phen})_2\text{qpy}](\text{PF}_6)_2$. The larger torsion angle of 53.2° that was reported for this compound is surmised to result from additional edge-to-face interactions of the pendent pyridyl with a co-crystallised benzene molecule positioned between the two arms of the quaterpyridine ligand.^[288]

Concerning the optimised geometries of $[\text{Ir}(\text{32})_2\text{Y}]^{3+}$ and $[\text{Ir}(\text{42})_2\text{Y}]^{3+}$ the two rings of the cyclometalated ligand are essentially planar, with a torsional angle of *ca.* 0.75°, whilst for complexes of 2-phenylpyridine this is increased to 2.1 – 3.6°. For $[\text{Ir}(\text{22})_2\text{Y}]^{3+}$ a torsional angle of *ca.* 7.5° is evident and attributed to the steric interaction of the *N*-methyl group. Whilst similar twisting was observed in the corresponding X-ray crystal structure, it was also observed for complexes of the other isomers of the bipyridinium ligands. No discernable trends regarding the magnitude of this angle were evident in the experimental data from which the origin of this twisting could be identified.

On examination of the interatomic distances between the hydrogens of the *N*-methyl substituent and the hydrogen in the 3-position of the pyridyl ring, values of 2.0 to 2.1 Å were predicted. This closely approximates those obtained from experimental structures, which

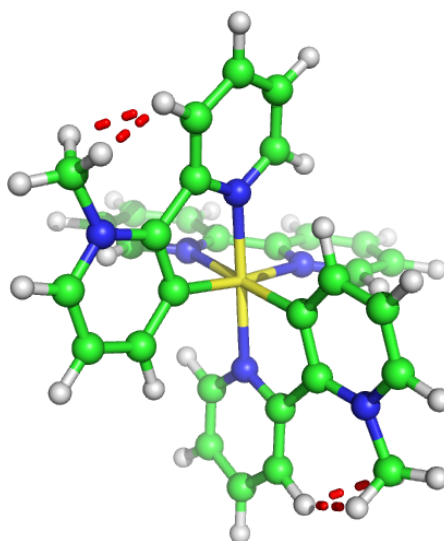


Fig. 4.20. Schematic of the optimised structure of $[\text{Ir}(\text{22})_2\text{Y}]^{3+}$; highlighting the interatomic distances between the *N*-methyl group of the bipyridinium ring and the hydrogen in the 3-position of the pyridyl ring. Image generated in MacPyMOL.

range from 1.925 to 2.094 Å. It should be noted that this represents the maximum distance between the two nuclei as rotation about the C–N bond by *ca.* 60° would bring one of the two hydrogens into closer proximity to that of the pyridyl ring. All values are within the 2.2 Å range expected for direct through-space coupling interactions to be in effect, thus lending credence to this mechanism being responsible for the long-range coupling observed in the 2D NMR spectra as discussed in section 4.2.2.1.3.

4.2.6.2. Absorption properties

Calculated $S_0 \rightarrow S_1$ transition energies and the respective MO contributions for complexes $[\text{Ir}(\text{22})_2\text{Y}]^{3+}$, $[\text{Ir}(\text{32})_2\text{Y}]^{3+}$, $[\text{Ir}(\text{42})_2\text{Y}]^{3+}$, $[\text{Ir}(\text{ppy})_2\text{qpy}]^+$ and $[\text{Ir}(\text{ppy})_2\text{Me}_2\text{qpy}]^{3+}$ are reported in Table 4.11. Comparisons of the experimental and simulated UV-visible spectra are shown in Fig. 4.21. for complexes of bipyridinium and Fig. 4.24 for those of 2-phenylpyridine. An energy level diagram comparing the frontier orbital energies of these complexes in addition to $[\text{Ir}(\text{22})_2\text{B}]^{3+}$ and $[\text{Ir}(\text{22})_2\text{F}]^{3+}$ is presented in Fig. 4.26. The calculated spectra are in good agreement with those obtained experimentally and successfully reproduce the trends therein.

For complexes of 2,2'-bipyridinium and 4,2'-bipyridinium the broad low energy bands of $\Delta E \leq 3.54$ eV are constructed primarily from three transitions of comparable oscillator strength and correspond to the HOMO \rightarrow LUMO, HOMO–1 \rightarrow LUMO and HOMO–2 \rightarrow LUMO+1 transitions, as listed in order of increasing energy. The HOMO is comprised of a combination of Ir $d_{3z^2-r^2}$ and $d_{x^2-y^2}$ orbitals that adopt an anti-bonding conformation with respect to the π -orbital of the cyclometalated ring of the bipyridinium ligand. The metal centre of the HOMO–1 is of similar composition with the exception that it is instead anti-bonding with respect to the pyridyl rings of the three ligands, although the contribution from each of these is minimal in comparison to that of the pyridinium moiety in the HOMO. The HOMO–2 is localised upon the iridium centre, being of d_{xy} and d_{yz} composition. The LUMO and LUMO+1 orbitals are centred about the bipyridinium cyclometalated ligands, with a minor metal component for the latter. As such these three transitions can be discussed in terms of MLCT processes that result in a redistribution of electron density from the metal centre to the π^* -orbitals of the cyclometalated ligands exclusively. However, due to the considerable contribution of the π -system of the cyclometalated ring towards the HOMO, it is perhaps more accurate to describe the processes that originate from this orbital as a mixed MLCT/LC transition with a potential ILCT component.

The influence of the ancillary ligand was successfully modeled with the data describing a bathochromic shift in the MLCT transitions upon increasing the $\text{p}K_a$ of the bipyridyl moiety. The increased electron density of the ligand affords a destabilisation of both the HOMO and LUMO, although the magnitude of the former is greater than that of the latter thus resulting in a net decrease of the HOMO – LUMO energy gap. The increase in energy of the HOMO is a result of the increased σ -donating ability of the ligand, whilst for the LUMO it is surmised to be a consequence of the decrease in the electronegativity of the metal centre that is induced by the

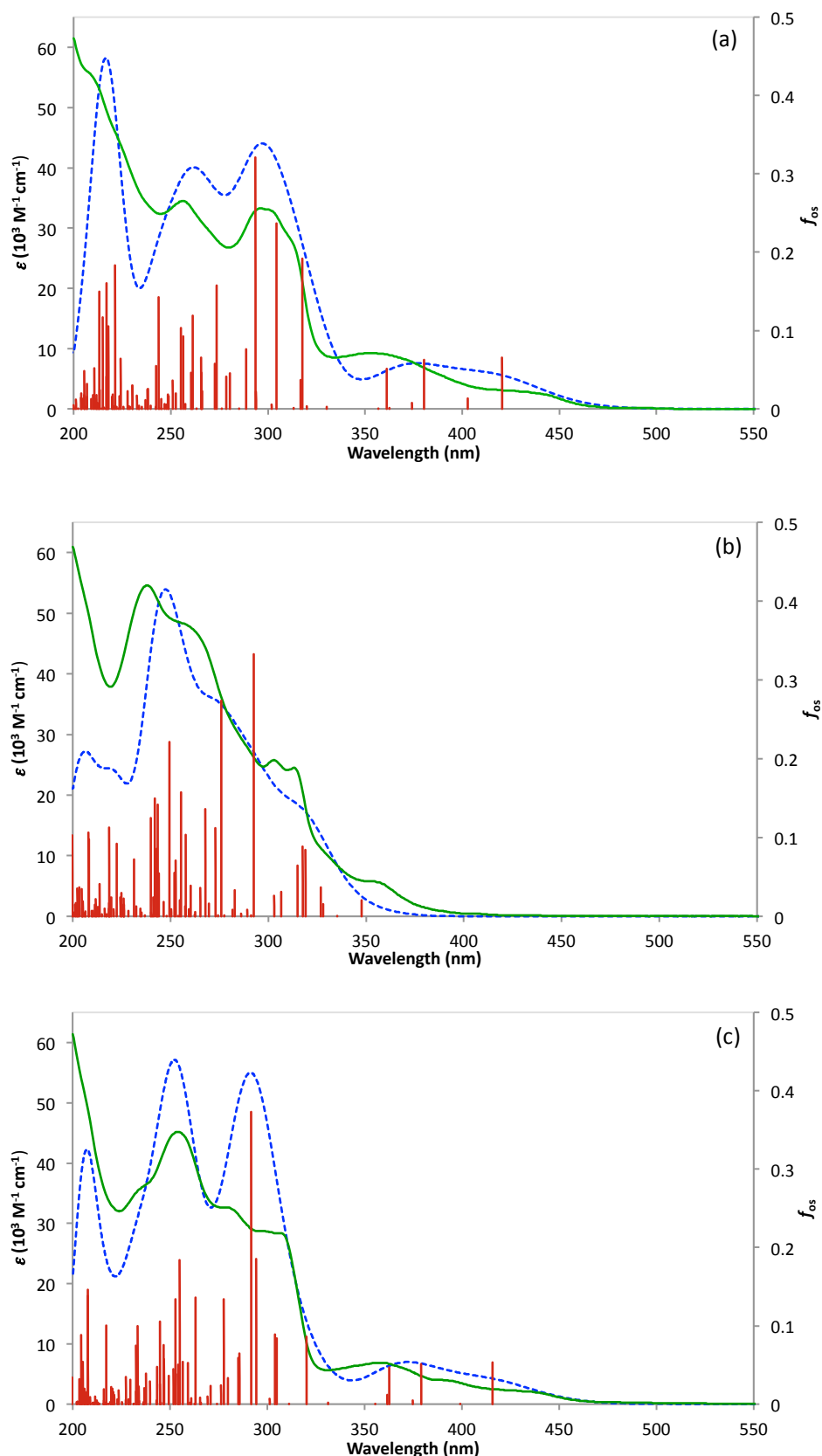


Fig. 4.21. Experimental (green) and the TD-DFT calculated (blue dash) UV-Visible spectra of **(a)** $[\text{Ir}(22)_2\text{Y}]^{3+}$, **(b)** $[\text{Ir}(32)_2\text{Y}]^{3+}$ and **(c)** $[\text{Ir}(42)_2\text{Y}]^{3+}$. Experimental data is plotted against the primary ϵ -axes with calculated spectra scaled to match to allow for comparison of absorption bands. Individual calculated vertical transitions (red) are plotted versus the secondary oscillator strength (f_{os}) axes.

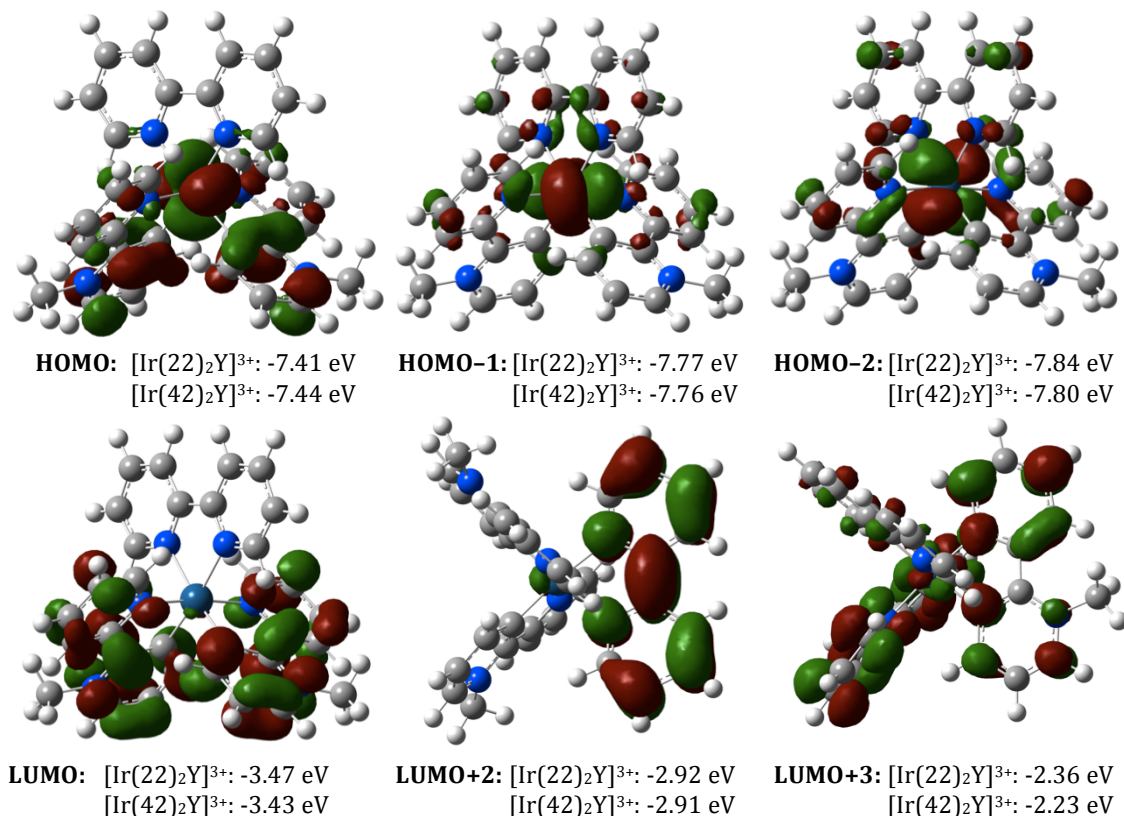


Fig. 4.22. DFT calculated electron density maps (isosurface value $0.03 \text{ e}/\text{\AA}^3$) and respective energies selected orbitals of $[\text{Ir}(22)_2\text{Y}]^{3+}$. Energies of corresponding orbitals of $[\text{Ir}(42)_2\text{Y}]^{3+}$ are also listed.

former interaction. Comparison of the lowest energy transition shows that $[\text{Ir}(22)_2\text{B}]^{3+}$ undergoes a bathochromic shift of 3.4 nm in relation to $[\text{Ir}(22)_2\text{Y}]^{3+}$, whilst $[\text{Ir}(22)_2\text{F}]^{3+}$ is hypsochromically shifted by 8 nm. The MLCT transitions to the π^* -orbitals of the ancillary ligand occur at higher energies, describing transitions to LUMO+2, the lowest lying orbital that is localised solely upon the bipyridyl moiety. The energy of this orbital is highly dependent upon the nature of the incorporated functional group, ranging from -3.3 eV for $[\text{Ir}(22)_2\text{F}]^{3+}$ to -2.74 eV in $[\text{Ir}(22)_2\text{B}]^{3+}$. The transitions of this type that are encompassed in the lower energy band originate from the HOMO, HOMO-1 and HOMO-2. Considering the composition of these orbitals the transitions are best referred to as a “mixed-metal/ligand-to-ligand” charge transfer (MML’CT)^[289-291] or a MLCT/LLCT.^[292] However, calculated transitions of HOMO \rightarrow LUMO+2 are of low oscillator strength and the bipyridinium contribution towards HOMO-1 and HOMO-2 is minimal by comparison, meaning the actual extent of LLCT character to this band is minimal. The lowest energy $S_0 \rightarrow S_1$ transition of notable contribution towards the LUMO+2 originates from the HOMO-2 in each of the complexes studied. The transition is subject to a hypsochromic shift of 25 nm upon substitution of the *tert*-butyl group of the ancillary ligand with trifluoromethyl owing to destabilisation of the LUMO+2. As the HOMO-2 is localised primarily upon the metal centre with minimal contribution from the cyclometalated ligands, the energy level of this orbital is affected to a greater degree by changes made to the ancillary ligand than either the HOMO or HOMO-1. As such it is also

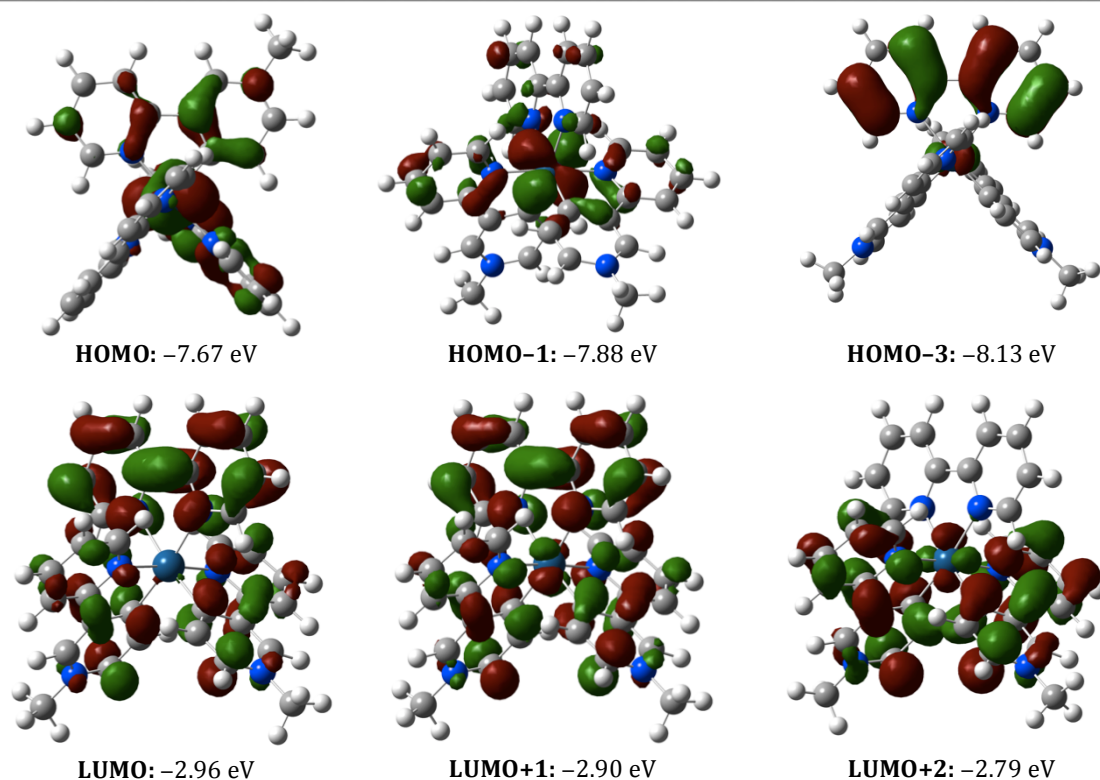


Fig. 4.23. DFT calculated electron density maps (isosurface value $0.03 \text{ e}/\text{\AA}^3$) and respective energies for selected orbitals of $[\text{Ir}(32)_2\text{Y}]^{3+}$.

subject to a notable destabilisation with decreasing $\text{p}K_{\text{a}}$ of the bipyridyl ligand, although the magnitude of this is smaller than that experienced by the LUMO+2. The transition correlates well with the additional feature observed in the experimental absorption spectra of $[\text{Ir}(22)_2\text{F}](\text{PF}_6)_3$ that resulted in the lack of a defined maxima for the MLCT band.

The intensely absorbing bands at shorter wavelengths are typically a combination of higher energy MLCT or $\pi-\pi^*$ transitions of both the cyclometalated and ancillary ligands. There is also evidence to support minor contributions from ILCT transitions within the cyclometalated ligand, whereby the pyridinium moiety acts as an electron donor towards the pyridyl ring resulting in the delocalisation of electron density across the entire ligand.

The lowest energy $S_0 \rightarrow S_1$ transition of $[\text{Ir}(32)_2\text{Y}]^{3+}$ corresponds to a HOMO \rightarrow LUMO or HOMO \rightarrow LUMO+1 transition. The HOMO is of comparable composition to those discussed previously, although it has been stabilised by *ca.* 0.25 eV and shows an additional electron density contribution from the pyridyl ring of the cyclometalated ligand. The isosymmetric LUMO and LUMO+1 orbitals have been destabilised by *ca.* 0.4-0.5 eV with the electron density now also delocalised across 2,2'-bipyridine, consequently exhibiting a lower contribution from the cyclometalated ligands. These transitions can therefore be characterised as a higher energy MLCT with a minor LLCT/ILCT component. All transitions of $\Delta E \leq 4.13 \text{ eV}$ are of similar character, the significant hypsochromic shift of these bands in relation to those of the other isomers is a consequence of the comparative stabilisation and destabilisation of the HOMO and LUMO respectively.

The energies and relative trends of the calculated HOMO and LUMO are in excellent agreement with results obtained from cyclic voltammetry experiments. On comparison of the potentials of the Ir^(III/IV) couple exhibited by [Ir(22)₂Y]³⁺, an anodic shift of *ca.* 0.2 V and 0.01 V is observed for [Ir(32)₂Y]³⁺ and [Ir(42)₂Y]³⁺ respectively. This correlates to the relative magnitude of the comparative destabilisation of the metal-based HOMOs for these two isomers. Likewise the increased energy of the ligand centred LUMO correlates to a cathodic shift of *ca.* 0.5 V and 0.04 V of the first reduction potentials of the 3,2'- and 4,2'- isomers. The calculated LUMO, LUMO+1 and LUMO+2 orbitals also corroborate the assignments made regarding the first three reduction couples, confirming that bipyridinium is typically expected to be more readily reduced than the ancillary ligand. Results for [Ir(32)₂Y]³⁺ remain unclear due to the near equal contribution from the cyclometalated and ancillary ligands towards the LUMO and LUMO+1. Although [Ir(32)₂F]³⁺ was not studied using TD-DFT, from the relative energy of the bipyridyl centred LUMO+2 in [Ir(22)₂F]³⁺ it is reasonable to suggest that the LUMO of the former would be localised about the ancillary ligand. This would allow for the first reductive process of [Ir(32)₂F]³⁺ to be assigned to the reduction of dCF₃bpy. Furthermore it is expected that the bipyridyl centred LUMO be shifted to an even lower energy in comparison to [Ir(22)₂F]³⁺ owing to the increased electronegativity of the metal centre in the [Ir(32)₂L]³⁺ series. This assignment would also explain the observed bathochromic shift of the MLCT bands in the UV-vis spectra for [Ir(32)₂F]³⁺, which is contrary to the hypsochromic shift evident for the other two isomers.

Due to the distinctly different properties in comparison to the bipyridinium compounds and to probe the origins of the effects of quaternisation of the ancillary ligand, additional calculations were undertaken for [Ir(ppy)₂qpy]⁺ and [Ir(ppy)₂Me₂qpy]³⁺. In both instances the low energy bands of $\lambda \geq 450$ nm and $\epsilon < 2000$ M⁻¹cm⁻³ are modelled about the HOMO → LUMO and HOMO-2 → LUMO transitions. The HOMOs of both these complexes are of comparable composition to one another and to [Ir(22)₂Y] and [Ir(42)₂Y]; the electron density localised about the metal centre and the cyclometalated moiety. By comparison, the HOMO has been destabilised by *ca.* 1.1 – 1.54 eV with respect to the bipyridinium compounds and is attributed to the increased electron density of the phenyl ring. The HOMO of [Ir(ppy)₂Me₂qpy]³⁺ has been stabilised by 0.18 eV as a result of changes made to the electron density at the metal centre, as brought about by the increased acceptor ability of [Me₂qpy]²⁺. Unlike the bipyridinium complexes, the LUMO is localised solely upon the ancillary ligand; in [Ir(ppy)₂qpy]⁺ this is centred upon the bipyridyl unit whilst for [Ir(ppy)₂Me₂qpy]³⁺ it is delocalised across the entire ligand, Fig 4.26. The L+1 and L+2 orbitals are likewise constructed though with a varying distribution of electron density between the bipyridyl and pendant pyridyl moieties. The LUMO of [Ir(ppy)₂qpy]⁺ is of comparable energy to the L+2 orbital of [Ir(22)₂Y], [Ir(22)₂B], and [Ir(42)₂Y], which are also localised upon the ancillary ligand. The LUMO, L+1 and L+2 of [Ir(ppy)₂Me₂qpy]³⁺ have all been significantly stabilised in comparison to the unquaternised analogue by 0.75, 1.23 and 0.63 eV respectively, resulting in

the observed bathochromic shift of the associated transitions. For $\Delta E \leq 3.10$ eV the transitions describe a redistribution of electron density from the metal and cyclometalating rings towards the ancillary ligand and are therefore assigned to an admixture of MLCT and LLCT processes. Interestingly the LUMO of $[\text{Ir}(\text{ppy})_2\text{Me}_2\text{qpy}]^{3+}$ is of more negative energy than those of the bipyridinium complexes. This suggests that the quaterpyridinium pro-ligands could be utilised to induce a bathochromic shift in the MLCT absorption profile of the complexes containing the bis(bipyridinium)iridium(III) moiety. It is also surmised that $[(\text{Pym})_2\text{qpy}]^{2+}$ may be used to further decrease the energy of the LUMO, as expected from the increased electron withdrawing ability of the pyrimidyl group and the comparative red-shift exhibited in the experimental UV-vis data of $\{\text{Ir}(\text{ppy})_2[(\text{Pym})_2\text{qpy}]\}^{3+}$.

At higher energies a contribution of MLCT processes associated with the cyclometalated ligands becomes apparent. The energy of the lowest lying unoccupied MO of ppy, L+3, is of considerably higher energy than the analogous orbital in complexes of

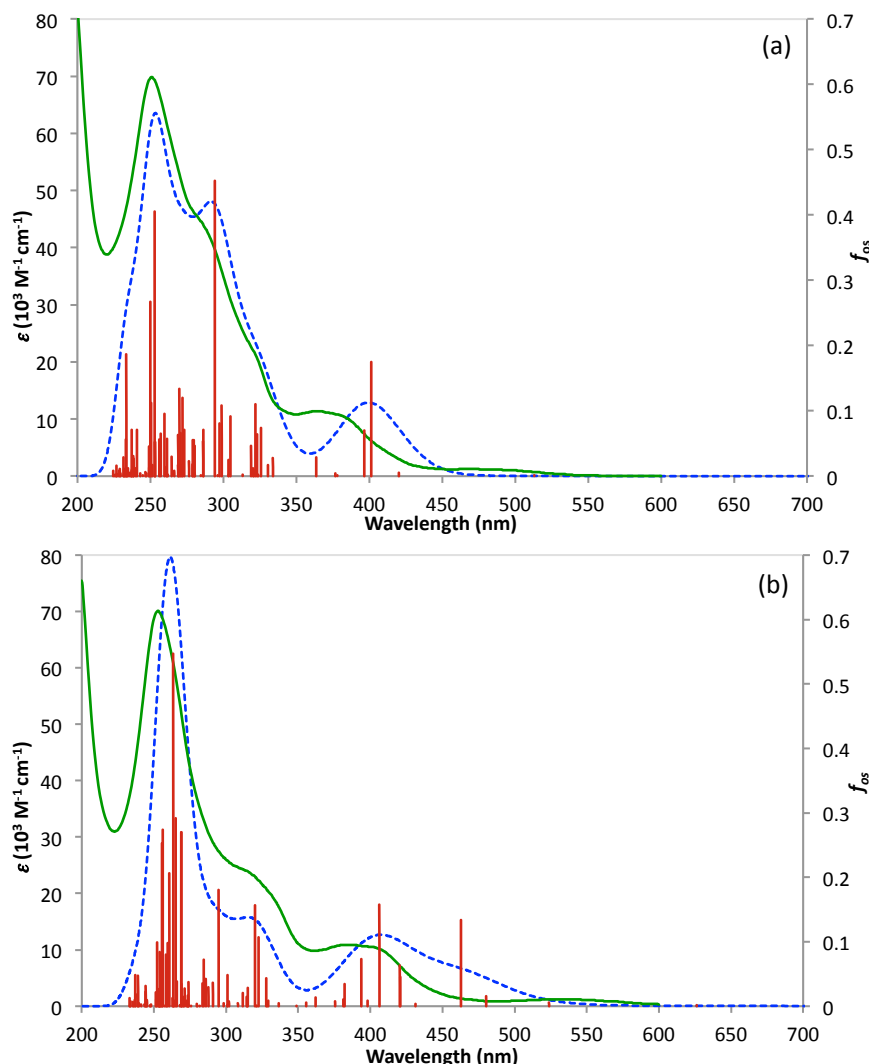


Fig. 4.24. Experimental (green) and the TD-DFT calculated (blue dash) UV-Visible spectra of **(a)** $[\text{Ir}(\text{ppy})_2\text{qpy}]^+$ and **(b)** $[\text{Ir}(\text{ppy})_2\text{Me}_2\text{qpy}]^{3+}$. Experimental data is plotted against the primary ϵ -axes with calculated spectra scaled to match to allow for comparison of absorption bands. Individual calculated vertical transitions (red) are plotted versus the secondary oscillator strength (f_{os}) axes.

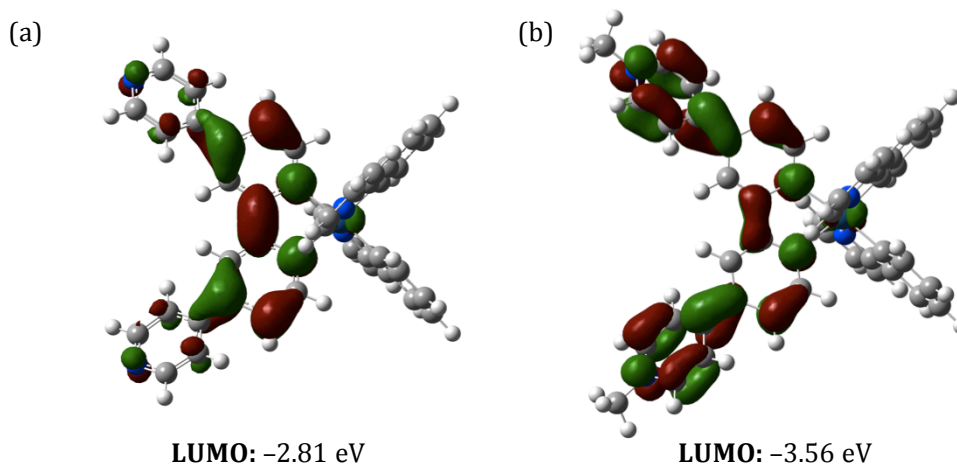


Fig. 4.25. TD-DFT calculated electron density maps (isosurface value $0.03 \text{ e}/\text{\AA}^3$) and respective energies for the LUMO of (a) $[\text{Ir}(\text{ppy})_2\text{qpy}]^+$ and (b) $[\text{Ir}(\text{ppy})_2\text{Me}_2\text{qpy}]^{3+}$.

bipyridinium and is destabilised by 0.86 to 1.54 eV. The L+3 orbital is centred across both rings of the phenylpyridine and is stabilised by 0.17 eV for $[\text{Ir}(\text{ppy})_2\text{Me}_2\text{qpy}]^{3+}$ in relation to the quaterpyridyl complex, owing to the influence of variations in the electronegativity of the metal centre. Despite this, the related HOMO \rightarrow L+3 transition occurs at slightly lower energy for $[\text{Ir}(\text{ppy})_2\text{qpy}]^+$ due to destabilisation of the HOMO. The transition is therefore ascribed to a combined MLCT/LC process with potential ILCT character as discussed previously.

The shoulder at *ca.* 325 nm can be assigned to the higher energy MLCT transitions towards both the ancillary and phenylpyridine ligands. Transitions of $\Delta E \geq 4.50$ eV are predominantly $\pi\text{-}\pi^*$ in character. The major component of the transition of high oscillator strength at 263.4 nm in $[\text{Ir}(\text{ppy})_2\text{Me}_2\text{qpy}]$ is an ILCT within the quaterpyridinium ligand in which the bipyridine unit acts as a donor towards the pyridinium acceptor.

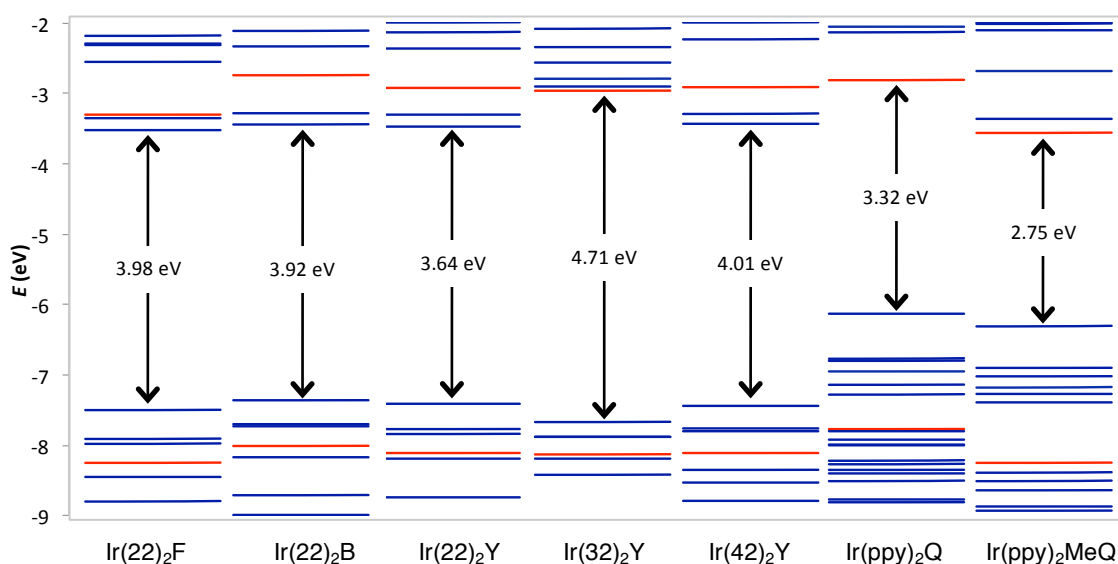


Fig. 4.26. Energy level diagram for complexes of the general formula $[\text{Ir}(\text{C}^{\wedge}\text{N})_2(\text{N}^{\wedge}\text{N})]^{n+}$ displaying the TD-DFT calculated MOs between -2.0 and -9.0 eV. Orbitals highlighted in red are the highest energy occupied and lowest energy unoccupied orbitals displaying considerable contribution from the ancillary ligand.

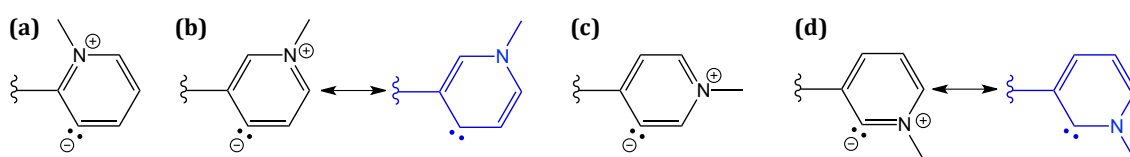
Table 4.9. Select vertical transitions obtained by TD-DFT calculations performed for the complex cations [Ir(22)₂Y]³⁺, [Ir(32)₂Y]³⁺, [Ir(42)₂Y]³⁺, [Ir(ppy)₂qpy]⁺ and [Ir(ppy)₂Me₂qpy]³⁺. Presented transitions chosen to represent the major contributors to each of the dominant bands in the UV-visible spectra.

Cation	λ /nm	ΔE /eV	f_{os}	Major Contributions	
[Ir(22) ₂ Y] ³⁺	420.5	2.95	0.0657	HOMO → LUMO (93 %)	
	402.8	3.08	0.0135	HOMO → L+1 (93 %)	
	380.4	3.26	0.0628	H-1 → LUMO (90 %)	
	361.2	3.43	0.0511	H-2 → L+1 (94 %)	
	317.7	3.90	0.1917	H-4 → LUMO (26 %), H-2 → L+2 (69 %)	
	304.4	4.07	0.2367	H-4 → L+1 (63%), HOMO → L+3 (29 %)	
	293.6	4.22	0.3206	H-3 → L+2 (73 %), H-1 → L+3 (18 %)	
	273.6	4.53	0.1572	H-2 → L+4 (62 %), H-2 → L+6 (10 %), H-2 → L+10 (11 %)	
	261.3	4.75	0.1186	H-6 → L+1 (11 %), H-1 → L+5 (66 %)	
	255.2	4.86	0.1035	H-2 → L+4 (13 %), H-2 → L+6 (67 %)	
	[Ir(32) ₂ Y] ³⁺	347.8	3.57	0.0201	HOMO → LUMO (37 %), HOMO → L+1 (53 %)
328.1		3.78	0.0156	H-1 → LUMO (56 %), H-1 → L+1 (28 %)	
326.9		3.79	0.0369	H-2 → LUMO (26 %), H-2 → L+1 (27 %), H-1 → L+2 (29 %)	
319.1		3.89	0.0844	H-2 → LUMO (57 %), H-1 → L+2 (23 %)	
306.6		4.04	0.0313	H-2 → L+2 (41 %), H-1 → L+1 (15 %), HOMO → L+2 (12 %), HOMO → L+4 (14 %)	
303.1		4.09	0.0263	HOMO → L+3 (82 %)	
292.6		4.24	0.3324	H-3 → LUMO (51 %), H-3 → L+1 (35 %)	
276.0		4.49	0.2736	H-4 → L+2 (58 %)	
267.9		4.63	0.1361	HOMO → L+5 (81 %)	
255.4		4.86	0.1577	H-5 → L+2 (53 %)	
[Ir(42) ₂ Y] ³⁺		415.8	2.98	0.0533	HOMO → LUMO (95 %)
	379.2	3.27	0.0514	H-1 → LUMO (92 %)	
	362.7	3.42	0.0465	H-2 → L+1 (95 %)	
	320.2	3.87	0.0864	H-2 → L+2 (95 %)	
	304.0	4.08	0.0887	H-5 → LUMO (12 %), H-4 → L+1 (29 %), HOMO → L+3 (47 %)	
	291.8	4.25	0.3728	H-4 → L+1 (20 %), H-3 → L+2 (42 %), HOMO → L+3 (24 %)	
	277.8	4.46	0.134	H-1 → L+3 (80 %)	
	263.2	4.71	0.1359	H-2 → L+4 (51 %), H-2 → L+11 (30 %)	
	255.1	4.86	0.184	H-7 → L+1 (18 %), H-1 → L+5 (38 %), HOMO → L+7 (14 %)	
	[Ir(ppy) ₂ qpy] ⁺	513.1	2.42	0.0009	HOMO->LUMO (98 %)
		401.4	3.09	0.1745	H-3->LUMO (15 %), H-1->LUMO (78 %)
396.6		3.13	0.0701	HOMO->L+3 (88 %)	
363.7		3.41	0.0288	H-3->LUMO (76 %), H-1->LUMO (14 %)	
325.8		3.81	0.0743	H-2->L+2 (22 %), H-1->L+1 (33 %), H-1->L+4 (18 %)	
323.1		3.84	0.0643	H-2->L+2 (23 %), H-2->L+3 (11 %), HOMO->L+5 (42 %)	
294.2		4.22	0.4521	H-8->LUMO (34 %), H-3->L+1 (23 %), H-3->L+4 (21 %)	
252.9		4.90	0.4049	H-14->LUMO (25 %), H-8->L+1 (36 %)	
[Ir(ppy) ₂ Me ₂ qpy] ²⁺	626.2	1.98	0.0017	HOMO->LUMO (94 %)	
	523.9	2.37	0.0052	HOMO->L+1 (98 %)	
	480.3	2.58	0.0152	H-2->LUMO (89 %)	
	462.8	2.68	0.1335	H-1->LUMO (89 %)	
	420.5	2.95	0.0635	H-1->L+1 (87 %)	
	406.3	3.05	0.158	H-3->LUMO (11 %), H-2->L+1 (84 %)	
	393.7	3.15	0.0732	HOMO->L+3 (90 %)	
	362.0	3.42	0.0139	H-4->L+1 (89 %)	
	320.0	3.87	0.1567	H-6->LUMO (13 %), H-2->L+3 (12 %), H-1->L+6 (51 %)	
	294.9	4.21	0.1803	H-4->L+3 (12 %), H-3->L+6 (51 %), H-2->L+7 (10 %)	

4.3. Further Discussion

The differences in properties observed between the complexes of the three isomers of bipyridinium might best be described in terms of resonance structures inherent within the pyridinium ring. The similarity of the $[\text{Ir}(22)_2\text{L}]^{3+}$ and $[\text{Ir}(42)_2\text{L}]^{3+}$ complexes may be expected on considering that in both instances the quaternised heteroatom is *meta* with respect to the Ir–C bond and will therefore exert similar electronic effects upon the carbanion. The differences exhibited between the two are afforded by a change in the position of the pyridyl ring in relation to the heteroatom and the slight variation in electron distribution that this affords. For 1-methyl-3-(2'-pyridyl)pyridinium the inherent resonance structures would place a partial positive charge upon the carbon of the cyclometalating bond thus decreasing the σ -donating ability of the ligand and potentially increasing the π -accepting ability. Consequently this would result in a net increase of electron density about the cyclometalated ligand with a concomitant decrease upon the metal centre. This would accurately describe the experimental observations made herein, although whether this effect is sufficient to afford differences of such magnitude is uncertain.

The second consideration is the additional resonance structures that may be accessed upon deprotonation of a pyridinium ring, whereby the moiety may act as a pyridine derived *N*-heterocyclic carbene (py-NHC).^[254] When the nitrogen is in the *meta* position with respect to the Ir – C bond, as it is for 1-methyl-2-(2'-pyridyl)pyridinium and 1-methyl-4-(2'-pyridyl)pyridinium, no additional resonance structures are available. This results in the formation of a zwitterionic ylidic-type structure containing a carbanion and iminium group. These are referred to as the abnormal carbenes as the presence of additional formal charges are required for some nuclei.



Scheme 4.6. Resonance structures of the deprotonated pyridinium ring of **(a)** 1-methyl-2-(2-pyridyl)pyridin-3-yl-ium **(b)** 1-methyl-3-(2-pyridyl)pyridin-4-yl-ium **(c)** 1-methyl-4-(2-pyridyl)pyridin-3-yl-ium and **(d)** 1-methyl-3-(2-pyridyl)pyridin-2-yl-ium. The pyridyl ring has been omitted for clarity.

1-methyl-3-(2'-pyridyl)pyridinium is unique in this series as it may also adopt a pyridinylidene structure to form a charge neutral carbene.^[293] This is true for both linkage isomers of the ligand, which are termed as the normal or remote carbenes when the heteroatom is in the *ortho* or *para* positions respectively. The term remote is used when a heteroatom is not present in the α -position of the deprotonated carbon, as such the abnormal carbenes may also be included in this class.^[254] The electronic spectra and electrochemical properties of the reported complexes are consistent with compounds of $[\text{Ir}(32)_2\text{L}]^{3+}$ forming a neutral carbene-like pyridylidene structure, unlike $[\text{Ir}(22)_2\text{L}]^{3+}$ and $[\text{Ir}(42)_2\text{L}]^{3+}$ which adopt a more zwitterionic character. The relative cathodic shift in the reduction potentials of

$[\text{Ir}(\text{32})_2\text{L}]^{3+}$ may therefore be attributed to the increasing energy of the π^* -orbitals that is afforded with increasing neutral carbene character. The enhanced π -back bonding that is also expected would result in the stabilisation of the metal based HOMO thus explaining the more positive oxidation potentials. These rationales are presented in the explanation of similar observations that were made concerning the properties of related ruthenium complexes containing the pyridinium functionality; $[\text{Ru}(\text{bpy})_2(\text{C}^{\wedge}\text{N})](\text{PF}_6)$ ^[243], $\text{Ru}(\text{terpy})(\text{N}^{\wedge}\text{N}^{\wedge}\text{C})$ ^[294, 295] and $[\text{Ru}(\text{N}^{\wedge}\text{C}^{\wedge}\text{N})(\text{napy-}\kappa^2\text{-N,N'})\text{CO}](\text{PF}_6)_2$ ^[296] where $\text{C}^{\wedge}\text{N}$ = 1-methyl-3-(2'-pyridyl)pyridinium and 1-methyl-4-(2'-pyridyl)pyridinium; $(\text{N}^{\wedge}\text{N}^{\wedge}\text{C})$ = *N''*-methyl-4'-methylthio-2,2':6',3'''-terpyridinium and *N''*-methyl-4'-methylthio-2,2':6',4'''-terpyridinium and $(\text{N}^{\wedge}\text{C}^{\wedge}\text{N})$ = *N*-methyl-3,5-di(2-pyridyl)pyridinium. By comparison, the relative magnitude of the shifts in both oxidation and reduction potentials were less than half of those noted in this investigation. It is surmised that this is owing to the inherent difference of the two metal centres and the accumulative effects that are afforded upon inclusion of two pyridinium moieties within a single complex. Regarding the previously discussed assignments of the redox processes, it should be noted that theoretical studies of NHC and py-NHC complexes have indicated that the M–C bond is primarily electrostatic in nature with a contribution of $\geq 65\%$.^[297-299] This lowered degree of covalency therefore suggests a decreased Ir–C[−] σ -bonding orbital contribution to the oxidation process.

Conclusions drawn from structural characterisation data are more ambiguous. Single crystal X-ray structures showed only a slight shortening of the Ir–C bond for $[\text{Ir}(\text{32})_2\text{L}](\text{PF}_6)_3$ which would be indicative of the neutral carbene. It is also expected that a variation in C–C bond lengths of the cyclometalating ring be apparent had a pyridylidene-type structure been adopted.^[297, 300-303] For $[\text{Ir}(\text{32})_2\text{Y}](\text{PF}_6)_3$ a shortening of both the C₂–C₃ and C₅–C₆ distances to *ca.* 1.36 Å is evident for one of the four distinct pyridinium moieties within the unit cell. This decrease of *ca.* 0.02 – 0.04 Å from typical values supports the existence of the neutral carbene structure although in all other instances no specific trends could be discerned.

The data obtained from ¹³C-NMR is likewise inconclusive. It has been reported that a downfield shift in δ_c values of the carbene resonance is indicative of an increased neutral carbene character. The observed chemical shifts for the A₆ carbon of $[\text{Ir}(\text{22})_2\text{Y}](\text{PF}_6)_3$ and $[\text{Ir}(\text{42})_2\text{Y}](\text{PF}_6)_3$ are in the range expected of an abnormal carbene signal, with a value of $\delta_c = 157.05 - 161.66$ ppm. Whilst this is deshielded by *ca.* 16 ppm for $[\text{Ir}(\text{32})_2\text{Y}](\text{PF}_6)_3$ it remains upfield of those typically reported for other remote NHCs and is instead closer to that of a normal py-NHC as in, for example, $[\text{Ir}(\text{COD})(3\text{-}(2\text{-pyridyl})\text{-4-methylpyridin-2-ylium-C}^2\text{,N}')\text{HX}]^+$ and $[\text{Ir}(\text{COD})(1\text{-}n\text{-butyl-3-(2-pyridyl)-4-methylpyridin-2-ylium-C}^2\text{,N}')\text{HX}]^+$ where $\delta_c = 180.0$ ^[304] and 182.5^[244] ppm respectively. It is expected that the remote py-NHCs undergo a comparative downfield shift in relation to the other conformations, although the magnitude of such a shift is yet to be fully established. Interestingly in the reported attempts to synthesise the related complexes of 1-*n*-butyl-3-(2'-pyridyl)pyridinium, the reaction yielded a number of isomers from which two distinct Ir–C resonances could be identified, with $\delta_c = 187.5$ and

178.3 ppm. The former is comparable to the equivalent shift in $[\text{Ir}(\text{COD})(1\text{-}n\text{-butyl-3-(2\text{-pyridyl)-4-methylpyridin-2-ylidene-}C^2,N')\text{HX}]^+$ on compensating for the inductive effect of the 4-methyl group. It may therefore be possible to assign the more up-field shift to the remote py-NHC linkage isomer, which would be in very good agreement with the value presented here for $[\text{Ir}(\text{32})_2\text{Y}](\text{PF}_6)_3$. Values of δ_{C} are perhaps not an accurate indicator of the favoured conformation as they are highly dependent upon numerous other factors.

The complexes presented here are unusual in that they contain two of the py-NHC moieties, thus making direct comparisons with literature precedent difficult as the metal centre is in a considerably different environment to those typically reported. On evaluation of the properties of the three distinct series of complexes discussed herein, it is evident that those of 1-methyl-3-(2'-pyridyl)pyridinium adopt a degree of neutral carbene character, although the precise extent to which this form is favoured cannot be quantified at present. Further NMR and crystallographic studies upon a broader range of compounds may prove useful, as would attempts to synthesise complexes of the alternate linkage isomer. This would allow insight into the properties of the normal carbene analogues to facilitate a complete comparative study.

4.4. Conclusions

Two distinct series of cationic cyclometalated iridium(III) complexes have been synthesised and successfully demonstrate the use of the pyridinium moiety towards improving aqueous solubility. Extensive NMR and crystallographic studies have allowed for unequivocal identification of these complexes, with the results further augmented by structural geometry optimisation calculations.

Incorporation of the viologen like quaterpyridinium ligands has yield compounds with low energy onset of absorption in the range of 556 – 685 nm. This originates from the stabilising effect of the pyridinium group upon the LUMO of the ancillary ligand and the resultant bathochromic shift this affords in the related MLCT transitions. The complexes of bipyridinium display distinct photophysical and electrochemical properties owing to the increased π -acceptor ability of the cyclometalated pyridinium ring in comparison to that of a substituted aryl. As such the compounds display high oxidation potentials and less commonly so are readily reduced at the cyclometalated ligand, with first reduction couples at potentials between -0.72 and -1.14 V. TD-DFT calculations confirm the nature of the photophysical processes and accurately predict trends observed in the experimental absorption profiles. Complexes of phenylpyridine are dominated by transitions of MLCT/LLCT character towards the ancillary ligand and are thus highly dependant upon changes in *N*-substituent of the quaterpyridyl moiety. The properties of the bipyridinium compounds instead arise from MLCT/LC transitions and are localised about the cyclometalated ligand.

4.5 Further Work

As has been discussed previously the properties of the cyclometalated iridium complexes are dominated by the choice of the cyclometalating ligand. The work reported here demonstrates but one particular means of fine-tuning these properties whilst still incorporating the quaternised pyridinium functionality. Literature has shown that by making alterations to the pyridyl ring in comparison to the cyclometalating moiety, it is possible to afford considerably different effects upon the properties of the complex. This would make the quaternised compounds of 2-phenylpyrimidine, 2-phenylpyrazine and 2-phenylpyridazine interesting targets for study. Furthermore, by modifying the relative electron-withdrawing or donating abilities of the *N*-substituent, it is possible to affect changes in the overall acceptor ability of the pyridinium unit. It is surmised this would provide the means to effectively manipulate the electron density of both the ligand and metal centre. Whilst attempts to utilise the *N*-(2,4-dinitrophenyl)bipyridinium pro-ligand failed as part of this study, there remains a wide scope of functional groups that may be incorporated for this purpose. The Zincke reaction has been successfully employed in the synthesis of a variety of mono and di-quaternised 4,4'-bipyridinium salts, although rates and yields are highly dependent upon a number of factors. Whilst the impact of variations in the electron density of the aryl amine were considered as part of this investigation, further attempts towards optimising this reaction are warranted as rates also vary with temperature, solvent and the counteranion of the pyridinium salt.^[305]

A final approach in modifying the cyclometalating ligands would be to include the quaternised functionality in the form of a pendant pyridinium group. It is expected such an approach would lead to some interesting photophysical properties as additional MLCT and potential ILCT character may be evident. Three potential ligands of interest would be 1-methyl-2'-phenyl-[4,4'-bipyridin]-1-ium, 1-methyl-4-(3-(pyridin-3-yl)phenyl)pyridin-1-ium and the quaterpyridinium analogue, 1-methyl-2'-(3-(1-methylpyridin-1-ium-4-yl)phenyl)-[4,4'-bipyridin]-1-ium, Fig. 4.27.

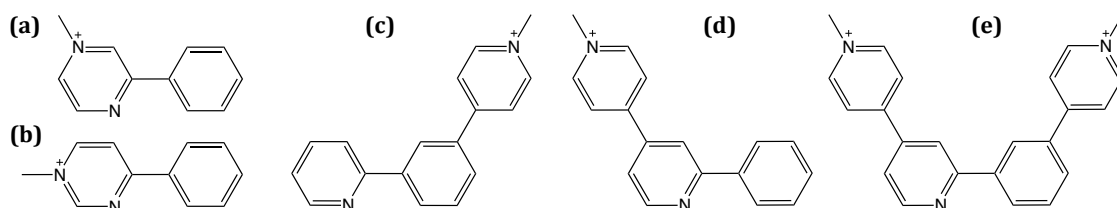


Fig. 4.27. Potential alternate cyclometalating ligands incorporating the pyridinium or a pyridinium-like moiety. **(a)** 1-methyl-3-phenylpyrazinium; **(b)** 1-methyl-4-phenylpyrimidinium; **(c)** 1-methyl-2'-phenyl-[4,4'-bipyridin]-1-ium; **(d)** 1-methyl-4-(3-(pyridin-3-yl)phenyl)pyridin-1-ium and **(e)** 1-methyl-2'-(3-(1-methylpyridin-1-ium-4-yl)phenyl)-[4,4'-bipyridin]-1-ium.

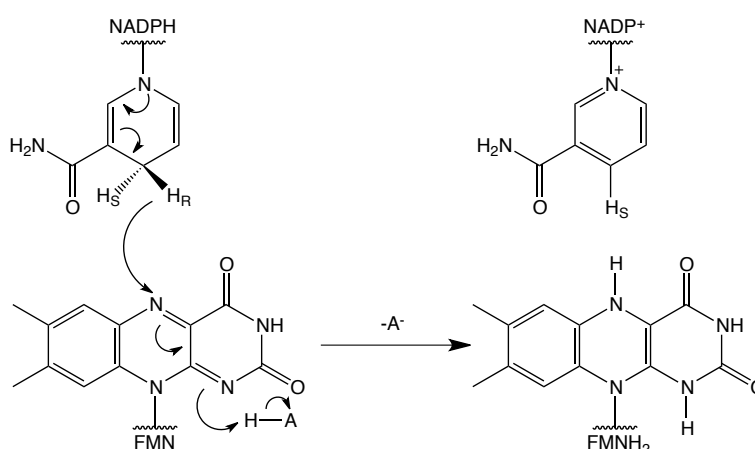
Another approach towards preparing photosensitisers with a broad a range of properties as possible would be to further expand the study beyond the transition metals presented thus far. One such example would be the complexes of rhenium, which have been previously shown to act as photosensitisers in a number of applications.^[306-311] In comparison

to Fe, Ru, Os and, to a lesser extent, Ir very few low valent polypyridyl complexes of rhenium are known. The majority that have been reported contain strong π -acid ligands, thus making direct comparisons with the metals investigated here difficult as a consequence of the relative differences in the ligands employed. Examples of tris-polypyridyl complexes of rhenium(II) have been reported and show interesting absorption and electrochemical properties, although the ability of such compounds to act as effective photosensitisers remains to be seen.^[312]

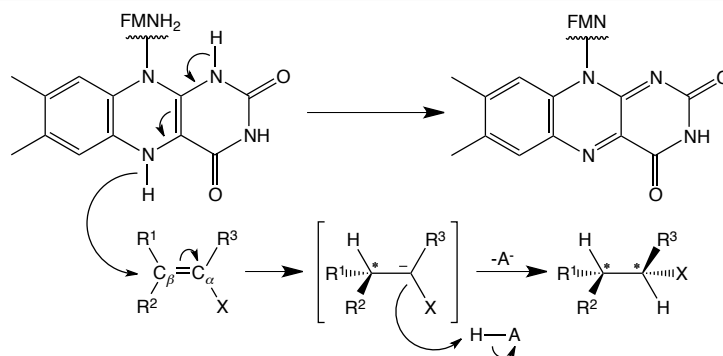
SECTION FIVE**DEVELOPMENT OF LIGHT-DRIVEN BIOCATALYTIC SYSTEMS****5.1 Introduction**

The old yellow enzyme (OYE) family is a series of flavin mononucleotide containing, NAD(P)H dependent oxidoreductases which show great potential for industrial and biotechnology applications. This has been made evident by a high efficiency towards the asymmetric reduction of a variety of industrially relevant activated alkenes. One such enzyme is the monomeric pentaerythritol tetranitrate reductase (PETNR) from *Enterobacter cloacae* st. PB2, so named as it was first isolated from soil rich in explosive chemical contaminants.^[313] This enzyme has demonstrated a high stability under a range of reaction conditions and is readily expressed to high levels in *Escherichia coli*.^[314] The crystal structure of PETNR has been solved to high resolution in the presence and absence of bound substrates and inhibitors.^[315-318] This extensive structural characterisation of the active site has afforded insights into the mechanistic details of the catalytic function and allowed the identification of key residues as targets towards site-directed mutagenesis studies with the aim of improving activity towards specific substrates or to afford different specificities.^[319, 320] As such these enzymes are prime candidates in the development of light-driven biocatalytic systems.

Typically the reactions of PETNR proceed via two successive half reactions. The first being the reduction of the FMN cofactor by NAD(P)H to yield the dihydroflavin. The proposed mechanism suggests formation of an enzyme-NADPH charge transfer complex prior to flavin reduction and subsequent dissociation of NAD(P)^+ .^[315] Complex formation is facilitated through π - π stacking interactions of the pyridinium and isoalloxazine rings of NADPH and FMN respectively. The proposed mechanism is supported by a characteristic, low energy, broad absorption band that is evident upon monitoring spectral changes concomitant with reduction of the enzyme. With the lack of absorbance changes associated with the population



Scheme 5.1. Mechanism for the reductive half reaction of the OYE family highlighting the reduction of the FMN cofactor by NAD(P)H.

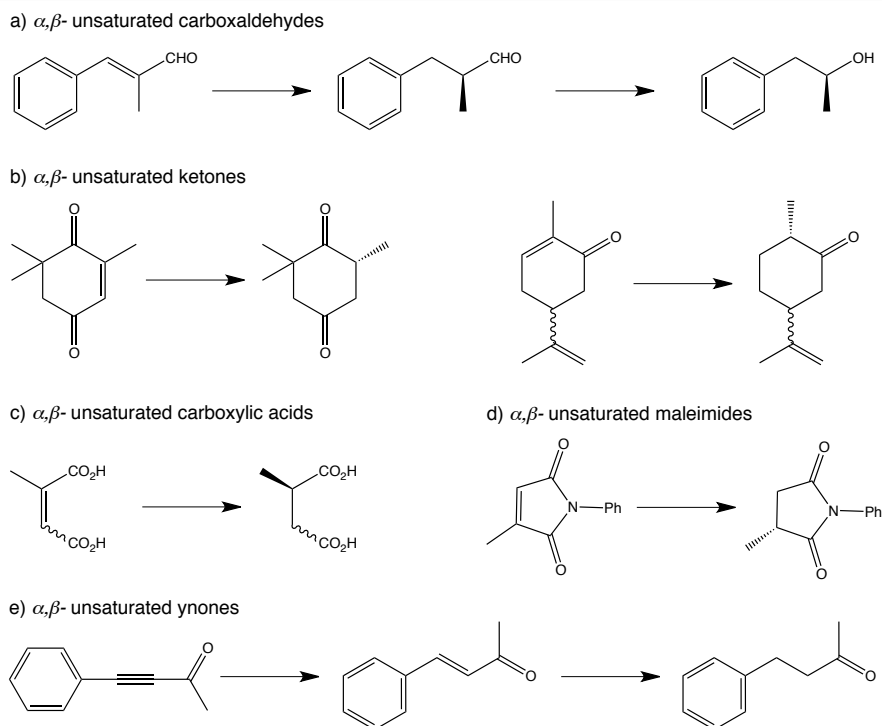


Scheme 5.2. Mechanism for the oxidative half-reaction of the OYE family, catalysing the reduction of an α , β -unsaturated alkene, where X = an electron withdrawing group and $H - A$ is a solvent molecule or enzyme residue.

of a singly reduced anionic semiquinone intermediate, as seen in other OYE homologues^[114, 321], it is therefore suggested that reduction occurs via a concerted two electron reduction by hydride transfer (H^-) similar to that of the bacterial morphinone reductase enzymes.^[322] There is also evidence to support the initial formation of a Michaelis complex, though whilst such a mechanism would fit the experimental data this has not yet been directly observed for PETNR.^[315]

The physiological oxidants of OYEs are as of yet unknown as the enzymes show high activity towards a diverse range of substrates, including the α,β -disubstituted unsaturated compounds. The oxidative half reaction proceeds via a stereoselective hydride transfer from the N5 of FMNH₂ to the C β of the bound substrate, subsequently resulting in reoxidation of the enzyme. Addition of [H₂] across the double bond is concluded on protonation of C α by a solvent derived proton.^[323] Structural analysis of the active site in OYE1 suggests that the tyrosine residue Y196 is in an ideal position to act as the proton donor towards C α ,^[324] with the analogous residue Y186 in PETNR surmised to act in a similar fashion.^[315, 316] Addition is expected to occur in a concerted and predominantly *anti*-fashion; the reaction considered to be comparable to an asymmetric Michael-type conjugate addition of a hydride to an activated alkene^[325] It is of note that for some related enzymes, examples of *syn*-addition have also been demonstrated.^[326, 327]

Substrate activity is dependent upon the presence of electron-withdrawing substituents to increase the susceptibility of the double bond towards nucleophilic attack. This has been demonstrated with a number of functional groups such as the aldehyde, ketone, nitro, carboxylic acid, ester, anhydride, lactone or imide groups.^[328, 329] For compounds such as 2-cyclohexen-1-one, the carbonyl group is also involved in extensive hydrogen bonding with two histidine residues within the active site, thus serving to further activate the double bond via polarisation. The prevalent substrates discussed in the literature in relation to the OYEs are those of the α,β -unsaturated carbonyl compounds. The α,β -unsaturated carboxyaldehydes or enals are of potential industrial importance due to extensive applications in the production of dispersants, detergents and fragrances. The biotransformations show a high tolerance for the



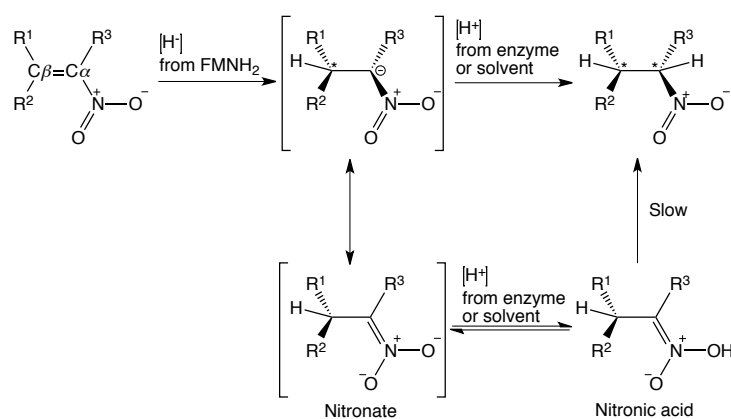
Scheme 5.3. Asymmetric bioreduction of a variety of α,β -unsaturated carbonyl compounds catalyzed by OYEs.

substitution of the R^1 and R^2 groups of C_β although less so for R^3 of C_α , as activity of the latter is limited to substituents of low steric bulk though is tolerant of electron withdrawing groups.

The cyclic and acyclic ketones are similarly good substrates for OYEs, with 2-cyclohex-1-enone and 2,6,6-trimethyl-cyclohex-2-en-1,4-dione proving to be of particular high activity; the latter being utilised in the large scale synthesis of (*R*)-levodione in the biocatalytic reduction by Baker's yeast. The α,β -unsaturated mono-carboxylic acids and esters tend to be poorer substrates for the OYEs, although activity can be improved on addition of electron withdrawing groups; the diacids and diesters for example show enhanced activity and are moderate to good substrates. Halides may also be incorporated as an activating group, though these are reductively eliminated on substitution at C_β .^[329] The chiral α -halogenated carboxylic acids and esters are reactive towards nucleophilic attack at C_α and are as such potential synthons in the preparation of ethers,^[330] thioethers,^[331] thiocarbonates^[332] and amines^[333].

Activity towards ynones was also demonstrated in the *trans* selective reduction of 4-phenyl-3-butyne-2-one by OYE 1-3 to yield (*E*)-4-phenyl-3-buten-2-one.^[334] OYE 3 showed the best reactivity with a theoretical yield of *ca.* 65 % after 5 hours. Further reduction to the saturated ketone was also evident, the rate of which was shown to increase significantly with decreasing concentration of the ynone in solution.

The related maleimides and acid anhydrides are extremely active towards PETNR and TOYE; the *N*-substituted maleimides showing K_m values in the range expected of a physiological substrate.^[125, 335] The resultant chiral succinimides may be used in a variety of chemical transformations that typically proceed via ring opening mechanisms on nucleophilic attack of one of the carbonyl groups thus forming new C-C, C-O, C-N and C-S linkages.^[336]



Scheme 5.4. The proposed mechanism for biocatalytic reduction of α,β -unsaturated nitroalkenes, by the OYE family, highlighting a potential decoupled reaction pathway via nitronate formation and subsequent protonation and tautomerisation. Where * indicates the presence of a newly formed chiral centre

Terpenoids are a series of natural products derived from the isoprene or 2-methyl-1,3-butadiene (C_5) unit and are produced as part of the biosynthetic pathways towards essential oils in a variety of plants, such as menthol/menthone in peppermint^[337] and carvone in the fruit of caraway.^[338] These acyclic or cyclic compounds may be considered as an equivalent to a substituted terpene, typically involving the shift or loss of carbon atoms and functionalisation by oxygen. The reduction of citral and carvone to yield citronellal and dihydrocarvone respectively has been demonstrated with a number of OYEs in moderate to excellent yields, although the resultant stereochemistry was dependent upon the enzyme employed.^[329] Typically these compounds have been utilised as valuable chiral synthons in the preparation of natural products and in the development of potential pharmaceuticals.^[339]

The electronegativity of the nitro group is such so as to sufficiently activate the double bond in $\alpha\text{-}\beta$ unsaturated nitroalkenes towards bioreduction by OYEs. The nitroalkanes are compounds of particular industrial relevance as they may be employed as precursors in the synthesis of various functional groups, including amines, hydroxylamines, aldehydes, carboxylic acids, and oximes.^[340] As such the formation of the nitroalkanes by enzymatic asymmetric reduction of nitroalkenes provides a synthetic route towards the introduction of up to two stereogenic centres with potential scope for further functionalisation. Issues pertaining to poor enantioselectivity have been encountered for these substrates and have been attributed to non-enzymatic product racemisation in aqueous solution,^[335] although through optimisation of reaction conditions the impact of such side reactions may be minimised.^[341] Studies concerning the reduction of 1-nitrocyclohexene by a number of OYEs show the reaction proceeds via decoupled hydride transfer and protonation steps. Results indicated the formation of a nitronate intermediate, which undergoes protonation to form the nitronic acid and subsequent tautomerisation to yield the corresponding nitroalkane product, Scheme 5.4.^[342, 343]

Another enzyme with potential applications in this study is an ene-reductase from *Thermoanaerobacter pseudethanolicus* E39.^[344] This thermostable old yellow enzyme (TOYE) was the first known to exist in multiple oligomeric states, with evidence to support the presence of octamers and dodecomers in solution.^[125] The crystal structure was determined to high resolution and showed that the enzyme adopts a homotetrameric structure, comprised of a two dimeric units, which is analogous to that of the tetrameric OYE, YqjM with which it shares 50% sequence homology.^[345]

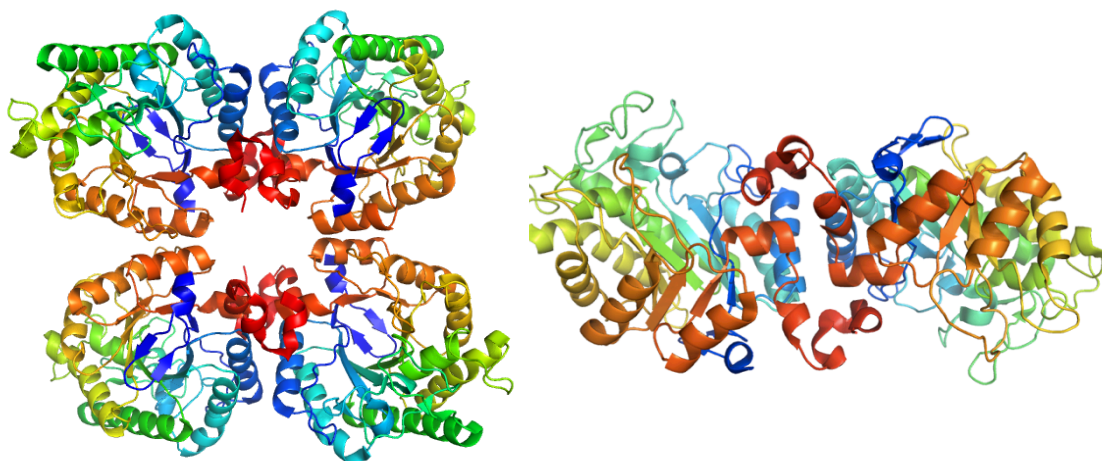


Fig. 5.1. Crystal structure of TOYE displayed as a rainbow coloured cartoon N- (blue) to C- (red) terminus. (A) Top view showing the complete tetrameric structure and (B) side view displaying the functional dimer. Image generated by MacPymol, (PDB code 3KRU).

The thermostability of TOYE was investigated using circular dichroism and differential scanning calorimetry techniques along with monitoring fluorescence changes associated with FMN and tryptophan residues. Results indicated that a loss of structural integrity begins at *ca.* 70°C with thermal denaturation occurring at 79°C and subsequent aggregation at 87°C. Whilst maintaining stability, activity towards biotransformation is significantly decreased on elevation of the reaction temperature; for example in the reduction of 2-methyl-1-pentanal, yields are reduced from 82 % to 38 % on increasing the temperature from 30°C to 50°C. This has been attributed to substrate/product decomposition and the likelihood of additional side reactions that may occur at elevated temperatures; the enantiomeric excess was likewise reduced from 55 % to 10 %. It was surmised that substrate binding or stereoselectivity might have been affected on increasing temperature, though a decrease in enantiomeric excess was particularly evident for those substrates that are known to undergo non-enzymatic racemisation, the rate of which would be increased with increasing temperature.

As had been previously demonstrated, thermophilic enzymes tend to offer improved stability towards organic solvents.^[346, 347] Steady-state reactions of TOYE in the presence of varying concentrations of ethanol showed 50 % loss of activity in a solution of 45 % ethanol and maintained *ca.* 20 % activity in an 80 % solution. In contrast PETNR showed similar deactivation in just a 20 % ethanolic solution and began to appreciably precipitate at

concentrations above 40%. TOYE also exhibited a high tolerance for a variety of other water-miscible organic solvents. Concerning the bioreduction of 2,6,6-trimethylcyclohex-2-ene-1,4-dione, comparable results were obtained for 10 % solutions of THF, methanol, ethanol and acetonitrile, with yields in the range of 65-69 %, although lower yields were observed for propanol (54 %), acetone (36 %) and DMF (37 %). The increased stability at elevated temperatures and in the presence of organic solvents significantly broadens the range of potential substrates that may be employed due to the related enhancement in solubilities. Furthermore, such properties are highly desirable towards increasing the compatibility of biotransformations with current industrial practices.

Herein the development and potential of light-driven biocatalytic systems based upon PETNR and TOYE using two distinct methods is discussed. The first of these is a diffusion controlled multicomponent system, which employs photosensitisers that are 'free' in solution. The second method involves the direct attachment of a photosensitiser to the enzyme via covalent bond formation. It has been shown that selective labeling of cysteinyl residues may be achieved upon using photosensitisers that incorporate the reactive α -bromomethyl group. This approach will be utilised in conjunction with site-directed mutagenesis studies to introduce new cysteinyl residues onto the surface of the enzyme so as to facilitate targeted labeling. Due to the extensive dimer interactions of TOYE and the implications this has for the active site, this approach will focus solely upon systems containing PETNR. As such, the design and preparation of a number of PETNR variants is described, along with details concerning the synthesis of appropriate ruthenium photosensitisers and subsequent labeling reactions thereof. The study will focus upon establishing the proof of principle that transition metal complexes can be utilised as effective photosensitisers towards enzymatic turnover and catalytic activity. Subsequent work will discuss the optimisation of said systems with the aim of maximising efficiencies and broadening the potential scope of this application towards a variety of substrates.

5.2 Results and Discussion

5.2.1 Site-Directed Mutagenesis of Pentaerythritol Tetranitrate Reductase.

5.2.1.1. Mutant Strand synthesis

On determination of potential sites for mutagenesis, a number of criteria must be considered. The first is that the residue be located near to the surface of the enzyme to ensure that it is sufficiently accessible to facilitate reaction with the ruthenium complex. The residue must also be in close proximity to the bound FMN cofactor, as it has been demonstrated that the distance between the two redox centres should be within 14 Å for optimal electron transfer to occur.^[348] Likewise the orientation of the side chain should be such so as to provide the correct spatial arrangement between the bound sensitiser and FMN. One of the most important considerations is that the mutation does not perturb the functionality of the enzyme, as such no residues involved in substrate/cofactor binding nor those in close proximity to such residues were considered for mutagenesis. From these criteria and studies of the crystal structure of the active site, three possible candidates of mutagenesis were identified, Q241, G301 and R324, Fig. 5.2. Primer sequences were subsequently designed for each of these mutations taking into consideration sequence length, melting temperatures and secondary structures, Table 5.1.

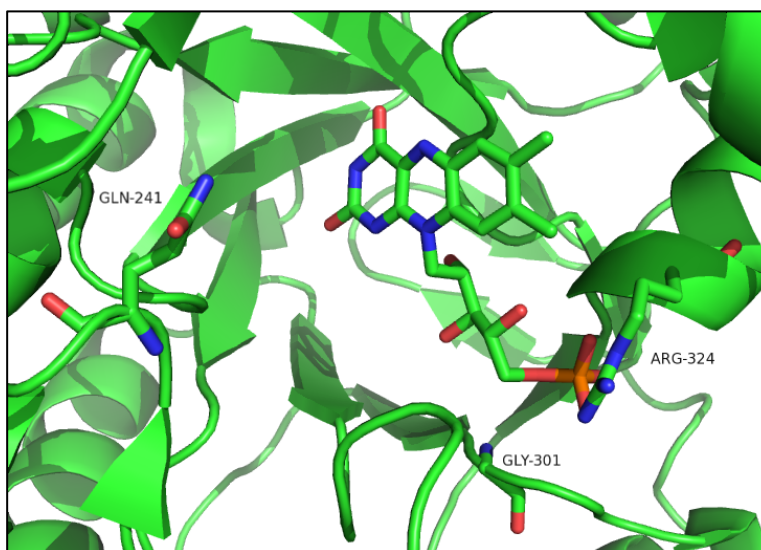


Fig. 5.2. The X-ray crystal structure of the active site of PETNR, highlighting the target residues for mutagenesis studies and their relative positions with respect to FMN. The image was generated in MacPyMol. The main chain is represented as a cartoon with the flavin cofactor and residues of interest shown as coloured sticks. (PDB code 1H50).

The secondary structures of the designed primers were of slightly higher melting temperatures than would be preferred, although these were amongst the better values calculated from a number of potential candidates. As such the initial PCR reactions were carried out at slightly elevated temperatures for both the annealing and extension phases, Table 5.2, Run 1. This proved unsuccessful as gel electrophoresis indicated that minimal quantities of DNA had been synthesised. It is believed that the temperature of the extension

phase may have been too high and that insufficient time had been allowed for complete polymerisation to occur. The conditions were therefore modified to incorporate a longer extension time at a lower temperature and, in the case of mutant R324C, DMSO added to the reaction mixture, Table 5.2 Run 2. The resultant PCR was much improved, with significant quantities of DNA with approximately the correct molecular weight being prepared, Fig. 5.3. Gel extraction and subsequent transformation of *E coli*. XL-10 gold ultracompetent cells was undertaken and the resultant mutated plasmid DNA purified using the QIAGEN® QIAprep® MiniPrep procedure. DNA sequencing results indicated successful mutant strand synthesis in each instance.

Table 5.1. List of primers used in the sequencing of PETNR variants, displaying both the forward and complementary sequences. The required alteration in the amino acid sequence to achieve each mutation is highlighted in red.

Mutation	Primer Sequence	Alteration	T _m	2°T _m
Q241CF	TCCCCGATCGGTACTTTCTGTAACGTCGACAACGGTCC	CAG ⇒ TGT	70	41
Q241CR	GGACCGTTGTCGACGTTACAGAAAGTACCGATCGGGGA	CTG ⇒ ACA		42
G301CF	GTGATTATCGGGGCGTGTGCGTATACGGCAGAG	GGT ⇒ TGT	68	38
G301CR	CTCTGCCGTATACGCACACGCCCGATAATCAC	ACC ⇒ ACA		39
R324CF	GCCGTGGCCTTTGGCTGTGACTACATTGCTAAC	CGT ⇒ TGT	67	45
R324CR	GTTAGCAATGTAGTCACAGCCAAAGGCCACGGC	ACG ⇒ ACA		43

Table 5.2. (Below) PCR cycling parameters used in the preparation of plasmid DNA towards the required PETNR variants. Where * denotes the addition of DMSO to the reaction mixture.

	Run One		Run Two		No. Cycles
	Temp/°C	Time/s	Temp/°C	Time/s	
Initialisation	94	120	94	120	1
Denaturation	94	15	94	15	18
Annealing	Q241C	30	54	30	
	G301C		54		
	R324C		55*		
Extension	72	100	68	270	
Final Extension	-	-	68	300	1
Hold	10	∞	10	∞	1

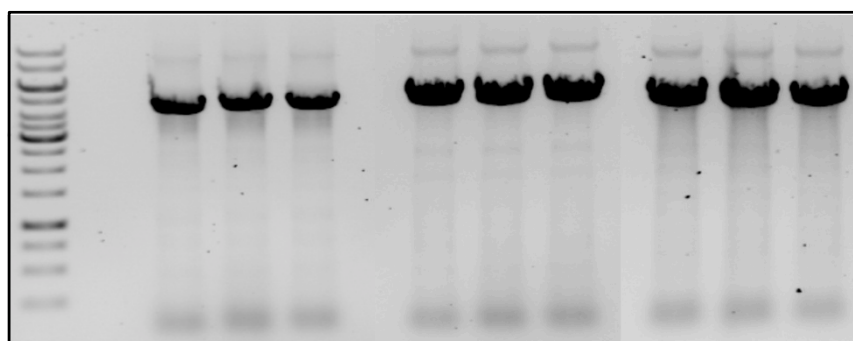


Fig. 5.3. Agarose gel showing final results achieved via PCR in the preparation of PETNR variants; (left to right) 1kb ladder (Fermentas; 250, 500, 750 bp, 1, 1.5, 2, 2.5, 3, 3.5, 4, 5, 6, 8, 10 kbp), PETNR_{Q241C}, PETNR_{G301C} and PETNR_{R324C}.

5.2.1.2. Expression and Purification of PETNR Variants.

Transformation of the plasmid DNA into *E. coli* JM109 cells was performed for each of the mutants, as described in section 2.4. Protein expression trials were undertaken with subsequent analysis by SDS-PAGE. Results indicated that expression had been successfully achieved for each of the mutants, although the yield of the G301C variant was comparatively poorer than those of Q241C and R324C, Fig. 5.5. In an attempt to improve results, the expression of G301C was repeated although the culture was this time inoculated with the original glycerol stock prepared using XL-10 Gold ultracompetent cells. It was thought that the characteristically high expression and toxicity resistance of this strain might aid in improving yields, although no beneficial effects were observed.

Each of the mutants was expressed on a larger scale in TB autoinduction media, with initial purification trials undertaken using PETNR_{Q241C}. After cell lysis the resultant mixture was centrifuged and the supernatants collected before the addition of excess FMN to maximise flavination of the enzyme. On dialysis the appearance of the solution changed from tan to golden yellow in colour, the latter characteristic of PETNR. The protein was then loaded onto a nickel affinity column pre-equilibrated with the wash buffer (50 mM KPO₄, 300 mM NaCl and 20 mM imidzole, pH 8). Purification was facilitated by nickel coordination of the histidine residues of the C-terminal His₈ tag incorporated into the protein. Elution with four column volumes of buffer afforded the removal of the unbound protein as a dilute tan band. On increasing the imidazole concentration to 50mM, the remaining protein was isolated as a bright yellow eluate. SDS-PAGE confirmed the removal of a majority of the impurities and that each of the collected yellow fractions was of the same composition. On combination and subsequent dialysis, the protein was loaded onto a Hi-Prep Q Sepharose column attached to an automated AKTA purifier 100 system that had been pre-equilibrated with 50 mM KPO₄, pH 8. It had been intended to perform an initial wash cycle using the same solution prior to commencing with a gradient of the elution buffer (1 M NaCl, 50 mM KPO₄, pH 8.0). However, on

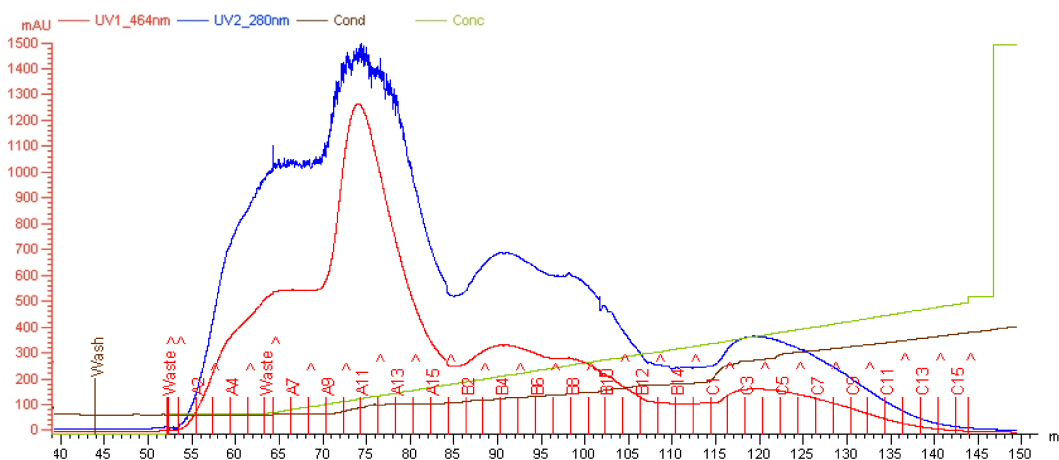


Fig. 5.4. UV-vis absorption profile recorded on purification of PETNR_{Q241C} by column chromatography utilising an AKTA purifier 100 system showing absorption at 280 (blue) and 464 nm (red). Additional information regarding solution conductivity (tan) and the concentration of elution buffer (green) is also shown.

starting the sequence, elution of the desired protein quickly became apparent. As such the gradient was initiated before a full wash cycle was completed. Measuring absorbance of the eluate at 280 and 464 nm provided the means to directly observe the total protein and flavin concentrations respectively. At this stage two distinctly different flavin containing species were identified, Fig. 5.4. SDS-PAGE confirmed that the main fraction was of pure PETNR, whilst samples taken from the later fractions contained a second minor component of higher molecular weight compared to that expected of the enzyme, Fig. 5.6. Therefore fractions A2 to A15 were combined as a single product and fractions B1 to C11 collected as another; fraction designations used as indicated in Fig. 5.4.

In an effort to distinguish the difference between these two fractions, native gel electrophoresis was performed and compared to a PETNR_{WT} standard, Fig. 5.7. This revealed that the first combined fraction contained a single species of a comparable size to the native enzyme, although its relative position would indicate that the mutant has adopted a slightly more open conformation. The precise reason for this is currently unknown, though the possibility of disulfide bond formation within the protein structure is considered unlikely. The second fraction contained two specific components and indicated the possibility of dimer formation via disulfide linkage between two monomeric units. As this issue is not normally a concern during preparation of PETNR, addition of β -mercaptoethanol and/or dithiothreitol (DTT) had not been considered in the originally developed procedure. Subsequent purification of PETNR_{G301C} was performed in the presence of 1.5 mM β -mercaptoethanol in all column and dialysis buffers, although the dimeric byproduct was again apparent. Further trials with PETNR_{R324C} were undertaken with 2 mM DTT included in the initial lysis buffer and 2 mM β -mercaptoethanol in all subsequent solutions. This proved sufficient to rectify the problem with no evidence to support the formation of the dimeric by-product and thus DTT was included in all further preparative procedures.

UV-vis absorption spectra were recorded at each stage of the purification process to establish the relative flavinated enzyme to total protein content of the samples. This was achieved on comparison of absorption at 280 and 464 nm, which indicated an increasing purity across successive purification steps. The final purified protein exhibited an absorption profile very similar to that of wild type PETNR, indicating that the mutation has had minimal effects on FMN and its binding. Using the collected absorption data, the concentration and relative purities of each sample were calculated, using an extinction coefficient value of $\epsilon_{464}=11.3 \times 10^3 \text{ M}^{-1}\text{cm}^{-1}$ for the flavinated enzyme (Table. 3.4). The total yield of the protein was 256 mg with 99.4% flavination. Similar results were obtained for PETNR_{R324C}, although yields were increased to 447 mg owing to the prevention of enzyme loss due to dimeric byproducts. Yields of PETNR_{G301C} were considerably poorer at 192 mg, thus reflecting the smaller expression band noted during the original trials.

Stage	Abs ₄₆₄	Concentration/ μM	Volume/mL	Moles	Mass Protein ^a /mg	Total Protein ^b /mg	% Flavination
Cell Extract	0.044	389.38	67	0.0261	1033.10	1675	61.68
First Dialysis	0.283	250.44	74	0.0185	733.90	932.4	78.71
Nickel Column	0.322	284.96	45	0.0128	507.79	702	72.33
Sepharose Frac 1	0.234	207.08	31	0.0064	254.22	255.75	99.40
Sepharose Frac. 2	0.086	7.61	59	0.0045	177.81	221.25	80.34

Table 5.3. Results of purification of PETNR Q241C variant, highlighting the respective protein content determined at each individual stage of the procedure. ^a Determined from monitoring absorption at 464 nm using an extinction coefficient of $\epsilon_{464} = 11.3 \times 10^3 \text{ M}^{-1} \text{ cm}^{-1}$. ^b Total protein was determined using the Bio-Rad Assay employing the Bradford reagent. Absorbance at 595 nm was recorded and the protein concentration extrapolated from known standards.

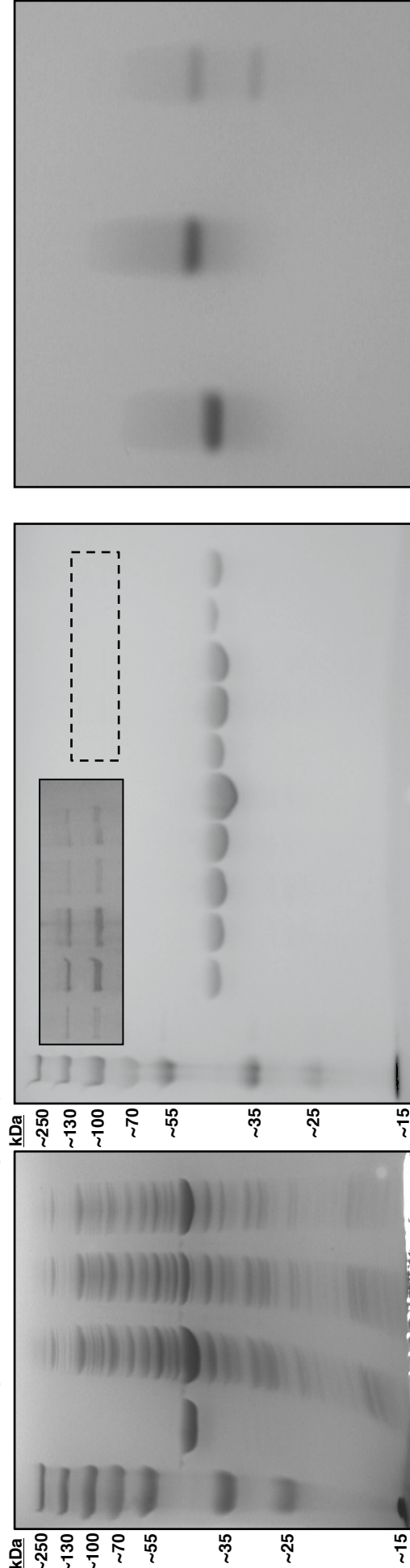


Fig. 5.5. SDS-PAGE of protein expression trials of the PETNR variants. Stained with Coomassie Brilliant Blue R250. (Left to right) Marker: PageRuler™ Plus prestained protein ladder (MW), WT PETNR, Q241C, G301C and R324C.

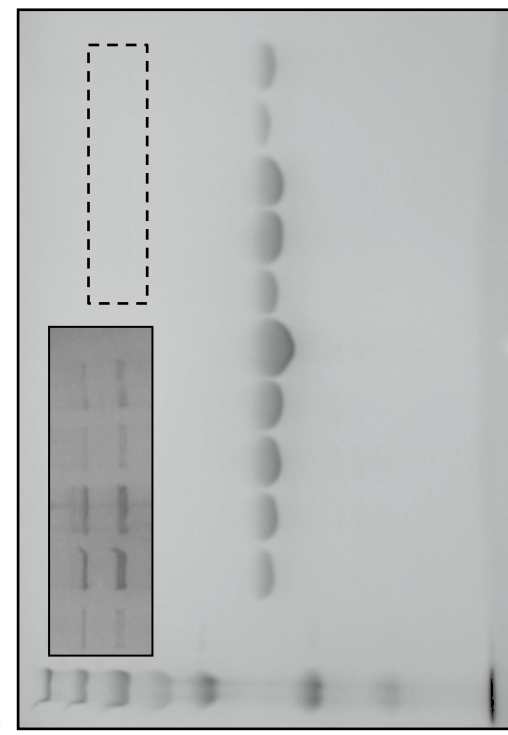


Fig. 5.6. SDS-PAGE of fractions collected on purification using a Hi-Prep Q Sepharose column. Stained with Coomassie Brilliant Blue R250. (Left to right) Ladder, Fractions A2, A4, A6, A9, B1, B4, B8, B14, C3 (as identified in Fig. 5.4.) and unbound protein. (Insert) Magnified image of highlighted area on staining using zinc/imidazole procedure

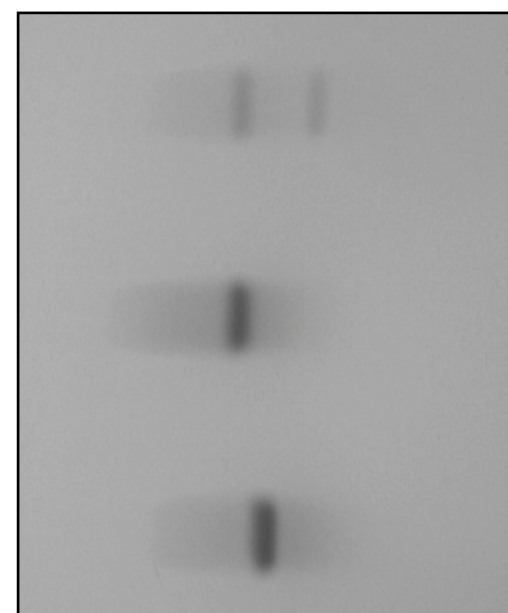
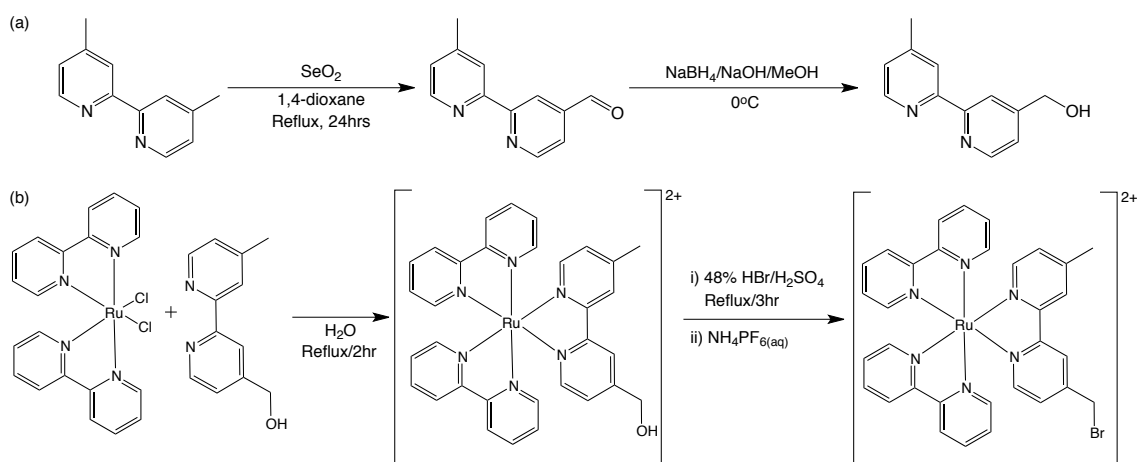


Fig. 5.7. Native PAGE of the two different products isolated on purification using a Hi-Prep Q Sepharose column stained with Coomassie Brilliant Blue R250. (Left to right) Wild Type, Combined Fraction 1 and Combined Fraction 2

5.2.2. Labelling studies of PETNR Variants.

5.2.2.1. Synthesis of Ruthenium Labels

Thioether linkages between the enzyme and the ruthenium labels are formed on reaction of the thiol group of a cysteinyl residue with an α -bromomethyl group incorporated into the complex. Due to the reactivity of the bromomethyl group towards hydrolysis, the final complex used in the labelling studies was prepared via the 4-hydroxymethyl-4'-methyl-2,2'-bipyridine analogue. The required pro-ligand is prepared by oxidation of 4,4'-dimethyl-2,2'-bipyridine in the presence of selenium dioxide, which selectively forms the monocarbaldehyde intermediate upon use of the correct stoichiometry.^[349] Subsequent transformation to the hydroxymethyl group is achieved using sodium borohydride as a reducing agent.^[350] The pro-ligand can then be coordinated to the bis-chelate dichlororuthenium(II) precursor to yield the required intermediary complex; this method was successfully employed in the synthesis of both $[\text{Ru}(\text{bpy})_2(4\text{-hydroxymethyl-4'-methyl-2,2'-bipyridine})](\text{PF}_6)_2$ and $[\text{Ru}(\text{bpz})_2(4\text{-hydroxymethyl-4'-methyl-2,2'-bipyridine})](\text{PF}_6)_2$.



Scheme 5.5 a) Synthesis of the 4-hydroxymethyl-4'-methyl-2,2'-bipyridine pro-ligand; b) Coordination of the pro-ligand to the $[\text{Ru}(\text{bpy})_2\text{Cl}_2]$ precursor and subsequent bromination reaction to yield the final complex to be used in labelling studies.

Substitution of the hydroxyl group using an appropriate brominating agent proceeds via a $\text{S}_{\text{N}}2$ mechanism. $[\text{Ru}(\text{bpy})_2(4\text{-bromomethyl-4'-methyl-2,2'-bipyridine})](\text{PF}_6)_2$ was prepared as described by Geren *et al.*^[36] using a 48% hydrogen bromide aqueous solution in the presence of concentrated sulphuric acid. However, attempts to use this procedure in conjunction with the bipyrazine analogue proved unsuccessful as the resultant material was typically a hygroscopic gel, which made subsequent filtration and isolation of the product as a solid problematic. On analysis of the material by $^1\text{H-NMR}$, it was evident that whilst bromination of the hydroxyl group had been achieved, the aromatic region of the spectra indicated the presence of a number of different components. It is therefore surmised that partial protonation of the distal nitrogens of the bipyrazine rings had occurred over the course of the reaction, alternate brominating agents were therefore investigated. Initial trials employing thionyl bromide (SOBr_2) proved unsuccessful, due to similar problems to those

observed during isolation of the product using the HBr procedure. The final method that was developed proceeded upon the reaction of phosphorus tribromide (PBr₃) with [Ru(bpy)₂(4-bromomethyl-4'-methyl-2,2'-bipyridine)](PF₆)₂ in acetonitrile at 65°C. The product was isolated on addition of diethyl ether to the reaction mixture with subsequent reprecipitation from methanol/DCM and metathesis to the hexafluorophosphate salt. The complex is stable as a solid when stored in a desiccator at room temperature for periods of two to three months without any adverse effects. Similarly the compound showed minimal evidence of hydrolysis when stored as an acetonitrile solution over a number of days, as shown by ¹H-NMR. This would suggest that the advised procedure of being stored under vacuum at -90°C as previously described in literature^[36] may be superfluous.

In an effort to prepare ruthenium labels of more varied properties, the potential of linker units other than 4-bromomethyl-4'-methyl-2,2'-bipyridine were investigated. Due to the reported high specificity of the α-bromomethyl group towards the labelling of cysteinyl residues,^[36] it was determined that this functionality should be incorporated into any new potential ligands. With the success achieved in tuning the redox potentials of the Ru(II/III) couple and the first reduction process in complexes of the quaternised quaterpyridyl ligands, these compounds were identified as ideal targets for this study. As such a new ligand, N'',N'''-di(4-hydroxymethylphenyl)-4,4':2',2'':4'',4'''-quaterpyridinium hexafluorophosphate, [(4-HOCH₂Ph)₂Qpy](PF₆)₂, was designed and synthesised; the procedure used to prepare both the ligand and the hydroxymethyl- precursor complex, in addition to complete characterisation data, is discussed in section 3.2. Cyclic voltammetry experiments and TD-DFT calculations suggested that upon photoexcitation, rapid electron transfer from the metal centre to the pyridinium moiety of the ancillary ligand would occur. By comparison to the complexes of 4-hydroxymethyl-4'-methyl-2,2'-bipyridine this would afford an increase of charge separation within the excited state. This behaviour is expected to increase the efficiency of the electron transfer process to the cofactor as the pyridinium group can act as a transfer mediator between the metal centre and FMN. Bromination of the hydroxymethyl group was achieved using phosphorus tribromide as described previously. The identity of the complex was confirmed using ¹H-NMR, which showed a up-field shift in the -CH₂- resonance of the methyl group with a concomitant change in the splitting pattern from a triplet to a singlet on loss of the hydroxyl proton. Mass spectroscopy results also indicated successful product formation as evident by the presence of species of *m/z* = 1503, 678 and 405; which are associated with [M-PF₆]⁺, [M-2PF₆]²⁺ and [M-3PF₆]³⁺ respectively.

5.2.2.2. Labelling trials

Labelling trials were undertaken using a modification of the procedure reported by Geren *et al.*^[36] in the study of cytochrome *c*. Initial studies focused upon the use of the PETNR_{Q241C} variant and [Ru(bpy)₂(4-bromomethyl-4'-methyl-2,2'-bipyridine)]Cl₂ as the labelling reagent. On completion of the reaction, unbound label could be readily removed on

passing the solution through a PD-10 desalting column containing Sephadex G-25. Eluting with a buffer of low ionic strength (*ca.* 5 mM Tris HCl) allowed for excellent separation of two distinct bands. The protein was first eluted as a yellow-orange solution, whilst unreacted label was collected on increasing the Tris-HCl concentration to 50 mM to afford a dark orange-red eluate. Each fraction was analysed by UV-visible spectroscopy to determine the composition by comparison with spectra of known standards. No free flavin was identified at any stage of the separation, indicating that cofactor binding had not been compromised during the labelling reaction. Successful labelling was achieved as indicated on comparison of the UV-vis spectra of the resultant enzyme-containing fraction to that of the native protein; the difference between the two equated to the absorption profile associated with the sensitiser. Assuming an additive contribution from the individual components, it was possible to extrapolate the enzyme to sensitiser ratio and thus determine the extent of labelling per equivalent of PETNR.

The results of the initial reaction between equimolar quantities of enzyme and sensitiser indicated that the reaction had not gone to completion, with an appreciable quantity of unlabelled enzyme present in the sample. In an effort to maximise labelling yields, additional trials investigating the impact of increasing the concentration of the sensitiser in the reaction mixture were undertaken. The highest yields and most consistent results were obtained using between 3 and 4 equivalents of the sensitiser. At higher concentrations significant precipitation of the enzyme was observed, with minimal quantities of protein remaining in solution on completion of the reaction when using *ca.* 10 equivalents.

It was at this time that additional sites of labelling became evident, as at higher concentrations the resultant product was consistent with doubly labelled protein. On examination of the crystal structure of PETNR, the native cysteine residue C222 was identified as the potential site of additional labelling. As the residue is located near to the surface of the enzyme it is thought to be sufficiently accessible to allow for reaction with the sensitiser.

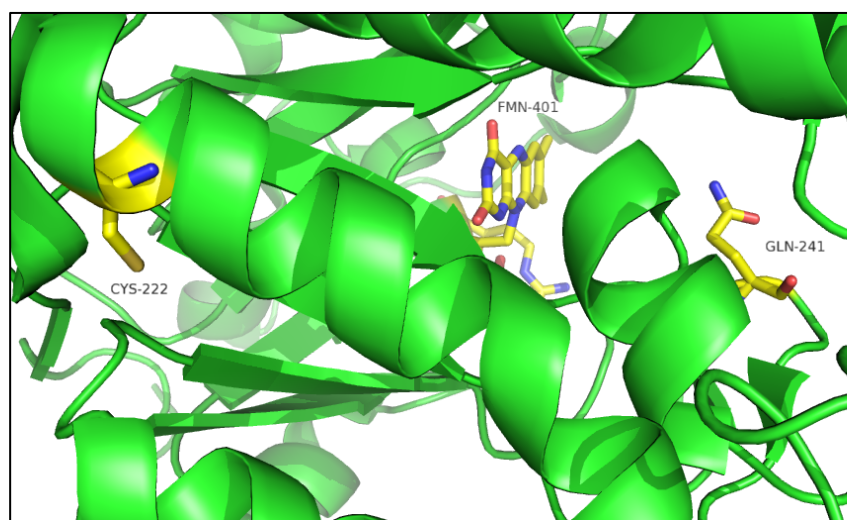


Fig. 5.8. *The x-ray crystal structure of PETNR, highlighting the relative positions of the C222 residue and the enzyme bound FMN of the active site. The image was generated in MacPyMol. The main chain is represented as a cartoon with the flavin cofactor and residues of interest shown as coloured sticks. (PDB code 1H50).*

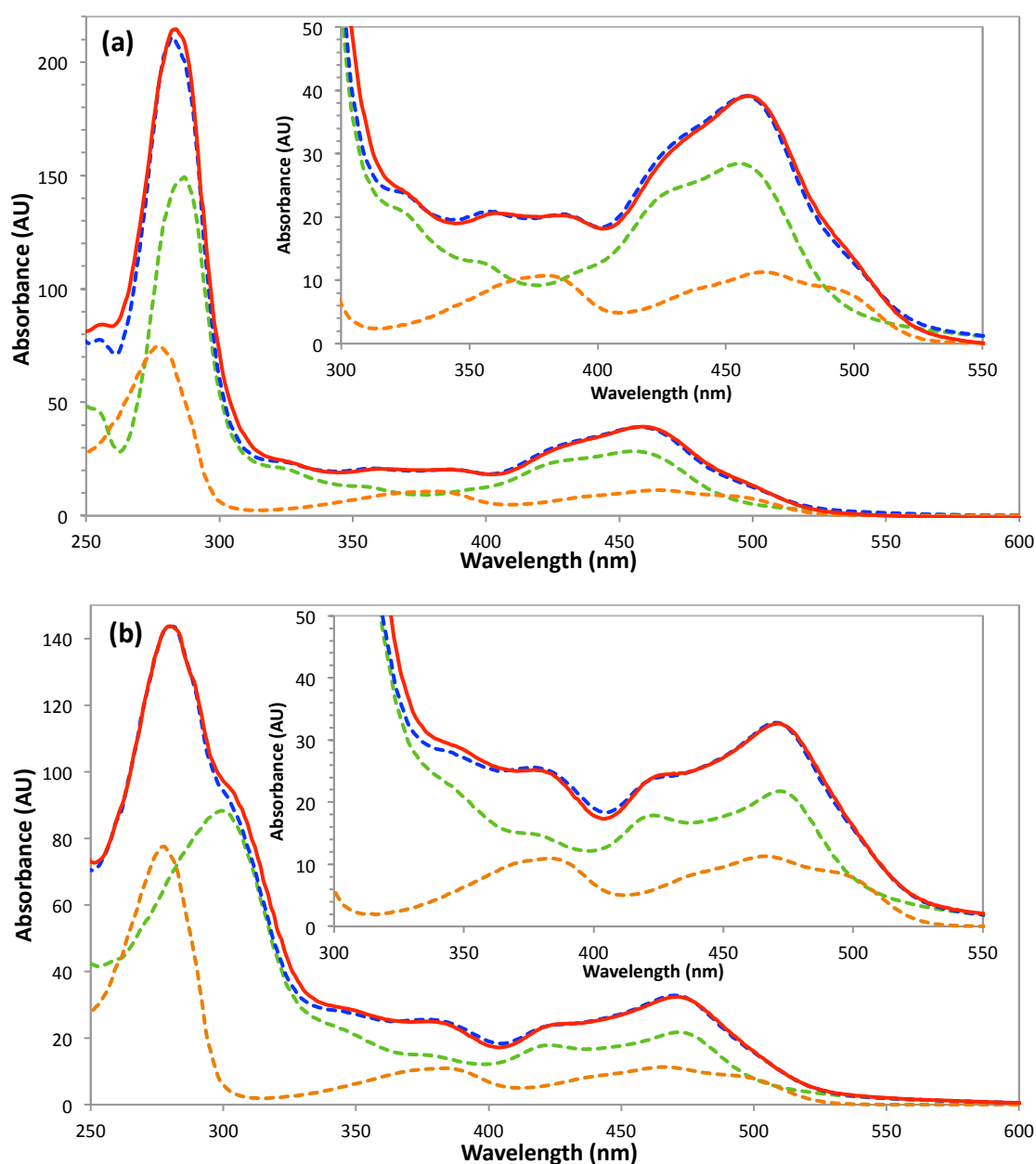


Fig. 5.9. UV-visible absorption spectra of the photosensitiser-PETNR_{Q241C} constructs using the labelling reagents **(a)** $[\text{Ru}(\text{bpy})_2(4\text{-hydroxymethyl-4'-methyl-2,2'-bipyridine})]^{2+}$ or **(b)** $[\text{Ru}(\text{bpz})_2(4\text{-hydroxymethyl-4'-methyl-2,2'-bipyridine})]^{2+}$. Illustrating the spectra of Ru-PETNR (red), PETNR_{Q241C} (orange), sensitiser (green) and the predicted spectra for Ru-PETNR calculated on addition of the individual components (blue). Calculated spectra were extrapolated from known extinction coefficient values for each of the individual components.

The site is spatially distant from the FMN cofactor and resides on the opposite side of the enzyme in relation to the active site. Considering its location it is surmised that should labelling occur, the bound sensitiser would be unable to contribute towards catalytic turnover of the enzyme.

With considerations of enzyme stability, studies into the effects of varying the temperature of the labelling reactions were also undertaken. Reactions performed at 4°C consistently gave poorer yields than those carried out at room temperature. Alternatively, it

had previously been demonstrated that upon employing slightly elevated temperatures it is possible to minimise the duration of the coupling reactions. However, those performed at 37°C over 3 – 4 h gave similarly poor results as those performed at 4°C. It is thought that at elevated temperatures, the hydrolysis of the α -bromomethyl group is sufficiently promoted to effectively compete with the coupling reaction.

Whilst reactions with the R324C variant also proceeded to give high yields of doubly labelled protein, attempts at labelling of the G301C mutant were far more inconsistent. On numerous instances, appreciable precipitation of the enzyme occurred over the 16 – 18 h time frame of the reaction. Whilst soluble labelled protein was obtained on a couple of occasions, this behaviour raised serious doubts concerning the stability of the construct, especially on consideration of the lower yields obtained for the enzyme itself upon expression. Due to these inconsistencies, this variant was not taken forward for biocatalytic trials.

The results obtained in labelling reactions of $[\text{Ru}(\text{bpz})_2(4\text{-bromomethyl-4'-methyl-2,2'-bipyridine})](\text{PF}_6)_2$ were comparable to those obtained for the bipyridyl analogue. However trials undertaken at approximately 4-5 equivalents of sensitiser indicated the possibility of triply labelled protein. Likewise during the control reactions performed using PETNR_{WT} , a ratio greater than 1:1 was observed, potentially indicating that the native enzyme was being labelled in more than one position.

Issues concerning precipitation were also encountered in the labelling studies using the $\{\text{Ru}(\text{bpz})_2[(\text{BrCH}_2\text{Ph})_2\text{qpy}]\}^{4+}$ sensitiser. Early in the reaction signs of complex precipitation became apparent, indicating poor solubility in aqueous solution that is most likely a consequence of the choice in counteranion. After further time had elapsed, signs of appreciable enzyme precipitation were also evident. Loss of protein could be minimised to a degree on using lower concentrations of sensitiser, although this inevitably gave poorer coupling yields. With the uncertainties pertaining to the selectivity of the reaction towards the incorporated cysteine over the native residues this was not an option that could be exploited. Attempts to improve the solubility of the complex on inclusion of increased concentrations of organic solvents further exacerbated the issues of protein precipitation.

It was initially thought that the sites of additional labelling might best be identified on obtaining x-ray crystal structures of the each of the labelled variants. Crystallisation studies were therefore undertaken in conjunction with enzymes labelled with the bipyridyl complex. Trials employed the sitting drop method that had been successfully used in previous crystallographic studies of PETNR . Solutions contained 1 M sodium acetate, 100 mM sodium cacodylate and various concentrations of PEG ($M_w = 3000$) and isopropyl alcohol, between 19 – 24 and 12 – 18 % respectively. Samples were incubated at 20°C for up to 30 days although in no instances was crystal growth observed. Additional trials were undertaken employing microseeding techniques from a seed stock created from the unlabelled wild-type enzyme. Again no evidence of crystallisation was noted, the samples instead yielding an amorphous precipitate. After multiple trials with similar results, further attempts were not pursued.

Consequently, the potential of mass spectroscopy as an alternate means of characterising these sensitiser-enzyme constructs was investigated. This technique proceeds via enzyme digestion and subsequent analysis and sequence determination of the resultant fragments. By comparison between unlabelled and labelled samples, the site of coupling can be determined by characteristic changes in mass. Unfortunately, at time of writing, further refinement of the experimental procedure is required before the technique can be successfully utilised in the analysis of construct of this type. As such, at present, no definitive assignment can be given for the sites of labelling, although from the consistently higher yields obtained for the coupling reactions of the prepared variants, it can be suggested that successful labelling of the incorporated cysteine residue has been achieved.

Once the additional sites have been identified, further optimisation of the coupling reaction may be undertaken. It has been suggested that multilabelled enzyme may be minimised upon reducing the number of equivalents of the labelling reagent however, a balance must be attained whereby the quantity of unlabelled protein is also minimised. The pH of solution has also been identified as an important factor, as in more basic conditions other residues are activated towards coupling; for example, at pH 10 – 10.5 lysine residues also readily undergo labelling.^[351]

5.2.3. Development of the photosynthetic system.

5.2.3.1. Diffusion controlled multicomponent systems

Initial trials of the diffusion controlled systems were undertaken in the presence of an electron transfer mediator, 1,1'-dimethyl-4,4'-bipyridinium dichloride, subsequently referred to as methyl viologen (MV^{2+}). This was chosen, as the compound has been extensively utilised in literature studies of both photosensitised electron transfer processes and the redox properties of a variety of biological systems. Previously unpublished work within the Scrutton group has also demonstrated that electrochemical generation of the singly reduced methyl viologen radical ($MV^{\cdot+}$) could be effectively used in the reduction of PETNR and subsequently biocatalytic turnover. Concerning the choice of photosensitiser, $[Ru(bpz)_2dClbpy]Cl_2$ was identified as the prime candidate to be used in initial studies, for two specific reasons. Firstly, both the ligand and complex could be prepared and isolated in good yields, more readily so than other compounds in the series. Secondly, the redox potentials of the complex represented an approximate mid-point value of those prepared at the time of undertaking these trials, thus it provided a good benchmark from which to begin the investigation. An aqueous solution of triethanolamine was used as the buffer solution in these reactions as it had been shown to act as an efficient sacrificial electron donor towards the photoexcited state of $[Ru(bpz)_3]Cl_2$.^[120]

5.2.3.1.1. Spectrophotometric Trials

In an effort to evaluate the viability of this approach, initial spectrophotometric trials were undertaken. This was possible as each of the individual components of the system show distinct absorption profiles in different redox states. Illumination of a sample containing $[Ru(bpz)_2dClbpy](Cl)_2$ (20 μM) and methyl viologen (0.5 mM) in the presence of triethanolamine (5 mM, pH 7), resulted in the rapid electron transfer to yield the reduced cationic radical of methyl viologen ($MV^{\cdot+}$). An accumulation of $MV^{\cdot+}$ was indicated as the solution developed a characteristic deep blue colour, which is associated with an increase in absorbance at 395 nm and 600 nm, Fig 5.10.A. Using known extinction coefficients, the concentration of $MV^{\cdot+}$ can be determined and the reaction monitored quantitatively. The radical persisted in solution for many minutes after illumination had ceased, though a slow reoxidation was noted overtime. On exposure to air, the deep blue colour was rapidly bleached indicating complete quenching of $MV^{\cdot+}$ by molecular oxygen. The rate of radical accumulation in a solution also containing PETNR (10 μM) was initially much slower and was accompanied by a decreasing absorbance at *ca.* 464 nm, Fig 5.10.B. The profile of the negative feature in the transient spectra was characteristic of the FMN cofactor of PETNR. After *ca.* 50 minutes of illumination no further decrease in absorbance was observed, it was also at this time that an increase in the rate of $MV^{\cdot+}$ formation was noted. This suggested that oxidised FMN had, up until that point, been acting as a quencher towards $MV^{\cdot+}$. Upon complete reduction of the enzyme the rate of $MV^{\cdot+}$ formation was no longer hindered by the effects of said quenching, thus explaining the concomitant increasing concentration of the radical.

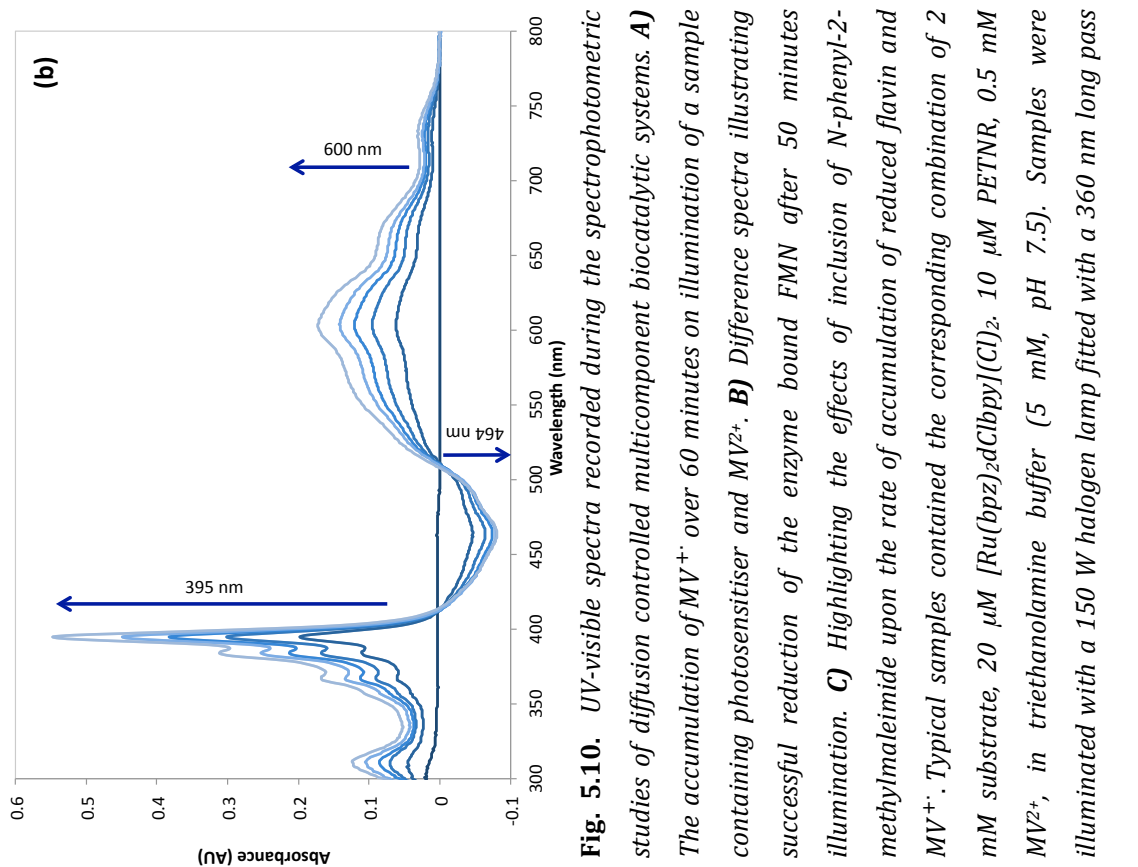


Fig. 5.10. UV-visible spectra recorded during the spectrophotometric studies of diffusion controlled multicomponent biocatalytic systems. **A)** The accumulation of MV^{2+} over 60 minutes on illumination of a sample containing photosensitizer and MV^{2+} . **B)** Difference spectra illustrating successful reduction of the enzyme bound FMN after 50 minutes illumination. **C)** Highlighting the effects of inclusion of N-phenyl-2-methylmaleimide upon the rate of accumulation of reduced flavin and MV^{2+} . Typical samples contained the corresponding combination of 2 mM substrate, 20 μM $[Ru(bpz)_2dCbpy](Cl)_2$, 10 μM PETNR, 0.5 mM MV^{2+} , in triethanolamine buffer (5 mM, pH 7.5). Samples were illuminated with a 150 W halogen lamp fitted with a 360 nm long pass

Inclusion of the substrate *N*-phenyl-2-methylmaleimide in solution further diminished the rate of accumulation of both MV^{+} and the reduced flavin cofactor, Fig. 5.10.C. The initial rate of change in absorption, measured after 10 minutes, was approximately half that seen for the substrate free assays. On further scans it was evident that both of the reduced species were being consumed at a more rapid rate as a gradual decrease in the associated absorption was observed until a steady state was reached after *ca.* 2 hours. The sample was illuminated for a further four hours with minimal changes to the transient spectra. Additional features at 316 and 345 nm were also observed, although the origins of these changes are unknown. Control samples lacking the presence of enzyme displayed MV^{+} formation of a rate similar to that in the absence of both PETNR and the substrate, indicating the reduced rate of MV^{+} accumulation was not a consequence of direct quenching by the substrate. These results suggest that successful electron transfer was achieved in the sequence of: photosensitiser \rightarrow MV^{2+} \rightarrow FMN \rightarrow substrate, thus resulting in catalytic turnover.

The initial aim had been to monitor catalytic activity spectrophotometrically. This was to gain insight into the ideal reaction conditions on directly monitoring the rate of substrate consumption/product formation via characteristic changes in the UV-visible absorption profiles associated with the compounds. However, it quickly became apparent from the control reactions that such a technique would be unusable with the current system due to the nature of the individual components employed. Typical substrates to be used in these assays exhibit high extinction coefficients primarily in the 200 – 300 nm region of the spectrum. Unfortunately this region is dominated by the $\pi - \pi^*$ transitions of the methyl viologen and the photosensitiser, the former displaying a single broad peak at 257 nm whilst the latter varies significantly depending upon the incorporated ligands. Additionally both of these components show appreciable fluctuations as a result of the formation of intermediary species during the reaction. This is exemplified by the decrease in absorption associated with methyl viologen consumption on reduction to the cationic radical. The use of triethanolamine as the sacrificial donor is fortuitous as this shows minimal absorption in the region of interest, although other donors such as aniline would exacerbate the situation further. Whilst it would be possible to monitor substrate consumption for particular compounds, doing so quantitatively would be problematic.

5.2.3.1.2. Light-driven Biocatalytic Trials

The initial assays and subsequent optimisation studies focused upon the bioreduction of 2-cyclohexen-1-one to yield the corresponding saturated cyclic ketone. 2-cyclohexenone has proven to be a good substrate for both enzymes of interest and has demonstrated a high stability in aqueous solution. In addition, both it and the product are widely commercially available thus allowing for extensive trials to be undertaken. In an effort to optimise the reaction conditions, the effects of changing the identity and/or concentrations of the individual components of the system were investigated. As such the standard reaction conditions were

slightly modified in comparison to those employed in the spectrophotometric assays. This was done so that the new conditions represented a midpoint between the two extremes to which the variables were to be altered. A standard reaction mixture was comprised of substrate (5 mM), enzyme (10 μ M), photosensitiser (20 μ M) and methyl viologen (0.1 mM) in a triethanolamine buffer (25 mM, pH 8.0) at a total volume of 3.5 mL and containing 5% ethanol to solubilise the substrate. Samples were illuminated with a 150 W halogen lamp fitted with a 360 nm long-pass filter to minimise direct photochemical reactions of the substrate and/or mediator.

5.2.3.1.2.1. Enzyme systems

With the aim of determining the relative activity of the respective systems, the first series of assays to be undertaken were those involving the different enzymes of interest to this study. The trials originally focused upon TOYE and PETNR_{WT} exclusively, though were later expanded to include the three PETNR variants that had been prepared. The latter were performed in an effort to establish a benchmark for subsequent biocatalytic trials of the covalently bound photosensitiser-enzyme constructs. The rates of reduction by TOYE were consistently greater than those of PETNR_{WT}, although the PETNR_{R324C} variant displayed enhanced activity compared to that of the native enzyme and the other mutants, Table 5.4.

Table 5.4. Comparison of the relative activities obtained for a number of OYEs towards the light-driven bioreduction of 2-cyclohexenone.

Enzyme	TOF [h ⁻¹] ^[a]	Conv. ^[b] [%]	Yield ^[b] [%]
TOYE	121.5	100	>99
PETNR	100.4	91	89
PETNR _{Q241C}	80.8	79	78
PETNR _{G301C}	81.1	88	85
PETNR _{R324C}	137.4	100	>99

^[a]Determined after 120 mins. ^[b] Conversions and yields determined by GC analysis from a calibration curve of known standards of the substrate/product and corrected using limonene as an internal standard. Calculated after 240 mins.

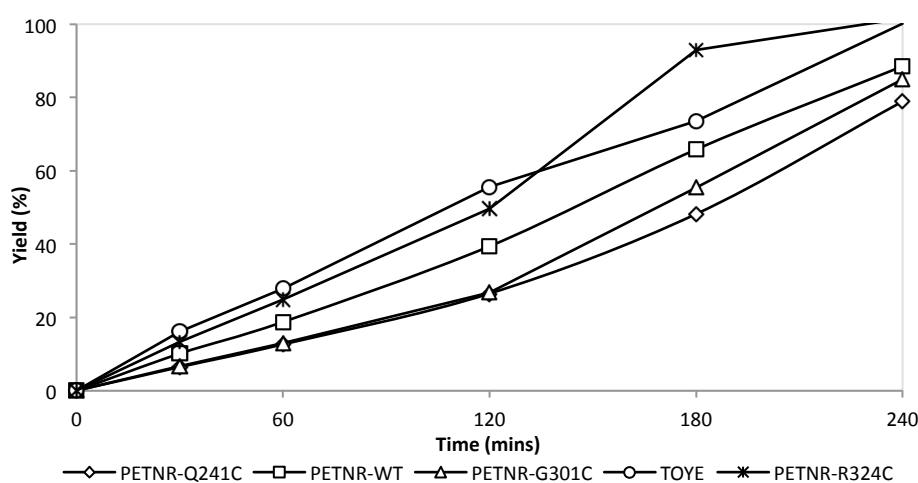


Fig. 5.11. Time course of the bioreduction of 2-cyclohexenone by a number of OYEs in conjunction with a light-driven biocatalytic system.

TOYE has been shown to have a relatively large active site in comparison to other OYEs. This is also true for the homologous YqjM and is one of the rationales provided regarding the utilisation of this enzyme in the light-driven biocatalytic systems discussed in section 1.4.3. Examination of the crystallographic data of PETNR_{WT} reveals a considerably smaller active site with the subsequently generated structures for the Q241C and G301C variants displaying minimal changes in the surface dimensions of the enzyme. Mutation of the R324 residue however results in a marked difference in the accessibility of the active site. Exchange of the comparatively large side chain of arginine with that of the thiol group of cysteine, affords a significant reduction in the steric bulk about the xylene ring of FMN. This essentially results in the formation of a new channel towards the cofactor, lying approximately perpendicular to the site of substrate binding. Such an arrangement is expected to be ideal, as effective interactions between the mediator and the cofactor may occur without hindering or being hindered by substrate binding, thus allowing for efficient electron transfer. It is unclear

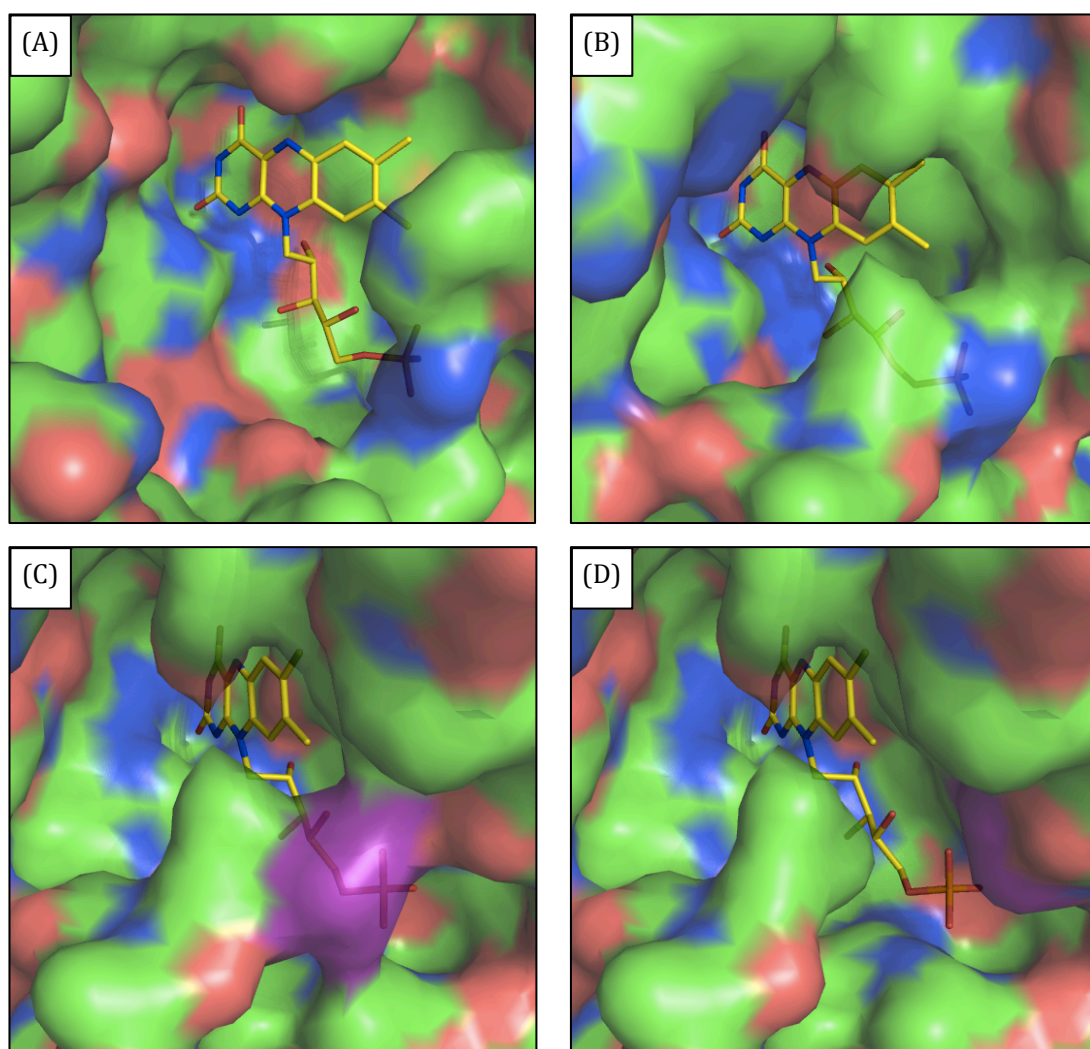
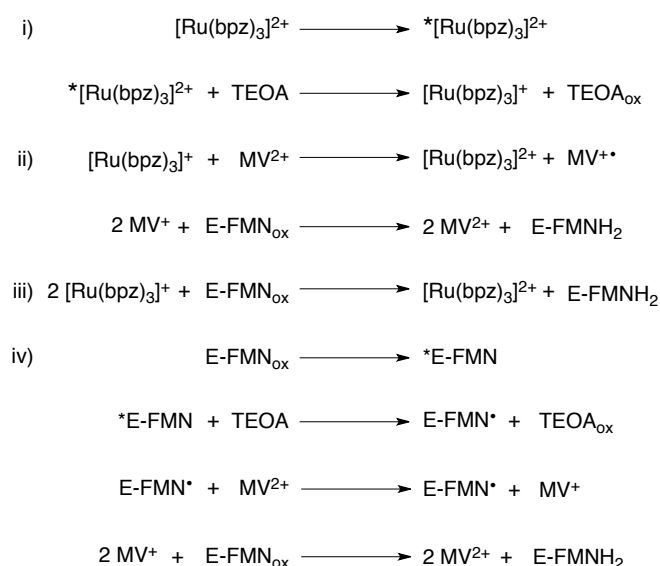


Fig. 5.12. Crystal structures of (A) TOYE (PDB code: 3KRU) and (B) PETNR (PDB code 1H50) focused upon the active site. (C) side view of the PETNR active site (D) R324C mutant 324 residue highlighted in purple All images and structural mutations generated using MacPyMOL.

whether the increased rates are solely a consequence of lowered steric hindrance as the side chain of arginine has a pK_a of 12.48 and remains positively charged even at elevated pH. This is expected to cause unfavourable electrostatic interactions with the positively charged viologen that may have acted towards perturbing electron transfer from the mediator.

5.2.3.1.2.2. Control Assays

To determine the sequence of electron transfer through the system, additional control reactions were undertaken in the absence of individual components. Non-illuminated reactions showed minimal to no catalytic turnover, the small quantity of product that was observed in some cases was attributed to illumination during sample preparation. Despite putting numerous counter measures in place to minimise unwanted light exposure, it could not be eliminated completely due to procedural limitations. No accumulation of the product was noted beyond this initial stage, indicating no catalytic turnover in the absence of light. On exclusion of the enzyme from the reaction mixture, no product formation was observed, although a slight decrease in substrate concentration, less than 5 % over 4h, indicated a potential minor side reaction. Further control assays for PETNR_{R324C} demonstrated minimal



Scheme 5.6. *Electron transfer processes that are proposed to contribute towards enzyme reduction, and ultimately total catalytic turnover, in the light-driven catalytic cycles of PETNR and TOYE. i) Photoexcitation of the ruthenium complex and subsequent reductive quenching of the excited state by triethanolamine. ii) Oxidation of the reduced complex on electron transfer to methyl viologen to yield the cationic radical, $\text{MV}^{\bullet+}$. The enzyme bound flavin is reduced to the dihydroquinone form via two successive single electron transfer steps from two viologen donors and proton abstraction from the solvent. iii) Direct electron transfer from the reduced photosensitiser to FMN. iv) Photoexcitation of the enzyme bound FMN and subsequent reductive quenching of the excited triplet state by TEOA. The unstable singly reduced form then undergoes rapid electron transfer to yield the oxidised flavin and $\text{MV}^{\bullet+}$. On sufficient accumulation of the reduced mediator, two sequential electron transfer steps proceed to afford the fully reduced cofactor.*

catalytic turnover upon exclusion of either the photosensitiser or the electron transfer mediator, which afforded cyclohexanone yields of *ca.* 4 % and <1 % respectively. Experiments of TOYE showed that similar catalytic turnover was achieved in the absence of MV²⁺, with slightly enhanced yields of *ca.* 8 %. These results suggest that direct electron transfer from the photosensitiser to the enzyme bound cofactor is possible, although flavin reduction occurs at a much slower rate. Unlike PETNR, similar activity was also observed in assays containing both the mediator and enzyme to yield cyclohexanone in 11 % yields. On consideration of the absorption profile of MV²⁺ and the lack of any appreciable absorbance at wavelengths longer than 300 nm, the fact that photocatalytic turnover is observed in the absence of a photosensitiser was initially somewhat surprising. It has been previously demonstrated that flavins may act as sensitisers in the photoreduction of methyl viologen,^[352] it is therefore surmised that catalytic turnover may, in this instance, be a consequence of MV⁺ formation on electron transfer from FMN. The increased activity of those assays using TOYE is primarily attributed to the increased accessibility of the active site and the subsequent variations this affords in the interactions of the cofactor with the various potential electron donors. There is also potential for additional interactions in TOYE that result from the enzyme adopting multiple oligomeric states in solution. The relatively poor rates that were achieved in these side reactions, confirms that the predominant electron transfer chain is that which was proposed in section 5.2.3.1.1 and is presented schematically in scheme 5.6.i. and 5.6.ii.

5.2.3.1.2.3. Photosensitisers

The influence of the photosensitiser was investigated on utilisation of a number of the prepared complexes. The sensitisers were selected to encompass a broad range of reduction potentials with the aim of determining optimal properties. The ruthenium complexes studied were [Ru(bpz)₂L]²⁺, where L = dNH₂bpy, d^tBubpy, dClbpy and bpz, in addition to [Ru(bpz)₂(Me₂qpy)]⁴⁺ and [Ru(bpy)(Me₂bpy)₂]⁶⁺. Of the iridium compounds [Ir(22)₂bpy]³⁺ and [Ir(32)₂dCF₃bpy]³⁺ were chosen to represent each of the two distinct series of the bipyridinium complexes. The latter was chosen as this was the only one of the 1-methyl-3-(2'-pyridyl)pyridinium complexes that exhibited a fully reversible first reduction process. Additional experiments were also undertaken using [Ru(bpy)₃]Cl₂ as a control standard as this is a photosensitiser that is typically used in systems similar to those discussed in section 1.

Comparisons of rates for the ruthenium complexes indicate a direct correlation to changes in the potential of the Ru^(II/III) couple, Fig. 5.13.B. The trend signified an increasing rate of catalytic turnover upon an anodic shift in the potential of the oxidative process. This may be attributed to a related anodic shift in the Ru^(*II/I) couple, which is a consequence of a stabilisation of the metal-based HOMO and the subsequent impact this has upon the properties of the excited state via changes in the HOMO-LUMO energy gap. It is expected that upon increasing the oxidising ability of the excited sensitiser that the rate of formation of the primary donor would likewise increase owing to improved reductive quenching by TEOA.

Table 5.5. *Influence of modifications made to the photosensitiser upon the activity of light driven biocatalytic systems in the reduction of 2-cyclohexenone by PETNR and TOYE.*

Photosensitiser	Enzyme	TOF. ^[a]	Conv. ^[b] [%]	Yield ^[b] [%]
[Ru(bpy) ₃] ²⁺	TOYE	25	23	16
	PETNR _{R324C}	-	5	0
[Ru(bpz) ₃] ²⁺	TOYE	235*	100	93
	PETNR _{R324C}	255*	100	95
[Ru(bpz) ₂ dNH ₂ bpy] ²⁺	TOYE	30	24	16
	PETNR _{R324C}	-	3	0
[Ru(bpz) ₂ d ^t Bubpy] ²⁺	TOYE	50	47	42
	PETNR _{R324C}	45	66	64
[Ru(bpz) ₂ dClbpy] ²⁺	TOYE	125	100	>99
	PETNR _{R324C}	135	100	>99
[Ru(bpz) ₂ (Me ₂ qpy)] ²⁺	TOYE	235*	100	>99
	PETNR _{R324C}	275*	100	>99
[Ru(bpy)(Me ₂ qpy) ₂] ²⁺	TOYE	85	66	64
	PETNR _{R324C}	95	76	69
[Ir(22) ₂ bpy] ³⁺	TOYE	120	100	>99
	PETNR _{R324C}	100	100	97
[Ir(32) ₂ dCF ₃ bpy] ³⁺	TOYE	-	5	0
	PETNR _{R324C}	-	4	0

^[a]Determined after 120 mins. * Determined after 60 minutes. ^[b] Conversions and yields determined by GC analysis from a calibration curve of known standards of the substrate/product and corrected using limonene as an internal standard. Calculated after 240 mins.

Due to the relative differences in redox potentials, the electron transfer processes of [Ru(bpy)₃]²⁺ are expected to proceed via an initial oxidative quenching by MV²⁺. The previously reported quantum yields of MV⁺ formation are relatively low in comparison to the bipyrazyl analogue and have been attributed to back electron transfer to the oxidised complex. Considering the redox potential of [Ru(bpz)₂dNH₂bpy]²⁺, a similar mechanism is surmised to be in effect, thus explaining the ineffectiveness of this sensitiser. Considering the complete lack of activity in the systems of both of these sensitisers with PETNR, it is thought that the observed turnover achieved with TOYE may be a result of the alternate electron transfer pathways discussed in section 5.2.3.1.2.2.

As is evident by the enhanced activity for the complexes containing the quaternised quaterpyridinium ligands, factors other than the potential of the Ru(II/III) couple contribute towards the overall activity of the sensitiser. Regarding the complexes of quaterpyridinium, two properties have been identified as potential reasons for this enhancement. The first is the ease with which the quaterpyridinium group is reduced and the resultant charge separation that is afforded in the excited state. The second is a consequence of the relative difference in the absorption profiles of the various complexes. Both [Ru(bpz)₂(Me₂qpy)]⁴⁺ and [Ru(bpy)(Me₂qpy)₂]⁶⁺ exhibit MLCT bands of significantly larger ϵ values compared to those of the ruthenium complexes of the unquaternised ancillary ligands, the increased activity may therefore be attributed to an increase in the efficiency of energy absorption by the sensitiser.

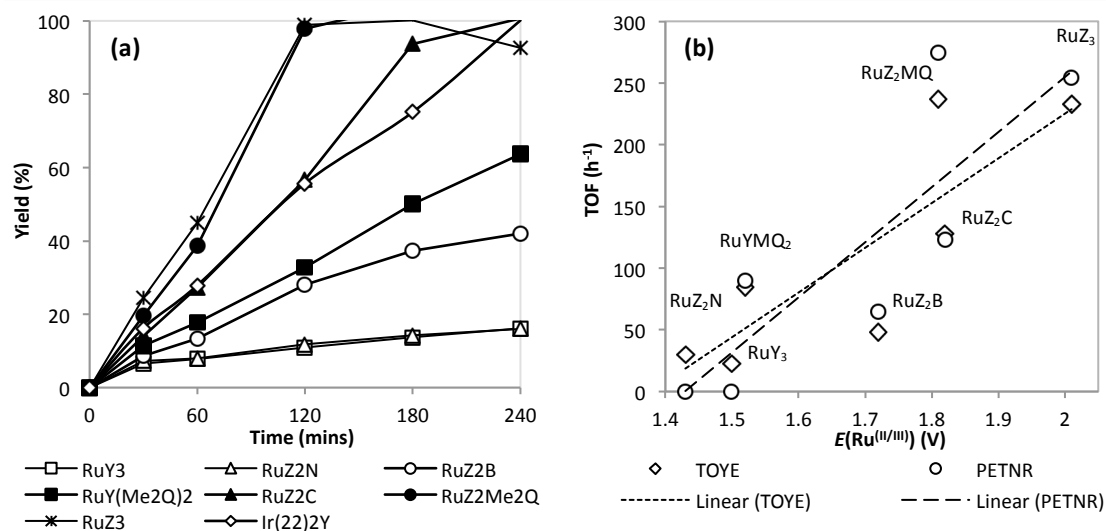


Fig. 5.13. (a) Time course illustrating the influence of changes in photosensitiser upon the bioreduction of 2-cyclohexenone by TOYE. **(b)** Plot of redox potentials of the Ru(II/III) couple vs TOF values obtained in the assays of both PETNR and TOYE. Where Y = bpy, Z = bpz, B = d^tBubpy, C = dClbpy, MeQ = [Me₂qpy]²⁺ and N = dNH₂bpy.

For the sensitisers displaying the highest activity it was noted that a degree of product decomposition may be evident on extended illumination after completion of the reaction. For example, in the assays of [Ru(bpz)₃]²⁺ a reduction of ca. 5-8 % in product yields was observed over the two hours after complete conversion of the substrate. This may be a consequence of the increased oxidising ability of these complexes or due to exposure of the product to high concentrations of MV⁺ for extended periods of time that may allow for unwanted side reactions to occur.

Whilst the process of electron transfer for the complexes of ruthenium is well established, the precise mechanism involved for the systems containing an iridium sensitiser remains unclear. In previous studies concerning photoinduced hydrogen production utilising cyclometalated iridium(III) complexes in conjunction with [Co(bpy)₃]²⁺ as an electron relay, a definitive mechanism of electron transfer could not be determined.^[226] Using TEOA as a sacrificial donor, it remained unclear whether the initial reaction of the excited sensitiser was that of oxidative quenching by [Co(bpy)₃]²⁺ or reductive quenching by TEOA. On consideration of the redox potentials of both the oxidative and reductive processes of [Ir(22)₂bpy]³⁺ and the nature of the cyclometalating ligand, it is proposed that, for the reactions described here, transfer occurs via a route analogous to the bis(2,2'-bipyrazyl)ruthenium(II) complexes. Regarding the reactions of [Ir(32)₂dCF₃bpy]³⁺ a significant degree of uncertainty remains, especially considering the inactivity of the species in the current system. Again it would be expected that the reaction predominately proceed via reductive quenching of the sensitiser, with the additional electron of the reduced state localised about the dCF₃bpy ancillary ligand. The scenario becomes more complicated when considering the related complexes of bpy and d^tBubpy as the first reduction potential is cathodically shifted by ca. 0.3-0.4 V. It is currently unknown whether the lack of activity of these complexes is due to unfavourable redox

potentials, an instability of the complex in the excited state or due to poor absorbance of the species within the region of the spectrum that is being illuminated.

5.2.3.1.2.4. Photosensitiser Concentration

Results for both PETNR and TOYE show a definitive increase in catalytic activity with increasing sensitiser concentration. In the presence of an excess of sacrificial donor and methyl viologen, it stands to reason that $MV^{+•}$ formation, and ultimately catalytic activity, be dependent upon the concentration of the photosensitiser and subsequently the primary donor of the system; the latter being the excited or singly reduced form of the complex, as dictated by the mechanism of electron transfer.

At high sensitiser concentrations an accumulation of $MV^{+•}$ rapidly occurred as the solution developed a dark blue-green colour within minutes of commencing illumination; the green tint is a result of the increased colouring of the solution owing to the ruthenium complex. This suggests that the rate of electron transfer to MV^{2+} is sufficient to generate a

Table 5.6. *Impact of changing photosensitiser concentration upon the rates of light driven biocatalytic reduction of 2-cyclohexenone by PETNR and TOYE.*

Enzyme	[PS] (μ M)	TOF ^[a]	Conv. ^[b] [%]	Yield ^[b] [%]
TOYE	5	85	86	85
	20	130	100	>99
	50	340	100	97
	100	360	100	>99
PETNR	5	45	39	37
	20	125	100	>99
	35	170	100	>99
	50	230	100	97

^[a]Determined after 120 mins. * Determined after 60 minutes. ^[b] Conversions and yields determined by GC analysis from a calibration curve of known standards of the substrate/product and corrected using limonene as an internal standard. Calculated after 240 mins.

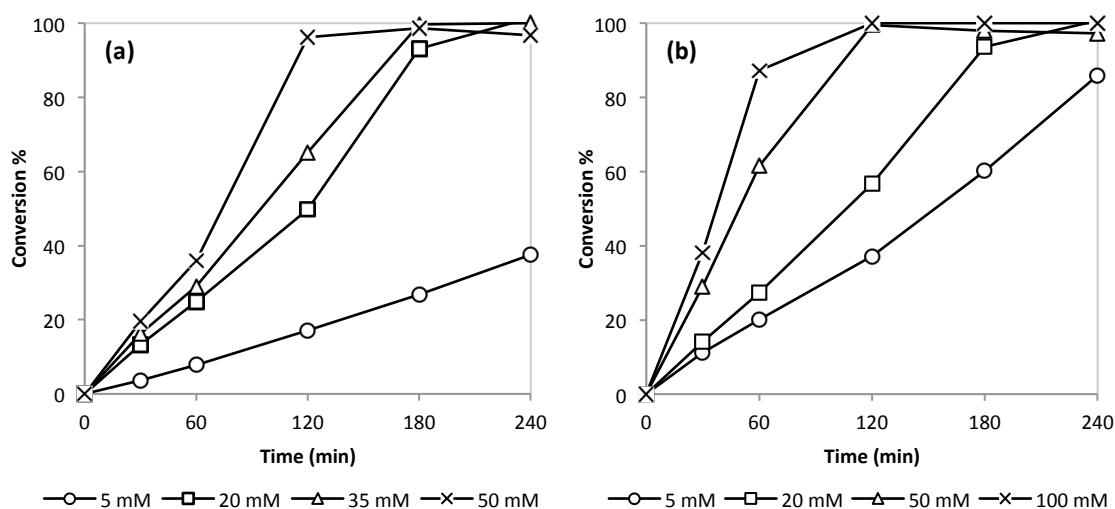


Fig. 5.14. *Time course indicating the influence of photosensitiser concentration upon the light-driven biocatalytic reduction of 2-cyclohexen-1-one by (a) PETNR and (b) TOYE.*

significant excess of the reduced mediator very early in the time course of the reaction. It is therefore surmised that, at these sensitiser concentrations, the rate of catalytic turnover is no longer limited by the rate of MV^{+} formation but is instead limited by the rate of electron transfer from the mediator to the enzyme bound FMN or due to the activity of the substrate itself. This is supported on consideration of the comparable TOFs obtained in the assays of TOYE at sensitiser concentrations of 50 and 100 μ M. It is expected that at higher sensitiser concentrations the rate of MV^{+} formation may also show a greater dependence upon other factors within the system, such as the concentration of MV^{2+} and the sacrificial electron donor.

5.2.3.1.2.5. Sacrificial Electron Donor Concentration

The influence of the sacrificial electron donor upon the system was investigated through a series of experiments containing varying initial concentrations of triethanolamine. The rates of reduction for systems of both $[Ru(bpz)_2dClbpy]^{2+}$ and $[Ir(22)_2bpy]^{3+}$ exhibited a distinct dependency upon the concentration of the donor; an increase in activity correlating to an increase in the concentration of TEOA. These results are consistent with the proposed mechanism that dictates that turnover be limited by the generation of the reduced sensitiser, which is dependent upon the bimolecular reaction between the excited sensitiser and TEOA. At low concentrations of the donor it is thought that activity may be further perturbed, as there is an increased probability that the excited sensitiser be reductively quenched by MV^{+} instead of TEOA, thus establishing a catalytically inactive cyclic transport chain within the system. The conclusions described here are contrary to those made in the study of the flavin sensitised light-driven systems of PAMO-P3 and YqjM, which both exhibited initial rates that were independent of donor concentration.^[108, 115] This difference in behaviour is surmised to be a consequence of the high FMN concentrations used in said assays and of the proposed electron transfer mechanism by which reduction of the flavin is achieved. EDTA concentration

Table 5.7. *Influence of changes in sacrificial electron donor concentrations upon the rates of light driven biocatalytic reduction of 2-cyclohexenone by PETNR and TOYE.*

[TEOA] [mM]	Enzyme	Photosensitiser	TOF ^[a]	Conv. ^[b] [%]	Yield ^[b] [%]
5	TOYE	$[Ru(bpz)_2dClbpy]^{2+}$	45	28	25
	PETNR	$[Ru(bpz)_2dClbpy]^{2+}$	45	36	34
	PETNR	$[Ir(22)_2bpy]^{3+}$	60	37	31
10	TOYE	$[Ru(bpz)_2dClbpy]^{2+}$	80	52	52
	PETNR	$[Ru(bpz)_2dClbpy]^{2+}$	80	70	65
	PETNR	$[Ir(22)_2bpy]^{3+}$	75	51	51
25	TOYE	$[Ru(bpz)_2dClbpy]^{2+}$	120	100	>99
	PETNR	$[Ru(bpz)_2dClbpy]^{2+}$	125	100	>99
	PETNR	$[Ir(22)_2bpy]^{3+}$	100	100	97
50	TOYE	$[Ru(bpz)_2dClbpy]^{2+}$	210	100	98
	PETNR	$[Ru(bpz)_2dClbpy]^{2+}$	230	100	>99
	PETNR	$[Ir(22)_2bpy]^{3+}$	190	100	>99

^[a]Determined after 120 mins. * Determined after 60 minutes. ^[b] Conversions and yields determined by GC analysis from a calibration curve of known standards of the substrate/product and corrected using limonene as an internal standard. Calculated after 240 mins.

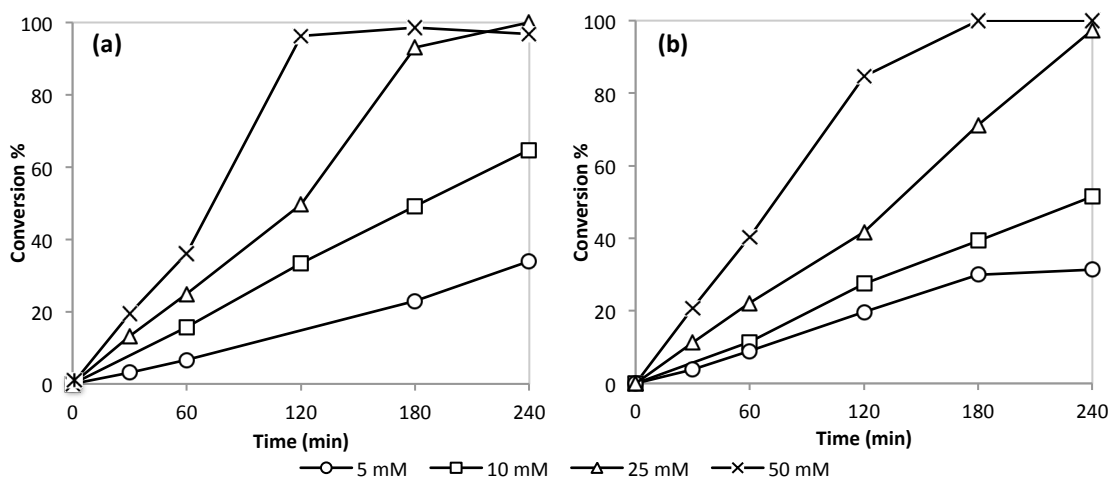


Fig. 5.15. Time course highlighting the impact of the concentration of TEOA in the light-driven PETNR catalysed reduction of 2-cyclohexen-1-one using (a) $[Ru(bpz)_2dClbpy]Cl_2$ and (b) $[Ir(22)zbpy]Cl_3$ as photosensitisers.

did however influence overall substrate conversion and was attributed to a complete consumption of the effective form of the donor prior to completion of the enzyme-catalysed reaction. Whilst comparable observations have not been made as part of this study it is expected that had the reaction time been extended, similar issues would have been encountered. It is thought that the rate of photosensitiser turnover at the donor concentrations that these issues become apparent is sufficiently slow so as the point of complete TEOA consumption is outside the 4-6 h time frame of these investigations. As such this is a factor that should be taken into consideration in any future studies.

5.2.3.1.2.6. pH Dependence

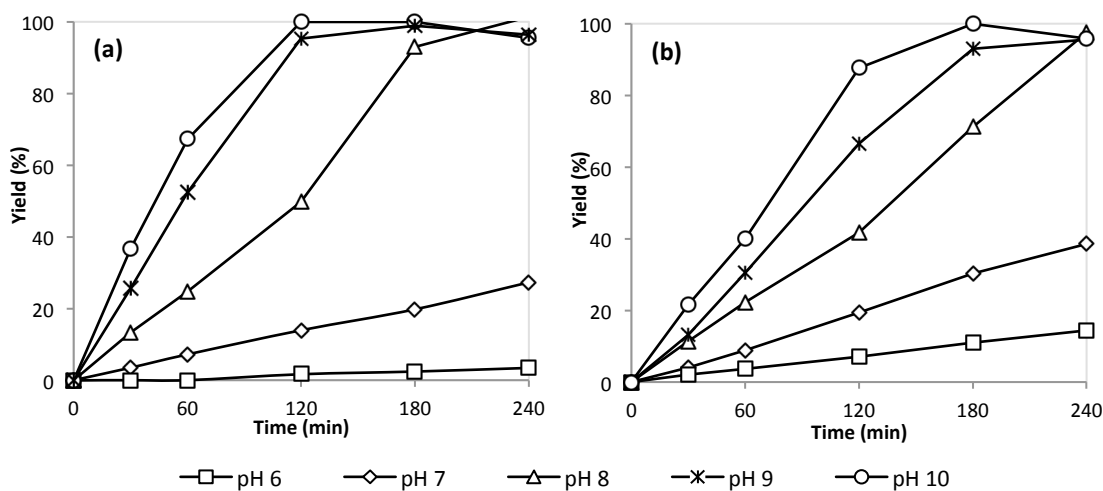
The impact of pH upon the activity of the system was investigated by employing TEOA buffer solutions in the range of pH 6.0 to 10.0. Whilst activity was demonstrated in all instances, a general decrease in product formation was associated with increasing acidity. As has previously been reported, the NAD(P)H driven reactions of PETNR demonstrate a broad pH activity profile, although a decrease in conversion rates was observed at pH < 7.^[335] On acidifying the solution beyond pH 6, activity is shown to be almost completely perturbed owing to the protonation of the imidazole ring of two key histidine residues that are involved in substrate binding.

In the present system, were enzyme deactivation the sole contributor to the poor performance at low pH, an accumulation of MV^{+} would be expected to occur due to perturbation of oxidative quenching by FMN. However, no appreciable concentration of MV^{+} was formed at any point during the assays performed at pH 6 and 7. This pH dependency may instead be attributed to the protonation of triethanolamine and subsequent changes in the concentration of the effective form of the sacrificial donor. As the pH decreases, the equilibrium shifts in favour of the protonated species which, as a consequence of changes in the reduction potential of the (TEOA/TEOA⁺) couple, is essentially ineffective as an electron

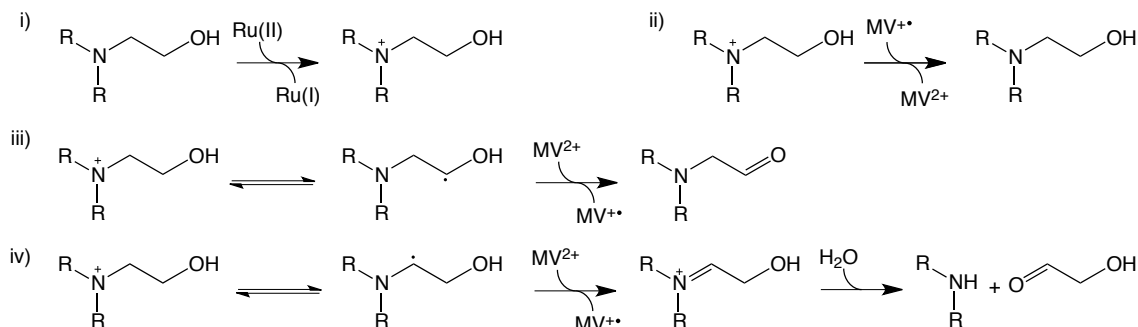
Table 5.8. pH dependency of the light driven biocatalytic reduction of 2-cyclohexenone by PETNR and TOYE.

pH	Enzyme	Photosensitiser	TOF. ^[a]	Conv. ^[b] [%]	Yield ^[b] [%]
6	TOYE	[Ru(bpz) ₂ dClbpy] ²⁺	10	10	10
	TOYE	[Ir(22) ₂ bpy] ³⁺	50	38	34
	PETNR _{R324C}	[Ru(bpz) ₂ dClbpy] ²⁺	5	4	3
	PETNR _{R324C}	[Ir(22) ₂ bpy] ³⁺	15	16	14
7	TOYE	[Ru(bpz) ₂ dClbpy] ²⁺	55	54	52
	TOYE	[Ir(22) ₂ bpy] ³⁺	70	74	73
	PETNR _{R324C}	[Ru(bpz) ₂ dClbpy] ²⁺	30	27	27
	PETNR _{R324C}	[Ir(22) ₂ bpy] ³⁺	40	39	38
8	TOYE	[Ru(bpz) ₂ dClbpy] ²⁺	130	100	>99
	TOYE	[Ir(22) ₂ bpy] ³⁺	125	100	>99
	PETNR _{R324C}	[Ru(bpz) ₂ dClbpy] ²⁺	125	100	>99
	PETNR _{R324C}	[Ir(22) ₂ bpy] ³⁺	100	100	97
9	TOYE	[Ru(bpz) ₂ dClbpy] ²⁺	250	100	>99
	TOYE	[Ir(22) ₂ bpy] ³⁺	155	100	96
	PETNR _{R324C}	[Ru(bpz) ₂ dClbpy] ²⁺	275	100	>99
	PETNR _{R324C}	[Ir(22) ₂ bpy] ³⁺	140	100	>99
10	TOYE	[Ru(bpz) ₂ dClbpy] ²⁺	290	100	98
	TOYE	[Ir(22) ₂ bpy] ³⁺	145	100	97
	PETNR _{R324C}	[Ru(bpz) ₂ dClbpy] ²⁺	210	100	96
	PETNR _{R324C}	[Ir(22) ₂ bpy] ³⁺	180	100	96

^[a]Determined after 120 mins. * Determined after 60 minutes. ^[b] Conversions and yields determined by GC analysis from a calibration curve of known standards of the substrate/product and corrected using limonene as an internal standard. Calculated after 240 mins.

**Fig. 5.16.** Time course indicating the influence of pH upon the light-driven PETNR catalysed reduction of 2-cyclohexen-1-one using (a) [Ru(bpz)₂dClbpy]Cl₂ and (b) [Ir(22)₂bpy]Cl₃.

donor towards the excited photosensitiser. The TEOA cation, formed on reductive quenching of the excited state complex, is also subject to an acid-base equilibrium in solution. At low pH the cationic form persists and may act as an oxidant towards MV^{•+}, thus perturbing the forward electron transfer within the catalytic cycle. Under basic conditions the cation is deprotonated to yield a neutral radical with the unpaired electron localised about the α -carbon of the amino or hydroxyl groups. The MV^{•+} reoxidation mechanism is effectively



Scheme 5.7. Reactions of the sacrificial electron donor in photosensitised assays also containing MV^{2+} as a transfer mediator. i) Reductive quenching of the excited photosensitiser leads to the formation of the TEOA cation; ii) reoxidation of the $MV^{\bullet+}$ by the resultant cationic species which persists in solution at low pH; iii) the acid-base equilibria of the TEOA cation to yield the α -hydroxyl radical and subsequent reduction of MV^{2+} ; iv) formation of the α -amino radical which is oxidised by MV^{2+} to yield the cationic immonium species which undergoes decomposition to give the respective amine and glycol aldehyde.

owing to the increased electron density of the species. The radical itself is an efficient reducing agent and readily undergoes electron transfer to yield $MV^{\bullet+}$ and the respective TEOA decomposition products. The latter process may be observed in transient absorption spectra as a second slower phase in the accumulation of $MV^{\bullet+}$.^[353] Similar observations and rationale have been made concerning systems employing EDTA as a sacrificial donor.^[354, 355]

By comparison, the activities of the bis-(bipyrazyl)ruthenium(II) complexes show a much greater dependence upon variations in pH than those of the iridium compounds. The stark contrast in activity on decreasing the basicity from pH 9 to pH 7 can be ascribed to deactivation of the photosensitiser upon protonation. The ligand centred radical that is formed upon reductive quenching by the sacrificial donor is readily protonated at sufficiently low pH to form the conjugate acid $[Ru(bpz)_2(\bullet bpzH)]^{2+}$, which has a $pK_a \approx 7.1$.^[356] The distal nitrogen of the pyrazyl radical is the most probable site of protonation although a H-adduct of the carbons in the three and five positions has also been suggested, as illustrated in Fig. 5.17.^[357] As a consequence, the redox potentials of the complex undergo an anodic shift of *ca.* 0.2 V, thus becoming insufficient to facilitate the reduction of MV^{2+} .^[356] This would explain the near inactivity of the system at pH 6, as at this point the majority of the complex is expected to have undergone protonation.

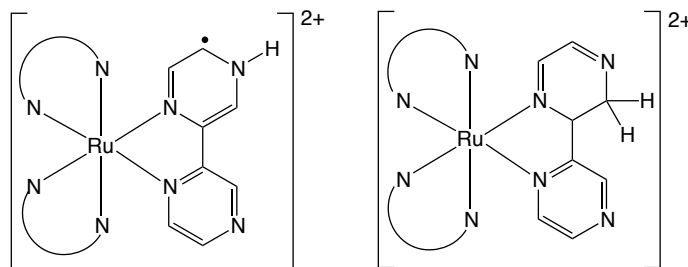


Fig. 5.17. Proposed structures for the protonated bpz ligand radical formed on excitation of $[Ru(bpz)_3]^{2+}$ in an acidic solution. a) N protonation b) H-adduct.

To improve the efficiencies in the range of pH 6.0 – 7.5 it is suggested that alternate complexes should be investigated. By focusing upon ligands that do not contain groups that may undergo protonation, it may be possible to minimise deactivation of the photosensitiser at lower pH. On comparison of a range of ruthenium(II) tris-homoleptic polypyridyl complexes, and taking into consideration the conclusions presented in section 5.2.3.1.2.3., dCF₃bpy was identified as a potential candidate for such studies. This was chosen as, of the simpler disubstituted bipyridyl pro-ligands, it is dCF₃bpy that yields complexes of redox potentials closest to those of bipyrazine; [Ru(dCF₃bpy)₃]²⁺ E(II/III) = +1.75 V and E(I/II) = -0.76 V.^[189]

5.2.3.1.3. Expanding the System: Selective Photoexcitation Towards Targeted Light-Driven Biocatalysis.

The extent to which the photophysical and redox properties of transition metal complexes may be manipulated, presents an opportunity to develop systems that utilise selective photoexcitation. It was surmised that on preparing photosensitisers of sufficiently varied absorption profiles there would be potential for the selective excitation of a particular sensitiser in preference to others within the same system. To test this hypothesis additional experiments using [Ru(bpy)(Me₂qpy)]⁴⁺, [Ru(bpz)₂dClbpy]²⁺, [Ir(22)₂bpy]³⁺ and [Ir(32)₂dCF₃bpy]³⁺ as photosensitisers towards the bioreduction of 2-cyclohexenone by PETNR_{R324C} were undertaken. These four complexes were chosen, as of all the compounds discussed in section 3 and 4, these exhibit the greatest diversity in absorption profiles, as displayed in Fig. 5.18. Experiments employed a series of long pass optical filters, which attenuate light of higher energy and allow for selective excitation of transitions that occur at longer wavelengths. Using filters of 305, 360, 460 and 530 nm it was possible to differentiate between the different sensitisers to various degrees.

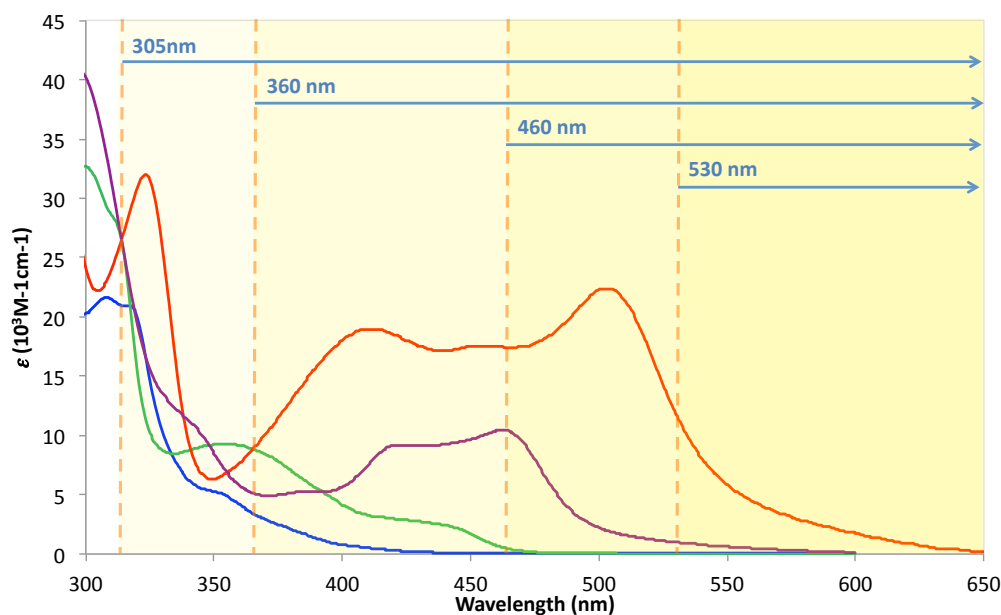


Fig. 5.18. UV-visible absorption spectra of [Ir(32)₂dCF₃bpy]Cl₃ (blue); [Ir(22)₂bpy]Cl₃ (green); [Ru(bpz)₂dClbpy]Cl₂ (purple) and [Ru(bpy)(Me₂qpy)₂]Cl₆ (red) recorded in deionised water and highlighting the various long pass filters employed in the study of selective photoexcitation.

Table 5.9. *Influence of the wavelength of incident irradiation in the light driven bioreduction of 2-cyclohexene by PETNR-R324C.*

Photosensitiser	Wavelength	TOF ^[a]	Conv. ^[b] [%]	Yield ^[b] [%]
[Ru(bpy)(Me ₂ qpy) ₂] ⁶⁺	530	40	30	28
	460	70	51	51
	360	90	76	69
	305	78.7	68	68
[Ru(bpz) ₂ dClbpy] ²⁺	530	27.0	20	19
	460	133.8	100	>99
	360	123.6	100	>99
	305	188.2	100	>99
[Ir(22) ₂ bpy] ³⁺	530	-	0	0
	460	28.1	23	23
	360	129.1	100	>99
	305	100.0	100	>99
[Ir(32) ₂ dCF ₃ bpy] ³⁺	530	-	0	0
	460	-	0	0
	360	-	0	0
	305	8.7	8	7

^[a]Determined after 120 mins. * Determined after 60 minutes. ^[b] Conversions and yields determined by GC analysis from a calibration curve of known standards of the substrate/product and corrected using limonene as an internal standard. Calculated after 240 mins.

Interestingly, absorption by the low intensity tailing of the MLCT band in [Ru(bpz)₂dClbpy]²⁺ was sufficient to afford appreciable product formation on irradiation with light of $\lambda \geq 530$ nm, with yields of 28 % after 4 h. In contrast, no substrate turnover was observed for either [Ir(22)₂bpy]³⁺ or [Ir(32)₂ dCF₃bpy]³⁺ upon illumination at these wavelengths. Of the four sensitiser, [Ru(bpy)(Me₂qpy)₂]⁶⁺ proved to be the most effective, although the difference in activity compared to [Ru(bpz)₂dClbpy]²⁺ was not proportional to the differences in absorption intensity; these results reflecting the poorer photosensitiser ability of the complex, as observed in section 5.2.3.1.2.3. It was also noted that the rate of protein precipitation was greatly enhanced in the presence of this sensitiser. On completion of the reaction signs of precipitation were already evident and if left at room temperature overnight a significant quantity of solid material was present in suspension. It is clear that some property of this particular complex is detrimental to the stability of the enzyme, although at present no specific explanation for this behavior has been determined.

Upon illumination at $\lambda \geq 460$ nm, a significant increase in the activity of both [Ru(bpy)(Me₂qpy)₂]⁶⁺ and [Ru(bpz)₂dClbpy]²⁺ was observed. This was most pronounced in the case of the latter and may be associated with excitation of the more intense MLCT transitions within the absorption profile of the complex. Initial activity of the [Ir(22)₂bpy]³⁺ was also evident, thus confirming that targeted excitation can be achieved towards the selective activation of catalytic turnover. It is thought that by using long-pass filters of *ca.* $\lambda \geq 500$ nm, it may be possible to further enhance the activity of the ruthenium complexes without initiating turnover within the [Ir(22)₂bpy]³⁺ sensitised systems. At $\lambda \geq 305$ nm, catalytic turnover using [Ir(32)₂dCF₃bpy]³⁺ as a sensitiser was finally achieved, although, despite a significant increase

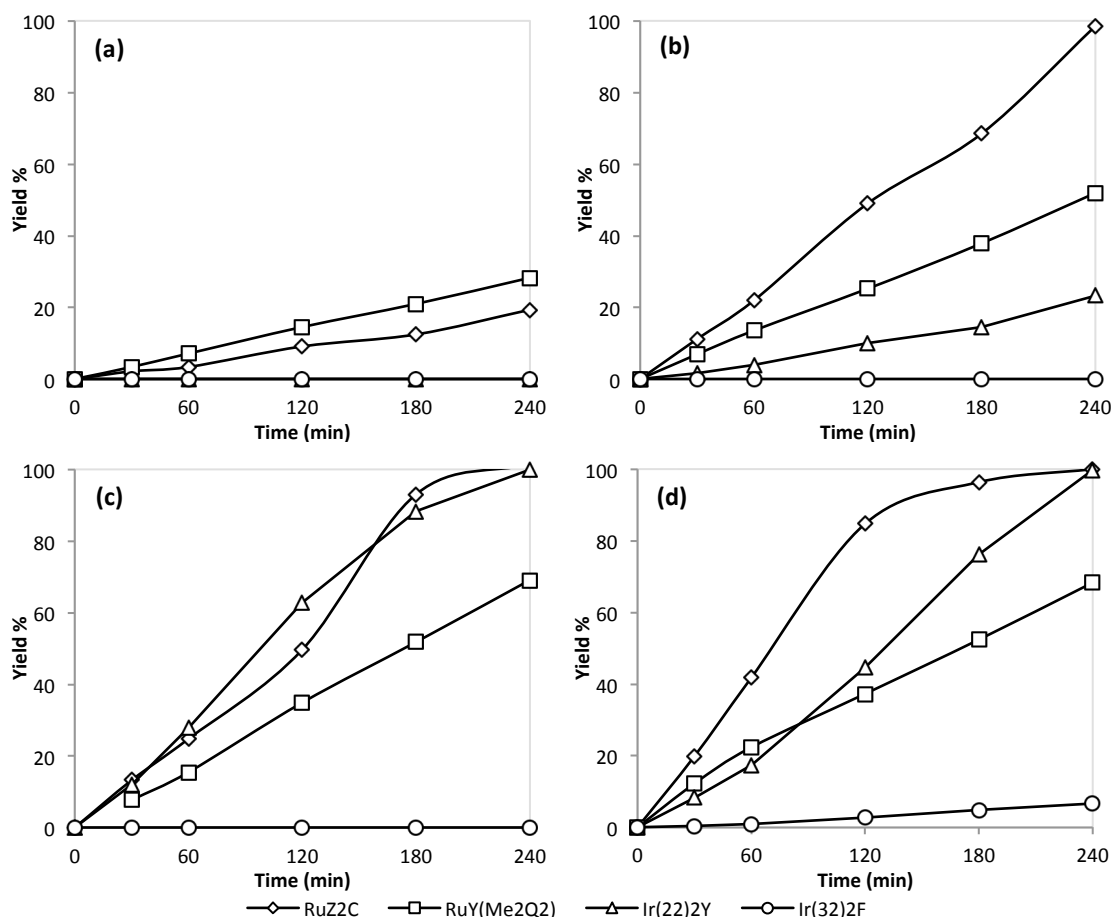


Fig. 5.19. The influence of photosensitisers and the wavelength of incident irradiation upon the activity of PETNR towards the bioreduction of 2-cyclohexen-1-one, as demonstrated employing long pass filters at **(a)** 530 **(b)** 460 **(c)** 360 and **(d)** 305 nm.

in absorbance, the activity of the system was relatively poor. From these results it is clear that the iridium complexes of 1-methyl-3-(2'-pyridyl)pyridinium are unsuitable as photosensitisers under the current reaction conditions.

Results indicate that initially, catalytic turnover increases upon changing the long-pass filter to one with an attenuation point of progressively shorter wavelength, this being attributed to an overall increase in the absorption of energy by the sensitiser. However, these trends are only apparent upon the initial excitation of the lowest energy MLCT band. After this point the trends become less clear as the changes in activity afforded by subsequent shifts in the wavelength of irradiation become less pronounced. It is thought that on excitation of higher energy MLCT bands, the resultant excited states have properties that make subsequent electron transfer towards catalytic turnover energetically unfavourable. These results suggest that sufficiently high levels of activity may be attained on excitation of the lower energy MLCT band alone. This would allow for the use of illumination across a much narrower range of wavelengths and thus afford an increase in the selectivity of targeted excitation. This has the additional benefit that, on illumination with light of as low an energy as possible, the likelihood of irreversible photochemical changes to the sensitiser may be minimised, thus enhancing the longevity of the catalytic system.

The capacity for selective excitation provides no tangible benefits towards the system in the current state. As electron transfer is diffusion controlled, targeted reduction of a specific terminal acceptor would be extremely difficult without extensive manipulation of the redox properties of each of the components present within the sample. There is also an extra level of complexity for those systems that rely upon the use of mediators to facilitate electron transfer, as these compounds readily undergo redox processes and make little to no distinction between the various donors and/or acceptors. However, if such an approach were used in conjunction with a covalently coupled sensitiser-enzyme construct, then targeted electron transfer to the enzyme bound cofactor may be achieved due to the close proximity of the two redox centres. The true potential of this premise is realised upon contemplating the preparation of multi-enzyme systems towards cascade reactions utilising sequential biocatalytic transformations.

5.2.4.1.4. Expanding the System: Applications Towards Other Substrates

With the optimal parameters and limits of the system established, attempts to broaden the potential scope of application were undertaken in the form of additional substrate assays. Four groups of potential compounds were identified and subsequently employed in light-driven biotransformations. It was noted during these assays that, under the employed reaction conditions, MV^{+} accumulation was dependent upon the reactivity of the substrate. For example, in assays of the poorer substrates an increased concentration of MV^{+} was evident early in the reaction, corresponding to a decreased rate in reoxidation of the mediator by FMN due to slower catalytic turnover. Likewise the more active substrates were characterised by a minimal accumulation of MV^{+} until complete substrate consumption was achieved. These observations suggest that in most instances the reaction conditions were sufficient to generate MV^{+} so as not to be significantly rate limiting of catalytic turnover.

Table 5.10. *Reduction of various activated alkenes by PETNR and TOYE in light-driven biocatalytic systems employing $(Ru(bpz)_2dClbpy)(Cl)_2$ as a photosensitiser.*

Substrate	Enzyme	TOF ^[a]	Conv. ^[b] [%]	Yield ^[b] [%]	Config.	ee ^[c] %
Cinnamaldehyde	PETNR _{R324C}	130	100	85	--	--
	TOYE	110	93	80	--	--
α -methylcinnamaldehyde	PETNR _{R324C}	36	56	22	(S)	37
	TOYE	190	100	68	(S)	9
2-methylpentenal	PETNR _{R324C}	105	100	65	(S)	85
	TOYE	130	100	73	(S)	6
Ketoisophorone	PETNR _{R324C}	190	100	95	(R)	40
	TOYE	260*	100	88	(R)	35
<i>N</i> -Ph-2-methylmaleimide	PETNR _{R324C}	10	81	10	(R)	>99
	TOYE	125	100	82	(R)	>99
trans- β -nitrostyrene	PETNR _{R324C}	--	100	0	--	--
	TOYE	--	100	0	--	--
(S)-Carvone	PETNR _{R324C}	15	24	5	(2R,5S)	>99
	TOYE	18	27	6	(2R,5S)	98

^[a]Determined after 120 mins. * Determined after 60 minutes. ^[b] Conversions and yields determined by GC analysis from a calibration curve of known standards of the substrate/product and corrected using limonene as an internal standard. Calculated after 240 mins. ^[c] Determined by GC analysis on comparison to known standards.

5.2.4.1.4.1. Aldehydes and Ketones

Each of the acyclic carbonyl compounds used as part of this study gave the desired product in moderate to good yields depending upon the enzyme employed. In the assays of cinnamaldehyde, PETNR exhibited slightly enhanced activity in comparison to TOYE, as evident by the incomplete conversion of the substrate in reactions of the latter. This is in agreement with the reported rates associated with this substrate in the native NADPH dependent biotransformations, at 4.7 and 0.39 s⁻¹ for PETNR and TOYE respectively.

The relative activities are reversed in assays of α -methylcinnamaldehyde, with TOYE demonstrating appreciably higher rates than PETNR, the latter only achieving *ca.* 56% substrate conversion over 4 h. This poor performance may be associated with substrate inhibition, which has been previously noted with PETNR in assays of α -methylcinnamaldehyde at concentrations in the low millimolar range.^[335] Unfortunately the kinetic constants for the analogous activity of TOYE have not been reported, so a direct comparison cannot be made. Quantitative conversion to the corresponding dihydrocinnamaldehyde was not achieved for either of the enzymes; in the assays of TOYE, despite complete consumption of the substrate, only modest yields of 68 % were attained. Decomposition of the substrate and/or product is suggested to be the source of these poor yields, owing to the susceptibility of the aldehyde group to nucleophilic attack.^[125] The poor *ees* obtained are likewise attributed to non-enzymatic activity, which has previously been noted in similar compounds with a stereogenic centre at C α .^[335] Racemisation of the product is prevalent at this position on account of its proximity to the electronegative carbonyl group and the associated increased acidity of the corresponding proton that facilitates rapid exchange with the aqueous media.^[95, 335, 358] The rate of this spontaneous racemisation is dependent upon the nature of the product and the reaction conditions employed. It has been shown that whilst the process occurs across a broad pH range, the rate is significantly enhanced in alkaline conditions.^[358] Loss of stereochemical information most probably occurs via tautomerisation; the increased rate observed at high pH suggests a base catalysed enolisation mechanism that is promoted on deprotonation of C α .

The related 2-methylpentenal was also subject to similar processes, with complete substrate consumption affording yields of 65–73 %. The disparity in the *ees* of the two systems can be explained in part by the enhanced rate of turnover demonstrated by TOYE. It is expected that this could prove detrimental to enantiopurity, as the product would be exposed to potential racemisation reactions for longer periods of time. However, the magnitude of the difference in the *ees* is much greater than that of the rates, therefore it is suggested that other contributing factors are also possibly in effect.

The reaction of 2,6,6-trimethyl-2-cyclohexen-1,4-dione, or ketoisophorone, rapidly proceeded to give levodione in near quantitative yields. The low *ees* that were obtained are expected, as the substrate has been shown to readily undergo reduction and to be subject to significant solvent catalysed racemisation in the assays of a number of OYEs.^[359] This issue is exacerbated in these photosensitised reactions as, unlike the other substrates employed in

this study, ketoisophorone undergoes a non-enzymatic reduction to afford racemic levodione in *ca.* 80 % yields. Observations of the control experiments undertaken in the absence of enzyme indicated a degree of quenching of $MV^{+\cdot}$, as the radical did not accumulate to concentrations typically expected under such conditions. The results suggest reduction occurs via electron transfer from $MV^{+\cdot}$ and, most likely, directly from the reduced photosensitiser. Between 210-240 minutes the solution became a much deeper blue as the radical cation accumulated to a greater concentration and was shown to coincide with near complete consumption of the substrate, as indicated by GC analysis. The readiness with which this substrate undergoes non-enzymatic reactions is thought to be a consequence of the activating effect of the two proximal carbonyl groups and the extended conjugation within the structure. Owing to the latter, multiple resonance forms may subsequently be adopted and act towards the stabilisation of intermediary species that could aid to facilitate reduction.

5.2.4.1.4.2. Maleimides

Two key issues were encountered during assays of *N*-phenyl-2-methylmaleimide. The first was one of aqueous solubility, which became apparent shortly after addition of the ethanolic stock solution to the reaction buffer. The resulting precipitate was observed to gradually redissolve over the course of the reaction, although this did not occur in all instances. For assays of TOYE, this issue was alleviated on increasing the ethanol concentration in the reaction buffer from 5 to 10 % and was possibly due to the increased solvent stability exhibited by the enzyme. The second issue pertained to a non-enzymatic side reaction, which was identified during control assays performed in the absence of enzyme and accounted for *ca.* 50 % substrate consumption during the course of a 4 hour reaction. No formation of *N*-phenyl-2-methylsuccinimide was observed nor could any additional species be distinguished from results obtained by GC analysis.

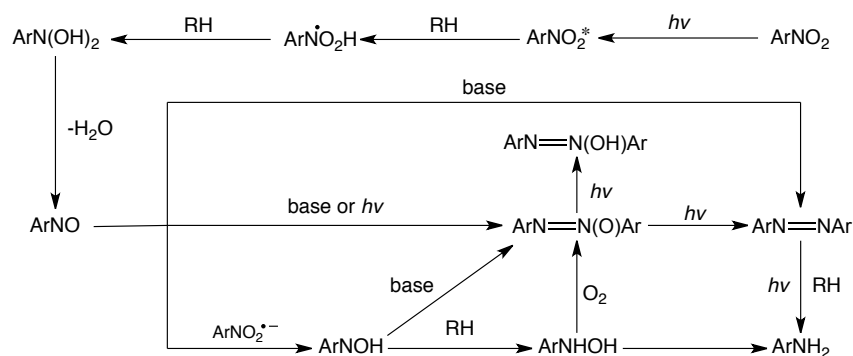
Reactions of PETNR showed minimal product formation despite near complete consumption of the substrate. The extracts were strongly coloured, taking on an increasingly orange/pink hue as the reaction progressed. Again no additional components were evident upon GC analysis preventing the identity of these impurities from being determined. In comparison, TOYE afforded complete substrate consumption to give near quantitative yields of the respective succinimide in less than 180 minutes. Unlike PETNR, prior to depletion of the substrate, no accumulation of $MV^{+\cdot}$ was observed. The lack of accumulation of $MV^{+\cdot}$ suggests that the generation of reducing equivalence was insufficient within the system and may have limited the rate of catalytic turnover. However, this may have proven beneficial for overall yields as further results suggested that the product itself was also subject to unwanted side reactions. After complete substrate reduction, a degradation of the resultant succinimide became apparent, as yields dropped from 93 % to just 82 % during the final hour of the assay. The pronounced difference in activities for these two systems towards *N*-phenyl-2-methylmaleimide again reflect the relative rates of catalytic turnover which have been

determined for the native NAD(P)H mediated reactions. Previous steady-state kinetic studies have shown that k_{cat} values for TOYE were over twice those reported for PETNR at $16.90 \pm 0.61 \text{ s}^{-1}$ and $7.65 \pm 0.13 \text{ s}^{-1}$ respectively.^[125, 335] It is this significant increase in the rate of activity that is thought to have allowed for substrate turnover to effectively compete with the apparent non-enzymatic reactions. The latter pathways have been attributed to either a direct reduction of the maleimide by MV^+ or a reaction with the decomposition products of TEOA. On consideration of the high yields obtained in assays of TOYE and the subsequent product decomposition, it is surmised that the reaction is predominant in the presence of an excess of MV^+ , as is the case throughout reactions of PETNR and during the latter stages of those with TOYE.

5.2.4.1.4.3. α,β -Unsaturated Nitroalkenes

Due to the electron withdrawing effects of the nitro group upon the extended conjugated system, the absorption maxima of the α,β -unsaturated nitroalkenes are significantly bathochromically shifted to the near-UV region of the spectrum. In an effort to minimise the likelihood of photochemical side reactions, 400 nm long-pass filters were used in all experiments involving these substrates. In addition to issues of *E/Z* isomerisation of the double bond, the photochemical reactions of the nitro group itself also had to be considered. It has been demonstrated that, upon irradiation, the nitro group is readily reduced to yield a mixture that is predominantly of the intermediary hydroxylamine or the fully reduced aniline. It is established that these reactions proceed via hydrogen abstraction from the solvent by the photoexcited $^3n,\pi^*$ state of the nitroalkene.^[360] A number of other minor products have also been identified although the precise decomposition products are dependant upon the reactions conditions employed, scheme 5.8.^[361, 362]

Initial observations in assays of *trans*- β -nitrostyrene again indicated that solubility of the substrate was of concern, as a fine precipitate began to form shortly after commencing the reaction. As such, attempts to improve the solubility were undertaken by substitution of the aryl ring with appropriate functionality, the first potential candidate being



Scheme 5.8. The proposed mechanism in the photochemical reduction of nitro-compounds, proceeding via hydrogen abstraction by the $^3n,\pi^*$ excited state. Where *Ar* = aryl and *RH* = hydrogen donor.^[360]

(*E*)-2-(2-nitrovinyl)phenol. However, initial trials with this substrate showed that whilst it exhibited improved solubility, an immediate colour change from pale yellow to deep red occurred on addition to the reaction mixture. This is a result of deprotonation of the highly acidic hydroxyl group owing to the slightly alkaline pH under which these reactions were performed. It was also noted that upon leaving the sample to stand over a number of hours that a slow precipitation of a yellow solid had occurred, implying that solubility remained an issue or that a chemical change may be occurring over time.

Inclusion of a higher concentration of the organic solvent within the reaction buffer sufficiently improved the solubility of *trans*- β -nitrostyrene to allow assays to be undertaken. Whilst GC analysis indicated that complete consumption of the substrate had been achieved, no product formation was evident nor could any volatile by-products be identified. This was true for all attempted assays, including those of a number of different nitro containing substrates. The ability of the viologens to act as electron transfer agents in the reduction of a variety of organic compounds has been previously reported, including the nitro aromatic compounds.^[363] It has been described that on using a DCM-water biphasic system containing dioctylviologen and sodium dithionite as an electron donor, near quantitative yields of the corresponding arylamines could be achieved. The reaction is suggested to proceed via the hydroxylamine intermediate in a manner analogous to that presented in Scheme 5.8. It was further demonstrated that in acetonitrile-water, tertiary nitroalkanes could be reduced to predominantly yield the corresponding hydroxylamine.^[364] Attempts to reduce a secondary nitro aliphatic compound, 1-nitro-1-phenylethane, resulted in the formation of acetophenone-*E*-oxime and acetophenone in 74 and 13 % yields respectively. This instead proceeded on initial reduction to the nitroso compound followed by rapid tautomerisation and subsequent conversion by a Retro-Henry reaction. This is in agreement with the observation made upon investigation of the NADPH mediated biotransformation of (*E*)-(1-nitroprop-1-en-2-yl)benzene by TOYE.^[125] The low yield of nitroalkane reported therein was accompanied by the formation of 2-phenylpropanal and the respective oxime, which indicated successful bioreduction of the double bond and subsequent transformation via the discussed mechanism. In addition to this, acetophenone was detected in both biotransformation assays and the associated control experiments, thus indicating a non-enzymatic side reaction that is suggested to occur via addition of water across the double bond.

Due to the potential instability in aqueous solution and the activity towards direct reduction by the photosensitiser and/or mediator under even biphasic conditions, it is suggested that these substrates are poor candidates for use in conjunction with the current light-driven biocatalytic systems.

5.2.4.1.4.4. Terpenoids

The assays of (*S*)-(+)-carvone demonstrated initial activity, as revealed by a steady consumption of the substrate to give near quantitative yields of the dihydrocarvone product.

The rate of turnover was fairly consistent between 0 – 30 and 30 – 60 minutes although after this time the reaction ceased, with minimal substrate consumption and no product formation occurring over the remaining three hours. This coincided with observations made regarding the relative quantities of MV^{+} present in solution during the course of the reaction. A minor accumulation of the radical initially occurred to attain a concentration that was typical of a system containing a moderately active substrate. After approximately 50 minutes, MV^{+} was gradually consumed until it was no longer apparent, implying a quenching of the photosensitised electron transfer process. The assays of the related substrate perillaldehyde showed similar behaviour, although product formation was considerably less and deactivation appeared to occur within the first 30 to 40 minutes.

The nature of this inhibitory activity remains unclear. As discussed previously, were this solely attributed to enzyme inhibition, complete quenching of MV^{+} would not be expected, thus suggesting an alternate pathway of deactivation. Likewise, the NADPH mediated reductions of (S)-(+)-carvone by PETNR proceeded to afford the dihydrocarvone in 95 % yields, with no evidence to support enzyme inhibition.^[335] Contrary to this, control assays in the absence of enzyme showed the rapid accumulation of MV^{+} with no evidence of significant quenching at any point during the reaction. It is therefore suggested that inhibition may be a result of an accumulation of dihydrocarvone or a byproduct formed due to enzymatic activity.

5.2.4.1.4. Expanding the System: Biphasic Assays

Additional trials were undertaken using a biphasic solvent system with the aim to curtail the apparent side reactions of the homogenous assays by minimising the exposure of the substrates and products to aqueous solution. This approach also has the benefit of circumventing issues of aqueous solubility of the substrates and would perhaps broaden the scope for new compounds to be used in conjunction with biotransformations. Three solvents were chosen as candidates to be used in this study, specifically, *iso*-octane, *n*-octanol and *tert*-butylmethyl ether (TBME). The first two of these have been previously used in the biphasic reactions of PETNR to great effect, although both are high boiling point solvents, which make subsequent isolation of the product more problematic. TBME has likewise been employed in studies concerning a number of OYEs towards the biotransformation of a variety of derivatised cinnamaldehydes.^[365] With a much lower boiling point of 55.2°C, the solvent may instead be readily removed by simple rotary evaporation or similar techniques.

As it is expected that the rate of reaction be significantly slowed due to the limitations of substrate diffusion across the phase boundary, longer reaction times would be required. Subsequently, it was decided that the biphasic reactions would be allowed to proceed for 24 hours in all instances. This was chosen in consideration of the broad range of activities evident for the substrates to be used in these trials. Additionally this provided more scope for comparison to literature precedent as most of the reported assays are performed over a similar time frame. As a consequence of these longer reactions times, the concentration of the

sacrificial electron donor was increased to 50 mM to ensure continued turn over of the photosensitiser throughout the entire procedure.

For comparison purposes, assays employing an enzyme coupled NADPH regeneration system were also undertaken for all combinations of substrates and solvents. The enzyme to be used was glucose-6-phosphate dehydrogenase (G6PDH), which has been previously shown to act as an effective means of regenerating the source of reducing equivalents for both PETNR^[335] and YqjM.^[365]

Under the majority of reaction conditions, assays of 2-cyclohexenone proceeded to afford complete substrate conversion and near quantitative yields of cyclohexanone. However, it was noted that for reactions containing TBME, precipitation of PETNR occurred after an extended period of time. Specific issues were encountered with assays of PETNR using the NADPH regeneration system, in which a significant quantity of a white solid was seen to form at the phase boundary. This was also apparent for the other substrates and in all instances the reactions failed to reach completion. Whilst protein precipitation was also evident for the photosensitised reactions, this did not impact the overall substrate turnover to the same degree, as near complete substrate consumption was typically observed. TOYE exhibited no visible signs of degradation during illumination assays, although in those of G6PDH a small quantity of white precipitate was observed. With a higher polarity index in comparison to *iso*-octane and *n*-octanol, it is thought that TBME is sufficiently water miscible to attain concentrations in aqueous solution so as to be of detriment to the enzyme. Therefore, the improved performance of TOYE in such assays may be discussed in terms of the enhanced solvent stability of the thermophilic enzymes.

The photosensitised biphasic assays of the three acyclic carbonyl compounds, cinnamaldehyde, α -methylcinnamaldehyde and 2-methylpentenal all displayed increased product yields in relation to the homogenous reactions, thus validating this approach towards minimising the impact of the side reactions associated with the aqueous media.

The relative activities of the two enzymes towards cinnamaldehyde were again made evident in these biphasic assays, as the reactions of TOYE displayed incomplete conversion of the substrate in both photosensitised and G6PDH mediated reactions of *n*-octanol and TBME. Interestingly, the reactions of *iso*-octane afforded complete conversion to give the saturated aldehyde in near quantitative yields. It is therefore suggested that the polarity of the organic solvents have some influence over the efficiency of these reactions. This is most probably a consequence of differences afforded in the rate of diffusion across the phase boundary and in the partitioning of the substrate between the two phases.

Regarding the reduction of α -methylcinnamaldehyde, the current biphasic conditions were ineffective towards improving the enantiopurity of the product. The poor *ees*, in the range of 0 – 23 %, reflect those of the homogenous assays and those previously reported in the studies of PETNR from literature.^[335] Whilst no such comparative assays have been previously

Table 5.11. Biphasic reduction of various activated alkenes by PETNR and TOYE using a photosensitiser or a NADP⁺/G6PDH co-factor regeneration system.^[a]

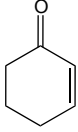
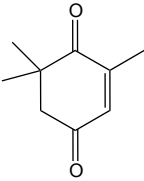
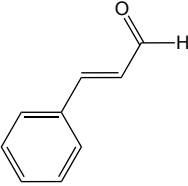
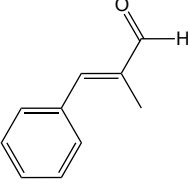
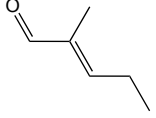
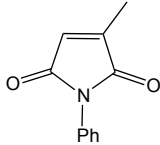
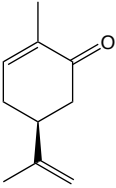
Substrate	Catalyst ^[a]	Solvent	Conv. ^[b] [%]	Yield ^[b] [%]	Config.	ee ^[c] %
	TOYE/Ru	<i>n</i> -octanol	100	>98	--	--
	TOYE/Ru	isooctane	100	>98	--	--
	TOYE/Ru	TBME	100	>98	--	--
	R324C/Ru	<i>n</i> -octanol	100	>98	--	--
	R324C/Ru	isooctane	100	>98	--	--
	R324C/Ru	TBME	100	>98	--	--
	TOYE/G6PDH	<i>n</i> -octanol	100	>98	--	--
	TOYE/G6PDH	isooctane	100	>98	--	--
	TOYE/G6PDH	TBME	100	>98	--	--
	R324C/G6PDH	<i>n</i> -octanol	100	>98	--	--
	R324C/G6PDH	isooctane	100	>98	--	--
	R324C/G6PDH	TBME	24	14	--	--
	TOYE/Ru	<i>n</i> -octanol	100	87	(<i>R</i>)	20
	TOYE/Ru	isooctane	100	89	(<i>R</i>)	26
	TOYE/Ru	TBME	100	75	(<i>R</i>)	23
	R324C/Ru	<i>n</i> -octanol	100	84	(<i>R</i>)	65
	R324C/Ru	isooctane	100	97	(<i>R</i>)	26
	R324C/Ru	TBME	100	87	(<i>R</i>)	29
	TOYE/G6PDH	<i>n</i> -octanol	100	90	(<i>R</i>)	67
	TOYE/G6PDH	isooctane	100	92	(<i>R</i>)	43
	TOYE/G6PDH	TBME	100	87	(<i>R</i>)	71
	R324C/G6PDH	<i>n</i> -octanol	100	86	(<i>R</i>)	66
	R324C/G6PDH	isooctane	100	92	(<i>R</i>)	43
	R324C/G6PDH	TBME	53	44	(<i>R</i>)	73
	TOYE/Ru	<i>n</i> -octanol	90	86	--	--
	TOYE/Ru	isooctane	100	>98	--	--
	TOYE/Ru	TBME	98	90	--	--
	R324C/Ru	<i>n</i> -octanol	100	96	--	--
	R324C/Ru	isooctane	100	>98	--	--
	R324C/Ru	TBME	100	>98	--	--
	TOYE/G6PDH	<i>n</i> -octanol	82	80	--	--
	TOYE/G6PDH	isooctane	100	>98	--	--
	TOYE/G6PDH	TBME	68	67	--	--
	R324C/G6PDH	<i>n</i> -octanol	100	96	--	--
	R324C/G6PDH	isooctane	100	97	--	--
	R324C/G6PDH	TBME	55	50	--	--
	TOYE/Ru	<i>n</i> -octanol	100	>98	(<i>S</i>)	15
	TOYE/Ru	isooctane	100	91	(<i>S</i>)	7
	TOYE/Ru	TBME	100	>98	(<i>S</i>)	13
	R324C/Ru	<i>n</i> -octanol	100	>98	(<i>S</i>)	23
	R324C/Ru	isooctane	100	95	(<i>S</i>)	6
	R324C/Ru	TBME	100	>98	(<i>S</i>)	0
	TOYE/G6PDH	<i>n</i> -octanol	76	76	(<i>S</i>)	22
	TOYE/G6PDH	isooctane	100	96	(<i>S</i>)	16
	TOYE/G6PDH	TBME	77	76	(<i>S</i>)	4
	R324C/G6PDH	<i>n</i> -octanol	100	98	(<i>S</i>)	13
	R324C/G6PDH	isooctane	100	95	(<i>S</i>)	12
	R324C/G6PDH	TBME	57	56	(<i>S</i>)	8
	TOYE/Ru	<i>n</i> -octanol	100	85	(<i>S</i>)	30
	TOYE/Ru	isooctane	100	>98	(<i>S</i>)	14
	TOYE/Ru	TBME	100	>98	(<i>S</i>)	8
	R324C/Ru	<i>n</i> -octanol	100	>98	(<i>S</i>)	90
	R324C/Ru	isooctane	100	93	(<i>S</i>)	89
	R324C/Ru	TBME			(<i>S</i>)	75
	TOYE/G6PDH	<i>n</i> -octanol	100	>98	(<i>S</i>)	30
	TOYE/G6PDH	isooctane	100	98	(<i>S</i>)	17
	TOYE/G6PDH	TBME	100	>98	(<i>S</i>)	7
	R324C/G6PDH	<i>n</i> -octanol	100	>98	(<i>S</i>)	87
	R324C/G6PDH	isooctane	100	96	(<i>S</i>)	84
	R324C/G6PDH	TBME			(<i>S</i>)	81

Table 5.11. (cont.) Biphasic reduction of various activated alkenes by PETNR and TOYE using a photosensitiser or a NADP⁺/G6PDH co-factor regeneration system.^[a]

Substrate	Catalyst ^[a]	Solvent	Conv. ^[b] [%]	Yield ^[b] [%]	Config.	ee ^[c] %	
	TOYE/Ru	<i>n</i> -octanol	100	54	(<i>R</i>)	> 99	
	TOYE/Ru	isooctane	--	--	--	--	
	TOYE/Ru	TBME	100	67	(<i>R</i>)	> 99	
	R324C/Ru	<i>n</i> -octanol	100	47	(<i>R</i>)	> 99	
	R324C/Ru	isooctane	--	--	--	--	
	R324C/Ru	TBME	81	28	(<i>R</i>)	> 99	
	TOYE/G6PDH	<i>n</i> -octanol	100	89	(<i>R</i>)	> 99	
	TOYE/G6PDH	isooctane	--	--	--	--	
	TOYE/G6PDH	TBME	100	66	(<i>R</i>)	> 99	
	R324C/G6PDH	<i>n</i> -octanol	100	81	(<i>R</i>)	> 99	
	R324C/G6PDH	isooctane	--	--	--	--	
	R324C/G6PDH	TBME	78	38	(<i>R</i>)	> 99	
		TOYE/Ru	<i>n</i> -octanol	94	90	(2 <i>R</i> ,5 <i>S</i>)	97
		TOYE/Ru	isooctane	90	86	(2 <i>R</i> ,5 <i>S</i>)	97
TOYE/Ru		TBME	98	95	(2 <i>R</i> ,5 <i>S</i>)	97	
R324C/Ru		<i>n</i> -octanol	100	97	(2 <i>R</i> ,5 <i>S</i>)	97	
R324C/Ru		isooctane	100	99	(2 <i>R</i> ,5 <i>S</i>)	96	
R324C/Ru		TBME	92	90	(2 <i>R</i> ,5 <i>S</i>)	93	
TOYE/G6PDH		<i>n</i> -octanol	97	92	(2 <i>R</i> ,5 <i>S</i>)	97	
TOYE/G6PDH		isooctane	100	98	(2 <i>R</i> ,5 <i>S</i>)	96	
TOYE/G6PDH		TBME	100	96	(2 <i>R</i> ,5 <i>S</i>)	97	
R324C/G6PDH		<i>n</i> -octanol	98	97	(2 <i>R</i> ,5 <i>S</i>)	96	
R324C/G6PDH		isooctane	99	84	(2 <i>R</i> ,5 <i>S</i>)	96	
R324C/G6PDH		TBME	47	46	(2 <i>R</i> ,5 <i>S</i>)	98	

^[a] Conditions for assays containing a photosensitizer: Enzyme (10 μ M), [Ru(bpz)₂dClbpy]Cl₂ (20 μ M) and methyl viologen (0.1 mM) in TEOA buffer (1.0 mL, 50 mM, pH 8.0). Conditions for assays containing G6PDH regeneration system: Enzyme (10 μ M), NADP⁺ (10 μ M), glucose-6-phosphate (15 mM) and glucose-6-phosphate dehydrogenase (10 U) in phosphate buffer (1.0 mL, 50 mM, pH 8.0). Substrate added as a solution of the indicated solvent (25 mM, 200 μ L). Assays undertaken at RT for 24 h at 450 rpm. ^[b] Conversions and yields determined by GC analysis from a calibration curve of known standards of the substrate/product and corrected using limonene as an internal standard. Calculated after 24 hours. ^[c] Determined by GC analysis on comparison to known standards

undertaken for TOYE, it has been shown that similarly poor *ees* were obtained for the homologous YqjM towards the biotransformation of *m,p*-methylenedioxy aldehyde.^[365]

As with the homogenous reactions, the enantiopurity of the products obtained upon the biphasic reduction of 2-methylpentenal showed a distinct dependence upon the enzyme. Typically assays of PETNR afforded considerably higher *ees* than TOYE, with values in the range of 75 – 90 % and 8 – 30 % respectively. By comparison to the homogenous reactions, a general improvement in the results obtained for TOYE had been achieved, specifically so when in conjunction with *n*-octanol as the organic solvent. Although these values do not match those that have been previously reported for this enzyme, the *ees* obtained for the photosensitised assays were comparable to those of the G6PDH mediated reactions performed as part of this study. On consideration of the continued differences in *ees* between the two enzymes and the consistently good results obtained for PETNR, it is suggested that TOYE display an inherently poorer stereoselectivity towards the synthesis of (*S*)-2-methylpentanal.

The influence of the non-enzymatic reduction of ketosiphorone is highlighted on comparison of the *ee* values obtained for the photosensitised and G6PDH mediated biphasic

assays. Whilst the former exhibits considerably lower stereoselectivity, the fact that the product is not racemic indicates that the enzymatic reduction is effectively competing with the direct electron transfer from the photosensitiser and/or MV^+ . It is therefore suggested that by increasing the enzyme concentration, it may be possible to promote the biotransformation pathway so as to make it the predominant mechanism of reduction within the system. Considering the expected increased rate of product formation, to sufficiently improve the enantiopurity of the product, this approach would have to be used in conjunction with significantly decreased reaction times so as to minimise the impact of non-enzymatic racemisation. It was shown for the G6PDH mediated assays that *ees* are also dependent upon the choice of organic solvent. Results describe that a decreasing polarity of the solvent, in the order TBME > *n*-octanol > *iso*-octane, correlates to a decreasing enantiopurity of the product, which can be discussed in terms of the relative partitioning of the substrate/product across the phase boundary. It is proposed that, owing to a decrease in solubility, for the less polar solvents the partitioning is shifted in favour of the aqueous phase, subsequently increasing the probability of non-enzymatic side reactions and racemisation.

Comparative assays for *N*-phenyl-2-methylmaleimide could not be undertaken using *iso*-octane due to insufficient substrate solubility; although preliminary trials were performed at concentrations *ca.* 40% of those typically employed to confirm successful activity. Despite obtaining good yields in the homogenous assays of TOYE, results of the biphasic reactions of TBME and *n*-octanol were somewhat disappointing, with yields in the range of 28-67 %. It is proposed that these poor yields are related to the product decomposition that was suggested in the final stage of the homogenous assays. These results highlight the need to optimise reaction times specifically for each of the individual substrates. As *N*-phenyl-2-methylmaleimide has proven to be an excellent substrate for both of these enzymes, it is expected that complete conversion be achieved relatively early within the time frame of these reactions. It is therefore proposed that, whilst the rate of decomposition is evidently slowed compared to the homogenous assays, the reaction times employed are sufficiently long to allow for appreciable loss of product on extended exposure to the aqueous phase. As such it is surmised that by decreasing the length of the reaction, a significant improvement in yields may be achieved.

Of particular interest are the similar yields obtained for assays of both PETNR and TOYE using *n*-octanol. Relatedly, extracts from the assays of PETNR showed no evidence of the strongly coloured impurities that had been noted in the homogenous reactions. These observations demonstrate that the use of a biphasic system can effectively minimise the impact of certain decomposition pathways. However, whilst the results of the light-driven assays in TBME were comparable to those using the G6PDH regeneration system, yields from the *n*-octanol reactions were considerably lowered by *ca.* 25-30 %. These observations potentially indicate a side reaction that is promoted by the photosensitised electron transfer process. Due to the susceptibility of the maleimides and succinimides to nucleophilic attack,

one such possibility is a direct reaction involving the hydroxyl group of *n*-octanol. However, considering the high pK_a of the solvent, this is potentially unlikely. A more probable explanation is that, due to the decreased polarity of *n*-octanol in comparison to TBME, the partitioning across the phase boundary is such so as to promote decomposition via the additional side reactions that are prevalent in the aqueous phase. This is perhaps corroborated by the results obtained from the attempted assays of *iso*-octane, which showed similarly decreased yields for the photosensitised system in comparison to the G6PDH mediated reactions, with yields of 7 % and 71 % respectively.

Interestingly the light-driven reduction of (S)-(+)-carvone proceeded to give near quantitative yields of the dihydrocarvone with excellent diastereomeric excesses in all instances. This demonstrates a further benefit of the biphasic systems as the organic phase acts as both a substrate reservoir and a product sink, effectively preventing the inhibitory effects that were observed in the homogenous reactions.

5.2.3.2. Covalently Bound Sensitiser-Enzyme Constructs.

5.2.3.2.1. Spectrophotometric Trials

Samples for spectrophotometric studies were exchanged into deoxygenated Tris-HCl buffer (5 mM, pH 8.0) using a PD-10 desalting column. Tris-HCl was chosen in preference to the TEOA buffer that is typically used for sample preparation, in an effort to minimise the likelihood of enzyme reduction prior to experiments. It was surmised that on exclusion of the sacrificial donor, turnover of the sensitiser could be perturbed; though as an extra precaution, care was taken to minimise exposure of the sample to light during preparation.

On illumination in the presence of triethanolamine, an initial decrease in absorbance was associated with the reduction of FMN, as identified by the characteristic profile of the extrapolated difference spectra. In the case of PETNR_{R324CRu}, a near complete reduction of the flavin was achieved in *ca.* 8 minutes to yield spectra that were comparable to the free complex in the region of 400 – 600 nm. After this time a continued decrease in absorbance was also evident, albeit at a slower rate. This bleaching of the MLCT of the complex continued over the course of the next twenty minutes, during which time additional features in the absorption profile also became apparent. The increases in absorbance at *ca.* 375 and 500 nm are consistent with the accumulation of the singly reduced sensitiser; the results comparable to observations made in the study of [Ru(bpz)₃]²⁺ in conjunction with either EDTA or TEOA as sacrificial donors.^[120, 366] The resultant spectra were also comparable to those obtained on chemical reduction of the sensitiser-enzyme construct on addition of an excess of sodium dithionite. Upon exposure to oxygen the spectra returned to the original state with minimal variations within the absorption profile, therefore indicating a general stability of the system despite extended periods of illumination. Samples of unlabelled enzyme were also illuminated under the same reaction conditions and showed minimal changes in absorbance over the same time frame, results indicating less than *ca.* 5 % reduction over 30 minutes.

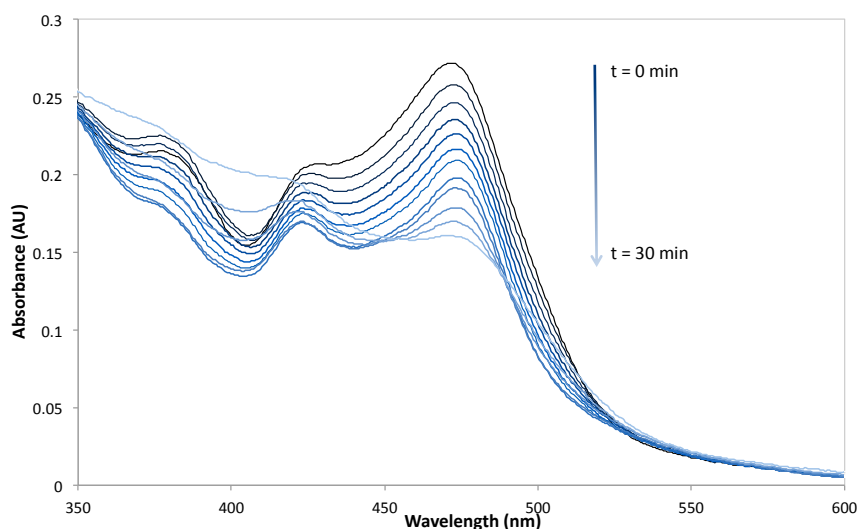


Fig. 5.20. Spectral changes afforded over the course of 30 minutes on illumination of a solution containing $PETNR_{R324CRu}$ in Tris-HCl (5 mM, pH 8.0) and in the presence of TEOA (25 mM, pH 8.0). The sample was illuminated using a 150 W halogen lamp fitted with a 360 nm long-pass filter.

5.2.3.2.2. Light-driven Biocatalytic Trials

The catalytic activities of the covalently bound sensitiser-enzyme constructs were poor in comparison to those of the diffusion-controlled analogues. In assays of 2-cyclohexenone the constructs prepared from $[Ru(bpz)_2(4\text{-bromomethyl-4'-methyl-2,2'-bipyridine})]^{2+}$ afforded minimal conversion to attain yields of *ca.* 6 – 10 %. The constructs of the bipyridyl analogue yielded no discernable quantity of the product, as in agreement with the conclusions made in section 5.2.3.1.2.3. Due to the uncertainties concerning the relative concentrations of active enzyme in each sample, a direct comparison of turnover rates between the different variants cannot be made.

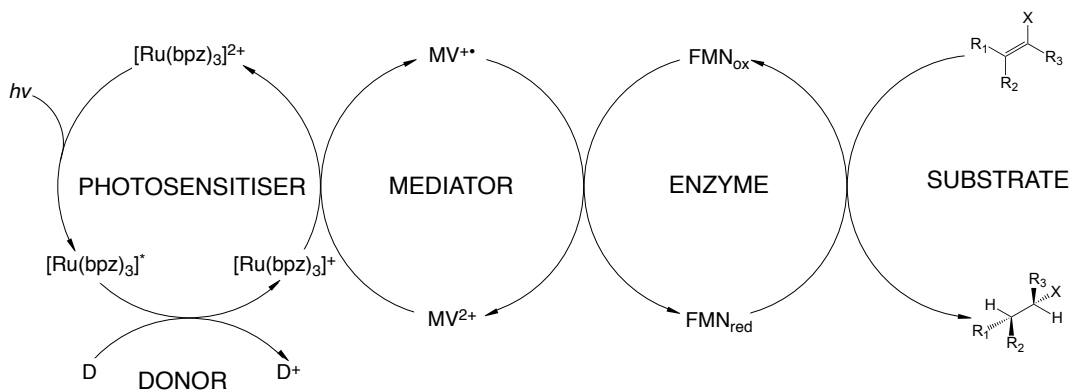
These poor results are in direct contrast to those typically reported in literature, which describe significant rate enhancements upon direct linking of individual components of an electron transport chain, as is discussed in section 1. The ineffectiveness of these systems may be attributed to the lack of an observed semiquinone in the catalytic cycle of PETNR. For the diffusion-controlled systems this is circumvented by the generation of an excess of reducing equivalents upon rapid accumulation of MV^+ . Catalytic activity is subsequently facilitated upon the rapid, near simultaneous, transfer of two electrons to yield the fully reduced cofactor and ultimately substrate reduction. In the covalently bound systems, activity is instead dependant upon two sequential transfer steps involving the photosensitiser; to wit a photoexcitation event with subsequent quenching by TEOA and reoxidation upon electron transfer to the cofactor. The suggested instability of the singly reduced form of the enzyme means that no intermediary exists in the system that may act to couple a single electron donor to a two electron acceptor.

Another consideration is the redox potential of the complex used in these studies. With an oxidation couple at *ca.* 1.72 V, the complex is expected to display poorer activity than $[Ru(bpz)_2dClbpy]Cl_2$ which has been used in the majority of assays thus far. It is instead

expected to show activity more comparable to that of $[\text{Ru}(\text{bpz})_2\text{d}^t\text{Bubpy}]\text{Cl}_2$, as discussed in section 5.2.3.1.2.3.

5.3. Conclusions

Herein, it has been shown that transition metal complexes are excellent candidates as photosensitisers towards light-driven biocatalytic systems, as demonstrated in the successful catalytic turnover of the oxidoreductase enzymes, TOYE and PETNR. Through extensive investigations the development of an effective diffusion-controlled multicomponent system utilising viologen transfer mediators has been achieved. The predominant electron transfer mechanism that is proposed to facilitate catalytic turnover is illustrated in Scheme 5.9.



Scheme 5.9. Proposed schematic for the light-driven biocatalytic reduction of activated alkenes by the flavin containing OYE using a transition metal photosensitiser and methyl viologen as an electron transfer mediator.

The impact of various factors upon the efficiency of these systems has been evaluated and optimal conditions identified; results indicated a dependence of activity upon the pH of solution and the concentration of both the sensitiser and sacrificial electron donor. Further work has also highlighted the extent to which the efficiency of catalytic turnover may be optimised upon manipulation of the redox potentials of the photosensitiser. Additionally, selective activation of catalysis has been effectively demonstrated through the targeted excitation of a complex upon altering the wavelength of the incident irradiation. Such an approach is of significant import in the development of light driven multi-enzyme systems towards cascade reactions in ‘one-pot’ syntheses. The systems have been successfully implemented in the reduction of a broad range of substrates under both aqueous and biphasic conditions, delivering yields and enantiomeric excesses comparable to those obtained utilising an enzyme coupled regeneration system.

Site directed mutagenesis has also been employed to prepare new cysteinyl variants of PETNR. Through the use of specifically designed ruthenium complexes, these variants were successfully used in the preparation of covalently bound sensitiser-enzyme constructs. Spectrophotometric studies indicated that direct electron transfer from the sensitiser to the FMN cofactor was achieved to afford complete reduction of the enzyme. Whilst these constructs show some catalytic activity, the rates are relatively poor compared to the

diffusion-controlled systems. There remains much scope to optimise the activity of these constructs and are as such, still viable candidates towards affording photosensitised biocatalysis.

The results presented here clearly demonstrate the potential of transition metal complexes in developing practical light-driven biocatalytic systems. It is expected that with further investigation this approach can be readily expanded to incorporate a variety of applications and provide an effective alternative to the use of costly redox cofactors and a reliance upon complex regeneration systems.

5.4 Further work

Concerning the diffusion controlled systems, further optimisation of the reaction conditions may prove effective towards maximising enantiomeric excesses and yields; this approach having been successfully demonstrated in assays employing enzyme-coupled regeneration techniques.^[335] Further work may also be undertaken to extend the number of substrates that can be utilised with this system, especially on consideration of the success achieved with the biphasic reactions and the broad range of potential new compounds this has subsequently made available.

As stated previously, there remains further scope towards optimising the performance of the covalently bound sensitiser systems, although the scale of such studies would be significant. The first option would be to investigate other enzymes as potential candidates for labelling; specifically those OYEs that exhibit a stable singly reduced semiquinone intermediate. This work would require additional mutagenesis studies for each of the new enzymes, involving the preparation of numerous cysteinyl variants to fully evaluate the impact of the relative positions upon the efficiencies of electron transfer.

Further mutagenesis studies of PETNR with the aim of incorporating multiple mutations may also be of worth. It is thought that on inclusion of multiple sensitisers about the active site it may be possible to greatly enhance the overall yield of reduced flavin and subsequently promote catalytic turnover. With such an approach, careful consideration of the target residues would be required as issues regarding steric hindrance are probable. Therefore, it may be that this method would be more effective with an enzyme that has an inherently larger active site so as to compensate for the influence of the exogenous labels. The native residues of PETNR that were identified as sites of additional labelling are also potential targets of mutagenesis. Replacement of these residues would aid in simplifying the absorption spectra of the resultant constructs and allow for more accurate determination of labelling yields. It would also allow scope for mechanistic studies using laser flash photolysis and time resolved spectroscopy, as the subsequent transient spectra would no longer be complicated by additional processes associated with the superfluous labels.

An investigation into the use of alternate labelling compounds is most certainly warranted. Whilst the bipyrazyl complexes show beneficial properties over the bipyridyl

analogues, further improvements are possible. The failure of the labelling studies with the quaterpyridinium complex was unfortunate, although with further manipulation of the ancillary ligand successful coupling of these quaternised species may still be achieved. One potential ligand of interest is 1''-(4-hydroxymethylphenyl)-2,2':4',4''-terpyridinium. Containing only a single bromomethyl group eliminates the possibility of additional side reactions that are associated with the inclusion of a second reactive site. Similarly incorporating only one pyridinium group lowers the overall charge of the complex and provides the means of ensuring that electron transfer into the pyridinium moiety is directed towards the surface of the enzyme and hence the terminal acceptor.

Another alternative would be to employ a covalently bound mediator, using a premise similar to that which was attempted with the quaterpyridinium linking unit and to that discussed in section 1 regarding the Ru-MV-cyt *c* triad complex. By introducing a saturated linker between the viologen type acceptor and the metal centre, it would be possible to further increase charge separation in the excited state and perhaps better facilitate electron transfer to FMN.

The possibility of covalently bound iridium compounds need also be explored, as this would allow the full potential of selective excitation of a complex to be determined. Whilst synthesis of the complexes of 4-hydroxymethyl-4'-methyl-2,2'-bipyridyl is expected to be relatively simple by employing the method discussed in section 4.2, subsequent bromination may prove problematic. The stability of the Ir–C bond is yet to be determined under acidic conditions at elevated temperatures, which are typically required during such reactions.

SECTION SIX

SUMMARY

Presented in Sections Three and Four is an extensive synthetic study into the preparation of a series of photosensitisers with a diverse range of photophysical and redox properties. The prepared compounds were identified using NMR and mass spectroscopies, elemental analysis and, in some instances, X-ray crystallography. All complexes were also subsequently analysed using UV-visible spectroscopy and cyclic voltammetry.

In Section Three a series of thirteen distinct tris(heteroaryl)ruthenium(II) compounds were synthesised containing the bis(2,2'-bipyrazyl)ruthenium(II) moiety. This work has developed new synthetic procedures that exhibit significant benefits over previously established methods towards the preparation of both 2,2'-bipyrazine and the associated complexes. The lessons learned from such work have already been adapted and utilised in the preparation of other pro-ligands and coordination compounds. The synthesis of complexes with general formula $[\text{Ru}(\text{bpz})_2(\text{N}^{\wedge}\text{N})]^{n+}$ have provided access to photosensitisers with a broad range of redox properties, as achieved via inducing changes in the energy of the metal-based HOMO upon varying the σ -donor ability of the ancillary ligand. Further complexes were synthesised incorporating the 4,4':2',2'':4'',4'''-quaterpyridinium ligands to attain complexes of higher overall positive charge with the aim of enhancing electrostatic interactions with the enzymatic systems. Additional studies into the preparation of bimetallic complexes were also undertaken, although these proved unsuccessful. This was primarily attributed to a deficiency of electron density at the metal centre of the bis(2,2'-bipyrazyl)ruthenium(II) moiety preventing formation of the multi-metallic species.

Section Four details the use of ligands containing the positively charged pyridinium moiety as a means of successfully preparing water soluble cationic cyclometalated iridium(III) coordination compounds. Upon incorporation of this functional group into either the cyclometalating or ancillary ligands, two distinct series of compounds were prepared. The initial complexes synthesised using the *N,N'*-disubstituted 4,4':2',2'':4'',4'''-quaterpyridinium compounds unequivocally confirmed the effectiveness of this approach towards improving aqueous solubility. Their use as ancillary ligands in future studies would provide the means to prepare a large number of water soluble iridium complexes by exploiting the existing catalogue of cyclometalating ligands that have already been published in the literature. Considering that the properties of complexes of this type are dominated by the choice of cyclometalating ligand, this potentially gives access to photosensitisers of greatly varied properties. Use of the monoquaternised bipyridinium compounds as pyridine derived *N*-heterocyclic carbene cyclometalating ligands has afforded a range of complexes with unusual and intriguing photophysical and redox properties. The distinct differences evident for complexes of 1-methyl-3-(2'-pyridyl)pyridinium highlights the influence that the site of

substitution within a ligand has upon the resultant electronic structure and subsequently the overall properties of a compound. The intense luminescence displayed by this series of complexes makes them ideal candidates for study using emission spectroscopic techniques and potential applications in OLEDs and LEECs. These complexes may also benefit from additional spectroelectrochemical studies to better understand the nature of the different oxidation states and the related electron transfer processes that may occur upon photoexcitation.

In Section Five, the prepared photosensitisers were successfully utilised to initiate light-driven catalytic turnover of the flavin dependent oxidoreductase enzymes, pentaerythritol tetranitrate reductase (PETNR) and the thermophilic old yellow enzyme (TOYE). The devised diffusion controlled multicomponent systems utilised methyl viologen as an electron transfer mediator between the photosensitiser and the FMN cofactor to ultimately facilitate enzyme turnover. This system was successfully employed in the biocatalytic reduction of seven substrates encompassing four families of α,β -substituted unsaturated compounds, including acyclic/cyclic aldehydes and ketones, maleimides and terpenoids. Through an extensive investigation, optimal reaction conditions have been identified and a mechanism of electron transfer has been proposed. The systems were successfully implemented using both aqueous and biphasic conditions, thus allowing a variety of procedures to be employed to best suit the requirements of the substrate or the restrictions of the experimental methods. In each instance, the obtained yields and enantiomeric excesses were typically comparable to those attained in the equivalent NAD(P)H dependent assays utilising an enzyme coupled regeneration system. A number of photosensitisers were tested in assays of both PETNR and TOYE and displayed an array of different activities towards catalytic turnover. The complexes of the general formula $[\text{Ru}(\text{bpz})_2(\text{N}^{\wedge}\text{N})]^{n+}$ demonstrated a distinct dependence of catalytic activity upon the redox potentials of the sensitiser, thus highlighting the importance of tuning the properties of the sensitiser to maximise the efficiency of electron transfer. The success of the iridium complexes is of particular relevance as their unique combination of high water solubility and unusual, though beneficial, redox properties makes them ideal alternatives as photosensitisers in biocatalytic systems, solar hydrogen production and potentially as probes in studying electron transfer in enzymes. Further manipulation of the complexes may be required to improve absorption in the visible region of the spectrum to aid in maximising the efficiency of sensitisation.

Overall, this investigation clearly demonstrates that transition metal complexes are excellent candidates as photosensitisers in developing practical light-driven biocatalytic systems. The results presented herein describe a system with a high activity towards a range of substrates far beyond those that have been previously reported. Whilst significant advances have been made in developing these light-driven biocatalytic systems, there remains much scope to achieve further progress in both the synthetic chemistry and biocatalytic aspects of this investigation; potential strategies towards these goals having been discussed in the

respective sections of this thesis. Perhaps the most significant of these suggestions is the continued investigation of the covalently bound photosensitiser-enzyme constructs. It is thought that should such systems be achieved the range of substrates could be greatly increased owing to the milder reaction conditions that consequently could be employed for photosensitised assays. Expanding the study to encompass other enzymes is also of utmost importance as this could significantly increase the range of chemical transformations that may be undertaken with these systems, thus increasing their industrial relevance.

It is expected that, should further investigation be undertaken, these artificial photosynthetic systems can be readily expanded to encompass a variety of applications and provide an effective alternative to the use of costly redox cofactors and a reliance upon complex regeneration techniques.

SECTION SEVEN: APPENDICES

APPENDIX A: SUMMARY OF SYNTHESISED PHOTOSENSITISERS

As part of this project a total of 14 ruthenium based photosensitisers have been prepared and fully characterised, the structures of which are presented in Fig. A.1.; A.2. and A.3. A further 12 cationic cyclometalated iridium(III) complex salts were synthesised utilising ligands containing positively charged functionality and are illustrated in Fig. A.4. and A.5.

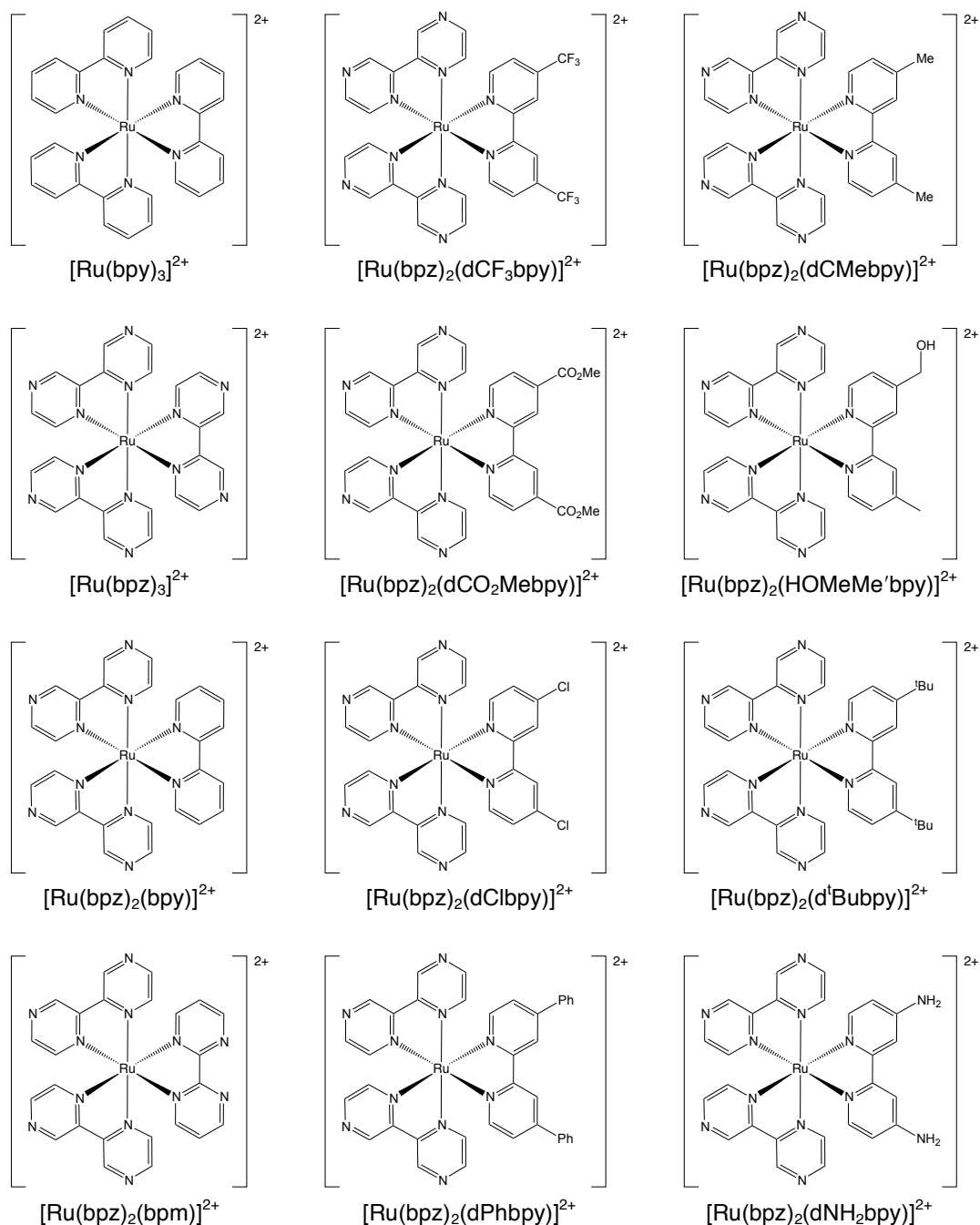


Fig. A.1. Representative structures of the prepared photosensitisers containing the bis(2,2'-bipyrazyl)ruthenium(II) moiety and a neutral polyheteroaryl ancillary ligand. Complexes were isolated as both the hexafluorophosphate and chloride salts.

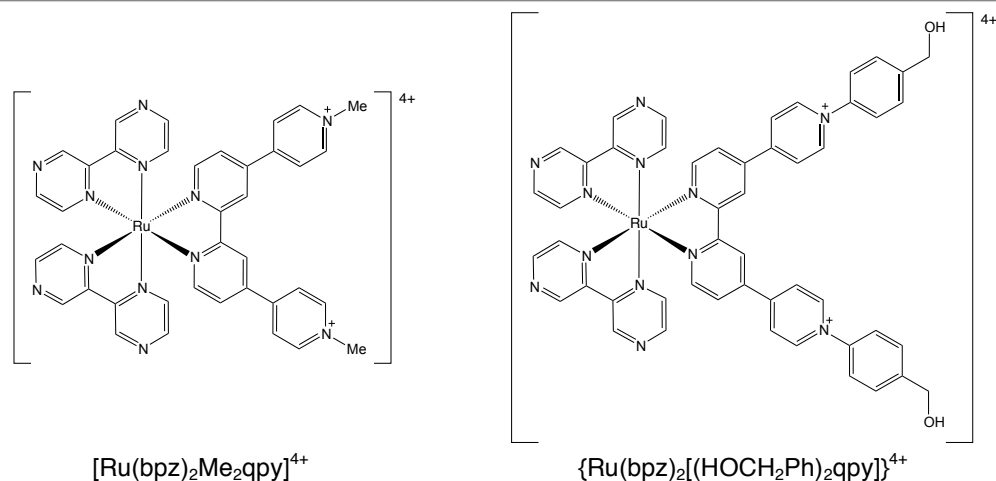


Fig. A.2. Representative structures of the prepared photosensitisers containing the bis(2,2'-bipyridyl)ruthenium(II) moiety and a 4,4':2':2'':4'':4'''-quaterpyridinium ancillary ligand. Complexes were isolated as both the hexafluorophosphate and chloride salts.

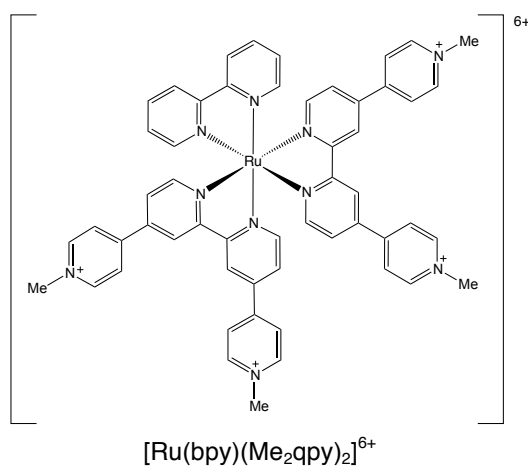


Fig. A.3. Structure of $[\text{Ru}(\text{bpy})(\text{Me}_2\text{qpy})_2]^{6+}$ that was prepared in an effort to access complex salts of higher overall positive charge. The complex was isolated as both the hexafluorophosphate and chloride salts.

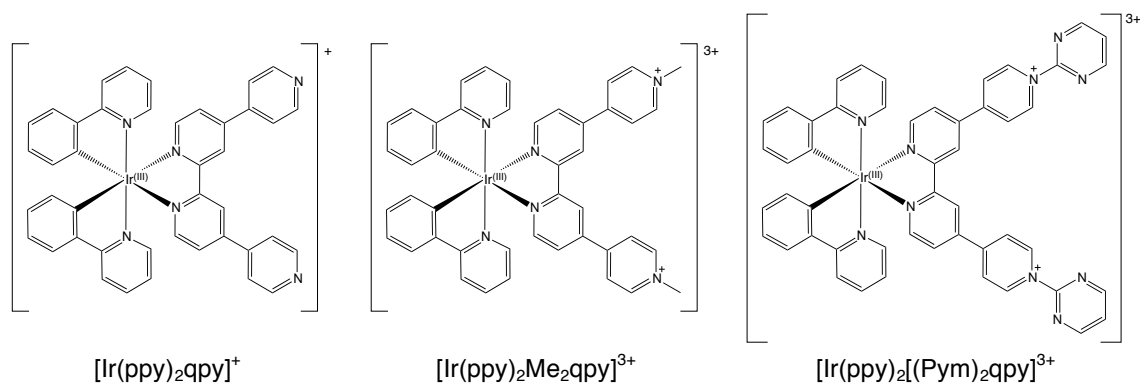


Fig. A.4. Representative structures of the cationic cyclometalated iridium(III) complexes of 2-phenylpyridine utilising the 4,4':2':2'':4'':4'''-quaterpyridyl or 4,4':2':2'':4'':4'''-quaterpyridinium ancillary ligands. The complexes were isolated as both the hexafluorophosphate and chloride salts.

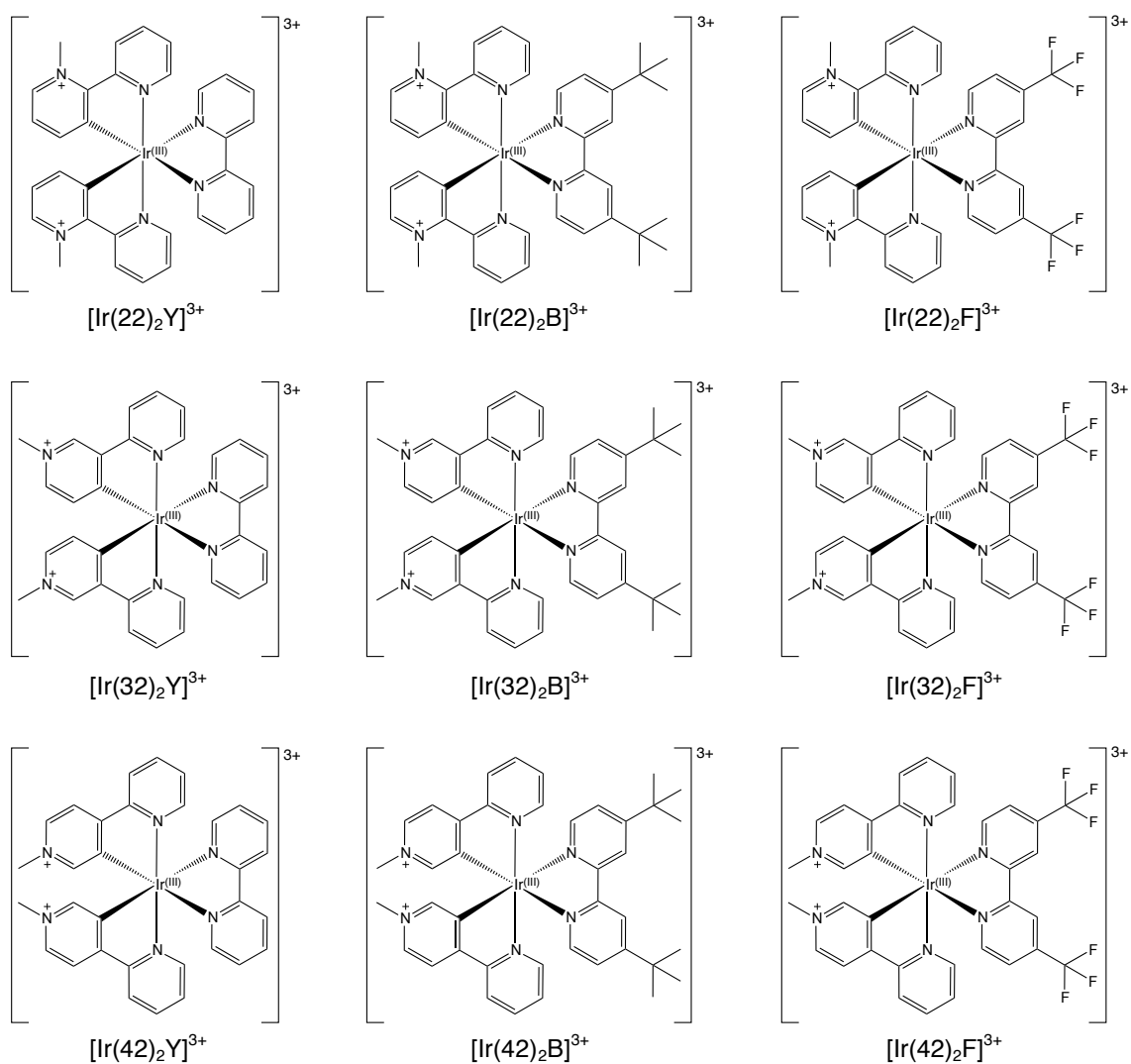


Fig. A.5. Representative structures of the bis cyclometalated iridium(III) complexes of the 2,2', 3,2' and 4,2'- isomers of methylated bipyridinium. The complexes were isolated as the hexafluorophosphate and chloride salts.

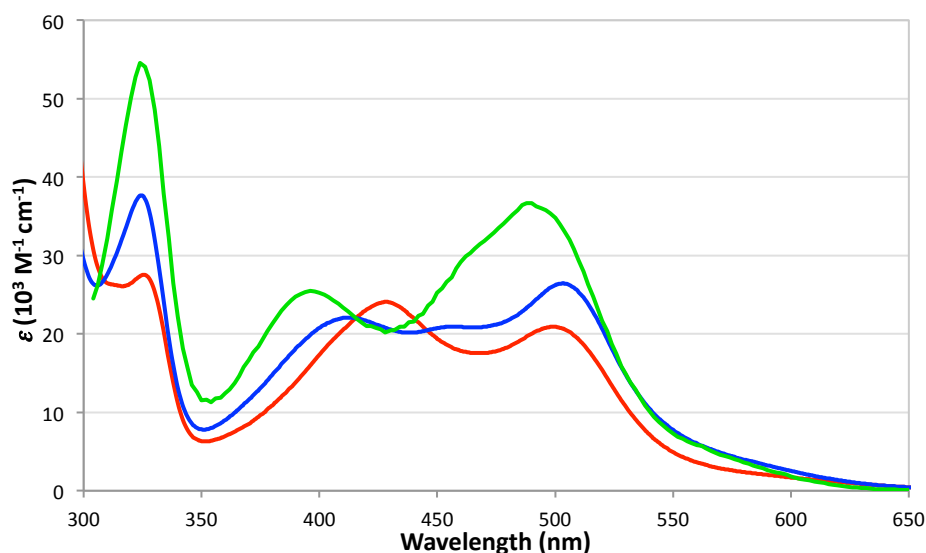
APPENDIX B:**Electronic Spectroscopy and Electrochemistry of the Ruthenium(II) Polypyridyl Complexes of [Me₂qpy]²⁺**

Fig. B.1. UV-visible absorption spectra of the complexes $[Ru(bpy)_2(Me_2qpy)](PF_6)_4$ ^[153] (red), $[Ru(bpy)(Me_2qpy)_2](PF_6)_6$ (blue) and $[Ru(Me_2qpy)_3](PF_6)_6$ ^[186] in acetonitrile at 298 K

Table B.1. Redox properties for compounds of the general formula $[Ru(bpy)_{3-n}(Me_2qpy)_n]^{(n+2)+}$.^a

Cation	Ru(III/II)	$E(n/n-1)$	$E(n-1/n-2)$	$E(n-2/n-3)$
$[Ru(bpy)_2(Me_2qpy)]^{4+}$	+1.41	-0.62	-0.73	--
$[Ru(bpy)(Me_2qpy)_2]^{6+}$	+1.52	-0.62 ^c	-0.72 ^c	-1.19 ^c
$[RuMe_2qpy)_3]^{8+}$	+1.61 ^b	-0.60	-0.74	--

^a $E = 0.5 \times (E_{pc} + E_{pa})$ vs Ag/AgCl; Measurements performed in acetonitrile, 0.1 M $[nBu_4N]PF_6$, with a scan rate of 100 mV s⁻¹ at RT; Solutions ca. 1.5×10^{-4} M with respect to analyte; F_c/F_c^+ internal reference, $E = 0.44$ V, $\Delta E_p = 70-90$ mV; Pt disc working electrode and Pt wire auxiliary electrode. ^b quasi-reversible process; ^c irreversible process, E_{pc} ; ^d irreversible process, E_{pa} ; as determined using differential pulse voltammetry techniques, potential increment = 2 mV; amplitude = 50 mV; pulse width = 0.01 s.

APPENDIX C:

X-Ray Crystallography

Data were collected on Oxford Diffraction XCalibur 2 or Bruker APEX CCD X-ray diffractometers by using MoK α radiation ($\lambda = 0.71073 \text{ \AA}$), and the data were processed by using the Oxford Diffraction CrysAlis Pro^[367], Bruker SAINT^[368], Bruker SMART^[368] and SADABS^[369] software packages. The structures were solved by direct methods by using SIR-2004^[370] via SHELXS-97,^[371] and refined by full-matrix least-squares on all F_0^2 data using SHELXL-97.^[372] All other calculations were carried out by using the SHELXTL package.^[373] All non-hydrogen atoms were refined anisotropically and hydrogen atoms were included in idealised positions by using the riding model, with thermal parameters 1.2 times those of aromatic parent carbon atoms, and 1.5 times those of methyl parent carbons.

Crystallographic data and refinement details for $[\text{Ir}(\text{ppy})_2\text{Pym}_2\text{qpy}](\text{PF}_6)_3$, $[\text{Ir}(22)_2\text{Y}](\text{PF}_6)_3$, $[\text{Ir}(22)_2\text{B}](\text{PF}_6)_3$, $[\text{Ir}(22)_2\text{F}](\text{PF}_6)_3$, $[\text{Ir}(32)_2\text{Y}](\text{PF}_6)_3$, $[\text{Ir}(32)_2\text{B}](\text{PF}_6)_3$, $[\text{Ir}(42)_2\text{Y}](\text{PF}_6)_3$ and $[\text{Ir}(22)_2\text{ClMeCN}](\text{PF}_6)_3$ are presented in Table A1. Concerning the structure of $[\text{Ir}(32)_2\text{Y}](\text{PF}_6)_3$, the obtained crystals were pseudo-merohedrally twinned, as such the twin matrix $(-1 \ 0 \ 0 / 0 \ -1 \ 0 / 1 \ 0 \ 1)$ was included in the instruction file to account for this and the scale factor refined to 0.314(9). Each twin component was also a racemic twin and the refined scale factors were 0.264(9) and 0.208(9). A problem regarding the pseudo-symmetry was also apparent which appears as an A alert on applying a CHECKCIF. Though most of the structure obeyed the lattice halving, one PF_6^- anion could not be refined satisfactorily, and the R value in the halved lattice was 10.0 % versus 6.4 % for the larger unit cell.

Table. C.1. Crystallographic data for complexes $\{Ir(ppy)_2[(Pym)_2qpy]\}(PF_6)_3$, $[Ir(22)_2Y](PF_6)_3$, $[Ir(22)_2B](PF_6)_3$, $[Ir(32)_2Y](PF_6)_3$, $[Ir(32)_2B](PF_6)_3$ and $[Ir(42)_2B](PF_6)_3$

	$[Ir(ppy)_2PQ](PF_6)_3$	$[Ir(22)_2Y](PF_6)_3$	$[Ir(22)_2B](PF_6)_3$	$[Ir(22)_2F](PF_6)_3$	$[Ir(32)_2Y](PF_6)_3$	$[Ir(32)_2B](PF_6)_3$	$[Ir(42)_2Y](PF_6)_3$
Empirical formula	$C_{56}H_{45}F_{18}IrN_{13}P_3$	$C_{37.5}H_{38.25}F_{18}IrN_6$ $O_{1.75}P_3$	$C_{48}H_{56}F_{18}IrN_{10}P_3$	$C_{41}H_{39.5}F_{24}IrN_{6.5}O_3P_3$	$C_{36}H_{34}F_{18}IrN_8P_3$	$C_{49}H_{62}F_{18}IrN_6O_3P_3$	$C_{38}H_{40}F_{18}IrN_7OP_3$
Formula weight	1527.16	1228.1	1400.14	1412.40	1205.82	1410.16	1237.88
Crystal appearance	Amber plate	Yellow Plate	Yellow Plate	Yellow Plate	Pale Yellow Plate	Yellow Plate	
<i>T</i> (K)	100(2)	100(2)	100(2)	100(2)	100(2)	100(2)	100(2)
<i>l</i> (Å)	0.71073	0.71073	0.71073	0.71073	0.71073	0.71073	0.71073
Crystal system	Monoclinic	Triclinic	Triclinic	Monoclinic	Monoclinic	Monoclinic	Monoclinic
Space group	<i>Cc</i>	$P\bar{1}$	$P\bar{1}$	<i>C2/c</i>	$P2_1$	$P2_1/n$	$P2_1/n$
Unit Cell Dimensions							
<i>a</i> (Å)	22.2647(16)	13.3456(19)	12.2728(19)	14.2871(4)	16.815(5)	10.5238(2)	12.2122(7)
<i>b</i> (Å)	14.6139(11)	13.3584(19)	12.369(2)	19.2131(5)	11.822(3)	43.9969(15)	21.6961(12)
<i>c</i> (Å)	18.6288(14)	13.788(2)	19.218(3)	37.1997(9)	22.655(12)	12.3994(3)	17.2606(9)
α (deg)	90	70.073(2)	98.396(3)	90	90	90	90
β (deg)	102.4440(10)	87.824(3)	101.854(3)	93.4620(1)	111.57(5)	99.663(2)	101.7760(10)
γ (deg)	90	80.281(2)	97.282(2)	90	90	90	90
Volume (Å ³)	5918.9(8)	2277.2(6)	2787.3(8)	10192.7(5)	4188(3)	5659.6(3)	4477.1(4)
<i>Z</i>	4	2	2	8	4	4	4
<i>D</i> _{calcd} / mg m ⁻³	1.714	1.791	1.668	1.841	1.912	1.655	1.837
Absorption coefficient (mm ⁻¹)	2.445	3.152	2.586	7.200	3.424	2.550	3.206
<i>F</i> (000)	3024	1207	1396	5544	2360	2824	2436
Crystal size/mm	0.25 × 0.20 × 0.03	0.55 × 0.40 × 0.20	0.45 × 0.40 × 0.10	0.19 × 0.15 × 0.08	0.30 × 0.22 × 0.10	0.45 × 0.2 × 0.2	0.40 × 0.30 × 0.20
θ range (deg)		2.06-26.43	1.69-26.44	3.86-66.59	1.72-25.35	2.93-25.03	1.88 - 26.36
Reflections collected	25080	13319	16345	34713	30758	111160	25575
Independent reflections (Rint)	13146 (0.0368)	9112 (0.0162)	11170 (0.0196)	8853 (0.0470)	15102 (0.0841)	9978 (0.0641)	9101 (0.0330)
θ max/ $^{\circ}$ (completeness)	25.00 (100 %)	25.00 (98.3 %)	26.44 (97.2 %)	66.59 (98.4 %)	25.35 (99.7 %)	25.03 (99.8 %)	25.00 (99.9 %)
Goodness-of-fit on <i>F</i> ²	1.003	1.042	1.025	1.055	0.993	1.142	1.017
Final <i>R</i> indices	<i>R</i> ₁ = 0.0409	<i>R</i> ₁ = 0.0314	<i>R</i> ₁ = 0.0311	<i>R</i> ₁ = 0.0403	<i>R</i> ₁ = 0.0641	<i>R</i> ₁ = 0.0793	<i>R</i> ₁ = 0.0379
$[I > 2\sigma(I)]$	<i>wR</i> ₂ = 0.0897	<i>wR</i> ₂ = 0.0818	<i>wR</i> ₂ = 0.0765	<i>wR</i> ₂ = 0.1025	<i>wR</i> ₂ = 0.1346	<i>wR</i> ₂ = 0.1556	<i>wR</i> ₂ = 0.0850
<i>R</i> indices (all data)	<i>R</i> ₁ = 0.0522	<i>R</i> ₁ = 0.0332	<i>R</i> ₁ = 0.0337	<i>R</i> ₁ = 0.0424	<i>R</i> ₁ = 0.1112	<i>R</i> ₁ = 0.0883	<i>R</i> ₁ = 0.0503
Peak and hole/ <i>e</i> Å ⁻³	<i>wR</i> ₂ = 0.0932	<i>wR</i> ₂ = 0.0831	<i>wR</i> ₂ = 0.0780	<i>wR</i> ₂ = 0.1040	<i>wR</i> ₂ = 0.1641	<i>wR</i> ₂ = 0.1610	<i>wR</i> ₂ = 0.0907
	1.235, -0.914	1.754, -0.798	1.726, -1.258	2.447, -1.130	2.620, -2.499	2.648, -4.096	1.356, -0.731

APPENDIX D:
Characterization data of $[\text{Ir}(\mathbf{22})_2\text{ClMeCN}](\text{PF}_6)_3$

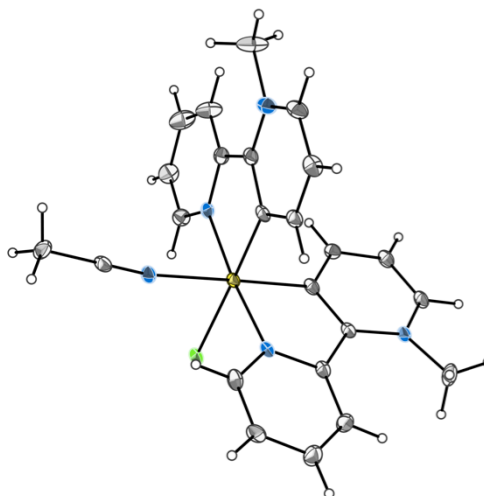


Fig. D.1. Representation of the crystal structure of $[\text{Ir}(\mathbf{22})_2\text{ClMeCN}](\text{PF}_6)_3$ with counter anions and solvent molecules omitted for clarity. Displacement ellipsoids are set at the 30 % probability level.

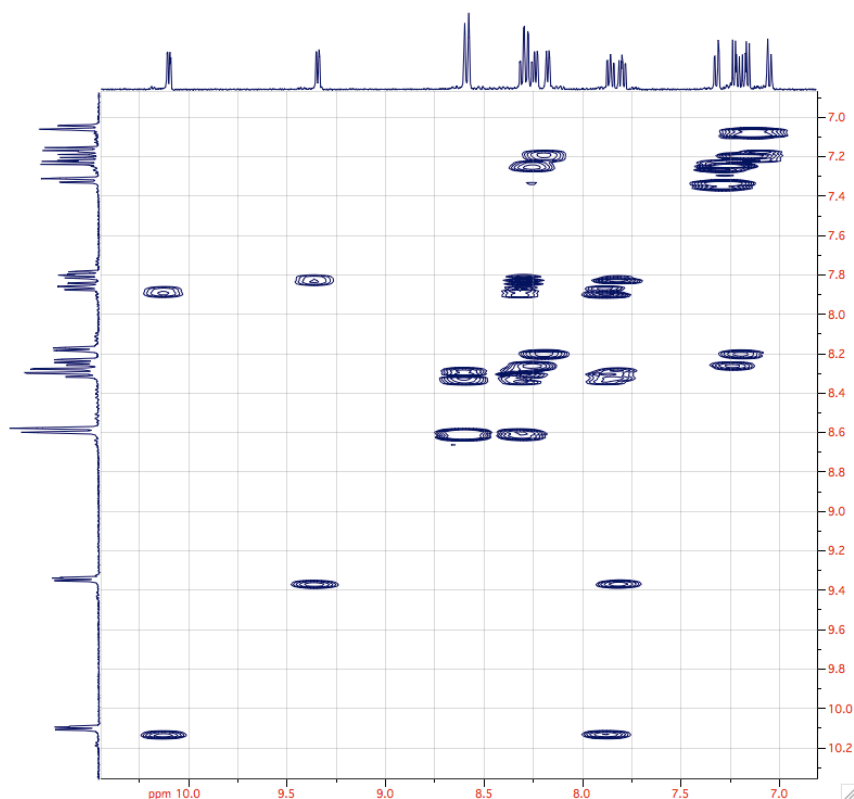


Fig. D.2. A section of the 2D-COSY spectrum of $[\text{Ir}(\mathbf{22})_2\text{Y}](\text{PF}_6)_3$ in the region 6.75 – 10.50 ppm used in the assignment of the ^1H -NMR resonances. Spectra recorded in CD_3CN .

Data: ^1H -NMR: δ_{H} (400 MHz, CD_3CN): 10.10 (1H, ddd, $J = 5.7, 1.7, 0.6$ Hz), 9.34 (1H, ddd, $J = 5.7, 1.6, 0.6$ Hz), 8.58 (2H, d, $J = 8.7$ Hz), 8.32-8.26 (2H, m), 8.23 (1H, dd, $J = 5.9, 0.8$ Hz), 8.18 (1H, dd, $J = 5.9, 0.7$ Hz), 7.86 (1H, ddd, $J = 7.6, 5.7, 1.2$ Hz), 7.80 (1H, ddd, $J = 7.6, 5.7, 1.2$ Hz), 7.32 (1H, dd, $J = 7.9, 5.9$ Hz), 7.22 (1H, dd, $J = 7.9, 5.9$ Hz), 7.17 (1H, dd, $J = 7.9, 5.9$ Hz), 7.05 (1H, dd, $J = 8.1, 1.3$ Hz), 4.60 (3H, s), 4.58 (3H, s), 2.09 (3H, s) ppm.

APPENDIX E:
Electronic Absorption and Electrochemistry of 1-Methyl-
bipyridinium pro-ligands.

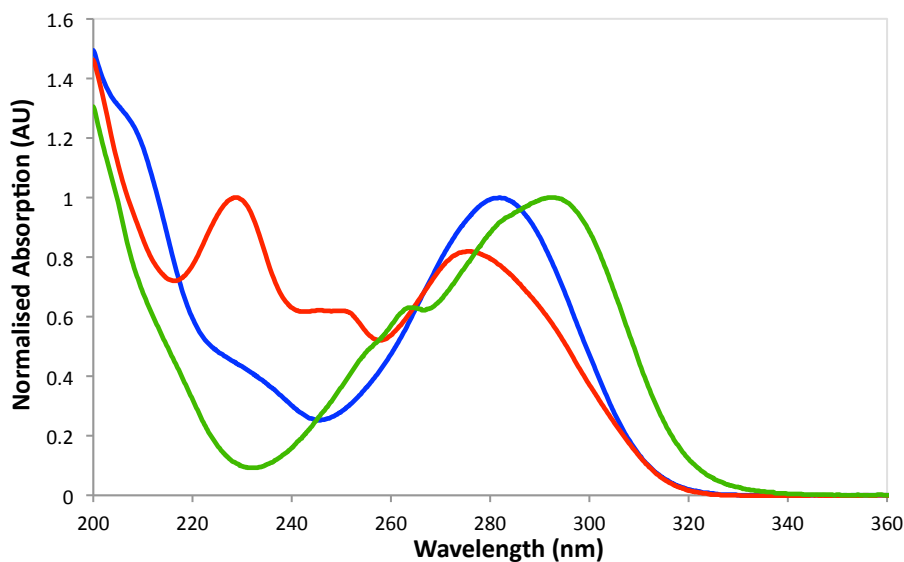


Fig. E.1. Normalized UV-visible absorption spectra of [1-Me-2,2'-bpy]PF₆ (blue), [1-Me-3,2'-bpy]PF₆ (red) and [1-Me-4,2'-bpy]PF₆ (green) displaying the region of $200 \leq \lambda \leq 360$ nm. Recorded in acetonitrile at 298 K.

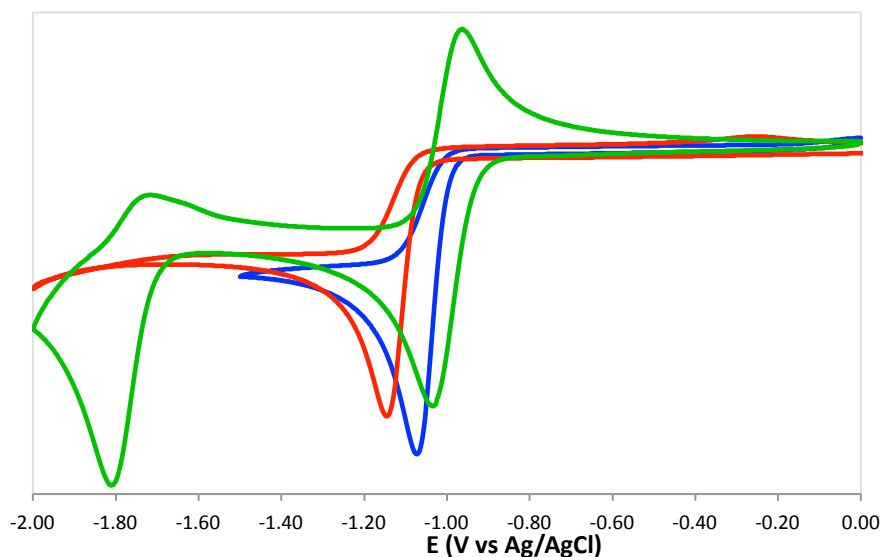


Fig. E.2. Cyclic voltammograms depicting the reduction processes of [1-Me-2,2'-bpy]PF₆ (blue), [1-Me-3,2'-bpy]PF₆ (red) and [1-Me-4,2'-bpy]PF₆ (green) recorded at 100 mVs^{-1} in $0.1 \text{ M } n\text{-Bu}_4\text{NPF}_6$ acetonitrile at 298 K.

APPENDIX F:
Theoretical studies of $[\text{Ir}(\text{22})_2\text{B}]$ and $[\text{Ir}(\text{22})_2\text{F}]$

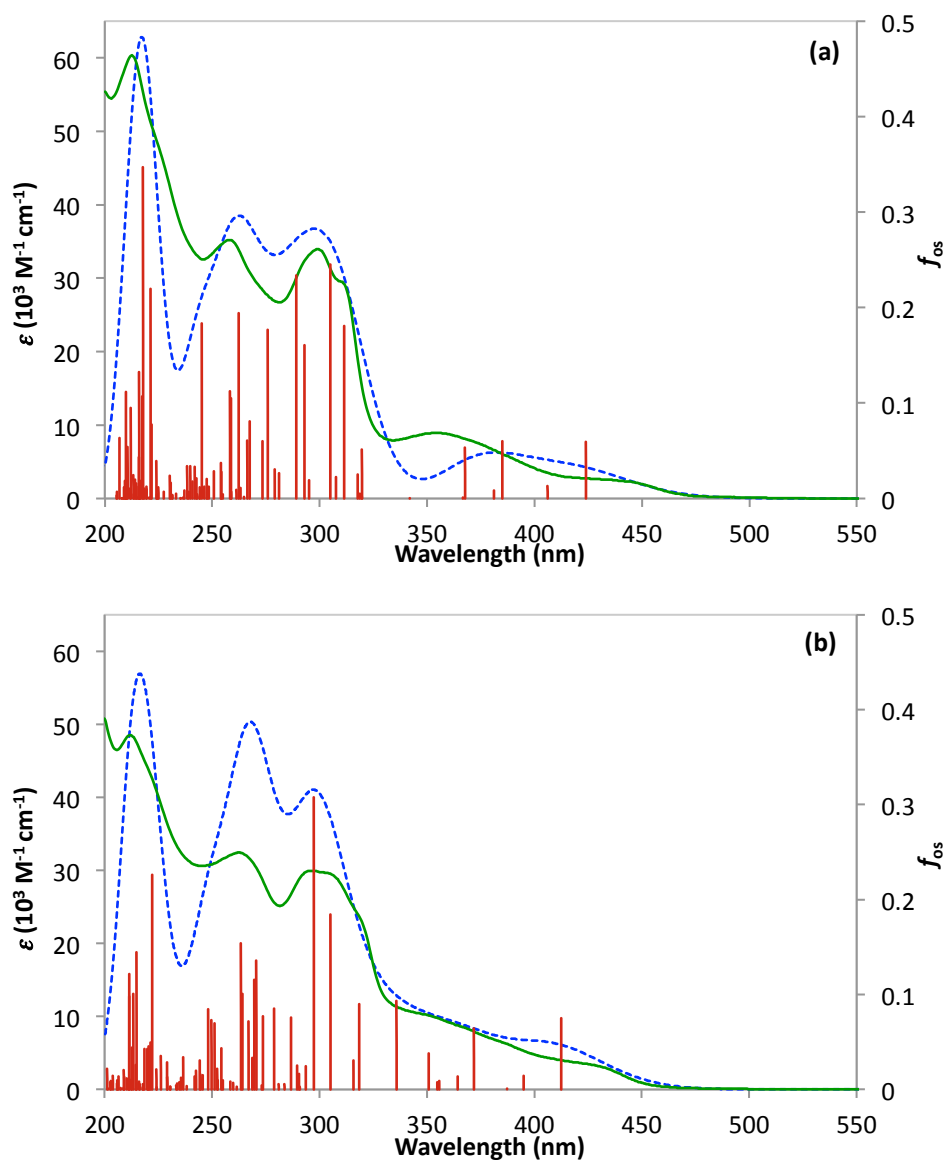


Fig. F.1. Experimental (green) and the TD-DFT calculated (blue dash) UV-Visible spectra of **(a)** $[\text{Ir}(\text{22})_2\text{B}]^{3+}$ and **(b)** $[\text{Ir}(\text{22})_2\text{F}]^{3+}$. Experimental data is plotted against the primary ϵ -axes with calculated spectra scaled to match to allow for comparison of absorption bands. Individual calculated vertical transitions (red) are plotted versus the secondary oscillator strength (f_{os}) axes

Table F.1. Select vertical transitions obtained by TD-DFT calculations performed for the complex cations $[\text{Ir}(\text{22})_2\text{F}]^{3+}$ and $[\text{Ir}(\text{22})_2\text{B}]^{3+}$. Presented transitions chosen to represent the major contributors to each of the dominant bands in the UV-visible spectra.

Cation	λ/nm	$\Delta E/\text{eV}$	f_{os}	Major Contributions
$[\text{Ir}(\text{22})_2\text{B}]^{3+}$	423.9	2.92	0.0595	HOMO->LUMO (93 %)
	406.1	3.05	0.0132	HOMO->L+1 (93 %)
	385.0	3.22	0.06	H-1->LUMO (90 %)
	381.1	3.25	0.0081	H-2->LUMO (92 %)
	367.7	3.37	0.0531	H-2->L+1 (93 %)
	319.7	3.88	0.0511	H-4->LUMO (91 %)
	311.4	3.98	0.1806	H-2->L+2 (88 %)
	305.0	4.07	0.2453	H-4->L+1 (66 %), HOMO->L+3 (27 %)
	292.9	4.23	0.1604	H-3->L+2 (26 %), H-1->L+3 (64 %)
	289.1	4.29	0.2335	H-3->L+2 (59 %), H-1->L+3 (20 %)
	275.9	4.50	0.1768	H-5->LUMO (15 %), H-2->L+4 (54 %), H-2->L+6 (11 %)
	262.3	4.73	0.1941	H-1->L+5 (65 %)
	258.7	4.79	0.1049	H-2->L+4 (12 %), H-2->L+6 (61 %)
	258.3	4.80	0.1122	H-1->L+6 (69 %)
	$[\text{Ir}(\text{22})_2\text{F}]^{3+}$	412.5	3.01	0.0751
395.0		3.14	0.0141	HOMO->L+1 (93 %)
371.9		3.33	0.0646	H-1->LUMO (92 %)
364.3		3.40	0.0138	H-2->LUMO (91 %)
355.7		3.49	0.0091	H-1->L+1 (81 %)
350.8		3.53	0.0383	H-2->L+1 (80 %), H-1->L+2 (17 %)
335.9		3.69	0.0933	H-2->L+2 (90 %)
305.1		4.06	0.1846	H-3->L+1 (60 %), HOMO->L+3 (31 %)
297.4		4.17	0.3078	H-4->L+2 (61 %), H-1->L+3 (15 %)
270.7		4.58	0.1359	H-5->L+1 (11 %), H-2->L+5 (35 %), H-1->L+4 (14 %), HOMO->L+7 (18 %)
269.7		4.60	0.1156	H-2->L+6 (52 %)
264.1		4.69	0.1005	H-5->L+2 (62 %), H-2->L+4 (25 %)
263.5		4.71	0.154	H-5->L+2 (33 %), H-2->L+4 (54 %)

APPENDIX G:
Electronic Absorption of Ruthenium Polyheteroaryl
Labelling Complexes

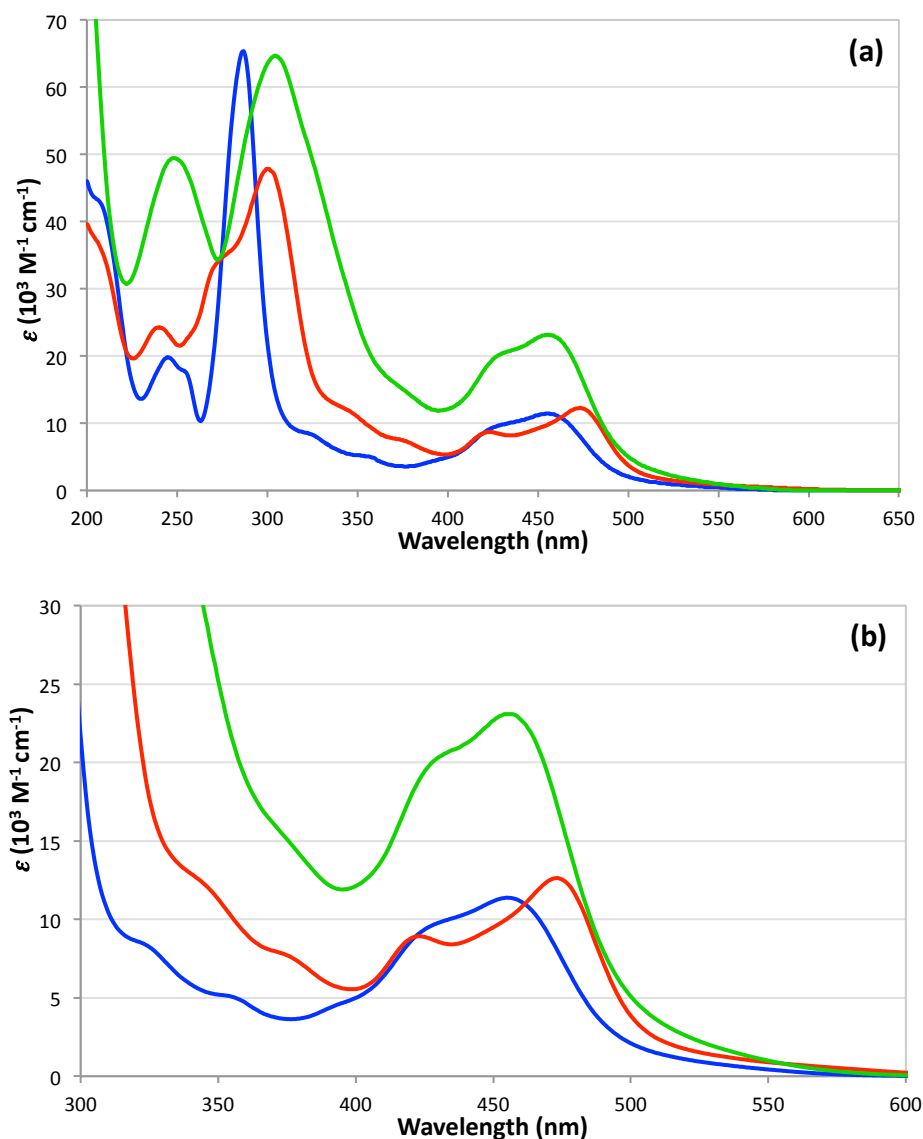


Fig. G.1. UV-visible absorption spectra of $[\text{Ru}(\text{bpy})_2(4\text{-hydroxymethyl-4'-methyl-2,2'-bipyridine})]\text{Cl}_2$ (blue), $[\text{Ru}(\text{bpz})_2(4\text{-hydroxymethyl-4'-methyl-2,2'-bipyridine})]\text{Cl}_2$ (red) and $\{[\text{Ru}(\text{bpz})_2(\text{HOCH}_2\text{Ph})_2\text{qpy}]\}\text{Cl}_4$ (green) in deionised water at 293 K displaying **a**) the full spectra and **b**) $300 \leq \lambda \leq 600\text{nm}$ expansion of the lower energy bands. Recorded in deionised water at 298 K.

Table G.1. UV-visible absorption data of the labelling reagents with the general formula $[Ru(L)_2(L)]^{n+}$.^a

Complex	λ_{\max} , nm	ϵ , $10^3 M^{-1} cm^{-1}$	E_{\max} , eV	λ_{onset} , nm	Assignment
[Ru(bpy) ₂ (HOMeMebpy)] ²⁺	245	19.9	5.06	577	$\pi \rightarrow \pi^*$
	287	65.1	3.57		$\pi \rightarrow \pi^*$
	429 ^{sh}	9.7	2.39		$d \rightarrow \pi^*$
	456	11.4	2.25		$d \rightarrow \pi^*$
[Ru(bpz) ₂ (HOMeMebpy)] ²⁺	240	23.8	5.17	613	$\pi \rightarrow \pi^*$
	275 ^{sh}	34.3	4.51		$\pi \rightarrow \pi^*$
	300	47.9	4.13		$\pi \rightarrow \pi^*$
	423	8.7	2.93		$d \rightarrow \pi^*$
	473	12.3	2.62		$d \rightarrow \pi^*$
{Ru(bpz) ₂ [(HOCH ₂ Ph) ₂ qpy]} ⁴⁺	254	54.0	4.88	594	$\pi \rightarrow \pi^*$
	298	64.5	4.16		$\pi \rightarrow \pi^*$
	427 ^{sh}	20.0	2.90		$d \rightarrow \pi^*$
	455	24.3	2.73		$d \rightarrow \pi^*$

^a Solutions ca. 1.0×10^{-5} - 1.0×10^{-4} M recorded in deionised water. λ_{onset} defined as the wavelength above which $\epsilon > 100 M^{-1} cm^{-1}$. ^{sh} denotes a shoulder or a poorly defined maximum.

APPENDIX H:
Homogeneous Light-Driven Biocatalytic Assays
Expanding the System: Applications Towards Other Substrates

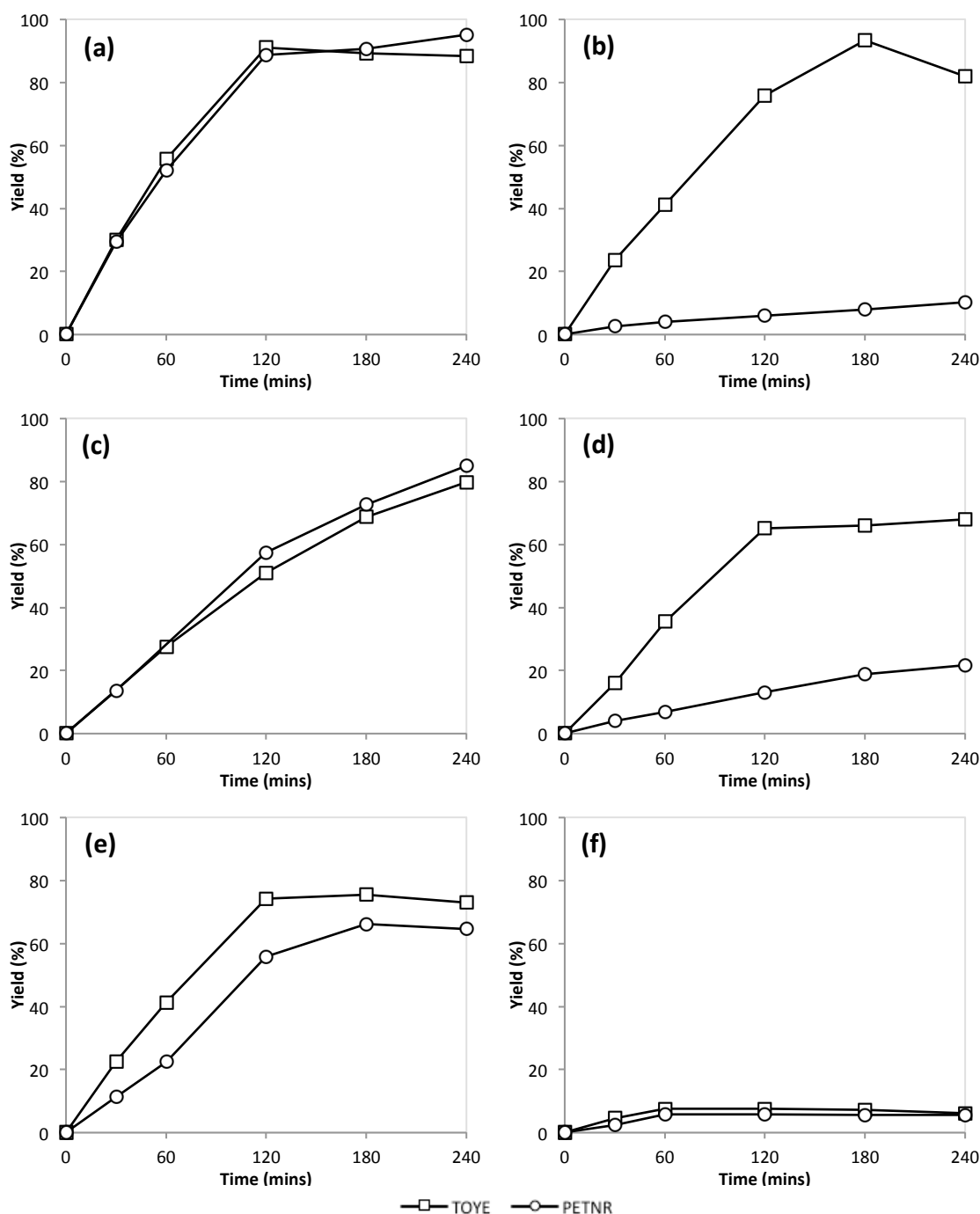


Fig. H.1. Time courses highlighting the relative activity of PETNR_{R324C} and TOYE in the homogenous light-driven bioreductions of a variety of α,β -disubstituted alkene substrates; **(a)** Ketoisophorone; **(b)** N-phenyl-2-methylmaleimide; **(c)** Cinnamaldehyde; **(d)** α -methylcinnamaldehyde; **(e)** 2-methylpentenal; **(f)** (R)-carvone.

REFERENCES

- (1) Skoog, D.A., Holler, F.J., and Crouch, S.R., *Principles of Instrumental Analysis*, **2007**, Thomson Brooks/Cole. p. 367-398.
- (2) Verhoeven, J.W., *Pure Appl. Chem.*, **1996**, 68(12): p. 2223-2286.
- (3) Wayne, C.E. and Wayne, R.P., *Photochemistry*, Oxford Chemistry Primers, **1996**, Oxford University Press, Oxford, UK.
- (4) Mathews, C.K., Van Holde, K.E., and Ahern, K.G., *Biochemistry*, **2000**, Benjamin Cummings. p. 594-626.
- (5) Antonkine, M.L. and Golbeck, J.H., *Photosystem I: FX, FA, and FB Iron-Sulfur Clusters*, in *Encyclopedia of Biological Chemistry*, J.L. Editors-in-Chief: William and M.D. Lane, Editors. **2004**, Elsevier: New York. p. 348-356.
- (6) Lubner, C.E., Grimme, R., Bryant, D.A., and Golbeck, J.H., *Biochemistry*, **2009**, 49(3): p. 404-414.
- (7) Hazzard, J.T., Poulos, T.L., and Tollin, G., *Biochemistry*, **1987**, 26(10): p. 2836-2848.
- (8) Tollin, G., *J. Bioenerg. Biomembr.*, **1995**, 27(3): p. 303-309.
- (9) Meyer, T.E., Przysiecki, C.T., Watkins, J.A., Bhattacharyya, A., Simonsen, R.P., Cusanovich, M.A., and Tollin, G., *Proc. Natl. Acad. Sci. U.S.A.*, **1983**, 80(22): p. 6740-6744.
- (10) Ahmad, I., Cusanovich, M.A., and Tollin, G., *Proc. Natl. Acad. Sci. U.S.A.*, **1981**, 78(11): p. 6724-6728.
- (11) Walker, M.C. and Tollin, G., *Biochemistry*, **1991**, 30(22): p. 5546-5555.
- (12) Walker, M.C., Pueyo, J., Navarro, J., Gómez-Moreno, C., and Tollin, G., *Arch. Biochem. Biophys.*, **1991**, 287(2): p. 351-358.
- (13) Hazzard, J.T., Marchesini, A., Curir, P., and Tollin, G., *Biochim. Biophys. Acta, Protein Struct. Mole. Enzymol.*, **1994**, 1208(1): p. 166-170.
- (14) Orii, Y., *Biochemistry*, **1993**, 32(44): p. 11910-11914.
- (15) Czochralska, B. and Lindqvist, L., *Chem. Phys. Lett.*, **1983**, 101(3): p. 297-299.
- (16) Buxton, G.V., Greenstock, C.L., Helman, W.P., and Ross, A.B., *J. Phys. Chem. Ref. Data*, **1988**, 17(2): p. 513-886.
- (17) Farrington, J.A., Land, E.J., and Swallow, A.J., *Biochim. Biophys. Acta, Bioenerg.*, **1980**, 590(2): p. 273-276.
- (18) Anderson, R.F., *Biochim. Biophys. Acta, Bioenerg.*, **1980**, 590(2): p. 277-281.
- (19) Girvan, H.M., Heyes, D.J., Scrutton, N.S., and Munro, A.W., *J. Am. Chem. Soc.*, **2007**, 129(20): p. 6647-6653.
- (20) Kotlyar, A.B., Borovok, N., and Hazani, M., *Biochemistry*, **1997**, 36(50): p. 15823-15827.
- (21) Graetzel, C.K., Jirousek, M., and Graetzel, M., *J. Phys. Chem.*, **1984**, 88(6): p. 1055-1058.
- (22) Kotlyar, A.B., Borovok, N., Khoroshyy, P., Tenger, K., and Zimányi, L.s., *Photochem. Photobiol.*, **2004**, 79(6): p. 489-493.

- (23) Tenger, K., Khoroshyy, P., Leitgeb, B.z., Rákhely, G.b., Borovok, N., Kotlyar, A., Dolgikh, D.A., and Zimányi, L.s., *J. Chem. Inf. Model.*, **2005**, 45(6): p. 1520-1526.
- (24) Heyes, D.J., Quinn, A.-M., Cullis, P.M., Lee, M., Munro, A.W., and Scrutton, N.S., *Chem. Commun. (Cambridge, U. K.)*, **2009**, (9): p. 1124-1126.
- (25) Kotlyar, A., Borovok, N., Hazani, M., Szundi, I., and Einarsdóttir, Ó., *Eur. J. Biochem.*, **2000**, 267(18): p. 5805-5809.
- (26) Zemel, H. and Hoffman, B.M., *J. Am. Chem. Soc.*, **1981**, 103(5): p. 1192-1201.
- (27) Dixit, B.P.S.N., Moy, V.T., and Vanderkooi, J.M., *Biochemistry*, **1984**, 23(9): p. 2103-2107.
- (28) Wallin, S.A., Stemp, E.D.A., Everest, A.M., Nocek, J.M., Netzel, T.L., and Hoffman, B.M., *J. Am. Chem. Soc.*, **1991**, 113(5): p. 1842-1844.
- (29) Millett, F. and Durham, B., *Biochemistry*, **2002**, 41(38): p. 11315-11324.
- (30) Durham, B. and Millett, F., *Biochim. Biophys. Acta, Bioenerg.*, **2012**, 1817(4): p. 567-574.
- (31) Winkler, J.R., Nocera, D.G., Yocom, K.M., Bordignon, E., and Gray, H.B., *J. Am. Chem. Soc.*, **1982**, 104(21): p. 5798-5800.
- (32) Isied, S.S., Worosila, G., and Atherton, S.J., *J. Am. Chem. Soc.*, **1982**, 104(26): p. 7659-7661.
- (33) Yocom, K.M., Shelton, J.B., Shelton, J.R., Schroeder, W.A., Worosila, G., Isied, S.S., Bordignon, E., and Gray, H.B., *Proc. Natl. Acad. Sci. U.S.A.*, **1982**, 79(22): p. 7052-7055.
- (34) Pan, L.P., Durham, B., Wolinska, J., and Millett, F., *Biochemistry*, **1988**, 27(19): p. 7180-7184.
- (35) Durham, B., Pan, L.P., Long, J.E., and Millett, F., *Biochemistry*, **1989**, 28(21): p. 8659-8665.
- (36) Geren, L., Hahm, S., Durham, B., and Millett, F., *Biochemistry*, **1991**, 30(39): p. 9450-9457.
- (37) Wang, K., Zhen, Y., Sadoski, R., Grinnell, S., Geren, L., Ferguson-Miller, S., Durham, B., and Millett, F., *J. Biol. Chem.*, **1999**, 274(53): p. 38042-38050.
- (38) Engstrom, G., Rajagukguk, R., Saunders, A.J., Patel, C.N., Rajagukguk, S., Merbitz-Zahradnik, T., Xiao, K., Pielak, G.J., Trumpower, B., Yu, C.-A., Yu, L., Durham, B., and Millett, F., *Biochemistry*, **2003**, 42(10): p. 2816-2824.
- (39) Ener, M.E., Lee, Y.-T., Winkler, J.R., Gray, H.B., and Cheruzel, L., *Proc. Natl. Acad. Sci. U.S.A.*, **2010**.
- (40) Nilsson, T., *Proc. Natl. Acad. Sci. U.S.A.*, **1992**, 89(14): p. 6497-6501.
- (41) Zaslavsky, D., Sadoski, R.C., Wang, K., Durham, B., Gennis, R.B., and Millett, F., *Biochemistry*, **1998**, 37(42): p. 14910-14916.
- (42) Downard, A.J., Honey, G.E., Phillips, L.F., and Steel, P.J., *Inorg. Chem.*, **1991**, 30(10): p. 2259-2260.
- (43) Cooper, J.B., MacQueen, D.B., Petersen, J.D., and Wertz, D.W., *Inorg. Chem.*, **1990**, 29(19): p. 3701-3705.
- (44) Boyde, S., Strouse, G.F., Jones, W.E., and Meyer, T.J., *J. Am. Chem. Soc.*, **1990**, 112(20): p. 7395-7396.
- (45) Shaw, J.R., Webb, R.T., and Schmehl, R.H., *J. Am. Chem. Soc.*, **1990**, 112(3): p. 1117-1123.
- (46) Brand, S.E., Rajagukguk, S., Ganesan, K., Geren, L., Fabian, M., Han, D., Gennis, R.B., Durham, B., and Millett, F., *Biochemistry*, **2007**, 46(50): p. 14610-14618.

- (47) O'Regan, B. and Gratzel, M., *Nature*, **1991**, 353(6346): p. 737-740.
- (48) Hagfeldt, A., Boschloo, G., Sun, L., Kloo, L., and Pettersson, H., *Chem. Rev. (Washington, DC, U. S.)*, **2010**, 110(11): p. 6595-6663.
- (49) Nazeeruddin, M.K. and Grätzel, M., *Conversion and Storage of Solar Energy using Dye-sensitized Nanocrystalline TiO₂ Cells*, in *Comprehensive Coordination Chemistry II*, J.A.M. Editors-in-Chief: and T.J. Meyer, Editors. **2003**, Pergamon: Oxford. p. 719-758.
- (50) Grätzel, M., *J. Photochem. Photobiol., C*, **2003**, 4(2): p. 145-153.
- (51) Polo, A.S., Itokazu, M.K., and Murakami Iha, N.Y., *Coord. Chem. Rev.*, **2004**, 248(13-14): p. 1343-1361.
- (52) Grätzel, M., *Inorg. Chem.*, **2005**, 44(20): p. 6841-6851.
- (53) Nazeeruddin, M.K., Kay, A., Rodicio, I., Humphry-Baker, R., Mueller, E., Liska, P., Vlachopoulos, N., and Graetzel, M., *J. Am. Chem. Soc.*, **1993**, 115(14): p. 6382-6390.
- (54) Ferrere, S. and Gregg, B.A., *J. Am. Chem. Soc.*, **1998**, 120(4): p. 843-844.
- (55) Sauv e, G., Cass, M.E., Coia, G., Doig, S.J., Lauermann, I., Pomykal, K.E., and Lewis, N.S., *J. Phys. Chem. B*, **2000**, 104(29): p. 6821-6836.
- (56) Chen, Y., Liu, W., Jin, J.-S., Liu, B., Zou, Z.-G., Zuo, J.-L., and You, X.-Z., *J. Organomet. Chem.*, **2009**, 694(5): p. 763-770.
- (57) Ning, Z., Zhang, Q., Wu, W., and Tian, H., *J. Organomet. Chem.*, **2009**, 694(17): p. 2705-2711.
- (58) Geary, E.A.M., Yellowlees, L.J., Jack, L.A., Oswald, I.D.H., Parsons, S., Hirata, N., Durrant, J.R., and Robertson, N., *Inorg. Chem.*, **2004**, 44(2): p. 242-250.
- (59) P echy, P., Renouard, T., Zakeeruddin, S.M., Humphry-Baker, R., Comte, P., Liska, P., Cevey, L., Costa, E., Shklover, V., Spiccia, L., Deacon, G.B., Bignozzi, C.A., and Gr tzel, M., *J. Am. Chem. Soc.*, **2001**, 123(8): p. 1613-1624.
- (60) Yella, A., Lee, H.-W., Tsao, H.N., Yi, C., Chandiran, A.K., Nazeeruddin, M.K., Diao, E.W.-G., Yeh, C.-Y., Zakeeruddin, S.M., and Gr tzel, M., *Science*, **2011**, 334(6056): p. 629-634.
- (61) Kitamura, T., Ikeda, M., Shigaki, K., Inoue, T., Anderson, N.A., Ai, X., Lian, T., and Yanagida, S., *Chem. Mater.*, **2004**, 16(9): p. 1806-1812.
- (62) Fontecilla-Camps, J.C., Amara, P., Cavazza, C., Nicolet, Y., and Volbeda, A., *Nature*, **2009**, 460(7257): p. 814-822.
- (63) Lubner, C.E., Kn rzer, P., Silva, P.J.N., Vincent, K.A., Happe, T., Bryant, D.A., and Golbeck, J.H., *Biochemistry*, **2010**, 49(48): p. 10264-10266.
- (64) Arnon, D.I., Mitsui, A. and Panegue, A., *Science*, **1961**, 134(3488): p. 1425-1437.
- (65) Tagawa, K. and Arnon, D.I., *Nature*, **1962**, 195(4841): p. 537-543.
- (66) Arnon, D.I., *Science*, **1965**, 149(3691): p. 1460-1470.
- (67) Benemann, J.R., Berenson, J.A., Kaplan, N.O., and Kamen, M.D., *Proc. Natl. Acad. Sci. U.S.A.*, **1973**, 70(8): p. 2317-2320.
- (68) Rosen, M.M. and Krasna, A.I., *Photochem. Photobiol.*, **1980**, 31(3): p. 259-265.
- (69) McTavish, H., *J. Biochem. (Tokyo, Jpn.)*, **1998**, 123(4): p. 644-649.

- (70) Ihara, M., Nishihara, H., Yoon, K.-S., Lenz, O., Friedrich, B., Nakamoto, H., Kojima, K., Honma, D., Kamachi, T., and Okura, I., *Photochem. Photobiol.*, **2006**, 82(3): p. 676-682.
- (71) Grimme, R.A., Lubner, C.E., Bryant, D.A., and Golbeck, J.H., *J. Am. Chem. Soc.*, **2008**, 130(20): p. 6308-6309.
- (72) Antonkine, M.L., Maes, E.M., Czernuszewicz, R.S., Breitenstein, C., Bill, E., Falzone, C.J., Balasubramanian, R., Lubner, C., Bryant, D.A., and Golbeck, J.H., *Biochim. Biophys. Acta, Bioenerg.*, **2007**, 1767(6): p. 712-724.
- (73) Grimme, R.A., Lubner, C.E., and Golbeck, J.H., *Dalton Trans.*, **2009**, (45): p. 10106-10113.
- (74) Lubner, C.E., Applegate, A.M., Knörzner, P., Ganago, A., Bryant, D.A., Happe, T., and Golbeck, J.H., *Proc. Natl. Acad. Sci. U.S.A.*, **2011**, 108(52): p. 20988-20991.
- (75) Okura, I., *Coord. Chem. Rev.*, **1985**, 68(0): p. 53-99.
- (76) Okura, I. and Kim-Thuan, N., *J. Mol. Catal.*, **1979**, 6(3): p. 227-230.
- (77) Okura, I. and Kim-Thuan, N., *J. Mol. Catal.*, **1979**, 5(4): p. 311-314.
- (78) Okura, I., Takeuchi, M., Kusunoki, S., and Aono, S., *Inorg. Chim. Acta*, **1982**, 63(0): p. 157-159.
- (79) Amao, Y., Tomonou, Y., Ishikawa, Y., and Okura, I., *Int. J. Hydrogen Energy*, **2002**, 27(6): p. 621-625.
- (80) Okura, I., Takeuchi, M., and Kim-Thuan, N., *Photochem. Photobiol.*, **1981**, 33(3): p. 413-416.
- (81) Okura, I., Takeuchi, M., and Kim-Thuan, N., *Chem. Lett.*, **1980**, 9(6): p. 765-766.
- (82) Okura, I., Kaji, N., Aono, S., Kita, T., and Yamada, A., *Inorg. Chem.*, **1985**, 24(4): p. 451-453.
- (83) Okura, I., Takeuchi, M., Kusunoki, S., and Aono, S., *Chem. Lett.*, **1982**, 11(2): p. 187-188.
- (84) Asakura, N., Hiraishi, T., Kamachi, T., and Okura, I., *J. Mol. Catal. A: Chem.*, **2001**, 172(1-2): p. 1-7.
- (85) Reisner, E., Fontecilla-Camps, J.C., and Armstrong, F.A., *Chem. Commun. (Cambridge, U. K.)*, **2009**, (5): p. 550-552.
- (86) Reisner, E., Powell, D.J., Cavazza, C., Fontecilla-Camps, J.C., and Armstrong, F.A., *J. Am. Chem. Soc.*, **2009**, 131(51): p. 18457-18466.
- (87) Woolerton, T.W., Sheard, S., Reisner, E., Pierce, E., Ragsdale, S.W., and Armstrong, F.A., *J. Am. Chem. Soc.*, **2010**, 132(7): p. 2132-2133.
- (88) Kadereit, D. and Waldmann, H., *Chem. Rev. (Washington, DC, U. S.)*, **2001**, 101(11): p. 3367-3396.
- (89) Weckbecker, A., Gröger, H., Hummel, W., *Regeneration of Nicotinamide Coenzymes: Principles and Applications for the Synthesis of Chiral Compounds*, in *Biosystems Engineering I: Advances in Biochemical Engineering/Biotechnology*, C. Wittmann and R. Krull, Editors. **2010**, Springer Berlin / Heidelberg. p. 195-242.
- (90) Servi, S., *Synthesis*, **1990**, 01(01): p. 1-25.
- (91) Wong, C.H. and Whitesides, G.M., *J. Org. Chem.*, **1982**, 47(14): p. 2816-2818.
- (92) Seelbach, K., Riebel, B., Hummel, W., Kula, M.-R., Tishkov, V.I., Egorov, A.M., Wandrey, C., and Kragl, U., *Tetrahedron Lett.*, **1996**, 37(9): p. 1377-1380.

- (93) Vrtis, J.M., White, A.K., Metcalf, W.W., and van der Donk, W.A., *Angew. Chem., Int. Ed.*, **2002**, 41(17): p. 3257-3259.
- (94) Eguchi, T., Kuge, Y., Inoue, K., Yoshikawa, N., Mochida, K., and Uwajima, T., *Biosci. Biotechnol. Biochem.*, **1992**, 56(5): p. 701-703.
- (95) Hall, M., Stueckler, C., Ehammer, H., Pointner, E., Oberdorfer, G., Gruber, K., Hauer, B., Stuermer, R., Kroutil, W., Macheroux, P., and Faber, K., *Adv. Synth. Catal.*, **2008**, 350(3): p. 411-418.
- (96) Stueckler, C., Hall, M., Ehammer, H., Pointner, E., Kroutil, W., Macheroux, P., and Faber, K., *Org. Lett.*, **2007**, 9(26): p. 5409-5411.
- (97) Kohlmann, C., Märkle, W., and Lütz, S., *J. Mol. Catal. B: Enzym.*, **2008**, 51(3-4): p. 57-72.
- (98) Hollmann, F., Lin, P.-C., Witholt, B., and Schmid, A., *J. Am. Chem. Soc.*, **2003**, 125(27): p. 8209-8217.
- (99) Lütz, S., *Transition Metal-Catalyzed Regeneration of Nicotinamide Cofactors*, in *The Handbook of Homogeneous Hydrogenation*, **2008**, Wiley-VCH Verlag GmbH, p. 1470-1482.
- (100) Wagenknecht, P.S., Penney, J.M., and Hembre, R.T., *Organometallics*, **2003**, 22(6): p. 1180-1182.
- (101) Monti, D., Ottolina, G., Carrea, G., and Riva, S., *Chem. Rev. (Washington, DC, U. S.)*, **2011**, 111(7): p. 4111-4140.
- (102) Gargiulo, S., Arends, I.W.C.E., and Hollmann, F., *ChemCatChem*, **2011**, 3(2): p. 338-342.
- (103) Jones, J.B. and Taylor, K.E., *J. Chem. Soc., Chem. Commun.*, **1973**, (6): p. 205-206.
- (104) Frisell, W.R., Chung, C.W., and Mackenzie, C.G., *J. Biol. Chem.*, **1959**, 234(5): p. 1297-1302.
- (105) Willner, I., Maidan, R., and Shapira, M., *J. Chem. Soc. Perk. Trans. 2*, **1990**, (4): p. 559-564.
- (106) Nam, D.H. and Park, C.B., *ChemBioChem*, **2012**, 13(9): p. 1278-1282.
- (107) Yadav, R.K., Baeg, J.-O., Oh, G.H., Park, N.-J., Kong, K.-j., Kim, J., Hwang, D.W., and Biswas, S.K., *J. Am. Chem. Soc.*, **2012**, 134(28): p. 11455-11461.
- (108) Taglieber, A., Schulz, F., Hollmann, F., Rusek, M., and Reetz, M.T., *ChemBioChem*, **2008**, 9(4): p. 565-572.
- (109) Hollmann, F., Taglieber, A., Schulz, F., and Reetz, M.T., *Angew. Chem., Int. Ed.*, **2007**, 46(16): p. 2903-2906.
- (110) Schulz, F., Leca, F.o., Hollmann, F., and Reetz, M.T., *Beilstein J. Org. Chem.*, **2005**, 1: p. 10.
- (111) Bocola, M., Schulz, F., Leca, F., Vogel, A., Fraaije, M.W., and Reetz, M.T., *Adv. Synth. Catal.*, **2005**, 347(7-8): p. 979-986.
- (112) Zilly, F.E., Taglieber, A., Schulz, F., Hollmann, F., and Reetz, M.T., *Chem. Commun. (Cambridge, U. K.)*, **2009**, (46): p. 7152-7154.
- (113) Massey, V., Stankovich, M., and Hemmerich, P., *Biochemistry*, **1978**, 17(1): p. 1-8.
- (114) Massey, V., Hemmerich, P., Knappe, W.R., Duchstein, H.J., and Fenner, H., *Biochemistry*, **1978**, 17(1): p. 9-17.
- (115) Grau, M.M., van der Toorn, J.C., Otten, L.G., Macheroux, P., Taglieber, A., Zilly, F.E., Arends, I.W.C.E., and Hollmann, F., *Adv. Synth. Catal.*, **2009**, 351(18): p. 3279-3286.

- (116) Perez, D.I., Grau, M.M., Arends, I.W.C.E., and Hollmann, F., *Chem. Commun. (Cambridge, U.K.)*, **2009**, (44): p. 6848-6850.
- (117) Churakova, E., Kluge, M., Ullrich, R., Arends, I., Hofrichter, M., and Hollmann, F., *Angew. Chem., Int. Ed.*, **2011**, 50(45): p. 10716-10719.
- (118) Burai, T.N., Panay, A.J., Zhu, H., Lian, T., and Lutz, S., *ACS Catalysis*, **2012**, 2(4): p. 667-670.
- (119) Pei, L., Liu, X., Gao, H., and Wu, Q., *Appl. Organomet. Chem.*, **2009**, 23(11): p. 455-459.
- (120) Crutchley, R.J. and Lever, A.B.P., *J. Am. Chem. Soc.*, **1980**, 102(23): p. 7128-7129.
- (121) Krejčík, M. and Vlček, A.A., *Inorg. Chem.*, **1992**, 31(12): p. 2390-2395.
- (122) Denti, G., Campagna, S., Sabatino, L., Serroni, S., Ciano, M., and Balzani, V., *Inorg. Chem.*, **1990**, 29(23): p. 4750-4758.
- (123) Bolger, J., Gourdon, A., Ishow, E., and Launay, J.-P., *Inorg. Chem.*, **1996**, 35(10): p. 2937-2944.
- (124) Anderson, P.A., Deacon, G.B., Haarmann, K.H., Keene, F.R., Meyer, T.J., Reitsma, D.A., Skelton, B.W., Strouse, G.F., and Thomas, N.C., *Inorg. Chem.*, **1995**, 34(24): p. 6145-6157.
- (125) Adalbjörnsson, B.V., Toogood, H.S., Fryszkowska, A., Pudney, C.R., Jowitt, T.A., Leys, D., and Scrutton, N.S., *ChemBioChem*, **2010**, 11(2): p. 197-207.
- (126) Gottlieb, H.E., Kotlyar, V., and Nudelman, A., *J. Org. Chem.*, **1997**, 62(21): p. 7512-7515.
- (127) Fulmer, G.R., Miller, A.J.M., Sherden, N.H., Gottlieb, H.E., Nudelman, A., Stoltz, B.M., Bercaw, J.E., and Goldberg, K.I., *Organometallics*, **2010**, 29(9): p. 2176-2179.
- (128) Kavanagh, P. and Leech, D.n., *Tetrahedron Lett.*, **2004**, 45(1): p. 121-123.
- (129) Guo, W. and Obare, S.O., *Tetrahedron Lett.*, **2008**, 49(33): p. 4933-4936.
- (130) Zhou, Z., Sarova, G.H., Zhang, S., Ou, Z., Tat, F.T., Kadish, K.M., Echegoyen, L., Guldi, D.M., Schuster, D.I., and Wilson, S.R., *Chem. – Eur. J.*, **2006**, 12(16): p. 4241-4248.
- (131) Sprecher, M., Breslow, R., Uziel, O., and Link, T.M., *Org. Prep. Proced. Int.*, **1994**, 26(6): p. 696-701.
- (132) Crutchley, R.J. and Lever, A.B.P., *Inorg. Chem.*, **1982**, 21(6): p. 2276-2282.
- (133) Rillema, D.P., Allen, G., Meyer, T.J., and Conrad, D., *Inorg. Chem.*, **1983**, 22(11): p. 1617-1622.
- (134) Crutchley, R.J., Lever, A.B.P., and Poggi, A., *Inorg. Chem.*, **1983**, 22(18): p. 2647-2650.
- (135) Lafferty, J.J. and Case, F.H., *J. Org. Chem.*, **1967**, 32(5): p. 1591-1596.
- (136) Bouilly, L., Turck, A., Plé, N., and Darabantu, M., *J. Heterocycl. Chem.*, **2005**, 42(7): p. 1423-1428.
- (137) Lin, S., Ischay, M.A., Fry, C.G., and Yoon, T.P., *J. Am. Chem. Soc.*, **2011**, 133(48): p. 19350-19353.
- (138) Fort, Y., Becker, S., and Caubère, P., *Tetrahedron*, **1994**, 50(41): p. 11893-11902.
- (139) Kong, K.C. and Cheng, C.H., *J. Am. Chem. Soc.*, **1991**, 113(16): p. 6313-6315.
- (140) Goodson, F.E., Wallow, T.I., and Novak, B.M., *Organic Synthesis Collective*, **2004**, 10: p. 501-506.

- (141) O'Keefe, D.F., Dannock, M.C., and Marcuccio, S.M., *Tetrahedron Lett.*, **1992**, 33(44): p. 6679-6680.
- (142) Hunt, A.R., Stewart, S.K., and Whiting, A., *Tetrahedron Lett.*, **1993**, 34(22): p. 3599-3602.
- (143) Vlád, G. and Horváth, I.T., *J. Org. Chem.*, **2002**, 67(18): p. 6550-6552.
- (144) Caton, M.P.L., Hurst, D.T., McOmie, J.F.W., and Hunt, R.R., *J. Chem. Soc. C*, **1967**: p. 1204-1209.
- (145) Wang, L., Zhang, Y., Liu, L., and Wang, Y., *J. Org. Chem.*, **2006**, 71(3): p. 1284-1287.
- (146) Burley, G.A., Davies, D.L., Griffith, G.A., Lee, M., and Singh, K., *J. Org. Chem.*, **2010**, 75(3): p. 980-983.
- (147) Mukhopadhyay, S., Rothenberg, G., Gitis, D., and Sasson, Y., *Org. Lett.*, **1999**, 2(2): p. 211-214.
- (148) ten Brink, G.-J., Arends, I.W.C.E., Hoogenraad, M., Verspui, G., and Sheldon, R.A., *Adv. Synth. Catal.*, **2003**, 345(4): p. 497-505.
- (149) Li, J.J., *Name Reactions: Schiemann reaction*, **2009**, Springer Berlin Heidelberg. p. 1-2.
- (150) Chan, K.S. and Tse, A.K.S., *Synth. Commun.*, **1993**, 23(14): p. 1929-1934.
- (151) McFarland, S.A., Lee, F.S., Cheng, K.A.W.Y., Cozens, F.L., and Schepp, N.P., *J. Am. Chem. Soc.*, **2005**, 127(19): p. 7065-7070.
- (152) Maury, O., Guegan, J.-P., Renouard, T., Hilton, A., Dupau, P., Sandon, N., Toupet, L., and Bozec, H.L., *New J. Chem.*, **2001**, 25(12): p. 1553-1566.
- (153) Coe, B.J., Harper, E.C., Helliwell, M., and Ta, Y.T., *Polyhedron*, **2011**, 30(11): p. 1830-1841.
- (154) Li, J.J., *Name Reactions - A Collection of Detailed Reaction Mechanisms*, **2006**, Springer Berlin Heidelberg. p. 637-639.
- (155) Jones, R.A., Roney, B.D., Sasse, W.H.F., and Wade, K.O., *J. Chem. Soc. B*, **1967**, (0): p. 106-111.
- (156) Wenkert, D. and Woodward, R.B., *J. Org. Chem.*, **1983**, 48(3): p. 283-289.
- (157) Donnici, C.L., Máximo Filho, D.H., Moreira, L.L.C., Reis, G.T.d., Cordeiro, E.S., Oliveira, I.M.F.d., Carvalho, S., and Paniago, E.B., *J. Braz. Chem. Soc.*, **1998**, 9: p. 455-460.
- (158) Moran, D.B., Morton, G.O., and Albright, J.D., *J. Heterocycl. Chem.*, **1986**, 23(4): p. 1071-1077.
- (159) Egbe, D.A.M., Amer, A.M., and Klemm, E., *Des. Monomers Polym.*, **2001**, 4(2): p. 169-175.
- (160) Iyoda, M., Otsuka, H., Sato, K., Nisato, N., and Oda, M., *Bull. Chem. Soc. Jpn.*, **1990**, 63(1): p. 80-87.
- (161) Polson, Matthew I.J., Lotoski, John A., Johansson, K.O., Taylor, Nicholas J., Hanan, Garry S., Hasenknopf, B., Thouvenot, R., Loiseau, F., Passalacqua, R., and Campagna, S., *Eur. J. Inorg. Chem.*, **2002**, 2002(10): p. 2549-2552.
- (162) Griffiths, P.M., Loiseau, F., Puntoriero, F., Serroni, S., and Campagna, S., *Chem. Commun. (Cambridge, U. K.)*, **2000**, (23): p. 2297-2298.
- (163) Jibril, I., Akasheh, T.S., and Shraim, A.M., *Polyhedron*, **1989**, 8(21): p. 2615-2619.
- (164) Zayat, L., Salierno, M., and Etchenique, R., *Inorg. Chem.*, **2006**, 45(4): p. 1728-1731.
- (165) McCusker, C.E. and McCusker, J.K., *Inorg. Chem.*, **2011**, 50(5): p. 1656-1669.

- (166) Losse, S., Görls, H., Groarke, R., Vos, J.G., and Rau, S., *Eur. J. Inorg. Chem.*, **2008**, 2008(28): p. 4448-4452.
- (167) Pichot, F., Beck, J.H., and Elliott, C.M., *J. Phys. Chem. A*, **1999**, 103(31): p. 6263-6267.
- (168) Coe, B.J., Harris, J.A., Jones, L.A., Brunschwig, B.S., Song, K., Clays, K., Garín, J., Orduna, J.s., Coles, S.J., and Hursthouse, M.B., *J. Am. Chem. Soc.*, **2005**, 127(13): p. 4845-4859.
- (169) Ta, Y.T., *Pyridinium Compounds as Sensitisers for Solar Cells*, in *Faculty of Engineering and Physical Sciences*, **2011**, University of Manchester: Manchester, UK.
- (170) Krause, R.A., *Inorg. Chim. Acta*, **1977**, 22(0): p. 209-213.
- (171) Ge, G., He, J., Guo, H., Wang, F., and Zou, D., *J. Organomet. Chem.*, **2009**, 694(19): p. 3050-3057.
- (172) Liu, Y., Turner, D.B., Singh, T.N., Angeles-Boza, A.M., Chouai, A., Dunbar, K.R., and Turro, C., *J. Am. Chem. Soc.*, **2008**, 131(1): p. 26-27.
- (173) Cox, R.H. and Bothner-By, A.A., *J. Phys. Chem.*, **1968**, 72(5): p. 1646-1649.
- (174) Bernstein, H.J. and Schneider, W.G., *J. Chem. Phys.*, **1956**, 24(2): p. 469-470.
- (175) Kowalewski, V.J., de Kowalewski, D.G., and Ferrá, E.C., *J. Mol. Spectrosc.*, **1966**, 20(3): p. 203-216.
- (176) Castellano, S., Sun, C., and Kostelnik, R., *J. Chem. Phys.*, **1967**, 46(1): p. 327-330.
- (177) Orellana, G., Alvarez Ibarra, C., and Santoro, J., *Inorg. Chem.*, **1988**, 27(6): p. 1025-1030.
- (178) Hartley, F.R., *Chem. Soc. Rev.*, **1973**, 2(2): p. 163-179.
- (179) Coe, B.J. and Glenwright, S.J., *Coord. Chem. Rev.*, **2000**, 203(1): p. 5-80.
- (180) Xie, X., Mulcahy, S.P., and Meggers, E., *Inorg. Chem.*, **2008**, 48(3): p. 1053-1061.
- (181) Danzer, G.D. and Kincaid, J.R., *J. Phys. Chem.*, **1990**, 94(10): p. 3976-3980.
- (182) Wu, J. and Kincaid, J.R., *J. Raman Spectrosc.*, **2004**, 35(11): p. 1001-1005.
- (183) Ferguson, J. and Herren, F., *Chem. Phys. Lett.*, **1982**, 89(5): p. 371-375.
- (184) Ceulemans, A. and Vanquickenborne, L.G., *J. Am. Chem. Soc.*, **1981**, 103(9): p. 2238-2241.
- (185) Coe, B.J., Foxon, S.P., Harper, E.C., Helliwell, M., Raftery, J., Swanson, C.A., Brunschwig, B.S., Clays, K., Franz, E., Garín, J., Orduna, J., Horton, P.N., and Hursthouse, M.B., *J. Am. Chem. Soc.*, **2010**, 132(5): p. 1706-1723.
- (186) Coe, B.J., Harris, J.A., Brunschwig, B.S., Asselberghs, I., Clays, K., Garín, J., and Orduna, J., *J. Am. Chem. Soc.*, **2005**, 127(38): p. 13399-13410.
- (187) Balk, R.W., Stufkens, D.J., Crutchley, R.J., and Lever, A.B.P., *Inorg. Chim. Acta*, **1982**, 64(0): p. L49-L50.
- (188) Lever, A.B.P., London, G., and McCarthy, P.J., *Can. J. Chem.*, **1977**, 55(17): p. 3172-3189.
- (189) Anderson, P.A., Anderson, R.F., Furue, M., Junk, P.C., Keene, F.R., Patterson, B.T., and Yeomans, B.D., *Inorg. Chem.*, **2000**, 39(13): p. 2721-2728.
- (190) Lever, A.B.P., *Inorg. Chem.*, **1990**, 29(6): p. 1271-1285.
- (191) Frisch, M.J., Trucks, G.W., Schlegel, H.B., Scuseria, G.E., Robb, M.A., Cheeseman, J.R., Scalmani, G., Barone, V., Mennucci, B., Petersson, G.A., Nakatsuji, H., Caricato, M., Li, X., Hratchian, H.P., Izmaylov, A.F., Bloino, J., Zheng, G., Sonnenberg, J.L., Hada, M., Ehara, M., Toyota, K., Fukuda, R., Hasegawa, J., Ishida, M., Nakajima, T., Honda, Y., Kitao, O., Nakai,

- H., Vreven, T., Montgomery, J.A., Peralta, J.E., Ogliaro, F., Bearpark, M., Heyd, J.J., Brothers, E., Kudin, K.N., Staroverov, V.N., Kobayashi, R., Normand, J., Raghavachari, K., Rendell, A., Burant, J.C., Iyengar, S.S., Tomasi, J., Cossi, M., Rega, N., Millam, J.M., Klene, M., Knox, J.E., Cross, J.B., Bakken, V., Adamo, C., Jaramillo, J., Gomperts, R., Stratmann, R.E., Yazyev, O., Austin, A.J., Cammi, R., Pomelli, C., Ochterski, J.W., Martin, R.L., Morokuma, K., Zakrzewski, V.G., Voth, G.A., Salvador, P., Dannenberg, J.J., Dapprich, S., Daniels, A.D., Farkas, Foresman, J.B., Ortiz, J.V., Cioslowski, J., and Fox, D.J., *Gaussian 09, Revision B.01*, **2009**: Wallingford CT.
- (192) Perdew, J.P., *Phys. Rev. B*, **1986**, 33(12): p. 8822-8824.
- (193) Becke, A.D., *Phys. Rev. A*, **1988**, 38(6): p. 3098-3100.
- (194) Becke, A.D., *J. Chem. Phys.*, **1993**, 98(7): p. 5648-5652.
- (195) Adamo, C. and Barone, V., *J. Chem. Phys.*, **1999**, 110(13): p. 6158-6170.
- (196) Zhao, Y. and Truhlar, D., *Theor. Chem. Acc.*, **2008**, 120(1-3): p. 215-241.
- (197) Weigend, F., Furche, F., and Ahlrichs, R., *J. Chem. Phys.*, **2003**, 119(24): p. 12753-12762.
- (198) Andrae, D., Häußermann, U., Dolg, M., Stoll, H., and Preuß, H., *Theor. Chem. Accounts Theor. Comput. Model. Theor. Chim. Acta*, **1990**, 77(2): p. 123-141.
- (199) Weigend, F. and Ahlrichs, R., *Phys. Chem. Chem. Phys.*, **2005**, 7(18): p. 3297-3305.
- (200) Barone, V. and Cossi, M., *J. Phys. Chem. A*, **1998**, 102(11): p. 1995-2001.
- (201) Cossi, M., Rega, N., Scalmani, G., and Barone, V., *J. Comput. Chem.*, **2003**, 24(6): p. 669-681.
- (202) O'Boyle, N.M., Tenderholt, A.L., and Langner, K.M., *J. Comput. Chem.*, **2008**, 29(5): p. 839-845.
- (203) Lai, H., Jones, D.S., Schwind, D.C., and Rillema, D.P., *J. Chem. Crystallogr.*, **1990**, 20(4): p. 321-325.
- (204) Alary, F., Heully, J.L., Bijeire, L., and Vicendo, P., *Inorg. Chem.*, **2007**, 46(8): p. 3154-3165.
- (205) Zheng, K.C., Wang, J.P., Peng, W.L., Liu, X.W., and Yun, F.C., *J. Mol. Struct. Theochem.*, **2002**, 582(1-3): p. 1-9.
- (206) Stoyanov, S.R., Villegas, J.M., and Rillema, D.P., *Inorg. Chem.*, **2002**, 41(11): p. 2941-2945.
- (207) Bonnet, S., Collin, J.-P., Gruber, N., Sauvage, J.-P., and Schofield, E.R., *Dalton Trans.*, **2003**, (24): p. 4654-4662.
- (208) Shen, Y., Walters, K.A., Abboud, K., and Schanze, K.S., *Inorg. Chim. Acta*, **2000**, 300-302(0): p. 414-426.
- (209) Matheis, W., Poppe, J., Kaim, W., and Zalis, S., *J. Chem. Soc., Perkin Trans. 2*, **1994**, (9): p. 1923-1928.
- (210) Kaim, W. and Matheis, W., *Chem. Ber.*, **1990**, 123(6): p. 1323-1325.
- (211) Baldo, M.A., O'Brien, D.F., You, Y., Shoustikov, A., Sibley, S., Thompson, M.E., and Forrest, S.R., *Nature*, **1998**, 395(6698): p. 151-154.
- (212) Evans, R.C., Douglas, P., and Winscom, C.J., *Coord. Chem. Rev.*, **2006**, 250(15-16): p. 2093-2126.

- (213) Lamansky, S., Djurovich, P., Murphy, D., Abdel-Razzaq, F., Lee, H.-E., Adachi, C., Burrows, P.E., Forrest, S.R., and Thompson, M.E., *J. Am. Chem. Soc.*, **2001**, *123*(18): p. 4304-4312.
- (214) Tsuboyama, A., Iwawaki, H., Furugori, M., Mukaide, T., Kamatani, J., Igawa, S., Moriyama, T., Miura, S., Takiguchi, T., Okada, S., Hoshino, M., and Ueno, K., *J. Am. Chem. Soc.*, **2003**, *125*(42): p. 12971-12979.
- (215) Constable, E.C., Housecroft, C.E., Schönhofer, E., Schönle, J., and Zampese, J.A., *Polyhedron*, **2012**, *35*(1): p. 154-160.
- (216) Nazeeruddin, M.K., Wegeh, R.T., Zhou, Z., Klein, C., Wang, Q., De Angelis, F., Fantacci, S., and Grätzel, M., *Inorg. Chem.*, **2006**, *45*(23): p. 9245-9250.
- (217) Lau, J.S.-Y., Lee, P.-K., Tsang, K.H.-K., Ng, C.H.-C., Lam, Y.-W., Cheng, S.-H., and Lo, K.K.-W., *Inorg. Chem.*, **2008**, *48*(2): p. 708-718.
- (218) Lo, K.K.-W., Chung, C.-K., Lee, T.K.-M., Lui, L.-H., Tsang, K.H.-K., and Zhu, N., *Inorg. Chem.*, **2003**, *42*(21): p. 6886-6897.
- (219) Lo, K.K.-W., Ng, D.C.-M., and Chung, C.-K., *Organometallics*, **2001**, *20*(24): p. 4999-5001.
- (220) Zhao, Q., Li, F., Liu, S., Yu, M., Liu, Z., Yi, T., and Huang, C., *Inorg. Chem.*, **2008**, *47*(20): p. 9256-9264.
- (221) Zhao, N., Wu, Y.-H., Shi, L.-X., Lin, Q.-P., and Chen, Z.-N., *Dalton Trans.*, **2010**, *39*(35): p. 8288-8295.
- (222) Baranoff, E., Yum, J.-H., Graetzel, M., and Nazeeruddin, M.K., *J. Organomet. Chem.*, **2009**, *694*(17): p. 2661-2670.
- (223) Mayo, E.I., Kilsa, K., Tirrell, T., Djurovich, P.I., Tamayo, A., Thompson, M.E., Lewis, N.S., and Gray, H.B., *Photochem. Photobiol. Sci.*, **2006**, *5*(10): p. 871-873.
- (224) King, K.A., Spellane, P.J., and Watts, R.J., *J. Am. Chem. Soc.*, **1985**, *107*(5): p. 1431-1432.
- (225) Cline, E.D., Adamson, S.E., and Bernhard, S., *Inorg. Chem.*, **2008**, *47*(22): p. 10378-10388.
- (226) Goldsmith, J.I., Hudson, W.R., Lowry, M.S., Anderson, T.H., and Bernhard, S., *J. Am. Chem. Soc.*, **2005**, *127*(20): p. 7502-7510.
- (227) Sajoto, T., Djurovich, P.I., Tamayo, A., Yousufuddin, M., Bau, R., Thompson, M.E., Holmes, R.J., and Forrest, S.R., *Inorg. Chem.*, **2005**, *44*(22): p. 7992-8003.
- (228) Dedeian, K., Djurovich, P.I., Garces, F.O., Carlson, G., and Watts, R.J., *Inorg. Chem.*, **1991**, *30*(8): p. 1685-1687.
- (229) Tamayo, A.B., Alleyne, B.D., Djurovich, P.I., Lamansky, S., Tsyba, I., Ho, N.N., Bau, R., and Thompson, M.E., *J. Am. Chem. Soc.*, **2003**, *125*(24): p. 7377-7387.
- (230) Baranoff, E., Curchod, B.F.E., Monti, F., Steimer, F.d.r., Accorsi, G., Tavernelli, I., Rothlisberger, U., Scopelliti, R., Grätzel, M., and Nazeeruddin, M.K., *Inorg. Chem.*, **2011**, *51*(2): p. 799-811.
- (231) Byun, Y., Lyu, Y.Y., Das, R.R., Kwon, O., Lee, T.W., and Park, Y.J., *Appl. Phys. Lett.*, **2007**, *91*(21).
- (232) Jiang, W., Gao, Y., Sun, Y., Ding, F., Xu, Y., Bian, Z., Li, F., Bian, J., and Huang, C., *Inorg. Chem.*, **2010**, *49*(7): p. 3252-3260.

- (233) Sun, P., Lu, X., Fan, Q., Zhang, Z., Song, W., Li, B., Huang, L., Peng, J., and Huang, W., *Macromolecules*, **2011**, 44(22): p. 8763-8770.
- (234) Ma, Y., Liu, S., Yang, H., Wu, Y., Yang, C., Liu, X., Zhao, Q., Wu, H., Liang, J., Li, F., and Huang, W., *J. Mater. Chem.*, **2011**, 21(47): p. 18974-18982.
- (235) Monk, P.M.S., *The viologens: physicochemical properties, synthesis, and applications of the salts of 4,4'-bipyridine*, **1998**: Wiley.
- (236) Dholakia, S., Gillard, R.D., and Wimmer, F.L., *Inorg. Chim. Acta*, **1983**, 69(0): p. 179-181.
- (237) Wimmer, F.L. and Wimmer, S., *Polyhedron*, **1985**, 4(9): p. 1665-1666.
- (238) Wimmer, F.L., Wimmer, S., and Castan, P., *J. Organomet. Chem.*, **1992**, 424(1): p. 99-104.
- (239) Yang, L., Wimmer, F.L., Wimmer, S., Zhao, J., and Braterman, P.S., *J. Organomet. Chem.*, **1996**, 525(1-2): p. 1-8.
- (240) Castan, P., Jaud, J., Wimmer, S., and Wimmer, F.L., *J. Chem. Soc., Dalton Trans.*, **1991**, (4): p. 1155-1158.
- (241) Braterman, P.S., Jae-Inh, S., Wimmer, F.M., and Wimmer, S., *Inorg. Chim. Acta*, **1991**, 189(1): p. 7-9.
- (242) Wimmer, F.L., *Inorg. Chim. Acta*, **1987**, 130(2): p. 259-264.
- (243) Koizumi, T.-a., Tomon, T., and Tanaka, K., *J. Organomet. Chem.*, **2005**, 690(5): p. 1258-1264.
- (244) Song, G., Zhang, Y., Su, Y., Deng, W., Han, K., and Li, X., *Organometallics*, **2008**, 27(23): p. 6193-6201.
- (245) Liu, C. and Yang, W., *Chem. Commun. (Cambridge, U. K.)*, **2009**, (41): p. 6267-6269.
- (246) Nonoyama, M., *Bull. Chem. Soc. Jpn.*, **1974**, 47(3): p. 767-768.
- (247) Gütz, C. and Lützen, A., *Synthesis*, **2010**, 2010(01): p. 85-90.
- (248) Heller, M. and Schubert, U.S., *J. Org. Chem.*, **2002**, 67(23): p. 8269-8272.
- (249) Luzung, M.R., Patel, J.S., and Yin, J., *J. Org. Chem.*, **2010**, 75(23): p. 8330-8332.
- (250) Jensen, A.E., Dohle, W., Sapountzis, I., Lindsay, D.M., Vu, V.A., and Knochel, P., *Synthesis*, **2002**, 2002(04): p. 0565,0569.
- (251) Ila, H., Baron, O., Wagner, A.J., and Knochel, P., *Chem. Commun. (Cambridge, U. K.)*, **2006**, (6): p. 583-593.
- (252) Nishigaki, J. and Deguchi, Y., *Oxonol compound, light-sensitive material and process for the synthesis of oxonol compound*, 2000, Fuji Photo Film Co., Ltd., Japan . p. 72 pp., Cont.-in-part of U.S. Ser. No. 896,064, abandoned.
- (253) Norrby, T., Borje, A., Zhang, L., and Akermark, B., *Acta Chem. Scand.*, **1998**, 52(0): p. 77-85.
- (254) Schuster, O., Yang, L., Raubenheimer, H.G., and Albrecht, M., *Chem. Rev. (Washington, DC, U. S.)*, **2009**, 109(8): p. 3445-3478.
- (255) McGee, K.A. and Mann, K.R., *Inorg. Chem.*, **2007**, 46(19): p. 7800-7809.
- (256) Katritzky, A.R. and Dega-Szafran, Z., *Magn. Reson. Chem.*, **1989**, 27(11): p. 1090-1093.
- (257) Joule, J.A. and Mills, K., *Heterocyclic Chemistry*. 5 ed, **2010**: John Wiley & Sons. 718.
- (258) Garces, F.O., Watts, R.J., *Magn. Reson. Chem.*, **1993**, 31(6): p. 529-536.

- (259) Garces, F.O., King, K.A., and Watts, R.J., *Inorg. Chem.*, **1988**, 27(20): p. 3464-3471.
- (260) Krumholz, P., *J. Am. Chem. Soc.*, **1951**, 73(7): p. 3487-3492.
- (261) Pérez-Hernández, N., Álvarez-Cisneros, C., Cerda-García-Rojas, C.M., Morales-Ríos, M.S., and Joseph-Nathan, P., *Magn. Reson. Chem.*, **2009**, 47(5): p. 437-442.
- (262) Rottendorf, H. and Sternhell, S., *Aust. J. Chem.*, **1964**, 17(12): p. 1315-1328.
- (263) Reddy, G.S., Hobgood, R.T., and Goldstein, J.H., *J. Am. Chem. Soc.*, **1962**, 84(3): p. 336-340.
- (264) Barfield, M. and Chakrabarti, B., *Chem. Rev. (Washington, DC, U. S.)*, **1969**, 69(6): p. 757-778.
- (265) Schröder, H. and Haslinger, E., *Magn. Reson. Chem.*, **1994**, 32(1): p. 12-15.
- (266) Schaefer, T. and Chum, K., *Can. J. Chem.*, **1976**, 54(14): p. 2231-2234.
- (267) Hilton, J. and Sutcliffe, L.H., *Prog. Nucl. Magn. Reson. Spectrosc.*, **1975**, 10(1): p. 27-39.
- (268) Myhre, P.C., Edmonds, J.W., and Kruger, J.D., *J. Am. Chem. Soc.*, **1966**, 88(11): p. 2459-2466.
- (269) Bhacca, N.S., Juneau, G.P., Lankin, D.C., Mukherjee, B., Seal, T., Escobedo, J.O., and Strongin, R.M., *Org. Lett.*, **2000**, 2(24): p. 3813-3815.
- (270) Lo, K.K.-W., Chung, C.-K., and Zhu, N., *Chem. – Eur. J.*, **2003**, 9(2): p. 475-483.
- (271) Neve, F., Crispini, A., Campagna, S., and Serroni, S., *Inorg. Chem.*, **1999**, 38(10): p. 2250-2258.
- (272) Il'inchik, E., Polyanskaya, T., and Volkov, V., *J. Struct. Chem.*, **2007**, 48(2): p. 300-309.
- (273) Snow, M.R. and Tiekink, E.R.T., *Z. Kristallogr.*, **1992**, 198(1-2): p. 148-150.
- (274) Castan, P., Dahan, F., Wimmer, S., and Wimmer, F.L., *J. Chem. Soc. Dalton Trans.*, **1990**, (10): p. 2971-2977.
- (275) Ohsawa, Y., Sprouse, S., King, K.A., DeArmond, M.K., Hanck, K.W., and Watts, R.J., *J. Phys. Chem.*, **1987**, 91(5): p. 1047-1054.
- (276) Calogero, G., Giuffrida, G., Serroni, S., Ricevuto, V., and Campagna, S., *Inorg. Chem.*, **1995**, 34(3): p. 541-545.
- (277) Collin, J.-P., Dixon, I.M., Sauvage, J.-P., Williams, J.A.G., Barigelletti, F., and Flamigni, L., *J. Am. Chem. Soc.*, **1999**, 121(21): p. 5009-5016.
- (278) Flamigni, L., Ventura, B., Barigelletti, F., Baranoff, E., Collin, J.-P., and Sauvage, J.-P., *Eur. J. Inorg. Chem.*, **2005**, 2005(7): p. 1312-1318.
- (279) Kahl, J.L., Hanck, K.W., and DeArmond, K., *J. Phys. Chem.*, **1978**, 82(5): p. 540-545.
- (280) King, K.A. and Watts, R.J., *J. Am. Chem. Soc.*, **1987**, 109(5): p. 1589-1590.
- (281) Didier, P., Ortmans, I., Kirsch-De Mesmaeker, A., and Watts, R.J., *Inorg. Chem.*, **1993**, 32(23): p. 5239-5245.
- (282) Weiner, M.A. and Basu, A., *Inorg. Chem.*, **1980**, 19(9): p. 2797-2800.
- (283) Jasinski, R.J., *J. Electrochem. Soc.*, **1977**, 124(5): p. 637-641.
- (284) Osawa, M. and Suetaka, W., *J. Electroanal. Chem. Interfac.*, **1989**, 270(1-2): p. 261-272.
- (285) Jasinski, R.J., *J. Electrochem. Soc.*, **1978**, 125(10): p. 1619-1623.
- (286) Bird, C.L. and Kuhn, A.T., *Chem. Soc. Rev.*, **1981**, 10(1): p. 49-82.

- (287) Shavaleev, N.M., Scopelliti, R., Baranoff, E., Grätzel, M., and Nazeeruddin, M.K., *Inorg. Chim. Acta*, **2012**, 383(0): p. 316-319.
- (288) Ahmad, H., Meijer, A.J.H.M., and Thomas, J.A., *Chemistry – An Asian Journal*, **2011**, 6(9): p. 2339-2351.
- (289) De Crisci, A.G., Lough, A.J., Multani, K., and Fekl, U., *Organometallics*, **2008**, 27(8): p. 1765-1779.
- (290) Cummings, S.D. and Eisenberg, R., *Inorg. Chem.*, **1995**, 34(8): p. 2007-2014.
- (291) Makedonas, C. and Mitsopoulou, C.A., *Inorg. Chim. Acta*, **2007**, 360(14): p. 3997-4009.
- (292) Makedonas, C., Veroni, I., and Mitsopoulou, C.A., *Eur. J. Inorg. Chem.*, **2007**, 2007(1): p. 120-131.
- (293) Strong, E.T.J., Price, J.T., and Jones, N.D., *Dalton Trans.*, **2009**, (42): p. 9123-9125.
- (294) Koizumi, T.-a., Tomon, T., and Tanaka, K., *Organometallics*, **2003**, 22(5): p. 970-975.
- (295) Koizumi, T.-a., Tomon, T., and Tanaka, K., *J. Organomet. Chem.*, **2005**, 690(19): p. 4272-4279.
- (296) Koizumi, T.-a., Tomon, T., and Tanaka, K., *Bull. Chem. Soc. Jpn.*, **2003**, 76(10): p. 1969-1975.
- (297) Schneider, S.K., Julius, G.R., Loschen, C., Raubenheimer, H.G., Frenking, G., and Herrmann, W.A., *Dalton Trans.*, **2006**, (9): p. 1226-1233.
- (298) Schneider, S.K., Roembke, P., Julius, G.R., Loschen, C., Raubenheimer, H.G., Frenking, G., and Herrmann, W.A., *Eur. J. Inorg. Chem.*, **2005**, 2005(15): p. 2973-2977.
- (299) Tonner, R., Heydenrych, G., and Frenking, G., *Chem. – Asian J.*, **2007**, 2(12): p. 1555-1567.
- (300) Owen, J.S., Labinger, J.A., and Bercaw, J.E., *J. Am. Chem. Soc.*, **2004**, 126(26): p. 8247-8255.
- (301) Álvarez, E., Conejero, S., Lara, P., López, J.A., Paneque, M., Petronilho, A., Poveda, M.L., del Río, D., Serrano, O., and Carmona, E., *J. Am. Chem. Soc.*, **2007**, 129(46): p. 14130-14131.
- (302) Álvarez, E., Conejero, S., Paneque, M., Petronilho, A., Poveda, M.L., Serrano, O., and Carmona, E., *J. Am. Chem. Soc.*, **2006**, 128(40): p. 13060-13061.
- (303) Conejero, S., Lara, P., Paneque, M., Petronilho, A., Poveda, M.L., Serrano, O., Vattier, F., Álvarez, E., Maya, C., Salazar, V., and Carmona, E., *Angew. Chem., Int. Ed.*, **2008**, 47(23): p. 4380-4383.
- (304) Song, G., Li, Y., Chen, S., and Li, X., *Chem. Commun. (Cambridge, U. K.)*, **2008**, (30): p. 3558-3560.
- (305) Cheng, W.-C. and Kurth, M.J., *Org. Prep. Proced. Int.*, **2002**, 34(6): p. 585-608.
- (306) Connick, W.B., Di Bilio, A.J., Hill, M.G., Winkler, J.R., and Gray, H.B., *Inorg. Chim. Acta*, **1995**, 240(1-2): p. 169-173.
- (307) Lam, L.S.M. and Chan, W.K., *ChemPhysChem*, **2001**, 2(4): p. 252-256.
- (308) Lo, K., *Exploitation of Luminescent Organometallic Rhenium(I) and Iridium(III) Complexes in Biological Studies Photophysics of Organometallics*, A.J. Lees, Editor **2010**, Springer Berlin / Heidelberg. p. 73-114.

- (309) Kumar, A., Sun, S.-S., and Lees, A., *Photophysics and Photochemistry of Organometallic Rhenium Diimine Complexes*, A.J. Lees, Editor **2010**, Springer Berlin / Heidelberg. p. 37-71.
- (310) Jiang, W., Liu, J., and Li, C., *Inorg. Chem. Commun.*, **2012**, 16(0): p. 81-85.
- (311) Liu, J.-H. and Jiang, W.-N., *Dalton Trans.*, **2012**, 41(32): p 9700-9707.
- (312) Helberg, L.E., Orth, S.D., Sabat, M., and Harman, W.D., *Inorg. Chem.*, **1996**, 35(19): p. 5584-5594.
- (313) Binks, P.R., French, C.E., Nicklin, S., and Bruce, N.C., *Appl. Environ. Microbiol.*, **1996**, 62(4): p. 1214-9.
- (314) French, C.E., Nicklin, S., and Bruce, N.C., *J. Bacteriol.*, **1996**, 178(22): p. 6623-7.
- (315) Khan, H., Harris, R.J., Barna, T., Craig, D.H., Bruce, N.C., Munro, A.W., Moody, P.C.E., and Scrutton, N.S., *J. Biol. Chem.*, **2002**, 277(24): p. 21906-21912.
- (316) Barna, T.M., Khan, H., Bruce, N.C., Barsukov, I., Scrutton, N.S., and Moody, P.C.E., *J. Mol. Biol.*, **2001**, 310(2): p. 433-447.
- (317) Khan, H., Barna, T., Harris, R.J., Bruce, N.C., Barsukov, I., Munro, A.W., Moody, P.C.E., and Scrutton, N.S., *J. Biol. Chem.*, **2004**, 279(29): p. 30563-30572.
- (318) Khan, H., Barna, T., Bruce, N.C., Munro, A.W., Leys, D., and Scrutton, N.S., *FEBS J.*, **2005**, 272(18): p. 4660-4671.
- (319) Fryszkowska, A., Toogood, H., Sakuma, M., Stephens, G.M., Gardiner, J.M., and Scrutton, N.S., *Catal. Sci. Tech.*, **2011**, 1(6): p. 948-957.
- (320) Toogood, H.S., Fryszkowska, A., Hulley, M., Sakuma, M., Mansell, D., Stephens, G.M., Gardiner, J.M., and Scrutton, N.S., *ChemBioChem*, **2011**, 12(5): p. 738-749.
- (321) Stewart, R.C. and Massey, V., *J. Biol. Chem.*, **1985**, 260(25): p. 13639-47.
- (322) Craig, D.H., Barna, T., Moody, P.C., Bruce, N.C., Chapman, S.K., Munro, A.W., and Scrutton, N.S., *Biochem. J.*, **2001**, 359(2): p. 315-323.
- (323) Vaz, A.D.N., Chakraborty, S., and Massey, V., *Biochemistry*, **1995**, 34(13): p. 4246-4256.
- (324) Kohli, R.M. and Massey, V., *J. Biol. Chem.*, **1998**, 273(49): p. 32763-32770.
- (325) Stuermer, R., Hauer, B., Hall, M., and Faber, K., *Curr. Opin. Chem. Biol.*, **2007**, 11(2): p. 203-213.
- (326) Bougioukou, D.J. and Stewart, J.D., *J. Am. Chem. Soc.*, **2008**, 130(24): p. 7655-7658.
- (327) Shimoda, K., Ito, D.I., Izumi, S., and Hirata, T., *J. Chem. Soc. Perkin Trans. 1*, **1996**, (4): p. 355-358.
- (328) Mueller, N.J., Stueckler, C., Hauer, B., Baudendistel, N., Housden, H., Bruce, N.C., and Faber, K., *Adv. Synth. Catal.*, **2010**, 352(2-3): p. 387-394.
- (329) Toogood, H.S., Gardiner, J.M., and Scrutton, N.S., *ChemCatChem*, **2010**, 2(8): p. 892-914.
- (330) Heseck, D., Lee, M., Zhang, W., Noll, B.C., and Mobashery, S., *J. Am. Chem. Soc.*, **2009**, 131(14): p. 5187-5193.
- (331) Seki, M., Yamanaka, T., and Kondo, K., *J. Org. Chem.*, **2000**, 65(2): p. 517-522.
- (332) Narendra, N., Lalithamba, H.S., and Sureshbabu, V.V., *Tetrahedron Lett.*, **2010**, 51(47): p. 6169-6173.

- (333) Righi, G., Ciambrone, S., D'Achille, C., Leonelli, A., and Bonini, C., *Tetrahedron*, **2006**, 62(50): p. 11821-11826.
- (334) Müller, A., Stürmer, R., Hauer, B., and Rosche, B., *Angew. Chem., Int. Ed.*, **2007**, 46(18): p. 3316-3318.
- (335) Fryszkowska, A., Toogood, H., Sakuma, M., Gardiner, J.M., Stephens, G.M., and Scrutton, N.S., *Adv. Synth. Catal.*, **2009**, 351(17): p. 2976-2990.
- (336) Katritzky, A.R., Yao, J., Qi, M., Chou, Y., Sikora, D.J., and Davis, S., *Heterocycles*, **1998**, 48(12): p. 2677-2691.
- (337) Davis, E.M., Ringer, K.L., McConkey, M.E., and Croteau, R., *Plant Physiol.*, **2005**, 137(3): p. 873-881.
- (338) Bouwmeester, H.J., Gershenzon, J., Konings, M.C.J.M., and Croteau, R., *Plant Physiol.*, **1998**, 117(3): p. 901-912.
- (339) Winkler, C.K., Tasnádi, G., Clay, D., Hall, M., and Faber, K., *J. Biotechnol.*, **2012**, 162(4): p. 381-389.
- (340) Ono, N., *Conversion of Nitro Compounds into Other Compounds*, in *The Nitro Group in Organic Synthesis*, **2002**, John Wiley & Sons, Inc. p. 159-181.
- (341) Toogood, H.S., Fryszkowska, A., Hare, V., Fisher, K., Roujeinikova, A., Leys, D., Gardiner, J.M., Stephens, G.M., and Scrutton, N.S., *Adv. Synth. Catal.*, **2008**, 350(17): p. 2789-2803.
- (342) Meah, Y. and Massey, V., *Proc. Natl. Acad. Sci. U.S.A.*, **2000**, 97(20): p. 10733-10738.
- (343) Mueller, F., Bruestlein, M., Hemmerich, P., Massey, V., and Walker, W.H., *Eur. J. Biochem.*, **1972**, 25(3): p. 573-80.
- (344) Onyenwoke, R.U., Kevbrin, V.V., Lysenko, A.M., and Wiegel, J., *Int. J. Syst. Evol. Microbiol.*, **2007**, 57(10): p. 2191-2193.
- (345) Fitzpatrick, T.B., Amrhein, N., and Macheroux, P., *J. Biol. Chem.*, **2003**, 278(22): p. 19891-19897.
- (346) Guagliardi, A., Manco, G., Rossi, M., and Bartolucci, S., *Eur. J. Biochem.*, **1989**, 183(1): p. 25-30.
- (347) Owusu, R.K. and Cowan, D.A., *Enzyme Microb. Technol.*, **1989**, 11(9): p. 568-574.
- (348) Page, C.C., Moser, C.C., and Dutton, P.L., *Curr. Opin. Chem. Biol.*, **2003**, 7(5): p. 551-556.
- (349) Trump, E.L. and Zhou, M.X., *Trans. Kans. Acad. Sci. (1903-)*, **1993**, 96(3/4): p. 167-180.
- (350) Berg, Katja E., Tran, A., Raymond, Mary K., Abrahamsson, M., Wolny, J., Redon, S., Andersson, M., Sun, L., Styring, S., Hammarström, L., Toftlund, H., and Åkermark, B., *Eur. J. Inorg. Chem.*, **2001**, 2001(4): p. 1019-1029.
- (351) Geren, L., Durham, B., and Millett, F., *Chapter 28 Use of Ruthenium Photoreduction Techniques to Study Electron Transfer in Cytochrome Oxidase*, in *Methods in Enzymology*, S.A. William and E.S. Immo, Editors. **2009**, Academic Press. p. 507-520.
- (352) Robinson, H.H. and Yocum, C.F., *Biochim. Biophys. Acta, Bioenerg.*, **1980**, 590(1): p. 97-106.
- (353) Kalyanasundaram, K., Kiwi, J., and Grätzel, M., *Helv. Chim. Acta*, **1978**, 61(7): p. 2720-2730.

- (354) Miller, D. and McLendon, G., *Inorg. Chem.*, **1981**, 20(3): p. 950-953.
- (355) Harriman, A. and Mills, A., *J. Chem. Soc., Faraday Trans. 2*, **1981**, 77(11): p. 2111-2124.
- (356) Venturi, M., Mulazzani, Q.G., Ciano, M., and Hoffman, M.Z., *Inorg. Chem.*, **1986**, 25(25): p. 4493-4498.
- (357) Mulazzani, Q.G., Venturi, M., and Hoffman, M.Z., *Int. J. Radiat. Applic. Instrum., C*, **1988**, 32(1): p. 71-78.
- (358) Sakai, K., Nakazawa, A., Kondo, K., and Ohta, H., *Agric. Biol. Chem.*, **1985**, 49(8): p. 2331-2335.
- (359) Hall, M., Stueckler, C., Hauer, B., Stuermer, R., Friedrich, T., Breuer, M., Kroutil, W., and Faber, K., *Eur. J. Org. Chem.*, **2008**, 2008(9): p. 1511-1516.
- (360) Barltrop, J.A. and Bunce, N.J., *J. Chem. Soc., C*, **1968**, p. 1467-1474.
- (361) Frolov, A.N., Kuznetsova, N.y.A., and El'tsov, A.V., *Russ. Chem. Rev.*, **1976**, 45(11): p. 1024.
- (362) Kjtaura, Y. and Matsuura, T., *Tetrahedron*, **1971**, 27(8): p. 1583-1595.
- (363) Park, K.K., Oh, C.H., and Joung, W.K., *Tetrahedron Lett.*, **1993**, 34(46): p. 7445-7446.
- (364) Park, K.K., Oh, C.H., and Sim, W.-J., *J. Org. Chem.*, **1995**, 60(19): p. 6202-6204.
- (365) Stueckler, C., Mueller, N.J., Winkler, C.K., Glueck, S.M., Gruber, K., Steinkellner, G., and Faber, K., *Dalton Trans.*, **2010**, 39(36): p. 8472-8476.
- (366) Prasad, D.R. and Hoffman, M.Z., *J. Am. Chem. Soc.*, **1986**, 108(10): p. 2568-2573.
- (367) *CrysAlisPro* (Ver. 1.171.34.44), Agilent Technologies Ltd., Yarnton, Oxfordshire, United Kingdom, **2010**.
- (368) *SMART* (Ver. 2.03a), Bruker AXS Inc., Madison, Wisconsin, USA, **2002**.
- (369) *SADABS* (Ver. 2.03a), Bruker AXS Inc., Madison, Wisconsin, USA, **2002**.
- (370) Burla, M.C., Caliendo, R., Camalli, M., Carrozzini, B., Cascarano, G.L., De Caro, L., Giacovazzo, C., Polidori, G., and Spagna, R., *J. Appl. Crystallogr.*, **2005**, 38(2): p. 381-388.
- (371) *SHELXS-97* (Ver. Sheldrick, G.M., University of Göttingen, Göttingen, Germany, **1997**.
- (372) *SHELXL-97* (Ver. Sheldrick, G.M., University of Göttingen, Göttingen, Germany, **1997**.
- (373) *SHELXTL* (Ver. 6.12), Bruker AXS Inc., Madison, Wisconsin, USA, **2001**.